

Supramolecular chemistry of fullerenes

Guest editors: Nazario Martín^a and Jean-François Nierengarten^b

^a*Grupo de Materiales Moleculares Orgánicos, Departamento de Química Orgánica, Facultad de Química, Universidad Complutense, E-28040 Madrid, Spain*

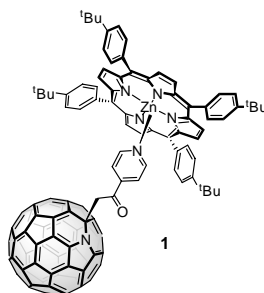
^b*Groupe de Chimie des Fullerènes et des Systèmes Conjugués, Laboratoire de Chimie de Coordination du CNRS 205, route de Nasbonne, 31077 Toulouse Cedex 4, France*

Contents

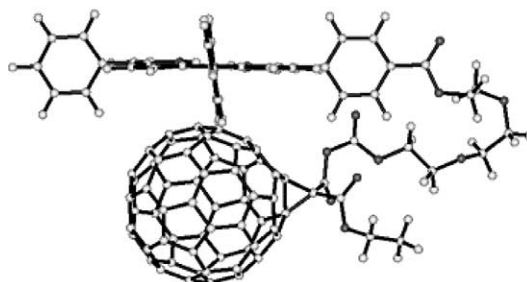
Announcement: Tetrahedron Symposia-in-Print	pp 1913–1915
Preface	p 1917
Foreword	p 1919
Foreword	p 1921

ARTICLES

Covalently linked heterofullerene–porphyrin conjugates; new model systems for long-lived intramolecular charge separation	pp 1923–1927
Frank Hauke, Stefan Atalick, Dirk M. Guldi* and Andreas Hirsch*	



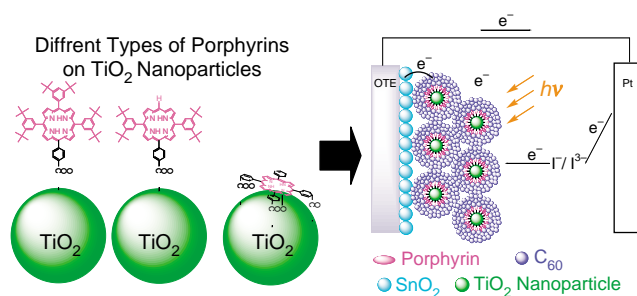
Synthesis and photophysics of porphyrin–fullerene donor–acceptor dyads with conformationally flexible linkers	pp 1928–1936
David I. Schuster,* Shaun MacMahon, Dirk M. Guldi, Luis Echegoyen and Silvia E. Braslavsky	



Supramolecular nanostructured assemblies of different types of porphyrins with fullerene using TiO₂ nanoparticles for light energy conversion

pp 1937–1946

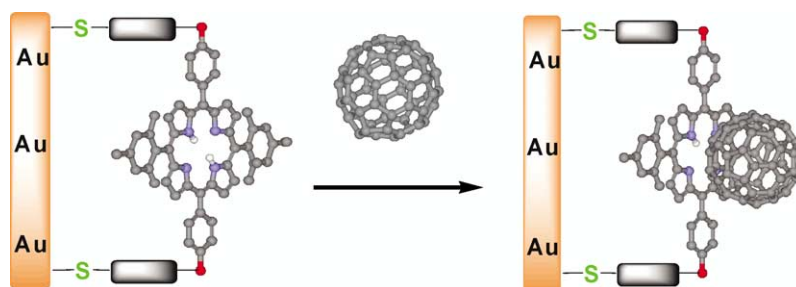
Taku Hasobe, Shigeki Hattori, Prashant V. Kamat* and Shunichi Fukuzumi*



Non-covalent immobilization of C₆₀ on gold surfaces by SAMs of porphyrin derivatives

pp 1947–1954

Sheng Zhang and Luis Echegoyen*

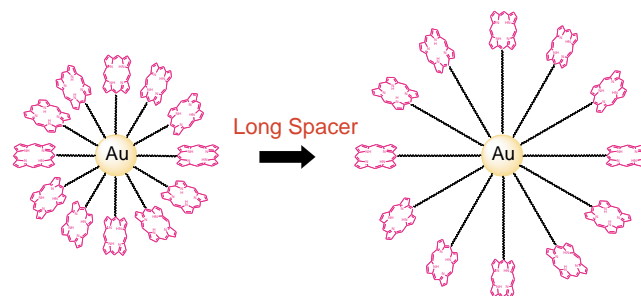


Structure and photoelectrochemical properties of nanostructured SnO₂ electrodes deposited electrophoretically with the composite clusters of porphyrin-modified gold nanoparticle with a long spacer and fullerene

pp 1955–1966

Hiroshi Imahori,* Atsushi Fujimoto, Soonchul Kang, Hiroki Hotta, Kaname Yoshida, Tomokazu Umeyama, Yoshihiro Matano and Seiji Isoda

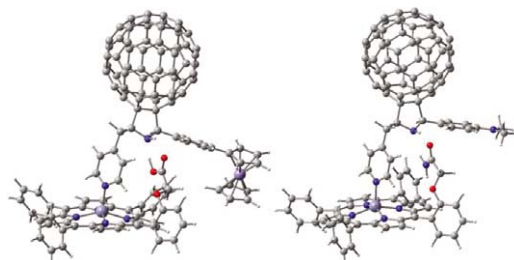
A three-dimensional porphyrin-monolayer-protected gold nanoparticle with a long spacer has been prepared to examine the structure and photoelectrochemical properties of the composite clusters with fullerene deposited electrophoretically onto a nanostructured SnO₂ electrode.



Supramolecular triads bearing porphyrin and fullerene via 'two-point' binding involving coordination and hydrogen bonding

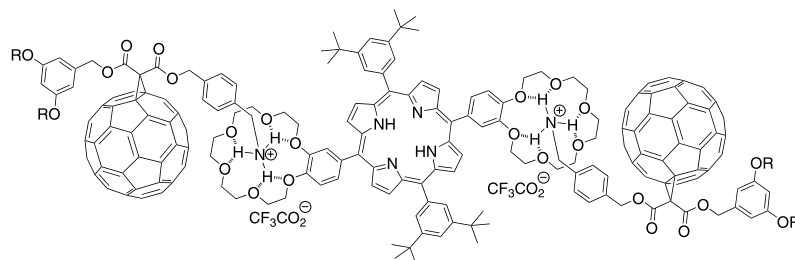
pp 1967–1978

Francis D'Souza,* Mohamed E. El-Khouly, Suresh Gadde, Melvin E. Zandler, Amy Lea McCarty, Yasuyuki Araki and Osamu Ito*

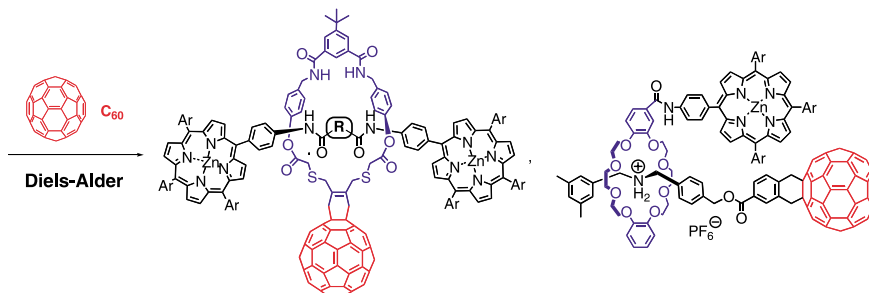


Supramolecular complexes obtained from porphyrin–crown ether conjugates and a fullerene derivative bearing an ammonium unit

pp 1979–1987

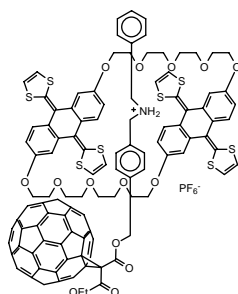
 Nathalie Solladié,* Mathieu E. Walther, Haiko Herschbach, Emmanuelle Leize, Alain Van Dorsselaer,*
 Teresa M. Figueira Duarte and Jean-François Nierengarten*

Synthesis of [60]fullerene-functionalized rotaxanes

pp 1988–1997

 Hisahiro Sasabe, Kei-ichiro Ikeshita, G. Abraham Rajkumar, Nobuhiro Watanabe, Nobuhiro Kihara,
 Yoshio Furusho, Kazuhiko Mizuno, Akiya Ogawa and Toshikazu Takata*

Supramolecular pseudo-rotaxane type complexes from π -extended TTF dimer crown ether and C₆₀

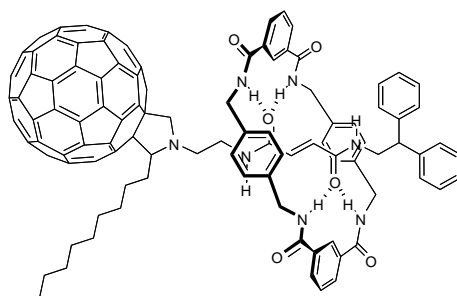
pp 1998–2002

Marta C. Díaz, Beatriz M. Illescas, Nazario Martín,* J. Fraser Stoddart, M. Angeles Canales, Jesús Jiménez-Barbero, Ginka Sarova and Dirk M. Guldi


Synthesis of a soluble fullerene–rotaxane incorporating a furamide template

pp 2003–2007

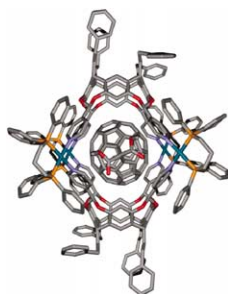
Aurelio Mateo-Alonso and Maurizio Prato*



Inclusion of methano[60]fullerene derivatives in cavitand-based coordination cages

pp 2008–2015

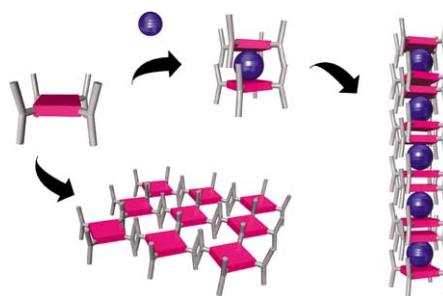
Laura Pirondini, Davide Bonifazi,* Barbara Cantadori, Paolo Braiuca, Mara Campagnolo, Rita De Zorzi, Silvano Geremia, François Diederich* and Enrico Dalcanale*

**Molecular programming of organogelators which can accept [60]fullerene by encapsulation**

pp 2016–2024

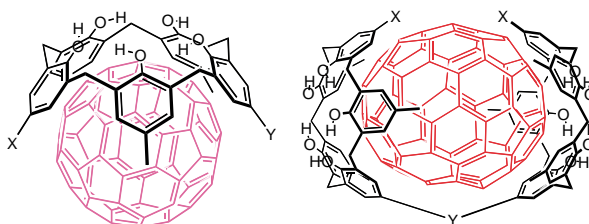
Michihiro Shirakawa, Norifumi Fujita, Hisashi Shimakoshi, Yoshio Hisaeda and Seiji Shinkai*

Porphyrin–fullerene interaction in the gel phase triggers morphological transformation from two-dimensional sheet-like structure to one-dimensional fibers of the gel tissue.

**Fullerene encapsulation with calix[5]arenes**

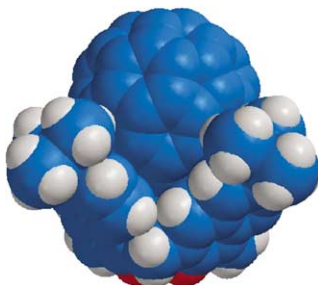
pp 2025–2035

Takeharu Haino,* Manabu Yanase, Chigusa Fukunaga and Yoshimasa Fukazawa*

**Supramolecular complexation studies of [60]fullerene with calix[4]naphthalenes—a reinvestigation**

pp 2036–2044

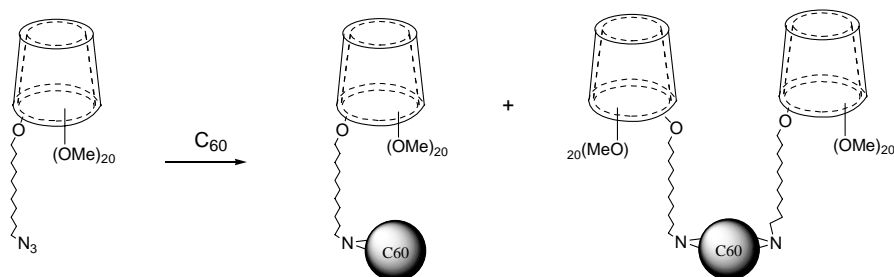
Paris E. Georghiou,* Anh Huu Tran, Skylar S. Stroud and David W. Thompson*



Synthesis of water-soluble 2-alkylcyclodextrin–C₆₀ conjugates and their inclusion complexation in aqueous solution

pp 2045–2049

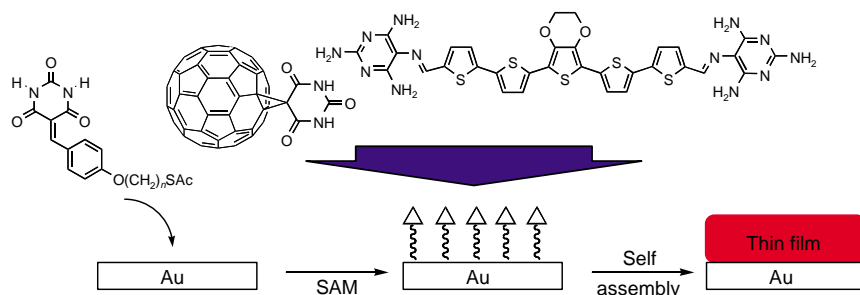
Yong Chen, Yali Wang, André Rassat, Pierre Sinaÿ, Yu Zhao and Yongmin Zhang*



Hierarchical self-assembly of all-organic photovoltaic devices

pp 2050–2059

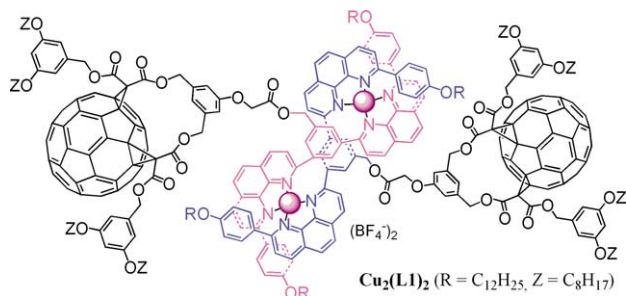
Chih-Hao Huang, Nathan D. McClenaghan, Alexander Kuhn, Georges Bravic and Dario M. Bassani*



Synthesis of fullerohelicates and fine tuning of the photoinduced processes by changing the number of addends on the fullerene subunits

pp 2060–2073

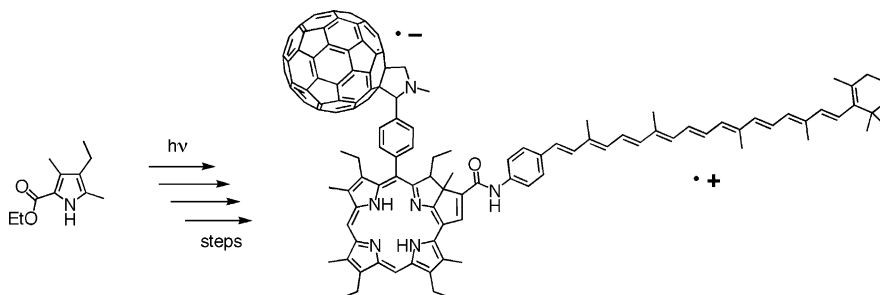
Michel Holler, François Cardinali, Hind Mamlouk, Jean-François Nierengarten,* Jean-Paul Gisselbrecht, Maurice Gross, Yannick Rio, Francesco Barigelletti and Nicola Armaroli*



Artificial photosynthetic reaction centers with carotenoid antennas

pp 2074–2096

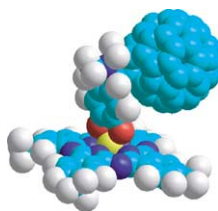
Stephanie L. Gould, Gerdenis Kodis, Paul A. Liddell, Rodrigo E. Palacios, Alicia Brune, Devens Gust,* Thomas A. Moore* and Ana L. Moore*



Synthesis and photophysical characterization of a titanium(IV) phthalocyanine–C₆₀ supramolecular dyad

pp 2097–2101

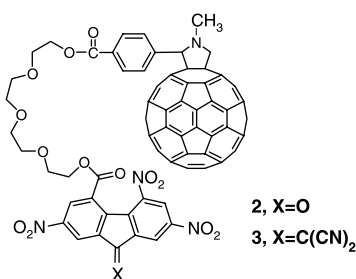
Beatriz Ballesteros, Gema de la Torre, Tomás Torres,* Gordon L. Hug, G. M. Aminur Rahman and Dirk M. Guldi*



Synthesis and characterization of new trinitrofluorene–fullerene dyads as photosensitizers in photorefractive polymer materials. Redox behavior and charge-transfer properties

pp 2102–2109

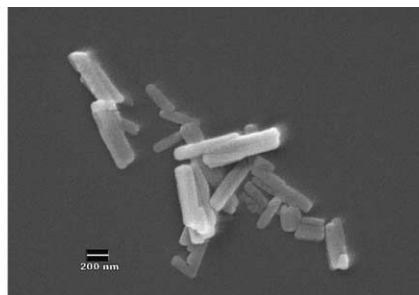
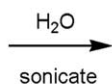
Luis Martín-Gomis, Javier Ortiz, Fernando Fernández-Lázaro, Ángela Sastre-Santos,* Bevan Elliott and Luis Echegoyen*



Self-organization of amphiphilic [60]fullerene derivatives in nanorod-like morphologies

pp 2110–2114

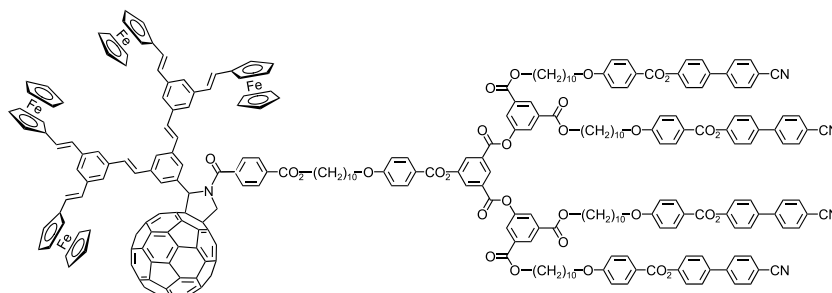
Peter Brough, Davide Bonifazi and Maurizio Prato*



Dendritic liquid-crystalline fullerene–ferrocene dyads

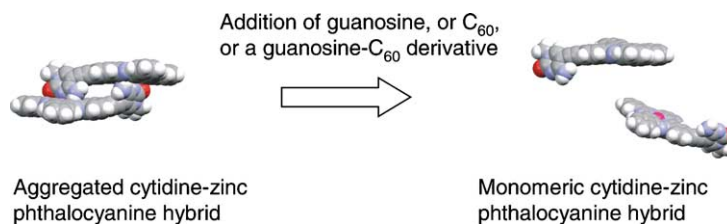
pp 2115–2122

Stéphane Campidelli, Laura Pérez, Julián Rodríguez-López, Joaquín Barberá,* Fernando Langa* and Robert Deschenaux*



Guanosine and fullerene derived de-aggregation of a new phthalocyanine-linked cytidine derivative pp 2123–2131

Jonathan L. Sessler,* Janarthanan Jayawickramarajah, Andreas Gouloumis, G. Dan Pantos, Tomás Torres* and Dirk M. Guldi*



Electronic absorption and fluorescence spectroscopies were used to study the aggregation and de-aggregation behavior of a novel cytidine tethered zinc phthalocyanine shown schematically above. De-aggregation of this conjugate, can be effected using guanosine, C₆₀, as well as via the addition of a synthetic guanosine-C₆₀ hybrid.

*Corresponding author

Supplementary data available via ScienceDirect

COVER

The Figure shows a new supramolecular pseudo-rotaxane type complex formed by a crown ether derivative containing two exTTF electron donor units and a threaded dibenzylammonium salt endowed with a [60]fullerene electron acceptor unit. This new ensemble as well as other related supramolecular structures contained in this issue are appealing systems for the study of photoinduced electron transfer processes mimicking the natural photosynthesis.

© 2005 N. Martín. Published by Elsevier Ltd.



Full text of this journal is available, on-line from **ScienceDirect**. Visit www.sciencedirect.com for more information.

CONTENTS
direct

This journal is part of **ContentsDirect**, the *free* alerting service which sends tables of contents by e-mail for Elsevier books and journals. You can register for **ContentsDirect** online at: <http://contentsdirect.elsevier.com>

Indexed/Abstracted in: AGRICOLA, Beilstein, BIOSIS Previews, CAB Abstracts, Chemical Abstracts. Current Contents: Life Sciences, Current Contents: Physical, Chemical and Earth Sciences, Current Contents Search, Derwent Drug File, Ei Compendex, EMBASE/Excerpta Medica, Medline, PASCAL, Research Alert, Science Citation Index, SciSearch



ELSEVIER

ISSN 0040-4020

Tetrahedron Symposia-in-Print

Series Editor

Professor H. H. Wasserman, Department of Chemistry, Yale University, P.O. Box 208107, New Haven, CT 06520-8107, U.S.A.

Tetrahedron Symposia-in-Print comprise collections of original research papers covering timely areas of organic chemistry.

Each symposium is organized by a Symposium Editor who will invite authors, active in the selected field, to submit original articles covering current research, complete with experimental sections. These papers will be rapidly reviewed and processed for publication by the Symposium Editor under the usual refereeing system.

Authors who have not already been invited, and who may have obtained recent significant results in the area of the announced symposium, may also submit contributions for Editorial consideration and possible inclusion. Before submitting such papers authors should send an abstract to the Symposium Editor for preliminary evaluation. Firm deadlines for receipt of papers will allow sufficient time for completion and presentation of ongoing work without loss of the freshness and timeliness of the research results.

Symposia-in-Print—already published

1. Recent trends in organic photochemistry, Albert Padwa, Ed. *Tetrahedron* **1981**, 37, 3227–3420.
2. New general synthetic methods, E. J. Corey, Ed. *Tetrahedron* **1981**, 37, 3871–4119.
3. Recent developments in polycyclopentanoid chemistry, Leo A. Paquette, Ed. *Tetrahedron* **1981**, 37, 4357–4559.
4. Biradicals, Josef Michl, Ed. *Tetrahedron* **1982**, 38, 733–867.
5. Electron-transfer initiated reactions, Gary B. Schuster, Ed. *Tetrahedron* **1982**, 38, 1025–1122.
6. The organic chemistry of animal defense mechanisms, Jerrold Meinwald, Ed. *Tetrahedron* **1982**, 38, 1853–1970.
7. Recent developments in the use of silicon in organic synthesis, Hans Reich, Ed. *Tetrahedron* **1983**, 39, 839–1009.
8. Linear tetrapyrroles, Ray Bonnett, Ed. *Tetrahedron* **1983**, 39, 1837–1954.
9. Heteroatom-directed metallations in heterocyclic synthesis, George R. Newcome, Ed. *Tetrahedron* **1983**, 39, 1955–2091.
10. Recent aspects of the chemistry of β -lactams, J. E. Baldwin, Ed. *Tetrahedron* **1983**, 39, 2445–2608.
11. New spectroscopic techniques for studying metabolic processes, A. I. Scott, Ed. *Tetrahedron* **1983**, 39, 3441–3626.
12. New developments in indole alkaloids, Martin E. Kuehne, Ed. *Tetrahedron* **1983**, 39, 3627–3780.
13. Recent aspects of the chemistry of nucleosides, nucleotides and nucleic acids, Colin B. Reese, Ed. *Tetrahedron* **1984**, 40, 1–164.
14. Bioorganic studies on receptor sites, Koji Nakanishi, Ed. *Tetrahedron* **1984**, 40, 455–592.
15. Synthesis of chiral non-racemic compounds, A. I. Meyers, Ed. *Tetrahedron* **1984**, 40, 1213–1418.
16. Control of acyclic stereochemistry, Teruaki Mukaiyama, Ed. *Tetrahedron* **1984**, 40, 2197–2344.
17. Recent aspects of anthracycline chemistry, T. Ross Kelly, Ed. *Tetrahedron* **1984**, 40, 4537–4794.
18. The organic chemistry of marine products, Paul J. Scheuer, Ed. *Tetrahedron* **1985**, 41, 979–1108.
19. Recent aspects of carbene chemistry, Matthew Platz, Ed. *Tetrahedron* **1985**, 41, 1423–1612.
20. Recent aspects of singlet oxygen chemistry of photooxidation, Isao Saito and Teruo Matsuura, Eds. *Tetrahedron* **1985**, 41, 2037–2236.
21. Synthetic applications of dipolar cycloaddition reactions, Wolfgang Oppolzer, Ed. *Tetrahedron* **1985**, 41, 3447–3568.
22. Selectivity and synthetic applications of radical reactions, Bernd Giese, Ed. *Tetrahedron* **1985**, 41, 3887–4302.
23. Recent aspects of organoselenium chemistry, Dennis Liotta, Ed. *Tetrahedron* **1985**, 41, 4727–4890.
24. Application of newer organometallic reagents to the total synthesis of natural products, Martin Semmelhack, Ed. *Tetrahedron* **1985**, 41, 5741–5900.
25. Formal transfers of hydride from carbon–hydrogen bonds, James D. Wuest, Ed. *Tetrahedron* **1986**, 42, 941–1208.
26. Synthesis of non-natural products: challenge and reward, Philip E. Eaton, Ed. *Tetrahedron* **1986**, 42, 1549–1916.
27. New synthetic methods—II, F. E. Ziegler, Ed. *Tetrahedron* **1986**, 42, 2777–3028.
28. Structure and reactivity of organic radical ions, Heinz D. Roth, Ed. *Tetrahedron* **1986**, 42, 6097–6350.
29. Organic chemistry in anisotropic media, V. Ramamurthy, J. R. Scheffer and N. J. Turro, Eds. *Tetrahedron* **1987**, 43, 1197–1746.
30. Current topics in sesquiterpene synthesis, John W. Huffman, Ed. *Tetrahedron* **1987**, 43, 5467–5722.
31. Peptide chemistry: design and synthesis of peptides, conformational analysis and biological functions, Victor J. Hruby and Robert Schwyzler, Eds. *Tetrahedron* **1988**, 44, 661–1006.
32. Organosilicon chemistry in organic synthesis, Ian Fleming, Ed. *Tetrahedron* **1988**, 44, 3761–4292.
33. α -Amino acid synthesis, Martin J. O'Donnell, Ed. *Tetrahedron* **1988**, 44, 5253–5614.
34. Physical-organic/theoretical chemistry: the Dewar interface, Nathan L. Bauld, Ed. *Tetrahedron* **1988**, 44, 7335–7626.
35. Recent developments in organocopper chemistry, Bruce H. Lipshutz, Ed. *Tetrahedron* **1989**, 45, 349–578.
36. Organotin compounds in organic synthesis, Yoshinori Yamamoto, Ed. *Tetrahedron* **1989**, 45, 909–1230.

37. Mycotoxins, Pieter S. Steyn, Ed. *Tetrahedron* **1989**, *45*, 2237–2464.
38. Strain-assisted syntheses, Léon Ghosez, Ed. *Tetrahedron* **1989**, *45*, 2875–3232.
39. Covalently linked donor–acceptor species for mimicry of photosynthetic electron and energy transfer, Devens Gust and Thomas A. Moore, Eds. *Tetrahedron* **1989**, *45*, 4669–4912.
40. Aspects of modern carbohydrate chemistry, S. Hanessian, Ed. *Tetrahedron* **1990**, *46*, 1–290.
41. Nitroalkanes and nitroalkenes in synthesis, Anthony G. M. Barrett, Ed. *Tetrahedron* **1990**, *46*, 7313–7598.
42. Synthetic applications of anodic oxidations, John S. Swenton and Gary W. Morrow, Eds. *Tetrahedron* **1991**, *47*, 531–906.
43. Recent advances in bioorganic chemistry, Dale L. Boger, Ed. *Tetrahedron* **1991**, *47*, 2351–2682.
44. Natural product structure determination, R. B. Bates, Ed. *Tetrahedron* **1991**, *47*, 3511–3664.
45. Frontiers in natural products biosynthesis. Enzymological and molecular genetic advances, D. E. Cane, Ed. *Tetrahedron* **1991**, *47*, 5919–6078.
46. New synthetic methods—III, S. E. Denmark, Ed. *Tetrahedron* **1992**, *48*, 1959–2222.
47. Organotitanium reagents in organic chemistry, M. T. Reetz, Ed. *Tetrahedron* **1992**, *48*, 5557–5754.
48. Total and semi-synthetic approaches to taxol, J. D. Winkler, Ed. *Tetrahedron* **1992**, *48*, 6953–7056.
49. Synthesis of optically active compounds—prospects for the 21st century, Kenji Koga and Takayuki Shioiri, Eds. *Tetrahedron* **1993**, *49*, 1711–1924.
50. Peptide secondary structure mimetics, Michael Kahn, Ed. *Tetrahedron* **1993**, *49*, 3433–3689.
51. Transition metal organometallics in organic synthesis, Anthony J. Pearson, Ed. *Tetrahedron* **1993**, *49*, 5415–5682.
52. Palladium in organic synthesis, Jan-E. Bäckvall, Ed. *Tetrahedron* **1994**, *50*, 285–572.
53. Recent progress in the chemistry of enediyne antibiotics, Terrence W. Doyle and John F. Kadow, Eds. *Tetrahedron* **1994**, *50*, 1311–1538.
54. Catalytic asymmetric addition reactions, Stephen F. Martin, Ed. *Tetrahedron* **1994**, *50*, 4235–4574.
55. Mechanistic aspects of polar organometallic chemistry, Manfred Schlosser, Ed. *Tetrahedron* **1994**, *50*, 5845–6128.
56. Molecular recognition, Andrew D. Hamilton, Ed. *Tetrahedron* **1995**, *51*, 343–648.
57. Recent advances in the chemistry of zirconocene and related compounds, Ei-ichi Negishi, Ed. *Tetrahedron* **1995**, *51*, 4255–4570.
58. Fluoroorganic chemistry: synthetic challenges and biomedicinal rewards, Giuseppe Resnati and Vadim A. Soloshonok, Eds. *Tetrahedron* **1996**, *52*, 1–330.
59. Novel applications of heterocycles in synthesis, A. R. Katritzky, Ed. *Tetrahedron* **1996**, *52*, 3057–3374.
60. Fullerene chemistry, Amos B. Smith III, Ed. *Tetrahedron* **1996**, *52*, 4925–5262.
61. New synthetic methods—IV. Organometallics in organic chemistry, István E. Markó, Ed. *Tetrahedron* **1996**, *52*, 7201–7598.
62. Cascade reactions, Ron Grigg, Ed. *Tetrahedron* **1996**, *52*, 11385–11664.
63. Applications of solid-supported organic synthesis in combinatorial chemistry, James A. Bristol, Ed. *Tetrahedron* **1997**, *53*, 6573–6706.
64. Recent applications of synthetic organic chemistry, Stephen F. Martin, Ed. *Tetrahedron* **1997**, *53*, 8689–9006.
65. Chemical biology, Gregory L. Verdine and Julian Simon, Eds. *Tetrahedron* **1997**, *53*, 11937–12066.
66. Recent aspects of S, Se, and Te chemistry, Richard S. Glass and Renji Okazaki, Eds. *Tetrahedron* **1997**, *53*, 12067–12318.
67. Modern organic chemistry of polymerization, H. K. Hall Jr., Ed. *Tetrahedron* **1997**, *53*, 15157–15616.
68. New synthetic methods—V, John L. Wood, Ed. *Tetrahedron* **1997**, *53*, 16213–16606.
69. New developments in organonickel chemistry, Bruce H. Lipshutz and Tien-Yau Luh, Eds. *Tetrahedron* **1998**, *54*, 1021–1316.
70. Solution phase combinatorial chemistry, David L. Coffen, Ed. *Tetrahedron* **1998**, *54*, 3955–4150.
71. Heterocycles in asymmetric synthesis, Alexandre Alexakis, Ed. *Tetrahedron* **1998**, *54*, 10239–10554.
72. Recent advances of phase-transfer catalysis, Takayuki Shioiri, Ed. *Tetrahedron* **1999**, *55*, 6261–6402.
73. Olefin metathesis in organic synthesis, Marc L. Snapper and Amir H. Hoveyda, Eds. *Tetrahedron* **1999**, *55*, 8141–8262.
74. Stereoselective carbon–carbon bond forming reactions, Harry H. Wasserman, Stephen F. Martin and Yoshinori Yamamoto, Eds. *Tetrahedron* **1999**, *55*, 8589–9006.
75. Applications of combinatorial chemistry, Miles G. Siegel and Stephen W. Kaldor, Eds. *Tetrahedron* **1999**, *55*, 11609–11710.
76. Advances in carbon–phosphorus heterocyclic chemistry, François Mathey, Ed. *Tetrahedron* **2000**, *56*, 1–164.
77. Transition metal organometallics in organic synthesis, Kenneth M. Nicholas, Ed. *Tetrahedron* **2000**, *56*, 2103–2338.
78. Organocopper chemistry II, Norbert Krause, Ed. *Tetrahedron* **2000**, *56*, 2727–2904.
79. Carbene complexes in organic chemistry, James W. Herndon, Ed. *Tetrahedron* **2000**, *56*, 4847–5044.
80. Recent aspects of the chemistry of β -lactams—II, Marvin J. Miller, Ed. *Tetrahedron* **2000**, *56*, 5553–5742.
81. Molecular assembly and reactivity of organic crystals and related structures, Miguel A. Garcia-Garibay, Vaidhyanathan Ramamurthy and John R. Scheffer, Eds. *Tetrahedron* **2000**, *56*, 6595–7050.
82. Protein engineering, Richard Chamberlin, Ed. *Tetrahedron* **2000**, *56*, 9401–9526.
83. Recent advances in peptidomimetics, Jeffrey Aubé, Ed. *Tetrahedron* **2000**, *56*, 9725–9842.
84. New synthetic methods—VI, George A. Kraus, Ed. *Tetrahedron* **2000**, *56*, 10101–10282.
85. Oxidative activation of aromatic rings: an efficient strategy for arene functionalization, Stéphane Quideau and Ken S. Feldman, Eds. *Tetrahedron* **2001**, *57*, 265–424.
86. Lewis acid control of asymmetric synthesis, Keiji Maruoka, Ed. *Tetrahedron* **2001**, *57*, 805–914.
87. Novel aromatic compounds, Lawrence T. Scott and Jay S. Siegel, Eds. *Tetrahedron* **2001**, *57*, 3507–3808.
88. Asymmetric synthesis of novel sterically constrained amino acids, Victor J. Hruby and Vadim A. Soloshonok, Eds. *Tetrahedron* **2001**, *57*, 6329–6650.
89. Recognition-mediated self-assembly of organic systems, Vincent M. Rotello, Ed. *Tetrahedron* **2002**, *58*, 621–844.
90. Synthesis of marine natural products containing polycyclic ethers, Masahiro Hiram and Jon D. Rainier, Eds. *Tetrahedron* **2002**, *58*, 1779–2040.

91. Fluorous chemistry, John A. Gladysz and Dennis P. Curran, Eds. *Tetrahedron* **2002**, *58*, 3823–4132.
92. Recent developments in chiral lithium amide base chemistry, Peter O'Brien, Ed. *Tetrahedron* **2002**, *58*, 4567–4734.
93. Beyond natural product synthesis (Tetrahedron Prize for Creativity in Organic Chemistry 2001 - Yoshito Kishi), Harry H. Wasserman and Stephen F. Martin, Eds. *Tetrahedron* **2002**, *58*, 6223–6602.
94. Strained heterocycles as intermediates in organic synthesis, Amy R. Howell, Ed. *Tetrahedron* **2002**, *58*, 6979–7194.
95. Molecular design of Lewis and Brønsted acid catalysts—the key to environmentally benign reagents (Tetrahedron Chair 2002), Hisashi Yamamoto, Ed. *Tetrahedron* **2002**, *58*, 8153–8364.
96. Recent developments in dendrimer chemistry, David K. Smith, Ed. *Tetrahedron* **2003**, *59*, 3787–4024.
97. Art, science and technology in total synthesis (Tetrahedron Prize for Creativity in Organic Chemistry 2002 - K. C. Nicolaou), Stephen F. Martin and Harry H. Wasserman, Eds. *Tetrahedron* **2003**, *59*, 6667–7070.
98. New synthetic methods—VII, Brian M. Stoltz, Ed. *Tetrahedron* **2003**, *59*, 8843–9030.
99. Oxiranyl and aziridinyl anions as reactive intermediates in synthetic organic chemistry, S. Florio, Ed. *Tetrahedron* **2003**, *59*, 9683–9864.
100. Recent advances in rare earth chemistry, Shū Kobayashi, Ed. *Tetrahedron* **2003**, *59*, 10339–10598.
101. Biocatalysts in synthetic organic chemistry, S. M. Roberts, Ed. *Tetrahedron* **2004**, *60*, 483–806.
102. Recent advances in the chemistry of zirconocenes, Keisuke Suzuki and Peter Wipf, Eds. *Tetrahedron* **2004**, *60*, 1257–1424.
103. Atropisomerism, Jonathan Clayden, Ed. *Tetrahedron* **2004**, *60*, 4325–4558.
104. Chemistry of biologically and physiologically intriguing phenomena, Daisuke Uemura, Ed. *Tetrahedron* **2004**, *60*, 6959–7098.
105. Olefin metathesis: a powerful and versatile instrument for organic synthesis (Tetrahedron prize for creativity in organic chemistry 2003 – R. H. Grubbs), Stephen F. Martin and Harry H. Wasserman, Eds. *Tetrahedron* **2004**, *60*, 7099–7438.
106. From synthetic methodology to biomimetic target assembly (Tetrahedron prize for creativity in organic chemistry 2003 – D. Seebach), Léon A. Ghosez, Ed. *Tetrahedron* **2004**, *60*, 7439–7794.
107. Solid and solution phase combinatorial chemistry, Rolf Breinbauer and Herbert Waldmann, Eds. *Tetrahedron* **2004**, *60*, 8579–8738.
108. Catalytic tools enabling total synthesis (Tetrahedron Chair 2004), Alois Fürstner, Ed. *Tetrahedron* **2004**, *60*, 9529–9784.
109. Synthesis and applications of non-racemic cyanohydrins and α -amino nitriles, Michael North, Ed. *Tetrahedron* **2004**, *60*, 10371–10568.
110. Synthetic receptors as sensors, Eric V. Anslyn, Ed. *Tetrahedron* **2004**, *60*, 11041–11316.
111. Functionalised organolithium compounds, Carmen Nájera and Miguel Yus, Eds. *Tetrahedron* **2005**, *61*, 3125–3450.
112. Applications of catalysis in academia and industry, Michael J. Krische, Ed. *Tetrahedron* **2005**, *61*, 6155–6472.
113. Development and application of highly active and selective palladium catalysts, Ian J. S. Fairlamb, Ed. *Tetrahedron* **2005**, *61*, 9647–9918.
114. Multicomponent reactions, Ilan Marek, Ed. *Tetrahedron* **2005**, *61*, 11299–11520.
115. Polymer-supported reagents and catalysts: increasingly important tools for organic synthesis, Patrick Toy and Min Shi, Eds. *Tetrahedron* **2005**, *61*, 12013–12192.
116. Organocatalysis in organic synthesis, Pavel Kočovský and Andrei V. Malkov, Eds. *Tetrahedron* **2006**, *62*, 243–502.
117. Supramolecular chemistry of fullerenes, Nazario Martín and Jean-François Nierengarten, Eds. *Tetrahedron* **2006**, *62*, 1905–2132.



Preface

Supramolecular chemistry of fullerenes

It was in 1987 when Jean-Marie Lehn together with two other supramolecular chemistry pioneers, Donald J. Cram and Charles J. Pedersen, received the Nobel Prize for the development and utilization of molecules with highly selective structure-specific interactions. One decade later, in 1996, another three great scientists, Sir Harold W. Kroto, Robert F. Curl and the late Richard E. Smalley were awarded with the Nobel Prize in 1996 for the discovery of the fullerenes. Both important branches of chemistry crossed each other to give rise to a new interdisciplinary field in which the imagination of chemists has been allowed to design and construct new and unprecedented fullerene-based supramolecular architectures.

It is in this year 2006 when we celebrate the 10th anniversary of the fullerenes award and, therefore, it is a good opportunity to think about the achievements and future goals in this field of chemistry. Although a detailed discussion on this fascinating topic is out of the scope of this preface, the wide variety of papers, reviews and books published during the last decade on fullerenes, as well as on the closely related carbon nanotube allotropes, give an idea of the unabated interest in this new avenue of chemistry. In this effervescent research, the application of the supramolecular principles to fullerenes has reached an outstanding position in its own right and we certainly believe that it constitutes a new interdisciplinary field with basic research interest and important potential applications. Therefore, in this timely special issue of *Tetrahedron Symposium-in-Print* entitled 'Supramolecular chemistry of fullerenes' we have gathered 23 original papers from leading groups actively engaged in supramolecular/fullerenes research, which shape a perfect mosaic on the state of the art in this new hybrid topic.

One of the major challenges that still lies in front of us is the control of weak forces, on a molecular basis, which will eventually lead to define the size and shape in relation to function of the resulting supramolecular ensembles. In this regard, the three dimensional rigid structure of fullerenes as well as their remarkable electronic properties result in a unique scaffold for the development of unprecedented architectures. For these purposes the different types of weak forces, namely hydrogen-bonding, π - π stacking, metal-mediated complexation and electrostatic interactions, have been used in the different articles gathered in this issue to construct new non-covalently bonded structures. A fundamental aspect in the construction of new architectures involving these biomimetic motifs is that, in contrast to covalently bonded structures, they are reversible and their binding energies can be tailored 'at will' by means of the chemical environment and temperature.

All the articles contained in this issue have been written by prominent scientists from all over the world. The guest editors want to express their gratitude to them for their collaboration and efforts to achieve this outstanding collection of manuscripts for the enjoyment of the reader. We hope that this group of scientific works on this new interdisciplinary theme will be considered a stimulus to further develop the huge possibilities that fullerenes have within the framework of supramolecular principles, and put new heart into other colleagues to develop new concepts in this central science that is chemistry.

We want to thank two of the above distinguished Nobel Prize scientists, Professors Lehn and Kroto for supporting this pleasant enterprise and for writing the encouraging Forewords for this issue. Needless to say that they are responsible, in a big part, for the science now presented in this editorial project.

It is fortuitous that as this special issue on fullerenes is being compiled, it coincides with the occasion of Fred Wudl's 65th birthday. Professor Wudl has been a key pioneer in the chemistry of fullerenes creating firstly a fullerene school in Santa Barbara and, later, the Institute for Exotic Materials in Los Angeles, where many young scientists discovered for the first time the fascinating field of fullerenes. Finally, our gratitude is also extended to the Scientific Editor of the *Tetrahedron Symposium-in-Print*, Professor Wasserman, as well as to Elsevier for their support and interest to come through this venture safely.

Nazario Martín

*Grupo de Materiales Moleculares Orgánicos,
Departamento de Química Orgánica,
Facultad de Química,
Universidad Complutense,
E-28040 Madrid,
Spain
E-mail address: nazmar@quim.ucm.es*

Jean-François Nierengarten

*Groupe de Chimie des Fullerènes et des Systèmes Conjugués,
Laboratoire de Chimie de Coordination du CNRS 205,
route de Narbonne,
31077 Toulouse Cedex 4,
France
E-mail address: jfnierengarten@lcc-toulouse.fr*

Available online 18 January 2006



Foreword

Supramolecular chemistry of fullerenes

The present special issue of Tetrahedron brings together two major areas of chemistry that emerged and experienced an extensive development over the last quarter of a century or so: supramolecular chemistry and fullerene chemistry. First came supramolecular chemistry, that opened a new era by taking power over the non-covalent bond and exploring chemistry beyond the molecule. Then, the discovery of the fullerenes provided an entirely new set of chemical substances of both wide scientific and high aesthetic appeal. Marrying the two areas has on one hand offered to fullerenes a novel playground for the generation of complex architectures of supramolecular nature. On the

other hand, it has led to the implementation of the intriguing physical and chemical features of fullerene substrates for the benefit of functional supramolecular chemistry. The present special issue assembles contributions from major players in the field, taking stock of the research performed at the interface between the two domains and opening perspectives for future developments.

Jean-Marie Lehn
Nobel Prize of Chemistry

Available online 18 January 2006



Foreword

Supramolecular chemistry of fullerenes

The novel carbon cage molecule (C_{60}), which was discovered in 1985 has the same icosahedral symmetry as the modern soccer ball. It was named Buckminsterfullerene after the designer of geodesic domes, which are constructed on the basis of the same structural principles. This discovery, together with that of its elongated cousins—the carbon nanotubes—heralded a totally new field of research into closed cage systems constructed from networks of atoms arrayed in 2d sheets. The importance of such structures was quite unexpected and the chemistry and physics of these new systems has turned out to be very rich indeed. They exhibit a very wide range of novel mechanical and electronic properties, which hold the promise of exciting applications in the not too distant future. For instance when macroscopic amounts of the molecule C_{60} suddenly became available in 1990 and it was possible to probe the chemistry and physics of this unique material one of the most fascinating and surprising discoveries was the discovery of high temperature superconductivity in the alkali metal doped material. In fact the electronic properties of these new materials, especially their ability to store electrons may well turn out to be some of their most important properties with intriguing possibilities for opening up the field of molecular electronics.

Although after some dozen or so years of research we have learned a lot there is still a much still not understood and the fascination with these materials is almost as great now as at it was when they were first isolated. The promise

will, however, only be fully realized if and when accurate structural control has been achieved for the synthesis of these new materials.

The fullerenes, highly symmetric C_{60} in particular, have a beauty and elegance, which excites the imagination of scientists and non-scientists alike as they bridge aesthetic gaps between the sciences, architecture, mathematics, engineering and the visual arts. Previously only two well-defined allotropes of carbon were known—diamond and graphite; the fullerenes constitute a third form and it is remarkable that their existence evaded discovery until almost the end of the twentieth century. The discovery has led to a paradigm shift in our understanding of the behaviour of sheet materials in general and, furthermore, has ushered in a new era of Nanoscience & Nanotechnology—the ‘New’ chemistry of complex 2d network cage systems that exhibit advanced materials behaviour. This issue provides a series of well-written and thoughtfully constructed accounts, which cover the present state of our knowledge and will undoubtedly catalyse new studies, which must result in not only the development of new understanding. This special issue is a lucid overview written by expert researchers who are leaders in their respective fields.

Harold W. Kroto
Nobel Prize of Chemistry

Available online 18 January 2006

Covalently linked heterofullerene–porphyrin conjugates; new model systems for long-lived intramolecular charge separation

Frank Hauke,^a Stefan Atalick,^{b,c} Dirk M. Guldi^{b,*} and Andreas Hirsch^{a,*}

^a*Institut für Organische Chemie, Henkestrasse 42, D-91054 Erlangen, Germany*

^b*Institut für Physikalische Chemie, Egerlandstr 3, D-91058 Erlangen, Germany*

^c*Radiation Laboratory, Notre Dame, IN 46556, USA*

Received 3 November 2004; revised 23 April 2005; accepted 25 April 2005

Available online 28 November 2005

Abstract—Attaching tetraphenyl porphyrins, with peripheral acetyl or malonate groups, to C₅₉N leads to the first covalently linked heterofullerene–porphyrin conjugates that exhibit long-lived intramolecular charge separation.

© 2005 Elsevier Ltd. All rights reserved.

One of the most intensively investigated areas of fullerene chemistry concerns the physico-chemical properties of fullerene derivatives covalently tethered to one or more photoactive electron donors.¹ In particular, porphyrins are electron donor/chromophores ideally suited for devising integrated, multicomponent model systems to transmit and process solar energy. A significant setback—when using fullerenes as electron-acceptor units—is the reduced electron affinity stemming from most functionalization reactions.²

Incorporating a heteroatom into the all carbon-framework of C₆₀ enhances its electron affinity and, thereby, overcomes some of the deficiencies encountered in conventional derivatization.³ The core functionalization of C₅₉N, on the other hand, is more demanding than that of the parent [60]fullerene.⁴ This is based on the fact that addition reactions to the C_s symmetrical C₅₉N framework may lead to up to 16 regioisomeric monoaddition products. However, the monoazaheterofullerene exhibits a highly regioselective functionalization pattern, which can exclusively be found with (C₅₉N)₂ as starting material.

The thermal cleavage of the inter dimer bond and subsequent oxidation of the formed C₅₉N radical yields the highly reactive C₅₉N⁺ cation. C₅₉N⁺ undergoes electrophilic substitution reactions with aromatics or enolizable compounds.⁵ In such monomeric C₅₉N derivatives the addend is connected to the heterofullerene

core by a sp³ carbon atom adjacent to the nitrogen atom. We have reported earlier on the formation of the supramolecular heterofullerene–porphyrin dyad **1**.⁶ In that system we used the functionalization technique mentioned above to connect an anchor group (acetylpyridine) to the C₅₉N framework. By an axial coordination of the pyridine nitrogen atom to the zinc atom of a tetraphenyl zinc porphyrin the dyad **1** was generated. Depending on the solvent either photoinduced singlet–singlet energy transfer or electron-transfer was observed for that supramolecular assembly of two redox-active components.

In the present contribution, we wish to report on the first examples of covalently linked heterofullerene–porphyrin conjugates as novel artificial light harvesting antenna and reaction center mimics. First, we synthesised functional porphyrins that carry suitable linking groups for the attachment to the C₅₉N core. Malonate functionalised tetraphenylporphyrin **2** and acetyl porphyrin derivative **3** (Fig. 1) are good target compounds, since they can be connected to the heterofullerene framework via the C-atom α to the carbonyl groups (Scheme 1).

The reaction of these two porphyrin derivatives (**2** and **3**) with an equimolar amount of (C₅₉N)₂ and 30 equiv of *p*-TsOH at 150 °C in *o*-dichlorobenzene (ODCB) in a constant stream of air afforded dyads **4** and **5** (Fig. 2) in moderate yields. **4** and **5** were purified by flash chromatography (silica gel, toluene) and were isolated in high purity (greater than 99%, determined by HPLC).

The structural characterisation of **2–5** was carried out by ¹H, ¹³C NMR, UV/vis and FT-IR spectroscopy as well as by

Keywords: Fullerenes; Porphyrins; Fluorescence quenching.

* Corresponding authors. Fax: +49 9131 8526864;

e-mail addresses: dirk.guldi@chemie.uni-erlangen.de;

hirsch@organik.uni-erlangen.de

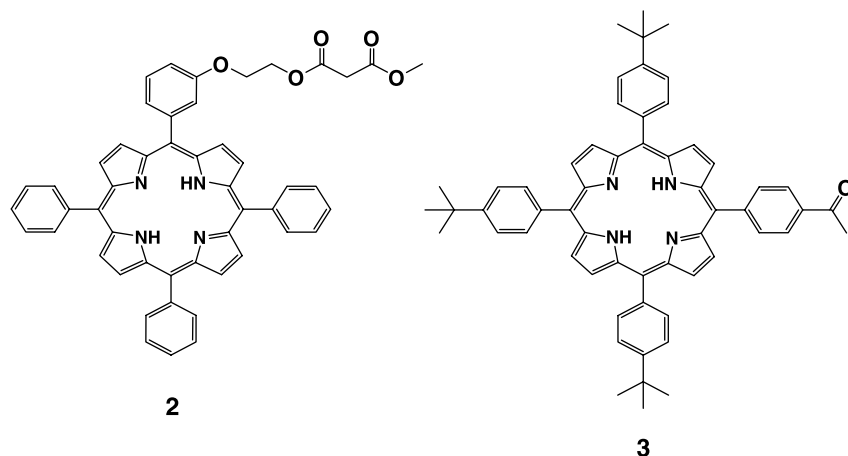
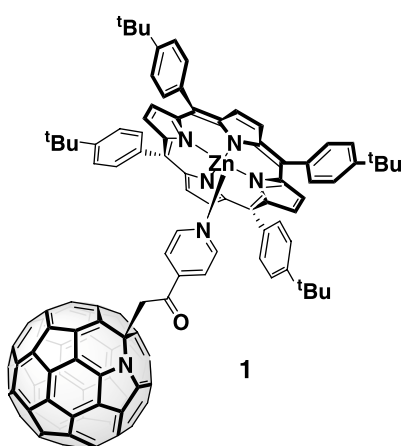


Figure 1. Tetraphenylporphyrins with malonate and acetyl groups.



Scheme 1. Structure of dyad 1.

FAB mass spectrometry.⁷ The UV/vis spectra of the $C_{59}N$ -porphyrin dyads **4** and **5** are, in first approximation, the superposition of the spectra of the $C_{59}N$ core^{3,4} and the respective porphyrin with the characteristic absorption bands at $\lambda = 257, 320$ nm of $C_{59}N$ and the Soret-Band and the four Q-bands of the porphyrins.

The 1H spectra of the dyads **4** and **5** are closely related to the spectra of the porphyrins **2** and **3**. Worth mentioning is the

downfield shift of the signals, which are associated with the methylene group in **2** and the methyl group in **3** by about 1.67 and 2.58 ppm, respectively. This effect is due to connecting the electron withdrawing $C_{59}N$ to porphyrins **2** and **3**. The ^{13}C NMR spectra allow assigning the symmetry of the heterofullerene–porphyrin dyads. Dyad **4**, for example, exhibits C_1 symmetry, due to the newly introduced asymmetric C-atom within the malonate group. Therefore, a set of 58 signals for the cage carbon atoms can be detected in the ^{13}C NMR spectrum.

Dyad **5** on the other hand exhibits C_s symmetry. The C-atoms of the heterofullerene framework, of the porphyrin core and of the four benzene rings resonate in the region between $\delta = 117$ –155. When comparing the signals of dyad **5** with those of porphyrin **3**, 30 signals, which are attributed to the resonances of the $C_{59}N$ core, can be sorted out. 28 signals have double intensity and two signals have single intensity, as they are located at the mirror plane of the $C_{59}N$ core. The characteristic resonance of the sp^3 -carbon atom of the $C_{59}N$ cage, which is also located at the mirror plane, occurs at $\delta = 78.40$. The carbonyl group of the ketone functionality resonates at $\delta = 194.78$ and the resonances of the α -methylene group are found at $\delta = 49.96$. Finally, the signals at $\delta = 34.49$ and 31.56 correspond to the carbon atoms of the three *t*-butyl groups.

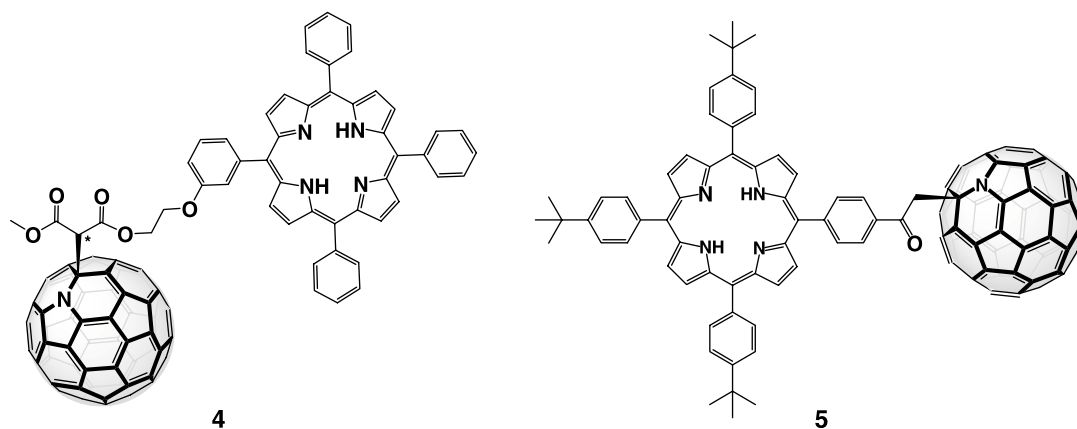


Figure 2. The two first covalently linked $C_{59}N$ -porphyrin dyads **4** and **5**.

Heterofullerene–porphyrin dyads **4** and **5** exhibit interesting photophysical properties. The porphyrin fluorescence—a sensitive probe for the magnitude of intramolecular electron transfer activation—is independent on the excitation (i.e., 414 nm Soret-band excitation or 520 nm Q-band excitation) quenched in both conjugates **4** and **5**—see Figures 3 and 4. Fluorescence quantum yields are on the order of $\sim 10^{-3}$ —relative to 0.10 for H₂P. In **4**, where the spacer connecting H₂P and C₅₉N allows for configurational flexibility, the solvent dependence on the fluorescence, that is, from toluene to THF and benzonitrile gives rise to invariant quenching (i.e., $\sim 2 \times 10^{-3}$). This suggests a solvent assisted through-space electron transfer mechanism. On the contrary, in **5** the data (i.e., toluene: 1.5×10^{-3} ; benzonitrile: 0.4×10^{-3}) is in line with a through-bond mechanism.⁸

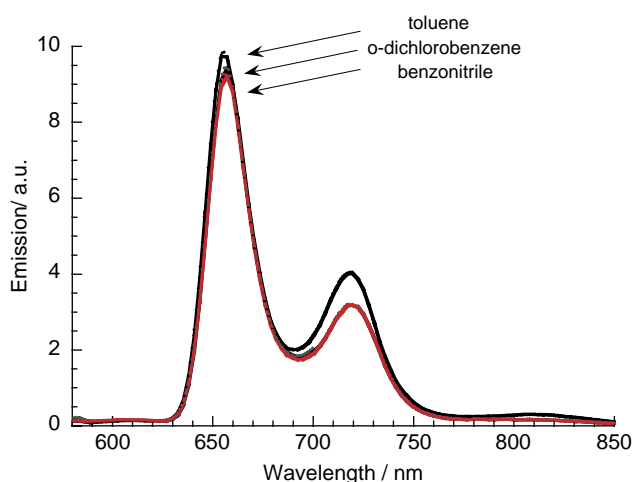


Figure 3. Fluorescence spectra of dyad **4** in different solvents (see labels for assignment) with matching absorption at the 427 nm excitation wavelength— $OD_{427\text{ nm}} = 0.5$.

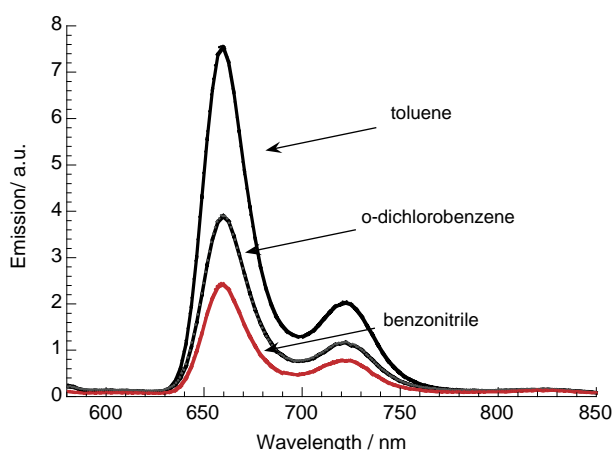


Figure 4. Fluorescence spectra of dyad **5** in different solvents (see labels for assignment) with matching absorption at the 427 nm excitation wavelength— $OD_{427\text{ nm}} = 0.5$.

In complementary transient absorption studies we probed the fate of the H₂P fluorescence quenching and looked into product identification. Pumping light into the H₂P's ground state in **4** and **5** with short laser pulses leads to the

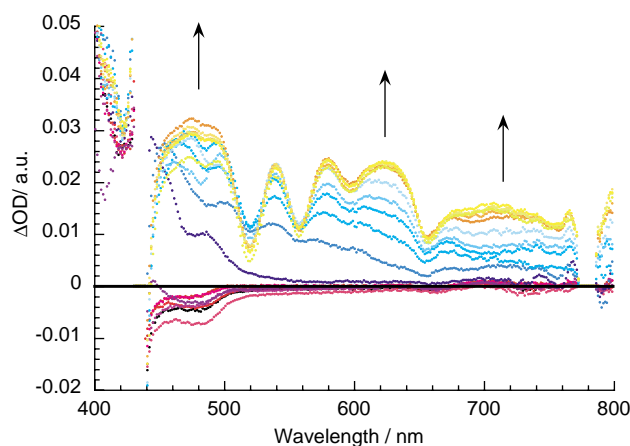


Figure 5. Differential absorption spectrum (visible and near-infrared) obtained upon femtosecond flash photolysis (382 nm) of $\sim 1.0 \times 10^{-5}$ M solutions of **5** in nitrogen saturated THF with a several time delay between -50 and 200 ps at room temperature. The spectrum corresponds to the changes that are associated with the transformation of the H₂P singlet excited state to the radical pair spectrum, H₂P^{•+}–C₅₉N^{•-}.

population of its singlet excited state, ¹*H₂P (1.9 eV). In **4** and **5** the lifetime of this intermediate state (< 0.4 ns) is shorter than in a H₂P reference (10 ns), since the lowest vibrational state of the singlet excited state undergoes exothermic electron transfer, generating the final (H₂P^{•+})–(C₅₉N)^{•-} state—see, for example, Figure 5. Interestingly, the singlet–singlet deactivation in **4** and **5** gives rise to trends, which resemble the fluorescence quenching: in **4** the singlet lifetimes (~ 0.35 ns) are invariant with respect to the solvent polarity, while for **5** shorter lifetimes were noted in polar benzonitrile (0.08 ns) relative to less polar THF (0.19 ns). Figure 6 illustrates the corresponding time-absorption profiles for **5**. Spectral characteristics of the charge-separated state comprise transient absorption in the visible and near-infrared with characteristic maxima in the 600–700 nm region (i.e., H₂P^{•+}) and at 1010 nm (i.e., C₅₉N^{•-}), respectively.

In oxygen-free solutions, the decays of the H₂P^{•+}/C₅₉N^{•-} radical ion pair transient absorption for **4** and **5** was best fitted by first-order kinetics. For all dyads, the higher the solvent polarity, the shorter the lifetime of the radical ion pair state. For example, in **5** the radical pair lifetimes were 260 and 155 ns in THF and benzonitrile, respectively—see Figure 7. Slightly larger were the lifetime values of **4** (i.e., THF: 445 ns; benzonitrile: 362 ns). As far as the thermodynamics are concerned, the larger the solvent polarity the less negative is the free energy ($-\Delta G^\circ$) associated with the charge recombination.^{1f} A decrease of $-\Delta G^\circ$ and faster charge recombination kinetics is typical of Marcus inverted region, where the electron transfer rates start to decrease with increasing free energy change.⁹

In summary, on the basis of available experimental results the proposed ensembles promise to be valuable to solar energy conversion and photovoltaics, specifically to novel chemical and light driven systems. Relative to previous systems, in which several arenes¹⁰ or C₆₀¹¹ itself were linked to the C₅₉N core, the choice of H₂P—as an excited state electron donor—is crucial to activate intramolecular charge separation. Particular important is the finding that

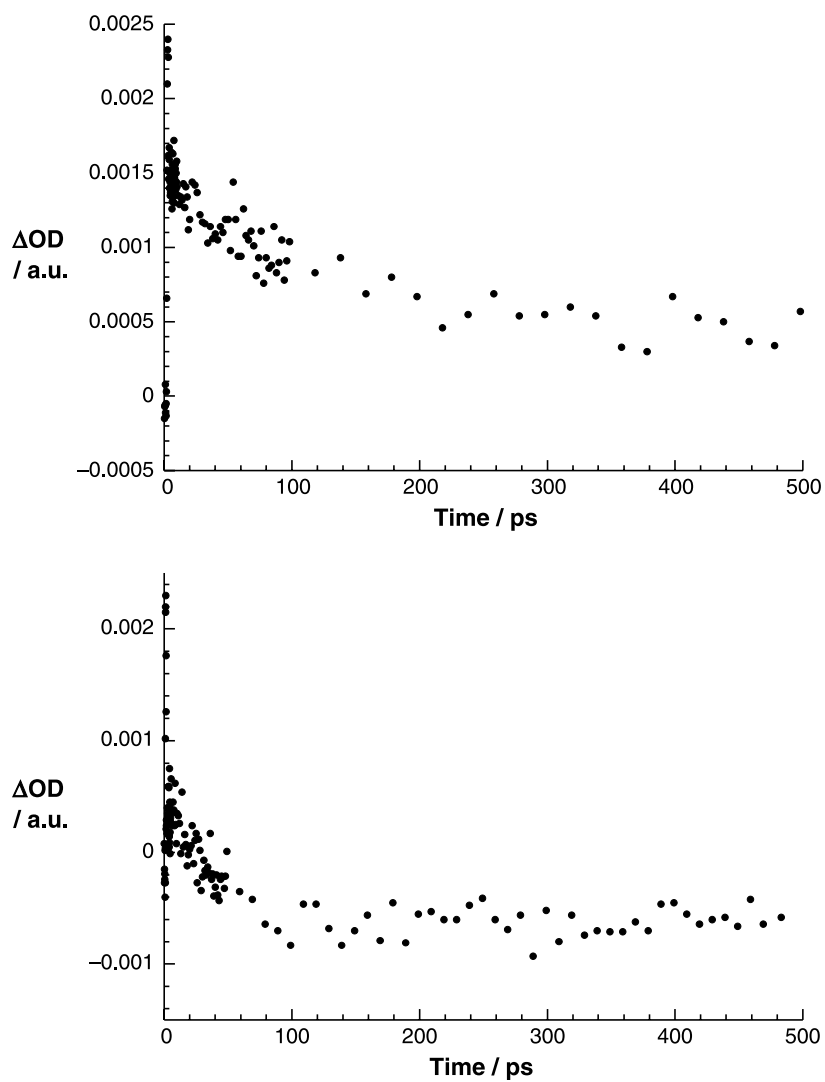


Figure 6. Time-absorption profile at 450 nm (upper figure) and 440 nm (lower figure) following the femtosecond flash photolysis (382 nm) of $\sim 1.0 \times 10^{-5}$ M solutions of **5** in nitrogen saturated THF and benzonitrile, respectively.

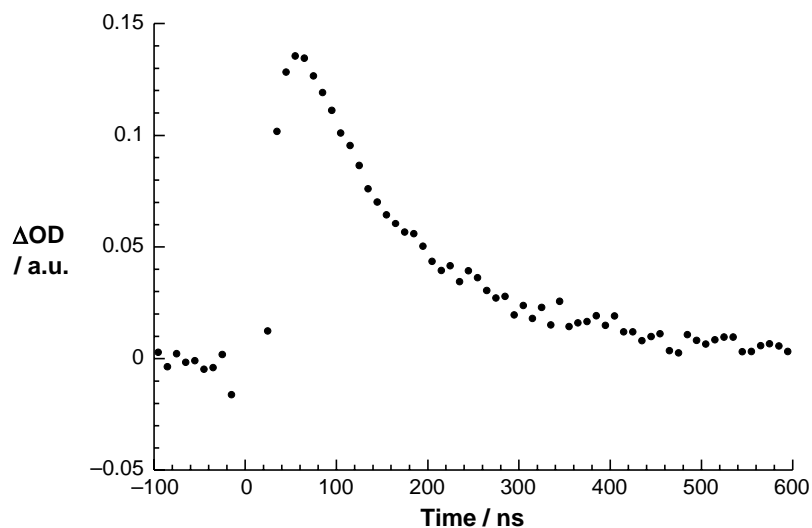


Figure 7. Time-absorption profile at 1010 nm following the nanosecond flash photolysis (532 nm) of $\sim 1.0 \times 10^{-5}$ M solutions of **5** in nitrogen saturated THF.

C₅₉N-based donor–acceptor ensembles exhibit small reorganization energies, a phenomenon typically encountered in C₆₀-based systems.¹ This assists in placing the energy wasting charge recombination dynamics into the Marcus inverted region and, in turn, to slow them down.

Acknowledgements

We thank the Deutsche Forschungsgemeinschaft (DFG), the Graduiertenkolleg ‘Homogener und heterogener Elektronentransfer’, and SFB 583 (Redoxaktive Metallkomplexe—Reaktivitätssteuerung durch molekulare Architekturen) for financial support. Part of this work was supported by the Office of Basic Energy Sciences of the US Department of Energy (NDRL No. 4650).

References and notes

- (a) Imahori, H.; Sakata, Y. *Adv. Mater.* **1997**, *9*, 537. (b) Prato, M. *J. Mater. Chem.* **1997**, *7*, 1097. (c) Martin, N.; Sanchez, L.; Illescas, B.; Perez, I. *Chem. Rev.* **1998**, *98*, 2527. (d) Imahori, H.; Sakata, Y. *Eur. J. Org. Chem.* **1999**, 2445. (e) Guldi, D. M. *Chem. Commun.* **2000**, 321. (f) Guldi, D. M.; Prato, M. *Acc. Chem. Res.* **2000**, *33*, 695. (g) Reed, C. A.; Bolskar, R. D. *Chem. Rev.* **2000**, *100*, 1075. (h) Gust, D.; Moore, T. A.; Moore, A. L. *J. Photochem. Photobiol., B* **2000**, *58*, 63. (i) Gust, D.; Moore, T. A.; Moore, A. L. *Acc. Chem. Res.* **2001**, *34*, 40. (j) Guldi, D. M. *Chem. Soc. Rev.* **2002**, *31*, 22. (k) Armaroli, N. *Photochem. Photobiol. Sci.* **2003**, *2*, 73. (l) Imahori, H.; Mori, Y.; Matano, Y. *J. Photochem. Photobiol., C* **2003**, *4*, 51.
- Echegoyen, L.; Echegoyen, L. E. *Acc. Chem. Res.* **1998**, *31*, 593.
- (a) Gruss, A.; Dinse, K.-P.; Hirsch, A.; Nuber, B.; Reuther, U. *J. Am. Chem. Soc.* **1997**, *119*, 8728. (b) Bellavia-Lund, C.; Keshavarz, M.; Collins, T.; Wudl, F. *J. Am. Chem. Soc.* **1997**, *119*, 8101. (c) Hummelen, J. C.; Bellavia-Lund, C.; Wudl, F. *Top. Curr. Chem.* **1999**, *199*, 93. (d) Nuber, B.; Hirsch, A. *Acc. Chem. Res.* **1999**, *32*, 795.
- Hauke, F.; Hirsch, A. *Chem. Commun.* **2001**, 1316.
- (a) Nuber, B.; Hirsch, A. *Chem. Commun.* **1998**, 406. (b) Hauke, F.; Hirsch, A. *Chem. Commun.* **1999**, 2199. (c) Hauke, F.; Hirsch, A. *Tetrahedron* **2001**, *57*, 3697.
- Hauke, F.; Swartz, A.; Guldi, D. M.; Hirsch, A. *J. Mater. Chem.* **2002**, *12*, 2088.
- Selected data for compound **4**: ν (KBr) (cm⁻¹) = 3052, 2920, 2850, 1741, 1637, 1595, 1574, 1551, 1471, 1438, 1348, 1316, 1287, 1215, 1176, 1155, 1071, 1031, 1000, 964, 799, 727, 700, 658, 579, 556, 524, 480, 469, 440 and 417; λ_{\max} (CH₂Cl₂) (nm) 257, 324, 402, 423, 517, 551, 591 and 648; ¹H NMR δ (400 MHz, CS₂/CDCl₃) = 8.74 (m, 8H, β H), 8.26 (d, 1H, ar), 8.19 (m, 3H, ar), 8.00 (d, 2H, ar), 7.94 (m, 1H, ar), 7.74 (m, 10H, ar), 7.47 (m, 1H, ar), 7.31 (m, 1H, ar), 5.32 (s, 1H, –CH–), 4.89 (dt, 2H, –CH₂–), 4.46 (t, 2H, –CH₂–), 4.01 (s, 3H, –CH₃), –3.02 (s, 2H, –NH); ¹³C NMR δ (100 MHz, CS₂/CDCl₃) 165.33/165.13 (each 1C, –C=O), 156.15, 154.19, 154.08, 146.08, 145.90, 145.79, 145.64, 145.60, 145.55, 145.52, 145.45, 145.32, 145.06, 144.94, 144.82, 144.71, 144.63, 144.60, 144.44, 144.34, 143.84, 143.58, 143.47, 143.34, 143.20, 143.06, 142.93, 142.88, 142.50, 142.26, 141.86, 141.76, 141.72, 141.67, 141.61, 141.50, 140.60, 140.48, 140.26, 140.11, 139.79, 139.71, 139.41, 139.30, 137.87, 136.04, 134.30, 134.27, 134.17, 133.97, 133.90, 127.40, 127.33, 127.23, 126.52, 126.41, 123.68, 123.58, 121.00, 119.96, 119.80, 119.73, 118.84, 114.55, 78.79 (1C, C-sp³), 65.83/64.27 (each 1C, –CH₂–), 61.34 (1C, –CH–), 52.63 (1C, –CH₃); *m/z* (FAB) 1496 [M]⁺ and 722 [C₅₉N]⁺. Selected data for **5**: ν (KBr) (cm⁻¹) 2956, 2925, 2901, 2863, 1684, 1598, 1560, 1500, 1457, 1421, 1397, 1361, 1264, 1185, 1106, 1023, 983, 966, 927, 877, 846, 798, 729, 580, 552, 523 and 420; λ_{\max} (CH₂Cl₂) (nm) 257, 322, 399, 420, 517, 552, 595 and 648; ¹H NMR δ (400 MHz, CS₂/CDCl₃) 8.91 (d, ³J = 4.9 Hz, 2H, β H), 8.83 (s, 4H, (H), 8.55 (d, ³J = 8.2 Hz, 2H, β H), 8.10 (m, 8H, ar), 7.75 (m, 8H, ar), 5.44 (s, 2H, –CH₂–), 1.64 (s, 9H, –CH₃), 1.61 (s, 18H, –CH₃), –2.87 (s, 2H, –NH); ¹³C NMR δ (100 MHz, CS₂/CDCl₃) 194.78 (1C, –C=O), 154.67 (2C, C₅₉N), 150.09 (3C, ar), 148.31 (1C, C₅₉N), 148.22 (2C, C₅₉N), 147.35 (1C, ar), 146.93 (2C, C₅₉N), 146.56 (2C, C₅₉N), 146.40 (2C, C₅₉N), 146.28 (2C, C₅₉N), 146.08 (2C, C₅₉N), 145.87 (2C, C₅₉N), 145.70 (2C, C₅₉N), 145.34 (2C, C₅₉N), 145.30 (1C, C₅₉N), 145.19 (2C, C₅₉N), 144.49 (2C, C₅₉N), 144.25 (2C, C₅₉N), 143.78 (2C, C₅₉N), 143.53 (2C, C₅₉N), 143.34 (2C, C₅₉N), 142.38 (2C, C₅₉N), 142.22 (2C, C₅₉N), 141.39 (2C, C₅₉N), 141.06 (2C, C₅₉N), 140.67 (2C, C₅₉N), 140.51 (2C, C₅₉N), 140.42 (2C, C₅₉N), 140.13 (2C, C₅₉N), 138.92/138.88 (1C/2C, ar), 138.76 (2C, C₅₉N), 136.90 (2C, C₅₉N), 135.52 (1C, ar), 135.14 (2C, ar), 134.27 (6C, ar), 134.09 (2C, C₅₉N), 126.82 (2C, ar), 124.29 (2C, C₅₉N), 123.57 (6C, ar), 120.77 (1C, porph), 120.39 (2C, porph), 117.45 (1C, porph), 78.40 (1C, C-sp³), 49.96 (1C, –CH₂–), 34.49 (3C, –CR₃), 31.56 (9C, –CH₃); *m/z* (FAB) 1547 [M]⁺, 1490 [M]⁺ – [tBu], 722 [C₅₉N]⁺.
- Only for **4** we found fluorescence lifetimes that fall within our experimental detection range of larger than 100 ns. The lifetime values were in toluene (0.33 ns), THF (0.33 ns) and benzonitrile (0.30 ns).
- Marcus, R. A. *Angew. Chem., Int. Ed., Engl.* **1993**, *32*, 11.
- Hauke, F.; Atalick, S.; Guldi, D. M.; Mack, J.; Scott, L.; Hirsch, A. *Chem. Commun.* **2004**, 766.
- Hauke, F.; Herranz, M. A.; Echegoyen, L.; Guldi, D. M.; Hirsch, A. *Chem. Commun.* **2004**, 600.

Synthesis and photophysics of porphyrin–fullerene donor–acceptor dyads with conformationally flexible linkers

David I. Schuster,^{a,*} Shaun MacMahon,^a Dirk M. Guldi,^b Luis Echegoyen^c
and Silvia E. Braslavsky^d

^aDepartment of Chemistry, New York University, New York, NY 10003, USA

^bInstitute for Physical and Theoretical Chemistry, University of Erlangen, 91058 Erlangen, Germany

^cDepartment of Chemistry, Clemson University, Clemson, SC 29634, USA

^dMax Planck Institute for Bioinorganic Chemistry (formerly Strahlenchemie), D 45413 Mülheim, Germany

Received 7 June 2005; revised 26 July 2005; accepted 30 July 2005

Available online 15 December 2005

Abstract—The synthesis and photophysics of a series of porphyrin–fullerene (P–C₆₀) dyads in which the two chromophores are linked by conformationally flexible polyether chains is reported. Molecular modeling indicates the two moieties adopt a stacked conformation in which the two chromophores are in close proximity. Photoexcitation of the free base dyads in polar solvents such as tetrahydrofuran and benzonitrile, causes electron transfer (ET) to generate charge-separated radical pair (CSRP) states, which were directly detected using transient absorption (TA) techniques. In nonpolar solvents such as toluene, where CSRP states were not directly detected, fullerene triplet state states were formed, according to TA studies as well as singlet oxygen sensitization measurements. The low value of the quantum efficiency for sensitized formation of singlet molecular oxygen [O₂(¹Δ_g)] in toluene and chloroform indicates that singlet energy transduction to give H₂P–¹C₆₀*, followed by intersystem crossing to H₂P–³C₆₀* and energy transfer to ³O₂, is not the operative mechanism. Rather, a mechanism is proposed involving ET to give CSRP states followed by exergonic charge recombination to eventually generate fullerene triplets. Such a mechanism has been demonstrated experimentally for structurally related P–C₆₀ dyads. For the corresponding ZnP–C₆₀ dyads with flexible linkers, only photoinduced ET to generate long-lived CSRP states is observed. Photoinduced charge separation in these dyad systems is extremely rapid, consistent with a through space rather than through-bond mechanism. Charge recombination is up to three orders of magnitude slower, indicating this process occurs in the inverted region of the Marcus curve that relates ET rates to the thermodynamic driving force. These observations once again demonstrate the advantages of incorporating fullerenes as electron acceptor components in photosynthetic model systems.

© 2005 Elsevier Ltd. All rights reserved.

1. Introduction

Fullerenes, C₆₀ in particular, have been found to make ideal acceptors in model photosynthetic systems, due to their unique photophysical, electrochemical, and chemical properties.¹ C₆₀ has been shown to reversibly accept up to six electrons in solution due to its three low lying degenerate lowest unoccupied molecular orbitals (LUMOs), with a first electrode potential resembling that of the quinone-derived electron acceptor in the photosynthetic reaction center.² Fullerenes accelerate charge separation and slow down charge recombination versus donor–acceptor (DA) dyads containing traditional two-dimensional electron acceptors such as quinones and imides. This phenomenon, which is general, has been rationalized by the small Marcus

reorganization energy (λ) accompanying electron transfer in fullerenes. Since the negative charge on the fullerene produced after photoexcitation of the donor moiety is delocalized over the entire π -system, the charge density is much lower than it would be on acceptors such as quinones, where the charge is concentrated mainly on the oxygens. The structural inflexibility of fullerene-based systems results in small internal reorganization energies (λ_v), while the charge dispersion minimizes the solvent reorganization energy (λ_s).³

For electron DA systems, Marcus theory predicts that as the free energy change (ΔG^0) for electron transfer (ET) becomes more negative, that is, increasingly exergonic, the ET rates increase, reaching a maximum when $-\Delta G_{ET} = \lambda$, the reorganization energy. As $-\Delta G_{ET}^0$ becomes more negative than the absolute value of λ , the ET rate decreases. For C₆₀ dyads, the maximum in the Marcus curve is reached at smaller values of $-\Delta G_{ET}^0$ compared to two-dimensional acceptors.

Keywords: Fullerenes; Porphyrins; Dyads.

* Corresponding author. Tel.: +1 212 998 8447; fax: +1 212 260 7905; e-mail: david.schuster@nyu.edu

Thus, charge separation (CS) rates for most fullerene-based DA dyads are located along the upward slope of the Marcus curve, near the maximum, leading to enhanced CS rates, whereas the large thermodynamic driving force for charge recombination (CR) places this process on the downward side of the Marcus parabola in the inverted region. This phenomenon causes a noticeable enhancement in the lifetime of charge-separated radical pair (CSRP) states in C₆₀-based DA systems versus analogous two-dimensional DA systems.⁴

Porphyrins are frequently used as donors in artificial photosynthetic systems. Porphyrins are synthetically accessible in a laboratory, (although their synthesis can be a rather arduous task),⁵ and they absorb light much more effectively than fullerenes in the visible region between 400 and 600 nm. Favorable van der Waals interactions between the curved π surface of the fullerene and the planar π surface of the porphyrin assist in the formation of supramolecular structures, overcoming the necessity to match a concave-shaped host to a convex-shaped guest.⁶ This unique intermolecular electronic interaction is observed in condensed media as well as in the solid state.

Attempts to suppress CR have led to the development of multi-chromophoric triads, tetrads and pentads, where ET can occur through a multi-step process, yielding CSRP with microsecond to second lifetimes.^{1c,d,7} An inherent problem is the synthetic challenge involved in the synthesis of such complicated assemblies. These multicomponent materials are far less efficient in the storage of energy than dyad systems, since sequential ET dissipates more and more of the initial excitation energy, lowering the capacity for energy storage.

Herein, we report on simple porphyrin–C₆₀ (P–C₆₀) dyads with flexible linkers, which are easily synthesized and which have many of the desirable properties of DA systems with respect to energy storage and CSRP state lifetimes.

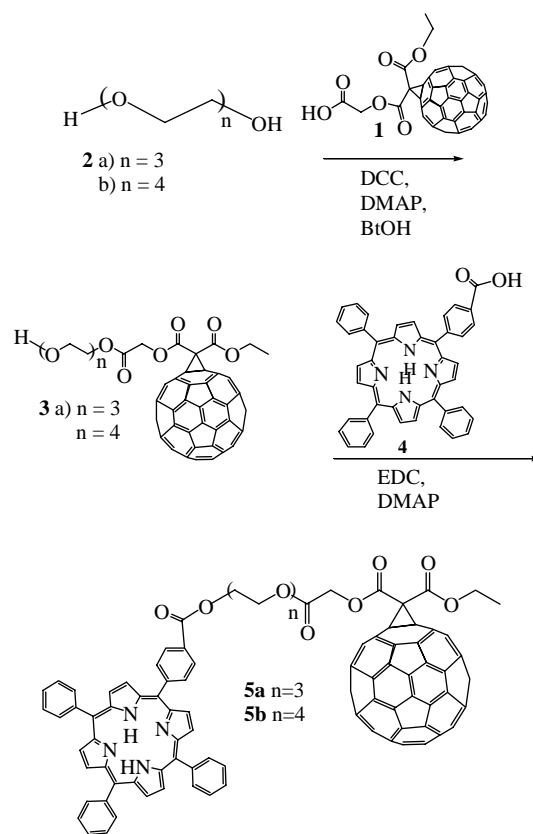
2. Free base porphyrin–fullerene dyads (H₂P–C₆₀)

2.1. Synthesis and structural characterization

Our initial foray into this area centered on the synthesis of porphyrin–fullerene (H₂P–C₆₀) dyads with flexible crown ether-like glycol linkers by a convergent route.⁸ Steady-state fluorescence spectra demonstrated rapid and efficient quenching of the porphyrin S₁ state by the fullerene, but the CS and CR kinetics were not measured on these phase I dyads. Among the synthetic problems encountered were the extremely low yields (i.e., ~30%) when using simple methanofullerene carboxylic acid, due to the acid poor solubility properties. Coupling of tetraphenylporphyrin carboxylic acid to the polyether linker also proved difficult, making it extremely challenging to generate dyads on a milligram scale.

In order to circumvent these problems, fullerene carboxylic acid **1**, originally reported by Diederich and Nierengarten,⁹ was used as the fullerene synthon. The strategy was to replace methanofullerene carboxylic acid by **1**, which would lead to flexibly linked H₂P–C₆₀ dyads with much better

solubility properties, as well as higher yields in the coupling reactions. Improved solubility would in turn allow more facile structural characterization. In the first series of reactions, summarized in Scheme 1, fullerene acid **1** was condensed with glycols **2a** and **2b** to give **3a** and **3b**, respectively, which were then condensed with 5,10,15,20-tetraphenylporphyrin carboxylic acid **4** to give dyads **5a** and **5b**, respectively. Details of these reactions are provided in an earlier paper dealing with the synthesis of a variety of P–C₆₀ dyads.¹⁰



Scheme 1.

¹H NMR spectra of **5a** and **5b** showed characteristic porphyrin bands between 7.5 and 9 ppm, glycol bands at 3.5–4 ppm, and distinctive peaks from the C₆₀ synthon **1**. Computer modeling using Insight II provided a prediction of the H₂P–C₆₀ geometry in the ground state (see Fig. 1).¹¹ Because of favorable porphyrin–fullerene π – π interactions, the glycol linker curves around, placing the porphyrin and fullerene within van der Waals contact range.

UV–vis spectra of dyads **5a** and **5b** in chloroform demonstrated strong ground state interactions. The porphyrin Soret bands at 422 nm were red shifted by approximately 5–10 nm relative to methyl ester **8**, indicating that the fullerene was close enough to the porphyrin in the ground state to perturb its absorption spectrum. Similar spectral shifts were also visible in the porphyrin Q-band region in both dyads. The broadness of the absorption in both the Soret and Q-band regions was surprising, and could indicate the presence of more than one conformation of these dyads in solution.

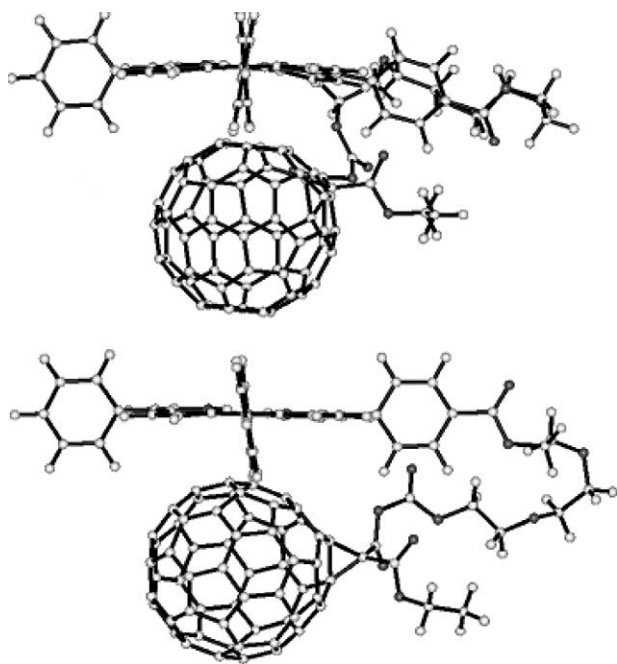


Figure 1. Insight II molecular mechanics calculations for dyads **5a** and **5b**.

Whereas substantial improvements in yield were observed in the coupling yields using fullerene carboxylic acid **1**, the porphyrin coupling step still proved to be extremely difficult. Moreover, the solubility of dyads **5a** and **5b**, though somewhat improved over the first generation dyads, still severely restricted the choice of solvents for photophysical studies. In order to improve the solubility characteristics of the porphyrin component, *tert*-butyl substituents were incorporated on the benzene rings, as in a large body of work in this field. The stepwise synthetic route to the solubilized porphyrin carboxylic acid **6** shown in Scheme 2 was developed. The first step involved preparation of a dipyrromethane derivative **7** from pyrrole and 3,5-di-*t*-butyl benzaldehyde, followed by condensation with 1 equiv each of this aldehyde and

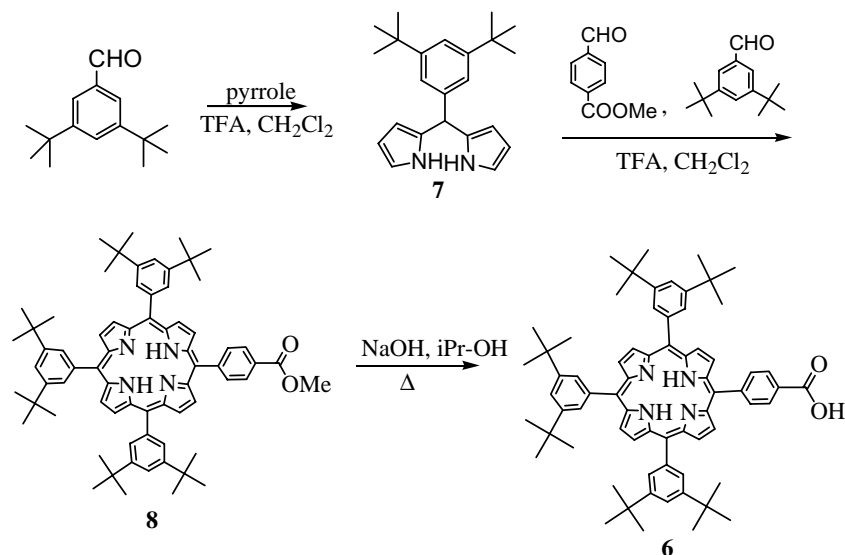
4-carboxymethylbenzaldehyde to give porphyrin methyl ester **8**. Overall yields of purified porphyrin were 17%. Hydrolysis gave carboxylic acid **6** in 94% yield.

Scheme 3 depicts the synthesis of the solubilized flexibly linked H₂P–C₆₀ dyads. The initial coupling reaction to fullerene acid **1** was carried out as before. Coupling of **3a** and **3b** to the porphyrin acid **6** using 1-(3-dimethylamino-propyl)-3-ethylcarbodiimide/dimethyl-aminopyridine (EDC/DMAP) gave the desired dyads **9a** and **9b** in 50% yield.

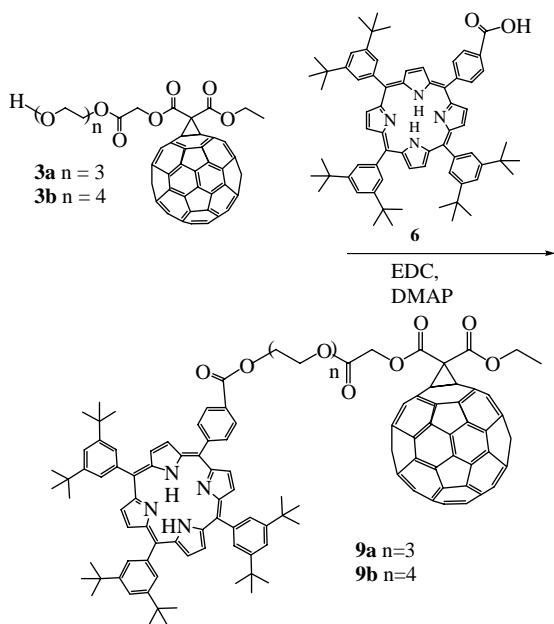
Intramolecular electronic interactions were again monitored using UV–vis spectroscopy. Bathochromic shifts of the porphyrin Soret band were pronounced, ranging from 6–10 nm depending on the solvent. The UV–vis spectra for dyads **9a** and **9b** were collected in solvents of greatly varying relative permittivity: toluene (2.0), THF (7.6), CH₂Cl₂ (9.1), and benzonitrile (PhCN) (26.0). An increase in the porphyrin–fullerene interaction was seen with increasing solvent polarity, particularly in **9b**. In relatively nonpolar solvents such as toluene and THF, the interaction between the chromophores in **9a** was stronger than in **9b**, according to shifts in the Soret band. As the solvent became more polar, the interaction in **9b** became comparable to that in **9a**. This may be because the chromophores are not as effectively solvated in polar media. It is remarkable that the interaction persists even in toluene, possibly because both the porphyrin and fullerene moieties are effectively solvated in aromatic solvents, and therefore must overcome a large entropic barrier to interact with each other. Such effects should be more pronounced with **9a** and **9b** versus **5a** and **5b** due to the presence of three di-*tert*-butylphenyl groups.

2.2. Electrochemistry

For **9a**, the first reductive redox couple of the C₆₀ center appears at –0.55 V versus Ag/AgCl, which is in good agreement with values typically observed for C₆₀ derivatives.¹² The first one-electron oxidation of the porphyrin



Scheme 2.



Scheme 3.

center occurs at +1.10 V, which is a bit more positive than that for tetraphenylporphyrins (typically +1.0 V). The small shifts are attributable to the intramolecular interactions in the dyad. Dyad **9b** showed a weak wave for the oxidation of the porphyrin center at 1.08 V, but no discernible peak for the reduction of the C₆₀ moiety was observed, probably due to the small amount of sample available. Similar measurements were not performed on **5a** and **5b**.

2.3. Steady-state fluorescence

The steady-state fluorescence properties of the flexibly linked H₂P–C₆₀ dyads were measured against that of a porphyrin standard, namely the methyl ester **8**, which has a fluorescence lifetime of 9 ns. Strong quenching in dyads **5a** and **5b** was seen relative to the standard in both benzene (Fig. 2) and chloroform (Fig. 3). To avoid signal saturation due to excessive absorption of the incident excitation light, the excitation was carried out at 550 nm, a region well separated from the Soret peak where the light is still absorbed exclusively by the porphyrin moiety. The other option available was to use extremely dilute solutions with

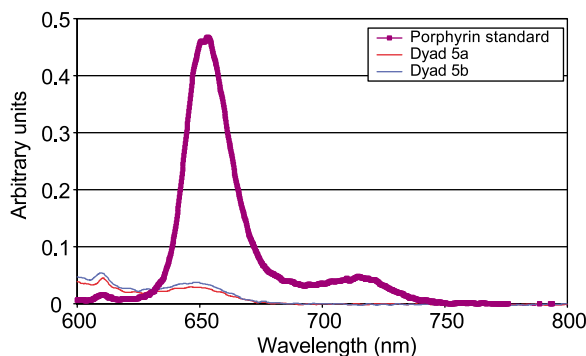


Figure 2. Fluorescence emission for dyads **5a** and **5b** in benzene (10 μ M). The porphyrin standard was methyl ester **8**.

excitation in the Soret band to the porphyrin S₂ state. The rate constant for fluorescence deactivation was higher in chloroform, which we ascribe to the increased rate of electron transfer quenching expected in the more polar solvent (*vide infra*). An increase in fluorescence quenching as a function of increasing solvent relative permittivity was observed. The quenching efficiency for dyads **5a** and **5b** both increase upon going from *o*-dichlorobenzene (ODCB) to PhCN to *N,N*-dimethylformamide (DMF).

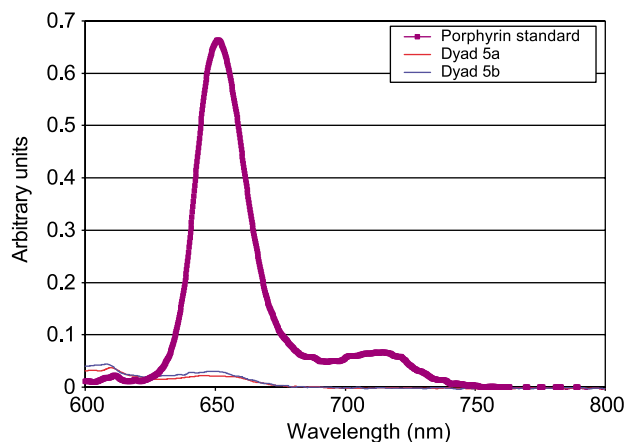


Figure 3. Fluorescence emission for dyads **5a** and **5b** in CHCl₃ (10 μ M). The porphyrin standard was methyl ester **8**.

The fluorescence properties of **9a** and **9b** were measured against that of the methyl ester of **6** as the porphyrin standard, with a fluorescence lifetime of 9 ns. Again, rapid and efficient quenching of porphyrin fluorescence in **9a** and **9b** was observed. The rate and efficiency of fluorescence quenching increased with increasing solvent polarity, as was seen with **5a** and **5b**.

2.4. Quantum yields for singlet oxygen formation

Quantum yields of sensitized singlet oxygen [O₂(¹ Δ_g)] formation (Φ_{Δ}) by dyads **5a** and **5b** upon excitation of air-saturated solutions at 532 nm are shown in Table 1. Full details of the procedure are given elsewhere.¹³ Quantum yields are reported relative to tetraphenylporphyrine (TPP) for which $\Phi_{\Delta} = 0.67 \pm 0.14$.¹⁴ The Φ_{Δ} value is an indirect way to measure ³C₆₀ formation, since ³C₆₀ transfer energy to ³O₂ to generate O₂(¹ Δ_g) occurs with unit efficiency, and for simple fullerene derivatives Φ_{Δ} is generally > 0.9.¹⁵ The Φ_{Δ} values for **5a** and **5b** are lower in chloroform than in toluene, where the values are the same for both dyads. The low Φ_{Δ} value in toluene indicates that singlet energy transduction to give H₂P–¹C₆₀^{*}, followed by intersystem crossing to H₂P–³C₆₀^{*} and energy transfer to ³O₂, is not operative.

Table 1. Quantum yields for O₂(¹ Δ_g) formation

Compound	Φ (relative) in PhMe	Φ (relative) in CHCl ₃
Porphyrin standard (TPP)	0.89	0.94
Dyad 5a	0.34	0.18
Dyad 5b	0.34	0.09

Excitation of air-saturated solutions at 532 nm. For procedural details, see Ref. 13.

If such a mechanism were operative, the values of Φ_{Δ} should have been much higher, in the range 0.9–1.0.¹⁵ Such a sequence has indeed been proposed for some H₂P–C₆₀ dyads in nonpolar solvents.^{16,17} However, another possible mechanism involves electron transfer in nonpolar solvents followed by back electron transfer to generate lower lying porphyrin and fullerene triplet states. Indeed, recent time-resolved electron paramagnetic resonance (TREPR) studies have established¹⁸ that the following stepwise mechanism is operative for a parachute-shaped ZnP–C₆₀ dyad system in toluene: (1) electron transfer to give a charge-separated state, (2) back electron transfer to give ³ZnP*–C₆₀, and finally (3) energy transfer to give the lower lying ZnP–³C₆₀*. Although we have no TREPR data as yet on dyads **5a** and **5b**, we propose that a similar mechanism is operative in the present case. It is interesting to note that the triethylene glycol-linked dyad **5a** generates twice as much O₂(¹Δ_g) as the tetraethylene glycol-linked compound **5b** in chloroform, which would be difficult to explain if the energy transduction pathway was operative, but makes sense in terms of a stepwise mechanism for O₂(¹Δ_g) formation where three distinct steps of variable efficiency are involved. Unfortunately, because of lack of material, similar studies were not done with dyads **9a** and **9b**.

In this context, it is worth noting that generation of fullerene triplets in high yield by an electron transfer/charge recombination pathway has also been reported by Armaroli et al. for a quite different type of dyad, namely one in which C₆₀ is covalently linked to a bipyridine (bipy) moiety complexed with Ru(II).¹⁹ Excitation of the metal complex moiety gives the lowest triplet metal-to-ligand-charge-transfer (MLCT) excited state, which is quenched by electron transfer (ET) to give the C₆₀ radical anion in quantitative yield. This is followed by charge recombination to generate ³C₆₀*, again in quantitative yield, as determined by luminescence, as above. It was noted that triplet–triplet energy transfer (EnT) from ³MLCT* to ³C₆₀* does not compete with ET, because the EnT process is highly exergonic and is therefore located in the Marcus inverted region.¹⁹

2.5. Transient absorption measurements

Characteristic transient singlet and triplet spectra were recorded in the pico-, nano-, and microsecond time regime following 532 nm laser excitation. Typically, in our ultrafast experiments (i.e., 20 ps laser pulses) it is possible to see singlet excited states formed instantaneously, namely, with kinetics faster than $5 \times 10^{10} \text{ s}^{-1}$. A fast intersystem crossing process (i.e., $k_{isc} \sim 1.0 \times 10^8 \text{ s}^{-1}$) governs the fate of the

metastable singlet excited states in H₂P, leading to the corresponding triplet manifold, which we see with our slower experiments (i.e., 10 ns laser pulses). Characteristic absorption for C₆₀ triplets was seen at 720 nm (data not shown).¹⁹ For experimental details, see previous work from this collaborative team.¹³ Time-resolved transient absorption measurements with the free base dyads **9a** and **9b** completely corroborated the steady-state fluorescence experiments. The rate of decay of the S₁ singlet excited state of H₂P in THF and PhCN is much faster than the typical intersystem crossing rate of H₂P, using ps excitation and detection in the ps and ns range. Moreover, the differential absorption changes at the end of the fast decay bear no resemblance with any of the typical singlet/triplet excited state characteristics for H₂P or C₆₀.¹⁹ Instead, broad H₂P π-radical cation absorption in the visible²⁰ and C₆₀ π-radical anion absorption in the near-infrared²¹ are observed (see Fig. 4), which were then employed as convenient markers to quantify the CS efficiency and CR dynamics.

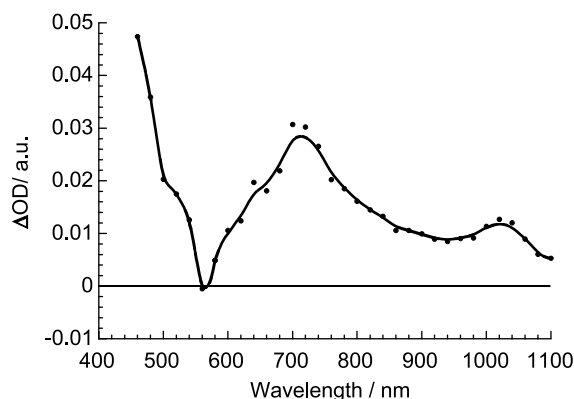


Figure 4. Differential absorption spectrum (visible and near-infrared) obtained upon nanosecond flash photolysis (532 nm) of $\sim 1.0 \times 10^{-5} \text{ M}$ solutions of **9b** in nitrogen-saturated THF with a time delay of 50 ns at room temperature. The spectrum corresponds to the radical pair H₂P^{•+}–C₆₀^{•-}.

The CS and CR dynamics in dyads **5a** and **5b**, along with the quantum yields for formation of the charge-separated states H₂P^{•+}–C₆₀^{•-} in five different solvents (Φ_{CS}), are summarized in Table 2. The lifetimes associated with CS decrease as the solvent polarity increases. Thus, the CS rates are highest in the most polar solvent, DMF, which is consistent with normal Marcus region behavior. Given that the CS rate constants vary only slightly with changes in solvent polarity, that is, they differ by less than a factor of three for both dyads, it is likely that CS in **5a** and **5b** is occurring

Table 2. Charge separation and recombination data for dyads **5a** and **5b**

Solvent	Dyad 5a			Dyad 5b		
	τ_{CS} (ns) ^a	τ_{CR} (ns) ^a	Φ_{CS} ^b	τ_{CS} (ns) ^a	τ_{CR} (ns) ^a	Φ_{CS} ^b
Toluene	0.188	373	0.19	0.222	396	0.33
THF	0.145	288	0.24	0.166	298	0.34
ODCB		246	0.50		270	0.67
PhCN	0.09	115	0.37	0.099	156	0.43
DMF	0.083	83	0.17	0.095	99	0.19

^a From formation and decay of C₆₀^{•-} absorption at 980–1020 nm.

^b From absorption at 1000 nm measured 20 ns after the flash, relative to reference dyad.

Table 3. Electron transfer dynamics for dyads **9a** and **9b**

Compound	τ_F (ns) ^a		τ_F (ns) ^b			τ_{CS} (ns)	
	THF	PhCN	PhMe	THF	PhCN	THF	PhCN
8			9.6	9.5	9.8		
9a	0.78	0.74	1.06	0.95	0.83		490
9b	0.94	0.83	1.93	1.81	1.28	725	450

^a Measured directly by disappearance of porphyrin S_1 state.

^b From steady-state fluorescence quenching data and fluorescence lifetime of porphyrin **6** methyl ester.

near the top of the Marcus curve, where rates are relatively insensitive to the thermodynamic driving force. However, CR is clearly occurring in the inverted region of the Marcus curve, as indicated by the fact that k_{CR} is slowest in the least polar solvent, toluene, and is highest in the most polar solvent, DMF. This is exactly the opposite of what would be expected if CR were occurring in the normal region of the Marcus curve. The value of Φ_{CS} is highest in *o*-dichlorobenzene.

The ET dynamics for dyads **9a** and **9b** are summarized in Table 3, along with fluorescence data for tetraphenylporphyrin methyl ester **8**. H_2P singlet excited state lifetimes, the inverse of the rates of charge separation, were measured in two different ways. The first column shows transient absorption data, following the rate of disappearance of singlet–singlet absorption of H_2P in the visible. The second set of lifetimes derives from measurements of the fluorescence lifetime of the H_2P standard, and determination of the extent of quenching in the dyads in three different solvents. The lifetime of the H_2P singlet excited state is then calculated by assuming that I/I_0 is equal to τ/τ_0 . Although the lifetimes determined by the two methods differ slightly, the trend is the same, namely k_{CS} increases with increasing solvent polarity, consistent with normal Marcus region behavior. The CR process, on the other hand, is clearly occurring in the Marcus inverted region, as the lifetime in THF far exceeds that in benzonitrile, a more polar solvent in which the CSRP state is lower in energy relative to the ground state than it is in THF. The very long lifetime of the CSRP state of **9b** in THF, namely 725 ns, is one of the longest ever measured for a simple P– C_{60} dyad in solution.^{16,22}

3. Zinc porphyrin–fullerene dyads (ZnP– C_{60})

3.1. Synthesis and structural characterization

Complexation of dyads **9a** and **9b** with zinc proceeded quantitatively using $Zn(OAc)_2$ in methanol, generating ZnP– C_{60} **9aZn** and **9bZn**. Since zinc porphyrins are in general better electron donors than their free base counterparts, **9aZn** and **9bZn** were expected to generate CSRP states more rapidly and with a higher quantum yield than their free base analogs. Electronic ZnP– C_{60} interactions in **9aZn** and **9bZn**, as monitored by UV–vis spectroscopy, are similar to those in **9a** and **9b**. Whereas red shifts in the absorption spectra were observed, the trend as a function of solvent polarity was not quite as clear as it was with the H_2P – C_{60} . An increase in solvent polarity increased the interaction, particularly in the dyad with

the longer linker, **9bZn**. Eventually, in the most polar solvents studied, the UV–vis spectra of ZnP– C_{60} display nearly identical interactions to those in the H_2P – C_{60} analogs. It is known that fullerene–porphyrin interactions are not as strong in metallated as in free base porphyrins, consistent with a larger distance between the chromophores in fullerene–metalloporphyrin co-crystals.⁹ Interchromophoric interactions prevail also in chelating solvents such as benzonitrile and THF, as clear shifts and bleaching in all absorption bands are observed upon comparison to the Zn-porphyrin standard.

3.2. Electrochemistry

For **9aZn**, the first oxidation (0.95 V) of the porphyrin center is shifted negatively by 150 mV and the reduction (–0.65 V) of C_{60} is shifted negatively by 100 mV relative to appropriate standards. For **9bZn**, the first one-electron oxidation of the porphyrin center occurs at 0.92 V and the first one-electron reduction of the C_{60} center appears at –0.59 V. There is a negative shift of 160 mV for the porphyrin center from **9b** to **9bZn**, consistent with the well known greater ease of oxidation of zinc versus free base porphyrins.

3.3. Steady-state fluorescence

Experiments for **9aZn** and **9bZn** were conducted using an excitation wavelength of 520 nm. The relative quenching efficiencies, relative to that of the ZnP standard, are similar to those observed in the corresponding H_2P – C_{60} . However, since the fluorescence lifetime of ZnP is typically on

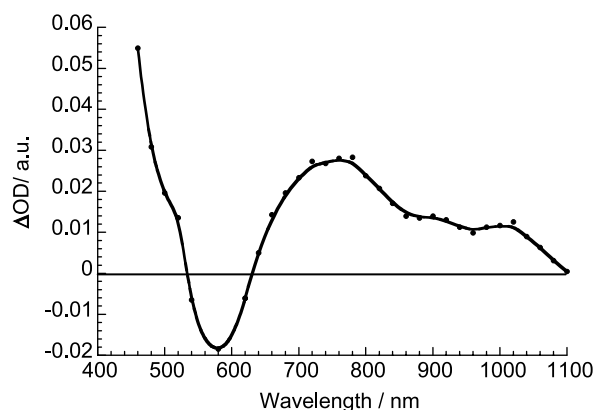


Figure 5. Differential absorption spectrum (visible and near-infrared) obtained upon nanosecond flash photolysis (532 nm) of $\sim 1.0 \times 10^{-5}$ M solutions of **9bZn** in nitrogen-saturated THF with a time delay of 50 ns at room temperature. The spectrum corresponds to the radical pair $ZnP^{\bullet+}-C_{60}^{\bullet-}$.

Table 4. Charge transfer dynamics for dyads **9aZn** and **9bZn**

Compound	τ_F (ns) ^a			τ_{CS} (ns)	
	PhMe	THF	PhCN	THF	PhCN
8Zn	2.1	2.1	2.1		
9aZn	0.24	0.21	0.11	490	180
9bZn	0.56	0.50	0.49	440	150

^a Measured by comparing steady-state fluorescence results to lifetime of Zn-porphyrin standard.

the order of ~ 2 ns, compared to 9 ns for the corresponding H₂P, the intramolecular CS rates in the ZnP–C₆₀ are clearly faster. As with the H₂P–C₆₀ analogues, increased quenching with increasing solvent polarity is observed for the ZnP–C₆₀.

3.4. Transient absorption measurements

The fate of the ZnP singlet excited state in **9aZn** and **9bZn** was also examined by pico-, nano-, and microsecond transient absorption spectroscopies. At early times (i.e., 50–100 ps), these are practically identical to those of the ZnTPP, disclosing strong bleaching at 550 nm and attesting to the formation of the ZnP singlet excited state. At a delay time of ca. 200 ps, a new transition around 640 nm starts to grow in, accompanied by another absorption in the near-infrared. Based on a spectral comparison, we ascribe the former to the ZnP π -radical cation, while the latter band belongs to the C₆₀ π -radical anion. The CSR absorption is persistent on the picosecond time scale and decays in the nano- to microsecond time regime (see Fig. 5).

The ET dynamics in several solvents are tabulated in Table 4. The rates of charge separation in **9aZn** and **9bZn** are consistently faster than those in **9a** and **9b**, by up to as much as an order of magnitude. This is hardly surprising since CS in the Zn-dyads is thermodynamically more favorable, which would lead to faster rates in an ET process occurring in the normal region of the Marcus curve. The charge recombination data again display inverted Marcus region behavior, as longer lifetimes are observed in THF than in benzonitrile.

4. Conclusions

The synthesis of a series of porphyrin–C₆₀ dyads with flexible polyether linkers of varying length has been accomplished using a standard set of reactions. Introduction of alkyl substituents on the porphyrin greatly increased the solubility and ease of handling of these compounds. Using steady-state and time resolved techniques, it was found that the rate constants for forward electron transfer in both free base (H₂P) and ZnP systems, are on average approximately three orders of magnitude greater than the rate constants associated with back electron transfer. The formation of C₆₀ triplet states in toluene for the free base dyads is attributed to ET followed by charge recombination, rather than a direct energy transfer mechanism, analogous to the situation in some other types of dyads. Fullerene triplets are not detected for the ZnP dyads in either polar or nonpolar solvents.

In these systems, the rapidity of the photoinduced ET process is best rationalized in terms of the molecular conformations of these dyads shown in Figure 1. It was reported by Armaroli et al.²⁴ that a doubly-linked face-to-face porphyrin–fullerene system and a related singly linked system show remarkably similar photophysical behavior, indicating that the donor and acceptor moieties in both these systems are in close proximity, and that through space rather than through-bond ET mechanisms dominate. On the other hand, there are some significant differences between the results of the present study and those reported for analogous doubly-linked dyads with parachute topology.¹³ The linkers in both cases are polyethers. The rates of charge separation in the present system are slightly slower than those in the parachute system by up to an order of magnitude, while the rates of charge recombination in the flexibly linked dyads are considerably slower, by closer to three orders of magnitude. For example, in THF the fluorescence lifetime of **5a** is 0.15 ns compared to 0.02–0.08 ns for the parachute dyad in the same solvent, while the CSR lifetime of **5a** is 300 ns, compared to 0.3 ns for the parachute compound. This difference can be rationalized in terms of significant differences in topology of the systems, but also suggests that through-bond ET processes may compete with through space mechanisms in the flexibly linked dyads, particularly with respect to charge recombination.

We conclude that the forward ET process in these flexibly linked donor–acceptor systems occurs near the peak of the Marcus parabola relating ET rates and thermodynamic driving force, while BET occurs deep in the inverted region, resulting in charge-separated radical pair (CSR) states with lifetimes approaching the microsecond time regime. This has obvious implications with respect to use of such systems in energy storage devices.²²

5. Experimental

All starting materials and solvents were purchased from Sigma-Aldrich and used without purification unless otherwise noted. ¹H NMR spectra were collected using a Gemini-200 MHz spectrometer. UV–vis spectra were collected using a Perkin-Elmer Lambda 35 UV–vis spectrometer. Fluorescence spectra were acquired using a Shimadzu RF-5301 PC fluorescence spectrophotometer. A gas chromatography mass spectrometer with an HP 5890 mass selective detector was used to acquire GC–MS data. MALDI–MS data were collected using an Omnix MALDI–TOF mass spectrometer. FAB–MS data were collected in collaboration with the Michigan State Mass Spectrometry Facility. HPLC was performed using a Milton-Roy 4000 obtained courtesy

of Prof. Ira Krull at Northeastern University. The HPLC column was a Buckyclutcher 1, using 15 μ L injections. Fluorescence lifetime data was collected using a Pico-Quant Fluo-Time 100 time-resolved spectrophotometer. Pico-second laser flash photolysis experiments were carried out with 532 nm laser pulses from a mode-locked, Q-switched Quantel YG-501 DP Nd:YAG laser system (18 ps pulse width, 2–3 mJ/pulse). Nanosecond Laser Flash Photolysis experiments were performed with laser pulses from a Quanta-Ray CDR Nd:YAG system (532 nm, 6 ns pulse width) in a front face excitation geometry.

5.1. Modified synthesis of 3,5-di-*tert*-butylbenzaldehyde

A solution of 3,5-di-*tert*-butyltoluene (21.84 g, 107 mmol) and *N*-bromosuccinimide (26.66 g, 150 mmol) in benzene (55 mL) was heated at reflux under visible light irradiation. The reaction was then cooled, filtered, the benzene was removed under reduced pressure and the residue was added to a solution of hexamethylenetetramine (45.00 g, 321 mmol) in a 1:1 H₂O/EtOH mixture (64 mL). The solution was heated at reflux for 4 h, concd HCl was added (21 mL) and heating at reflux was continued for 30 min. The ethanol was removed under reduced pressure, and the remaining aqueous layer was extracted with ether. The ether layer was dried (MgSO₄) and the solvent was removed under reduced pressure. Recrystallization from EtOH yielded the desired product as white crystals (66%).

5.1.1. 3,5-Di-*tert*-butylphenyl dipyrromethane 7.

A solution of the above aldehyde (3.581 g, 16.4 mmol) and freshly distilled pyrrole (28.4 mL, 409 mmol) was stirred under Ar at room temperature. Trifluoroacetic acid (0.13 mL, 16.4 mmol) was added dropwise, and the solution was stirred an additional 30 min. An excess of triethylamine (0.3 mL) was added to quench the reaction, and the pyrrole was removed under reduced pressure. The crude product was dissolved in CH₂Cl₂ and extracted with 0.1 M aqueous NaOH and water, dried (Na₂SO₄) and the solvent was removed under reduced pressure. Flash chromatography yielded the dipyrromethane derivative as a sticky light brown solid (51%) (SiO₂, 85:14:1 Cyclohexane/EtOAc/Et₃N, *R*_f=0.5). The material was characterized by its 200 MHz ¹H NMR spectrum, 50 MHz ¹³C NMR spectrum and GC/MS analysis.²³

5.1.2. 5-(4'-Carboxymethylphenyl)-10,15,20-tris-(3,5-di-*tert*-butyl-phenyl)porphyrin 6. A solution of dipyrromethane **6** (3.00 g, 9.0 mmol), 3,5-di-*tert*-butylbenzaldehyde (0.979 g, 4.5 mmol), and 4-carboxymethyl benzaldehyde (0.736 g, 4.5 mmol) in dry CH₂Cl₂ (900 mL) was stirred at room temperature under Ar. Trifluoroacetic acid (0.69 mL, 16 mmol) was added dropwise and the mixture was stirred an additional 1 h. Excess 2,3-dichloro-5,6-dicyano-1,4-benzoquinone (DDQ) (3 g) was added and the solution was stirred open to the air for an additional 2 h. The solvent was removed under reduced pressure and the product was purified via flash chromatography (17%) (6:4 Hexanes/EtOAc, *R*_f=0.5). The porphyrin ester **8** was characterized by ¹H NMR and MALDI-MS analysis.²³

A solution of **8** (250 mg) in isopropanol was heated at reflux. A solution of KOH (1.4 g) in water (12.5 mL)

was added dropwise, and the solution was heated at reflux for 6 h. The solvent was removed under reduced pressure, the residue was dissolved in CH₂Cl₂ and then extracted sequentially with 1 M HCl and water. After drying over Na₂SO₄, the solvent was removed under reduced pressure, and the final porphyrin carboxylic acid **6** was purified via flash chromatography (yield 94%) (SiO₂, 1:9 MeOH/CH₂Cl₂, *R*_f=0.5). The material was characterized by ¹H NMR and MALDI-MS analysis.²³

5.1.3. Glycol-C₆₀ adducts 3a and 3b. General procedure: bromobenzene was added to an Ar-purged flask containing fullerene carboxylic acid **1** (1 equiv), DMAP (0.2 equiv), 1-hydroxybenzotriazole hydrate (1.1 equiv) and dicyclohexylcarbodiimide (DCC) (10 equiv). The appropriate diol (10 equiv) was added in DMSO, and the reaction was held at 50 °C with stirring for 18 h. Bromobenzene was removed under reduced pressure and the crude product was dissolved in CH₂Cl₂ and extracted sequentially with water, 10% aqueous CaSO₄ and brine. The final solution was dried (Na₂SO₄) and the solvent was removed under reduced pressure. The residue was purified by flash chromatography (SiO₂, 10% EtOAc/PhMe) to give **3a** (61%) and **3b** (64%), respectively.

5.1.4. Synthesis of dyads 9a and 9b. General procedure for EDC/DMAP coupling: to a solution of porphyrin acid **6** (1.01 equiv), EDC (1.01 equiv) and DMAP (1.01 equiv) in the minimum amount of dry CH₂Cl₂, a solution of C₆₀ carboxylic acid derivative **3a** or **3b** (1 equiv) in CH₂Cl₂ was added at room temperature. The mixture was stirred for 18 h, diluted with CH₂Cl₂ (20 mL), washed with a solution of saturated aqueous NH₄Cl (3×20 mL) and brine (2×20 mL), dried (Na₂SO₄) and finally evaporated to give the crude dyad, which was purified via flash chromatography to give the pure material. Dyad **9a**: 51% (10% EtOAc/PhMe, *R*_f=0.25); Dyad **9b**: 47% (10% EtOAc/PhMe, *R*_f=0.2). The final products were characterized by ¹H NMR and MALDI-MS analysis.²³

5.2. Singlet molecular oxygen emission measurements

These experiments were done following the procedure described in a previous paper in this series.¹³

Acknowledgements

D.I.S. and S.M. are grateful to the US National Science Foundation for support of their work at NYU, under grant CHE-009789. L.E. also gratefully acknowledges NSF support for the work at Clemson.

References and notes

- (a) Imahori, H.; Sakata, Y. *Adv. Mater.* **1997**, *9*, 537. (b) Prato, M. *J. Mater. Chem.* **1997**, *7*, 1097. (c) Martin, N.; Sánchez, L.; Illescas, B.; Pérez, I. *Chem. Rev.* **1998**, *98*, 2527. (d) Imahori, H.; Sakata, Y. *Eur. J. Org. Chem.* **1999**, 2445. (e) Diederich, F.; Gómez-López, M. *Chem. Soc. Rev.* **1999**, *28*, 263. (f) Guldi, D. M. *Chem. Commun.* **2000**, 321. (g) Reed, C. A.; Bolskar, R. D. *Chem. Rev.* **2000**, *100*, 1075. (h) Gust, D.;

- Moore, T. A.; Moore, A. L. *J. Photochem. Photobiol., B* **2000**, *58*, 63. (i) Gust, D.; Moore, T. A.; Moore, A. L. *Acc. Chem. Res.* **2001**, *34*, 40. (j) Guldi, D. M.; Martin, N. *J. Mater. Chem.* **2002**, *12*, 1978–1992. (k) Guldi, D. M. *Chem. Soc. Rev.* **2002**, *31*, 22. (l) Imahori, H.; Mori, Y.; Matano, Y. *J. Photochem. Photobiol., C* **2003**, *4*, 51. (m) Nierengarten, J. F. *Top. Curr. Chem.* **2003**, *228*, 87. (n) Guldi, D. M. *Pure Appl. Chem.* **2003**, *75*, 1069. (o) El-Khouly, M. E.; Ito, O.; D'Souza, F. *J. Photochem. Photobiol., C* **2004**, *5*, 79. (p) Guldi, D. M.; Prato, M. *Chem. Commun.* **2004**, 2517.
2. Xie, Q.; Perez-Cordero, E.; Echegoyen, L. *J. Am. Chem. Soc.* **1992**, *114*, 3978.
3. Imahori, H.; Hagiwara, K.; Akiyama, T.; Aoki, M.; Taniguchi, S.; Okada, T.; Shirakawa, M.; Sakata, Y. *Chem. Phys. Lett.* **1996**, *263*, 545.
4. (a) Guldi, D. M.; Luo, C.; Prato, M.; Dietel, E.; Hirsch, A. *Chem. Commun.* **2000**, 373. (b) Imahori, H.; Tamaki, K.; Guldi, D. M.; Luo, C.; Fujitsuka, M.; Fukuzumi, S. *J. Am. Chem. Soc.* **2001**, *123*, 2607. (c) Imahori, H.; Yamada, H.; Guldi, D. M.; Endo, Y.; Shimomura, A.; Kundu, S.; Yamada, K.; Okada, T.; Sakata, Y.; Fukuzumi, S. *Angew. Chem., Int. Ed.* **2002**, *41*, 2344. (d) Ohkubo, K.; Imahori, H.; Shao, J. G.; Ou, Z. P.; Kadish, K. M.; Chen, Y. H.; Zheng, G.; Pandey, R. K.; Fujitsuka, M.; Ito, O.; Fukuzumi, S. *J. Phys. Chem. A* **2002**, *106*, 10991. (e) Fukuzumi, S.; Ohkubo, K.; Imahori, H.; Guldi, D. M. *Chem. Eur. J.* **2003**, *9*, 1585.
5. (a) Lindsey, J. S.; Schreiman, I. C.; Hsu, H. C.; Kearney, P. C.; Marguerettaz, A. M. *J. Org. Chem.* **1987**, *52*, 827. (b) Lee, C. H.; Lindsey, J. S. *Tetrahedron* **1994**, *50*, 11427. (c) Littler, B. J.; Ciringh, Y.; Lindsey, J. S. *J. Org. Chem.* **1999**, *64*, 2864. (d) Smith, K. M. *J. Porphyrins Phthalocyanines* **2000**, *4*, 319.
6. Boyd, P. D. W.; Hodgson, M. C.; Rickard, C. E. F.; Oliver, A. G.; Brothers, P. J.; Chaker, L.; Bolskar, R. D.; Tham, F. S.; Reed, C. A. *J. Am. Chem. Soc.* **1999**, *121*, 10487.
7. Imahori, H.; Guldi, D. M.; Tamaki, K.; Yoshida, Y.; Luo, C.; Sakata, Y.; Fukuzumi, S. *J. Am. Chem. Soc.* **2001**, *123*, 6617.
8. Baran, P. S.; Monaco, R. R.; Khan, A. U.; Schuster, D. I.; Wilson, S. R. *J. Am. Chem. Soc.* **1997**, *119*, 8363. Schuster, D. I. *Carbon* **2000**, *38*, 1607.
9. Nierengarten, J.-F.; Herrmann, A.; Tykwinski, R. R.; Ruttimann, M.; Diederich, F.; Boudon, C.; Gisselbrecht, J. P.; Gross, M. *Helv. Chim. Acta* **1997**, *80*, 293.
10. (a) MacMahon, S.; Wilson, S. R.; Schuster, D. I. *Proc. Electrochem. Soc.* **2000**, *8*, 155. (b) MacMahon, S.; Fong, R.; Baran, P. S.; Safonov, I.; Wilson, S. R.; Schuster, D. I. *J. Org. Chem.* **2001**, *66*, 5449.
11. Schuster, D. I.; Jarowski, P. D.; Kirschner, A. N.; Wilson, S. R. *J. Mater. Chem.* **2002**, *12*, 2041.
12. Bourgeois, J.-P.; Diederich, F.; Echegoyen, L.; Nierengarten, J.-F. *Helv. Chim. Acta* **1998**, *81*, 1835.
13. Schuster, D. I.; Cheng, P.; Jarowski, P. D.; Guldi, D. M.; Luo, C.; Echegoyen, L.; Pyo, S.; Holzwarth, A. R.; Braslavsky, S. E.; Williams, R. M.; Klihm, G. *J. Am. Chem. Soc.* **2004**, *126*, 7257.
14. Ogilby, P. R.; Foote, C. S. *J. Am. Chem. Soc.* **1982**, *104*, 2069.
15. Arbogast, J. W.; Darmanyan, A. P.; Foote, C. S.; Rubin, Y.; Diederich, F. N.; Alvarez, M. M.; Anz, S. J.; Whetten, R. L. *J. Phys. Chem.* **1991**, *95*, 11. Bensasson, R. V.; Bienvenue, E.; Dellinger, M.; Leach, S.; Seta, P. *J. Phys. Chem.* **1994**, *98*, 3492.
16. For a review, see: Bracher, P. J.; Schuster, D. I. In *Fullerenes: From Synthesis to Optoelectronic Properties*; Guldi, D. M., Martin, N., Eds.; Kluwer Academic: Dordrecht, 2002; pp 163–212.
17. Kuciauskas, D.; Lin, S.; Seely, G. R.; Moore, A. L.; Moore, T. A.; Gust, D.; Drovetskaya, T.; Reed, C. A.; Boyd, P. D. W. *J. Phys. Chem.* **1996**, *100*, 15926–15932.
18. Galili, T.; Regev, A.; Levanon, H.; Schuster, D. I.; Guldi, D. M. *J. Phys. Chem. A* **2004**, *108*, 10632–10639.
19. Armaroli, N.; Accorsi, G.; Felder, D.; Nierengarten, J.-F. *Chem. Eur. J.* **2002**, *8*, 2314–2323.
20. Guldi, D. M.; Prato, M. *Acc. Chem. Res.* **2000**, *33*, 695.
21. (a) Guldi, D. M.; Luo, C.; Da Ros, T.; Prato, M.; Dietel, E.; Hirsch, A. *Chem. Commun.* **2000**, 375. (b) Luo, C.; Guldi, D. M.; Imahori, H.; Tamaki, K.; Sakata, Y. *J. Am. Chem. Soc.* **2000**, *122*, 6535. (c) Guldi, D. M.; Luo, C.; Prato, M.; Dietel, E.; Hirsch, A. *Chem. Commun.* **2000**, 373. (d) Imahori, H.; Tamaki, K.; Guldi, D. M.; Luo, C.; Fujitsuka, M.; Ito, O.; Sakata, Y.; Fukuzumi, S. *J. Am. Chem. Soc.* **2001**, *123*, 2607. (e) Imahori, H.; Guldi, D. M.; Tamaki, K.; Yoshida, Y.; Luo, C.; Sakata, Y.; Fukuzumi, S. *J. Am. Chem. Soc.* **2001**, *123*, 6617. (f) Imahori, H.; Yamada, H.; Guldi, D. M.; Endo, Y.; Shimomura, A.; Kundu, S.; Yamada, K.; Okada, T.; Sakata, Y.; Fukuzumi, S. *Angew. Chem., Int. Ed.* **2002**, *41*, 2344. (g) Guldi, D. M.; Scheloske, M.; Dietel, E.; Hirsch, A.; Troisi, A.; Zerbetto, F.; Prato, M. *Chem. Eur. J.* **2003**, *9*, 4968. (h) Balbinot, D.; Atalick, S.; Guldi, D. M.; Hatzimarinaki, M.; Hirsch, A.; Jux, N. *J. Phys. Chem.* **2003**, *107*, 13273.
22. Guldi, D. M. *Chem. Soc. Rev.* **2002**, *31*, 22.
23. For details, see: MacMahon, S. Ph.D. Dissertation, New York University, 2004.
24. Armaroli, N.; Marconk, G.; Echegoyen, L.; Bourgeois, J.-P.; Diederich, F. *Chem. Eur. J.* **2000**, *6*, 1629–1645.

Supramolecular nanostructured assemblies of different types of porphyrins with fullerene using TiO₂ nanoparticles for light energy conversion

Taku Hasobe,^{a,b,†} Shigeki Hattori,^a Prashant V. Kamat^{b,*} and Shunichi Fukuzumi^{a,*}

^aDepartment of Material and Life Science, Graduate School of Engineering, Osaka University, SORST, Japan Science and Technology Agency, Suita, Osaka 565-0871, Japan

^bRadiation Laboratory and Department of Chemical and Biomolecular Engineering, University of Notre Dame, Notre Dame, Indiana 46556, USA

Received 10 May 2005; revised 27 May 2005; accepted 30 May 2005

Available online 13 December 2005

Abstract—TiO₂ nanoparticles were modified with porphyrin derivatives, 5-[4-benzoic acid]-10,15,20-tris[3,5-di-*tert*-butylphenyl]-21*H*,23*H*-porphyrin (**Ar-H₂P-COOH**), 5-[4-benzoic acid]-10,20-tris[3,5-di-*tert*-butylphenyl]-21*H*,23*H*-porphyrin (**H-H₂P-COOH**), and 5,10,15,20-tetra[4-benzoic acid]-21*H*,23*H*-porphyrin (**H₂P-4COOH**). The porphyrin-modified TiO₂ nanoparticles were deposited on nanostructured OTE/SnO₂ electrode together with nanoclusters of fullerene (C₆₀) in acetonitrile–toluene (3/1, v/v) using an electrophoretic deposition technique to afford the porphyrin-modified TiO₂ composite electrode denoted as OTE/SnO₂/(porphyrin-modified TiO₂ nanoparticle + C₆₀)_n. The porphyrin-modified TiO₂ composite electrodes have efficient light absorbing properties in the visible region, exhibiting the photoactive response under visible light excitation using I₃⁻/I⁻ redox couple. The incident photon-to-photocurrent efficiency (IPCE) values of supramolecular nanostructured electrodes of porphyrin-modified TiO₂ nanoparticles with fullerene [OTE/SnO₂/(**Ar-H₂P-COO-TiO₂ + C₆₀)_n, OTE/SnO₂/(**H-H₂P-COO-TiO₂ + C₆₀)_n, and OTE/SnO₂/(**H₂P-4COO-TiO₂ + C₆₀)_n] are much larger than those of the reference systems of porphyrin-modified TiO₂ nanoparticles without C₆₀ [OTE/SnO₂/(**Ar-H₂P-COO-TiO₂)_n, OTE/SnO₂/(**H-H₂P-COO-TiO₂)_n, and OTE/SnO₂/(**H₂P-4COO-TiO₂)_n]. In particular, the maximum IPCE value (41%) is obtained for OTE/SnO₂/(**H-H₂P-COO-TiO₂ + C₆₀)_n under the bias potential of 0.2 V versus SCE. This indicates that the formation of supramolecular complexes between porphyrins and fullerene on TiO₂ nanoparticles plays an important role in improvement of the light energy conversion properties.**************

© 2005 Elsevier Ltd. All rights reserved.

1. Introduction

Increasing attention towards solar energy conversion has resulted in the development of efficient solar cells.^{1–6} The construction of such efficient photovoltaic devices requires an enhanced light-harvesting efficiency of chromophore molecules throughout the solar spectrum together with a highly efficient conversion of the harvested light into electrical energy.^{1–6}

Porphyrinoid chromophores have been involved in a number of important biological electron transfer systems including the primary photochemical reactions of chlorophylls in the photosynthetic reaction centers.⁷ Rich and

extensive absorption features of porphyrinoid systems result in increased absorption cross-sections and an efficient use of the solar spectrum.^{8–10} In purple photosynthetic bacteria, visible light is harvested efficiently by the antenna complexes composed of a wheel-like array of chlorophylls.¹¹ Since porphyrins contain an extensively conjugated two-dimensional π -system, they are suitable not only for synthetic light-harvesting systems, but also for efficient electron transfer, because the uptake or release of electrons results in minimal structural and solvation change upon electron transfer.¹² In contrast with the two-dimensional porphyrin π -system, fullerenes contain an extensively conjugated three-dimensional π system.^{13–15} Buckminsterfullerene (C₆₀), for example, is described as having a closed-shell configuration consisting of 30 bonding molecular orbitals with 60 π -electrons,^{13–15} which is also suitable for the efficient electron transfer reduction because of the minimal changes of structure and solvation associated with the electron transfer.¹⁶ Judging from the excellent light-harvesting properties of porphyrins and the efficient electron transfer properties of both porphyrins and fullerenes, combination of porphyrins and fullerenes seems to

Keywords: Porphyrin; Fullerene; TiO₂ nanoparticle; Light energy conversion.

* Corresponding authors. Tel.: +81 6 6879 7368; fax: +81 6 6879 7370 (S. F.); tel.: +1 574 631 5411; fax: +1 574 631 8068 (P. V. K.); e-mail addresses: pkamat@nd.edu; fukuzumi@ap.chem.eng.osaka-u.ac.jp

† Present address: School of Materials Science, Japan Advanced Institute of Science and Technology, Ishikawa 932–1292, Japan

be ideal for fulfilling an enhanced light-harvesting efficiency of chromophores throughout the solar spectrum and a highly efficient conversion of the harvested light into the photocurrent generation. In addition, porphyrins are known to form supramolecular complexes with C_{60} , which contain closest contacts between one of the electron-rich 6:6 bonds of the guest fullerene and the geometric center of the host porphyrins.^{17–20} The strong interaction between porphyrins and fullerenes is likely to be a good driving force for the formation of supramolecular complexes between porphyrins and C_{60} .²¹ Self-assembled monolayers (SAMs) of fullerenes and porphyrins have thereby merited special attention as artificial photosynthetic materials and photonic molecular devices.^{22–24} However, such monolayer assemblies possess poor light-harvesting capability, exhibiting only low values of the incident photon-to-photocurrent efficiency (IPCE). In addition, the synthetic difficulty has precluded practical application of such artificial photosynthetic model compounds to develop low-cost photovoltaic devices.

In order to overcome these problems, we have previously reported a simple and new approach to prepare composite clusters of porphyrins and fullerene in a mixture of polar and nonpolar solvents, which are assembled as multilayers on a nanostructured SnO_2 electrode using an electrophoretic deposition technique.²⁵ The photoelectrochemical properties of the composite systems of porphyrins and fullerene are superior to those of the single component system.^{25a}

In particular, multi-porphyrin arrays such as porphyrin dendrimers and porphyrin-modified gold nanoclusters with fullerenes exhibit much improved photoelectrochemical properties as compared with the composite clusters of monomeric porphyrin and fullerene.²⁶

On the other hand, assembly of dye-modified TiO_2 nanoparticles on electrodes using the electrophoretic deposition technique has also been reported to be useful for preparation of organic thin films to obtain good electron acceptor materials.^{3c,d,27,28} The electrophoretic deposition of dye-modified TiO_2 nanoparticles on electrodes is an attractive method for preparation of organic multilayer films. However, assembly of porphyrin-modified TiO_2 nanoparticles on electrodes using the electrophoretic deposition technique has yet to be applied to construct the supramolecular electrodes with C_{60} .

We report herein, a new type of organic solar cells based on composite nanoclusters of porphyrin-modified TiO_2 nanoparticles and fullerene and the photoelectrochemical properties, which are different depending on the type of porphyrins shown in Figure 1: 5-[4-benzoic acid]-10,15,20-tris[3,5-di-*tert*-butylphenyl]-21*H*,23*H*-porphyrin (**Ar-H₂P-COOH**), 5-[4-benzoic acid]-10,20-di[3,5-di-*tert*-butylphenyl]-21*H*,23*H*-porphyrin (**H-H₂P-COOH**), 5,10,15,20-tetra[4-benzoic acid]-21*H*,23*H*-porphyrin (**H₂P-4COOH**). The porphyrin (**H₂P**) moieties are modified with carboxylic acid group (**Ar-H₂P-COOH**, **H-H₂P-COOH** and

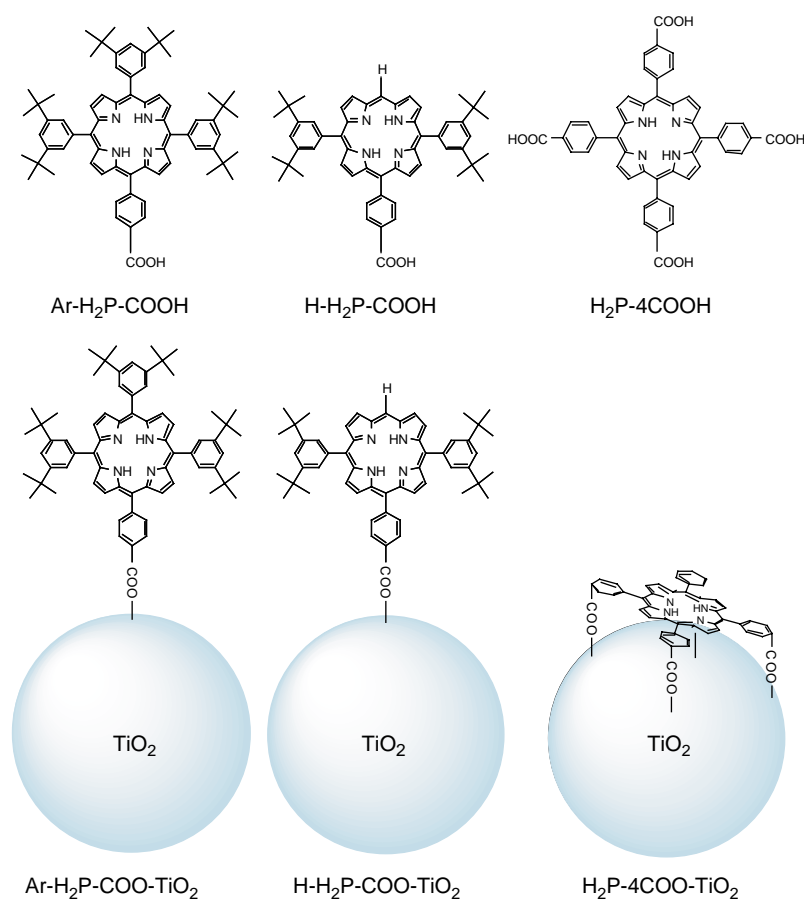
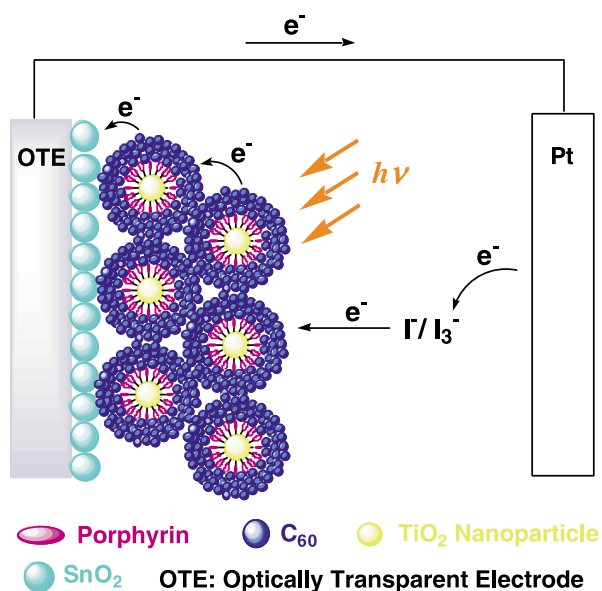


Figure 1. TiO_2 nanoparticles modified with porphyrin dyes and the reference compounds employed in this study.

$\text{H}_2\text{P-4COOH}$ in Fig. 1) in order to be assembled on TiO_2 nanoparticles [denoted as $\text{Ar-H}_2\text{P-COO-TiO}_2$, $\text{H-H}_2\text{P-COO-TiO}_2$, and $\text{H}_2\text{P-4COO-TiO}_2$ in Fig. 1, respectively].

The porphyrin-modified TiO_2 nanoparticles and fullerene nanoclusters are deposited as thin films on optically transparent electrode (OTE) of nanostructured SnO_2 (OTE/ SnO_2) using an electrophoretic method as shown in Scheme 1. We examined the photoelectrochemical properties of composite cluster system using porphyrin-modified TiO_2 nanoparticles ($\text{Ar-H}_2\text{P-COO-TiO}_2$, $\text{H-H}_2\text{P-COO-TiO}_2$, and $\text{H}_2\text{P-4COO-TiO}_2$) and fullerene (C_{60}) on OTE/ SnO_2 electrode [denoted as OTE/ SnO_2 /($\text{Ar-H}_2\text{P-COO-TiO}_2 + \text{C}_{60}$) $_n$, OTE/ SnO_2 /($\text{H-H}_2\text{P-COO-TiO}_2 + \text{C}_{60}$) $_n$, and OTE/ SnO_2 /($\text{H}_2\text{P-4COO-TiO}_2 + \text{C}_{60}$) $_n$, respectively] relative to the reference systems containing porphyrin-modified TiO_2 nanoparticles without C_{60} [OTE/ SnO_2 /($\text{Ar-H}_2\text{P-COO-TiO}_2$) $_n$, OTE/ SnO_2 /($\text{H-H}_2\text{P-COO-TiO}_2$) $_n$, and OTE/ SnO_2 /($\text{H}_2\text{P-4COO-TiO}_2$) $_n$]. The morphology and light energy conversion properties including the mechanism of these composite cluster systems are described in this paper.



Scheme 1.

2. Experimental

2.1. General

Chemicals used in this study are of the best grade available, supplied by Tokyo Chemical Industries, Wako Pure Chemical, or Sigma Aldrich Co. ^1H NMR spectra were recorded on a JNM-AL300 (JEOL) instrument at 300 MHz. Matrix-assisted laser desorption/ionization (MALDI) time-of-flight (TOF) mass spectra were measured on a Kratos Compact MALDI I (Shimadzu). TiO_2 nanoparticles (P25, $d=21$ nm) were purchased from Nippon Aerogel Co. $\text{H}_2\text{P-4COOH}$ was purchased from Sigma Aldrich Co. Preparation of $\text{Ar-H}_2\text{P-COOH}$ and $\text{H-H}_2\text{P-COOH}$ have been described elsewhere.^{29,30}

2.2. Preparation of TiO_2 nanoparticles modified with porphyrin moieties

TiO_2 nanoparticles modified with porphyrin moieties ($\text{Ar-H}_2\text{P-COO-TiO}_2$, $\text{H-H}_2\text{P-COO-TiO}_2$, and $\text{H}_2\text{P-4COO-TiO}_2$) were prepared by mixing TiO_2 nanoparticles (80–100 °C) and 3.0×10^{-4} mol dm $^{-3}$ of $\text{Ar-H}_2\text{P-COOH}$, $\text{H-H}_2\text{P-COOH}$, and $\text{H}_2\text{P-4COOH}$ in acetonitrile (10 ml) for 12h. After adsorbing $\text{Ar-H}_2\text{P-COOH}$, $\text{H-H}_2\text{P-COOH}$, and $\text{H}_2\text{P-4COOH}$, TiO_2 nanoparticles were filtered, and the subsequent washing with acetonitrile and dried to obtain samples of $\text{Ar-H}_2\text{P-COO-TiO}_2$, $\text{H-H}_2\text{P-COO-TiO}_2$, and $\text{H}_2\text{P-4COO-TiO}_2$, respectively. The dye molecules were completely desorbed from TiO_2 nanoparticles into solution by immersing the dye-modified TiO_2 nanoparticles in methanol overnight. The amounts of $\text{Ar-H}_2\text{P-COOH}$, $\text{H-H}_2\text{P-COOH}$, and $\text{H}_2\text{P-4COOH}$ adsorbed on TiO_2 nanoparticles relative to the total weight were determined as 2.98×10^{-5} , 2.98×10^{-5} , and 2.97×10^{-5} mol/g, respectively.²⁸ The molecular packing densities of porphyrins on TiO_2 nanoparticles are approximately the same.

2.3. Electrophoretic deposition of composite clusters on electrode

C_{60} is soluble in nonpolar solvents such as toluene. In mixed solvents (acetonitrile/toluene), however, they aggregate to form large size clusters with diameter of 100–300 nm.³¹ The C_{60} cluster and TiO_2 nanoparticles were electrophoretically deposited onto SnO_2 films under an applied potential as reported previously.^{28,31}

Nanostructured SnO_2 films were cast on an optically transparent electrode (OTE) by using a dilute (1–2%) colloidal solution (Alfa Chemicals), followed by annealing of the dried film at 673 K. Details about the electrode preparation and its properties have been described elsewhere.³² These films are highly porous and electrochemically active to conduct charges across the film. The SnO_2 film electrode (OTE/ SnO_2) and an OTE plate were introduced in a 1 cm path length cuvette and were connected to positive and negative terminals of the power supply, respectively. A known amount (~ 2 mL) of C_{60} , porphyrin-modified TiO_2 nanoparticles ($\text{Ar-H}_2\text{P-COO-TiO}_2$, $\text{H-H}_2\text{P-COO-TiO}_2$, and $\text{H}_2\text{P-4COO-TiO}_2$), or the mixed cluster suspension in acetonitrile–toluene (3/1, v/v) immediately after the ultrasonication was transferred to a 1 cm cuvette in which two electrodes (viz. OTE/ SnO_2 and OTE) were kept at a distance of ~ 6 mm using a Teflon spacer. A dc voltage (500 V) was applied between the two electrodes for 2 min using a Fluke 415 power supply. The deposition of the film can be visibly seen as the solution becomes colorless with simultaneous brown coloration of the SnO_2 /OTE electrode. The SnO_2 /OTE electrodes coated with porphyrin-modified TiO_2 nanoparticles ($\text{Ar-H}_2\text{P-COO-TiO}_2$, $\text{H-H}_2\text{P-COO-TiO}_2$, and $\text{H}_2\text{P-4COO-TiO}_2$) and C_{60} clusters are referred to OTE/ SnO_2 /($\text{Ar-H}_2\text{P-COO-TiO}_2 + \text{C}_{60}$) $_n$, OTE/ SnO_2 /($\text{H-H}_2\text{P-COO-TiO}_2 + \text{C}_{60}$) $_n$, and OTE/ SnO_2 /($\text{H}_2\text{P-4COO-TiO}_2 + \text{C}_{60}$) $_n$, respectively.

The UV–visible spectra were recorded on a Shimadzu 3101 spectrophotometer. Images were recorded using a Hitachi

H600 transmission electron microscope. The morphology of the mesoporous electrodes was characterized by a scanning electron micrograph (SEM; JEOL, JSM-6700F).

2.4. Photoelectrochemical measurements

Photoelectrochemical measurements were performed using a standard three-compartment cell consisting of a working electrode and Pt wire gauze counter electrode and saturated calomel reference electrode (SCE). All photoelectrochemical measurements were performed in acetonitrile containing 0.5 mol dm^{-3} NaI and 0.01 mol dm^{-3} I_2 with a Keithley model 617 programmable electrometer. A collimated light beam from a 150 W Xenon lamp with a 400 nm cut-off filter was used for excitation of the composite cluster films cast on SnO_2 electrodes. A Bausch and Lomb high intensity grating monochromator was introduced into the path of the excitation beam for selecting wavelength. A Princeton Applied Research (PAR) model 173 potentiostat and Model 175 universal programmer were used for recording IV characteristics. The IPCE values were calculated by normalizing the photocurrent values for incident light energy and intensity using Eq. 1,²⁵

$$\text{IPCE}(\%) = 100 \times 1240 \times I_{\text{sc}} / (W_{\text{in}} \times \lambda) \quad (1)$$

where I_{sc} is the short circuit photocurrent (A/cm^2), W_{in} is the incident light intensity (W/cm^2), and λ is the wavelength (nm).

3. Results and discussion

3.1. Preparation of the composite cluster films of porphyrin-modified TiO_2 nanoparticles and C_{60}

Porphyrins and C_{60} are soluble in nonpolar solvents such as toluene, but much less soluble in polar solvents such as acetonitrile.^{25,26} By the proper choice of polar to nonpolar solvent, we can achieve a controlled aggregation in the form of the composite nanoclusters. Detailed information of composite nanoclusters of porphyrins and C_{60} has been described elsewhere.^{25,31} Porphyrin-modified TiO_2 nanoparticles and C_{60} were electrophoretically deposited onto the electrode in suspended solution.²⁸ Upon subjecting the resultant cluster suspension to a high electric dc field (500 V for 2 min), mixed porphyrin-modified TiO_2 nanoparticles ($\text{Ar-H}_2\text{P-COO-TiO}_2$, $\text{H-H}_2\text{P-COO-TiO}_2$, and $\text{H}_2\text{P-4COO-TiO}_2$) and fullerene clusters [$(\text{H}_2\text{P-COO-TiO}_2 + \text{C}_{60})_n$] were deposited onto an optically transparent electrode (OTE) of a nanostructured SnO_2 electrode (OTE/SnO_2), to obtain the modified electrode. As the deposition continues we can visually observe decoloration of the solution, accompanied by coloration of the electrode that is connected to positive terminal of the dc power supply. A mixed cluster suspension of porphyrin-modified TiO_2 nanoparticles ($\text{Ar-H}_2\text{P-COO-TiO}_2$, $\text{H-H}_2\text{P-COO-TiO}_2$, and $\text{H}_2\text{P-4COO-TiO}_2$) and C_{60} were prepared in the total concentration range from 0.025 to $0.13 \text{ mmol dm}^{-3}$ (molecular ratio of $\text{H}_2\text{P}:\text{C}_{60}=1:5$) in acetonitrile-toluene (3/1, v/v). In this case, the mixed clusters were first prepared using different amounts of H_2P on TiO_2 nanoparticle and C_{60} to maintain their molar ratio as 1:5. The absorption spectrum of $\text{OTE/SnO}_2/(\text{H}_2\text{P-4COO-TiO}_2 + \text{C}_{60})_n$ shows

that incident light is absorbed strongly in the visible and near-infrared regions (spectrum a in Fig. 2). A broad absorption is observed in $\text{OTE/SnO}_2/(\text{H}_2\text{P-4COO-TiO}_2 + \text{C}_{60})_n$ in the visible region as compared with the reference system without C_{60} [$\text{OTE/SnO}_2/(\text{H}_2\text{P-4COO-TiO}_2)_n$]. Such a broad absorption property of $\text{OTE/SnO}_2/(\text{H}_2\text{P-COO-TiO}_2 + \text{C}_{60})_n$ may be ascribed to charge-transfer (CT) absorption between porphyrins and C_{60} .^{25,26,33} Absorption properties of $\text{OTE/SnO}_2/(\text{Ar-H}_2\text{P-COO-TiO}_2 + \text{C}_{60})_n$ and $\text{OTE/SnO}_2/(\text{H-H}_2\text{P-COO-TiO}_2 + \text{C}_{60})_n$ are similar to that of $\text{OTE/SnO}_2/(\text{H}_2\text{P-4COO-TiO}_2 + \text{C}_{60})_n$.

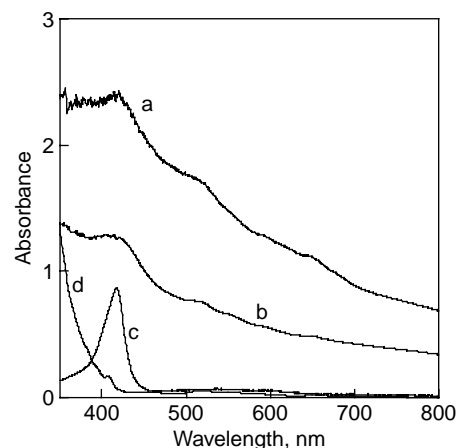


Figure 2. (A) Absorption spectra of (a) $\text{OTE/SnO}_2/(\text{H}_2\text{P-4COO-TiO}_2 + \text{C}_{60})_n$ ($[\text{H}_2\text{P}]=0.025 \text{ mmol dm}^{-3}$, $[\text{C}_{60}]=0.13 \text{ mmol dm}^{-3}$); (b) $\text{OTE/SnO}_2/(\text{H}_2\text{P-4COO-TiO}_2)_n$ ($[\text{H}_2\text{P}]=0.025 \text{ mmol dm}^{-3}$); (c) $\text{H}_2\text{P-4COOH}$ in toluene-*tert*-butanol (v/v, 1/1) ($10 \mu\text{mol dm}^{-3}$) and (d) C_{60} in toluene ($15 \mu\text{mol dm}^{-3}$).

3.2. Morphology of $\text{OTE/SnO}_2/(\text{H-H}_2\text{P-COO-TiO}_2 + \text{C}_{60})_n$

Scanning electron micrograph (SEM) was used to examine the morphology of the $\text{OTE/SnO}_2/(\text{H-H}_2\text{P-COO-TiO}_2 + \text{C}_{60})_n$ film (Fig. 3c). The $\text{OTE/SnO}_2/(\text{H-H}_2\text{P-COO-TiO}_2 + \text{C}_{60})_n$ film is composed of closely packed clusters of about 20–200 nm size with a networked structure, which may result from a supramolecular CT interaction between

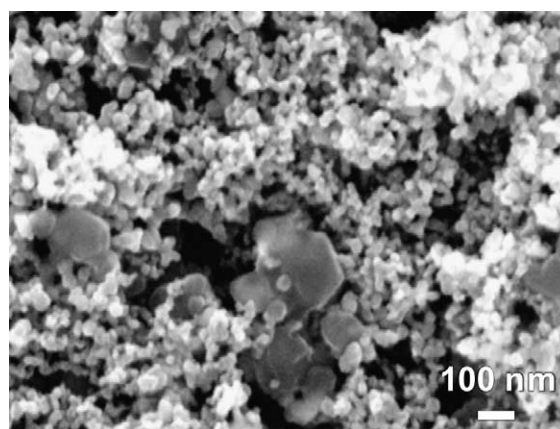


Figure 3. Scanning electron micrograph (SEM) image of $\text{OTE/SnO}_2/(\text{H-H}_2\text{P-COO-TiO}_2 + \text{C}_{60})_n$ ($[\text{H}_2\text{P}]=0.025 \text{ mmol dm}^{-3}$, $[\text{C}_{60}]=0.13 \text{ mmol dm}^{-3}$).

H_2P and C_{60} on TiO_2 nanoparticles. In contrast with the $\text{OTE}/\text{SnO}_2/(\text{H}-\text{H}_2\text{P}-\text{COO}-\text{TiO}_2 + \text{C}_{60})_n$ film, the $\text{OTE}/\text{SnO}_2/(\text{C}_{60})_n$ film without porphyrin-modified TiO_2 nanoparticles contain a large size (100–300 nm) of nanoclusters as reported previously^{28,31b}. Based on these SEM images we can conclude that TiO_2 nanoparticles play an important role in the cluster formation on the films.

3.3. Photoelectrochemical properties of the composite cluster films of porphyrin-modified TiO_2 nanoparticles and C_{60} on OTE/SnO_2 electrodes

The photoelectrochemical performance was examined using the composite cluster films of porphyrin-modified TiO_2 nanoparticles ($\text{Ar}-\text{H}_2\text{P}-\text{COO}-\text{TiO}_2$, $\text{H}-\text{H}_2\text{P}-\text{COO}-\text{TiO}_2$, and $\text{H}_2\text{P}-4\text{COO}-\text{TiO}_2$) and C_{60} as a photoanode in a photoelectrochemical cell. Photocurrent measurements were performed in acetonitrile containing NaI (0.5 mol dm^{-3}) and I_2 (0.01 mol dm^{-3}) as redox electrolyte and Pt gauge counter electrode. The photovoltage and photocurrent responses recorded following the excitation of $\text{OTE}/\text{SnO}_2/(\text{H}-\text{H}_2\text{P}-\text{COO}-\text{TiO}_2 + \text{C}_{60})_n$ electrode the visible region ($\lambda > 400 \text{ nm}$) are shown in Figure 4A and B, respectively. The photocurrent response is prompt, steady and reproducible during repeated on/off cycles of the visible illumination. The short circuit photocurrent density (I_{sc}) is 0.095 mA/cm^2 , and open circuit voltage (V_{oc}) is 240 mV were reproducibly obtained during these measurements. Blank experiments conducted with OTE/SnO_2 (i.e., by excluding composite clusters ($\text{H}-\text{H}_2\text{P}-\text{COO}-\text{TiO}_2 + \text{C}_{60})_n$) produced no detectable photocurrent under the similar experimental conditions. These experiments confirmed the important role of ($\text{H}-\text{H}_2\text{P}-\text{COO}-\text{TiO}_2 + \text{C}_{60})_n$ assembly toward harvesting light energy and generating photocurrent during the operation of a photoelectrochemical cell.

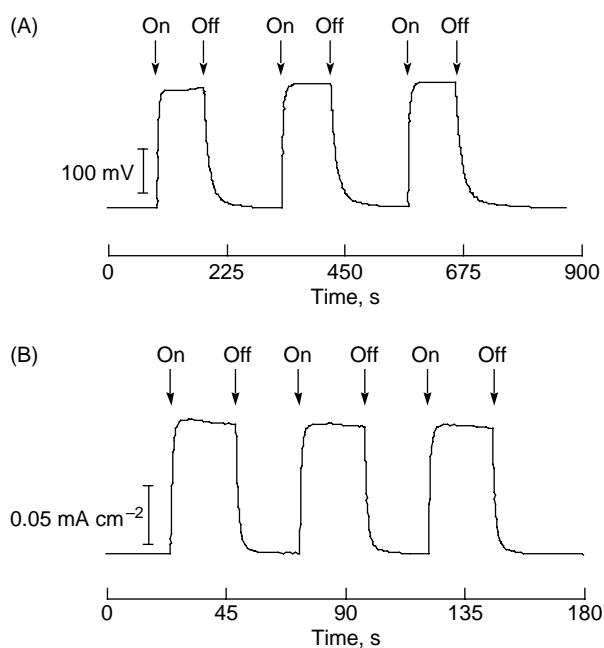


Figure 4. (A) Photovoltage and (B) photocurrent generation at $\text{OTE}/\text{SnO}_2/(\text{H}-\text{H}_2\text{P}-\text{COO}-\text{TiO}_2 + \text{C}_{60})_n$ ($[\text{H}_2\text{P}] = 0.025 \text{ mmol dm}^{-3}$, $[\text{C}_{60}] = 0.13 \text{ mmol dm}^{-3}$) under illumination of white light ($\lambda > 400 \text{ nm}$); electrolyte: 0.5 mol dm^{-3} NaI and 0.01 mol dm^{-3} I_2 in acetonitrile; input power: 6.8 mW cm^{-2} .

The charge separation in the $\text{OTE}/\text{SnO}_2/(\text{H}-\text{H}_2\text{P}-\text{COO}-\text{TiO}_2 + \text{C}_{60})_n$ electrode can be further modulated by the application of an electrochemical bias potential. Figure 5 shows $I-V$ characteristics of the $\text{OTE}/\text{SnO}_2/(\text{H}-\text{H}_2\text{P}-\text{COO}-\text{TiO}_2 + \text{C}_{60})_n$ and $\text{OTE}/\text{SnO}_2/(\text{H}-\text{H}_2\text{P}-\text{COO}-\text{TiO}_2)_n$ electrodes under the visible light illumination. The photocurrent increases as the applied potential is scanned toward more positive potentials. Increased charge separation and the facile transport of charge carriers under a positive bias potential are responsible for enhanced photocurrent generation. The ratio of net photocurrent generation of $\text{OTE}/\text{SnO}_2/(\text{H}-\text{H}_2\text{P}-\text{COO}-\text{TiO}_2 + \text{C}_{60})_n$ at $+0.2 \text{ V}$ versus SCE to that of $\text{OTE}/\text{SnO}_2/(\text{H}-\text{H}_2\text{P}-\text{COO}-\text{TiO}_2 + \text{C}_{60})_n$ at 0 V versus SCE (Fig. 5A) is much larger than the case of $\text{OTE}/\text{SnO}_2/(\text{H}-\text{H}_2\text{P}-\text{COO}-\text{TiO}_2)_n$ (Fig. 5B). This demonstrates that C_{60} works as an electron acceptor in the supramolecular complex to enhance the photocurrent generation. At potentials greater than $+0.4 \text{ V}$ versus SCE, the direct electrochemical oxidation of iodide interferes with the photocurrent measurement.

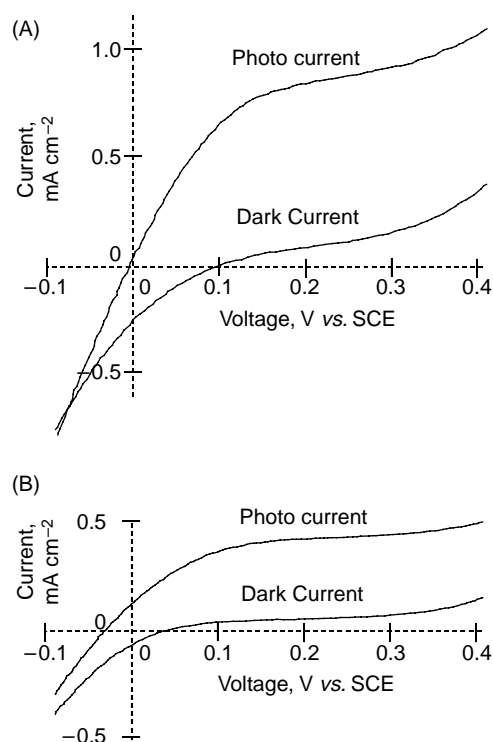


Figure 5. $I-V$ characteristics of (A) $\text{OTE}/\text{SnO}_2/(\text{H}-\text{H}_2\text{P}-\text{COO}-\text{TiO}_2 + \text{C}_{60})_n$ ($[\text{H}_2\text{P}] = 0.025 \text{ mmol dm}^{-3}$, $[\text{C}_{60}] = 0.13 \text{ mmol dm}^{-3}$) and (B) $\text{OTE}/\text{SnO}_2/(\text{H}-\text{H}_2\text{P}-\text{COO}-\text{TiO}_2)_n$ ($[\text{H}_2\text{P}] = 0.025 \text{ mmol dm}^{-3}$) under illumination of white light ($\lambda > 400 \text{ nm}$); electrolyte: 0.5 mol dm^{-3} NaI and 0.01 mol dm^{-3} I_2 in acetonitrile; input power: 27.8 mW cm^{-2} .

A series of photocurrent action spectra were recorded in order to evaluate the photoresponse of the composite clusters towards the photocurrent generation. First, we measured the photocurrent action spectra of $\text{OTE}/\text{SnO}_2/(\text{Ar}-\text{H}_2\text{P}-\text{COO}-\text{TiO}_2)_n$, $\text{OTE}/\text{SnO}_2/(\text{H}-\text{H}_2\text{P}-\text{COO}-\text{TiO}_2)_n$, and $\text{OTE}/\text{SnO}_2/(\text{H}_2\text{P}-4\text{COO}-\text{TiO}_2)_n$ as shown in Figure 6. Photocurrent generation is observed under no applied bias potential using a standard two-compartment cell consisting of a working electrode and Pt wire gauze counter electrode to attain 2–6% of maximum IPCE values (spectra a in Fig. 6A–C, respectively). We also measured

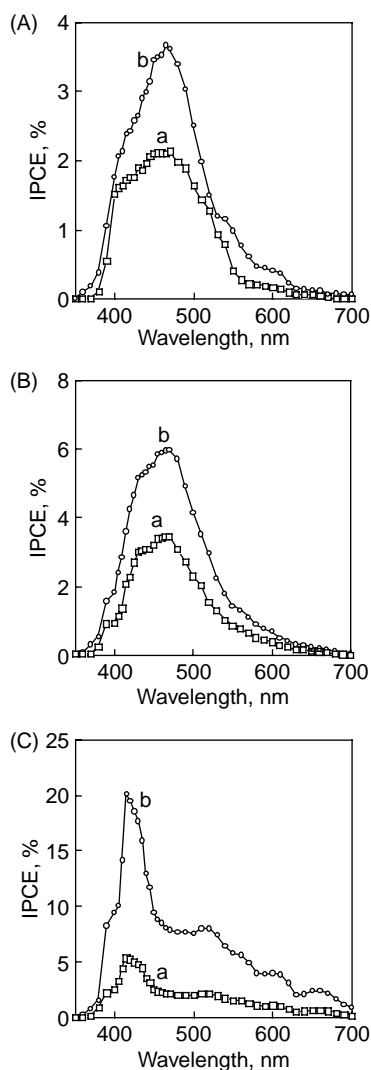


Figure 6. (A) Photocurrent action spectra of OTE/SnO₂/(Ar-H₂P-COO-TiO₂)_n ([H₂P]=0.025 mmol dm⁻³) (a) with no applied bias potential and (b) at an applied bias potential of 0.2 V versus SCE. (B) Photocurrent action spectra of OTE/SnO₂/(H-H₂P-COO-TiO₂)_n ([H₂P]=0.025 mmol dm⁻³) (a) with no applied bias potential and (b) at an applied bias potential of 0.2 V versus SCE. (C) Photocurrent action spectra of OTE/SnO₂/(H₂P-4COO-TiO₂)_n ([H₂P]=0.025 mmol dm⁻³) (a) with no applied bias potential and (b) at an applied bias potential of 0.2 V versus SCE. Electrolyte: 0.5 mol dm⁻³ NaI and 0.01 mol dm⁻³ I₂ in acetonitrile.

the photocurrent action spectra of OTE/SnO₂/(Ar-H₂P-COO-TiO₂)_n, OTE/SnO₂/(H-H₂P-COO-TiO₂)_n, and OTE/SnO₂/(H₂P-4COO-TiO₂)_n under an applied bias potential of 0.2 V versus SCE using a standard three-compartment cell as a working electrode along with Pt wire gauze counter electrode and saturated calomel reference electrode (SCE) (spectra b in Fig. 6A–C, respectively). The maximum IPCE value (~20%) is obtained for OTE/SnO₂/(H₂P-4COO-TiO₂)_n, which is much larger than those of OTE/SnO₂/(Ar-H₂P-COO-TiO₂)_n (~3.5%) and OTE/SnO₂/(H-H₂P-COO-TiO₂)_n (~6%). This demonstrates that the difference in the IPCE values results from different electron injection properties from the excited state of porphyrins to the conduction band of TiO₂ semiconductor nanocrystallites. From the structural point of view between porphyrin moieties and TiO₂ nanoparticles, porphyrin moieties definitely lie on the TiO₂ surface because of

four-point connection in the case of H₂P-4COO-TiO₂, whereas porphyrin moieties may stand on the TiO₂ surface in the cases of OTE/SnO₂/(Ar-H₂P-COO-TiO₂)_n and OTE/SnO₂/(H-H₂P-COO-TiO₂)_n as shown in Figure 1. The close distance between porphyrins and TiO₂ surface in H₂P-4COO-TiO₂ relative to that of Ar-H₂P-COO-TiO₂ or H-H₂P-COO-TiO₂ may result in an efficient electron transfer from the excited state of the porphyrin moiety of H₂P-4COO-TiO₂ to the conduction band of TiO₂ semiconductor nanocrystallites.

We have also measured the photocurrent action spectra of OTE/SnO₂/(Ar-H₂P-COO-TiO₂+C₆₀)_n, OTE/SnO₂/(H-H₂P-COO-TiO₂+C₆₀)_n, and OTE/SnO₂/(H₂P-4COO-TiO₂+C₆₀)_n in order to evaluate the effect of C₆₀ on the IPCE values as shown in Figure 7. IPCE values of these composite cluster systems under an applied bias potential of 0.2 V versus SCE become larger than those under no applied potential, as observed for porphyrin-modified TiO₂ nanoparticle films without C₆₀ (Fig. 6). The IPCE values of composite cluster electrodes (Fig. 7A–C) also become larger than those of the individual systems [OTE/SnO₂/(C₆₀)_n (Fig. 7D) or OTE/SnO₂/(porphyrin-modified TiO₂ nanoparticle)_n (Fig. 6)]. In particular, the maximum IPCE value of OTE/SnO₂/(H-H₂P-COO-TiO₂+C₆₀)_n under the bias of 0.2 V versus SCE (~42%) is much larger than the sum of two individual IPCE values (spectrum c in Fig. 7B: ~12%) of OTE/SnO₂/(H-H₂P-COO-TiO₂)_n (spectrum b in Fig. 6B) and OTE/SnO₂/(C₆₀)_n (spectrum b in Fig. 7D) with the same concentrations of H₂P and C₆₀. This indicates that the interaction between H₂P and C₆₀ contributes significantly to an increase in the IPCE value.

We have further compared the action spectrum of OTE/SnO₂/(H-H₂P-COO-TiO₂+C₆₀)_n with those of OTE/SnO₂/(Ar-H₂P-COO-TiO₂+C₆₀)_n and OTE/SnO₂/(H₂P-4COO-TiO₂+C₆₀)_n. It should be noted that the molecular packing densities of porphyrins on TiO₂ nanoparticles are approximately the same in OTE/SnO₂/(H-H₂P-COO-TiO₂+C₆₀)_n, OTE/SnO₂/(Ar-H₂P-COO-TiO₂+C₆₀)_n, and OTE/SnO₂/(H₂P-4COO-TiO₂+C₆₀)_n (vide supra). In the case of comparison between OTE/SnO₂/(H-H₂P-COO-TiO₂+C₆₀)_n and OTE/SnO₂/(Ar-H₂P-COO-TiO₂+C₆₀)_n under the bias of 0.2 V versus SCE, the IPCE value of OTE/SnO₂/(H-H₂P-COO-TiO₂+C₆₀)_n (spectrum b in Fig. 7B) is much larger than that of OTE/SnO₂/(Ar-H₂P-COO-TiO₂+C₆₀)_n (spectrum b in Fig. 7A). The absence of 3,5-di-*tert*-butylphenyl substituent at the 15-*meso* position of porphyrin ring in H-H₂P-COO-TiO₂ may enhance the interaction with C₆₀, which can be inserted between two porphyrin rings of the porphyrin assembly on TiO₂ nanoparticles (Scheme 2), as compared with Ar-H₂P-COO-TiO₂ in which the *meso* positions are fully substituted. The stronger interaction between the less bulky porphyrins and C₆₀ leads to an increase in the IPCE value. Such a sandwiched structure of C₆₀ inserted between two porphyrin rings in Scheme 2 may be impossible in the case of OTE/SnO₂/(H₂P-4COO-TiO₂+C₆₀)_n because of the four-point connection of the porphyrin ring onto the TiO₂ surface. This may be the reason why the IPCE values of OTE/SnO₂/(H₂P-4COO-TiO₂)_n under an applied bias potential of 0.2 V versus SCE (spectrum b in Fig. 7C) are

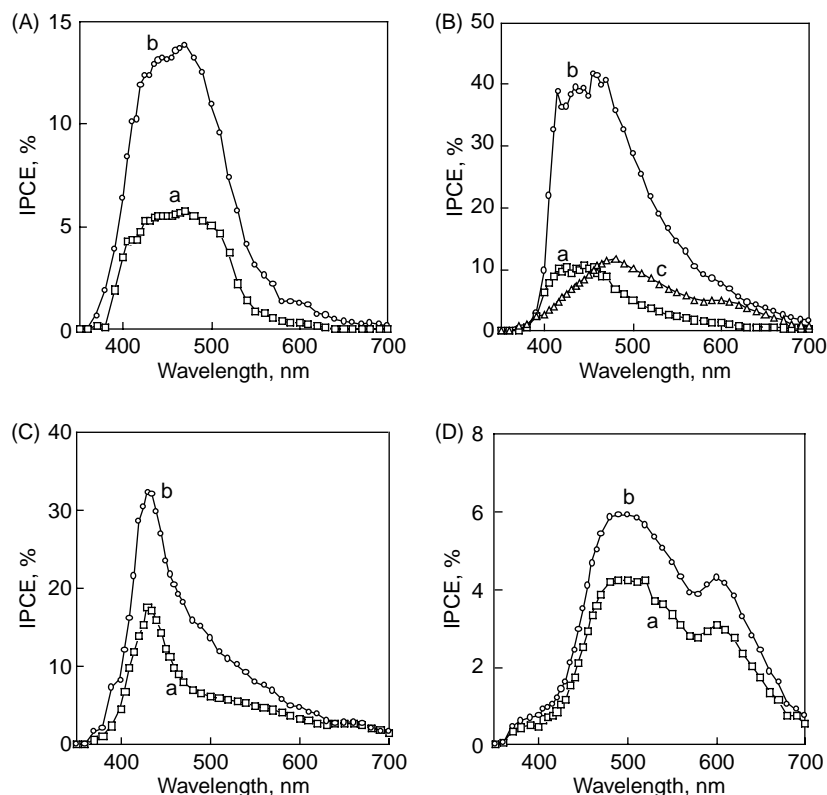


Figure 7. (A) Photocurrent action spectra of OTE/SnO₂/(Ar-H₂P-COO-TiO₂ + C₆₀)_n ([H₂P]=0.025 mmol dm⁻³, [C₆₀]=0.13 mmol dm⁻³) (a) with no applied bias potential and (b) at an applied bias potential of 0.2 V versus SCE. (B) Photocurrent action spectra of OTE/SnO₂/(H-H₂P-COO-TiO₂ + C₆₀)_n ([H₂P]=0.025 mmol dm⁻³, [C₆₀]=0.13 mmol dm⁻³) (a) with no applied bias potential and (b) at an applied bias potential of 0.2 V versus SCE. (c) Sum of two individual IPCE values of OTE/SnO₂/(H-H₂P-COO-TiO₂)_n (spectrum b in Fig. 6B) and OTE/SnO₂/(C₆₀)_n (spectrum b in Fig. 7D) at an applied bias potential of 0.2 V versus SCE. (C) Photocurrent action spectra of OTE/SnO₂/(H₂P-4COO-TiO₂ + C₆₀)_n ([H₂P]=0.025 mmol dm⁻³, [C₆₀]=0.13 mmol dm⁻³) (a) with no applied bias potential and (b) at an applied bias potential of 0.2 V versus SCE. (D) Photocurrent action spectra of OTE/SnO₂/(C₆₀)_n ([C₆₀]=0.13 mmol dm⁻³) (a) with no applied bias potential and (b) at an applied bias potential of 0.2 V versus SCE. Electrolyte: 0.5 mol dm⁻³ NaI and 0.01 mol dm⁻³ I₂ in acetonitrile.

smaller than those of OTE/SnO₂/(H-H₂P-COO-TiO₂)_n (spectrum b in Fig. 7B).³⁴ Based on these results, we can conclude that three-dimensional steric control between

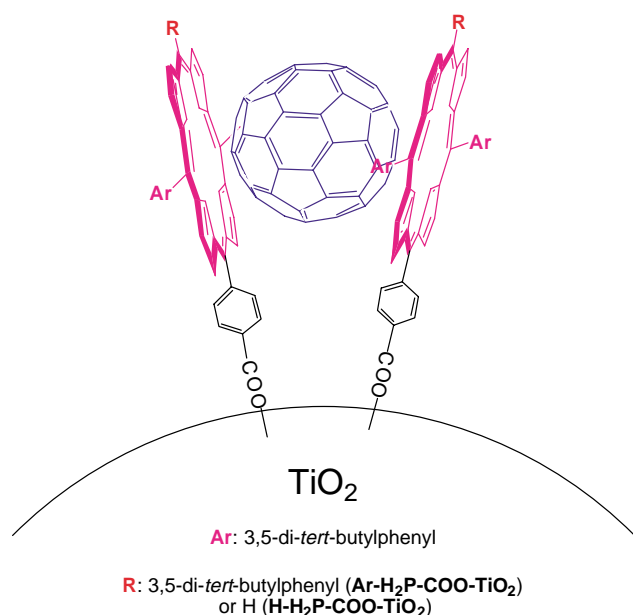
donor and acceptor moieties is a key factor for construction of efficient organic solar devices.

3.4. Power conversion efficiency

The power conversion efficiency (η) of the photoelectrochemical cell was determined by varying the load resistance with use of Eq. 2,^{25a}

$$\eta = ff \times I_{sc} \times V_{oc} / W_{in} \quad (2)$$

where the fill factor (ff) is defined as $ff = P_{max} / (V_{oc} \times I_{sc})$; P_{max} is the maximum power output of the cell, V_{oc} is the open circuit photovoltage, I_{sc} is the short circuit photocurrent. A decrease in the photovoltage accompanied by an increase in the photocurrent is observed with decreasing the load resistance (Fig. 8c). The detailed characteristics of the OTE/SnO₂/(H-H₂P-COO-TiO₂)_n, OTE/SnO₂/(H-H₂P-COO-TiO₂ + C₆₀)_n, and OTE/SnO₂/(H₂P-4COO-TiO₂ + C₆₀)_n electrodes are summarized in Table 1. The I_{sc} and V_{oc} values of OTE/SnO₂/(H-H₂P-COO-TiO₂ + C₆₀)_n are much larger than those of OTE/SnO₂/(H-H₂P-COO-TiO₂)_n, leading to more than four times improvement of the η value (0.11%) as compared with that of OTE/SnO₂/(H-H₂P-COO-TiO₂)_n (0.025%). Furthermore, the η value of organized OTE/SnO₂/(H-H₂P-COO-TiO₂ + C₆₀)_n using TiO₂ nanoparticles is about three times greater than that of non-organized composite cluster system of porphyrin and fullerene without TiO₂ (~0.03%).^{25a,26a,b} The η value



Scheme 2. Illustration of supramolecular assembly between porphyrins and C₆₀ in (Ar-H₂P-COO-TiO₂ + C₆₀)_n and (H-H₂P-COO-TiO₂ + C₆₀)_n.

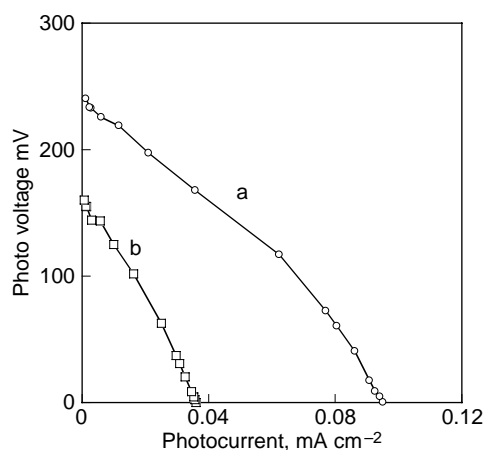


Figure 8. Power characteristics of (a) OTE/SnO₂/(H-H₂P-COO-TiO₂ + C₆₀)_n ([H₂P]=0.025 mol dm⁻³, [C₆₀]=0.13 mol dm⁻³) and (b) OTE/SnO₂/(H-H₂P-COO-TiO₂)_n ([H₂P]=0.025 mol dm⁻³) under white light illumination (λ > 400 nm); electrolyte: 0.5 mol dm⁻³ NaI and 0.01 mol dm⁻³ I₂ in acetonitrile; input power: 6.8 mW cm⁻².

Table 1. Performance characteristics of OTE/SnO₂/(H-H₂P-COO-TiO₂)_n, OTE/SnO₂/(H-H₂P-COO-TiO₂ + C₆₀)_n, and OTE/SnO₂/(H₂P-4COO-TiO₂ + C₆₀)_n

System	V _{oc} (mV)	I _{sc} (mA cm ⁻²)	ff	η ^a
(H-H ₂ P-COO-TiO ₂) _n	160	0.035	0.31	0.025
(H-H ₂ P-COO-TiO ₂ + C ₆₀) _n	240	0.095	0.33	0.11
(H ₂ P-4COO-TiO ₂ + C ₆₀) _n	220	0.11	0.29	0.10

^a Electrolyte: 0.5 mol dm⁻³ NaI and 0.01 mol dm⁻³ I₂ in acetonitrile; white light illumination (λ > 400 nm); input power: 6.8 mW cm⁻².

of OTE/SnO₂/(H₂P-4COO-TiO₂ + C₆₀)_n (0.10%) is about the same as that of OTE/SnO₂/(H-H₂P-COO-TiO₂ + C₆₀)_n (0.11%).

3.5. Photocurrent generation mechanism

The photocurrent generation mechanism in composite cluster systems of porphyrin and fullerene has previously been reported to be initiated by ultrafast electron transfer from the singlet excited state of porphyrin to C₆₀ in the femtosecond time domain.^{25,26} In the case of the reference systems without C₆₀ [OTE/SnO₂/(Ar-H₂P-COO-TiO₂)_n, OTE/SnO₂/(H-H₂P-COO-TiO₂)_n, and OTE/SnO₂/(H₂P-4COO-TiO₂)_n], the photoexcitation of H₂P moiety results in electron injection from the singlet excited state of the dye into the conduction band and/or trap states of TiO₂ nanoparticles to produce the porphyrin radical cation (H₂P^{•+}). The electrons collected on TiO₂ nanoparticles are furthermore injected into SnO₂ nanocrystallites (E_{CB} = 0 V vs NHE)^{25a} to produce the photocurrent in the circuit. The resulting porphyrin radical cation (H₂P^{•+}) produced in the photoinduced electron injection to the conduction band of TiO₂ is reduced by electrolyte (I₃⁻/I⁻ = 0.5 V vs NHE) in the multilayer film.²⁵ At the counter electrode, the electron reduces the oxidized electrolyte (I₃⁻), leading to the photocurrent generation.

In the cases of OTE/SnO₂/(H-H₂P-COO-TiO₂ + C₆₀)_n, OTE/SnO₂/(H-H₂P-COO-TiO₂ + C₆₀)_n, and OTE/SnO₂/(H₂P-4COO-TiO₂ + C₆₀)_n, not only TiO₂ nanoparticles,

but also C₆₀ molecules (C₆₀/C₆₀^{•-} = -0.2 V vs NHE)^{25a} act as an electron acceptor, leading to the enhancement of the photocurrent generation efficiency in composite cluster systems (porphyrin-modified TiO₂ nanoparticle and C₆₀) as compared with the systems without C₆₀. The major pathway contributing to the enhanced photocurrent generation is the intermolecular charge-transfer between excited H₂P and C₆₀ within the supramolecular complex to produce H₂P^{•+} and C₆₀^{•-}. Photoinduced electron transfer from the porphyrin singlet excited state (¹H₂P*) to C₆₀ is thermodynamically feasible as evident from the oxidation potential of ¹H₂P* (¹H₂P*/H₂P^{•+} = -0.7 V vs NHE),²⁵ which is more negative than the reduction potential of C₆₀ (C₆₀/C₆₀^{•-} = -0.2 V vs NHE).^{25a} Such photoinduced electron transfer from the excited porphyrins to C₆₀ has been well established by earlier studies.^{16,26} C₆₀^{•-} is also generated from the interaction between excited C₆₀ (C₆₀^{*}) and iodide ions present in the electrolyte. Collectively, these C₆₀^{•-} species accumulated in clusters transfer electrons to SnO₂ nanocrystallites (E_{CB} = 0 V vs NHE),^{25,31} to produce the current in the circuit. The regeneration of H₂P (H₂P/H₂P^{•+} = 1.2 V vs NHE)²⁵ is achieved by the triiodide/iodide couple (I₃⁻/I⁻ = 0.5 V vs NHE)²⁵ present in the electrolyte system. The ability of C₆₀/C₆₀^{•-} to act as an electron shuttle and mediate the electron transfer process has been demonstrated in earlier studies.³⁵ The improvement of IPCE values under an applied bias potential of 0.2 V versus SCE relative to the corresponding systems under no applied potential results from an increase of driving force of electron transfer from C₆₀^{•-} to SnO₂ nanocrystallites using a standard three-compartment cell.

4. Conclusion

We have successfully constructed supramolecular photo-voltaic cells composed of molecular nanocluster assemblies of porphyrin and fullerene, which are well organized with TiO₂ nanoparticles. The IPCE values of the composite cluster systems of porphyrins and C₆₀ with TiO₂ nanoparticles [OTE/SnO₂/(H-H₂P-COO-TiO₂ + C₆₀)_n, OTE/SnO₂/(H-H₂P-COO-TiO₂ + C₆₀)_n, and OTE/SnO₂/(H₂P-4COO-TiO₂ + C₆₀)_n] are greater than the reference systems [OTE/SnO₂/(H-H₂P-COO-TiO₂)_n, OTE/SnO₂/(H-H₂P-COO-TiO₂)_n, and OTE/SnO₂/(H₂P-4COO-TiO₂)_n]. The largest η value is achieved with the porphyrin-modified TiO₂ nanoparticles and C₆₀ clusters.

Acknowledgements

This work was partially supported by a Grant-in-Aid (No. 16205020) and by a COE program of Osaka University (Integrated Ecochemistry) from the Ministry of Education, Culture, Sports, Science, and Technology, Japan. PVK acknowledges the support from the Office of Basic Energy Science of the US Department of the Energy. TH acknowledges the support of Japan Society for the Promotion of Science Research Fellowship for Young Scientist. This is contribution no. NDRL 4605 from the Notre Dame Radiation Laboratory and from Osaka University. We are

grateful to Dr. Yuji Wada, Osaka University, for helping preparation of TiO₂ nanoparticles modified with dyes.

References and notes

- (a) O'Regan, B.; Grätzel, M. *Nature* **1991**, *353*, 737. (b) Bach, U.; Lupo, D.; Comte, P.; Moser, J. E.; Weissörtel, F.; Salbeck, J.; Spreitzer, H.; Grätzel, M. *Nature* **1998**, *395*, 583. (c) Hagfeldt, A.; Grätzel, M. *Chem. Rev.* **1995**, *95*, 49. (d) Hagfeldt, A.; Grätzel, M. *Acc. Chem. Res.* **2000**, *33*, 269.
- (a) Velusamy, M.; Justin Thomas, K. R.; Lin, J. T.; Hsu, Y.-C.; Ho, K.-C. *Org. Lett.* **2005**, *7*, 1899. (b) Padinger, F.; Rittberger, R. S.; Sariciftci, N. S. *Adv. Funct. Mater.* **2003**, *13*, 85. (c) Schmidt-Mende, L.; Fechtenkötter, A.; Müllen, K.; Moons, E.; Friend, R. H.; MacKenzie, J. D. *Science* **2001**, *293*, 1119.
- (a) Huynh, W. U.; Dittmer, J. J.; Alivisatos, A. P. *Science* **2002**, *295*, 2425. (b) Liu, J.; Tanaka, T.; Sivula, K.; Alivisatos, A. P.; Frechet, J. M. J. *J. Am. Chem. Soc.* **2004**, *126*, 6550. (c) Zhang, D.; Yoshida, T.; Minoura, H. *Chem. Lett.* **2002**, *31*, 874. (d) Zhang, D.; Yoshida, T.; Minoura, H. *Adv. Mater.* **2003**, *15*, 814.
- (a) Bignozzi, C. A.; Argazzi, R.; Kleverlaan, C. J. *Chem. Soc. Rev.* **2000**, *29*, 87. (b) Liu, J.; Kadnikova, E. N.; Liu, Y.; McGehee, M. D.; Frechet, J. M. J. *J. Am. Chem. Soc.* **2004**, *126*, 9486. (c) Smith, A. P.; Smith, R. R.; Taylor, B. E.; Durstock, M. F.; Durstock, M. F. *Chem. Mater.* **2004**, *16*, 4687.
- (a) Yang, F.; Shtein, M.; Forrest, S. R. *Nat. Mater.* **2005**, *4*, 37. (b) Halls, J. J. M.; Walsh, C. A.; Greenham, N. C.; Marseglia, E. A.; Friend, R. H.; Moratti, S. C.; Holmes, A. B. *Nature* **1995**, *376*, 498.
- (a) Wienk, M. M.; Kroon, J. M.; Verhees, W. J. H.; Knol, J.; Hummelen, J. C.; van Hal, P. A.; Janssen, R. A. J. *Angew. Chem., Int. Ed.* **2003**, *42*, 3371. (b) Peumans, P.; Uchida, S.; Forrest, S. R. *Nature* **2003**, *425*, 158. (c) Eckert, J.-F.; Nicoud, J.-F.; Nierengarten, J.-F.; Liu, S.-G.; Echegoyen, L.; Barigelletti, F.; Armaroli, N.; Ouali, L.; Krasnikov, V.; Hadziioannou, G. *J. Am. Chem. Soc.* **2000**, *122*, 7467.
- (a) Barber, J. *Nature* **1988**, *333*, 114. (b) *The Photosynthetic Reaction Center*; Deisenhofer, J., Norris, J. R., Eds.; Academic: San Diego, 1993. (c) *Anoxygenic Photosynthetic Bacteria*; Blankenship, R. E., Madigan, M. T., Bauer, C. E., Eds.; Kluwer Academic: Dordrecht, 1995.
- (a) Gust, D.; Moore, T. A.; Moore, A. L. *Acc. Chem. Res.* **1993**, *26*, 198. (b) Gust, D.; Moore, T. A.; Moore, A. L. *Acc. Chem. Res.* **2001**, *34*, 40. (c) Gust, D.; Moore, T. A. In Kadish, K. M., Smith, K. M., Guillard, R., Eds.; *The Porphyrin Handbook*; Academic: San Diego, CA, 2000; Vol. 8, pp 153–190.
- (a) Wagner, R. W.; Lindsey, J. S. *Pure Appl. Chem.* **1996**, *68*, 1373. (b) Sazanovich, I. V.; Kirmaier, C.; Hindin, E.; Bocian, D. F.; Linsey, J. S.; Holten, D. *J. Am. Chem. Soc.* **2004**, *126*, 2664. (c) *Photoinduced Electron Transfer*; Fox, M. A., Channon, M., Eds.; Elsevier: Amsterdam, 1988.
- (a) Bar-Haim, A.; Klafter, J.; Kopelman, R. *J. Am. Chem. Soc.* **1997**, *119*, 6197. (b) Sadamoto, R.; Tomioka, N.; Aida, T. *J. Am. Chem. Soc.* **1996**, *118*, 3978. (c) Jiang, D.-L.; Aida, T. *J. Am. Chem. Soc.* **1998**, *120*, 10895. (d) Choi, M.-S.; Aida, T.; Yamazaki, T.; Yamazaki, I. *Chem. Eur. J.* **2002**, *8*, 2668. (e) Capitosti, G. J.; Guerrero, C. D.; Binkley, D. E., Jr.; Rajesh, C. S.; Modarelli, D. A. *J. Org. Chem.* **2003**, *68*, 247. (f) Harth, E. M.; Hecht, S.; Helms, B.; Malmstrom, E. E.; Frechet, J. M. J.; Hawker, C. J. *J. Am. Chem. Soc.* **2002**, *124*, 3926.
- (a) McDermott, G.; Prince, S. M.; Freer, A. A.; Hawthornthwaite-Lawless, A. M.; Papiz, M. Z.; Cogdell, R. J.; Isaacs, N. W. *Nature* **1995**, *374*, 517. (b) Koepke, J.; Hu, X.; Muenke, C.; Schulten, K.; Michel, H. *Structure* **1996**, *4*, 581. (c) Pullerits, T.; Sundstrom, V. *Acc. Chem. Res.* **1996**, *29*, 381.
- (a) Fukuzumi, S. In Kadish, K. M., Smith, K. M., Guillard, R., Eds.; *The Porphyrin Handbook*; Academic: San Diego, 2000; Vol. 8, pp 115–152. (b) Fukuzumi, S.; Endo, Y.; Imahori, H. *J. Am. Chem. Soc.* **2002**, *124*, 10974.
- Kroto, H. W.; Heath, J. R.; O'Brien, S. C.; Curl, R. F.; Smalley, R. E. *Nature* **1985**, *318*, 162.
- (a) Haddon, R. C. *Acc. Chem. Res.* **1988**, *21*, 243. (b) Haddon, R. C. *Science* **1993**, *261*, 1545.
- Echegoyen, L.; Echegoyen, L. E. *Acc. Chem. Res.* **1998**, *31*, 593.
- (a) Fukuzumi, S.; Guldi, D. M. In Balzani, V., Ed.; *Electron Transfer in Chemistry*; Wiley-VCH: Weinheim, 2001; Vol. 2, pp 270–337. (b) Fukuzumi, S.; Imahori, H. In Balzani, V., Ed.; *Electron Transfer in Chemistry*; Wiley-VCH: Weinheim, 2001; Vol. 2, pp 927–975.
- (a) Ishii, T.; Aizawa, N.; Yamashita, M.; Matsuzaka, H.; Kodama, T.; Kikuchi, K.; Ikemoto, I.; Iwasa, Y. *J. Chem. Soc., Dalton Trans.* **2000**, 4407. (b) Diederich, F.; Gómez-López, M. *Chem. Soc. Rev.* **1999**, *28*, 263.
- (a) Boyd, P. D. W.; Reed, C. A. *Acc. Chem. Res.* **2005**, *38*, 235. (b) Boyd, P. D. W.; Hodgson, M. C.; Rickard, C. E. F.; Oliver, A. G.; Chaker, L.; Brothers, P. J.; Bolskar, R. D.; Tham, F. S.; Reed, C. A. *J. Am. Chem. Soc.* **1999**, *121*, 10487. (c) Sun, D.; Tham, F. S.; Reed, C. A.; Chaker, L.; Burgess, M.; Boyd, P. D. W. *J. Am. Chem. Soc.* **2000**, *122*, 10704. (d) Sun, D.; Tham, F. S.; Reed, C. A.; Chaker, L.; Boyd, P. D. W. *J. Am. Chem. Soc.* **2002**, *124*, 6604.
- (a) Olmstead, M. M.; Costa, D. A.; Maitra, K.; Noll, B. C.; Phillips, S. L.; Van Calcar, P. M.; Balch, A. L. *J. Am. Chem. Soc.* **1999**, *121*, 7090. (b) Olmstead, M. M.; deBettencourt-Dias, A.; Duchamp, J. C.; Stevenson, S.; Marciu, D.; Dorn, H. C.; Balch, A. L. de Bettencourt-Dias. *Angew. Chem., Int. Ed.* **2001**, *40*, 1223.
- (a) Zheng, J.-Y.; Tashiro, K.; Hirabayashi, Y.; Kinbara, K.; Saigo, K.; Aida, T.; Sakamoto, S.; Yamaguchi, K. *Angew. Chem., Int. Ed.* **2001**, *40*, 1857. (b) Eichhorn, D. M.; Yang, S.; Jarrell, W.; Baumann, T. F.; Beall, L. S.; White, A. J. P.; Williams, D. J.; Barrett, A. G. M.; Hoffman, B. M. *J. Chem. Soc., Chem. Commun.* **1995**, 1703.
- Wang, Y.-B.; Lin, Z. *J. Am. Chem. Soc.* **2003**, *125*, 6072.
- (a) Caldwell, W. B.; Chen, K.; Mirkin, C. A.; Babinec, S. J. *Langmuir* **1993**, *9*, 1945. (b) Shon, Y.-S.; Kelly, K. F.; Halas, N. J.; Lee, T. R. *Langmuir* **1999**, *15*, 5329. (c) Hirayama, D.; Takimiya, K.; Aso, Y.; Otsubo, T.; Hasobe, T.; Yamada, H.; Imahori, H.; Fukuzumi, S.; Sakata, Y. *J. Am. Chem. Soc.* **2002**, *124*, 532.
- (a) Lahav, M.; Gabriel, T.; Shipway, A. N.; Willner, I. *J. Am. Chem. Soc.* **1999**, *121*, 258. (b) Hutchison, J. E.; Postlethwaite, T. A.; Chen, C.-h.; Hathcock, K. W.; Ingram, R. S.; Ou, W.; Linton, R. W.; Murray, R. W.; Tyvoll, T. A.; Chng, L. L.; Collman, J. P. *Langmuir* **1997**, *13*, 2143. (c) Gryko, D. T.; Zhao, F.; Yasserli, A. A.; Roth, K. M.; Bocian, D. F.; Kuhr, W. G.; Lindsey, J. S. *J. Org. Chem.* **2000**, *65*, 7356.

24. (a) Imahori, H.; Norieda, H.; Yamada, H.; Nishimura, Y.; Yamazaki, I.; Sakata, Y.; Fukuzumi, S. *J. Am. Chem. Soc.* **2001**, *123*, 100. (b) Imahori, H.; Hasobe, T.; Yamada, H.; Nishimura, Y.; Yamazaki, I.; Fukuzumi, S. *Langmuir* **2001**, *17*, 4925. (c) Hasobe, T.; Imahori, H.; Ohkubo, K.; Yamada, H.; Sato, T.; Nishimura, Y.; Yamazaki, I.; Fukuzumi, S. *J. Porphyrins Phthalocyanines* **2003**, *7*, 296.
25. (a) Hasobe, T.; Imahori, H.; Fukuzumi, S.; Kamat, P. V. *J. Phys. Chem. B* **2003**, *107*, 12105. (b) Hasobe, T.; Imahori, H.; Fukuzumi, S.; Kamat, P. V. *J. Mater. Chem.* **2003**, *13*, 2515.
26. (a) Hasobe, T.; Imahori, H.; Kamat, P. V.; Fukuzumi, S. *J. Am. Chem. Soc.* **2003**, *125*, 14962. (b) Hasobe, T.; Kashiwagi, Y.; Absalom, M. A.; Sly, J.; Hosomizu, K.; Crossley, M. J.; Imahori, H.; Kamat, P. V.; Fukuzumi, S. *Adv. Mater.* **2004**, *16*, 975. (c) Hasobe, T.; Kamat, P. V.; Troiani, V.; Solladie, N.; Ahn, T. K.; Kim, S. K.; Kim, D.; Kongkanand, A.; Kuwabata, S.; Fukuzumi, S. *J. Phys. Chem. B* **2005**, *109*, 19. (d) Hasobe, T.; Imahori, H.; Kamat, P. V.; Ahn, T. K.; Kim, S. K.; Kim, D.; Fujimoto, A.; Hirakawa, T.; Fukuzumi, S. *J. Am. Chem. Soc.* **2005**, *127*, 1216.
27. (a) Matsumoto, Y.; Noguchi, M.; Matsunaga, T.; Kamada, K.; Koinuma, M.; Yamada, S. *Electrochemistry* **2001**, *69*, 314. (b) Miyasaka, T.; Kijitori, Y.; Murakami, T. N.; Kimura, M.; Uegusa, S. *Chem. Lett.* **2002**, *31*, 1250. (c) Xu, D.; Xu, Y.; Chen, D.; Guo, G.; Gui, L.; Tang, Y. *Adv. Mater.* **2000**, *12*, 520.
28. Hasobe, H.; Hattori, S.; Kamat, P. V.; Wada, Y.; Fukuzumi, S. *J. Mater. Chem.* **2005**, *15*, 372.
29. Hasobe, T.; Imahori, H.; Yamada, H.; Sato, T.; Ohkubo, K.; Fukuzumi, S. *Nano Lett.* **2003**, *3*, 409.
30. Yamada, H.; Imahori, H.; Nishimura, Y.; Yamazaki, I.; Ahn, T. K.; Kim, S. K.; Kim, D.; Fukuzumi, S. *J. Am. Chem. Soc.* **2003**, *125*, 9129.
31. (a) Kamat, P. V.; Barazzouk, S.; Thomas, K. G.; Hotchandani, S. *J. Phys. Chem. B* **2000**, *104*, 4014. (b) Barazzouk, S.; Hotchandani, S.; Kamat, P. V. *Adv. Mater.* **2001**, *13*, 1614.
32. Bedja, I.; Hotchandani, S.; Kamat, P. V. *J. Phys. Chem.* **1994**, *98*, 4133.
33. Tkachenko, N. V.; Lemmetyinen, H.; Sonoda, J.; Ohkubo, K.; Sato, T.; Imahori, H.; Fukuzumi, S. *J. Phys. Chem. A* **2003**, *107*, 8834.
34. The IPCE values in Figure 7C are particularly smaller than those in Figure 7B in the longer wavelength region because of the more unfavorable interaction between $\text{H}_2\text{P-4COO-TiO}_2$ and C_{60} as compared with that between $\text{H-H}_2\text{P-COO-TiO}_2$ and C_{60} .
35. Kamat, P. V.; Haria, M.; Hotchandani, S. *J. Phys. Chem. B* **2004**, *108*, 5166.

Non-covalent immobilization of C₆₀ on gold surfaces by SAMs of porphyrin derivatives

Sheng Zhang and Luis Echegoyen*

Department of Chemistry, Clemson University, Clemson, SC 29634, USA

Received 6 May 2005; revised 25 May 2005; accepted 27 May 2005

Available online 15 November 2005

Abstract—Three porphyrin derivatives, one containing thioctic ester groups (**3**) and the other two with thioether chains (**4** and **5**), were synthesized. The cyclic voltammograms of the porphyrin compounds exhibit two reversible reduction processes and one reversible oxidation. Stable self-assembled monolayers (SAMs) of the porphyrin compounds were formed on gold surfaces. Non-covalent immobilization of C₆₀ was accomplished upon incubation of some of the porphyrin SAMs in solutions of C₆₀.

© 2005 Elsevier Ltd. All rights reserved.

1. Introduction

The highly symmetric three-dimensional structure and unique electronic properties of [60]fullerene make it an attractive candidate to construct novel materials.¹ While dramatic, systematic and rapid progress has been made in the covalent functionalization of C₆₀,² supramolecular interactions with C₆₀ are attracting increasing interest in recent times. [60]Fullerenesupramolecules were first detected as cocrystallized complexes with π -electron rich compounds.^{3–5} Ermer first reported the supramolecular complexation of hydroquinone with C₆₀ in hot benzene solution.³ Subsequently, cocrystallizations of fullerenes with ferrocene⁴ and bis(ethylenedithio)tetrathiafulvalene⁵ were investigated to prepare the corresponding solid state complexes. Solid state complexes of fullerene with inorganic materials like S₈ and P₄ have also been investigated.⁶ The driving force for the formation of such supramolecules is the weak charge transfer interaction between the electron deficient C₆₀ and electron rich molecules.

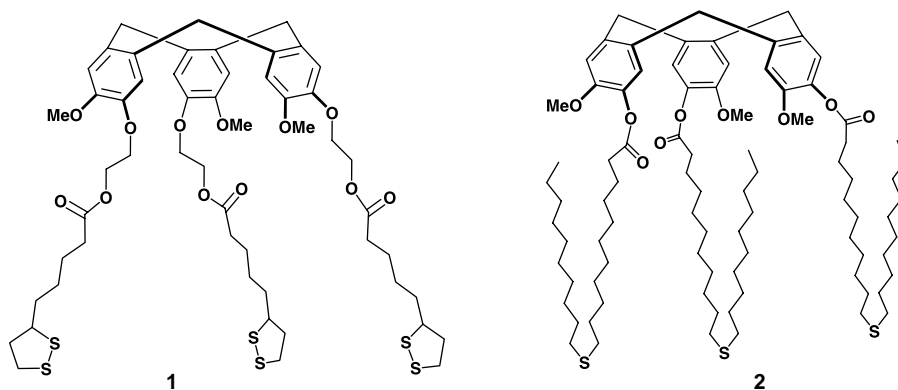
π -Stacking enhances the weak charge transfer interaction and induces the curved surface of C₆₀ prone to form convex–concave supramolecules with other interesting targets. Since covalent functionalization of C₆₀ changes some of its desirable electronic properties, supramolecular complexation is attractive to orient C₆₀ and yet preserve these interesting properties. The first reported inclusion

complex of C₆₀ was the incorporation of a single C₆₀ molecule into the cavities of two γ -cyclodextrin molecules.⁷ Calixarenes are organic molecules with preorganized arrays of aromatic rings. Concave–convex π -stacking interactions as well as donor–acceptor interactions play a key role in forming ball and socket complex structures of calixarenes with C₆₀. Selective complexation of crude fullerene soot with *p*-*tert*-butylcalix[8]arene has been utilized to purify C₆₀.⁸ Evaporation of solutions of C₆₀ or C₇₀ in the presence of calix[6]arene yields 2C₆₀·(calix[6]arenes) or 2C₇₀·(calix[6]arenes).⁹ Upon addition of calix[5]arene to C₆₀ in several solvents, a color change from purple to pale yellow has been observed.¹⁰ The complexation of a covalently linked calix[5]arene dimer shows to date the largest binding constant value for C₆₀ in organic solvents (76,000 M⁻¹).¹¹ However, not all calixarenes can form ball and socket structures with fullerenes. Calix[4]arenes have cavities that are too small to incorporate fullerenes.¹² Another kind of macrocyclic compound possessing the ability to complex C₆₀ is cyclotrimeratrylene (CTV). Addition of cyclotrimeratrylene to a solution of C₆₀ in toluene afforded black crystals of 1.5C₆₀·(CTV)(toluene).¹³ The X-ray structure shows that C₆₀ stands well above the cavity of the CTV derivative. In addition, the host–guest interaction of C₆₀ with polybenzyl ether dendrimer functionalized CTV derivatives has been investigated by Nierengarten et al.¹⁴

Fullerenes can also interact with porphyrins and metalloporphyrins through an interaction between a curved surface and a flat surface, the so-called planar–convex interaction. This non-covalent recognition element was first confirmed by a crystal structure of a covalently linked

Keywords: Porphyrins; Fullerenes; Cyclic voltammetry; SAMs; Non-covalent immobilization.

* Corresponding author. Tel.: +1 864 656 0778; fax: +1 864 656 6613; e-mail: luis@clemson.edu



Scheme 1. Cyclotrimeratrylene (CTV) derivatives **1** and **2**.

tetraphenylporphyrin– C_{60} dyad.¹⁵ Following that, a series of metalloporphyrin– C_{60} supramolecules were systematically studied.¹⁶ Favorable van der Waals attractions between the convex π -surfaces of fullerenes and the planar π -surfaces of porphyrins contribute to the supramolecular recognition. To inhibit fullerene aggregation, a porphyrin cyclic dimer¹⁷ and a porphyrin jaw¹⁸ were also prepared to complex C_{60} . A very selective extraction method for higher fullerenes has been developed using cyclic dimers of zinc porphyrins.¹⁹ Very recently, the first example of ‘supramolecular peapods’²⁰ composed of a linear Zinc porphyrin nanotube and fullerenes has been developed based on the same recognition concept.

Because of their potential usefulness in photovoltaic cells, superconductivity and biological system, thin films of fullerene-based materials have been actively investigated. Self-assembled monolayers (SAMs) have demonstrated obvious advantages to form well defined and highly ordered fullerene arrays on surfaces. Many reports have been published describing how to covalently construct densely packed C_{60} monolayers.^{21–26} Mirkin and coworkers first reported the well-ordered SAMs of a C_{60} thiol derivative on gold surfaces and SAMs of C_{60} on cysteamine modified ITO surfaces.²¹ Imahori and Fukuzumi have prepared a series of self-assembled monolayers of porphyrin–fullerene dyads and triads and systematically investigated their photoelectric conversion properties.²² Some reports have pointed out that pyridyl nitrogens, like thiol sulfurs, can strongly adsorb on gold surfaces.²³ Echegoyen et al. have reported SAMs of a fullerene derivative containing a 1,10-phenanthroline adduct on gold surfaces.²⁴ They also prepared stable SAMs of oligothiophene–fulleropyrrolidine dyads by the spontaneous adsorption on Au (111).²⁵ They also described an alternative methodology to prepare thin films of fullerene derivatives by utilizing a defined molecular recognition event, the complexation between the primary ammonium cations and an 18-crown-6 moiety.²⁶

Immobilization of fullerene derivatives onto surfaces can also be achieved through electrostatic interactions. The first example involving electrostatic interactions was the binding of a C_{60} modified by cationic headgroups with anionic duplex DNA.²⁷ Another example was the construction of photoactive ITO electrodes using a layer by layer approach. C_{60} bearing positively charged groups was deposited on

ITO surfaces driven electrostatically by poly(styrene-4-sulfonate) anions.²⁸ In all of those cases, covalent functionalization of C_{60} was required, which partially destroys the electronic π -delocalization of the molecule due to introduction of the adduct. In addition, C_{60} has a high aggregation tendency, which affects its molecular electronic properties. To overcome both of those problems, Shinkai et al. accomplished the non-covalent incorporation of isolated C_{60} molecules by complexation with homo-oxacalix[3]arenes on surfaces, combining electrostatic and π -stacking.²⁹ The photocurrent flow of such photoactive ITO electrodes exhibited a very high quantum yield (21%) upon irradiation. In this case, C_{60} was not functionalized and presumably not self-aggregated.

In our very recent research, we reported non-covalent immobilization of C_{60} on gold surfaces by SAMs of two cyclotrimeratrylene (CTV) derivatives (Shown in Scheme 1), one containing thioctic esters (**1**) and the other with thioether groups (**2**) by taking advantage of the host–guest interaction between C_{60} and the CTV derivatives.³⁰ Self-assembled monolayers (SAMs) of **1** and **2** were formed on gold surfaces and were characterized by CV blocking experiments, impedance spectroscopy and electrochemical reductive desorption. Non-covalent immobilization of C_{60} on gold surfaces was obtained with SAMs of the two CTV

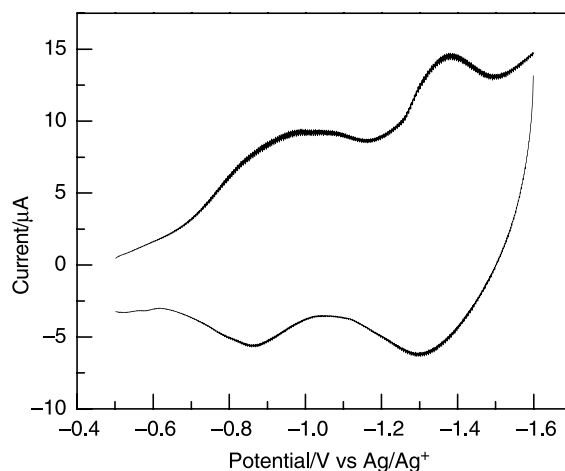


Figure 1. CV recorded in CH_3CN of SAMs of **1** after the incubation in solution of C_{60} . Supporting electrolyte: 0.1 M Bu_4NPF_6 . Scan rate: 0.1 V/s.

derivatives. SAMs of **1** can bind C_{60} after they are formed or during formation. As shown in Figure 1, two well-defined reversible redox waves at $E_{1/2} = -0.93$ and -1.34 V versus Ag/Ag^+ were observed, which correspond to the first and second reduction processes of C_{60} , respectively, confirming the incorporation of C_{60} in the SAMs. However, SAMs of **2** could not incorporate C_{60} by incubation of the monolayers in solutions of C_{60} . If the mixture of **2** and C_{60} was kept for 2 weeks and then SAMs were formed from the resulting solution, C_{60} was detected in the SAMs, as shown in Figure 2. The cyclic voltammogram recorded in CH_3CN exhibits two broad waves at $E_{1/2} = -1.06$ and -1.45 V versus Fc/Fc^+ , which correspond to the first two reduction processes of C_{60} .

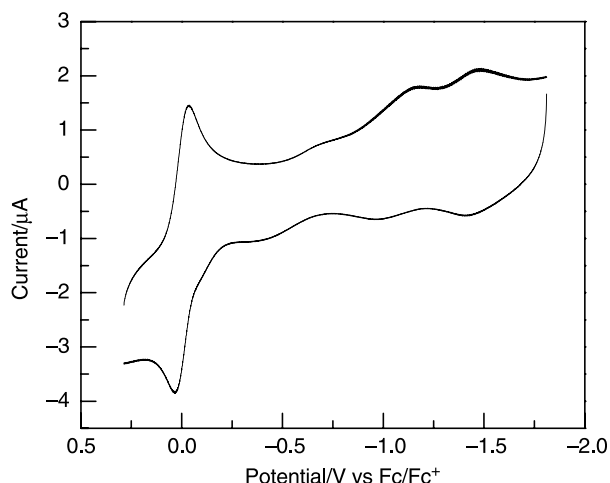


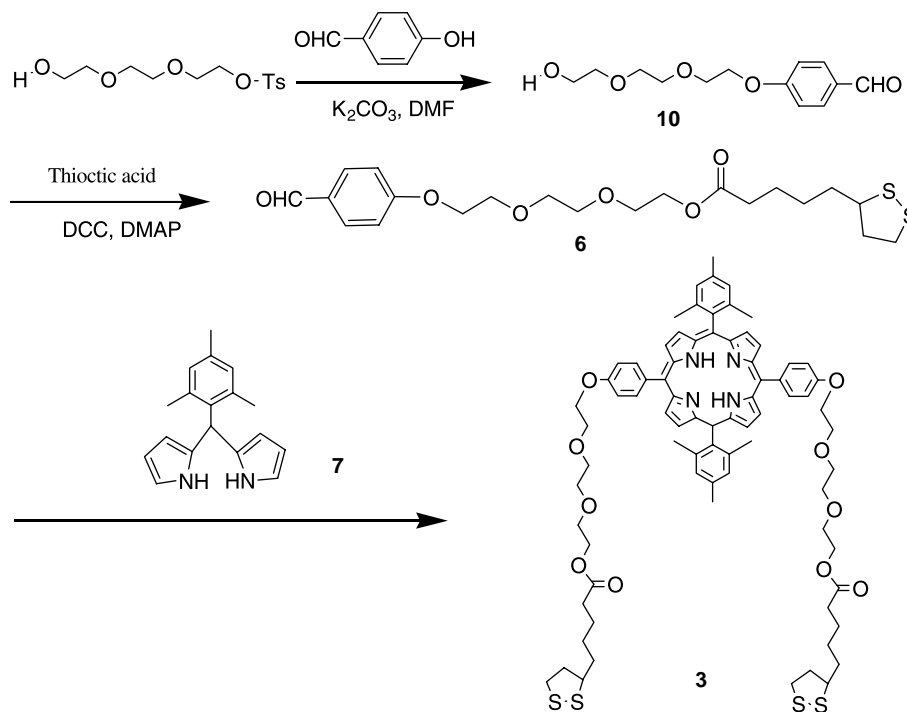
Figure 2. CV recorded in CH_3CN of SAMs grown from the mixture of C_{60} and **2** for two weeks. Supporting electrolyte: 0.1 M Bu_4NPF_6 . Scan rate: 0.1 V/s.

Here we further explore the use of non-covalent interactions between porphyrin receptors and C_{60} to immobilize fullerene on surfaces. Three porphyrin derivatives (**3–5**) with surface anchoring groups were prepared. All compounds were fully characterized by 1H and ^{13}C NMR and MS spectroscopies. SAMs of these porphyrin compounds were formed on gold surfaces. Stable SAMs of these porphyrin compounds were used to supramolecularly incorporate C_{60} on gold surfaces.

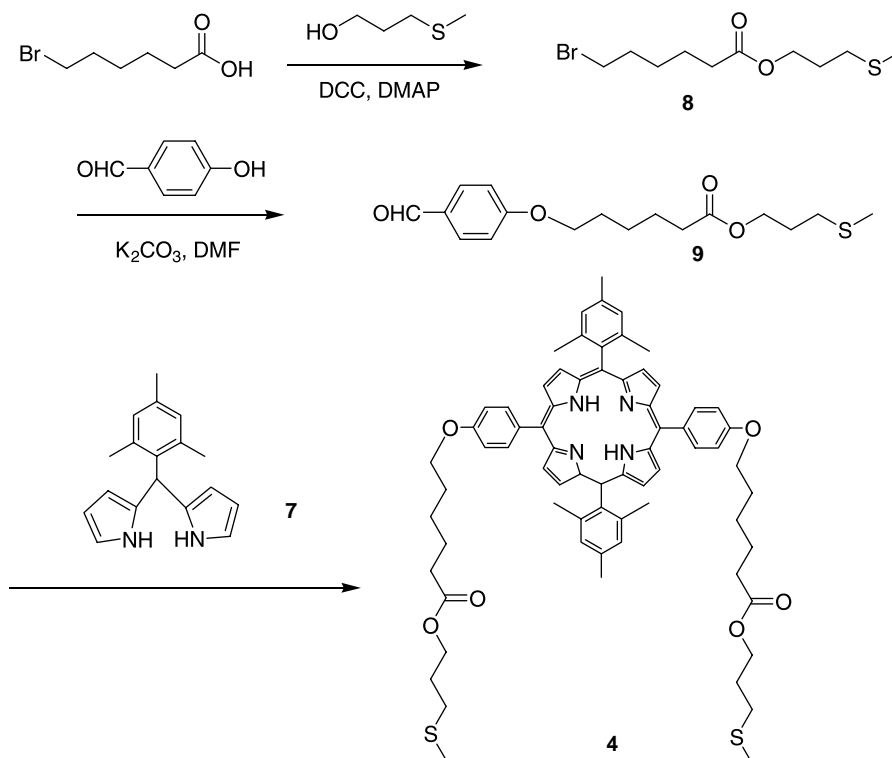
2. Results and discussions

The synthetic methods used for the preparation of porphyrin derivatives **3–5** are shown in Schemes 2–4. Compound **3** was obtained by the condensation of *meso*-(mesityl)dipyrromethane **7** with aldehyde **6** followed by oxidation with DDQ in anhydrous CH_2Cl_2 .³¹ Aldehyde **6** was prepared by coupling compound **10**³² with thioctic acid in the presence of DCC and DMAP. Compound **10** was synthesized by the treatment of 4-hydroxybenzaldehyde with triethylene glycol monotosylate in the presence of K_2CO_3 . As shown in Scheme 3, compound **8**³³ was prepared by the reaction of 6-bromohexanoic acid with 3-(methylthio)-1-propanol. Subsequent treatment of **8** with 4-hydroxybenzaldehyde afforded aldehyde **9**. Condensation of compound **9** with **7** afforded bis-thioether porphyrin derivative **4**. Treatment of **8** with tetrahydroxyphenylporphyrin in DMF using K_2CO_3 as base produced **5**.

The solution electrochemistry of compounds **3–5** was investigated by cyclic voltammetry in CH_2Cl_2 . The cyclic voltammogram of **4** (Fig. 3) features two reversible one-electron reduction couples at -1.79 and -2.13 V versus Fc/Fc^+ , respectively. The first reversible oxidation wave was observed at 0.46 V versus Fc/Fc^+ . The second



Scheme 2. Synthesis of porphyrin derivative **3**.

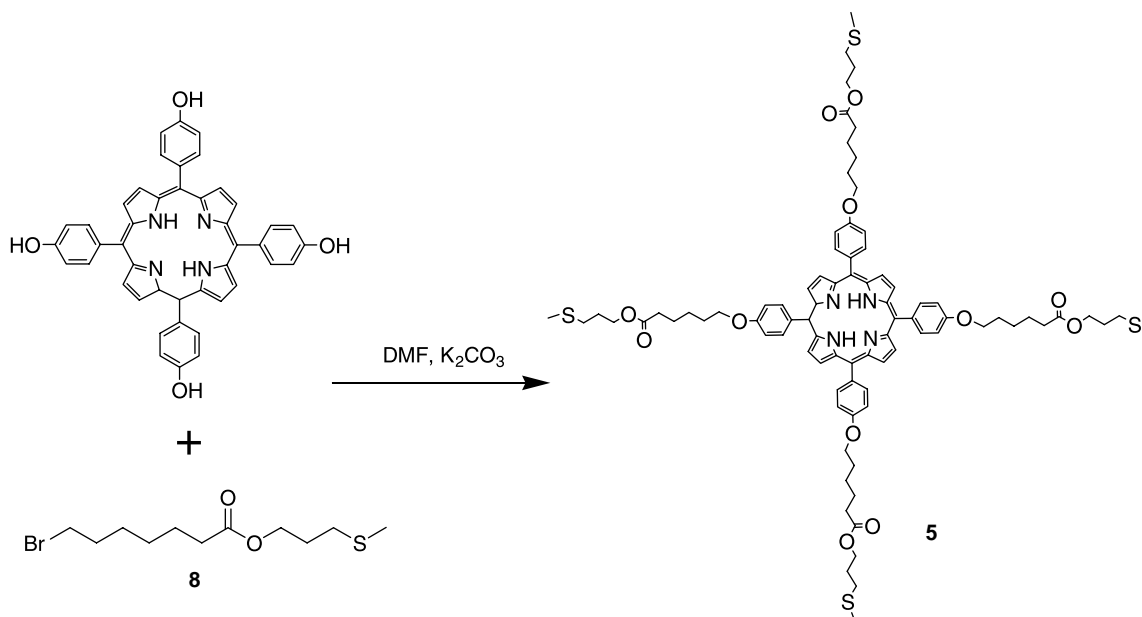


Scheme 3. Synthesis of porphyrin derivative **4**.

oxidation of this porphyrin compound is not reversible, which is probably due to the introduction of long alkyl or OEG chains. Compounds **3** and **5** exhibit very similar electrochemical behavior. All the redox potentials measured for these three porphyrin derivatives are summarized in Table 1.

SAMs of compounds **3–5** were formed on gold surfaces by dipping gold bead electrodes into CH₂Cl₂ solutions of the target compounds. All the monolayers were characterized

by cyclic voltammetry. The CV (Fig. 4) of the gold electrode modified with SAMs of **3** shows the expected two one-electron reduction processes at potentials -1.57 and -1.95 V versus Ag/Ag⁺, respectively. The oxidation waves of SAMs of **3–5** are not reversible. The potentials were not referenced to internal Fc/Fc⁺ since the SAMs blocked this compound from approaching the electrode surface. All peak potentials are proportional to the sweep rate, which was varied between 0.1 and 0.8 V/s, indicating surface-confined behavior due to the immobilization of the



Scheme 4. Synthesis of porphyrin derivative **5**.

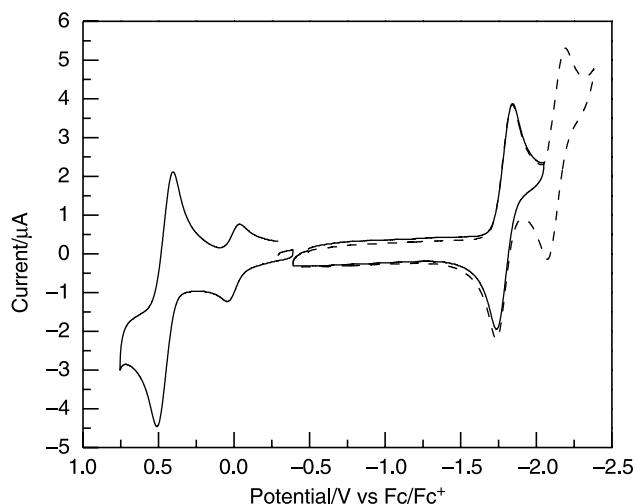


Figure 3. CV recorded in CH_2Cl_2 of **4**. Supporting electrolyte: 0.1 M Bu_4NPF_6 . Scan rate: 0.1 V/s.

Table 1. Redox potentials of **3–5** and their SAMs

	Potentials versus Fc/Fc^+			Potentials versus Ag/Ag^+	
	$E_{\text{ox.1}}^{1/2}$	$E_{\text{red.1}}^{1/2}$	$E_{\text{red.2}}^{1/2}$	$E_{\text{red.1}}^{1/2}$	$E_{\text{red.2}}^{1/2}$
4	0.46	-1.79	-2.13	SAMs of 4 -1.57	-1.94
3	0.46	-1.78	-2.12	SAMs of 3 -1.57	-1.95
5	0.44	-1.78	-2.14	SAMs of 5 -1.50	-1.85

electroactive porphyrin derivative on the surfaces. The peak-to-peak separations of the first and second reduction waves are 22 and 34 mV, respectively, indicative of electrochemically reversible processes on the surfaces.

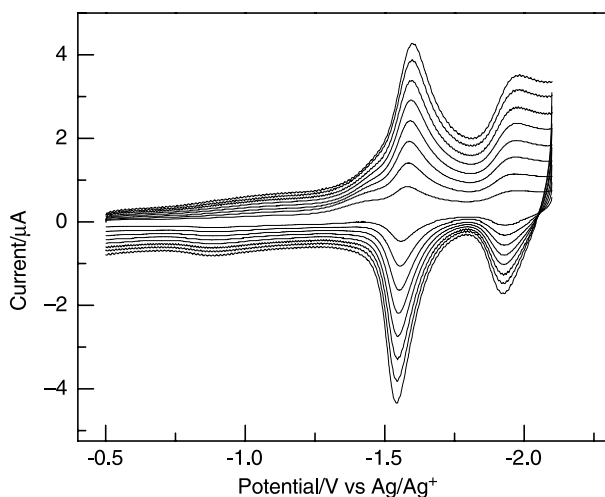


Figure 4. CV recorded in CH_3CN of SAMs grown from **3** at variable scan rates (0.1–0.8 V/s). Supporting electrolyte: 0.1 M Bu_4NPF_6 .

Figure 5 shows the electrochemistry of SAMs of **4**. Two pairs of reversible reduction peaks were observed at -1.57 and -1.94 V versus Ag/Ag^+ , respectively, which correspond to the first two reduction processes of **4**. The peak-to-peak separations of the first and second reduction waves are 16 and 19 mV, respectively. The electrochemical response of monolayers of **4** is also consistent with a redox

system confined to the gold electrode surfaces. Compared to the second reduction, the first one is sharper, like the case of SAMs of **3**. SAMs of the four-legged porphyrin derivative **5** exhibit very similar electrochemical behavior. The redox potentials of all the monolayers are included in **Table 1**. It should be noted that the SAMs of **3–5** are very stable and their electrochemical responses remain essentially unchanged after multiple scans, which makes it possible to investigate the potential interactions with C_{60} .

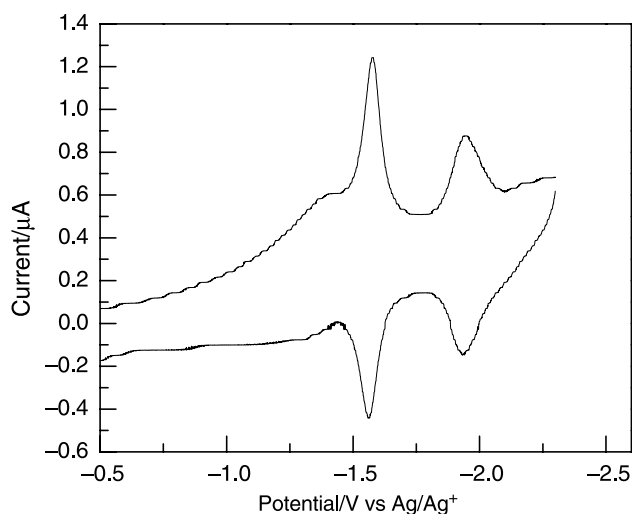


Figure 5. CV recorded in CH_3CN of SAMs of **4**.

SAMs of porphyrin compounds **3–5** were immersed into 1,2-dichlorobenzene solutions of C_{60} for 10 h. After washing the gold bead electrodes with copious 1,2-dichlorobenzene, toluene, and CH_2Cl_2 and drying under a flow of Argon, they were investigated by cyclic voltammetry. **Figure 6** shows the electrochemistry of SAMs of **3** after the incubation in 1,2-dichlorobenzene solutions of C_{60} . In the first scan, four reduction peaks were observed at -0.94 , -1.33 , -1.56 and -1.93 V versus Ag/Ag^+ , respectively. The first two reduction potentials are almost the same as those observed for C_{60} immobilized on gold surfaces by CTV derivatives, which correspond to the first two reduction processes of C_{60} , thus confirming the incorporation of C_{60} on gold surfaces by SAMs of **3**. The first and second reoxidation peaks are, compared to their corresponding reductions, very weak. The third and fourth redox waves are reversible redox processes with peak-to-peak separations of 31 and 33 mV, respectively, which correspond to the first and second reduction processes of the porphyrin moiety. Compared to the redox responses of free SAMs of **3**, the reduction peaks of the porphyrin after incorporation of C_{60} are broader and a shoulder peak at -1.67 V was observed. These results probably indicate formation of C_{60} –porphyrin complex on gold surfaces. Observations of additional reoxidation peaks at around -1.37 and -1.78 V versus Ag/Ag^+ also support this assumption. Unfortunately these surface-confined complexes are not very stable since the peak intensities of the first two reduction peaks keep decreasing upon successive scans and eventually only the redox responses for porphyrin group were observed after several scans.

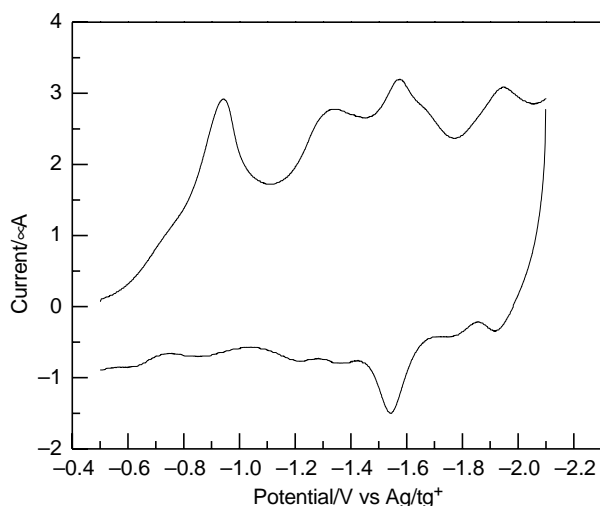


Figure 6. CV recorded in CH_3CN of SAMs of **3** after dipping into a solution of C_{60} .

Attempts to trap C_{60} on gold surfaces by SAMs of **4** were also tried. **Figure 7** shows the electrochemistry of the SAMs of **4** after incubation in solutions of C_{60} . The first scan (solid line, **Fig. 7**) exhibits a rather complex electrochemical response with several broad peaks, probably due to the overlapping of the reductions of porphyrin and C_{60} in different complexation modes. The CV changed dramatically upon successive scans, indicating some structural rearrangement of the porphyrin– C_{60} complexes, and/or the injection of TBA^+ or release of solvent trapped during the assembly process in the SAMs. The dashed line in **Figure 7** corresponds to the fourth cycle. Compared to the first scan, the peak currents of the fourth scan are drastically decreased. Four reduction peaks were observed in the fourth scan. The first and second reductions at -1.01 and -1.31 V versus Ag/Ag^+ probably correspond to the first two reduction processes of C_{60} , respectively, indicative of the incorporation of C_{60} into the SAMs of **4**. The third and fourth reductions at -1.56 and -1.93 V versus Ag/Ag^+ are reversible redox waves attributed to the first and second reduction processes of compound **4**. SAMs of

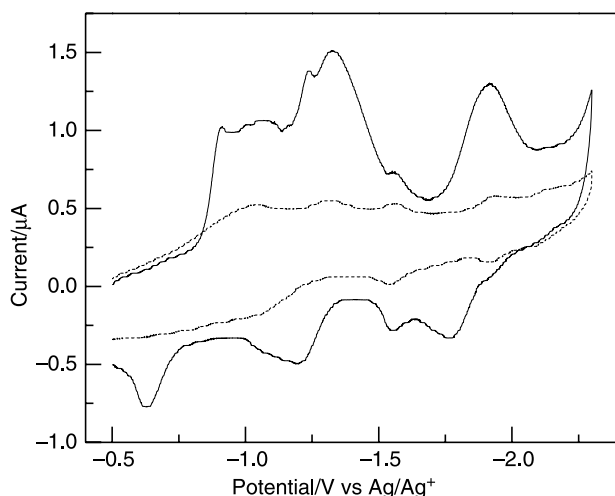


Figure 7. CV recorded in CH_3CN of SAMs of **4** after dipping into a solution of C_{60} (solid line: first scan; dashed line: fourth scan). Supporting electrolyte: 0.1 M Bu_4NPF_6 . Scan rate: 0.1 V/s.

the four-legged porphyrin derivative **5** were also tested for C_{60} binding in the same way. However, no redox response assignable to C_{60} was observed after immersing the SAMs of **5** into a 1,2-dichlorobenzene solution of C_{60} . These observations probably indicated that the four chains in the immobilized compound hinder the incorporation of C_{60} due to steric constraint.

3. Conclusion

Three porphyrin derivatives with sulfur anchoring groups were synthesized. Cyclic voltammograms of these target compounds exhibit two reversible reduction processes and one reversible oxidation peaks for **3–5**. The second oxidation of these compounds is not reversible. SAMs of **3–5** were formed on gold surfaces and investigated by cyclic voltammetry. SAMs of **3** and **4** can trap C_{60} on gold surfaces, as detected by observing the first two reduction processes of C_{60} . SAMs of **5**, however, were not effectively at trapping C_{60} on gold surfaces in the same way. Electrochemical studies also show that such surface complexes of C_{60} are not stable upon successive reductive scans, probably due to the weak binding interaction.

4. Experimental

4.1. General

^1H and ^{13}C NMR spectra were recorded on a Bruker AC 300 spectrometer. Mass spectroscopy was recorded with an Omni Flex MALDI-TOF spectrometer. Elemental analyses were performed using a Carlo Erba EA 1106. Deionized water was prepared with a nanopure infinity ultrapure water system. The gold beads were prepared and electrochemically cleaned as reported previously.³⁴ Monolayers on gold were prepared by the immersion of freshly prepared gold beads in 1 mM solutions of compounds **3–5** in CH_2Cl_2 . All electrochemical measurements were performed with the CHI 660 Electrochemical Workstation. 0.1 M tetrabutylammonium hexafluorophosphate in CH_2Cl_2 (redistilled) was used as the supporting electrolyte (degassed with Argon). Platinum wire was employed as the counter electrode. An Ag/Ag^+ electrode or Ag wire was used as the reference for the monolayer and solution electrochemistry, respectively. In the case of solution electrochemistry, Ferrocene (Fc) was added as an internal reference and the potentials were referenced relative to the Fc/Fc^+ couple. The potentials of monolayer electrochemistry were referenced relative to the Ag/Ag^+ couple. A glassy carbon electrode, polished with aluminum paste and ultrasonicated in deionized water and CH_2Cl_2 bath, was used as the working electrode for the solution electrochemistry. SAM modified gold bead electrodes were used as working electrodes for monolayer electrochemistry.

4.1.1. Synthesis of 10. 4-Hydroxybenzaldehyde (0.86 g, 7.04 mmol), triethylene glycol monotosylate (1.46 g, 4.8 mmol), K_2CO_3 (5.40 g, 39.1 mmol) and DMF (20 ml) were refluxed under Ar for 48 h. After removing the solvent, the brownish residue was treated with 10% aqueous HCl and dichloromethane. The organic layer was washed three times

with water and dried over anhydrous MgSO_4 . After filtration and evaporation, the crude residue was chromatographed on silica gel using 20% $\text{AcOEt}/\text{CH}_2\text{Cl}_2$ as eluent to give a pale yellow oil **10**. Yield: 78%. ^1H NMR (CDCl_3 , ppm): 9.18 (s, 1H), 7.79–7.59 (d, 2H, $J=8.6$ Hz), 6.99–6.96 (d, 2H, $J=8.6$ Hz), 4.18–4.15 (t, 2H, $J=4.8$ Hz), 3.86–3.83 (t, 2H, $J=4.8$ Hz), 3.69–3.61 (m, 6H), 3.57–3.54 (t, 2H, $J=4.8$ Hz), 2.99 (s, 1H). ^{13}C NMR (CDCl_3 , ppm): 190.69, 163.59, 131.78, 129.84, 114.68, 72.33, 70.65, 70.11, 69.22, 67.48, 61.45.

4.1.2. Synthesis of 6. Thioctic acid (1.04 g, 5.04 mmol) and **10** (0.86 g, 3.38 mmol) were dissolved in CH_2Cl_2 (30 ml). The mixture was stirred for 30 min at 0 °C under Ar. Then 1,3-dicyclohexylcarbodiimide (DCC) (1.04 g, 5.03 mmol) and 4-(dimethylamino)-pyridine (DMAP) (0.13 g, 1.06 mmol) were added, and the mixture was stirred for another 30 min at 0 °C. The cooling bath was then removed and the solution allowed to warm to room temperature. After being stirred for 48 h under Ar, the reaction mixture was filtered through a fine glass frit to afford a clear filtrate and the insoluble urea byproduct as a white solid. The filtrate was washed three times with water and dried over MgSO_4 . After filtration and evaporation, the residue was chromatographed on silica gel using 20% $\text{AcOEt}/\text{CH}_2\text{Cl}_2$ as eluent to give a pale yellow oil **6** (1.29 g, 86%). ^1H NMR (CDCl_3 , ppm): 9.72 (s, 1H), 7.68–7.65 (d, 2H, $J=8.6$ Hz), 6.88–6.86 (d, 2H, $J=8.6$ Hz), 4.09–4.06 (m, 4H), 3.75–3.71 (t, 2H, $J=4.8$ Hz), 3.59–3.55 (m, 6H), 3.42–3.38 (m, 1H), 3.00–2.92 (m, 2H), 2.29–2.26 (m, 1H), 2.20–2.15 (t, 2H, $J=7.4$ Hz), 1.89–1.27 (m, 7H). ^{13}C NMR (CDCl_3 , ppm): 190.14, 172.72, 163.26, 131.35, 129.44, 114.34, 70.26, 69.98, 68.90, 68.60, 67.25, 62.82, 55.76, 39.65, 37.93, 33.99, 33.33, 28.12, 24.04.

4.1.3. Synthesis of 3. 5-Mesityldipyrromethane **7** (0.13 g, 0.50 mmol) and **6** (0.22 g, 0.50 mmol) were dissolved in CH_2Cl_2 (10 ml) and then TFA (0.10 g, 0.89 mmol) was added slowly over 30 s. The mixture was stirred at room temperature for 30 min. DDQ (0.11 g, 0.50 mmol) was added and the mixture was stirred at room temperature for another hour. The complete reaction mixture was poured onto a pad of alumina and eluted with a mixture of $\text{AcOEt}/\text{CH}_2\text{Cl}_2$ from 0 to 50% until the eluting solution was pale brown. The solvent was removed under vacuum to give a dark purple solid, which was dissolved in toluene and heated under reflux for 1 h in the presence of DDQ (0.11 g, 0.50 mmol) to oxidize any remaining chlorine. After cooling to room temperature, the reaction mixture was purified by column chromatography (SiO_2 , 10% $\text{AcOEt}/\text{CH}_2\text{Cl}_2$) to afford compound **3** (0.23 g, 32%). ^1H NMR (CDCl_3 , ppm): 8.82–8.81 (d, 4H, $J=4.8$ Hz), 8.70–8.69 (d, 4H, $J=4.8$ Hz), 8.13–8.12 (d, 4H, $J=8.3$ Hz), 7.31–7.30 (d, 4H, $J=8.3$ Hz), 7.28 (s, 4H), 4.43 (t, 4H, $J=4.8$ Hz), 4.31 (t, 4H, $J=4.8$ Hz), 4.06 (t, 4H, $J=4.8$ Hz), 3.87 (t, 4H, $J=4.8$ Hz), 3.80 (m, 8H), 3.62–3.48 (m, 2H), 3.18–3.05 (m, 4H), 2.63 (s, 6H), 2.40–2.39 (m, 6H), 1.84 (s, 12H), 1.83–1.27 (m, 14H). ^{13}C NMR (CDCl_3 , ppm): 173.61, 158.66, 139.50, 138.62, 137.78, 135.58, 134.69, 127.84, 119.11, 118.24, 112.93, 71.09, 70.84, 70.11, 69.42, 67.80, 63.62, 56.42, 40.29, 38.55, 34.70, 34.09, 28.85, 24.75, 21.75, 21.59. m/z (MALDI): 1371 ($\text{M}^+ + \text{H}$). Anal. Calcd for $\text{C}_{78}\text{H}_{90}\text{O}_{10}\text{N}_4\text{S}_4$: C, 68.29; H, 6.62. Found: C, 68.87; H, 6.21.

4.1.4. Synthesis of 8. 6-Bromohexanoic acid (2.56 g, 13.12 mmol) and 3-(methylthio)-1-propanol (1.16 g, 10.92 mmol) were dissolved in CH_2Cl_2 (40 ml). Then 1,3-dicyclohexylcarbodiimide (DCC) (3.39 g, 16.43 mmol) and 4-(dimethylamino)-pyridine (DMAP) (0.40 g, 3.27 mmol) were added, and the mixture was stirred at 0 °C for 30 min. The cooling bath was then removed and the solution allowed to warm to room temperature. After being stirred for 48 h under Ar, the reaction mixture was filtered through a fine glass frit to afford a clear filtrate and the insoluble urea byproduct as a white solid. The filtrate was washed three times with water, and dried over MgSO_4 . After filtration and evaporation, the residue was chromatographed on silica gel using CH_2Cl_2 as eluent to give a pale yellow oil **8** (2.60 g, 84%). ^1H NMR (CDCl_3 , ppm): 4.11–4.09 (t, 2H, $J=6.8$ Hz), 3.35–3.33 (t, 2H, $J=6.8$ Hz), 2.51–2.48 (t, 2H, $J=6.8$ Hz), 2.28–2.25 (t, 2H, $J=6.8$ Hz), 2.04 (s, 3H), 1.87–1.85 (m, 4H), 1.62–1.59 (m, 2H), 1.45–1.42 (m, 2H). ^{13}C NMR (CDCl_3 , ppm): 173.44, 63.00, 34.08, 33.60, 32.45, 30.68, 28.25, 27.70, 24.14, 15.58.

4.1.5. Synthesis of 9. 4-Hydroxybenzaldehyde (0.55 g, 4.50 mmol), **8** (1.06 g, 3.74 mmol), K_2CO_3 (4.15 g, 30 mmol) and DMF (30 ml) were refluxed under Ar for 48 h. After removing the solvent, the brownish residue was treated with 5% aqueous HCl and dichloromethane. The organic layer was washed three times with water and dried over anhydrous MgSO_4 . After filtration and evaporation, the crude residue was chromatographed on silica gel using 3% $\text{AcOEt}/\text{CH}_2\text{Cl}_2$ as eluent to give a pale yellow oil **9** (1.04 g, 86%). ^1H NMR (CDCl_3 , ppm): 9.90 (s, 1H), 7.86–7.83 (d, 2H, $J=8.6$ Hz), 7.02–6.99 (d, 2H, $J=8.6$ Hz), 4.21–4.18 (t, 2H, $J=6.0$ Hz), 4.10–4.06 (t, 2H, $J=7.2$ Hz), 2.59–2.57 (t, 2H, $J=6.0$ Hz), 2.39–2.35 (t, 2H, $J=7.2$ Hz), 2.12 (s, 3H), 1.96–1.74 (m, 6H), 1.59–1.54 (m, 2H). ^{13}C NMR (CDCl_3 , ppm): 190.73, 173.25, 163.28, 131.95, 130.33, 114.71, 68.01, 62.88, 34.07, 30.57, 28.72, 28.16, 25.55, 24.60, 15.46.

4.1.6. Synthesis of 4. Condensation of 5-mesityldipyrromethane **7** (0.14 g, 0.52 mmol) and **9** (0.17 g, 0.52 mmol) in CH_2Cl_2 (10 ml) with TFA (0.11 g, 0.96 mmol) by following the procedure described for **3** afforded a purple solid **4** (180 mg, 30%). ^1H NMR (CDCl_3 , ppm): 8.85–8.84 (d, 4H, $J=4.8$ Hz), 8.71–8.69 (d, 4H, $J=4.8$ Hz), 8.15–8.12 (d, 4H, $J=8.4$ Hz), 7.30 (s, 4H), 7.29–7.27 (d, 4H, $J=8.4$ Hz), 4.30–4.24 (m, 8H), 2.65 (s, 6H), 2.64–2.61 (m, 4H), 2.50–2.45 (t, 4H, $J=7.5$ Hz), 2.16 (s, 6H), 2.07–1.99 (m, 12H), 1.89 (s, 12H), 1.86–1.84 (m, 4H). ^{13}C NMR (CDCl_3 , ppm): 173.77, 158.91, 139.52, 139.41, 138.39, 135.62, 135.06, 127.83, 119.79, 118.67, 112.78, 68.00, 63.07, 34.39, 30.77, 29.31, 28.36, 25.99, 24.96, 21.74, 21.59, 15.66. m/z (MALDI): 1134 (M^+). Anal. Calcd for $\text{C}_{70}\text{H}_{78}\text{O}_6\text{N}_4\text{S}_2$: C, 74.04; H, 6.93. Found: C, 74.67; H, 6.45.

4.1.7. Synthesis of 5. Tetra-(*p*-hydroxyphenyl)porphyrin (50 mg, 0.074 mmol), **8** (0.40 g, 1.41 mmol), K_2CO_3 (0.31 g, 2.24 mmol) and DMF (freshly distilled over CaH_2 , 30 ml) were refluxed under Ar for 3 days. After removing the solvent, the residue was treated with water and dichloromethane. The organic layer was washed three times with water and dried over anhydrous MgSO_4 . After filtration and evaporation, the crude residue was chromatographed on

silica gel using 5–7% AcOEt/CH₂Cl₂ containing 0.3% Et₃N as eluent to yield purple solid **5** (60 mg, 55%). ¹H NMR (CDCl₃, ppm): 8.79 (s, 8H), 8.04–8.02 (d, 8H, *J*=8.4 Hz), 7.19–7.17 (d, 8H, *J*=8.6 Hz), 4.16–4.13 (m, 16H), 2.53–2.50 (t, 8H, *J*=7.4 Hz), 2.39–2.36 (t, 8H, *J*=7.4 Hz), 2.04 (s, 12H), 1.93–1.53 (m, 32H). ¹³C NMR (CDCl₃, ppm): 178.01, 173.75, 158.92, 135.90, 135.70, 132.44, 130.52, 119.86, 112.76, 69.40, 63.04, 34.67, 34.38, 30.74, 29.79, 29.39, 29.29, 29.08, 28.33, 25.98, 24.94, 23.02, 15.63. *m/z* (MALDI): 1134 (M⁺). Anal. Calcd for C₈₄H₁₀₂O₁₂N₄S₄: C, 67.80; H, 6.91. Found: C, 67.01; H, 6.02.

Acknowledgements

Financial support from the National Science Foundation, (Grant no. CHE-0135786) is greatly appreciated.

References and notes

- Dresselhaus, M. S.; Dresselhaus, G.; Eklund, P. C. *Science of Fullerenes and Carbon Nanotubes*; Academic: San Diego, 1996.
- (a) Hirsch, A. *The chemistry of the Fullerenes*; Thieme: Stuttgart, 1994. (b) Diederich, F.; Thilgen, C. *Science* **1996**, *271*, 317.
- Ermer, O. *Helv. Chim. Acta* **1991**, *74*, 1339.
- Crane, J. D.; Hitchcock, P. B.; Kroto, H. W.; Taylor, R.; Walton, D. R. M. *J. Chem. Soc., Chem. Commun.* **1992**, 1746.
- Izuoka, A.; Tachikawa, T.; Sugawara, T.; Suzuki, Y.; Konno, M.; Saito, Y.; Shinohara, H. *J. Chem. Soc., Chem. Commun.* **1992**, 1472.
- (a) Burgi, H. B.; Venugopalan, P.; Schwarzenbach, D.; Diederich, F.; Thigen, C. *Helv. Chim. Acta* **1993**, *76*, 2115. (b) Douthwaite, R. E.; Green, M. L. H.; Heyes, S. J.; Rosseinsky, M. J.; Turner, J. F. C. *J. Chem. Soc., Chem. Commun.* **1994**, 1367.
- (a) Anderson, T.; Nilsson, K.; Sundahl, M.; Westman, G.; Wennerstrom, O. *J. Chem. Soc., Chem. Commun.* **1992**, 604. (b) Yoshida, Z.; Takekuma, H.; Takekuma, S.-I.; Matsubara, Y. *Angew. Chem., Int. Ed. Engl.* **1994**, *33*, 1597.
- Atwood, J. L.; Koutsantonis, G. A.; Raston, C. L. *Nature* **1994**, *368*, 229.
- Raston, C. L.; Atwood, J. L.; Nichols, P. J.; Sudria, I. B. N. *Chem. Commun.* **1996**, 2615.
- Haino, T.; Yanase, M.; Fukazawa, Y. *Angew. Chem., Int. Ed.* **1997**, *36*, 259.
- Haino, T.; Yanase, M.; Fukazawa, Y. *Angew. Chem., Int. Ed.* **1998**, *37*, 997.
- Ikeda, A.; Yoshimura, M.; Shinkai, S. *Tetrahedron Lett.* **1997**, *38*, 2107.
- (a) Steed, J. W.; Junk, P. C.; Atwood, J. L.; Barnes, M. J.; Raston, C. L.; Burkhalter, R. S. *J. Am. Chem. Soc.* **1994**, *116*, 10346. (b) Atwood, J. L.; Barnes, M. J.; Gardiner, M. G.; Raston, C. L. *Chem. Commun.* **1996**, 1449.
- (a) Nierengarten, J.-F.; Oswald, L.; Eckert, J.-F.; Nicoud, J.-F.; Armaroli, N. *Tetrahedron Lett.* **1999**, *40*, 5681. (b) Felder, D.; Heinrich, B.; Guillon, D.; Nicoud, J.-F.; Nierengarten, J.-F. *Chem. Eur. J.* **2000**, *6*, 3501. (c) Rio, Y.; Nierengarten, J.-F. *Tetrahedron Lett.* **2002**, *43*, 4321.
- Sun, Y.; Drovetskaya, T.; Bolskar, R. D.; Bau, R.; Boyd, P. D. W.; Reed, C. A. *J. Org. Chem.* **1997**, *62*, 3642.
- (a) Evans, D. R.; Fackler, N. L. P.; Xie, Z.; Richard, C. E. F.; Boyd, P. D. W.; Reed, C. A. *J. Am. Chem. Soc.* **1999**, *121*, 8466. (b) Olmstead, M. M.; Costa, D. A.; Maitra, K.; Noll, B. C.; Phillips, S. L.; van Calcar, P. M.; Balch, A. L. *J. Am. Chem. Soc.* **1999**, *121*, 7090. (c) Boyd, P. D. W.; Hodgson, M. C.; Richard, C. E. F.; Oliver, A. G.; Chaker, L.; Brothers, P. J.; Bolskar, R. D.; Tham, F. S.; Reed, C. A. *J. Am. Chem. Soc.* **1999**, *121*, 10487. (d) Ishii, T.; Aizawa, N.; Yamashita, M.; Matsuzaka, H.; Kodama, T.; Kikuchi, K.; Ikemoto, I.; Iwasa, Y. *J. Chem. Soc., Dalton Trans.* **2000**, 4407.
- Tashiro, K.; Aida, T.; Zheng, J.-Y.; Kinbara, K.; Saigo, K.; Sakamoto, S.; Yamaguchi, K. *J. Am. Chem. Soc.* **1999**, *121*, 9477.
- Sun, D. Y.; Tham, F. S.; Reed, C. A.; Chaker, L.; Burgess, M.; Boyd, P. D. W. *J. Am. Chem. Soc.* **2000**, *122*, 10704.
- Shoji, Y.; Tashiro, K.; Aida, T. *J. Am. Chem. Soc.* **2004**, *126*, 6570.
- Yamaguchi, T.; Ishii, N.; Tashiro, K.; Aida, T. *J. Am. Chem. Soc.* **2003**, *125*, 13934.
- (a) Chen, K.; Caldwell, W. B.; Mirkin, C. A. *J. Am. Chem. Soc.* **1993**, *115*, 1193. (b) Shi, X.; Caldwell, W. B.; Chen, K.; Mirkin, C. A. *J. Am. Chem. Soc.* **1994**, *116*, 11598.
- (a) Imahori, H.; Fukuzumi, S. *Adv. Funct. Mater.* **2004**, *14*, 525. (b) Imahori, H.; Azuma, T.; Ozawa, S.; Yamada, H.; Ushida, K.; Ajavakom, A.; Norieda, H.; Sakata, Y. *Chem. Commun.* **1999**, 557. (c) Imahori, H.; Yamada, H.; Nishimura, Y.; Yamazaki, I.; Sakata, Y. *J. Phys. Chem. B* **2000**, *104*, 2099.
- (a) Hudson, J. E.; Abruna, H. D. *J. Phys. Chem.* **1996**, *100*, 1036. (b) Cunha, F.; Tao, N. J.; Wang, X. W.; Jin, Q.; Duong, B.; D'Agnese, J. *Langmuir* **1996**, *12*, 6410. (c) Zhang, S.; Dong, D.; Gan, L.-B.; Liu, Z. F.; Huang, C. H. *New J. Chem.* **2001**, *25*, 606.
- Dominguez, O.; Echegoyen, L.; Cunha, F.; Tao, N. J. *Langmuir* **1998**, *14*, 821.
- Liu, S.-G.; Marineau, C.; Raimundo, J.-M.; Roncali, J.; Echegoyen, L. *Chem. Commun.* **2001**, 913.
- Arias, F.; Godinez, L. A.; Wilson, S. R.; Kaifer, A. E.; Echegoyen, L. *J. Am. Chem. Soc.* **1996**, *118*, 6086.
- (a) Cassel, A. M.; Scrivens, W. A.; Tour, J. M. *Angew. Chem., Int. Ed.* **1998**, *37*, 1528. (b) Takenaka, S.; Yamashita, K.; Takagi, M.; Hatta, T.; Tanaka, A.; Tsuge, O. *Chem. Lett.* **1999**, 319.
- Luo, C.; Guldi, D. M.; Maggini, M.; Menna, E.; Mondini, S.; Kotov, N. A.; Prato, M. *Angew. Chem., Int. Ed.* **2000**, *39*, 3905.
- (a) Hatano, T.; Ikeda, A.; Akiyama, T.; Yamada, S.; Sano, M.; Kanekiyo, Y.; Shinkai, S. *J. Chem. Soc., Perkin Trans. 2* **2000**, 909. (b) Ikeda, A.; Hatano, T.; Shinkai, S.; Akiyama, T.; Yamada, S. *J. Am. Chem. Soc.* **2001**, *123*, 4855.
- Zhang, S.; Palkar, A.; Fragoso, A.; Prados, P.; de Mendoza, J.; Echegoyen, L. *Chem. Mater.* **2005**, *17*, 2063.
- (a) Littler, B. J.; Ciringh, Y.; Lindsey, J. S. *J. Org. Chem.* **1999**, *64*, 2864. (b) Littler, B. J.; Miller, M. A.; Hung, C.-H.; Wagner, R. W.; O'Shea, D. F.; Boyle, P. D.; Lindsey, J. S. *J. Org. Chem.* **1999**, *64*, 1391. (c) Lindsey, J. S.; Schreiman, I. C.; Hsu, H. C.; Kearney, P. C.; Marguerettaz, A. M. *J. Org. Chem.* **1987**, *52*, 827. (d) Lee, C.-L.; Lindsey, J. S. *Tetrahedron* **1994**, *50*, 11427.
- Davidson, R. S.; Palmer, S. J.; Pratt, J. E.; Wilson, S. P. WO 9733202, 1997, CAN 127301279.
- Zhang, M. J.; Vedantham, P.; Flynn, D. L.; Hanson, P. R. *J. Org. Chem.* **2004**, *69*, 8340.
- (a) Zhang, S.; Echegoyen, L. *J. Am. Chem. Soc.* **2005**, *127*, 2006. (b) Zhang, S.; Echegoyen, L. *Org. Lett.* **2004**, *6*, 791. (c) Zhang, S.; Song, F.; Echegoyen, L. *Eur. J. Org. Chem.* **2004**, 2936.

Structure and photoelectrochemical properties of nanostructured SnO₂ electrodes deposited electrophoretically with the composite clusters of porphyrin-modified gold nanoparticle with a long spacer and fullerene

Hiroshi Imahori,^{a,b,c,*} Atsushi Fujimoto,^a Soonchul Kang,^a Hiroki Hotta,^b Kaname Yoshida,^d Tomokazu Umeyama,^a Yoshihiro Matano^a and Seiji Isoda^d

^aDepartment of Molecular Engineering, Graduate School of Engineering, Kyoto University, Nishikyo-ku, Kyoto 615-8510, Japan

^bPRESTO, JAPAN Science and Technology Agency (JST), Japan

^cFukui Institute for Fundamental Chemistry, Kyoto University, 34-4, Takano-Nishihiraki-cho, Sakyo-ku, Kyoto 606-8103, Japan

^dInstitute for Chemical Research, Kyoto University, Uji, Kyoto 611-0011, Japan

Received 10 May 2005; revised 27 May 2005; accepted 30 May 2005

Available online 18 November 2005

Abstract—Structure and photoelectrochemical properties of nanostructured SnO₂ electrodes deposited electrophoretically with the composite clusters of porphyrin-modified gold nanoparticle with a long, flexible spacer and C₆₀ molecules have been examined to obtain basic information on the development of organic solar cells with a high performance. The photoelectrochemical system with the long, flexible spacer between the porphyrin and the gold nanoparticle in the porphyrin-modified gold nanoparticle exhibited comparable external quantum yield in the UV–vis regions relative to porphyrin-modified gold nanoparticle with a relatively short spacer—C₆₀ composite reference system. These results demonstrate that a suitable spacer to incorporate C₆₀ molecules efficiently between the porphyrins in porphyrin-modified gold nanoparticles is a prerequisite for improving the performance of porphyrin and fullerene-based organic solar cells. © 2005 Elsevier Ltd. All rights reserved.

1. Introduction

The interest in organic solar cells has been motivated by the need to replace fossil fuels with the clean and renewable solar energy.^{1–7} In this context, one of the most promising strategies is the development of organic solar cells that mimic natural photosynthesis in the conversion and storage of solar energy. The structures of photosynthetic reaction centers of bacteria and other organisms have given important hints on the design of organic solar cells mimicking photosynthesis.^{8,9} Natural antennae including chlorophylls and carotenoids collect a large amount of solar energy and redirect it as electronic excitation energy to reaction center where subsequent conversion into redox chemical energy takes place through redox active molecules such as chlorophylls and quinones across photosynthetic membrane.¹⁰ The components in the natural system are highly organized in protein matrix, whereas well-controlled

organization of donor (D) and acceptor (A) molecules on electrode surfaces has been often limited in molecular photovoltaics because of the synthetic difficulty and the lack of basic information for the organization.

Recently, we have established porphyrin–alkanethiolate monolayer protected-gold nanoparticles (MPPs) where ~100 porphyrin molecules are assembled three-dimensionally on a gold nanoparticle.¹¹ The porphyrin MPPs exhibit high light-harvesting capability and suppress undesirable energy transfer quenching of the porphyrin singlet excited state by the gold surface relative to the bulk gold.¹¹ More importantly, pre-organized porphyrin molecules on gold nanoparticle have a flexible host space^{11d,12} between the porphyrin moieties, which can incorporate guest acceptor molecules. C₆₀ is highly promising as a guest molecule, since the combination of porphyrin and C₆₀ results in a small reorganization energy, which allows to accelerate photoinduced charge separation and to slow down charge recombination, leading to the efficient production of a long-lived, charge-separated state.^{13–16} Moreover, porphyrin and C₆₀ are known to make a supramolecular complex in solutions as well as in solid state.^{12,17–22} Accordingly, C₆₀ is

Keywords: Nanoparticles; Fullerenes; Porphyrinoids.

* Corresponding author. Address: PRESTO, JAPAN Science and Technology Agency (JST), Japan. Tel.: +81 75 383 2566; fax: +81 75 383 2571; e-mail: imahori@scl.kyoto-u.ac.jp

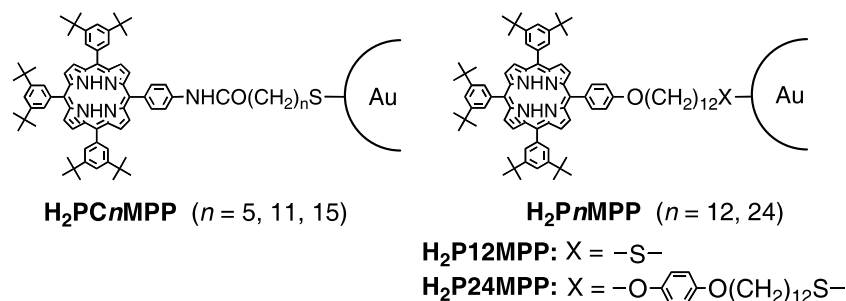
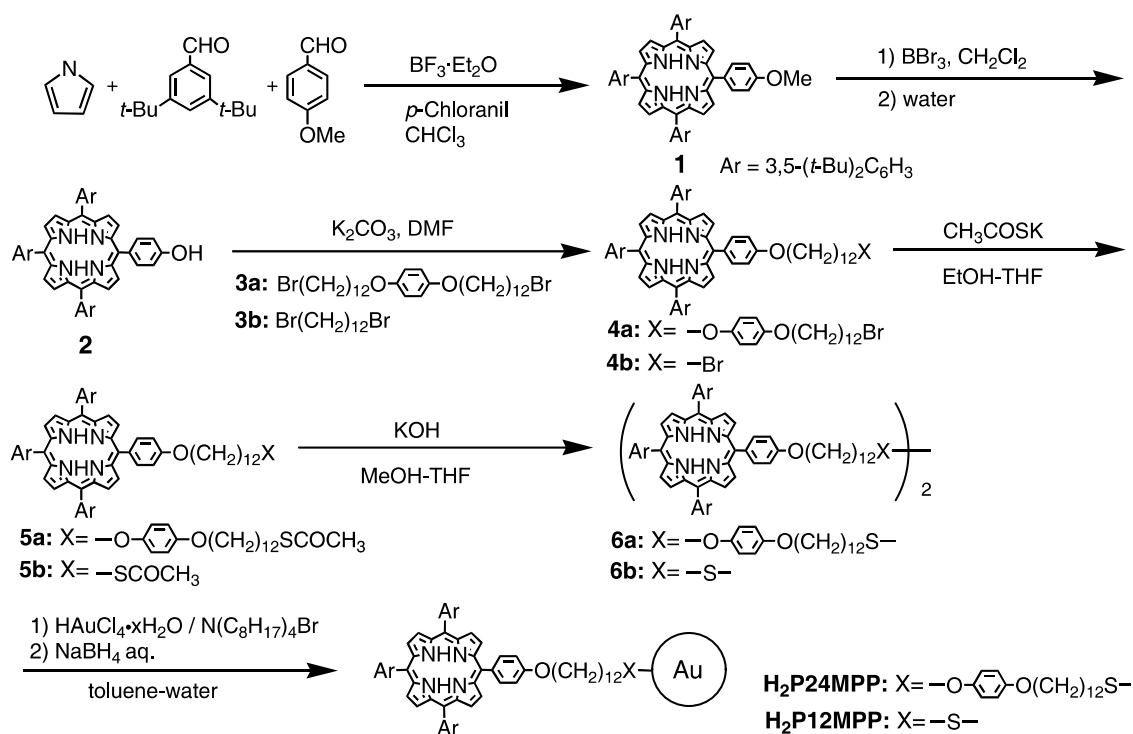


Figure 1. Molecular structures of porphyrin-modified gold nanoparticles **H₂PC_nMPP** ($n = 5, 11, 15$, left) and **H₂P_nMPP** ($n = 12, 24$, right).

expected to be incorporated into the host cavity of porphyrin MPPs, which results in the formation of D–A alternating supramolecular complex.

On the basis of the concept described above, we have recently reported novel organic solar cells, composed of porphyrin MPPs [**H₂PC_nMPP** ($n = 5, 11, 15$); Fig. 1] and C₆₀, which are prepared using stepwise self-organization of porphyrin and C₆₀ molecules with gold nanoparticles on SnO₂ electrodes using an electrophoretic deposition method.²³ Namely, porphyrin MPPs are prepared starting from porphyrin-alkanethiol or equivalent (primary organization). The porphyrin MPPs form supramolecular complexes with C₆₀ molecules (secondary organization) and they are associated in acetonitrile/toluene mixed solvent (tertiary organization). Then, the highly colored composite clusters can be assembled as three-dimensional arrays onto nanostructured SnO₂ films to afford the SnO₂ electrode modified with the composite clusters of the porphyrin and C₆₀ molecules using the electrophoretic deposition method

(quaternary organization). The film of the composite clusters with the gold nanoparticles and C₆₀ molecules exhibits an incident photon-to-photocurrent efficiency (IPCE) as high as 54%, which is much higher than the reference systems consisting of a simple combination of porphyrin and C₆₀ single components.²³ The IPCE values are dependent on the spacer length between the porphyrin and the gold nanoparticle.²³ Although the IPCE values increase with increasing the number of methylene spacer ($n = 5, 11, 15$), the IPCE values in the present system have not been optimized so far. Herein, we report the structure and photoelectrochemical properties of **H₂P_nMPP-C₆₀** ($n = 24$) composite electrodes (Fig. 1). A long spacer between the porphyrin and the gold nanoparticle is expected to affect both the capability of incorporating C₆₀ molecules into **H₂P24MPP** and the photoelectrochemical properties. The structure and photoelectrochemical properties of the **H₂P24MPP-C₆₀** composite electrodes are compared with those of **H₂P12MPP-C₆₀** ($n = 12$) composite reference electrodes (Fig. 1).



Scheme 1.

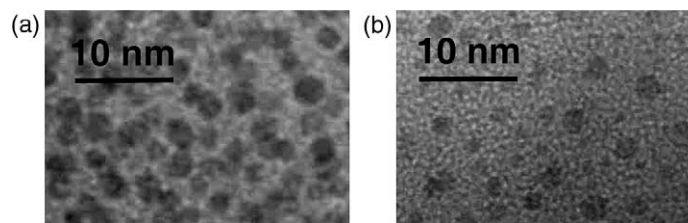


Figure 2. TEM images of (a) **H₂P24MPP** and (b) **H₂P12MPP**. The samples were formed by solvent evaporation from a toluene solution containing the compound. The dark spots correspond to the gold cores.

2. Results and discussion

2.1. Preparation and characterization

The preparation of **H₂P24MPP** and **H₂P12MPP** were carried out as shown in Scheme 1. Methoxy porphyrin **1** was prepared by condensation of pyrrole with 3,5-di-*tert*-butylbenzaldehyde²⁴ and 4-methoxybenzaldehyde in the presence of BF₃·OEt₂.²⁵ Methoxy group in porphyrin **1** was deprotected to give **2**.²⁶ Hydroxyporphyrin **2** was linked to 1,4-bis(12-bromododecyloxy)benzene **3a**²⁷ and 1,12-dibromododecane **3b**, respectively, to yield bromoporphyrins **4a** and **4b**.²⁶ Bromides **4a** and **4b** were converted to disulfides **6a** and **6b**, respectively, via nucleophilic substitution with potassium thioacetate and subsequent base deprotection of **5a** and **5b**.²⁶ Porphyrin MPPs **H₂P_nMPC** (*n* = 12, 24) were directly prepared by reduction of HAuCl₄ with NaBH₄ in toluene/water containing porphyrin disulfide (**6**:HAuCl₄ = 1:2) to increase the extent of functionalization.¹¹ Their structures were verified by spectroscopic analyses (see Section 4). Methoxy porphyrin **1** was used as a reference porphyrin.

The mean diameters of the gold core determined by TEM were $2R_{\text{CORE}} = 2.4$ nm (with a standard deviation $\sigma = 0.4$ nm) for **H₂P24MPP** (Fig. 2a) and $2R_{\text{CORE}} = 2.2$ nm ($\sigma = 0.5$ nm) for **H₂P12MPP** (Fig. 2b). Taking the gold core as a sphere with density ρ_{Au} (58.01 atoms/nm³)²⁸ covered with an outermost layer of hexagonally close-packed gold atoms (13.89 atoms/nm²)²⁸ with a radius of $R_{\text{CORE}} - R_{\text{Au}}$ ($R_{\text{Au}} = 0.145$ nm),²⁸ the model predicts that the cores of **H₂P24MPP** and **H₂P12MPP** contain 420 and 323 Au atoms, respectively, of which 194 and 159 lie on the Au surface (Table 1). Given the values for elemental analyses of **H₂P24MPP** and **H₂P12MPP** (see Section 4), the numbers of porphyrin alkanethiolate chains on gold surface of **H₂P24MPP** and **H₂P12MPP** are determined as 155 and 80, respectively. The difference in the estimated number of porphyrin alkanethiolate chains on the gold surfaces may

result from the experimental errors and have little influence on the complexation with C₆₀ (vide infra). It should be noted here that the TEM image of **H₂P24MPP** exhibits close packing of the gold cores relative to **H₂P12MPP**. Slow solvent evaporation on the TEM grid may allow the porphyrin moieties with a long spacer in **H₂P24MPP** to become entangled with each other, resulting in the close disposition of the gold cores.

¹H NMR spectra of porphyrin MPPs were measured in CDCl₃. ¹H NMR spectra of **H₂P24MPP** and **H₂P12MPP** are shown with those of porphyrin disulfide dimers **6a** and **6b** in CDCl₃ (Fig. 3). The broadening of $-S-CH_2-$ and $-CH_2O-$ signals in **H₂P24MPP** and **H₂P12MPP** as compared with those of **6a** and **6b** indicates that all the porphyrin alkanethiolates are covalently linked to the gold surface to leave no parent molecules **6a** and **6b**. The NMR resonances due to the methylene spacer in **H₂P24MPP** and **H₂P12MPP** are also much broader than those of the terminal porphyrin moiety. Such broadening of the NMR signal is typical characteristic of MPPs.²⁹ It is noteworthy that the signals in **H₂P24MPP** are much sharper than those of **H₂P12MPP**. This indicates that the movement of the porphyrin moieties including the spacer is less restricted in **H₂P24MPP** relative to **H₂P12MPP**.

2.2. Electrochemical and photophysical properties

Cyclic voltammograms of **H₂P24MPP** and **H₂P12MPP** are also compared with that of porphyrin reference **1** (1.0×10^{-4} M based on the number of the porphyrins) in CH₂Cl₂ containing 0.1 M *n*-Bu₄NPF₆ with a sweep rate of 0.1 V s⁻¹. The first oxidation potential of **H₂P24MPP** (0.44 V vs Fc/Fc⁺) is the same as that of **1** (0.44 V vs Fc/Fc⁺). The first oxidation potential of **H₂P12MPP** (0.43 V vs Fc/Fc⁺) is also virtually the same as that of **1**.

UV–vis spectra of porphyrin MPPs were taken in THF (Fig. 4). The absorption due to the surface plasmon

Table 1. Diameter, composition of Au atom and porphyrin, spectroscopic and electrochemical data of porphyrin MPPs and porphyrin reference

Compound	Diameter, $2R_{\text{core}}$ (standard deviation) (nm) ^a	Number of gold atoms (number of porphyrin) ^b	$E_{\text{ox}}^{0/+}$ /V versus Fc/Fc ⁺ ^c	λ_{max} of Soret band (nm) ^d	Half bandwidth (cm ⁻¹) ^{d,e}
H₂P24MPP	2.4 (0.4)	420 (155)	0.44	419	6.8×10^5
H₂P12MPP	2.2 (0.5)	323 (80)	0.43	418	8.6×10^5
1			0.44	419	5.1×10^5

^a From TEM measurements.

^b Estimated from the results on TEM and elemental analysis.

^c The oxidation potentials due to the porphyrin moiety were determined by cyclic voltammetry measurements in CH₂Cl₂ containing 0.1 M *n*-Bu₄NPF₆ with a sweep rate 0.1 V s⁻¹; glassy carbon working electrode, platinum wire counter electrode, and Ag/AgNO₃ (0.01 M in acetonitrile) reference electrode.

^d In THF.

^e From the Soret band.

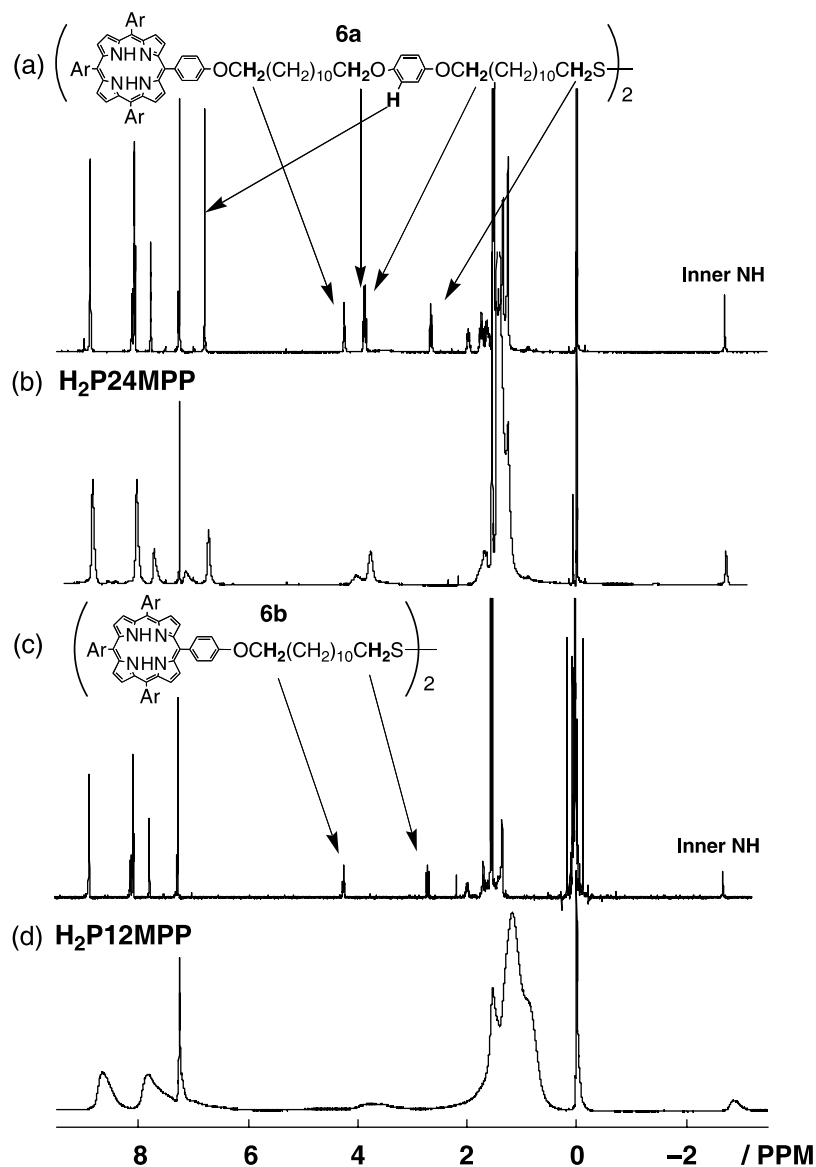


Figure 3. ^1H NMR spectra of (a) **6a**, (b) **H₂P24MPP**, (c) **6b**, and (d) **H₂P12MPP** in CDCl_3 .

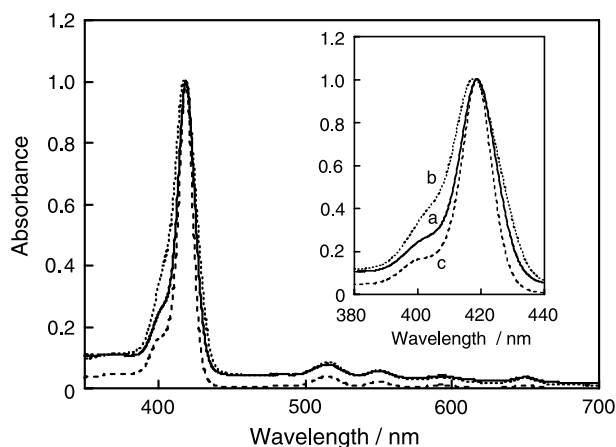


Figure 4. UV-vis absorption spectra of (a) **H₂P24MPP** (solid line), (b) **H₂P12MPP** (dotted line), and (c) **1** (dash line) in THF. The spectra were normalized at the Soret band for comparison.

resonance of the gold nanoparticle is much weaker than that of the absorption due to the porphyrin moiety. The λ_{max} value of the Soret band (419 nm) of **H₂P24MPP** in THF is identical to that of porphyrin reference **1** (419 nm), whereas the λ_{max} value of **H₂P12MPP** is slightly blue-shifted (1 nm) relative to that of **1** in THF (Table 1). In accordance with the results, the half bandwidths of the Soret band are in the order of **1** ($5.1 \times 10^5 \text{ cm}^{-1}$) < **H₂P24MPP** ($6.8 \times 10^5 \text{ cm}^{-1}$) < **H₂P12MPP** ($8.6 \times 10^5 \text{ cm}^{-1}$). These indicate that there is less interaction between the porphyrins in **H₂P24MPP** with a long spacer in comparison with **H₂P12MPP** with a relatively short spacer.

Steady-state fluorescence spectra of porphyrin MPPs and **1** were measured in THF with the excitation of the Soret peak where the absorbance was adjusted to be identical. Peak position (655 nm) and shape of the emission are similar, but the moderate quenching of the steady-state fluorescence of

porphyrin MPPs is seen relative to **1** (Fig. 5). This agrees with the previous results that the porphyrin excited singlet state on the gold surface is quenched by energy transfer (EN).¹¹ The relative fluorescence intensity of porphyrin MPPs versus **1** in THF decreases with decreasing the spacer length in the order: **H₂P24MPP** (32%) > **H₂P12MPP** (6.5%). In other words, the EN quenching of the porphyrin excited singlet state is suppressed in **H₂P24MPP** relative to **H₂P12MPP** due to the long separation distance between the porphyrin and the gold surface in **H₂P24MPP**.

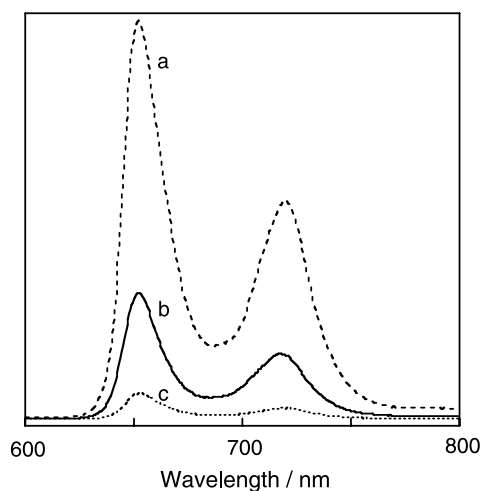


Figure 5. Steady-state fluorescence spectra of (a) **1** (dash line), (b) **H₂P24MPP** (solid line), and (c) **H₂P12MPP** (dotted line) in THF. The spectra were measured with the excitation of the Soret peak where the absorbance was adjusted to be identical.

2.3. Assembly of porphyrin MPPs and C₆₀ composite clusters in mixed solvents

Figure 6 shows visible-near infrared (IR) absorption spectra of a mixture of porphyrin MPPs and C₆₀ in toluene. CT absorption is seen in the absorption spectra of a mixture of **H₂PnMPP** ($n = 12, 24$) and C₆₀ (spectrum a) relative to the superposition of the component spectra (spectrum d, dotted line). Such CT absorption does not appear in a mixture of porphyrin reference **1** and C₆₀ in toluene (Fig. 6C(a)). The broad absorption in the visible and near IR regions is characteristic of π -complex formed between porphyrins and fullerenes.^{22b,d-f} Similar CT interactions leading to such an extended absorption have been observed for porphyrin-C₆₀ dyads linked at close proximity.^{22b,d-f} Thus, we can control the three-dimensional array of porphyrins and C₆₀ molecules by using gold nanoparticles. It is interesting to note that the CT absorption of **H₂P24MPP** and C₆₀ composite is weaker than that of **H₂P12MPP** and C₆₀ composite. This indicates that the spacer in **H₂P24MPP** is too long and flexible to incorporate C₆₀ molecules efficiently into the host cavity (vide infra).

Absorption spectra of a mixture of **H₂PnMPP** ($n = 12, 24$) and C₆₀ in acetonitrile–toluene (1/2, v/v) are compared with superpositions of the absorption spectra of **H₂PnMPP** ($n = 12, 24$) and C₆₀ in toluene, as shown in Figure 7. The absorption spectra of the mixture of **H₂PnMPP** ($n = 12, 24$) and C₆₀ in acetonitrile–toluene (1/2, v/v) exhibit broader absorption in the visible and near IR regions than those of

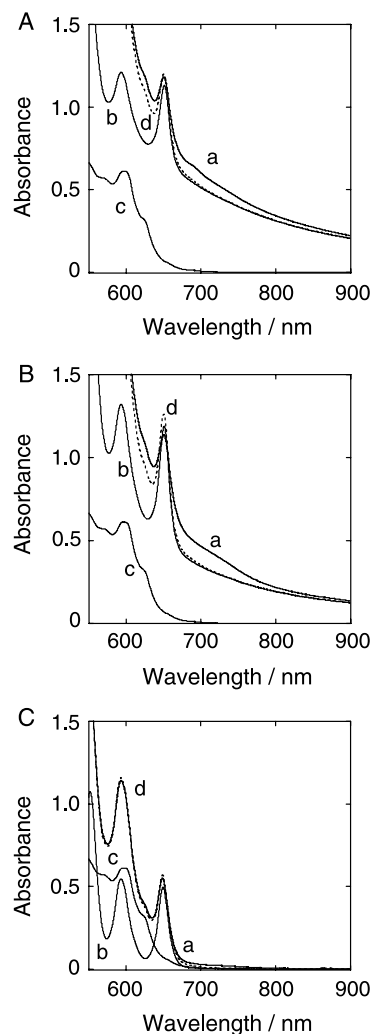


Figure 6. (A) Visible-near infrared absorption spectra of (a) a mixture of **H₂P24MPP** and C₆₀ ([H₂P]=0.13 mM, [C₆₀]=0.76 mM), (b) **H₂P24MPP** ([H₂P]=0.13 mM), (c) C₆₀ ([C₆₀]=0.76 mM), and (d) a superposition of the spectra of (b) and (c) (dotted line) in toluene. (B) Visible-near infrared absorption spectra of (a) a mixture of **H₂P12MPP** and C₆₀ ([H₂P]=0.13 mM, [C₆₀]=0.76 mM), (b) **H₂P12MPP** ([H₂P]=0.13 mM), (c) C₆₀ ([C₆₀]=0.76 mM), and (d) a superposition of the spectra of (b) and (c) (dotted line) in toluene. (C) Visible-near infrared absorption spectra of (a) a mixture of **1** and C₆₀ ([H₂P]=0.13 mM, [C₆₀]=0.76 mM), (b) **1** ([H₂P]=0.13 mM), (c) C₆₀ ([C₆₀]=0.76 mM), and (d) a superposition of the spectra of (b) and (c) in toluene (dotted line).

the respective superposition of the absorption spectra of **H₂P24MPP** and C₆₀ and **H₂P12MPP** and C₆₀ in toluene. This demonstrates the formation of composite clusters in the mixed solvent [denoted as (**H₂P24MPP** + C₆₀)_m and (**H₂P12MPP** + C₆₀)_m].^{23,30} It should be emphasized here that the Soret band of (**H₂P12MPP** + C₆₀)_m is significantly red-shifted relative to that in the superposition of the absorption spectra of **H₂P12MPP** and C₆₀ in toluene, whereas the Soret band of (**H₂P24MPP** + C₆₀)_m remains in the same position in comparison with the reference system. This demonstrates that **H₂P12MPP** can incorporate C₆₀ molecules more effectively than **H₂P24MPP** as a result of suitable spacer length in **H₂P12MPP** for the binding of C₆₀ molecules (vide supra).

Steady-state fluorescence spectra were measured for the mixture of porphyrin MPPs and C₆₀ in toluene and

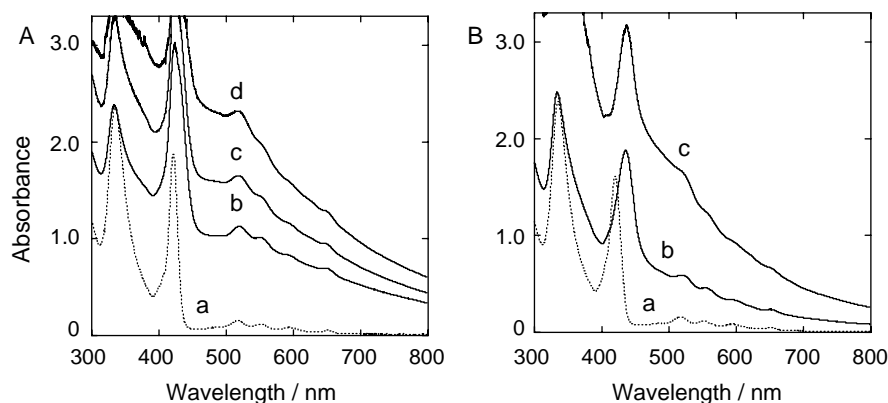


Figure 7. (A) (a) A superposition of UV-vis absorption spectra of **H₂P24MPP** and C₆₀ ([H₂P]=5.0 μM, [C₆₀]=40 μM; [H₂P]/[C₆₀]=1:8) in toluene (dotted line) and UV-vis absorption spectra of (**H₂P24MPP**+C₆₀)_m (b) ([H₂P]=0.13 mM, [C₆₀]=0.50 mM; [H₂P]/[C₆₀]=1:4), (c) ([H₂P]=0.13 mM, [C₆₀]=0.75 mM; [H₂P]/[C₆₀]=1:6), and (d) ([H₂P]=0.13 mM, [C₆₀]=1.00 mM; [H₂P]/[C₆₀]=1:8) in acetonitrile-toluene (1/2, v/v, solid line). (B) (a) A superposition of UV-vis absorption spectra of **H₂P12MPP** and C₆₀ ([H₂P]=5.0 μM, [C₆₀]=40 μM; [H₂P]/[C₆₀]=1:8) in toluene (dotted line) and UV-vis absorption spectra of (**H₂P12MPP**+C₆₀)_m (b) ([H₂P]=0.13 mM, [C₆₀]=0.50 mM; [H₂P]/[C₆₀]=1:4) and (c) ([H₂P]=0.13 mM, [C₆₀]=1.00 mM; [H₂P]/[C₆₀]=1:8) in acetonitrile-toluene (1/2, v/v, solid line).

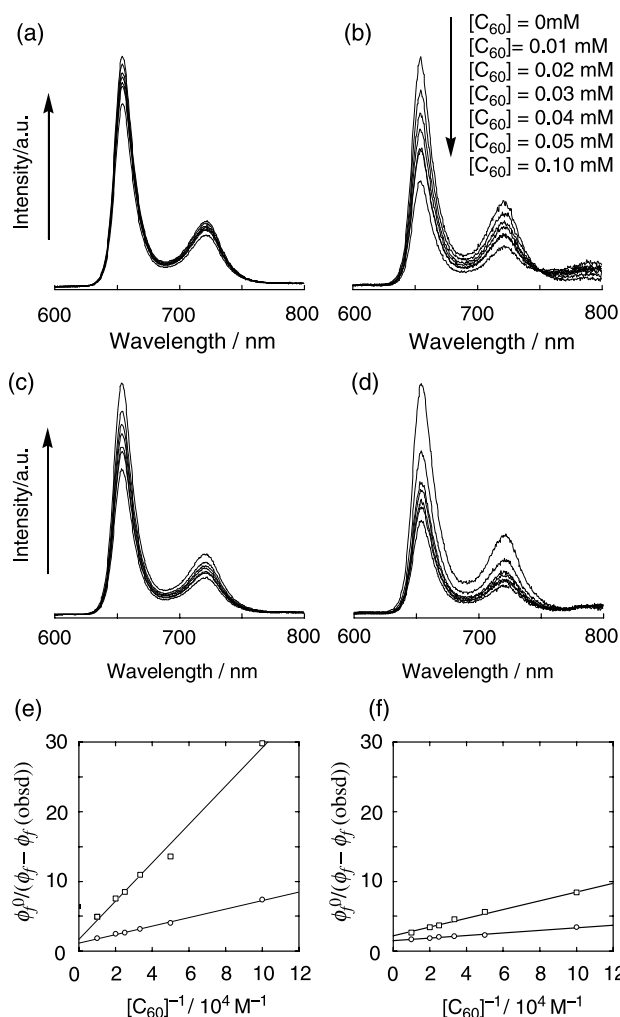
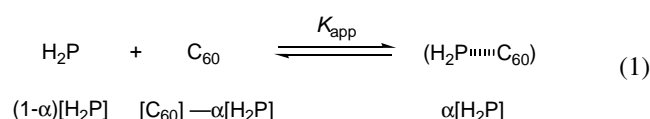


Figure 8. Steady-state fluorescence spectra of (a) **H₂P24MPP** and (b) **H₂P12MPP** in toluene and (c) **H₂P24MPP**, and (d) **H₂P12MPP** in acetonitrile-toluene=1/2 (v/v) at various concentrations of C₆₀ ([H₂P]=5.0 μM, [C₆₀]=0–0.10 mM, λ_{ex}=435 nm). Dependence of $\phi_f^0/(\phi_f - \phi_f(\text{obsd}))$ on the reciprocal concentration of C₆₀ for (e) **H₂P24MPP** (solid line with square circles) and **H₂P12MPP** (solid line with open circles) in toluene and (f) **H₂P24MPP** (solid line with square circles) and **H₂P12MPP** (solid line with open circles) in acetonitrile/toluene=1:2 (v/v).

acetonitrile/toluene ([H₂P]=5 μM, [C₆₀]=0–0.10 mM, λ_{ex}=435 nm), as shown in Figure 8a–d. Weak CT emission due to the π-complexation between the porphyrin and C₆₀ molecules is seen around 800 nm²² only for the mixture of **H₂P12MPP** and C₆₀ in toluene (Fig. 8b), which is consistent with the observation of relatively strong CT absorption in a mixture of **H₂P12MPP** and C₆₀ in toluene. Assuming the apparent 1:1 complexation of porphyrin and C₆₀, the apparent association constants for the formation of supramolecular complexes between porphyrin MPPs and C₆₀ molecules (Eq. 1) in toluene and mixed solvent (acetonitrile/toluene=1:2) are determined by the analysis of the fluorescence quenching of porphyrin MPPs by C₆₀ in order to estimate the degree of accommodation of C₆₀ into the porphyrin MPPs.²³ Under the experimental conditions, the fluorescence quenching of porphyrin reference **1** by C₆₀ is negligible. On the other hand, in the case of **H₂P24MPP** and **H₂P12MPP** in both toluene and the mixed solvent, the fluorescence from the porphyrin moiety decreases with increasing C₆₀ concentration.



where α is the degree of association between H₂P and C₆₀.

The observed fluorescence quantum yield ($\phi_f(\text{obsd})$) of H₂P in solution can be related to the fluorescence yields of uncomplexed (ϕ_f^0) and complexed (ϕ_f') molecules of H₂P by the following equation (Eq. 2),

$$\phi_f(\text{obsd}) = (1-\alpha)\phi_f^0 + \alpha\phi_f' \quad (2)$$

Eq. 2 can be simplified to the form:

$$\phi_f^0 - \phi_f(\text{obsd}) = \alpha\phi_f^0 - \phi_f' \quad (3)$$

At relatively high concentrations of $[\text{C}_{60}] \gg [\text{H}_2\text{P}]$, α is given by:

$$\alpha = \frac{K_{\text{app}}[\text{C}_{60}]}{1 + K_{\text{app}}[\text{C}_{60}]} \quad (4)$$

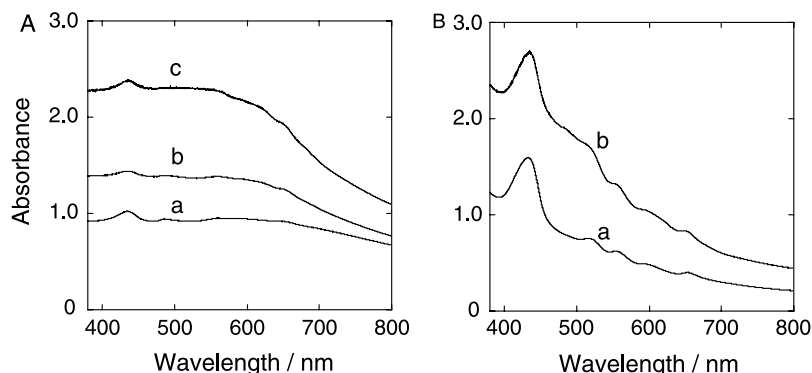


Figure 9. (A) Absorption spectra of ITO/SnO₂/(H₂P24MPP + C₆₀)_m (a) ([H₂P]=0.13 mM, [C₆₀]=0.50 mM; [H₂P]/[C₆₀]=1:4), (b) ([H₂P]=0.13 mM, [C₆₀]=0.75 mM; [H₂P]/[C₆₀]=1:6), and (c) ([H₂P]=0.13 mM, [C₆₀]=1.00 mM; [H₂P]/[C₆₀]=1:8). (B) Absorption spectra of ITO/SnO₂/(H₂P12MPP + C₆₀)_m (a) ([H₂P]=0.13 mM, [C₆₀]=0.50 mM; [H₂P]/[C₆₀]=1:4) and (b) ([H₂P]=0.13 mM, [C₆₀]=1.00 mM; [H₂P]/[C₆₀]=1:8).

From Eqs. 3 and 4, we obtain the following relation (Eq. 5). By using Eq. 5, a linear dependence of $1/(\phi_f^0 - \phi_f(\text{obsd}))$ on $[C_{60}]^{-1}$ is obtained.

$$\frac{1}{\phi_f^0 - \phi_f(\text{obsd})} = \frac{1}{\phi_f^0 - \phi_f'} + \frac{1}{K_{\text{app}}(\phi_f^0 - \phi_f')[C_{60}]} \quad (5)$$

The K_{app} values of H₂P24MPP and H₂P12MPP determined from the double reciprocal plots are 6.0×10^3 and $1.9 \times 10^4 \text{ M}^{-1}$ in toluene and 3.4×10^4 and $7.7 \times 10^4 \text{ M}^{-1}$ in the mixed solvent (acetonitrile/toluene=1:2), respectively (Fig. 8e and f). The K_{app} values in the mixed solvent are larger than those in toluene. Strong lyophobic interaction between the porphyrin and C₆₀ molecules is responsible for the high complexation between the porphyrin MPPs and C₆₀ molecules in the mixed solvent. It should be noted here that the K_{app} values of H₂P24MPP are significantly smaller than those of H₂P12MPP in both toluene and the mixed solvent. This also supports that H₂P24MPP has small binding property for C₆₀ molecules relative to H₂P12MPP due to the long, flexible spacer (vide supra).

2.4. Electrophoretic deposition

As shown earlier,²³ clusters of porphyrin and C₆₀ prepared in acetonitrile/toluene mixed solvent can be assembled electrophoretically as thin films onto a nanostructured SnO₂ electrode surface on an ITO electrode (denoted as ITO/SnO₂). Upon application of a DC electric field of 200 V between

the ITO/SnO₂ and ITO electrodes, which are immersed together in a mixed acetonitrile–toluene (1/2, v/v) solution containing (H₂P24MPP + C₆₀)_m or (H₂P12MPP + C₆₀)_m clusters, the mixed clusters are deposited on the SnO₂ nanocrystallites [denoted as ITO/SnO₂/(H₂PnMPP + C₆₀)_m ($n=12, 24$)]. As the deposition continues, the discoloration of the solution is observed, accompanied by concomitant coloration of the electrode that is connected to positive terminal of a DC power supply.

Absorption spectra of ITO/SnO₂/(H₂PnMPP + C₆₀)_m ($n=12, 24$) electrodes prepared using the mixed clusters (H₂PnMPP + C₆₀)_m ($n=12, 24$) in acetonitrile–toluene (1/2, v/v) are shown in Figure 9. The light-harvesting capability of ITO/SnO₂/(H₂PnMPP + C₆₀)_m ($n=12, 24$; spectra a–c) is high in the near infrared region as well as the UV–vis region. Absorption spectra of ITO/SnO₂/(H₂PnMPP + C₆₀)_m ($n=12, 24$) largely reflect those of (H₂PnMPP + C₆₀)_m ($n=12, 24$) in acetonitrile/toluene=1:2, indicating that the cluster solution is effectively deposited on ITO/SnO₂.

The AFM images of ITO/SnO₂/(H₂P24MPP + C₆₀)_m and ITO/SnO₂/(H₂P12MPP + C₆₀)_m reveal the aggregation of the clusters with 100–300 nm size as shown in Figure 10. These results also suggest that the electrophoretic deposition of (H₂PnMPP + C₆₀)_m ($n=12, 24$) leads to the association of clusters on nanostructured SnO₂ electrodes growing into larger ones.²³

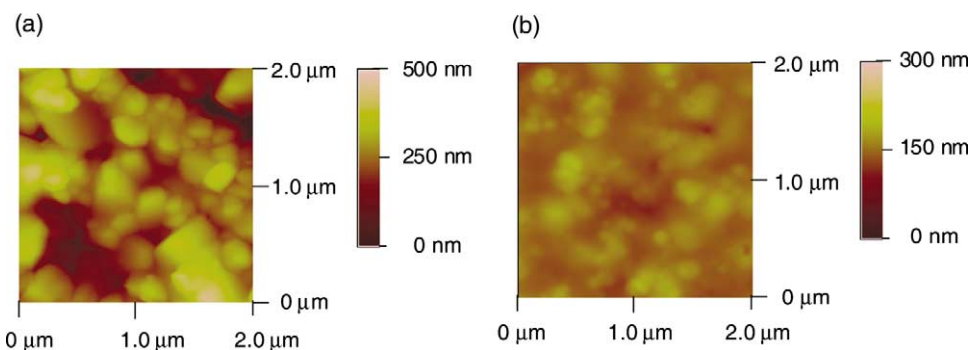


Figure 10. AFM images of (a) ITO/SnO₂/(H₂P24MPP + C₆₀)_m ([H₂P]=0.13 mM, [C₆₀]=1.00 mM; [H₂P]/[C₆₀]=1:8) and (b) ITO/SnO₂/(H₂P12MPP + C₆₀)_m ([H₂P]=0.13 mM, [C₆₀]=0.50 mM; [H₂P]/[C₆₀]=1:4).

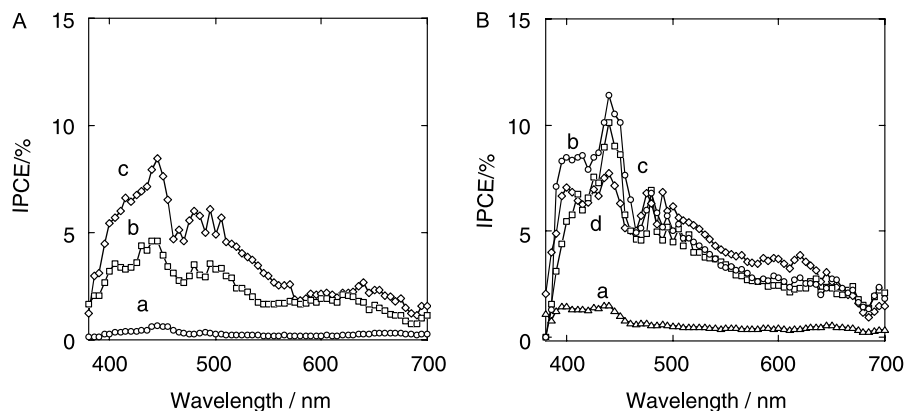


Figure 11. The photocurrent action spectra (IPCE vs wavelength) of (A) ITO/SnO₂/(H₂P24MPP + C₆₀)_m and (B) ITO/SnO₂/(H₂P12MPP + C₆₀)_m. Potential: +0.06 V versus SCE; Electrolyte: 0.5 M LiI and 0.01 M I₂. (A) [H₂P] = 0.13 mM, (a) [C₆₀] = 0.50 mM (circle), (b) [C₆₀] = 0.75 mM (square), and (c) [C₆₀] = 1.00 mM (diamond). (B) [H₂P] = 0.13 mM, (a) [C₆₀] = 0.25 mM (upper triangle), (b) [C₆₀] = 0.50 mM (circle), (c) [C₆₀] = 0.75 mM (square), and (d) [C₆₀] = 1.00 mM (diamond) in acetonitrile/toluene = 1:2 (v/v).

2.5. Comparison of photoelectrochemical properties

To evaluate the photoelectrochemical performance of the (H₂P_nMPP + C₆₀)_m (*n* = 12, 24) films, we used ITO/SnO₂/(H₂P_nMPP + C₆₀)_m electrode as a working electrode, a Pt wire counter electrode, and a Ag/AgNO₃ reference electrode containing 0.5 M LiI and 0.01 M I₂ in acetonitrile as the electrolyte in a photoelectrochemical device. Photocurrent action spectra of ITO/SnO₂/(H₂P_nMPP + C₆₀)_m (*n* = 12, 24) devices with various C₆₀ concentrations are shown in Figure 11. The overall photoelectrochemical response of ITO/SnO₂/(H₂P_nMPP + C₆₀)_m (*n* = 12, 24) parallels the broad absorption spectral features, indicating the involvement of both H₂P_nMPP and C₆₀ in the photocurrent generation. The IPCE values of ITO/SnO₂/(H₂P24MPP + C₆₀)_m exhibit a monotonous increase with increasing the relative ratio of C₆₀ to reach the maximum IPCE of 8.5% at 445 nm with the ratio of [H₂P]/[C₆₀] = 1:8 in the mixed solvent (Fig. 11A). In contrast, with increasing the relative ratio of C₆₀, the IPCE values of ITO/SnO₂/(H₂P12MPP + C₆₀)_m device initially increase and exhibit 11% as a maximum at 440 nm with the ratio of [H₂P]/[C₆₀] = 1:4 and become constant under the same experimental conditions (Fig. 11B). The spacer between the porphyrin and the gold core in H₂P24MPP is long and flexible so that efficient supramolecular complexation between the porphyrin and C₆₀ molecules is rather inhibited. This may explain the comparable IPCE values in the two photoelectrochemical devices irrespective of the large difference in the spacer length between the porphyrin and the gold nanoparticle.

Considering the well-established photodynamics of porphyrin-fullerene systems,^{13–16} the porphyrin excited singlet state may be quenched by C₆₀ via electron transfer or partial charge transfer in the supramolecular porphyrin-C₆₀ complex rather than by gold nanocluster via energy transfer. Thus, photocurrent generation in the present system is initiated by ultrafast charge separation or partial charge transfer from the porphyrin excited singlet state (¹H₂P*/H₂P⁺ = -0.7 V vs NHE)²³ to C₆₀ (C₆₀/C₆₀⁻ = -0.2 V vs NHE)²³ in the supramolecular complex rather than direct electron injection to conduction band of SnO₂ (0 V vs NHE)²³ system. The resultant

reduced C₆₀ injects electrons into the SnO₂ nanocrystallites, whereas the oxidized porphyrin (H₂P/H₂P⁺ = 1.2 V vs NHE)²³ undergoes the electron transfer reduction with the iodide (I₃⁻/I⁻ = 0.5 V vs NHE)²³ in the electrolyte system.

3. Conclusions

In summary, we have examined the structure and photoelectrochemical properties of nanostructured SnO₂ electrodes deposited electrophoretically with the composite clusters of porphyrin MPP with the long spacer and C₆₀ molecules. This system exhibits comparable photoresponse in the UV–vis regions and IPCE values relative to the porphyrin MPP and C₆₀ reference system with the relatively short spacer. The design of pre-organized nanostructured porphyrins with a suitable spacer to incorporate C₆₀ molecules efficiently between the porphyrins will be necessary for improving the performance of porphyrin and fullerene-based organic solar cells.

4. Experimental

4.1. General methods

Melting points were recorded on a Yanagimoto micro-melting point apparatus and are not corrected. ¹H and ¹³C NMR spectra were measured on a JEOL EX-270 (270 MHz) or a JEOL JMN-AL300 (300 MHz). Matrix-assisted laser desorption/ionization (MALDI) time-of-flight mass spectra (TOF) were measured on a Shimadzu KOMPACT MALDI II. FAB mass spectra were measured on a JEOL JMS-HS100 spectrometer using 3-nitrobenzyl alcohol as a matrix. Elemental analyses were performed at the Microanalytical Laboratory of Kyoto University. UV–vis–near IR absorption spectra were recorded using a Lambda 900 spectrophotometer (Perkin Elmer, USA). Steady-state fluorescence spectra were acquired on a SPEX FluoroMAX-3 spectrometer. Transmission electron micrographs (TEM) of the clusters were recorded by applying a drop of the sample to carbon-coated copper grid. Images were recorded using a JEOL JEM-200CX

transmission electron microscope. AFM measurements were carried out using a Digital Nanoscope III in the tapping mode.

4.2. Materials

All solvents and chemicals were of reagent grade quality, obtained commercially and used without further purification unless otherwise noted (*vide infra*). HAuCl₄ (99.999%) and tetraoctylammonium bromide (98%) were purchased from Aldrich. Tetrabutylammonium hexafluorophosphate (*n*-Bu₄NPF₆) used as a supporting electrolyte for the electrochemical measurements was obtained from Tokyo Kasei Organic Chemicals. THF was purchased from Wako Pure Chemical Ind., Ltd, and purified by successive distillation over sodium benzophenone ketyl before use. Thin-layer chromatography (TLC) and flash column chromatography were performed with 25 DC-Alufolien Aluminiumoxid 60 F₂₅₄ Neutral (Merck) and Silica gel 60N (Kanto Chemicals), respectively.

4.3. Synthesis

The compounds used in this study were prepared according to the literature.^{11,24–27}

4.3.1. 5-(4-Methoxyphenyl)-10,15,20-tris(3,5-di-*tert*-butylphenyl)porphyrin (1). 3,5-Di-*tert*-butylbenzaldehyde (3.49 g, 18 mmol), 4-methoxybenzaldehyde (0.73 g, 6 mmol), pyrrole (1.59 g, 24 mmol) and borontrifluoride ethylether complex (0.32 μ L) were added to 800 mL of chloroform, which was degassed by bubbling with Ar for 1 h before the addition. The reaction vessel was shielded from ambient light. After stirring for 1 h, 2,3,5,6-tetrachloro-1,4-benzoquinone (5.92 mmol, 24 mmol) was added to the reddish black reaction mixture, and then, the resulting mixture was stirred for 1 h. After 1.0 mL of triethylamine was added, the reaction mixture was passed through a short column of activated alumina. Flash column chromatography on silica gel with dichloromethane/hexane = 1:1 (v/v) as the eluent afforded the products, which were washed with methanol and dried to give **1** as a purple red solid (1.02 g, 1.1 mmol, 18%). Mp > 300 °C; ¹H NMR (CDCl₃) δ 8.90 (s, 4H), 8.87 (s, 4H), 8.15 (d, *J* = 8.4 Hz, 2H), 8.09 (d, *J* = 2 Hz, 4H), 8.07 (d, *J* = 2 Hz, 2H), 7.90 (m, 3H), 7.29 (d, *J* = 8.4 Hz, 2H), 4.10 (s, 3H), 1.52–1.55 (m, 54H), –2.70 (s, 2H); MALDI-TOF-MS *m/z* 982 (M + H⁺). Anal. Found: C, 84.42; H, 8.18; N, 5.65. Calcd for: C₆₉H₈₀N₄O: C, 84.44; H, 8.22; N, 5.71.

4.3.2. 5-(4-Hydroxyphenyl)-10,15,20-tris(3,5-di-*tert*-butylphenyl)porphyrin (2). Porphyrin **1** (1.04 g, 1.05 mmol) was dissolved in dry CH₂Cl₂ (13 mL) at –78 °C (dry ice–acetone bath), followed by the addition of BBr₃ (1.4 μ L, 10 mmol) under Ar. The resulting green solution was vigorously stirred for 12 h, then cautiously, water was added to the suspension and the mixture was washed with 0.1 M HCl aqueous solution, and neutralized with saturated NaHCO₃ aqueous solution. The organic layer was separated and dried over anhydrous Na₂SO₄. The solution was removed and reprecipitated with dichloromethane/methanol to yield **2** as a purple red solid (944 mg, 0.98 mmol, 93%).²⁶

4.3.3. 1,4-Bis(12-bromododecyloxy)benzene (3a). 1,4-Hydroquinone (1.1 g, 10 mmol) and 1,12-dibromododecane

(16.4 g, 50 mmol) were dissolved in hot ethanol (50 mL). Then, anhydrous potassium carbonate (2.9 g, 20 mmol) was added under reflux and stirred for 2 h. The reaction mixture was extracted with CH₂Cl₂, and washed with saturated NaCl aqueous solution. The organic layer was dried with Na₂SO₄ and removed under reduced pressure. The reprecipitation from dichloromethane/methanol gave **3a** as a white solid (2.8 g, 4.7 mmol, 47%). Mp = 86–87 °C; ¹H NMR (CDCl₃) δ 6.82 (s, 4H), 3.89 (t, *J* = 6.8 Hz, 4H), 3.41 (t, *J* = 6.8 Hz, 4H), 1.85 (quintet, *J* = 6.8 Hz, 4H), 1.75 (quintet, *J* = 6.8 Hz, 4H), 1.42 (m, 8H), 1.28 (m, 24H); ¹³C NMR (CDCl₃) δ 26.02, 28.14, 28.73, 29.36, 29.39, 29.47, 29.48, 29.51, 32.79, 34.05, 68.54, 115.21, 152.97; FAB-MS *m/z* 604.3 (M + H⁺). Anal. Found: C, 8.65; H, 59.14; Br, 26.44. Calcd for C₃₀H₅₂O₂Br₂: C, 8.67; H, 59.60; Br, 26.43.

4.3.4. Compound 4a. Porphyrin **2** (485 mg, 0.50 mmol), **3a** (604 mg, 1.0 mmol), and potassium carbonate anhydrous (140 mg, 1 mmol) were dissolved in DMF (40 mL), then the mixture was warmed up to 90 °C for 1.5 h. After cooling the solution, the mixture was extracted with CH₂Cl₂ and washed with water. The organic layer was dried over anhydrous Na₂SO₄. The solution was removed and then purified by flash column chromatography (CH₂Cl₂) and high-performance liquid chromatography (JAIGEL-3H, 4H, CHCl₃). Reprecipitation from dichloromethane/methanol gave **4a** as a purple red solid (310 mg, 0.21 mmol, 42%). Mp > 300 °C; ¹H NMR (CDCl₃) δ 8.89 (s, 4H), 8.88 (s, 4H), 8.13 (d, *J* = 8.8 Hz, 2H), 8.09 (d, *J* = 2 Hz, 4H), 8.08 (d, *J* = 2 Hz, 2H), 7.79 (m, 3H), 7.27 (d, *J* = 8.8 Hz, 2H), 6.81 (s, 4H), 4.25 (t, *J* = 6.8 Hz, 2H), 3.90 (t, *J* = 6.4 Hz, 2H), 3.87 (t, *J* = 6.4 Hz, 2H), 3.40 (t, *J* = 6.8 Hz, 2H), 1.98 (quintet, *J* = 7.2 Hz, 2H), 1.2–1.9 (m, 92H), –2.69 (s, 2H); FAB-MS *m/z* 1491.0 (M + H⁺). Anal. Found: C, 8.76; H, 78.78; N, 3.76. Calcd for: C₉₈H₁₂₉BrN₄O₃: C, 8.72; H, 78.94; N, 3.76.

4.3.5. Compound 4b. Porphyrin **2** (484 mg, 0.50 mmol), 1,12-dibromododecane **3b** (820 mg, 2.5 mmol), and potassium carbonate anhydrous (346 mg, 2.5 mmol) were dissolved in 40 mL of DMF and the mixture was warmed up to reflux for 2 h. After cooling, the mixture was extracted with CH₂Cl₂ and washed with water. The organic layer was dried with anhydrous Na₂SO₄. The solvent was removed under reduced pressure. Flash column chromatography on silica gel and subsequent reprecipitation from dichloromethane/methanol gave **4b** as a purple red solid (422 mg, 0.35 mmol, 69%). Mp > 300 °C; ¹H NMR (CDCl₃) δ 8.89 (s, 4H), 8.88 (s, 4H), 8.13 (d, *J* = 8.4 Hz, 2H), 8.08 (d, *J* = 2 Hz, 4H), 8.07 (d, *J* = 2 Hz, 2H), 7.79 (m, 3H), 7.27 (d, *J* = 8.4 Hz, 2H), 4.25 (t, *J* = 6.4 Hz, 2H), 3.42 (t, *J* = 6.8 Hz, 2H), 1.99 (quintet, *J* = 7.2 Hz, 2H), 1.87 (quintet, *J* = 7.2 Hz, 2H), 1.7–1.2 (m, 70H), –2.70 (s, 2H); FAB-MS *m/z* 1214.8 (M + H⁺). Anal. Found: C, 7.91; H, 79.61; N, 4.56. Calcd for C₈₀H₁₀₁BrN₄O: C, 8.38; H, 79.11; N, 4.61.

4.3.6. Compounds 5a and 5b. A solution of **4a** (280 mg, 0.19 mmol) and potassium thioacetate (123 mg, 1.1 mmol) in ethanol–THF (1/1 = v/v 20 mL) was heated to reflux for 2 h. The solvent was removed under reduced pressure and the residue was added to a small amount of dichloromethane. The organic layer was washed with water and saturated sodium chloride solution, and dried over anhydrous sodium sulfate. After filtration, dichloromethane was

removed on a rotary evaporator, and flush column chromatography on silica gel (neutral) with dichloromethane/methanol and subsequent reprecipitation from dichloromethane/methanol gave **5a** as a purple red solid (241 mg, 0.16 mmol, 87%).

Compound **5a**. Mp > 300 °C; ¹H NMR (CDCl₃) δ 8.89 (s, 4H), 8.88 (s, 4H), 8.13 (d, *J* = 8.8 Hz, 2H), 8.08 (d, *J* = 2 Hz, 4H), 8.07 (d, *J* = 2 Hz, 2H), 7.79 (m, 3H), 7.27 (d, *J* = 8.8 Hz, 2H), 6.81 (s, 4H), 4.25 (t, *J* = 6.4 Hz, 2H), 3.90 (t, *J* = 6.4 Hz, 2H), 3.87 (t, *J* = 6.4 Hz, 2H), 2.85 (t, *J* = 7.6 Hz, 2H), 2.31 (s, 3H), 1.98 (quintet, *J* = 7.2 Hz, 2H), 1.75 (m, 4H), 1.3–1.7 (m, 88H), –2.69 (s, 2H); FAB-MS *m/z* 1487.1 (M+H⁺). Anal. Found: C, 8.84; H, 80.51; N, 3.67. Calcd for C₁₀₀H₁₃₂N₄O₄S: C, 8.95; H, 80.81; N, 3.77.

Compound **5b**. Mp > 300 °C; ¹H NMR (CDCl₃) δ 8.90 (s, 4H), 8.89 (s, 4H), 8.30 (d, *J* = 8.4 Hz, 2H), 8.09 (d, *J* = 2 Hz, 4H), 8.08 (d, *J* = 2 Hz, 2H), 7.79 (m, 3H), 7.27 (d, *J* = 8.4 Hz, 2H), 4.24 (t, *J* = 6.4 Hz, 2H), 2.87 (t, *J* = 7.6 Hz, 2H), 2.31 (s, 3H), 1.98 (quintet, *J* = 7.2 Hz, 2H), 1.3–1.7 (m, 72H), –2.69 (s, 2H); FAB-MS *m/z* 1209.9 (M+H⁺). Anal. Found: C, 8.04; H, 80.71; N, 4.33. Calcd for C₈₂H₁₀₄N₄O₂S: C, 8.66; H, 81.41; N, 4.63.

4.3.7. Compounds 6a and 6b. A solution of **5a** (464 mg, 0.31 mmol) and KOH (158 mg, 2.8 mmol) in methanol–THF (7/3 = v/v, 100 mL) was refluxed under Ar in the dark for 10 min. After cooling, the mixture was poured onto brine and extracted with toluene. The extract was dried over anhydrous Na₂SO₄, and the solvent was removed under reduced pressure to give **6a** as a purple red solid (352 mg, 0.24 mmol, 78%).

Compound **6a**. Mp > 300 °C; ¹H NMR (CDCl₃) δ 8.89 (s, 8H), 8.88 (s, 8H), 8.12 (d, *J* = 8.8 Hz, 4H), 8.08 (d, *J* = 2 Hz, 8H), 8.07 (d, *J* = 2 Hz, 4H), 7.78 (m, 6H), 7.27 (d, *J* = 8.8 Hz, 4H), 6.80 (s, 8H), 4.24 (t, *J* = 6.4 Hz, 4H), 3.89 (t, *J* = 6.4 Hz, 4H), 3.86 (t, *J* = 6.4 Hz, 4H), 2.66 (t, *J* = 7.6 Hz, 4H), 1.98 (quintet, *J* = 7.2 Hz, 4H), 1.7–1.8 (m, 8H), 1.6–1.7 (m, 8H), 1.2–1.6 (m, 168H), –2.70 (s, 4H); MALDI-TOF-MS *m/z* 2886 (M+H⁺). Anal. Found: C, 8.95; H, 81.48; N, 3.91. Calcd for C₁₉₆H₂₅₈N₈O₆S₂: C, 9.01; H, 81.56; N, 3.88.

Compound **6b**. Mp > 300 °C; ¹H NMR (CDCl₃) δ 8.90 (s, 8H), 8.89 (s, 8H), 8.12 (d, *J* = 8.4 Hz, 4H), 8.08 (d, *J* = 2 Hz, 8H), 8.07 (d, *J* = 2 Hz, 4H), 7.79 (m, 6H), 7.26 (d, *J* = 8.4 Hz, 4H), 4.25 (t, *J* = 6.8 Hz, 4H), 2.69 (t, *J* = 7.4 Hz, 4H), 1.98 (quintet, *J* = 7.0 Hz, 4H), 1.7–1.3 (m, 144H), –2.70 (s, 4H); MALDI-TOF-MS *m/z* 2332 (M+H⁺). Anal. Found: C, 8.60; H, 81.72; N, 4.91. Calcd for C₁₆₀H₂₀₂N₈O₂S₂: C, 8.73; H, 82.35; N, 4.80.

4.3.8. H₂P24MPP and H₂P12MPP. Compound **6** (180 mg) was dissolved in a mixture of HAuCl₄ (11.5 mM) and tetraoctylammonium bromide (19.2 mM) in toluene (11 mL). With vigorous stirring to the resultant solution was added 7 mL of sodium borohydride aqueous solution (0.55 M). After further stirring for 24 h, the organic phase was separated and washed with water. The extract was dried over anhydrous Na₂SO₄, the solvent was removed under reduced pressure. The residue was purified by gel permeation chromatography (Bio-beads S-X1 200–400

mesh, toluene) and high performance liquid chromatography (JAIGEL-3H,4H, CHCl₃), and reprecipitated from hexane/2-propanol to give **H₂PnMPP** as a purple red solid (34 mg (*n* = 12), 55 mg (*n* = 24)).

H₂P24MPP. Mp > 300 °C. Anal. Found: C, 59.89; H, 6.63; N, 2.57. Calcd for (C₉₈H₁₂₉N₄O₃S)₁₅₅Au₄₂₀: C, 59.53; H, 6.59; N, 2.83.

H₂P12MPP. Mp > 300 °C. Anal. Found: C, 49.18; H, 5.07; N, 2.85. Calcd for (C₈₀H₁₀₁N₄OS)₈₀Au₃₂₃: C, 48.97; H, 5.20; N, 2.86.

4.4. Preparation of clusters and their deposition onto the ITO/SnO₂ electrode

H₂P24MPP, **H₂P12MPP** and C₆₀ are readily soluble in nonpolar solvent such as toluene. In mixed solvents, however, they aggregate and form larger clusters. Nanostructured SnO₂ films were cast on an optically transparent indium–tin oxide (ITO) electrode by applying a dilute (1.5%) colloidal solution (Chemat) and annealing the dried film at 673 K. These films are highly porous and are electrochemically active to conduct charges across the film. The SnO₂ film electrode (ITO/SnO₂) and an ITO plate were introduced in a 1 cm path length cuvette and were connected to positive and negative terminals of the power supply, respectively. A known amount (~1.5 mL) of the cluster solution in acetonitrile–toluene (1/2, v/v) was transferred to the cuvette in which the two electrodes (viz, ITO/SnO₂ and ITO) were kept at a distance of ~6 mm using Teflon spacer. A DC voltage (200 V) was applied between these two electrodes using ATTO AE-8750 power supply. The deposition of the film can be visibly seen as the solution becomes colorless with simultaneous coloration of the ITO/SnO₂ electrode.

4.5. Photoelectrochemical measurements

The photoelectrochemical measurements were performed in a one-compartment Pyrex UV cell (5 mL) with a standard three electrodes arrangement consisting of a working electrode, a Pt wire counter electrode, and a Ag/AgNO₃ reference electrode containing 0.5 M LiI and 0.01 M I₂ in acetonitrile as the electrolyte. Photocurrent measurements were made with an ALS 630A electrochemical analyzer. A monochromatic light through a monochromator (Ritsu MC-10N) by a 500 W xenon lamp (Ushio XB-50101AA-A) was used for excitation of the thin films cast on SnO₂ electrodes. The IPCE values were calculated by normalizing the photocurrent values for incident light energy and intensity and using the expression: IPCE (%) = 100 × 1240 × *I* / (W_{in} × λ), where *I* is the photocurrent, W_{in} is the incident light intensity, and λ is the excitation wavelength.

Acknowledgements

This work was supported by Grant-in-Aid (No. 16310073 to H.I.) from MEXT, Japan. H.I. also thanks Grant-in-Aid from MEXT, Japan (21st Century COE on Kyoto University Alliance for Chemistry) for financial support. A part of this work was supported by ‘Nanotechnology Support Project’

of the Ministry of Education, Culture, Sports, Science and Technology (MEXT), Japan.

References and notes

- (a) Hagfeldt, A.; Grätzel, M. *Acc. Chem. Res.* **2000**, *33*, 269. (b) Grätzel, M. *Nature* **2001**, *414*, 338. (c) Bignozzi, C. A.; Argazzi, R.; Kleverlaan, C. J. *Chem. Soc. Rev.* **2000**, *29*, 87.
- (a) Yu, G.; Gao, J.; Hummelen, J. C.; Wudl, F.; Heeger, A. J. *Science* **1995**, *270*, 1789. (b) Wudl, F. *J. Mater. Chem.* **2002**, *12*, 1959.
- (a) Shaheen, S. E.; Brabec, C. J.; Sariciftci, N. S.; Padinger, F.; Fromherz, T.; Hummelen, J. C. *Appl. Phys. Lett.* **2001**, *78*, 841. (b) Padinger, F.; Rittberger, R. S.; Sariciftci, N. S. *Adv. Funct. Mater.* **2003**, *13*, 85.
- (a) Schmidt-Mende, L.; Fechtenkötter, A.; Müllen, K.; Moons, E.; Friend, R. H.; MacKenzie, J. D. *Science* **2001**, *293*, 1119. (b) Halls, J. J. M.; Walsh, C. A.; Greenham, N. C.; Marseglia, E. A.; Friend, R. H.; Moratti, S. C.; Holmes, A. B. *Nature* **1995**, *376*, 498.
- (a) Granström, M.; Petritsch, K.; Arias, A. C.; Lux, A.; Andersson, M. R.; Friend, R. H. *Nature* **1998**, *395*, 257. (b) Huynh, W. U.; Dittmer, J. J.; Alivisatos, A. P. *Science* **2002**, *295*, 2425. (c) Scher, E. C.; Manna, L.; Alivisatos, A. P. *Philos. Trans. R. Soc. A* **2003**, *361*, 241. (d) Liu, J.; Tanaka, T.; Sivula, K.; Alivisatos, A. P.; Fréchet, J. M. J. *J. Am. Chem. Soc.* **2004**, *126*, 6550.
- (a) Wienk, M. M.; Kroon, J. M.; Verhees, W. J. H.; Knol, J.; Hummelen, J. C.; van Hal, P. A.; Janssen, R. A. J. *Angew. Chem., Int. Ed.* **2003**, *42*, 3371. (b) Dhanabalan, A.; van Duren, J. K. J.; van Hal, P. A.; van Dongen, J. L. J.; Janssen, R. A. J. *Adv. Funct. Mater.* **2001**, *11*, 255. (c) Peumans, P.; Uchida, S.; Forrest, S. R. *Nature* **2003**, *425*, 158.
- (a) Eckert, J.-F.; Nicoud, J.-F.; Nierengarten, J.-F.; Liu, S.-G.; Echegoyen, L.; Barigelletti, F.; Armaroli, N.; Ouali, L.; Krasnikov, V.; Hadziioannou, G. *J. Am. Chem. Soc.* **2000**, *122*, 7467. (b) Lahav, M.; Heleg-Shabtai, V.; Wasserman, J.; Katz, E.; Willner, I.; Dürr, H.; Hu, Y.-Z.; Bossmann, S. H. *J. Am. Chem. Soc.* **2000**, *122*, 11480.
- Ermler, U.; Fritsch, G.; Buchanan, S. K.; Michel, H. *Structure* **1994**, *2*, 925.
- (a) Deisenhofer, J.; Michel, H. *Science* **1989**, *245*, 1463. (b) Hoff, A. J.; Deisenhofer, J. *Phys. Rep.* **1997**, *287*, 1.
- Williams, L. C.; Taguchi, A. K. W. Genetic Manipulation of Purple Photosynthetic Bacteria. In *Anoxygenic Photosynthetic Bacteria*; Blankenship, R. E., Madigan, M. T., Bauer, C. E., Eds.; Kluwer Academic: Dordrecht, The Netherlands, 1995; p 1029.
- (a) Imahori, H.; Arimura, M.; Hanada, T.; Nishimura, Y.; Yamazaki, I.; Sakata, Y.; Fukuzumi, S. *J. Am. Chem. Soc.* **2001**, *123*, 335. (b) Imahori, H.; Kashiwagi, Y.; Endo, Y.; Hanada, T.; Nishimura, Y.; Yamazaki, I.; Araki, Y.; Ito, O.; Fukuzumi, S. *Langmuir* **2004**, *20*, 73. (c) Imahori, H.; Kashiwagi, Y.; Hanada, T.; Endo, Y.; Nishimura, Y.; Yamazaki, I.; Fukuzumi, S. *J. Mater. Chem.* **2003**, *13*, 2890. (d) Fukuzumi, S.; Endo, Y.; Kashiwagi, Y.; Araki, Y.; Ito, O.; Imahori, H. *J. Phys. Chem. B* **2003**, *107*, 11979.
- (a) Evans, D. R.; Fackler, N. L. P.; Xie, Z.; Rickard, C. E. F.; Boyd, P. D. W.; Reed, C. A. *J. Am. Chem. Soc.* **1999**, *121*, 8466. (b) Sun, D.; Tham, F. S.; Reed, C. A.; Chaker, L.; Burgess, M.; Boyd, P. D. W. *J. Am. Chem. Soc.* **2000**, *122*, 10704. (c) Nishioka, T.; Tashiro, K.; Aida, T.; Zheng, J.-Y.; Kinbara, K.; Saigo, K.; Sakamoto, S.; Yamaguchi, K. *Macromolecules* **2000**, *33*, 9182. (d) Tashiro, K.; Aida, T.; Zheng, J.-Y.; Kinbara, K.; Saigo, K.; Sakamoto, S.; Yamaguchi, K. *J. Am. Chem. Soc.* **1999**, *121*, 9477. (e) Shoji, Y.; Tashiro, K.; Aida, T. *J. Am. Chem. Soc.* **2004**, *126*, 6570.
- Gust, D.; Moore, T. A.; Moore, A. L. *Acc. Chem. Res.* **2001**, *34*, 40.
- (a) Choi, M.-S.; Aida, T.; Luo, H.; Araki, Y.; Ito, O. *Angew. Chem., Int. Ed.* **2003**, *42*, 4060. (b) Li, K.; Schuster, D. I.; Guldi, D. M.; Herranz, M. A.; Echegoyen, L. *J. Am. Chem. Soc.* **2004**, *126*, 3388. (c) D'Souza, F.; Deviprasad, G. R.; El-Khouly, M. E.; Fujitsuka, M.; Ito, O. *J. Am. Chem. Soc.* **2001**, *123*, 5277. (d) Armaroli, N.; Marconi, G.; Echegoyen, L.; Bourgeois, J.-P.; Diederich, F. *Chem. Eur. J.* **2000**, *6*, 1629. (e) D'Souza, F.; Smith, P. M.; Zandler, M. E.; McCarty, A. L.; Itou, M.; Araki, Y.; Ito, O. *J. Am. Chem. Soc.* **2004**, *126*, 7898. (f) de la Torre, G.; Giacalone, F.; Segura, J. L.; Martín, N.; Guldi, D. M. *Chem. Eur. J.* **2005**, *11*, 1267.
- (a) Fukuzumi, S.; Imahori, H. In Balzani, V., Ed.; *Electron Transfer in Chemistry*; Wiley-VCH: Weinheim, 2001; Vol. 2, pp 927–975. (b) Imahori, H.; Sakata, Y. *Eur. J. Org. Chem.* **1999**, 2445. (c) Fukuzumi, S.; Guldi, D. M. In Balzani, V., Ed.; *Electron Transfer in Chemistry*; Wiley-VCH: Weinheim, 2001; Vol. 2, pp 270–337. (d) Imahori, H. *Org. Biomol. Chem.* **2004**, *2*, 1425. (e) Imahori, H. *J. Phys. Chem. B* **2004**, *108*, 6130. (f) Imahori, H.; Fukuzumi, S. *Adv. Funct. Mater.* **2004**, *14*, 525.
- (a) Imahori, H.; Tamaki, K.; Guldi, D. M.; Luo, C.; Fujitsuka, M.; Ito, O.; Sakata, Y.; Fukuzumi, S. *J. Am. Chem. Soc.* **2001**, *123*, 2607. (b) Imahori, H.; Guldi, D. M.; Tamaki, K.; Yoshida, Y.; Luo, C.; Sakata, Y.; Fukuzumi, S. *J. Am. Chem. Soc.* **2001**, *123*, 6617.
- Diederich, F.; Gómez-López, M. *Chem. Soc. Rev.* **1999**, *28*, 263.
- (a) Boyd, P. D. W.; Hodgson, M. C.; Rickard, C. E. F.; Oliver, A. G.; Chaker, L.; Brothers, P. J.; Bolskar, R. D.; Tham, F. S.; Reed, C. A. *J. Am. Chem. Soc.* **1999**, *121*, 10487. (b) Sun, D.; Tham, F. S.; Reed, C. A.; Chaker, L.; Boyd, P. D. W. *J. Am. Chem. Soc.* **2002**, *124*, 6604.
- Sun, D.; Tham, F. S.; Reed, C. A.; Boyd, P. D. W. *Proc. Natl. Acad. Sci. U.S.A.* **2002**, *99*, 5088.
- (a) Olmstead, M. M.; Costa, D. A.; Maitra, K.; Noll, B. C.; Phillips, S. L.; Van Calcar, P. M.; Balch, A. L. *J. Am. Chem. Soc.* **1999**, *121*, 7090. (b) Olmstead, M. M.; de Bettencourt-Dias, A.; Duchamp, J. C.; Stevenson, S.; Marciu, D.; Dorn, H. C.; Balch, A. L. *Angew. Chem., Int. Ed.* **2001**, *40*, 1223.
- (a) Tashiro, K.; Aida, T.; Zheng, J.-Y.; Kinbara, K.; Saigo, K.; Sakamoto, S.; Yamaguchi, K. *J. Am. Chem. Soc.* **1999**, *121*, 9477. (b) Zheng, J.-Y.; Tashiro, K.; Hirabayashi, Y.; Kinbara, K.; Saigo, K.; Aida, T.; Sakamoto, S.; Yamaguchi, K. *Angew. Chem., Int. Ed.* **2001**, *40*, 1857. (c) Shirakawa, M.; Fujita, N.; Shinkai, S. *J. Am. Chem. Soc.* **2003**, *125*, 9902.
- (a) Guldi, D. M.; Luo, C.; Prato, M.; Troisi, A.; Zerbetto, F.; Scheloske, M.; Dietel, E.; Bauer, W.; Hirsch, A. *J. Am. Chem. Soc.* **2001**, *123*, 9166. (b) Imahori, H.; Hagiwara, K.; Aoki, M.; Akiyama, T.; Taniguchi, S.; Okada, T.; Shirakawa, M.; Sakata, Y. *J. Am. Chem. Soc.* **1996**, *118*, 11771. (c) Wang, Y.-B.; Lin, Z. *J. Am. Chem. Soc.* **2003**, *125*, 6072. (d) Imahori, H.; Tkachenko, N. V.; Vehmanen, V.; Tamaki, K.; Lemmetyinen, H.; Sakata, Y.; Fukuzumi, S. *J. Phys. Chem. A* **2001**, *105*, 1750. (e) Tkachenko, N. V.; Guenther, C.; Imahori, H.; Tamaki, K.; Sakata, Y.; Fukuzumi, S.; Lemmetyinen, H. *Chem. Phys. Lett.* **2000**, *326*, 344. (f) Vehmanen, V.;

- Tkachenko, N. V.; Imahori, H.; Fukuzumi, S.; Lemmetyinen, H. *Spectrochim. Acta, Part A* **2001**, *57*, 2229.
23. (a) Hasobe, T.; Imahori, H.; Kamat, P. V.; Fukuzumi, S. *J. Am. Chem. Soc.* **2003**, *125*, 14962. (b) Hasobe, T.; Imahori, H.; Kamat, P. V.; Ahn, T. K.; Kim, S. K.; Kim, D.; Fujimoto, A.; Hirakawa, T.; Fukuzumi, S. *J. Am. Chem. Soc.* **2005**, *127*, 1216.
24. (a) Miyamoto, T. K.; Tsuzuki, S.; Hasegawa, T.; Sakata, Y. *Chem Lett.* **1983**, 1587. (b) Chardon-Noblat, S.; Sauvage, J.-P.; Mathis, P. *Angew. Chem., Int. Ed. Engl.* **1989**, *28*, 593. (c) Mammel, D.; Kautz, C.; Müllen, K. *Chem. Ber.* **1990**, *123*, 1353. (d) Tamiaki, H.; Suzuki, S.; Maruyama, K. *Bull. Chem. Soc. Jpn.* **1993**, *66*, 2633.
25. Lindsey, J. S.; Schreiman, I. C.; Hsu, H. C.; Kearney, P. C.; Marguerettaz, A. M. *J. Org. Chem.* **1987**, *52*, 827.
26. Yamada, H.; Imahori, H.; Fukuzumi, S. *J. Mater. Chem.* **2002**, *12*, 2034.
27. Kunitake, T.; Tsuge, A.; Takarabe, K. *Polym. J.* **1985**, *17*, 633.
28. Terrill, R. H.; Postlethwaite, T. A.; Chen, C.-h.; Poon, C.-D.; Terzis, A.; Chen, A.; Hutchison, J. E.; Clark, M. R.; Wignall, G.; Londono, J. D.; Superfine, R.; Falvo, M.; Johnson, C. S., Jr.; Samulski, E. T.; Murray, R. W. *J. Am. Chem. Soc.* **1995**, *117*, 12537.
29. Templeton, A. C.; Wuelfing, W. P.; Murray, R. W. *Acc. Chem. Res.* **2000**, *33*, 27.
30. (a) Thomas, K. G.; Biju, V.; Guldi, D. M.; Kamat, P. V.; George, M. V. *J. Phys. Chem. B* **1999**, *103*, 8864. (b) Kamat, P. V.; Barazzouk, S.; Hotchandani, S.; Thomas, K. G. *Chem. Eur. J.* **2000**, *6*, 3914.



Supramolecular triads bearing porphyrin and fullerene via ‘two-point’ binding involving coordination and hydrogen bonding

Francis D’Souza,^{a,*} Mohamed E. El-Khouly,^{b,c} Suresh Gadde,^a Melvin E. Zandler,^a
Amy Lea McCarty,^a Yasuyuki Araki^b and Osamu Ito^{b,*}

^aDepartment of Chemistry, Wichita State University, 1845 Fairmount, Wichita KS 67260-0051, USA

^bInstitute of Multidisciplinary Research for Advanced Materials, Tohoku University, Katahira, Sendai 980-8577, Japan

^cDepartment of Chemistry, Graduate School of Science, Tohoku University, Aoba, Sendai 980-8587, Japan

Received 20 April 2005; accepted 4 May 2005

Available online 21 November 2005

Abstract—Supramolecular triads composed of fullerene (C₆₀) as primary electron acceptor, zinc porphyrin (ZnP) as primary electron donor, and either a ferrocene (Fc), or *N,N*-dimethylaminophenyl (DMA), or *N,N*-diphenylaminophenyl (DPA) entity as a second electron donor were constructed via a ‘two-point’ binding motif involving axial coordination and hydrogen bonding. The B3LYP/3-21G(*) optimized structures revealed disposition of the three entities of the triads in a triangular fashion. The redox behavior of the different components was studied using cyclic voltammetry in *o*-dichlorobenzene containing 0.1 M (*n*-C₄H₉)₄NClO₄. The oxidation potentials of the second electron donor followed the trend: Fc < DMA < DPA, and the free-energy calculations suggested the possibility of the occurrence of sequential hole transfer in these triads. Efficient electron transfer from the excited singlet state of zinc porphyrin to the fullerene entity was observed in all of the studied triads in *o*-dichlorobenzene. Longer charge-separated states were observed for zinc porphyrin with a carboxylic acid compared with that having an amide group. The ratios of the experimentally determined forward to reverse electron transfer rates, k_{CS}/k_{CR} were evaluated to be 10³ for triads formed by zinc porphyrin with a carboxylic acid, suggesting charge stabilization in these triads.
© 2005 Elsevier Ltd. All rights reserved.

1. Introduction

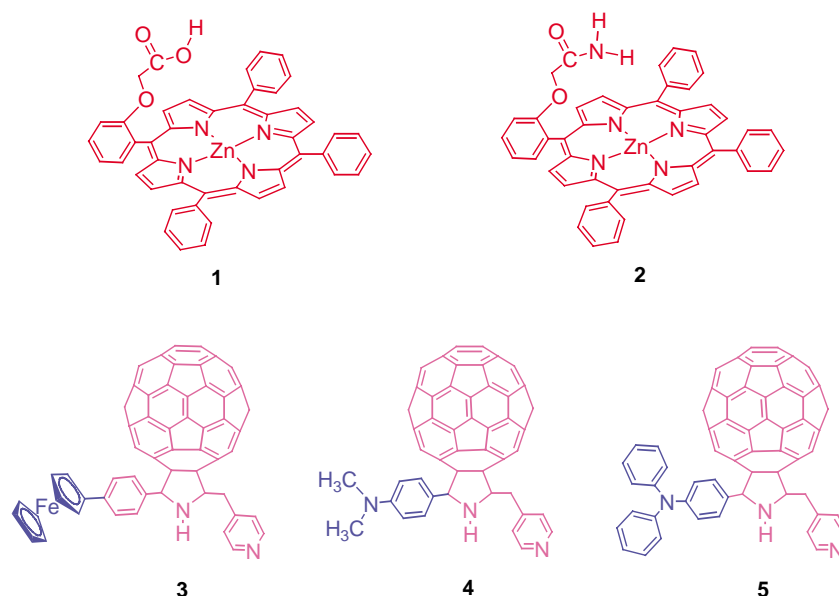
In nature, the photosynthetic reaction centers perform multi-step electron transfer processes with high quantum efficiency and long lifetimes of the final charge separated states of around 1 s.¹ Toward designing artificial photosynthetic reaction centers to harvest solar energy, meaningful incentives have been borrowed from the organization principle derived from the study of the natural photosynthetic reaction centers where the different photo- and redox-active components are assembled via non-covalent interactions in a protein matrix. One of the commonly used strategies to achieve long-lived charge-separated states during photoinduced electron transfer in model compounds involves promoting multi-step electron transfer reactions along well-defined redox gradients (e.g., triads, tetrads, pentads, etc.).^{2–5} However, to control the rates and yields of electron transfer reactions, and to eliminate the energy wasting charge-recombination

reactions, a better control over the separation, angular relationships, electronic coupling, and composition in donor–acceptor assemblies at a molecular level is desired. Utilization of biomimetic methodologies such as hydrogen bonding, metal–ligand complexation, electrostatic interactions, and π – π stacking would provide the much needed control over the composition and architecture of these complexes. Hence, self-assembled donor–acceptor assemblies are considered to be a viable alternative for the covalently linked molecular polyads in order to achieve an increased rate and yield of the charge-separation process, and prolongation of the lifetime of the charge-separated state.²

Several methodologies have been reported in the literature to self-assemble fullerenes⁶ and fullerene bearing donor–acceptor systems in solution and on electrode surfaces.^{7–12} High yields of photoelectrochemical currents have been reported when modified electrodes bearing porphyrin–fullerene systems were utilized for light energy conversion purposes.¹⁰ Recently, we reported supramolecular triads composed of zinc porphyrin (ZnP), fullerene (C₆₀) and *N,N*-dimethylaminophenyl (DMA) entities by a ‘two-point’ binding strategy involving axial coordination and hydrogen

Keywords: Supramolecule; Photoinduced charge-separation; Charge recombination; Zinc porphyrin; Fullerene; Supramolecular triads.

* Corresponding authors. Tel.: +1 316 978 7380; fax: +1 316 978 3431 (F.D.); fax: +81 22 217 5608 (O.I.);
e-mail addresses: francis.dsouza@wichita.edu; ito@tagen.tohoku.ac.jp



Scheme 1. Structure of the zinc porphyrin and fullerene derivatives utilized for constructing self-assembled supramolecular triads by the ‘two-point’ binding motif.

bonding.¹¹ In this approach, zinc porphyrin was functionalized with a pendant arm having either a carboxylic acid or an amide terminal group (compounds **1** and **2** in Scheme 1). The fullerene was functionalized to possess a pyridine coordinating ligand and a secondary donor, DMA (compound **4** in Scheme 1). During the self-assembly process, the pyridine entity coordinated to the zinc ion of the porphyrin, and the pendant carboxylic acid (or amide group) formed hydrogen bonds with the pyrrolidine amine group thus forming stable conjugates via the ‘two-point’ binding motif. The equilibrium constants evaluated from spectroscopic studies supported such stabilization of the supramolecules by ‘two-point’ binding strategy. The photochemical and photophysical studies revealed that the lifetimes of the radical ion-pairs were in the range of 30–40 ns in *o*-dichlorobenzene. This was unlike the simple dyads involving zinc porphyrin and fullerene held by an axial coordination bond, where the lifetimes of the radical ion-pairs were shorter than 10 ns.¹²

To gain further insights into the charge stabilization process in these triads, in the present study, we have extended this approach of constructing supramolecular triads by replacing the second donor (D), DMA by a ferrocene (Fc) or a *N,N*-diphenylaminophenyl (DPA) entity (compounds **3** and **5** in Scheme 1). Assembling porphyrins, **1** or **2** to either of the fullerenes, **3**, **4** or **5** is expected to result in the formation of stable supramolecular triads. The second electron donor, ferrocene in **3** has a lower oxidation potential than the primary donor, zinc porphyrin, thus satisfying the conditions of charge migration along the redox-gradient. Interestingly, the DPA entity in **5** has a higher oxidation potential than ZnP, and hence, sequential hole transfer leading to charge separated state may not be possible when ZnP is excited. Alternatively, a hole transfer from the DPA radical cation to the ZnP entity is thermodynamically possible when the C₆₀ is excited. Due to the employed ‘two-point’ binding strategy, these triads are expected to have similar supramolecular structures with respect to the

distance and orientation between the entities, with only a change in the type of second electron donor. Hence, a comparison between the spectral and photochemical behavior of these triads should shed light into the mechanistic aspects of charge stabilization in these novel supramolecular triads.

2. Results and discussion

2.1. Optical absorption studies

The ‘two-point’ binding in the self-assembled supramolecular triads was established from ¹H NMR and UV–visible absorption, and ab initio computational modeling studies. UV–visible absorption titrations involving either of porphyrins **1** or **2**, and, either of fullerenes, **3**, **4** or **5** exhibited spectral changes characteristic of axially coordinated species, that is, they exhibited red shifted Soret and visible absorption bands with the appearance of isosbestic points.¹³ Typical spectral changes observed for **2** on increasing addition of **3** are shown in Figure 1. Job’s plots by the method of continuous variation confirmed 1:1 complex formation. The formation constants, *K*, for the porphyrin–fullerene conjugates, determined from the UV–visible spectral data by Scatchard plots¹⁴ (Fig. 1 inset) are listed in Table 1. The *K* values range (1–10) × 10⁴ M⁻¹ for the two point bound triads, and are an order of magnitude higher than that observed for the one-point bound through axial coordination of zinc tetraphenylporphyrin, ZnTPP dyads and triads.^{8,12} The higher values of *K* indicate stable complex formation as a result of the employed ‘two-point’ binding motif.^{9,11} Generally, the *K* values for fullerenes binding to **1** are larger than those involving **2**. This could be rationalized based on the strength of the hydrogen bonds between carboxylic acid and pyrrolidino N–H groups for the former case compared with that between amide and pyrrolidino N–H groups in the latter case (See Scheme 2). The ‘two-point’ binding in

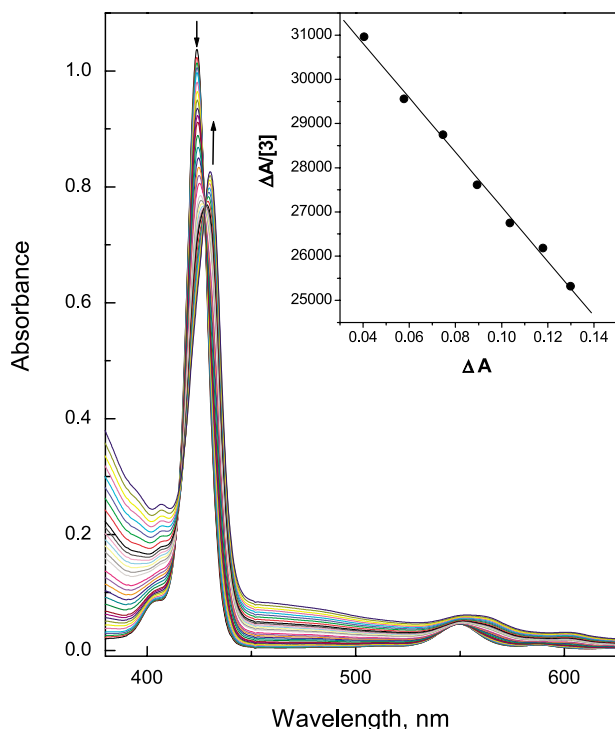


Figure 1. UV-visible spectral changes observed for **2** (4.85 μM) on increasing addition of **3** (0.3 μM each addition) in *o*-dichlorobenzene. The figure inset shows the Scatchard plot of the data analysis monitored at 423 nm.

Table 1. Formation constants calculated from Scatchard plots of absorbance data for the 'two-point' bound supramolecular dyads and triads in *o*-dichlorobenzene at 298 K

Compound ^a	K (M^{-1}) ^b			
	3	4 ^c	5	C_{60}Py ^d
ZnTPP ^e	6.8×10^3	7.8×10^3	9.8×10^3	$7.7 \times 10^{3,f}$
1	4.2×10^4	10.0×10^4	7.7×10^4	1.3×10^4
2	6.1×10^4	3.1×10^4	5.1×10^4	1.1×10^4

^a See Scheme 1 for structures of the porphyrin and fullerene derivatives.

^b Error = $\pm 10\%$.

^c Previously reported systems (Ref. 11); however, these data were re-measured in the present study.

^d 2-(4'-Pyridyl)fulleropyrrolidine.

^e *meso*-Tetraphenylporphyrinatozinc(II).

^f Ref. 12.

the supramolecular triads has also been established from ^1H NMR spectral studies detailed in our previous contribution.¹¹

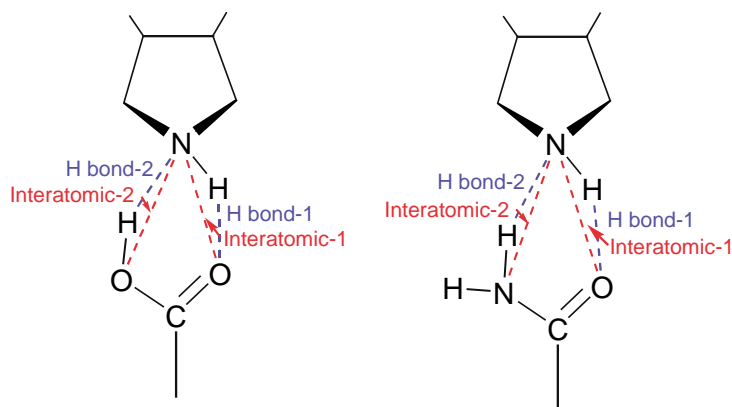
2.2. Ab initio B3LYP/3-21G(*) studies

To gain insights into the geometry of the self-assembled triads, computational studies were performed by using density functional methods (DFT) at the B3LYP/3-21G(*) level. In our calculations, all of the porphyrin–fullerenes complexes were fully optimized to a stationary point on the Born–Oppenheimer potential energy surface. Figure 2 presents the optimized structures of representative **1:3**, **1:4**, **1:5**, and **2:4** triads, from which the key geometric parameters were evaluated as given in Table 2.

In the optimized structures, the distance between the zinc atom and nitrogen atom of pyridine was found to be 2.02 Å, close to that obtained earlier for the self-assembled $\text{C}_{60}\text{Py}:\text{ZnP}$ dyad by X-ray crystallography,^{8m} and shorter than the 2.06–2.09 Å Zn–N distances of the zinc porphyrin. The inter-atomic distances for the hydrogen-bonding functionalities, as shown in Scheme 2, are also listed in Table 2. Short distances of H–O (H-bond-1 in Scheme 2) and H–N (H-bond-2) were observed suggesting the existence of hydrogen bonding in all of the investigated triads. Short inter-atomic distances of O–N (interatomic-1) or N–N and O–N (interatomic-2) also may be caused by the hydrogen bonding. The center-to-center, Ct-to-Ct, distances between the entities were evaluated as a measure of spatial disposition of these photo- and redox-active entities. It was observed that the three entities of the triads were positioned approximately in a triangular fashion with the entities 10–12 Å apart from each other. This arrangement of the entities differed from the majority of the covalently linked triads reported in the literature where the entities were arranged in a linear fashion.¹⁵ It is important to note that the Ct-to-Ct distances were slightly larger between ZnP and C_{60} compared to the distances between ZnP and the second electron donor entity.

2.3. Electrochemical studies

Cyclic voltammetric (CV) studies were performed to evaluate the potentials of the different redox entities utilized to form the supramolecular triads as shown in Figure 3.



Scheme 2. Hydrogen bonds and inter-atomic distances used in Table 2.

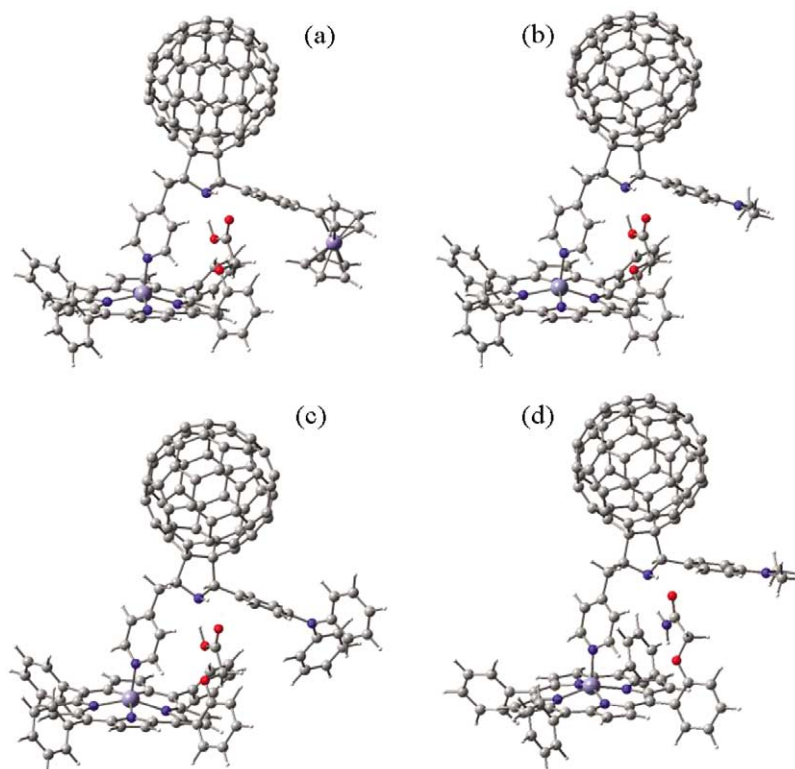


Figure 2. Ab initio B3LYP/3-21G(*) optimized structures of supramolecular triads: (a) **1:3**, (b) **1:4**, (c) **1:5**, and (d) **2:4**.

Table 2. B3LYP/3-21G(*) optimized geometric parameters of the investigated supramolecular triads

Triad ^a	Ct-to-Ct distance (Å)						
	ZnP–C ₆₀ ^b	ZnP–D2 ^c	C ₆₀ –D2 ^c	H–O ^d	H–N ^e	O–N ^f	O–N ^g or (N–N) ^g
1:3	12.29	11.73	11.26	2.06	1.57	2.86	2.61
1:4^h	12.27	11.02	9.42	2.04	1.57	2.85	2.61
1:5	12.25	10.86	9.42	2.02	1.58	2.84	2.61
2:4^h	12.33	11.43	9.23	1.89	2.09	2.86	2.96

^a See Figure 1 for abbreviations.

^b Zinc center to the center of fullerene sphere.

^c D2 = central atom of the second donor (Fe for ferrocene and N for *N,N*-dimethylaminophenyl and *N,N*-diphenylaminophenyl entities).

^d H-bond-1 (See Scheme 2).

^e H-bond-2 (See Scheme 2).

^f Interatomic-1 (See Scheme 2).

^g Interatomic-2 (See Scheme 2).

^h Previously reported systems (Ref. 11); however, these data were calculated in the present study.

The redox potentials corresponding to the oxidation (E_{ox}) of ZnTPP were located at 0.28 and 0.62 V vs Fc/Fc⁺, while the potentials corresponding to the reduction were located at –1.92 and –2.23 V versus Fc/Fc⁺, respectively, in *o*-dichlorobenzene. These potentials are not much different from the ZnP moieties in **1** and **2** employed in the present study¹¹ indicating little or no electronic interactions between the porphyrin π -system and the pendant amide or carboxylic acid groups. During the cathodic scan, the voltammograms of the functionalized fullerenes **3–5** revealed three one-electron reductions (E_{red}) within the potential window of the solvent. These waves were located at $E_{\text{red}} = -1.17$, -1.55 and -2.07 V vs Fc/Fc for **3**.¹¹ The first E_{red} values were located at -1.17 , -1.18 and -1.17 V vs Fc/Fc for **3**, **4**, and **5**, respectively. During the anodic scan of the potential, peaks corresponding to the oxidation of the second electron donor entities were also observed. For **3** bearing a ferrocene entity, the oxidation was

fully reversible and was located at $E_{\text{ox}} = 0.01$ V versus Fc/Fc⁺, which is lesser than $E_{\text{ox}} = 0.28$ V of ZnTPP. However, for compounds **4** and **5** bearing DMA and DPA entities, respectively, the oxidation process was found to be irreversible (Fig. 3); the peak potentials were located at $E_{\text{pa}} = 0.38$ V for **4** and $E_{\text{pa}} = 0.53$ V vs Fc/Fc⁺ for **5**, respectively. The oxidation potentials of the different electron donors followed the trend: Fc < ZnP < DMA < DPA.

A comparison between the redox potentials of the different entities suggests that the potential values of the primary electron donor, zinc porphyrin and the acceptor, fullerene entities remain almost the same irrespective of the macrocycle substitution and the appended second electron donor on the fullerene. That is, electronic effects of the pendant arm on the porphyrin and that of the second electron donor on the fullerene were quite small in the ground state.

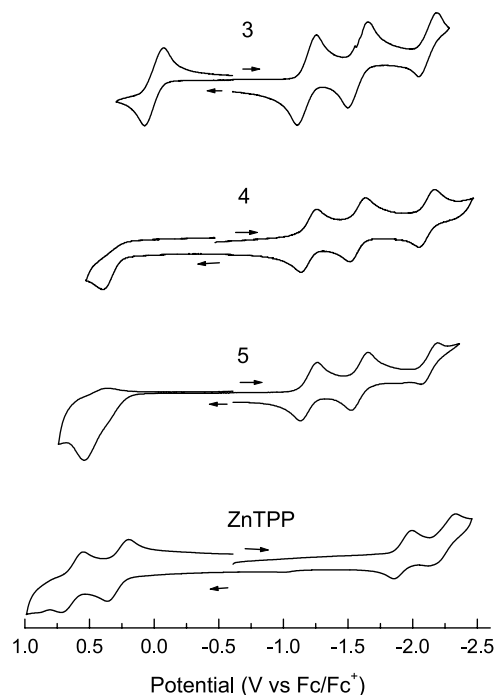


Figure 3. Cyclic voltammograms of compounds **3**, **4**, **5**, and ZnTPP in *o*-dichlorobenzene containing 0.1 M $(n\text{-C}_4\text{H}_9)_4\text{NClO}_4$. Scan rate = 100 mV/s.

The energy levels of the charge-separated states (ΔG_{RIP}) were evaluated using the Weller-type approach utilizing the redox potentials, center-to-center distance, and dielectric constant of the solvent as listed in Table 3.¹⁶ By comparing these energy levels of the charge-separated states with the energy levels of the excited states, the driving forces (ΔG_{CS}) were evaluated (Table 3). The generation of $\text{ZnP}^{\cdot+}:\text{C}_{60}^{\cdot-}$ is exothermic via $^1\text{ZnP}^*$ and $^1\text{C}_{60}^*$ in *o*-dichlorobenzene for all of the triads. The negative driving forces for the generation of $\text{ZnP}^{\cdot+}:\text{C}_{60}^{\cdot-}$ were also calculated via $^3\text{ZnP}^*$ and $^3\text{C}_{60}^*$. The charge-separation leading to the formation of $\text{D}^{\cdot+}:\text{C}_{60}^{\cdot-}$ is exothermic via $^3\text{C}_{60}^*$ for **3** and **4**, but not **5**. A hole shift from $\text{ZnP}^{\cdot+}$ to Fc is possible in the supramolecule, but in the case of DMA and DPA bearing triads, an opposite hole shift from $\text{D2}^{\cdot+}$ (formed via $^1\text{C}_{60}^*$) to ZnP is conceivable.

2.4. Emission studies

The photochemical behavior of the ‘two-point’ bound supramolecular triads was investigated, first, by using steady-state fluorescence measurements. On addition of either of compounds **3**, **4** or **5** to an argon saturated *o*-dichlorobenzene solution of zinc porphyrins, **1** or **2**, the fluorescence intensity of the ZnP entity decreased. Representative fluorescence spectral changes of **2** on increasing addition of **5** are shown in Figure 4a; fluorescence intensity of the ZnP entity decreased until about 25% of the original intensity without shifts of peaks. The Stern-Volmer plots¹⁷ constructed from the fluorescence quenching data are shown in Figure 4b, which exhibits an upward curvature at higher concentrations of fullerenes. The Stern-Volmer quenching constants, K_{SV} calculated from the linear segment of the plots at lower concentration of fullerene were 3–4 orders of magnitude higher than that expected for bimolecular diffusion-controlled quenching. Such large quenching rates indicate the occurrence of intramolecular quenching processes in these triads. It may also be mentioned here that the efficiency of quenching was much higher than that reported earlier for ‘single-point’ bound zinc porphyrin–fullerene dyads.¹²

The functionalized fullerenes, **3**, **4** or **5** revealed a weak fluorescence band in the longer wavelength region around 720 nm corresponding to the $^1\text{C}_{60}^*$ emission.¹⁸ The intensity of this band for each of the fullerene dyads, **3**, **4** or **5** was found to be much smaller than that observed for fulleropyrrolidine bearing no second electron donor entity (viz. 2-phenyl fulleropyrrolidine), suggesting charge-separation from the $^1\text{C}_{60}^*$ entity to the appended second electron donor. Addition of zinc porphyrins, **1** or **2**, to the solution of **3**, **4** or **5**, masked the weak fluorescence of the C_{60} entity by the tail of the strong fluorescence of the ZnP entity, prohibiting further data analysis.

Emission time-profiles of the singlet excited state of zinc porphyrins in the absence and presence of fullerenes are shown in Figure 5a. Zinc porphyrins **1**, and **2** in deaerated *o*-dichlorobenzene revealed monoexponential decay with lifetimes of 1.92, 2.35, and 1.97 ns, respectively. Upon forming the supramolecular triads by complexing with the functionalized fullerenes, two-component fluorescence

Table 3. Energy levels of the charge-separated states (ΔG_{RIP}), free-energy changes for charge-separation (ΔG_{CS}), and hole shift (ΔG_{HS}) for supramolecular triads in *o*-dichlorobenzene

Porphyrins	Fullerenes	$-\Delta G_{\text{RIP(P-C)}}^a$ (eV) ^a	$-\Delta G_{\text{RIP(D-C)}}^a$ (eV) ^a	$-\Delta G_{\text{CS(P-C)}}^b$ (eV) ^b	$-\Delta G_{\text{CS(P-C*)}}^b$ (eV) ^b	$-\Delta G_{\text{CS(C*-D)}}^b$ (eV) ^b	$-\Delta G_{\text{HS(P-D)}}^b$ (eV)
1	3	1.33	1.05	0.74	0.39	0.54	0.28
	4 ^c	1.35	1.41	0.72	0.37	0.16	−0.06
	5	1.36	1.58	0.71	0.36	−0.01	−0.22
2	3	1.33	1.05	0.74	0.39	0.54	0.28
	4 ^c	1.35	1.41	0.72	0.37	0.16	−0.06
	5	1.36	1.58	0.71	0.36	−0.01	−0.22
ZnTPP	4 ^c	1.35		0.74	0.39		
ZnTPP	C_{60}PY^d	1.35		0.74	0.37		

^a $\Delta G_{\text{RIP}} = E_{\text{ox}} - E_{\text{red}} + \Delta G_{\text{S}}$, where $\Delta G_{\text{S}} = -e^2/(4\pi\epsilon_0\epsilon_{\text{R}}R_{\text{Ct-Ct}})$ and ϵ_0 and ϵ_{R} refer to vacuum permittivity and dielectric constant of *o*-dichlorobenzene.

^b $-\Delta G_{\text{CS}} = \Delta E_{0-0} - \Delta G_{\text{RIP}}$, where ΔE_{0-0} is the energy of the lowest excited states (2.07 eV for $^1\text{ZnP}^*$, 1.72 eV for $^1\text{C}_{60}^*$). Although the values of $\Delta G_{\text{CS}}^{\text{†}}$ are not listed, they can be easily calculated using $\Delta E_{0-0} = 1.50$ eV for $^3\text{ZnP}^*$ and $^3\text{C}_{60}^*$.

^c Ref. 11.

^d Ref. 12.

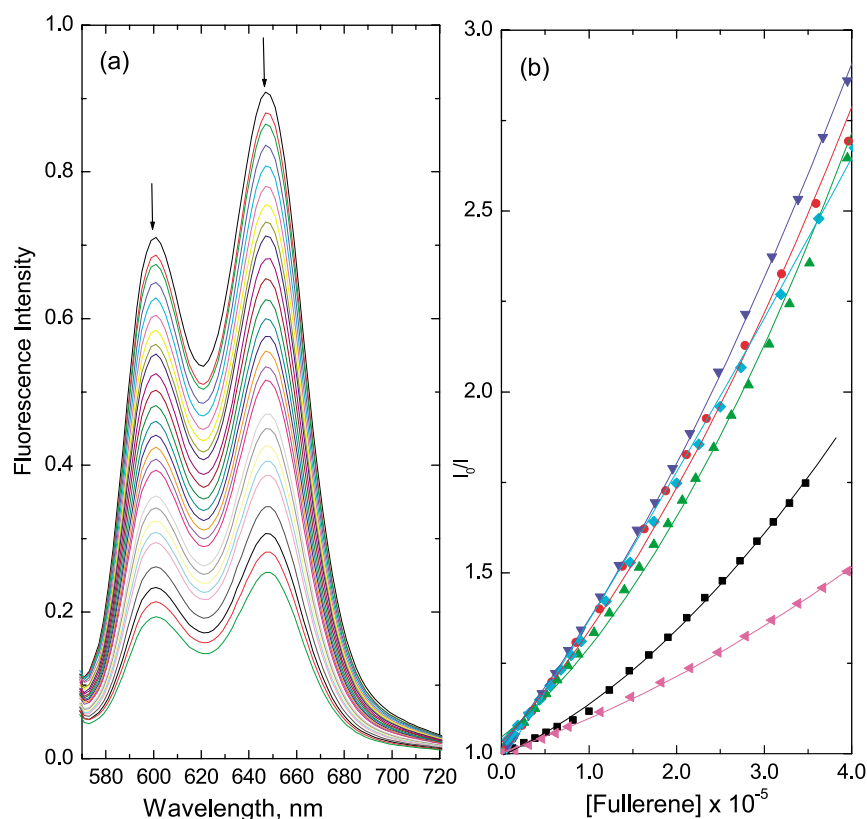


Figure 4. (a) Fluorescence spectra of **2** ($4 \mu\text{M}$) in the presence of various amounts of **3** ($0.3 \mu\text{M}$ each addition) in *o*-dichlorobenzene ($\lambda_{\text{ex}} = 549 \text{ nm}$). (b) Stern-Volmer plots for the fluorescence quenching of (i) **2** by **5** (\blacktriangledown), (ii) **2** by **3** (\blacktriangle), (iii) **1** by **3** (\bullet), (iv) **1** by **5** (\blacklozenge), (v) ZnP by **3** (\blacksquare), and (vi) ZnP by **5** (\blacktriangleleft) in *o*-dichlorobenzene (See Scheme 1 for abbreviations and structures).

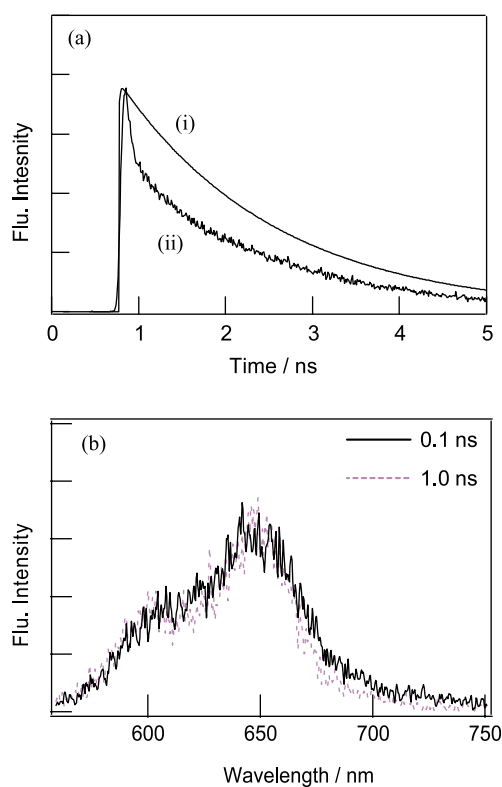


Figure 5. (a) Fluorescence decay profiles of (i) **1** and (ii) **1** in the presence of 2 equiv of **5** in *o*-dichlorobenzene: $\lambda_{\text{ex}} = 410 \text{ nm}$ and $\lambda_{\text{em}} = 600 \text{ nm}$. (b) Time-resolved fluorescence spectra of the supramolecular triad **2:3** in *o*-dichlorobenzene.

decays of ZnP were observed. The quick fluorescence decay could arise either due to the charge-separation or energy transfer from the $^1\text{ZnP}^*$ moiety to the C_{60} moiety in supramolecular triads. In a control experiment, no clear shortening of the fluorescence lifetime of ZnTPP was observed for a dyad formed by coordinating C_{60}py (bearing no hydrogen bonding entity and second electron donor entity) to ZnP, indicating that the hydrogen bonding and the second electron donor are essential to accelerate the fluorescence quenching. The slow fluorescence decay rates seem to be similar to the ZnTPP moiety, and hence may be attributed to the uncomplexed ZnP moiety. The fraction of the short fluorescence lifetime for **1** having larger K value was larger than that for **2** having smaller K value.

In order to verify the occurrence of energy transfer from the $^1\text{ZnP}^*$ to the fullerene entity, time-resolved fluorescence spectra of a representative supramolecular triad, **1:5** were recorded in *o*-dichlorobenzene. As shown in Figure 5b, the time-resolved fluorescence spectrum of **1:5** at 0.1 ns time-interval, that is, immediately after excitation revealed bands at 600 and 650 nm corresponding to the singlet emission of the ZnP moiety. After a time interval of 2.0 ns, the spectral features were found to be unchanged with no new peaks around 720 nm corresponding to the emission of the C_{60} moiety. These results suggest absence of energy transfer from the $^1\text{ZnP}^*$ moiety to the C_{60} moiety as a possible fluorescence quenching mechanism in the supramolecular triads.

In the absence of any energy transfer, the observed short fluorescence lifetimes of $^1\text{ZnP}^*$ were attributed to

Table 4. Fluorescence lifetimes (τ_f),^a charge-separation rate constants (k_{CS})^b, and charge-separation quantum yields (Φ_{CS})^b via ¹ZnP*, and charge recombination rate constants (k_{CR}) for supramolecular triads in *o*-dichlorobenzene

Porphyrins	Fullerenes	Lifetimes (ps)	k_{CS} (s^{-1}) ^c	Φ_{CS} ^c	k_{CR} (s^{-1}) (τ_{RIP} (ns))	k_{CS}/k_{CR}
1	3	160 (62%)	5.8×10^9	0.93	5.6×10^6 (170)	1040
		2550 (38%)				
	4^d	110 (75%) ^c	8.6×10^9	0.99	1.0×10^8 (10) ^{c,e}	86
		2280 (25%)				
		5				
2	3	130 (65%)	7.3×10^9	0.94	4.5×10^6 (220) ^c	1600
		2700 (35%)				
	4^d	80 (51%)	7.8×10^9	0.96	4.9×10^7 (20) ^c	160
		1500 (49%)				
		5				
ZnP^d	4^d	69 (81%)	1.4×10^{10}	0.96	3.1×10^7 (30) ^c	100
		1600 (19%)				
		5				
ZnTPP^f	C₆₀Py^f	104 (60%)	1.0×10^{10}	0.94	4.6×10^7 (20) ^c	200
		1700 (40%)				
		71 (27%)	—	—	3.4×10^7 (30)	—
		2030 (73%)	—	—	—	—
		1850 (100%)	$< 2 \times 10^7$	< 0.04	—	—

^a The singlet lifetime of ZnTPP, **1** and **2** (see Scheme 1 for structures) in deaerated *o*-dichlorobenzene were found to be 1.92, 2.35, and 1.97 ns, respectively.

^b $k_{CS} = (1/\tau_f)_{\text{complex}} - (1/\tau_f)_{\text{ZnP}}$; $\Phi_{CS} = [(1/\tau_f)_{\text{complex}} - (1/\tau_f)_{\text{ZnP}}]/(1/\tau_f)_{\text{complex}}$.

^c These values calculated from the fast decay component.

^d Ref. 11.

^e Two component decays; initial fast decay was reported in our previous paper (Ref. 6). Slow decay was analyzed in the present study.

^f Ref. 12.

the occurrence of an electron-transfer process within the supramolecular triads. The charge-separation rate-constants (k_{CS}) and quantum yields (Φ_{CS}) via ¹ZnP* were evaluated in the usual manner employed in the intramolecular electron-transfer process (equations are cited in the margin under Table 4).^{11,12} High values of both k_{CS} and Φ_{CS} were obtained for all of the studied supramolecular triads (Table 4).

In agreement with the steady-state fluorescence behavior, the lifetimes of fullerenes **3–5** were found to be efficiently quenched. The lifetime of fullerenes, **4** and **5** was found to be 250 and 150 ps, respectively, as major fractions (60–80%) in two-component decays. These lifetimes are shorter than those of fulleropyrrolidines bearing no electron donors (1300 ns),¹⁸ suggesting occurrence of charge-separation between the C₆₀ and the second electron donor via the ¹C₆₀* moiety. These lifetimes gave the k_{CS} and Φ_{CS} values via the ¹C₆₀* moiety to be $(3.4–6.0) \times 10^9 s^{-1}$ and 0.82–0.89, respectively. In the case of **3**, fluorescence lifetimes of the ¹C₆₀* moiety was too short to observe suggesting efficient charge-separation between Fc and the ¹C₆₀* moiety. Further analysis of the data in the presence of zinc porphyrins, **1** or **2**, could not be accomplished since the strong ZnP emission masked the weaker C₆₀ emission.

2.5. Nanosecond transient absorption studies

Figure 6 shows transient spectra and time profiles obtained for the triads **1:5** and **1:3**. The spectrum recorded at 100 ns after the laser light pulse showed the radical anion of the C₆₀ moiety around 1020 nm. The absorption bands at 700 and 870 nm correspond to the triplet states of C₆₀ and ZnP, respectively.¹⁹ The absorption band of zinc porphyrin cation radical, expected to appear around 625 nm, was masked by the peaks of the ZnP fluorescence in the 500–650 nm region. Furthermore, the absorption band of the cation radical of ZnP may be overlapped with the absorption bands of the triplet states of the C₆₀ and ZnP moieties in this wavelength region. The time profile monitored for the C₆₀^{•-} entity at

1020 nm band⁶ revealed complete decay of the C₆₀^{•-} moiety within about 2 μ s thus giving the charge-recombination rate constants, k_{CR} of $(4.5–5.6) \times 10^6 s^{-1}$. The lifetimes of the charge-separated states (τ_{RIP}) evaluated from the k_{CR} values ($\tau_{RIP} = 1/k_{CR}$) were found to range from 170 to 220 ns. On the other hand, the absorption bands in the region of 700–850 nm did not show appreciable decay within 1.5 μ s

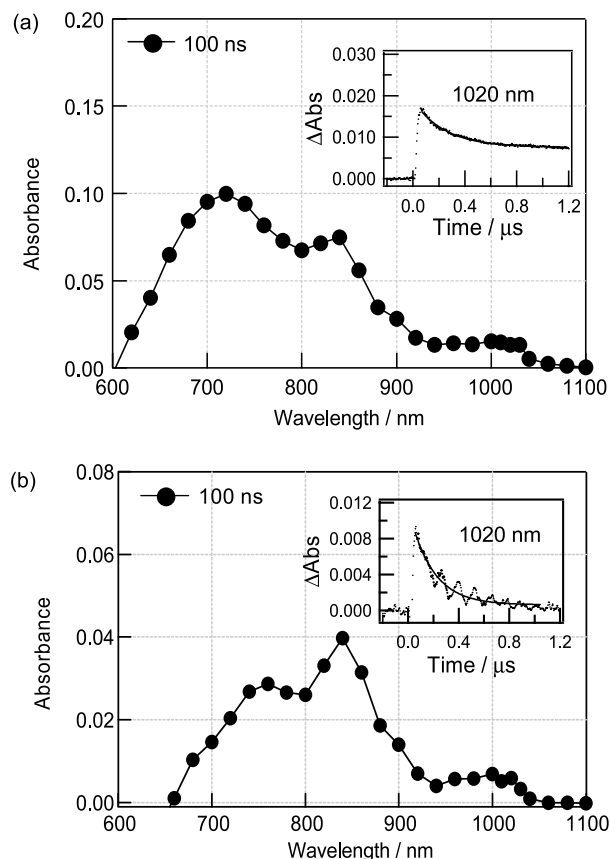


Figure 6. Transient absorption spectra obtained by 532 nm laser light photolysis of **1** (0.05 mM) with (a) **5** (0.05 mM) and (b) **3** (0.05 mM) in *o*-dichlorobenzene.

due to the overlap of the triplet absorption bands in the wavelength range.

Transient absorption spectra obtained for the triads **2:5** and **2:3** are shown in Figure 7. A quick decay was observed in the 1020 nm region, while the 700–850 nm region exhibited slow decay typical of the triplet absorption bands.¹⁸ From the plots of the absorbance at 10 ns, the quick decay process at the 1020 nm band has been attributed to the charge-recombination. From the analysis of the decay curve the k_{CR} values were calculated to be in the range of $4.6\text{--}10 \times 10^7 \text{ s}^{-1}$, which resulted in the τ_{RIP} values shorter than 20 ns. Additionally, the k_{CR} values obtained using donor **1**, were found to be smaller than those obtained by using donor **2** suggesting that larger K values correlate with longer τ_{RIP} values.

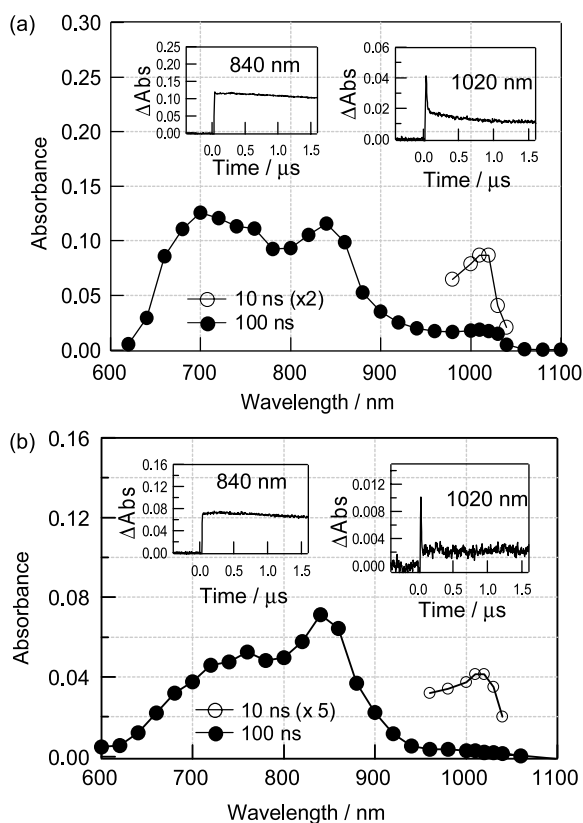


Figure 7. Transient absorption spectra of **2** (0.1 mM) in the presence of **5** (0.12 mM) in Ar-saturated *o*-dichlorobenzene by the excitation of 532 nm laser light.

The nanosecond transient absorption spectra of the fullerene derivatives, **4** and **5**, in the absence of added ZnP revealed a peak at 700 nm corresponding to the formation of ${}^3\text{C}_{60}^*-\text{D2}$, but not at 1000 nm region corresponding to $\text{C}_{60}^{\cdot-}$, suggesting the occurrence of rapid charge-recombination of $\text{C}_{60}^{\cdot-}-\text{D2}^{\cdot+}$ going to ${}^3\text{C}_{60}^*-\text{D2}$ in *o*-dichlorobenzene. In the case of **3**, the transient absorption band of ${}^3\text{C}_{60}^*-\text{D2}$ at 700 nm was not observed, suggesting rapid charge-recombination of $\text{C}_{60}^{\cdot-}-\text{D2}^{\cdot+}$ leading to the ground state $\text{C}_{60}-\text{D2}$ species in *o*-dichlorobenzene.²⁰ On complexing these fullerene derivatives with zinc porphyrins **1** or **2**, the transient absorption spectra revealed features similar to the ones shown in Figure 7, when the samples

were excited with a 335 nm laser light for selective excitation of C_{60} . These observations indicate that the rate of through-space hole shift from $\text{C}_{60}^{\cdot-}-\text{D2}^{\cdot+}$ to ZnP entity is not fast enough compared with the rapid through-bond charge-recombination in the supramolecular triads.

The ratio of the experimentally determined charge-separation rate via ${}^1\text{ZnP}^*$ to the charge recombination rate, k_{CS}/k_{CR} , a measure of excellence of charge stabilization, in the studied triads is given in Table 4. Such analysis indicates better charge stabilization in the triads having larger K values. That is, triads formed by donor **1** having a pendant carboxylic acid group H-bonded to the full-erypyrrolidine N–H site, in addition to the coordination of pyridine to the Zn center. This ratio for triads involving carboxylic acid on porphyrins is almost similar to that obtained for covalently linked dyads involving the ZnP and C_{60} moieties.^{8f} This effect is better defined in the case of carboxylic acid functionality bearing ZnP: C_{60} –DMA and ZnP: C_{60} –DPA triads. The second electron donor attached to C_{60} moiety also seems to affect indirectly the photophysical events of the conjugates as hole transfer reagents.

2.6. Energetic considerations and charge stabilization

The energy level diagram for the occurrence of electron transfer from the singlet excited zinc porphyrin is shown in Figure 8. The values of different energy levels are cited from Table 3. Electron transfer from the singlet excited zinc porphyrin to the fullerene entity to create the initial radical ion-pair, $\text{ZnP}^{\cdot+}:\text{C}_{60}^{\cdot-}$ is energetically favorable for all of the studied triads. A hole transfer from the $\text{ZnP}^{\cdot+}$ to the second electron donor (D2) is energetically favorable in case of **3** bearing ferrocene as second electron donor moiety. Thus, the observed k_{CR} values may include both a CR-1 process for $\text{ZnP}^{\cdot+}:\text{C}_{60}^{\cdot-}$ and hole-shift process to $\text{D2}^{\cdot+}:\text{C}_{60}^{\cdot-}$. Unfortunately, in the present study, we could not detect transient spectral signals of the ferrocene cation because of its low molar absorptivity.¹⁵ Considering the lower energy levels of $\text{ZnP}^{\cdot+}:\text{C}_{60}^{\cdot-}-\text{D2}$ compared to those of

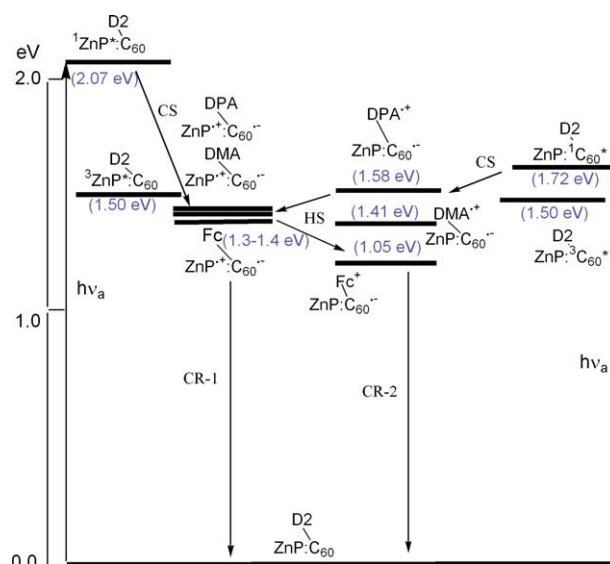


Figure 8. Energy-level diagram showing the different photochemical events of the investigated supramolecular triads.

ZnP:C₆₀⁻-D2⁺ for DMA and DPA, a hole transfer from the ZnP⁺ to DMA and DPA is not conceivable.

Electron transfer from the second electron donor, D2 to the singlet excited C₆₀ is also possible in these triads, generating ZnP:C₆₀⁻-D2⁺. Furthermore, hole-shift process to ZnP⁺:C₆₀⁻-D2 is thermodynamically possible for DMA and DPA. However, we could not obtain such experimental verifications, since the charge-recombination of ZnP:C₆₀⁻-D2⁺ seems to be faster than the hole-shift process. Additionally the time-resolved fluorescence studies revealed that the energy transfer from the singlet excited ZnP to C₆₀ was a minor process in the presently investigated triads.

3. Summary

Supramolecular triads have been formed by the 'two-point' binding strategy involving axial coordination and hydrogen bonding. Analysis of the optical spectral data revealed higher binding constants compared to the zinc porphyrin-diyad held by only metal–ligand axial coordination, and the B3LYP/3-21G(*) studies revealed structures of the triads in which the different entities were arranged in a triangular fashion. Electrochemical studies allowed evaluation of the redox potentials of the different entities and the oxidation potential of the second electron donor of the triads followed the trend: ferrocene < *N,N*-dimethylaminophenyl < *N,N*-diphenylaminophenyl. Time-resolved emission studies revealed efficient charge separation from the singlet excited state of zinc porphyrin in the studied triads. Nanosecond transient absorption studies provided proof of electron transfer and revealed slower charge recombination in the case of triads having hydrogen-bonding with the carboxylic acid group. In the case of triads having amide hydrogen-bonding, appreciable prolongation of the charge-separated state was not observed. The ratio of the experimentally measured k_{CS}/k_{CR} values revealed ability of some of these triads for light induced generation of charged species, especially in the case of porphyrins bearing carboxylic acid functionality. The second electron donor attached to C₆₀ moiety also seems to affect indirectly the photophysical events of the conjugates as hole transfer reagents.

4. Experimental

4.1. Chemicals

Buckminsterfullerene, C₆₀ (+99.95%) was from SES Research, (Houston, TX). All the chromatographic materials and solvents were procured from Fisher Scientific and were used as received. D-4-Pyridylalanine was from Pep Tech Corp (CA). Tetra-*n*-butylammonium perchlorate (*n*-C₄H₉)₃NCIO₄, was from Fluka Chemicals. All other chemicals utilized in the synthesis were from Aldrich Chemicals (Milwaukee, WI), and were used as received. Porphyrins **1** and **2**, and fullerene, **4** were synthesized according to earlier published methods.¹¹

4.1.1. Synthesis of 3. To a 150 ml toluene containing 100 mg of C₆₀, 100 mg of 4-ferrocenylbenzaldehyde

(2.5 equiv) and 46 mg of 4-pyridylalanine (2 equiv) was added, and the solution was refluxed for 15 h. The solvent was removed under vacuum and the product was adsorbed on silica gel. The product was purified on a silica gel column using 80:20 v/v toluene and ethyl acetate eluent. Yield: 57%. ¹H NMR (CHCl₃-*d*, δ ppm): 8.7 (s broad, 2H Py), 7.76 (d, 2H Py), 7.45, 7.55 (d, d, 4H, -Ph-Fe), 5.70 (s, 1H), 5.05, 4.05 (d, d, 2H pyrrolidineH), 3.57 (t, 2H, -CH₂-Py), 3.9, 4.25, 4.59 (s, t, t, 9H, ferrocene). ESI mass in CH₂Cl₂, calcd: 1113.8; found: *m/z* 1114.7.

4.1.2. Synthesis of 5. To a 170 ml of toluene, 100 mg of C₆₀, 120 mg of 4-(diphenylamino)benzaldehyde (3 equiv) and 46 mg of 4-pyridylalanine (2 equiv) was added and the solution was refluxed for 18 h. At the end, the solvent was removed under vacuum and the product was purified on a silica gel column using toluene–ethylacetate (7/3 v/v) as eluent. Yield=60%. ¹H NMR (CHCl₃-*d*, δ ppm): 8.7 (s broad, 2H, Py), 7.7 (d, 2H, py), 7.52 (d, 2H, Ph), 7.05 (d, 2H, Ph), 6.9–7.2 (10H, N-2Ph), 5.69 (s, 1H) 5.05, 4.05 (d, d, 2H pyrrolidineH), 3.5 (t, 2H, -CH₂-Py). ESI mass in CH₂Cl₂, calcd: 1097.5; found: *m/z* 1098.3.

4.2. Instrumentation

The UV–visible spectral measurements were carried out with a Shimadzu Model 1600 UV–visible spectrophotometer. The fluorescence emission was monitored by using a Spex Fluorolog-tau spectrometer. The ¹H NMR studies were carried out on a Varian 400 MHz spectrometer. Tetramethylsilane (TMS) was used as an internal standard. Cyclic voltammograms were recorded on a EG&G Model 263A potentiostat using a three electrode system. A platinum button or glassy carbon electrode was used as the working electrode. A platinum wire served as the counter electrode and a Ag/AgCl was used as the reference electrode. Ferrocene/ferrocenium (Fc/Fc⁺) redox couple was used as an internal standard. All the solutions were purged prior to electrochemical and spectral measurements using argon gas. The ESI-Mass spectral analyses of the newly synthesized compounds were performed by using a Fennigan LCQ-Deca mass spectrometer. For this, the compounds (about 0.1 mM) were prepared in CH₂Cl₂, freshly distilled over calcium hydride.

4.2.1. Molecular orbital calculations. The computational calculations were performed by ab initio B3LYP/3-21G(*) methods with GAUSSIAN 03 software package on high speed computers.²¹

4.2.2. Time-resolved emission and transient absorption measurements. The picosecond time-resolved fluorescence spectra were measured using an argon-ion pumped Ti:sapphire laser (Tsunami) and a streak scope (Hamamatsu Photonics). The details of the experimental setup are described elsewhere.²² Nanosecond transient absorption spectra in the NIR region were measured by means of laser-flash photolysis; 532 light and 355 nm light from a Nd:YAG laser were used as the exciting source for zinc porphyrin and fullerene, respectively. A Ge-avalanche-photodiode module was used for detecting the monitoring light from a pulsed Xe-lamp as described in our previous report.²²

Acknowledgements

The authors are thankful to the donors of the Petroleum Research Fund administered by the American Chemical Society and National Institutes of Health (GM 59038). This research was partially supported by a Grant-in-Aid for the COE project (to M.E.K.), and for Scientific Research on Priority Area (417) from the Ministry of Education, Science, Sport and Culture of Japan (to O.I. add Y.A.) for support of this work.

References and notes

- (a) Diefenhofer, J.; Michel, H. *Angew. Chem., Int. Ed. Engl.* **1989**, *28*, 829. (b) Feher, G.; Allen, J. P.; Okamura, M. Y.; Rees, D. C. *Nature* **1989**, *339*, 111. (c) McDermott, G.; Prince, S. M.; Freer, A. A.; Hawthornethwaite-Lawles, A. M.; Papiz, M. Z.; Cogdell, R. J.; Isaacs, N. W. *Nature* **1995**, *374*, 517. (d) Marcus, R. A.; Sutin, N. *Biochim. Biophys. Acta* **1985**, *811*, 265.
- (a) Sessler, J. S.; Wang, B.; Springs, S. L.; Brown, C. T. In *Comprehensive Supramolecular Chemistry*; Atwood, J. L., Davies, J. E. D., MacNicol, D. D., Vögtle, F., Eds.; Pergamon: New York, 1996; Chapter 9. (b) Ward, M. W. *Chem. Soc. Rev.* **1997**, *26*, 365. (c) Hayashi, T.; Ogoshi, H. *Chem. Soc. Rev.* **1997**, *26*, 355. (d) Piotrowiak, P. *Chem. Soc. Rev.* **1999**, *28*, 143. (e) Guldi, D. M. *Chem. Soc. Rev.* **2002**, *31*, 22. (f) Guldi, D. M. *Chem. Commun.* **2000**, 321. (g) Meijer, M. D.; van Klink, G. P. M.; van Koten, G. *Coord. Chem. Rev.* **2002**, *230*, 141. (h) El-Khouly, M. E.; Ito, O.; Smith, P. M.; D'Souza, F. *J. Photochem. Photobiol. C* **2004**, *5*, 79. (i) D'Souza, F.; Ito, O., *Coord. Chem. Rev.* **2005**, *249*, 1410.
- (a) Sutin, N. *Acc. Chem. Res.* **1983**, *15*, 275. (b) Wasielewski, M. R. *Chem. Rev.* **1992**, *92*, 435. (c) Gust, D.; Moore, T. A.; Moore, A. L. *Acc. Chem. Res.* **1993**, *26*, 198. (d) Paddon-Row, M. N. *Acc. Chem. Res.* **1994**, *27*, 18. (e) McLendon, G.; Hake, R. *Chem. Rev.* **1992**, *92*, 481. (f) Gould, I. R.; Farid, S. *Acc. Chem. Res.* **1996**, *29*, 522. (g) Mataga, N.; Miyasaka, H. *Adv. Chem. Phys.* **1999**, *107*, 431. (h) Lewis, F. D.; Letsinger, R. L.; Wasielewski, M. R. *Acc. Chem. Res.* **2001**, *34*, 159. (i) Harriman, A.; Sauvage, J.-P. *Chem. Soc. Rev.* **1996**, *26*, 41. (j) Blanco, M.-J.; Jiménez, M. C.; Chambron, J.-C.; Heitz, V.; Linke, M.; Sauvage, J.-P. *Chem. Soc. Rev.* **1999**, *28*, 293. (k) Balzani, V.; Juris, A.; Venturi, M.; Campagna, S.; Serroni, S. *Chem. Rev.* **1996**, *96*, 759. (l) *Electron Transfer in Chemistry*; Balzani, V., Ed.; Wiley-VCH: Weinheim, 2001. (m) Martín, N.; Sánchez, L.; Illescas, B.; Pérez, I. *Chem. Rev.* **1998**, *98*, 2527.
- (a) Miller, J. R.; Calcaterra, L. T.; Closs, G. L. *J. Am. Chem. Soc.* **1984**, *106*, 3047. (b) Closs, G. L.; Miller, J. R. *Science* **1988**, *240*, 440. (c) Connolly, J. S.; Bolton, J. R. In *Photoinduced Electron Transfer*; Fox, M. A., Chanon, M., Eds.; Elsevier: Amsterdam, 1988; pp 303–393; Part D. (d) Wasielewski, M. R. In *Photoinduced Electron Transfer*; Fox, M. A., Chanon, M., Eds.; Elsevier: Amsterdam, 1988; pp 161–206; Part A. (e) Verhoeven, J. W. *Adv. Chem. Phys.* **1999**, *106*, 603. (f) Maruyama, K.; Osuka, A.; Mataga, N. *Pure Appl. Chem.* **1994**, *66*, 867. (g) Osuka, A.; Mataga, N.; Okada, T. *Pure Appl. Chem.* **1997**, *69*, 797. (h) Sun, L.; Hammarström, L.; Åkermark, B.; Styring, S. *Chem. Soc. Rev.* **2001**, *30*, 36.
- (a) Imahori, H.; Sakata, Y. *Adv. Mater.* **1997**, *9*, 537. (b) Imahori, H.; Sakata, Y. *Eur. J. Org. Chem.* **1999**, 2445. (c) Balch, A. L.; Olmstead, M. M. *Chem. Rev.* **1998**, *98*, 2123. (d) Imahori, H.; Fukuzmi, S. *Adv. Funct. Mater.* **2004**, *14*, 525. (e) Boyd, P. D.; Reed, C. A. *Acc. Chem. Res.* **2005**, *38*, 235.
- (a) Hong, H.; Davidov, D.; Kallinger, C.; Lemmer, U.; Feldmann, J.; Harth, E.; Gugel, A.; Mullen, K. *Synth. Met.* **1999**, *102*, 1537. (b) Haino, T.; Araki, H.; Yamanaka, Y.; Fukazawa, Y. *Tetrahedron Lett.* **2001**, *42*, 3203. (c) Georgakilas, V.; Pellarini, F.; Prato, M.; Guldi, D. M.; Melle-Franco, M.; Zerbetto, F. *Proc. Natl. Acad. Sci. U.S.A.* **2002**, *99*, 5075. (d) Diederich, F.; Gomez-Lopez, M. *Chem. Soc. Rev.* **1999**, *28*, 263. (e) Schubert, U. S.; Weidl, C. H.; Rapta, P.; Harth, E.; Mullen, K. *Chem. Lett.* **1999**, *9*, 949. (f) Liu, Y.; Wang, H.; Liang, P.; Zhang, H.-Y. *Angew. Chem., Int. Ed.* **2004**, *43*, 2690. (g) Rispens, M. T.; Sanchez, L.; Beckers, E. H. A.; van Hal, P. A.; Schenning, A. P. H. J.; Abdelkrim, E.-G.; Peeters, E.; Meijer, E. W.; Janssen, R. A. J.; Hummelen, J. C. *Synth. Met.* **2003**, *135*, 801.
- (a) Camps, X.; Dietel, E.; Hirsch, A.; Pyo, S.; Echegoyen, L.; Hackbarth, S.; Roder, B. *Chem. Eur. J.* **1999**, *5*, 2362. (b) Boyd, P. D. W.; Hodgson, M. C.; Rickard, C. E. F.; Oliver, A. G.; Chaker, L.; Brothers, P. J.; Bolskar, R. D.; Tham, F. S.; Reed, C. A. *J. Am. Chem. Soc.* **1999**, *121*, 10487. (c) Chukharev, V.; Tkachenko, N. V.; Efimov, A.; Guldi, D. M.; Hirsch, A.; Scheloske, M.; Lemmetyinen, H. *J. Phys. Chem. B* **2004**, *108*, 16377. (d) Sun, D.; Tham, F. S.; Reed, C. A.; Boyd, P. D. W. *Proc. Natl. Acad. Sci. U.S.A.* **2002**, *99*, 5088. (e) Kimura, M.; Saito, Y.; Ohta, K.; Hanabusa, K.; Shirai, H.; Kobayashi, N. *J. Am. Chem. Soc.* **2002**, *124*, 5274. (f) Sun, D.; Tham, F. S.; Reed, C. A.; Chaker, L.; Boyd, P. D. W. *J. Am. Chem. Soc.* **2002**, *124*, 6604. (g) Guldi, D. M.; Da Ros, T.; Braiuca, P.; Prato, M.; Alessio, E. *J. Mater. Chem.* **2002**, *12*, 2001. (h) Watanabe, N.; Kihara, N.; Furusho, Y.; Takata, T.; Araki, Y.; Ito, O. *Angew. Chem., Int. Ed.* **2003**, *42*, 681. (i) Guldi, D. M. *Pure Appl. Chem.* **2003**, *75*, 1069. (j) Yamaguchi, T.; Ishii, N.; Tashiro, K.; Aida, T. *J. Am. Chem. Soc.* **2003**, *125*, 13934. (k) Hoshino, S.; Ishii, K.; Kobayashi, N.; Kimura, M.; Shirai, H. *Chem. Phys. Lett.* **2004**, *386*, 149. (l) Dudic, M.; Lhotak, P.; Stibor, I.; Petrickova, H.; Lang, K. *New J. Chem.* **2004**, *28*, 85. (m) Li, K.; Schuster, D. I.; Guldi, D. M.; Herranz, M. A.; Echegoyen, L. *J. Am. Chem. Soc.* **2004**, *126*, 3388. (n) Litvinov, A. L.; Konarev, D. V.; Kovalevsky, A. Y.; Lapshin, A. N.; Yudanov, E. I.; Coppens, P.; Lyubovskaya, R. N. *Fullerenes, Nanotubes, and Carbon Nanostructures* **2004**, *12*, 215. (o) Schuster, D. I.; Li, K.; Guldi, D. M.; Ramey, J. *Org. Lett.* **2004**, *6*, 1919. (p) Schuster, D. I.; Cheng, P.; Jarowski, P. D.; Guldi, D. M.; Luo, C.; Echegoyen, L.; Pyo, S.; Holzwarth, A. R.; Braslavsky, S. E.; Williams, R. M.; Klihm, G. *J. Am. Chem. Soc.* **2004**, *126*, 7257. (q) Chukharev, V.; Tkachenko, N. V.; Efimov, A.; Guldi, D. M.; Hirsch, A.; Scheloske, M.; Lemmetyinen, H. *J. Phys. Chem. B* **2004**, *108*, 16377. (r) Kim, H. J.; Park, K.-M.; Ahn, T. K.; Kim, S. K.; Kim, K. S.; Kim, D.; Kim, H.-J. *Chem. Commun.* **2004**, 2594. (s) Charvet, R.; Jiang, D.-L.; Aida, T. *Chem. Commun.* **2004**, 2664. (t) Sandanayaka, A. S. D.; Watanabe, N.; Ikeshita, K.-I.; Araki, Y.; Kihara, N.; Furusho, Y.; Ito, O.; Takata, T. *J. Phys. Chem. B* **2005**, *109*, 2516. (u) Sessler, J. L.; Jayawickramarajah, J.; Gouloumis, A.; Torres, T.; Guldi, D. M.; Maldonado, S.; Stevenson, K. J. *Chem. Commun.* **2005**, *14*, 1892.
- (a) D'Souza, F.; Deviprasad, G. R.; Rahman, M. S.; Choi, J.-P. *Inorg. Chem.* **1999**, *38*, 2157. (b) Armaroli, N.; Diederich, F.;

- Echegoyen, L.; Habicher, T.; Flamigni, L.; Marconi, G.; Nierengarten, J.-F. *New J. Chem.* **1999**, *77*. (c) Da Ros, T.; Prato, M.; Guldi, D. M.; Alessio, E.; Ruzzi, M.; Pasimeni, L. *Chem. Commun.* **1999**, 635. (d) D'Souza, F.; Deviprasad, G. R.; Zandler, M. E.; El-Khouly, M. E.; Fujitsuka, M.; Ito, O. *J. Phys. Chem. B* **2002**, *106*, 4952. (e) D'Souza, F.; Gadde, S.; Zandler, M. E.; Arkady, K.; El-Khouly, M. E.; Fujitsuka, M.; Ito, O. *J. Phys. Chem. A* **2002**, *106*, 12393. (f) D'Souza, F.; Deviprasad, G. R.; El-Khouly, M. E.; Fujitsuka, M.; Ito, O. *J. Am. Chem. Soc.* **2001**, *123*, 5277. (g) El-Khouly, M. E.; Gadde, S.; Deviprasad, G. R.; Fujitsuka, M.; Ito, O.; D'Souza, F. *J. Porphyrins Phthalocyanines* **2003**, *7*, 1. (h) El-Khouly, M. E.; Rogers, M. E.; Zandler, M. E.; Gadde, S.; Fujitsuka, M.; Ito, O.; D'Souza, F. *ChemPhysChem* **2003**, *4*, 474. (i) Wilson, S. R.; MacMahon, S.; Tat, F. T.; Jarowski, P. D.; Schuster, D. I. *Chem. Commun.* **2003**, 226. (j) D'Souza, F.; Smith, P. M.; Zandler, M. E.; McCarty, A. L.; Itou, M.; Araki, Y.; Ito, O. *J. Am. Chem. Soc.* **2004**, *126*, 7898. (k) D'Souza, F.; Smith, P. M.; Gadde, S.; McCarty, A. L.; Kullman, M. J.; Zandler, M. E.; Itou, Y.; Araki, Y.; Ito, O. *J. Phys. Chem. B* **2004**, *108*, 11333. (l) D'Souza, F.; El-Khouly, M. E.; Gadde, S.; McCarty, A. L.; Karr, P. A.; Zandler, M. E.; Araki, Y.; Ito, O. *J. Phys. Chem.* **2005**, *109*, 10107. (m) D'Souza, F.; Rath, N. P.; Deviprasad, G. R.; Zandler, M. E. *Chem. Commun.* **2001**, 267.
9. (a) D'Souza, F.; Gadde, S.; Zandler, M. E.; Itou, M.; Araki, Y.; Ito, O. *Chem. Commun.* **2004**, 2276. (b) D'Souza, F.; Chitta, R.; Gadde, S.; Zandler, M. E.; Sandanayaka, A. S. D.; Araki, Y.; Ito, O. *Chem. Commun.* **2005**, 1279. (c) D'Souza, F.; Chitta, R.; Gadde, S.; Zandler, M. E.; Sandanayaka, A. S. D.; Araki, Y.; Ito, O. *Chem. Eur. J.* **2005**, *11*, 4416.
10. (a) Takahashi, K.; Etoh, K.; Tsuda, Y.; Yamaguchi, T.; Komura, T.; Ito, S.; Murata, K. *J. Electroanal. Chem.* **1997**, *426*, 85. (b) Imahori, H.; Yamada, H.; Ozawa, S.; Sakata, Y.; Ushida, K. *Chem. Commun.* **1999**, 1165. (c) Imahori, H.; Yamada, H.; Nishimura, Y.; Yamazaki, I.; Sakata, Y. *J. Phys. Chem. B* **2000**, *104*, 2099. (d) Nishioka, T.; Tashiro, K.; Aida, T.; Zheng, J.-Y.; Kinbara, K.; Saigo, K.; Sakamoto, S.; Yamaguchi, K. *Macromolecules* **2000**, *33*, 9182. (e) Imahori, H.; Norieda, H.; Yamada, H.; Nishimura, Y.; Yamazaki, I.; Sakata, Y.; Fukuzumi, S. *J. Am. Chem. Soc.* **2001**, *123*, 100. (f) Ikeda, A.; Hatano, T.; Shinkai, S.; Akiyama, T.; Yamada, S. *J. Am. Chem. Soc.* **2001**, *123*, 4855. (g) Fungo, F.; Otero, L.; Borsarelli, C. D.; Durantini, E. N.; Silber, J. J.; Sereno, L. *J. Phys. Chem. B* **2002**, *106*, 4070. (h) Yamada, H.; Imahori, H.; Nishimura, Y.; Yamazaki, I.; Ahn, T. K.; Kim, S. K.; Kim, D.; Fukuzumi, S. *J. Am. Chem. Soc.* **2003**, *125*, 9129. (i) Hasobe, T.; Imahori, H.; Kamat, P. V.; Fukuzumi, S. *J. Am. Chem. Soc.* **2003**, *125*, 14962. (j) Guldi, D. M.; Zilbermann, I.; Anderson, G. A.; Kordatos, K.; Prato, M.; Tafuro, R.; Valli, L. *J. Mater. Chem.* **2004**, *14*, 303. (k) Imahori, H.; Kashiwagi, Y.; Hasobe, T.; Kimura, M.; Hanada, T.; Nishimura, Y.; Yamazaki, I.; Araki, Y.; Ito, O.; Fukuzumi, S. *Thin Solid Films* **2004**, *451–452*, 580. (l) Hasobe, T.; Kashiwagi, Y.; Absalom, M. A.; Sly, J.; Hosomizu, K.; Crossley, M. J.; Imahori, H.; Kamat, P. V.; Fukuzumi, S. *Adv. Mater.* **2004**, *16*, 975. (m) Imahori, H.; Kimura, M.; Hosomizu, K.; Fukuzumi, S. *J. Photochem. Photobiol., A* **2004**, *166*, 57. (n) Hasobe, T.; Kamat, P. V.; Absalom, M. A.; Kashiwagi, Y.; Sly, J.; Crossley, M. J.; Hosomizu, K.; Imahori, H.; Fukuzumi, S. *J. Phys. Chem. B* **2004**, *108*, 12865. (o) Imahori, H.; Liu, J.-C.; Hosomizu, K.; Sato, T.; Mori, Y.; Hotta, H.; Matano, Y.; Araki, Y.; Ito, O.; Maruyama, N.; Fujita, S. *Chem. Commun.* **2004**, 2066. (p) Imahori, H.; Kimura, M.; Hosomizu, K.; Sato, T.; Ahn, T. K.; Kim, S. K.; Kim, D.; Nishimura, Y.; Yamazaki, I.; Araki, Y.; Ito, O.; Fukuzumi, S. *Chem. Eur. J.* **2004**, *10*, 5111. (q) Yoshimoto, S.; Saito, A.; Tsutsumi, E.; D'Souza, F.; Ito, O.; Itaya, K. *Langmuir* **2004**, *20*, 11046. (r) Hasobe, T.; Imahori, H.; Kamat, P. V.; Ahn, T. K.; Kim, S. K.; Kim, D.; Fujimoto, A.; Hirakawa, T.; Fukuzumi, S. *J. Am. Chem. Soc.* **2005**, *127*, 1216. (s) Cho, Y.-J.; Ahn, T. K.; Song, H.; Kim, K. S.; Lee, C. Y.; Seo, W. S.; Lee, K.; Kim, S. K.; Kim, D.; Park, J. T. *J. Am. Chem. Soc.* **2005**, *127*, 2380. (t) Bae, A.-H.; Hatano, T.; Sugiyasu, K.; Kishida, T.; Takeuchi, M.; Shinkai, S. *Tetrahedron Lett.* **2005**, *46*, 3169.
11. D'Souza, F.; Deviprasad, G. R.; Zandler, M. E.; El-Khouly, M. E.; Fujitsuka, M.; Ito, O. *J. Phys. Chem. A* **2003**, *107*, 4801.
12. D'Souza, F.; Deviprasad, G. R.; Zandler, M. E.; Hoang, V. T.; Arkady, K.; Van Stipdonk, M.; Perera, A.; El-Khouly, M. E.; Fujitsuka, M.; Ito, O. *J. Phys. Chem. A* **2002**, *106*, 3243.
13. (a) Nappa, M.; Valentine, J. S. *J. Am. Chem. Soc.* **1978**, *100*, 5075. (b) D'Souza, F.; Hsieh, Y.-Y.; Deviprasad, G. R. *Inorg. Chem.* **1996**, *35*, 5747.
14. (a) Scatchard, G. *Ann. N.Y. Acad. Sci.* **1949**, *51*, 661. (b) Harris, D. C. *Quantitative Chemical Analysis*, 6th ed.; Freeman: New York, 2003; pp 439–440.
15. Imahori, H.; Tamaki, K.; Guldi, D. M.; Luo, C.; Fujitsuka, M.; Ito, O.; Sakata, Y.; Fukuzumi, S. *J. Am. Chem. Soc.* **2001**, *123*, 2607.
16. (a) Rehm, D.; Weller, A. *Isr. J. Chem.* **1970**, *7*, 259. (b) Mataga, N.; Miyasaka, H. In *Electron Transfer*; Jortner, J., Bixon, M., Eds.; Wiley: New York, 1999; pp 431–496; Part 2.
17. Lakowicz, J. R. *Principles of Fluorescence Spectroscopy*, 2nd ed.; Kluwer/Plenum: New York, 1999.
18. Luo, C.; Fujitsuka, M.; Watanabe, A.; Ito, O.; Gan, L.; Huang, Y.; Huang, C. H. *J. Chem. Soc., Faraday Trans.* **1998**, *84*, 572.
19. (a) Ghosh, H. N.; Pal, H.; Sapre, A. V.; Mittal, J. P. *J. Am. Chem. Soc.* **1993**, *115*, 11722. (b) Nojiri, T.; Watanabe, A.; Ito, O. *J. Phys. Chem. A* **1998**, *102*, 5215. (c) Fujitsuka, M.; Ito, O.; Yamashiro, T.; Aso, Y.; Otsubo, T. *J. Phys. Chem. A* **2000**, *104*, 4876.
20. (a) D'Souza, F.; Zandler, M. E.; Smith, P. M.; Deviprasad, G. R.; Arkady, K.; Fujitsuka, M.; Ito, O. *J. Phys. Chem. A* **2002**, *106*, 649. (b) D'Souza, F.; Zandler, M. E.; Smith, P. M.; Deviprasad, G. R.; Arkady, K.; Fujitsuka, M.; Ito, O. *J. Org. Chem.* **2002**, *67*, 9122. (c) Fujitsuka, M.; Tsuboya, N.; Hamasaki, R.; Ito, M.; Onodera, S.; Ito, O.; Yamamoto, Y. *J. Phys. Chem. A* **2003**, *107*, 1452.
21. Frisch, M. J.; Trucks, G. W.; Schlegel, H. B.; Scuseria, G. E.; Robb, M. A.; Cheeseman, J. R.; Montgomery, J. A., Jr.; Vreven, T.; Kudin, K. N.; Burant, J. C.; Millam, J. M.; Iyengar, S. S.; Tomasi, J.; Barone, V.; Mennucci, B.; Cossi, M.; Scalmani, G.; Rega, N.; Petersson, G. A.; Nakatsuji, H.; Hada, M.; Ehara, M.; Toyota, K.; Fukuda, R.; Hasegawa, J.; Ishida, M.; Nakajima, T.; Honda, Y.; Kitao, O.; Nakai, H.; Klene, M.; Li, X.; Knox, J. E.; Hratchian, H. P.; Cross, J. B.; Adamo, C.; Jaramillo, J.; Gomperts, R.; Stratmann, R. E.; Yazyev, O.; Austin, A. J.; Cammi, R.; Pomelli, C.; Ochterski, J. W.; Ayala, P. Y.; Morokuma, K.; Voth, G. A.; Salvador, P.; Dannenberg, J. J.; Zakrzewski, V. G.; Dapprich, S.; Daniels, A. D.; Strain, M. C.; Farkas, O.; Malick, D. K.; Rabuck, A. D.; Raghavachari, K.; Foresman, J. B.; Ortiz, J. V.; Cui, Q.; Baboul, A. G.; Clifford, S.; Cioslowski, J.; Stefanov, B. B.; Liu, G.; Liashenko, A.; Piskorz, P.; Komaromi, I.; Martin, R. L.; Fox, D. J.; Keith, T.; Al-Laham, M. A.; Peng, C. Y.;

- Nanayakkara, A.; Challacombe, M.; Gill, P. M. W.; Johnson, B.; Chen, W.; Wong, M. W.; Gonzalez, C.; Pople, J. A. *Gaussian 03*, Revision A.2, Gaussian, Inc., Pittsburgh, PA, 2003.
22. (a) Matsumoto, K.; Fujitsuka, M.; Sato, T.; Onodera, S.; Ito, O. *J. Phys. Chem. B* **2000**, *104*, 11632. (b) Komamine, S.; Fujitsuka, M.; Ito, O.; Morikawa, K.; Miyata, T.; Ohno, T. *J. Phys. Chem. A* **2000**, *104*, 11497. (c) Yamazaki, M.; Araki, Y.; Fujitsuka, M.; Ito, O. *J. Phys. Chem. A* **2001**, *105*, 8615. (d) Nishikawa, H.; Kojima, S.; Kodama, T.; Ikemoto, I.; Suzuki, S.; Kikuchi, K.; Fujitsuka, M.; Luo, H.; Araki, Y.; Ito, O. *J. Phys. Chem. A* **2004**, *108*, 1881.

Supramolecular complexes obtained from porphyrin–crown ether conjugates and a fullerene derivative bearing an ammonium unit

Nathalie Solladié,^{a,*} Mathieu E. Walther,^a Haiko Herschbach,^b Emmanuelle Leize,^b
Alain Van Dorsselaer,^{b,*} Teresa M. Figueira Duarte^c and Jean-François Nierengarten^{c,*}

^a*Groupe de Synthèse de Systèmes Porphyriniques, Laboratoire de Chimie de Coordination du CNRS, 205 route de Narbonne, 31077 Toulouse Cedex 4, France*

^b*Laboratoire de Spectrométrie de Masse Bio-organique, Ecole de Chimie, Polymères et Matériaux (ECPM), Université Louis Pasteur and CNRS, 25 rue Becquerel, 67087 Strasbourg Cedex 2, France*

^c*Groupe de Chimie des Fullerènes et des Systèmes Conjugués, Laboratoire de Chimie de Coordination du CNRS, 205 route de Narbonne, 31077 Toulouse Cedex 4, France*

Received 8 April 2005; revised 26 April 2005; accepted 30 April 2005

Available online 14 November 2005

Abstract—A methanofullerene derivative with an ammonium subunit (**1**) has been prepared and its ability to form a supramolecular complex with a porphyrin–crown ether conjugate evidenced by NMR, UV–vis, electrospray mass spectrometry (ES-MS) and luminescence experiments. Interestingly, in addition to the ammonium–crown ether recognition, intramolecular stacking of the fullerene moiety and the porphyrin subunit has been evidenced. Due to this additional recognition element, the association constant for the supramolecular complex is increased by two orders of magnitude when compared to the K_a values found for the complexation of **1** with benzo-18-crown-6. Finally, non-covalent systems resulting from the association of cation **1** with porphyrin derivatives bearing two crown ether subunits have been investigated. Intramolecular C₆₀–porphyrin interactions have also been evidenced within these supramolecular complexes. As a result, the 2:1 complexes are very stable as shown by the ES-MS studies.

© 2005 Elsevier Ltd. All rights reserved.

1. Introduction

Owing to their particular electrochemical and electronic properties, C₆₀ and porphyrins are interesting building blocks for the construction of new photochemical molecular devices.¹ Indeed, the synthesis of covalently linked porphyrin–fullerene hybrids have generated significant research efforts in the last few years.^{2,3} Their photophysical properties have been studied in details and intramolecular processes such as electron and energy transfer evidenced in such multicomponent hybrid systems.^{2,3} Importantly, excited-state dynamic investigations on C₆₀–porphyrin conjugates have revealed that the fullerene sphere is a particularly interesting electron acceptor in artificial photosynthetic models.⁴ The characteristics of C₆₀ are effectively in stark contrast with those of common acceptors with smaller size such as benzoquinone. Actually,

accelerated charge separation and decelerated charge recombination has been observed in a fullerene-based acceptor–donor system when compared to the equivalent benzoquinone-based system.⁴ This has been interpreted by the smaller reorganization energy (λ) of C₆₀ compared with those of small acceptors: the smaller reorganization energy of C₆₀ positions the photoinduced charge separation rate upward along the normal region of the Marcus parabolic curve, while forcing the charge recombination rate downward in the inverted region. The efficient photogeneration of long lived charge-separated states by photoinduced electron transfer is of particular interest for solar energy conversion and photovoltaic devices prepared from porphyrin–fullerene systems have shown promising energy conversion efficiencies.⁵

Whereas research focused on covalently bound C₆₀–porphyrin derivatives has received considerable attention, only a few related examples of non-covalent assemblies have been described so far.^{6,7} In most cases, these non-covalent assemblies have been obtained from a C₆₀ derivative bearing a pyridyl moiety and a metalloporphyrin through coordination to the metal ion.⁶ Due to the apical

Keywords: Binding studies; Crown ether; Fullerene; Porphyrin; Supramolecular chemistry.

* Corresponding authors. Tel.: +33 561 33 31 00; fax: +33 561 55 30 03; e-mail addresses: solladie@lcc-toulouse.fr; vandors@chimie.u-strasbg.fr; jfnierengarten@lcc-toulouse.fr

binding on the porphyrin subunit, the attractive van der Waals interaction of the fullerene sphere with the planar π -surface of the porphyrin seen for several covalent C_{60} -porphyrin derivatives⁸ or in the solid state structures of porphyrin–fullerene co-crystals⁹ is not possible in such arrays. It can also be mentioned here that the π - π stacking between C_{60} and porphyrin moieties is capable of enhancing the efficiency of the end-capping reactions of pseudo-rotaxanes and C_{60} thus leading to [2]-rotaxanes in higher yields.¹⁰ As part of this research, we have recently shown that π -stacking of the two chromophores can have a dramatic effect on the recognition interactions in non-covalent C_{60} -porphyrin ensembles.⁷ Specifically, a supramolecular complex has been obtained from porphyrin–crown ether conjugate **2** and methanofullerene derivative **1** bearing an ammonium function (Fig. 1). In addition to the ammonium–crown ether interaction, intramolecular stacking of the fullerene moiety and the porphyrin subunit has been evidenced in the supramolecular system. Due to this additional recognition element, the association constant (K_a) for the complex obtained from **1** and **2** is increased by two orders of magnitude when compared to K_a values previously found for the complexation of **1** with other crown ether derivatives. In this paper, we now report a full account on this work. In addition, we also show that more complex supramolecular systems are easily accessible by using similar interactions as illustrated by the association of cation **1** with porphyrin derivatives **3** and **4** bearing two crown ether subunits (Fig. 1).

2. Results and discussion

2.1. Synthesis

The synthesis of the functionalized methanofullerene derivative **1** is depicted in Scheme 1. Commercially available methyl 4-(aminomethyl)benzoate hydrochloride was converted to its *t*-butylcarbonyl (Boc) derivative **5** as previously reported.¹¹ $LiAlH_4$ reduction of compound **5** afforded compound **6** in 93% yield. Reaction of acid **7**¹² with benzylic alcohol **6** under esterification conditions using *N,N'*-dicyclohexylcarbodiimide (DCC) and 4-dimethylaminopyridine (DMAP) led to malonic ester **8** in 78% yield. The functionalization of C_{60} with **8** is based on the Bingel reaction.¹³ Nucleophilic addition of a stabilized α -halocarbocation to the C_{60} core, followed by an intramolecular nucleophilic substitution, leads to clean cyclopropanation of C_{60} .¹⁴ It has been shown that the α -halomalonate can be generated in situ, and direct treatment of C_{60} with malonates in the presence of I_2 under basic conditions affords the corresponding methanofullerenes in good yields.¹⁵ Treatment of C_{60} with **8**, iodine and 1,8-diazabicyclo[5.4.0]-undec-7-ene (DBU) in toluene at room temperature afforded methanofullerene **9** in 57% yield. Finally, removal of the Boc group with CF_3CO_2H afforded the targeted derivative **1** as its trifluoroacetate salt in a quantitative yield.

The synthesis of the porphyrin–crown ether derivatives **2**, **3**, and **4** is depicted in Scheme 2. Porphyrin **2** was obtained

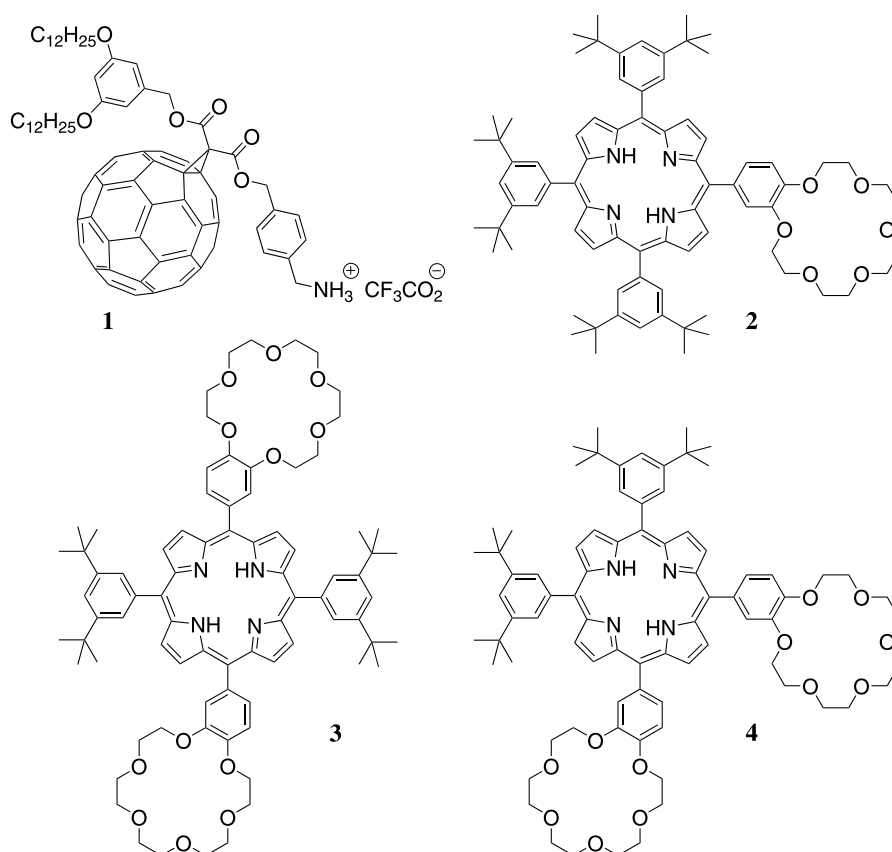
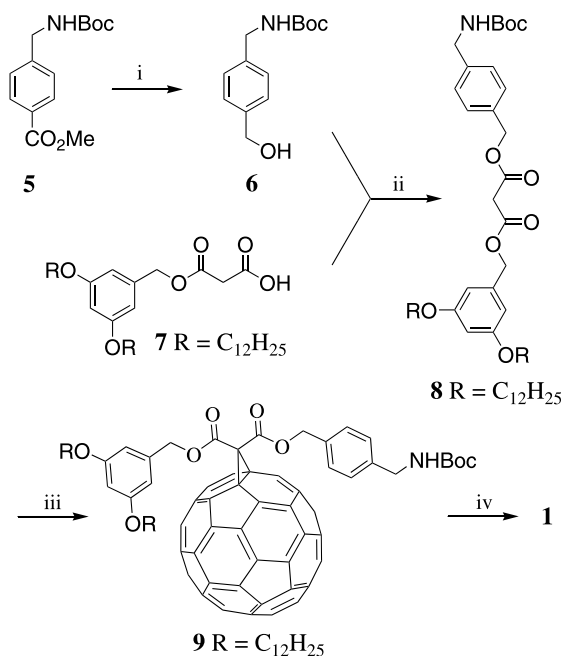
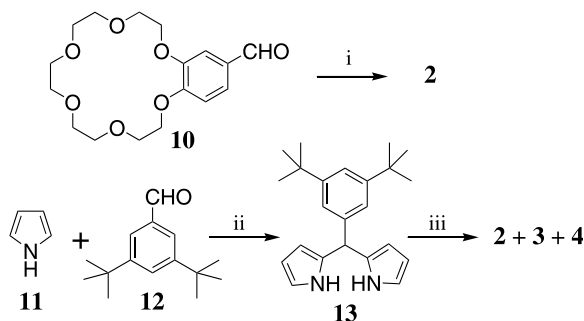


Figure 1. Compounds 1–4.



Scheme 1. Reagents and conditions: (i) LiAlH_4 , THF, 0°C (93%); (ii) DCC, DMAP, CH_2Cl_2 , 0°C to rt (78%); (iii) C_{60} , I_2 , DBU, toluene, rt (57%); (iv) $\text{CF}_3\text{CO}_2\text{H}$, CH_2Cl_2 , rt (99%).

under the classical conditions developed by Lindsey.¹⁶ Condensation of aldehydes **10**¹⁷ (1 equiv) and **12** (3 equiv) with pyrrole (4 equiv) in CHCl_3 in the presence of $\text{BF}_3 \cdot \text{Et}_2\text{O}$ as catalyst was followed by the oxidation of the porphyrinogens by *p*-chloranil. Compound **2** was thus obtained in 13% yield after purification.



Scheme 2. Reagents and conditions: (i) **12** (3 equiv), **11** (4 equiv), $\text{BF}_3 \cdot \text{Et}_2\text{O}$, CHCl_3 , rt then *p*-chloranil, Δ (13%); (ii) $\text{BF}_3 \cdot \text{Et}_2\text{O}$, rt (69%); (iii) **10**, $\text{BF}_3 \cdot \text{Et}_2\text{O}$, CHCl_3 , rt then *p*-chloranil, Δ (**2**: 14%; **3**: 11%; **4**: 12%)

The selective preparation of *trans*- A_2B_2 porphyrin **3** was attempted by the condensation of dipyrromethane **13** and aldehyde **10**. Compound **13** was obtained in a good yield by acid catalyzed condensation of aldehyde **12** with an excess pyrrole in solvent free conditions. Treatment of dipyrromethane **13** with aldehyde **10** in CHCl_3 in the presence of a catalytic amount of $\text{BF}_3 \cdot \text{Et}_2\text{O}$ yielded a mixture of porphyrins **2**, **3**, and **4**. Indeed, under these conditions, polypyrrolic rearrangement reactions took place as often observed during the condensation of aldehydes with 5-substituted dipyrromethane derivatives containing an unhired aryl substituent (lacking β -substituents).¹⁸ As a result of this scrambling process, the desired *trans*- A_2B_2 porphyrin **3** was obtained together with other porphyrin

derivatives. Indeed, compounds **2**, **3**, and **4** were isolated after tedious chromatographic purifications.

2.2. Binding studies

The ability of the fullerene derivative **1** to form supramolecular complexes with crown ether derivatives was first investigated with commercially available benzo-18-crown-6 (**14**) by NMR studies. As shown in Figure 2, the ^1H NMR spectra of **1** in CDCl_3 showed dramatic changes upon successive addition of **14**. The complexation-induced changes in chemical shifts were particularly important for the aromatic protons of the 4-(aminomethyl)benzyl moiety in **1** (H_c and H_d). Indeed, the signal of H_{c-d} in **1** was shifted upfield when benzo-18-crown-6 (**14**) was added. The latter observation may be ascribed to the proximity of the aromatic unit of guest **14** within the supramolecular complex [**1**·(**14**)] in good agreement with the proposed structure. The association constant for the 1:1 complex based on the H_b chemical shifts of **1** was determined as $K_a = 2100 \pm 100 \text{ M}^{-1}$, corresponding to a Gibbs free energy of complexation $\Delta G^0 = -4.5 \text{ kcal/mol}$. Identical results within the error range were obtained when the complexation-induced changes in chemical shifts were monitored for the other protons of **1**.

The binding behavior of ammonium **1** to porphyrin **2** was also investigated by ^1H NMR titration in CDCl_3 at 298 K. As depicted in Figure 3A, the comparison between the ^1H NMR spectra of **1**, **2** and mixtures of both components revealed the apparition of new sets of signals as well as complexation-induced changes in chemical shifts. This is particularly visible for the pyrrolic protons of the porphyrin moiety and the signals arising from the crown ether subunit. The latter observations suggest the existence of two conformers for the supramolecular complex obtained upon association of the two components, one being in fast exchange with uncomplexed **1** and **2** on the NMR time-scale, the other one in slow exchange as shown in Figure 3B. On the one hand, the initial ammonium–crown ether association leading to conformer **A** is responsible for the observed complexation-induced changes in chemical shifts upon addition of ammonium **1** to solutions of **2**. In principle, association of the two molecular units should be possible by π -stacking of the two chromophores only. However, no significant changes in chemical shifts were observed in the ^1H NMR spectrum of **1** upon addition of compound **9** thus showing that the C_{60} –porphyrin interaction does not take place in the absence of ammonium–crown ether recognition. On the other hand, the new sets of signals seen in the ^1H NMR spectra correspond to conformer **B**. The dramatic upfield shift observed for the pyrrolic protons in **B** must be the result of the close proximity of the fullerene sphere suggesting that supramolecule [**1**·(**2**)] adopts a conformation in which the C_{60} subunit is located atop the porphyrin macrocycle. Further evidence for C_{60} –porphyrin interactions came from UV–vis measurements. Addition of **1** to a CH_2Cl_2 solution of **2** causes a red shift of the Soret band, no further spectral changes being observed beyond the addition of ca. 5 equiv of **1** ($\lambda_{\text{max}} = 421$ and 427 nm before and after addition of **1**, respectively). The latter observation confirmed the existence of the C_{60} –porphyrin interactions in [**1**·(**2**)]. Effectively, red shifts in

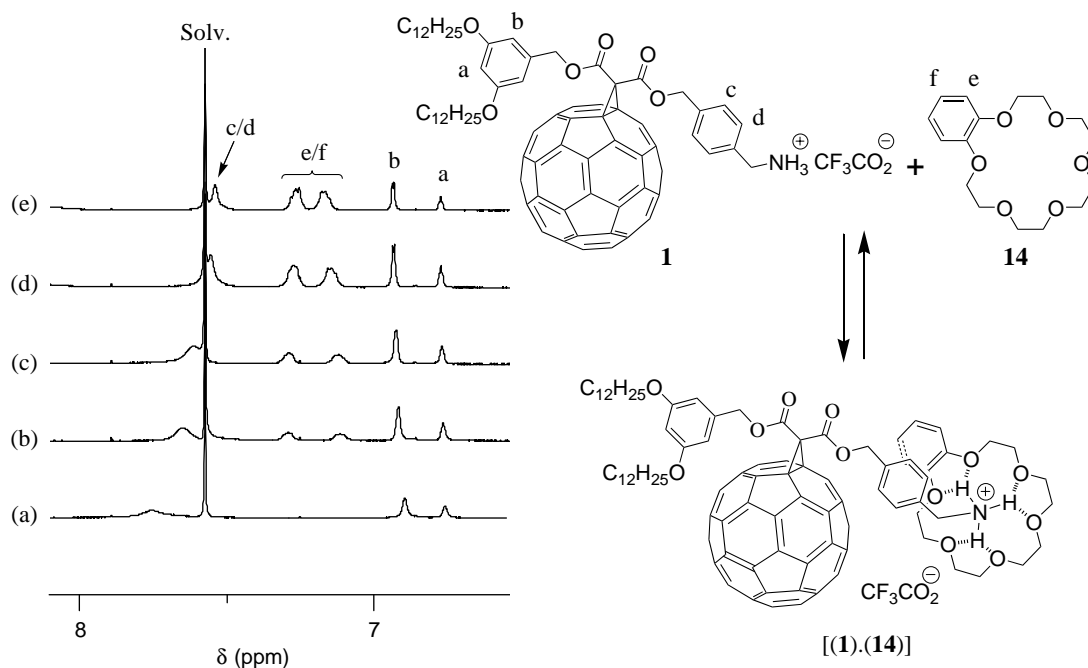


Figure 2. ^1H NMR spectra (300 MHz, CDCl_3 , 298 K) of **1** with 0 (a), 0.25 (b), 0.5 (c), 1.25 (d) and 2 equiv (e) of **14**.

the Soret band have been observed for covalent C_{60} -porphyrin conjugates due to intramolecular π -stacking of the two chromophores.⁸ As reported in detail in the preliminary communication,⁷ the K_a value for the binding of **1** to **2** was determined by a fluorescence titration. A surprisingly high value for the association constant $K_a = 375,000 \text{ M}^{-1}$ was obtained. Effectively, the association constant between porphyrin **2** and fullerene **1** is unexpectedly increased by two orders of magnitude when compared to the K_a value found for the complexation of **1** with crown ether **14**. Such a stabilization of the supramolecular complex formed between **1** and **2**, which can be attributed to an additional intramolecular interaction, provides further evidence for the π -stacking of the fullerene moiety and the porphyrin subunit in $[(\mathbf{1})\cdot(\mathbf{2})]$ suggested by the NMR studies.

The binding behavior of **1** to porphyrins **3** and **4** was also investigated by ^1H NMR in CDCl_3 at 298 K. As discussed for the NMR binding studies of **1** to **2**, apparition of new sets of signals and complexation-induced changes in chemical shifts were observed in the ^1H NMR spectra of **3** and **4** upon addition of ammonium **1** revealing the effective formation of supramolecular structures. However, the interpretation of the NMR spectra appeared difficult due to the possible formation of 1:1 and 2:1 complexes. It must, however, be noted that, as in the case of $[(\mathbf{1})\cdot(\mathbf{2})]$, intramolecular C_{60} -porphyrin interactions were evidenced for the supramolecular complexes obtained from the association of both **3** and **4** with ammonium **1**. Effectively, some signals corresponding to the pyrrolic protons were dramatically up-field shifted in the ^1H NMR spectra of **3** and **4** upon addition of methanofullerene **1**. Furthermore, by adding increasing amount of **1** to CH_2Cl_2 solutions of **3** and **4**, the characteristic red shift of the Soret band due to the C_{60} -porphyrin interactions was observed in the UV-vis spectra.

2.3. Mass spectrometric characterization

The supramolecular complexes obtained from fullerene derivative **1** and the porphyrin-crown ether conjugate **2-4** were further characterized in the gas phase by electrospray mass spectrometry (ES-MS). Unlike other mass spectrometric methods, ES-MS allows pre-existing ions in solution to be transferred to the gas phase without fragmentation. This soft ionization technique, mainly developed by Fenn and co-workers,¹⁹ is now commonly applied to the study of large non-covalent assemblies²⁰ and appears as ideally suited to characterize the non-covalent complexes formed from **1** and **2-4**. The positive ES mass spectrum (Fig. 4) recorded from a 1:1 mixture of **1** and **2** displayed a singly charged ion peak at $m/z = 2587.2$, which can be assigned to the 1:1 complex after loss of the trifluoroacetate counteranion (calculated $m/z = 2587.24$).

As shown in Figure 5, the positive ES mass spectrum obtained under mild conditions (extracting cone voltage $V_c = 50 \text{ V}$) from a 2:1 mixture of **1** and **4** is characterized by a doubly charged ion peak at $m/z = 2055.2$, which can be assigned to the 2:1 complex after loss of the two trifluoroacetate counteranions (calculated $m/z = 2055.45$). The peak corresponding to the 1:1 complex could almost not be detected under these conditions thus suggesting that the self-assembled array $[(\mathbf{1})\cdot(\mathbf{3})_2]$ is the most abundant species in the analysed solution.

ES-MS analysis of a 2:1 mixture of **1** and **3** gave similar results. At low V_c , only the signal corresponding to the supramolecular complex $[(\mathbf{1})\cdot(\mathbf{3})_2]$ was observed (Fig. 6). Under more brutal conditions ($V_c = 180 \text{ V}$), the spectrum was still dominated by the doubly charged ion peak at $m/z = 2055.6$ but a singly charged ion peak attributed to the 1:1 complex was also observed at $m/z = 2709.6$ (calculated $m/z = 2709.28$). The intensity of the latter signal is increased

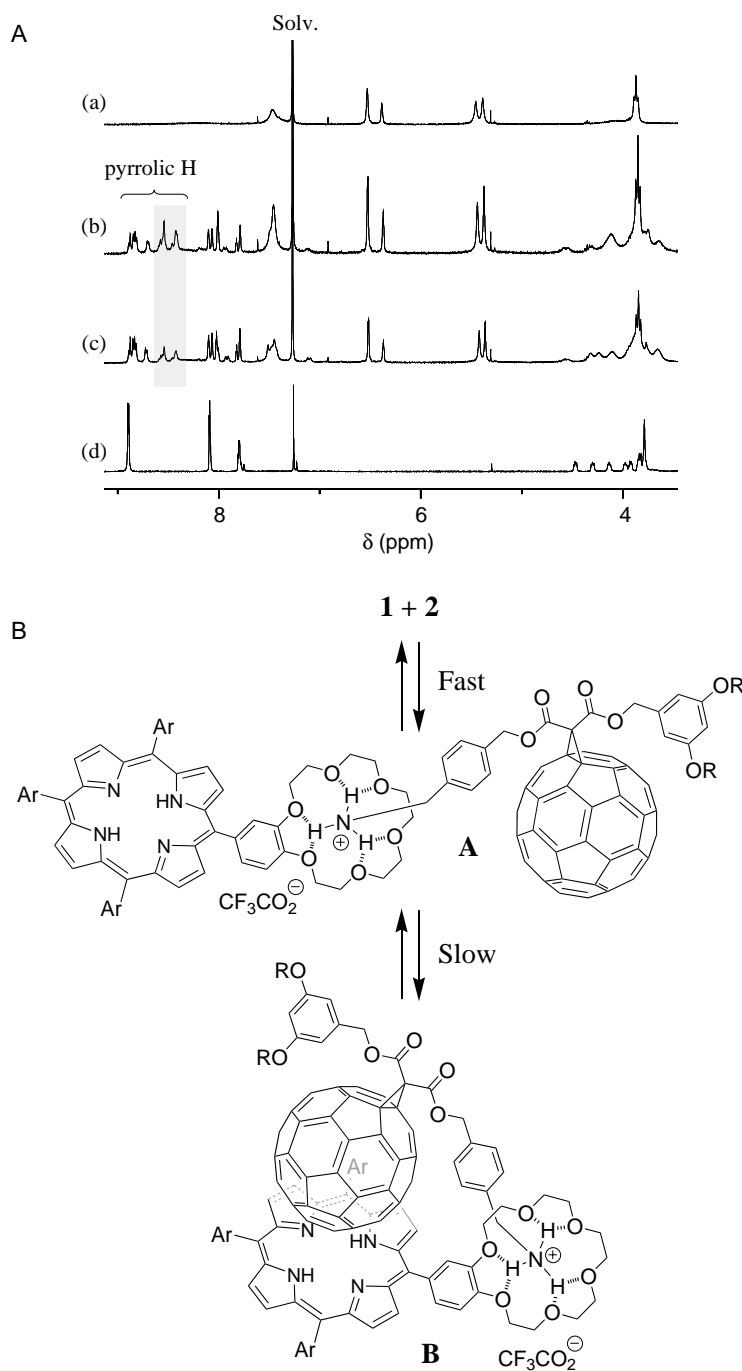


Figure 3. (A) ¹H NMR spectra (CDCl₃, 300 MHz, 298 K) of **1** (a), **2** (d), a 2:1 mixture of **1** and **2** (b) and a 1:1 mixture of **1** and **2** (c); the signals of the pyrrolic protons of **B** are highlighted. (B) Schematic representation of the two conformers of the supramolecular complex obtained upon association of **1** and **2**. **A** is in fast exchange with uncomplexed **1** and **2** on the NMR time-scale and **B** in slow exchange.

as the V_c value is increased, thus the peak corresponding to [(**1**)·(**3**)] must result from the fragmentation of the 2:1 supramolecular complex [(**1**)·(**3**)₂] initially present in solution. A similar behavior was also observed for the ES mass spectra of the 2:1 mixture of **1** and **4** recorded at various V_c values. In both cases, the fragmentation is still limited thus showing the high stability of the non-covalent arrays [(**1**)·(**3**)₂] and [(**1**)·(**4**)₂]. This observation further corroborates the existence of intramolecular stacking interactions between the fullerene moiety and the porphyrin subunit in [(**1**)·(**3**)₂] and [(**1**)·(**4**)₂] as suggested by the NMR and UV–vis data.

2.4. Preliminary fluorescence studies

The complexation between **1** and **2–4** was finally investigated in CH₂Cl₂ by luminescence studies. A large decrease in intensity of the characteristic porphyrin emission was observed when the fullerene ammonium salt **1** was added to a CH₂Cl₂ solution of **2**, **3** or **4**. This decrease can be attributed, at least in part, to the reabsorption of the porphyrin luminescence by the fullerene derivative **1**. However, experiments carried out in parallel with mixtures of **2**, **3** or **4** and methanofullerene **9**, which are not able to form a supramolecular complex show that the decrease in

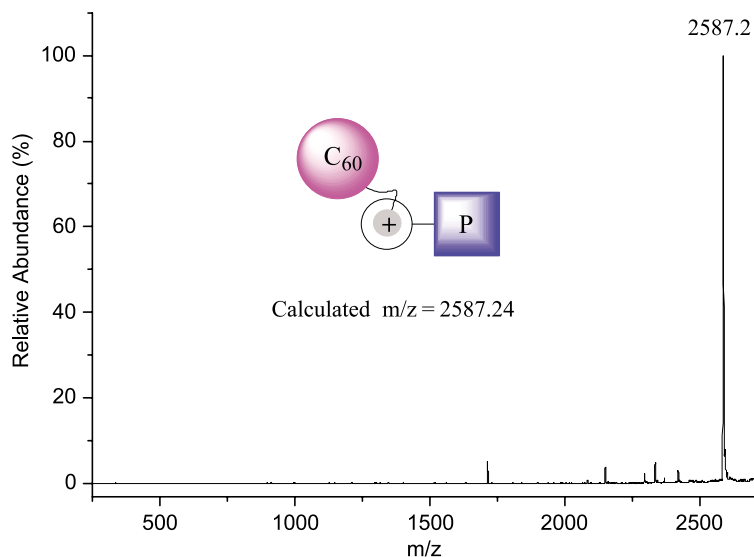


Figure 4. ES mass spectrum ($V_c=20$ V) recorded from an equimolar mixture (10^{-5} M) of **1** and **2** in CH_2Cl_2 .

luminescence intensity could mainly originate from an intramolecular photoinduced process in the supramolecular C_{60} –porphyrin conjugates. Further evidence for an intramolecular quenching of the porphyrin excited-state by the fullerene moiety in $[(\mathbf{1})\cdot(\mathbf{2})]$, $[(\mathbf{1})\cdot(\mathbf{3})_2]$ and $[(\mathbf{1})\cdot(\mathbf{4})_2]$ was obtained from the following experiments. Addition of DBU to mixtures of **1** and **2**, **3** or **4** in CH_2Cl_2 causes an increase of the porphyrin emission. Actually, the fluorescence intensity of the resulting solution was found to be similar to that of the reference solution containing **9** and **2**, **3** or **4**. In other words, the treatment with a base deprotonates the ammonium moiety of **1** and, thereby, disrupts the non-covalent bonding interactions that brought the components together. Addition of trifluoroacetic acid to the CH_2Cl_2 solution regenerates the ammonium center, thus allowing the formation of the supramolecular complexes, and the luminescence intensity of final solution is the same as that of the starting mixture of **1** and **2**, **3** or **4**. The observed decrease in luminescence intensity originates from either energy or electron transfer from the photoexcited porphyrin

to the C_{60} acceptor in the supramolecular complexes. Steady state measurements are not sufficient to determine the nature of the quenching because the residual porphyrin emission overlaps the much weaker fullerene emission, thus prohibiting clean excitation spectroscopy. Detailed photo-physical studies are currently under investigation and will be reported in due time.

3. Conclusions

A methanofullerene derivative bearing an ammonium unit (**1**) was synthesized. Its ability to form supramolecular complexes with crown ether derivatives was first evidenced with commercially available benzo-18-crown-6 (**14**) by NMR studies. The value found for the association constant is quite low (2100 M^{-1} in CDCl_3 at 298 K) but consistent with association constants already reported for supramolecular associates resulting from ammonium–crown ether interactions.^{20d,21} The assembly of the C_{60} –ammonium

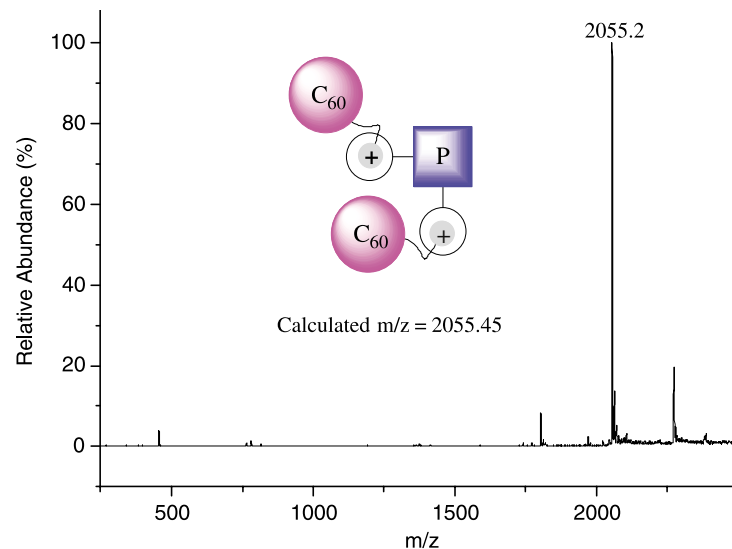


Figure 5. ES mass spectrum ($V_c=50$ V) recorded from a 2:1 mixture of **1** and **4** in CH_2Cl_2 .

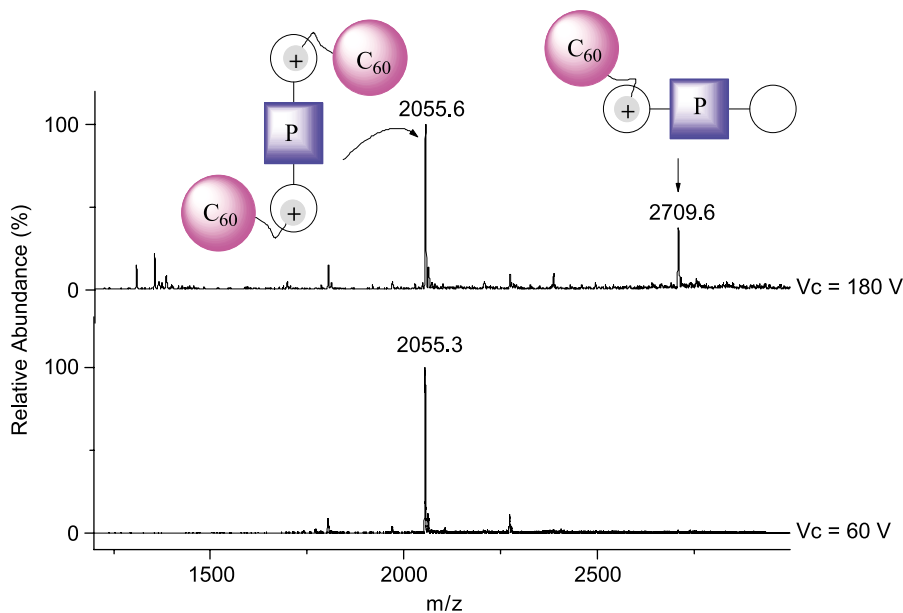


Figure 6. ES mass spectra recorded at different V_c from a 2:1 mixture of **1** and **3** in CH_2Cl_2 .

cation **1** with a porphyrin derivative bearing one crown ether moiety (**2**) was also investigated. The NMR and UV–vis binding studies revealed an interesting behavior. Effectively, in addition to the ammonium–crown ether recognition, intramolecular stacking of the fullerene moiety and the porphyrin subunit has been evidenced. Due to this additional recognition element, the association constant for the supramolecular complex is increased by two orders of magnitude when compared to the K_a values found for the complexation of **1** with crown ether **14**. Finally, more complex non-covalent systems resulting from the association of cation **1** with porphyrin derivatives **3** and **4** bearing two crown ether subunits were investigated. Intramolecular C_{60} –porphyrin interactions have also been evidenced within the resulting supramolecular complexes. As a result, the 2:1 complexes are very stable as shown by the ES-MS studies. These supramolecular arrays containing two fullerene subunits appear to be particularly interesting candidates for photophysical studies. Effectively, the beneficial effect resulting from the presence of a second fullerene moiety on the properties of C_{60} -dumbbells has been recently highlighted by Martin and co-workers.²²

In conclusion, this work paves the way toward the construction of new stable non-covalent supramolecular arrays combining porphyrin and fullerene units. Upon a suitable choice of the molecular components, new supramolecular architectures displaying interesting photoinduced intercomponent processes can be envisaged. Work in this direction is under progress in our laboratories.

4. Experimental

4.1. General

Reagents and solvents were purchased as reagent grade and used without further purification. THF was distilled over sodium benzophenone ketyl. Compounds **5**,¹¹ **7**,¹² and **10**¹⁷

were prepared as previously reported. All reactions were performed in standard glassware under an inert Ar atmosphere. Evaporation and concentration were done at water aspirator pressure and drying in vacuo at 10^{-2} Torr. Column chromatography: silica gel 60 (230–400 mesh, 0.040–0.063 mm) was purchased from Merck. Thin-layer chromatography (TLC) was performed on glass sheets coated with silica gel 60 F_{254} purchased from Merck, visualization by UV light. UV–vis spectra were recorded on a Hitachi U-3000 spectrophotometer. NMR spectra were recorded on a Bruker AC 300 with solvent peaks as reference. Elemental analyses were performed by the analytical service at the Institut Charles Sadron, Strasbourg.

4.1.1. Compound 6. A 1 M LiAlH_4 solution in dry THF (4 mL, 4.0 mmol) was added dropwise to a stirred solution of **5** (0.9 g, 3.39 mmol) in dry THF (100 mL) at 0°C . The resulting mixture was stirred for 5 h at 0°C , then MeOH was carefully added. The resulting mixture was filtered (Celite) and evaporated. Column chromatography (SiO_2 , CH_2Cl_2 /2% MeOH) yielded **6** (0.75 g, 93%) as a colorless glassy product. ^1H NMR (300 MHz, CDCl_3): 7.31 (AB, $J=7$ Hz, 4H), 4.83 (broad s, 1H), 4.69 (d, $J=6$ Hz, 2H), 4.31 (d, $J=6$ Hz, 2H), 1.67 (broad s, 1H), 1.46 (s, 9H); ^{13}C NMR (75 MHz, CDCl_3): 155.9, 140.0, 138.2, 127.6, 127.2, 79.5, 64.9, 44.3, 28.3. Anal. Calcd for $\text{C}_{13}\text{H}_{19}\text{O}_3\text{N}$: C 65.80, H 8.07, N 5.90. Found: C 66.52, H 8.18, N 6.03.

4.1.2. Compound 8. DCC (2.57 g, 12.6 mmol) was added to a stirred solution of **6** (0.745 g, 3.14 mmol), **7** (1.94 g, 3.45 mmol) and DMAP (0.153 g, 1.26 mmol) in CH_2Cl_2 (100 mL) at 0°C . After 1 h, the mixture was allowed to slowly warm to room temperature (within 1 h), then stirred for 12 h, filtered and evaporated to dryness. Column chromatography (SiO_2 , CH_2Cl_2 /hexane 4:1) yielded **8** (1.93 g, 78%) as a colorless oil. ^1H NMR (300 MHz, CDCl_3): 7.28 (AB, $J=7$ Hz, 4H), 6.46 (d, $J=2$ Hz, 2H), 6.41 (t, $J=2$ Hz, 1H), 5.16 (s, 2H), 5.09 (s, 2H), 4.84 (broad s, 1H), 4.31 (d, $J=6$ Hz, 2H), 3.91 (t, $J=7$ Hz, 4H), 3.47 (s,

2H), 1.75 (m, 4H), 1.44 (s, 9H), 1.30 (m, 36H), 0.88 (t, $J=7$ Hz, 6H); ^{13}C NMR (75 MHz, CDCl_3): 166.2, 160.4, 155.8, 139.3, 137.1, 134.3, 128.6, 127.6, 106.4, 101.1, 79.5, 68.1, 67.2, 66.9, 44.3, 41.5, 31.9, 29.65, 29.6, 29.5, 29.4, 29.3, 29.2, 28.4, 26.0, 22.7, 14.1.

4.1.3. Compound 9. DBU (0.16 mL, 1.04 mmol) was added to a stirred solution of C_{60} (300 mg, 0.41 mmol), I_2 (116 mg, 0.45 mmol) and **8** (326 mg, 0.41 mmol) in toluene (500 mL) at room temperature. The solution was stirred for 12 h at room temperature, filtered through a short plug of SiO_2 (toluene) and evaporated. Column chromatography (SiO_2 , CH_2Cl_2 /hexane 7:3) yielded **9** (0.71 g, 57%) as a dark brown solid. UV–vis (CH_2Cl_2): 256 (125,500), 325 (35,900), 425 (3300), 688 (190); ^1H NMR (300 MHz, CDCl_3): 7.35 (AB, $J=7$ Hz, 4H), 6.56 (d, $J=2$ Hz, 2H), 6.42 (t, $J=2$ Hz, 1H), 5.47 (s, 2H), 5.39 (s, 2H), 4.87 (broad s, 1H), 4.32 (d, $J=6$ Hz, 2H), 3.89 (t, $J=7$ Hz, 4H), 1.75 (m, 4H), 1.43 (s, 9H), 1.30 (m, 36H), 0.88 (t, $J=7$ Hz, 6H); ^{13}C NMR (75 MHz, CDCl_3): 163.3, 163.2, 160.4, 155.8, 145.1, 145.05, 145.0, 144.95, 144.85, 144.8, 144.6, 144.5, 144.4, 143.8, 143.7, 143.0, 142.9, 142.8, 142.1, 141.8, 141.7, 140.8, 140.7, 139.6, 139.1, 138.8, 136.4, 133.6, 129.1, 127.7, 107.0, 101.6, 79.5, 71.3, 68.8, 68.5, 68.1, 51.7, 44.3, 31.9, 29.7, 29.6, 29.4, 29.3, 29.2, 28.4, 26.1, 22.7, 14.1. Anal. Calcd for $\text{C}_{107}\text{H}_{73}\text{O}_8\text{N}$: C 85.64, H 4.90, N 0.93. Found: C 85.41, H 4.90, N 0.84.

4.1.4. Compound 1. A solution of **9** (393 mg, 0.26 mmol) and $\text{CF}_3\text{CO}_2\text{H}$ (20 mL) in CH_2Cl_2 (40 mL) was stirred at room temperature for 4 h. The mixture was then washed with water, dried (MgSO_4), filtered and evaporated to dryness. Recrystallization from CH_2Cl_2 /hexane yielded **1** (397 mg, 99%) as a dark brown solid. UV–vis (CH_2Cl_2): 257 (130,200), 326 (36,900), 425 (3200), 687 (180); ^1H NMR (300 MHz, CDCl_3): 7.46 (AB, $J=8$ Hz, 4H), 6.51 (d, $J=2$ Hz, 2H), 6.37 (t, $J=2$ Hz, 1H), 5.46 (s, 2H), 5.37 (s, 2H), 4.16 (s, 2H), 3.86 (t, $J=7$ Hz, 4H), 1.67 (m, 4H), 1.25 (m, 36H), 0.87 (t, $J=7$ Hz, 6H); ^{13}C NMR (75 MHz, CDCl_3): 163.4, 163.3, 160.4, 145.2, 145.1, 144.9, 144.6, 144.4, 143.8, 142.9, 142.1, 141.8, 141.7, 140.9, 140.8, 139.3, 138.6, 136.4, 136.1, 129.4, 129.1, 107.3, 101.8, 71.2, 69.0, 68.2, 51.6, 31.9, 29.7, 29.5, 29.4, 29.3, 26.2, 22.7, 14.2; FAB-MS: 1401.5 ($[\text{M}-\text{CF}_3\text{CO}_2]^-$), calcd for $\text{C}_{102}\text{H}_{66}\text{O}_6\text{N}$: 1401.6. Anal. Calcd for $\text{C}_{104}\text{H}_{66}\text{O}_8\text{NF}_3 \cdot 0.8 \text{CH}_2\text{Cl}_2$: C 79.54, H 4.31, N 0.89. Found: C 79.74, H 4.35, N 0.83.

4.1.5. Compound 2. A 3.2 M solution of $\text{BF}_3 \cdot \text{OEt}_2$ (200 μL) in CHCl_3 was added to a stirred solution of **10** (170 mg, 0.50 mmol), **11** (140 μL , 2.02 mmol) and **12** (331 mg, 1.51 mmol) in CHCl_3 (200 mL) at room temperature under argon. The resulting solution was stirred for 1 h and *p*-chloranil (382 mg, 1.56 mmol) added. The mixture was then refluxed for 1 h and evaporated. Column chromatography (SiO_2 , CH_2Cl_2 /MeOH 90:10) gave **2** (75 mg, 13%) as a dark purple solid. UV–vis (CH_2Cl_2): 421 (455,000), 517 (16,500), 553 (9800), 592 (5300), 648 (5300); ^1H NMR (CDCl_3 , 300 MHz): 8.90 (s, 8H), 8.09 (d, $J=2$ Hz, 4H), 8.08 (d, $J=2$ Hz, 2H), 7.80 (t, $J=2$ Hz, 2H), 7.79 (d, $J=2$ Hz, 1H), 7.78 (t, $J=2$ Hz, 1H), 7.76 (dd, $J=7$, 2 Hz, 1H), 7.24 (d, $J=7$ Hz, 1H), 4.47 (t, $J=6$ Hz, 2H), 4.30 (t, $J=6$ Hz, 2H), 4.14 (t, $J=6$ Hz, 2H), 3.98 (t, $J=$

6 Hz, 2H), 3.93 (m, 2H), 3.85 (m, 4H), 3.79 (m, 6H), 1.54 (s, 36H), 1.53 (s, 18H), -2.69 (broad s, 2H).

4.1.6. Compound 13. A 3.2 M solution of $\text{BF}_3 \cdot \text{OEt}_2$ (0.28 mL) in CHCl_3 was added to a stirred mixture of **12** (804 mg, 3.68 mmol) and pyrrole (10 mL, 36.6 mmol) at room temperature under argon. After 2 h, the resulting dark brown solution was evaporated. The residue was dissolved in CH_2Cl_2 , washed with a 1 M aqueous NaOH solution ($2 \times$) and evaporated. Column chromatography (SiO_2 , hexane/ CH_2Cl_2 /Et₃N 94:5:1) gave **13** (848 mg, 69%) as a brown oil. ^1H NMR (CDCl_3 , 300 MHz): 7.87 (broad s, 2H), 7.49 (t, $J=2$ Hz, 1H), 7.22 (d, $J=2$ Hz, 2H), 6.73 (m, 2H), 6.29 (m, 2H), 6.06 (m, 2H), 5.52 (s, 1H), 1.46 (s, 18H).

4.1.7. Compounds 2, 3, and 4. A 3.2 M solution of $\text{BF}_3 \cdot \text{OEt}_2$ (0.2 mL) in CHCl_3 was added to a stirred solution of **13** (334 mg, 1 mmol) and **10** (340 mg, 1 mmol) in CHCl_3 (200 mL) at room temperature under argon. The resulting dark red solution was stirred for 1 h and *p*-chloranil (367 mg, 1.5 mmol) added. The mixture was then refluxed for 1 h and evaporated. Column chromatography (SiO_2) gave **2** (eluent: CH_2Cl_2 /MeOH 90:10, 54 mg, 14%), **3** (eluent: CH_2Cl_2 /MeOH 88:12, 73 mg, 11%), **4** (eluent: CH_2Cl_2 /MeOH 85:15, 80 mg, 12%).

Compound 3. Dark purple solid. UV–vis (CH_2Cl_2): 422 (230,000), 519 (10,700), 546 (7300), 594 (6500), 645 (6600); ^1H NMR (CDCl_3 , 300 MHz): 8.88 (s, 8H), 8.07 (d, $J=2$ Hz, 4H), 7.80 (t, $J=2$ Hz, 2H), 7.77 (broad s, 2H), 7.74 (broad d, $J=7$ Hz, 2H), 7.23 (d, $J=7$ Hz, 2H), 4.46 (t, $J=6$ Hz, 4H), 4.29 (t, $J=6$ Hz, 4H), 4.13 (t, $J=6$ Hz, 4H), 3.97 (t, $J=6$ Hz, 4H), 3.93 (m, 4H), 3.81 (m, 8H), 3.78 (m, 12H), 1.53 (s, 36H), -2.74 (broad s, 2H).

Compound 4. Dark purple solid. UV–vis (CH_2Cl_2): 422 (280,000), 520 (19,400), 552 (14,300), 594 (9700), 646 (9500); ^1H NMR (CDCl_3 , 300 MHz): 8.88 (m, 8H), 8.08 (d, $J=2$ Hz, 2H), 8.07 (d, $J=2$ Hz, 2H), 7.81 (t, $J=2$ Hz, 1H), 7.80 (t, $J=2$ Hz, 1H), 7.78 (m, 2H), 7.74 (m, 2H), 7.23 (m, 2H), 4.46 (m, 4H), 4.29 (m, 4H), 4.12 (m, 4H), 3.97 (m, 4H), 3.90 (m, 4H), 3.82 (m, 8H), 3.78 (m, 12H), 1.54 (s, 18H), 1.53 (s, 18H), -2.73 (broad s, 2H).

4.2. ES-MS

Samples for ES-MS were prepared from stock solutions of **1**, **2**, **3**, and **4** in CH_2Cl_2 to achieve a concentration of 10^{-5} M. Positive ES mass spectra were obtained on an ES triple quadrupole mass spectrometer Quattro II with a mass-to-charge (m/z) ratio range extended to 8000 (Micromass, Altrincham, UK). The electrospray source was heated to 40°C . Sample solutions were introduced into the mass spectrometer source with a syringe pump (Harvard type 55 1111: Harvard Apparatus Inc., South Natick, MA, USA) with a flow rate of $3 \mu\text{L min}^{-1}$. The extraction cone voltage (V_c) was systematically changed from 20 to 180 V. Calibration was performed using protonated horse myoglobin. Scanning was performed in the MCA (Multi Channel Analyzer) mode, and several scans were summed to obtain the final spectrum.

4.3. Determination of the association constant K_a by NMR titration

The ^1H NMR binding studies were performed at 298 K in CDCl_3 . The concentration of **1** was kept constant (0.5 mM). Increasing amounts of **14** were added (0.2–2 mM; 12 data points) and the chemical shift (δ) of the aromatic protons in **1** were observed. The complexation-induced variation of the chemical shift ($\Delta\delta$) was plotted against the concentration of **14**. The complexation data (K_a , ΔG^0 , $\Delta\delta_{\text{sat}}$) were obtained by iteration using a nonlinear regression analysis curve-fitting software developed in the laboratories of Prof. François Diederich.²³ The experiment was performed in duplicate.

Acknowledgements

This work was supported by the CNRS and the French Ministry of Research (ACI Jeunes Chercheurs to N.S.).

References and notes

- (a) Martín, N.; Sánchez, L.; Illescas, B.; Pérez, I. *Chem. Rev.* **1998**, *98*, 2527–2547. (b) Nierengarten, J.-F. *Sol. Energy Mater. Sol. Cells* **2004**, *83*, 187–199. (c) Segura, J. L.; Martín, N.; Guldi, D. M. *Chem. Soc. Rev.* **2005**, *34*, 31–47. (d) Bendikov, M.; Wudl, F.; Perepichka, D. F. *Chem. Soc. Rev.* **2004**, *104*, 4891–4945. (e) Nierengarten, J.-F. *New J. Chem.* **2004**, *28*, 1177–1191.
- Guldi, D. M. *Chem. Soc. Rev.* **2002**, *31*, 22–36 and references therein.
- (a) Imahori, H.; Sakata, Y. *Eur. J. Org. Chem.* **1999**, 2445–2457. (b) Gust, D.; Moore, T. A.; Moore, A. L. *Acc. Chem. Res.* **2001**, *34*, 40–48. (c) Imahori, H. *J. Phys. Chem. B* **2004**, *108*, 6130–6143. (d) Imahori, H. *Org. Biomol. Chem.* **2004**, *2*, 1425–1433.
- Imahori, H.; Hagiwara, K.; Akiyama, T.; Aoki, M.; Taniguchi, S.; Okada, T.; Shirakawa, M.; Sakata, Y. *Chem. Phys. Lett.* **1996**, *263*, 545–550.
- Imahori, H.; Fukuzumi, S. *Adv. Funct. Mater.* **2004**, *14*, 525–536 and references therein.
- (a) Armaroli, N.; Diederich, F.; Echegoyen, L.; Habicher, T.; Flamigni, L.; Marconi, G.; Nierengarten, J.-F. *New J. Chem.* **1999**, *23*, 77–83. (b) D'Souza, F.; Deviprasad, G. R.; Rahman, M. S.; Choi, J.-P. *Inorg. Chem.* **1999**, *38*, 2157–2160. (c) Da Ros, T.; Prato, M.; Guldi, D. M.; Alessio, E.; Ruzzi, M.; Pasimeni, L. *Chem. Commun.* **1999**, 635–636. (d) Guldi, D. M.; Da Ros, T.; Braiuca, P.; Prato, M.; Alessio, E. *J. Mater. Chem.* **2002**, *12*, 2001–2008. (e) Wilson, S. R.; MacMahon, S.; Tat, F. T.; Jarowski, P. D.; Schuster, D. I. *Chem. Commun.* **2003**, 226–227.
- Solladié, N.; Walther, M. E.; Gross, M.; Figueira Duarte, T. M.; Bourgogne, C.; Nierengarten, J.-F. *Chem. Commun.* **2003**, 2412–2413.
- (a) Schuster, D. I.; Jarowski, P. D.; Kirschner, A. N.; Wilson, S. R. *J. Mater. Chem.* **2002**, *12*, 2041–2047. (b) Armaroli, N.; Marconi, G.; Echegoyen, L.; Bourgeois, J.-P.; Diederich, F. *Chem. Eur. J.* **2000**, *6*, 1629–1645.
- Boyd, P. D. W.; Reed, C. A. *Acc. Chem. Res.* **2005**, *38*, 235–242 and references therein.
- Sasabe, H.; Kihara, N.; Furusho, Y.; Mizuno, K.; Ogawa, A.; Takata, T. *Org. Lett.* **2004**, *6*, 3957–3960.
- Zistler, A.; Kock, S.; Schlüter, A. D. *J. Chem. Soc., Perkin Trans 1* **1999**, 501–508.
- Felder, D.; Gutiérrez Nava, M.; del Pilar Carreon, M.; Eckert, J.-F.; Luccisano, M.; Schall, C.; Masson, P.; Gallani, J.-L.; Heinrich, B.; Guillon, D.; Nierengarten, J.-F. *Helv. Chim. Acta* **2002**, *85*, 288–319.
- Bingel, C. *Chem. Ber.* **1993**, *126*, 1957–1959.
- Nierengarten, J.-F. In *Fullerenes: from Synthesis to Optoelectronic Applications*; Guldi, D. M., Martin, N., Eds.; Kluwer Academic: Dordrecht (The Netherlands), 2002; pp 51–79.
- Nierengarten, J.-F.; Gramlich, V.; Cardullo, F.; Diederich, F. *Angew. Chem., Int. Ed.* **1996**, *35*, 2101–2103.
- Lindsey, J. S.; Wagner, R. W. *J. Org. Chem.* **1989**, *54*, 828.
- Handyside, T. M.; Lockhart, J. C.; McDonnell, M. B.; Rao, P. V. S. *J. Chem. Soc., Dalton Trans.* **1982**, 2331–2336.
- (a) Littler, B. J.; Ciringh, Y.; Lindsey, J. S. *J. Org. Chem.* **1999**, *64*, 2864–2872. (b) Geier, G. R., III; Littler, B. J.; Lindsey, J. S. *J. Chem. Soc., Perkin Trans. 2* **2001**, 701–711.
- Fenn, J. B.; Mann, M.; Meng, C. K.; Wong, S. F.; Whitehouse, C. M. *Science* **1989**, *246*, 64–66.
- (a) Nierengarten, H.; Rojo, J.; Leize, E.; Lehn, J.-M.; Van Dorsselaer, A. *Eur. J. Inorg. Chem.* **2002**, 573–579. (b) Rogniaux, H.; Van Dorsselaer, A.; Barth, P.; Biellmann, J.-F.; Barbanton, J.; van Zandt, M.; Chevriér, B.; Howard, E.; Mitschler, A.; Potier, N.; Urzhumtseva, L.; Moras, D.; Poodjary, A. *J. Am. Soc. Mass Spectrom.* **1999**, *10*, 209–212. (c) Gutiérrez-Nava, M.; Jaeggy, M.; Nierengarten, H.; Masson, P.; Guillon, D.; Van Dorsselaer, A.; Nierengarten, J.-F. *Tetrahedron Lett.* **2003**, *44*, 3039–3042. (d) Gutiérrez-Nava, M.; Nierengarten, H.; Masson, P.; Van Dorsselaer, A.; Nierengarten, J.-F. *Tetrahedron Lett.* **2003**, *44*, 3043–3046. (e) Schalley, C. A. *Int. J. Mass Spectrom.* **2000**, *194*, 11–39.
- Lehn, J.-M. *Supramolecular Chemistry, Concepts and Perspectives*; VCH: Weinheim, Germany, 1995.
- Sanchez, L.; Herrantz, A.; Martin, N. *J. Mater. Chem.* **2005**, *15*, 1409–1421.
- Peterson, B. Associate V.1.6, Ph.D. Thesis, University of California, Los Angeles, 1994.

Synthesis of [60]fullerene-functionalized rotaxanes

Hisahiro Sasabe,^a Kei-ichiro Ikeshita,^a G. Abraham Rajkumar,^c Nobuhiro Watanabe,^a
 Nobuhiro Kihara,^a Yoshio Furusho,^b Kazuhiko Mizuno,^a Akiya Ogawa^a
 and Toshikazu Takata^{c,*}

^aDepartment of Applied Chemistry, Osaka Prefecture University, Sakai, Osaka 599-8531, Japan

^bYashima Super-structured Helix Project, ERATO, JST, Moriyama-ku, Nagoya 552-8555, Japan

^cDepartment of Organic and Polymeric Materials, Tokyo Institute of Technology, O-okayama, Meguro-ku, Tokyo 152-8552, Japan

Received 2 June 2005; revised 16 September 2005; accepted 18 September 2005

Available online 28 November 2005

Abstract—Synthesis of [60]fullerene (C₆₀)-functionalized rotaxanes via Diels–Alder reactions with C₆₀ is described. Diels–Alder reaction of C₆₀ and sulfone moiety as masked diene attached on the wheels of rotaxanes results in high yields of C₆₀ incorporation. Rotaxanes are prepared by tin-catalyzed urethane-forming end-capping reaction with isocyanate of pseudorotaxane having the wheel carrying C₆₀ functionality as introduced by the Diels–Alder reaction. The Diels–Alder reaction was accomplished as end-capping reaction between C₆₀ and pseudorotaxane bearing sulfone moiety as masked diene on the axle terminal. A variety of C₆₀-containing [2]rotaxanes was prepared in moderate to good yields by these Diels–Alder protocols.

© 2005 Elsevier Ltd. All rights reserved.

1. Introduction

Supramolecular fullerene chemistry is a rapidly emerging field with fascinating scientific and technological perspectives.¹ Interlocked compounds such as rotaxanes and catenanes as supramolecular systems are characterized by their unique structural features as extraordinary freedom and mobility of their components, which are linked by ‘non-covalent linkage’ but not by covalent linkage (or sometimes called as ‘mechanical linkage’, ‘topological linkage’, and so on).² Therefore, the utilization of the interlocked molecules in a variety of systems such as molecular switches and machines has long been studied. We have recently reported several important applications of the interlocked compounds, where through-space chirality transfer in rotaxane systems has been first demonstrated,^{3a,b} while reversible crosslinking polymer system based on the rotaxane framework has been prepared.^{3c} From significance of development of efficient charge separation systems for photovoltaic applications,⁴ we have elaborated to synthesize a number of C₆₀-containing interlocked compounds,^{5–8} because photo-induced through-space electron transfer might give rise to the construction of effective systems for solar energy conversion. In this paper, we wish to disclose the syntheses

of a series of rotaxanes containing C₆₀ moiety on its wheel or axle through the efficient Diels–Alder reactions of C₆₀ (Fig. 1).

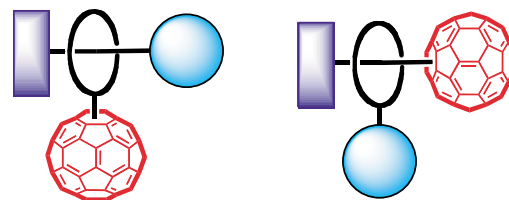


Figure 1. Two types of C₆₀-containing rotaxanes as synthetic targets.

2. Results and discussion

Rotaxanes can be prepared by several methods, which are categorized mainly as two essentially different approaches: kinetic and thermodynamic ones (Fig. 2).⁹ The kinetic method requires an irreversible process for construction of rotaxane in final step (Figs. 2, 1–3), while the thermodynamic one undergoes an equilibrium step to rotaxane in final step (Figs. 2, 4–6). Among them, the most straightforward process is the threading-capping approach via the end-capping of axle terminal of intermediary pseudorotaxane. LUMO level of C₆₀ is low enough to undergo easy Diels–Alder reaction.¹⁰ The present study utilizes the Diels–Alder protocol for C₆₀-introduction either directly and indirectly

Keywords: Rotaxane; [60]Fullerene; Diels–Alder reaction; End-capping; Synthesis; Wheel; Axle.

* Corresponding author. Tel.: +81 3 5734 2898; fax: +81 3 5734 2888; e-mail: ttakata@polymer.titech.ac.jp

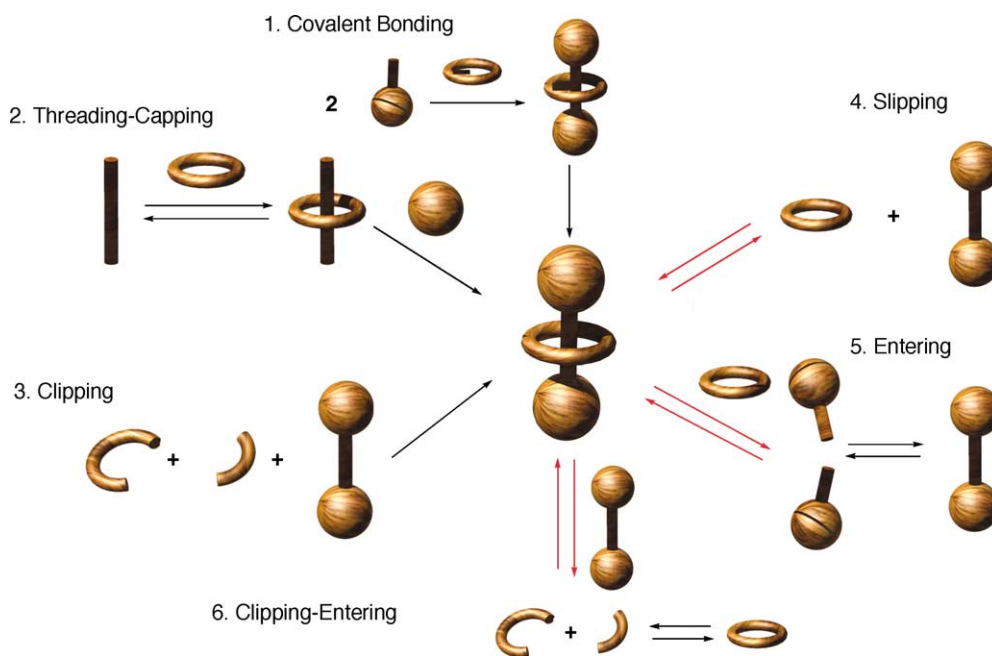


Figure 2. Typical synthetic methods of rotaxane.

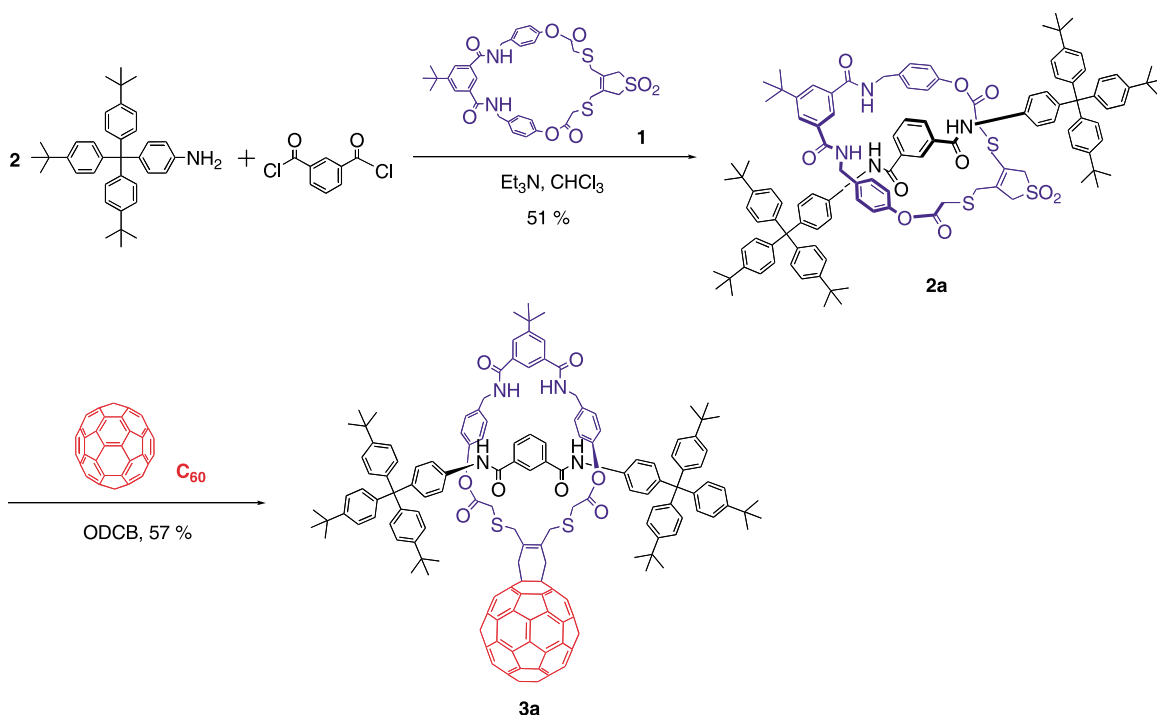
into rotaxanes, as constructed according to ‘threading-capping’ approach.

2.1. Rotaxanes containing [60]fullerene-functionalized wheel

*C*₆₀-Introduction via Diels–Alder reaction on rotaxane wheel.

*C*₆₀-Functionalization by Diels–Alder reaction can be characterized as neutral introduction protocol among

several typical effective functionalizations. As a macrocycle for the introduction of *C*₆₀ by Diels–Alder reaction, *exo*-sulfolene moiety-carrying compound **1** was synthesized by the reported method,⁵ where the sulfolene moiety acts as a masked diene, since *C*₆₀ is served as a dienophile. The corresponding rotaxanes **2** were prepared according to the method utilizing the hydrogen bonding interaction between amide groups of the wheel and axle during the axle-forming reaction (Scheme 1). A mixture of *C*₆₀ (1.5 equiv) and rotaxane **2** was heated in refluxing *o*-dichlorobenzene (ODCB) to afford corresponding *C*₆₀-containing rotaxane



Scheme 1.

Table 1. Synthesis of rotaxanes and introduction of C₆₀ moiety by Diels–Alder reaction to macrocycle carrying sulfone moiety

Axle	2		3	
	Time (h)	Yield (%)	Time (h)	Yield (%)
	12	51 (2a)	3	57 (3a)
	12	23 (2b)	3	54 (3b)
	5	17 (2c , M=H ₂) ^a	1.5	69 (3c , M=H ₂) ^a 82 (3cz , M=Zn) ^b
	5	9 (2d , M=H ₂) ^a	1.5	74 (3d , M=H ₂) ^a 86 (3dz , M=Zn) ^b
	5	51 (2e , M=H ₂) ^a	1.5	70 (3e , M=H ₂) ^a 88 (3ez , M=Zn) ^b

^a Data from Ref. 5b.^b The compounds **3cz**, **3dz**, and **3ez** were prepared by the reaction of **3c–3e** with Zn(OAc)₂.

3 in a good yield. The C₆₀ moiety was successfully introduced into a few rotaxanes (**2b–2e**) possessing triarylamine and porphyrin-terminated axles in high yields, independent of presence of the triarylamine and porphyrin functional groups (Table 1). The yields of the C₆₀ introduction via the Diels–Alder reaction were almost high enough to confirm it as a reliable general method under neutral conditions. The present method through the introduction of C₆₀ at the final step would have advantages to minimize the solubility problem of C₆₀ and to make the procedure easy, since the product has high solubility. The rotaxane structure of **3a** was fully characterized by ¹H NMR and MS spectra in addition to elemental analysis.

It seems convenient to develop C₆₀-carrying rotaxane component with high solubility, because versatile synthetic procedures can be employed at any stage in the synthetic

route to rotaxane. Remarkably enhanced solubility of C₆₀-containing crown ether was found in the system consisting of ethoxycarbonyl-substituted dibenzo[24]crown-8-ether (DB24C8), which was converted to C₆₀-containing crown ether **5** by the Diels–Alder reaction of C₆₀ and 3,4-bis(bromomethyl)benzo moiety-containing crown ether as a diene precursor.⁶ The solubility of **5** was more than 320 mM (400 mg/mL) in chloroform, indicating its easy use as a building block in molecular architecture. In particular, end-capping approach of pseudorotaxane to rotaxane requires high concentration of its components owing to the pseudorotaxane formation in the equilibrium being strongly dependent of concentration.

The predominant formation of pseudorotaxane **7** in an equilibrium between *sec*-ammonium axle and DB24C8 wheel under neutral or acidic condition is well known as

a result of highly strong attractive hydrogen bonding interaction between the ammonium and crown ether. [2]Rotaxanes **9** carrying C₆₀ on their wheels were synthesized in good yields by the end-capping reaction using bulky isocyanates **8** via dibutyltin dilaurate (DBTDL)-catalyzed urethane-forming reaction of a pseudorotaxane formed in situ from **5**¹¹ and **6**.

A chloroform solution of **6**¹² and a slight excess of **5** was treated with 1.5 equiv of 3,5-dimethylphenyl isocyanate **8** and 10% of the catalyst DBTDL in chloroform at room temperature to end-cap the terminal hydroxy group of **7**. The target [2]rotaxane **9a** thus formed was easily isolated by preparative GPC (eluent: chloroform) in 73% yield (Scheme 2). Photo- and electroactive ferrocene or triphenylamine moiety was similarly introduced using the corresponding bulky isocyanates **8b** and **8c** to give dyad rotaxanes **9b** in 65% yield and **9c**⁶ in 76% yield, respectively. The high yields of **9** clearly suggest the high concentration of the intermediary pseudorotaxane, which is resulting from the high solubility of the wheel **5**. The rotaxanes **9** were similarly characterized by ¹H NMR and MS spectra and elemental analysis.

Synthesis of a rotaxane bearing a differently C₆₀-functionalized crown ether wheel **12** was achieved by the Diels–Alder reaction of sulfolene-*pendant* DB24C8 **11** and C₆₀ (Scheme 3). As shown in Scheme 4, **11** was obtained by the reaction of acid chloride of DB24C8 with aminomethyl sulfolene in 93% yield, followed by the Diels–Alder

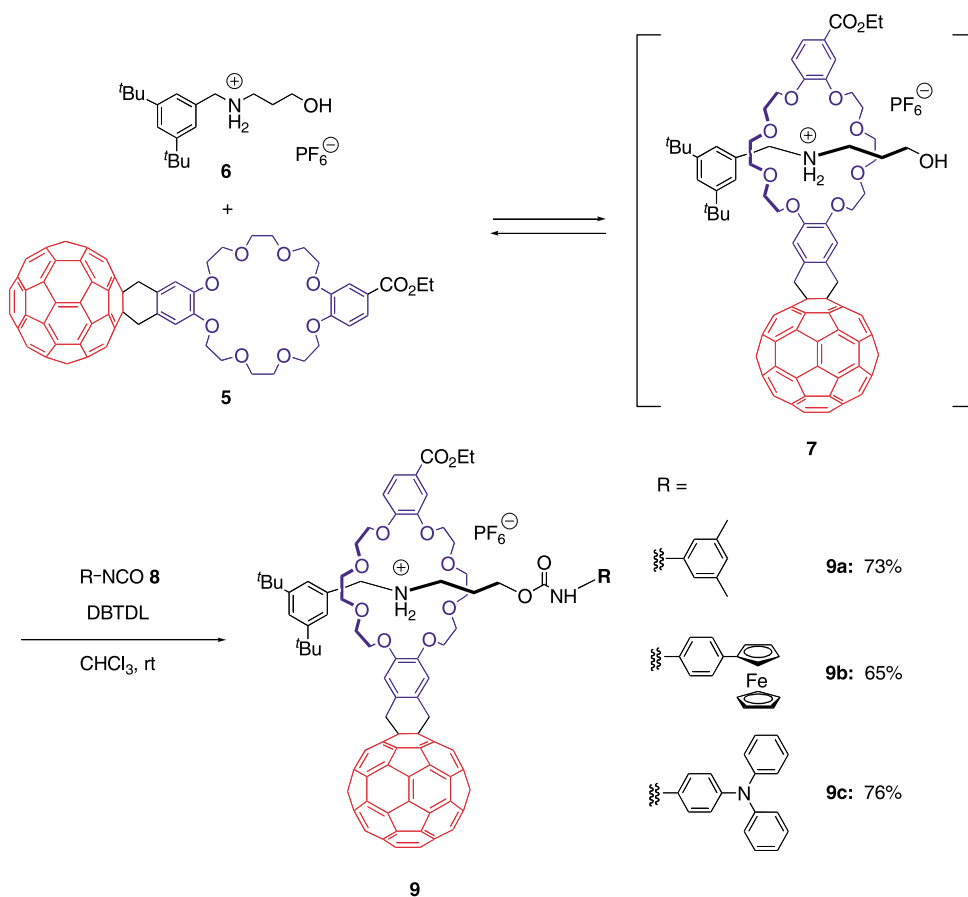
reaction with C₆₀, in 65% yield. Scheme 3 summarizes the two independent routes to C₆₀-functionalized rotaxane **14** via **12** and **13**, that is, either the initial C₆₀-introduction to the wheel and subsequent end-capping, and the initial end-capping followed by the C₆₀-introduction. The both routes were effective enough to obtain good yields of C₆₀-functionalized rotaxanes, as listed in Table 2.

C₆₀-Introduction via Bingel reaction on rotaxane wheel.

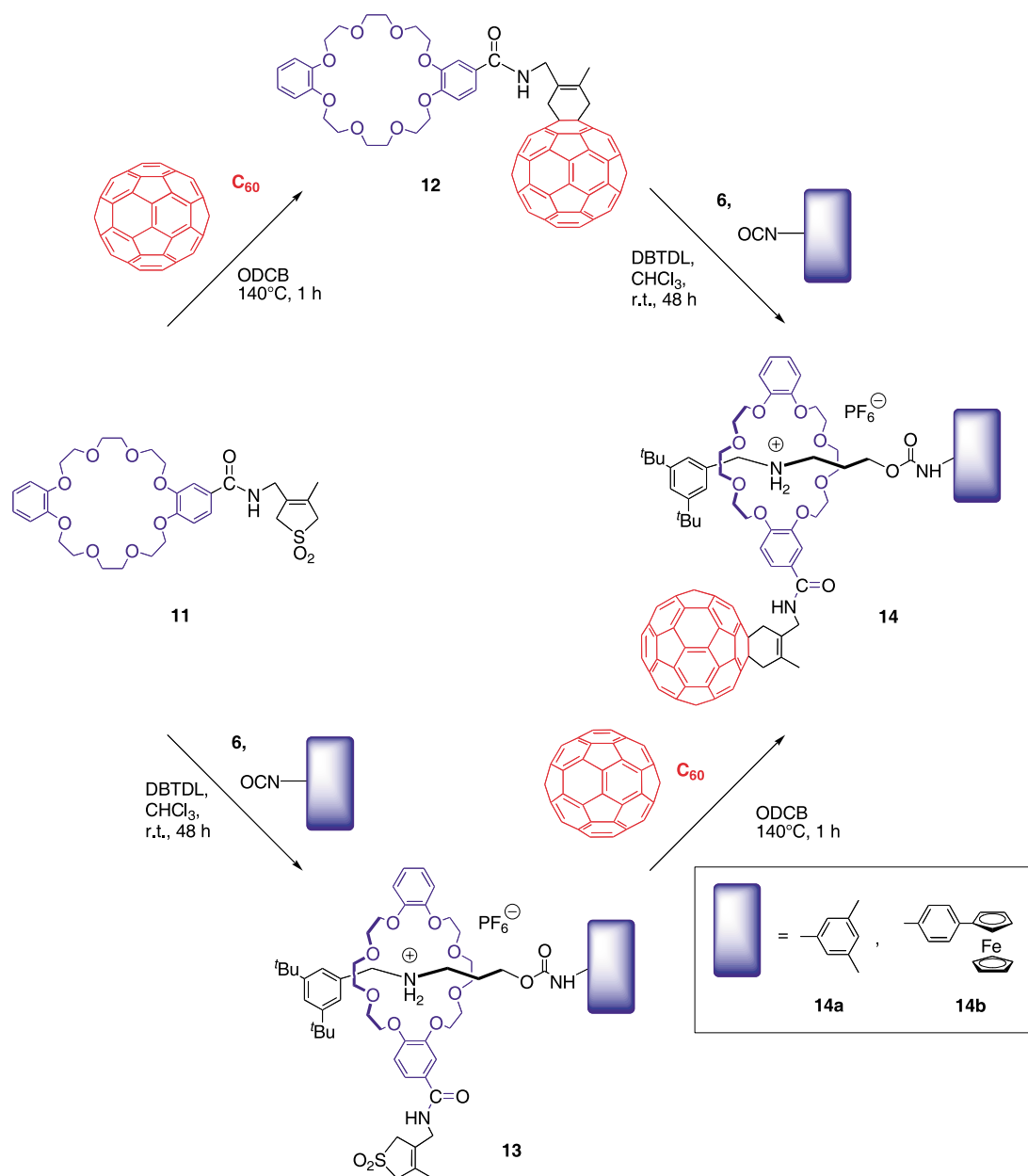
Crown ether **15**¹³ derived by the Bingel reaction with C₆₀ was also available as a wheel for C₆₀-rotaxane **16** via the typical end-capping reaction of pseudorotaxane **6**·**15** with bulky isocyanate **8a**. When crown ether **15** was used, corresponding rotaxane **16** was obtained in 16% yield (Scheme 5).

C₆₀-Introduction via Diels–Alder reaction on the axle end of rotaxane.

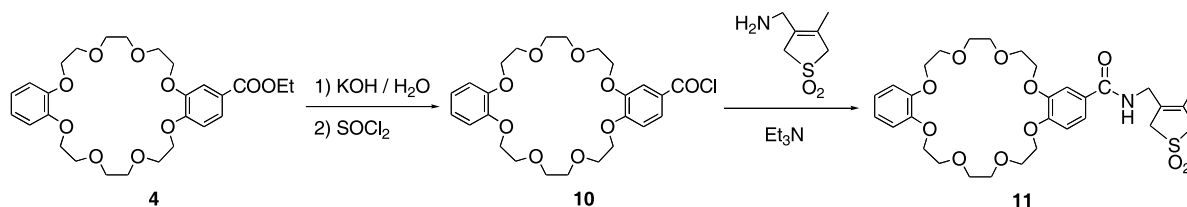
The Diels–Alder end-capping protocol with C₆₀ was applied to the preparation of simple [2]rotaxane containing the C₆₀ moiety at the axle terminal.¹⁴ Benzosultine function serves as quinodimethane via thermal extrusion of SO₂ capable of undergoing smooth Diels–Alder reaction with dienophile. The reaction of *sec*-ammonium salt having the terminal sultine moiety (**17a**) with 1.5 equiv of C₆₀ in the presence of 2.0 equiv of DB24C8 at 80 °C in ODCB gave the corresponding C₆₀-containing [2]rotaxane **18** in 33% yield (Table 3). The yield of **18** depends upon the efficiency of the Diels–Alder



Scheme 2.



Scheme 3.



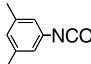
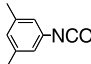
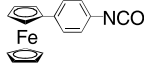
Scheme 4.

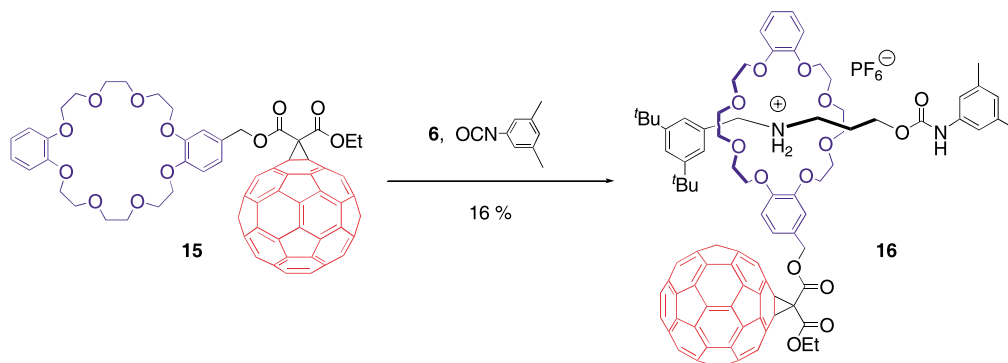
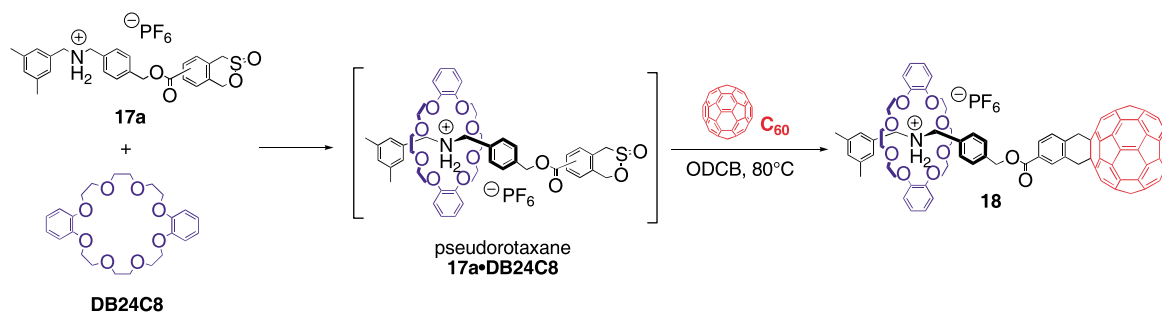
reaction with C_{60} of the intermediary pseudorotaxane **17a**·DB24C8, which is formed in the equilibrium between **17a** and DB24C8, where the equilibrium does not so largely incline to **17a**·DB24C8 because of high temperature required for the extrusion of SO_2 . In general high temperature decreases ratio of pseudorotaxane as equilibrium intermediate. Rotaxane **19** was obtained in 23% yield, when **17b** was used as the axle.

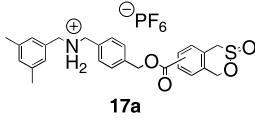
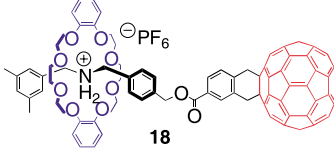
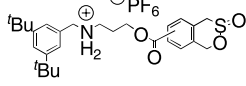
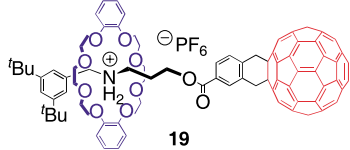
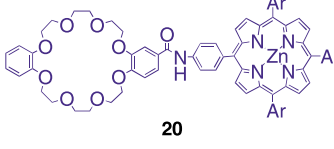
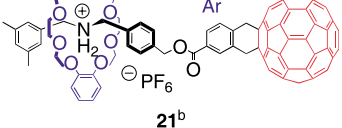
The lowered yield would be attributed to the low efficiency of pseudorotaxane formation due to the bulkiness of **17b**.

The Diels–Alder reaction can be promoted by using well known strong charge-transfer (CT) interaction between C_{60} and a porphyrin group attached to the wheel.¹⁵ The reaction of pseudorotaxane **17a**·**20** with C_{60} afforded C_{60} –zinc

Table 2. Synthesis of C₆₀-functionalized rotaxanes by Diels–Alder reaction to the crown ether wheel via two processes according to Scheme 3

Isocyanate	12		13		14	
	Time (h)	Yield (%)	Time (h)	Yield (%)	Time (h)	Yield (%)
	1	65 (12)	48	71 (13a)	48	66 (14a)
					1	42 (14a)
	2	65 (12)	48	49 (13b)	48	42 (14b)
					1	22 (14b)

**Scheme 5.****Table 3.** Synthesis of rotaxanes by the Diels–Alder reaction with C₆₀ at the axle terminal of pseudorotaxane formed in situ^a

Axle	Wheel	Product	Yield (%)
	DB24C8		33
	DB24C8		23
17a	 20 Ar = 3,5-di- <i>t</i> -butylphenyl		46

^a A mixture of axle, wheel (2.0 equiv), and C₆₀ (1.5 equiv) in ODCB was heated at 80 °C for 12 h.

^b Data from Ref. 14.

porphyrin dyad [2]rotaxane **21** in 46% yield (Table 3). The apparent increase in yield in the Diels–Alder reaction is in good agreement with the intervention of the attractive interaction between C₆₀ and the porphyrin moieties of pseudorotaxane **17a·20**.

3. Conclusion

In the present study, we have discussed the efficient introduction of C₆₀ into rotaxane wheel or axle. The Diels–Alder protocol for the introduction of C₆₀ to rotaxane resulted in the successful synthesis of a variety of C₆₀-functionalized rotaxanes. The advantage of the protocol is that the reaction proceeds under neutral condition, which does not disturb the weak interaction for the formation of supramolecular architectures such as pseudorotaxane. The pre-introduction of C₆₀ into wheel component with high solubility overcame the solubility problem of C₆₀ to give good yields of C₆₀-functionalized rotaxanes.

4. Experimental

4.1. General

Melting points were measured on a Yanagimoto micro melting point apparatus and were uncorrected. IR spectra were recorded on a JASCO FT-IR model 230 spectrometer. ¹H NMR measurements were performed on JEOL JNM-GX-270 and JNM-L-400 spectrometers in CDCl₃ with tetramethylsilane as an internal reference. FAB-MS measurements were carried out with a Finnigan TSQ-70 instrument. UV–vis spectra were measured on a Jasco FP-6300 spectrometer. For preparative HPLC, a JAICO LC-908 system using columns JAIGEL 1 (ϕ 20×600 mm) and JAIGEL 2 (ϕ 20×600 mm) was employed. Compounds **3c(3cz)**⁵, **3d(3dz)**⁵, **3e(3ez)**⁵, **5**⁶, **6**¹², **9c**⁶, **15**¹³, **17a**¹⁴, **17b**¹⁴, and **20**¹⁴ were prepared according to the methods described previously. [60]Fullerene (C₆₀) was purchased from Frontier Carbon Corporation. Other materials of reagent grade were used without further purification.

4.1.1. Synthesis of rotaxane 2a. To a stirring solution of (4-aminophenyl)tris(4-*tert*-butylphenyl)methane (756 mg, 1.5 mmol) and triethylamine (0.21 mL, 1.5 mmol) in chloroform (30 mL) at 0 °C was added dropwise a solution of a mixture of isophthaloyl dichloride (81 mg, 0.4 mmol) and macrocycle **1** (108 mg, 0.15 mmol) in chloroform (50 mL) over a period of 1 h. A chloroform (20 mL) solution of isophthaloyl chloride (71 mg, 0.35 mmol) was added dropwise to the mixture over a period of 1 h. The mixture was stirred at 0 °C for 1 h and at room temperature for 1 h. After evaporation of solvent, the residual mixture was subjected to the separation by column chromatography on silica gel (eluent: chloroform) to afford **2a** as white solid. Yield 125 mg (51%). Mp 231–234 °C (decomp.); IR (NaCl) 3356, 2962, 1735, 1644, 1507, 1323, 1268, 1251, 1193, 822 cm⁻¹; ¹H NMR (400 MHz, CDCl₃) δ = 8.94 (s, 1H, Ar-H), 8.41 (s, 2H, NH), 8.35 (s, 2H, Ar-H), 7.94 (s, 1H, Ar-H), 7.81 (d, *J* = 7.8 Hz, 2H, Ar-H), 7.78 (t, *J* = 4.1 Hz, 2H, NH), 7.38 (d, *J* = 8.5 Hz, 4H, Ar-H), 7.35 (t, *J* = 7.8 Hz, 1H, Ar-H), 7.29 (d, *J* = 8.6 Hz, 12H, Ar-H), 7.22

(d, *J* = 4.1 Hz, 2H, NH), 7.16 (d, *J* = 8.8 Hz, 4H, Ar-H), 7.16 (d, *J* = 8.5 Hz, 12H, Ar-H), 6.66 (d, *J* = 8.6 Hz, 4H, Ar-H), 6.29 (d, *J* = 8.6 Hz, 4H, Ar-H), 4.33 (d, *J* = 3.9 Hz, 4H, CH₂), 3.88 (s, 4H, CH₂), 3.72 (s, 4H, CH₂), 3.17 (s, 4H, CH₂), 1.38 (s, 9H, *t*-Bu), 1.32 (s, 54H, *t*-Bu) ppm; ¹³C NMR (100 MHz, CDCl₃) δ = 170.9, 166.8, 164.7, 152.7, 149.0, 148.5, 144.1, 143.7, 135.5, 134.7, 134.1, 133.3, 131.5, 130.7, 130.5, 130.4, 129.7, 128.9, 128.4, 125.6, 124.3, 121.2, 121.0, 118.5, 63.5, 58.2, 44.5, 35.1, 34.3, 31.3, 31.2, 30.4, 29.6 ppm; FAB-MS (matrix: mNBA) *m/z* 1862 [M+H]⁺. Anal. Calcd for C₁₁₈H₁₃₀N₄O₁₀S₃; C, 76.18; H, 7.04; N, 3.01. Found C, 76.22; H, 7.01; N, 2.93.

4.1.2. Synthesis of C₆₀-rotaxane 3a. A mixture of **2a** (100 mg, 0.058 mmol), C₆₀ (116 mg, 0.16 mmol), and hydroquinone (1 mg) in 1,2-dichlorobenzene (5 mL) was refluxed for 3 h. The mixture was evaporated and the residue was subjected to the purification by silica gel column chromatography (eluent: chloroform). The roughly purified material was further purified by preparative HPLC to give **3a** as brown solid. Yield 80 mg (57%). Mp > 300 °C (decomp.); IR (NaCl) 3353, 2961, 1732, 1644, 1506, 1268, 822 cm⁻¹; ¹H NMR (400 MHz, CDCl₃, 323 K) δ = 8.97 (s, 1H, Ar-H), 8.36 (s, 2H, Ar-H), 8.32 (s, 2H, Ar-H), 8.07 (s, 1H, Ar-H), 7.90 (d, *J* = 7.8 Hz, 2H, Ar-H), 7.75 (t, 2H, *J* = 3.5 Hz, NH), 7.45 (t, *J* = 7.8 Hz, 1H, Ar-H), 7.43 (d, *J* = 8.1 Hz, 4H, Ar-H), 7.27 (d, *J* = 8.3 Hz, 12H, Ar-H), 7.22 (d, *J* = 8.6 Hz, 4H, Ar-H), 7.15 (d, *J* = 8.3 Hz, 12H, Ar-H), 6.74 (d, *J* = 8.0 Hz, 4H, Ar-H), 6.37 (d, *J* = 7.8 Hz, 4H, Ar-H), 4.38 (d, *J* = 3.5 Hz, 4H, CH₂), 4.14 (s, 4H, CH₂), 4.09 (s, 4H, CH₂), 3.31 (s, 4H, CH₂), 1.39 (s, 9H, *t*-Bu), 1.30 (s, 9H, *t*-Bu) ppm; ¹³C NMR (100 MHz, CDCl₃) δ = 171.6, 166.9, 164.9, 152.8, 149.2, 148.6, 147.7, 146.6, 146.3, 145.8, 145.6, 145.5, 145.3, 144.7, 144.2, 143.8, 143.2, 142.7, 142.12, 142.10, 141.7, 140.3, 135.5, 135.3, 135.0, 134.8, 134.0, 133.3, 131.7, 131.2, 130.6, 129.9, 129.0, 128.7, 125.3, 124.3, 124.2, 121.4, 121.2, 118.9, 65.9, 63.6, 44.74, 44.68, 35.2, 34.3, 34.0, 31.4, 31.3, 31.1 ppm; FAB-MS (matrix: mNBA) *m/z* 2516 [M+H]⁺.

4.1.3. Synthesis of rotaxane 2b. To a solution of 4-(*N,N*-bis(4-*tert*-butylbiphenyl)amino)aniline (210 mg, 0.400 mmol) and triethylamine (56.0 μL, 0.401 mmol) in chloroform (20.0 mL) was added a mixture of macrolactam **1**⁵ (72.3 mg, 0.100 mmol) and isophthaloyl chloride (20.4 mg, 0.100 mmol) in chloroform (20.0 mL) over a period of 1 h at 0 °C. Then, an additional chloroform solution (10.0 mL) of isophthaloyl chloride (20.3 mg, 0.100 mmol) was added over a period of 1 h at 0 °C. After being stirred at 0 °C for 1 h and then at room temperature overnight, the mixture was evaporated to dryness. The residue was purified by column chromatography on silica gel (chloroform, *R*_f = 0.05) and preparative HPLC to afford **2b** (43.0 mg, 22.6 μmol, 23% yield based on the macrolactam **1**) as a yellow solid. Mp 173–179 °C; ¹H NMR (400 MHz, CDCl₃) δ = 8.89 (s, 1H), 8.33 (s, 2H), 8.27 (s, 2H), 7.99 (s, 1H), 7.87 (d, *J* = 7.6 Hz, 2H), 7.80 (m, 2H), 7.56–7.53 (m, 16H), 7.46 (d, *J* = 8.8 Hz, 8H), 7.44 (m, 1H), 7.40 (d, *J* = 8.8 Hz, 4H), 7.18 (d, *J* = 8.8 Hz, 8H), 7.11 (d, *J* = 8.8 Hz, 4H), 6.84 (d, *J* = 8.2 Hz, 4H), 6.45 (d, *J* = 8.2 Hz, 4H), 4.44 (s, 4H), 3.98 (s, 4H), 3.64 (s, 4H), 3.20 (s, 4H), 1.36 (s, 36H), 1.35 (s, 9H) ppm; IR (KBr) 3365, 2959, 1649, 1601, 1499, 1319, 1272, 1193, 1115, 819 cm⁻¹; FAB-MS (matrix: mNBA) *m/z* 1901 [M]⁺.

4.1.4. Synthesis of C₆₀-rotaxane 3b. A mixture of C₆₀ (61.1 mg, 84.9 μmol), **2b** (32.2 mg, 16.9 μmol) and hydroquinone (0.800 mg, 7.26 μmol) in 1,2-dichlorobenzene (15.0 mL) was refluxed for 3 h. The reaction mixture was evaporated to dryness. The residue was chromatographed on silica gel (chloroform, *R_f*=0.10) and the crude product was purified by preparative HPLC to afford **3b** (23.4 mg, 9.14 μmol, 54%) as a blackish brown solid. Mp 277–280 °C (dec); ¹H NMR (400 MHz, CDCl₃, 333 K) δ=8.97 (s, 1H), 8.44 (s, 2H), 8.37 (s, 2H), 8.16 (s, 1H), 7.99 (d, *J*=7.2 Hz, 2H), 7.78 (t, *J*=4.0 Hz, 2H), 7.52–7.48 (m, 21H), 7.40 (d, *J*=8.4 Hz, 8H), 7.18–7.09 (m, 12H), 6.87 (d, *J*=8.2 Hz, 4H), 6.52 (d, *J*=8.2 Hz, 4H), 4.51 (d, *J*=4.0 Hz, 4H), 4.16 (s, 8H), 3.38 (s, 4H), 1.38 (s, 9H), 1.34 (s, 36H) ppm; IR (KBr) 3422, 2958, 1652, 1496 cm⁻¹; FAB-MS (matrix: mNBA) *m/z* 2560 [M+H]⁺. Anal. Calcd for C₁₈₀H₁₂₀N₆O₈S₂·0.25CHCl₃: C, 83.62; H, 4.68; N, 3.25; S, 2.48%. Found C, 83.33; H, 4.68; N, 3.36; S, 2.45%.

4.1.5. Synthesis of C₆₀-rotaxane 9a. In the dark, to a solution of axle **6** (6.3 mg, 15 μmol) and crown ether **5** (20 mg, 16 μmol) in CHCl₃ (0.30 mL) was added 3,5-dimethylphenyl isocyanate **8a** (3.0 μL, 20 μmol). After dibutyltin dilaurate (1.0 μL, 1.6 μmol) was added, the mixture was stirred at room temperature for 20 h and evaporated to dryness. The residue was subjected to preparative GPC (eluent: CHCl₃) to afford rotaxane **9a** as a dark brown solid (20 mg, 73%). ¹H NMR (270 MHz, CDCl₃, 333 K) δ=7.64 (dd, 1H, *J*=1.8, 8.4 Hz), 7.54–7.23 (m, 9H), 7.12 (br s, 2H), 6.91 (d, 1H, *J*=8.6 Hz), 6.64 (s, 1H), 4.79–4.74 (m, 2H), 4.56–4.17 (m, 14H), 4.04–3.70 (m, 16H), 3.57–3.51 (m, 6H), 2.25 (br s, 6H), 2.03–1.97 (m, 2H), 1.39–1.21 (m, 21H) ppm; IR (NaCl) 2952, 1722, 1668, 1612, 1506, 1456, 1220, 1107, 1057, 954, 843, 754, 557 cm⁻¹; FAB-MS (matrix: mNBA) *m/z* 1693 [M-PF₆]⁺. Anal. Calcd for C₁₁₆H₇₉F₆N₂O₁₂P·(CHCl₃)_{0.25}: C, 74.76; H, 4.28; N, 1.50%. Found: C, 74.65; H, 4.44; N, 1.52%.

4.1.6. C₆₀-Rotaxane 9b. The title compound was prepared similarly to **9a**. Yield 65%. A dark brown solid. ¹H NMR (400 MHz, CDCl₃, 333 K) δ=7.65 (d, 1H, *J*=6.9 Hz), 7.53 (s, 1H), 7.37–7.34 (m, 8H), 7.25–7.08 (m, 3H), 7.08 (br, 1H), 6.90 (d, 1H, *J*=8.8 Hz), 4.76–4.73 (m, 2H), 4.55–4.16 (m, 17H), 4.06–3.71 (m, 20H), 3.54–3.53 (m, 6H), 2.01–1.98 (m, 2H), 1.38–1.34 (m, 3H), 1.24 (s, 18H) ppm; IR (film) 2960, 1716, 1592, 1535, 1510, 1457, 1268, 1207, 1105, 955, 843 cm⁻¹; FAB-MS (matrix: mNBA) *m/z* 1994 [M+H]⁺, 1849 [M-PF₆]⁺. Anal. Calcd for C₁₂₄H₈₃F₆FeN₂O₁₂P·(CHCl₃)_{1.0}: C, 71.05; H, 4.01; N, 1.33%. Found: C, 71.45; H, 4.38; N, 1.49%.

4.1.7. Synthesis of 11. To a solution of 3-aminomethyl-4-methylsulfolene (295 mg, 1.83 mmol) and Et₃N (557 mg, 5.50 mmol) in THF (10 mL), a solution of 3-chlorocarbonylDB24C8 (920 mg, 1.80 mmol) in THF (50 mL) was added at 0 °C. After 1 h the ice bath was removed and the reaction mixture was stirred at room temperature for 4 h. After completion of the reaction (TLC; 20% MeOH in EtOAc), then the reaction mixture was diluted with 200 mL CHCl₃ and washed with 1 M HCl (75 mL) and water (75 mL). Evaporation of the solvent gave the crude product, which was chromatographed over silica gel (eluent: 10% MeOH/EA) to give **11** as a white solid (1.07 g, 93%).

¹H NMR (CDCl₃, 270 MHz) δ=7.28 (m, 1H, Ar-H), 7.2 (m, 1H, Ar-H), 6.79–6.83 (m, 5H, Ar-H), 6.32 (br s, 1H, -NH), 3.68–4.11 (m, 30H, CH₂ of DB24C8 and sulfolene), 1.97 (s, 3H, CH₃)

4.1.8. Synthesis of C₆₀-crown ether 12. **11** (141 mg, 0.22 mmol) and fullerene (480 mg, 0.67 mmol) in 1,2-dichlorobenzene (30 mL) were refluxed for 2 h. After completion of the reaction, the reaction mixture was passed thro a short column of silica gel. Elution with toluene removes all the unreacted fullerene and finally elution with 5% MeOH/CHCl₃ gives the crude product, which was purified by HPLC to afford **12** as a purple solid (184 mg, 65%). ¹H NMR (CDCl₃, 270 MHz) δ=7.32 (m, 1H, Ar-H), 6.67 (m, 1H, Ar-H), 6.95 (dd, 1H, Ar-H, *J*'=2.16 Hz, *J*''=1.9 Hz), 6.83 (m, 4H, Ar-H), 6.31 (br s, 1H, -NH), 4.63 (d, 2H, CH₂, *J*=5.7 Hz), 3.76–4.11 (m, 28H, CH₂ of DB24C8 and sulfolene), 2.4 (s, 3H, CH₃) ppm.

¹³C NMR (CDCl₃, 100 MHz) δ=167.1 156.6, 148.8, 148.6, 147.6, 146.5, 146.2, 145.7, 145.5, 145.4, 145.4, 145.3, 144.9, 144.7, 144.6, 143.1, 142.6, 142.5, 142.3, 142.3, 142.2, 142.0, 141.9, 141.6, 141.5, 140.2, 140.1, 137.0, 136.6, 135.5, 135.5, 131.7, 121.4, 114.7, 114.0, 113.1, 112.5, 112.5, 71.2, 70.2, 69.9, 69.8, 69.7, 69.5, 69.4, 69.2, 66.3, 66.1, 59.2, 55.7, 46.7, 42.9, 40.4, 30.8, 23.6, 19.5 ppm; FAB-MS; *m/z*: 1292 (M⁺) IR cm⁻¹: 1654 (CO-NH) calculated for C₉₁H₄₁NO₉ (CHCl₃)₁ (H₂O)₄: C, 74.47; H, 3.40; N, 0.94%. Found C, 74.58; H, 3.31; N, 1.10%

4.1.9. Synthesis of rotaxane 13a. To a solution of the axle (**6**) (84.7 mg, 0.20 mmol) and DB24C8 having sulfolene unit **11** (153 mg, 0.24 mmol) in chloroform (1.2 mL), 3,5-dimethylphenyl isocyanate (51 μL, 0.36 mmol) and di-*n*-butyltin dilaurate (DBTDL) (18 μL, 0.030 mmol) were added and the reaction mixture under Ar atmosphere was stirred at room temperature for 48 h. After the removal of solvent the residue was subjected to HPLC to give the rotaxane (**13a**) (172 mg, 71%). Mp 98.8–100 °C; ¹H NMR (CDCl₃, 270 MHz) δ=7.52 (br s, 1H, -NH), 7.45–7.27 (m, 3H, Ar-H of axle), 7.09–7.0 (m, 4H, Ar-H of end-cap and wheel), 6.88 (s, 6H, Ar-H of wheel), 6.66 (br s, 1H, -NH), 4.70–4.64 (m, 2H, CH₂ of axle), 4.40–3.34 (m, 34H, CH₂ of axle and wheel), 2.24 (s, 6H CH₃ of end-cap), 1.90 (s, 3H, CH₃ of wheel) ppm, 1.82 (br s, 2H, CH₂ of axle), 1.21 (s, 18H, *t*-butyl of axle) ppm ¹³C NMR (CDCl₃, 100 MHz) δ=166.8, 153.2, 151.4, 150.2, 147.4, 147.3, 147.1, 138.5, 137.8, 131.4, 128.7, 127.4, 127.1, 125.1, 124.0, 123.3, 122.0, 121.9, 116.5, 112.9, 112.8, 112.1, 111.5, 77.5, 77.1, 76.8, 70.6, 70.6, 70.5, 70.2, 70.1, 70.0, 69.1, 69.8, 68.5, 68.4, 68.3, 68.1, 61.3, 60.9, 58.2, 52.9, 46.2, 37.5, 34.8, 34.7, 34.6, 31.6, 31.3, 31.1, 26.2, 21.4, 14.6; FAB-MS *m/z* 1060.7 [M-PF₆+H]⁺, 100%, 996.4 [(M-PF₆+H)-SO₂]⁺, 68%; IR (KBr) 3423, 3166, 1718, 1654, 1322, 1124, 842 cm⁻¹. Anal. Calcd for C₅₈H₈₁F₆N₃O₁₃PS (H₂O)_{1.9}: C, 56.19; H, 6.90; N 3.39%. Found C, 56.36; H, 6.90; N, 3.16%.

4.1.10. Synthesis of rotaxane 13b. To the solution of the axle (**6**) (43 mg, 0.10 mmol) and DB24C8 having sulfolene unit conjugate **11** (76 mg, 0.12 mmol) in chloroform (0.6 mL), were added 4-ferrocenylphenyl isocyanate (61 mg, 0.20 mmol) and di-*n*-butyltin dilaurate (DBTDL)

(12 μL , 0.020 mmol). The reaction mixture under Ar atmosphere was stirred at room temperature for 48 h. After the removal of solvent the residue was subjected to HPLC to give the rotaxane (**13b**) (67 mg, 49%). Mp 132–134 °C (decomp.); ^1H NMR (CDCl_3 , 270 MHz) δ = 7.58 (m, 2H, Ar-H of end-cap), 7.44 (br s, 1H, –NH), 7.36–7.28 (m, 8H, Ar-H of end-cap, axle and wheel), 6.93–6.88 (m, 4H, Ar-H of wheel), 6.85 (br s, 1H, –NH), 4.6–3.24 (m, 45H, CH_2 of axle and wheel, $\text{CH}=\text{}$ of end-cap), 1.91 (s, 3H, CH_3 of wheel), 1.78 (br s, 2H, CH_2 of axle), 1.20 (s, 18H, *t*-butyl of axle) ppm ^{13}C NMR (CDCl_3 , 100 MHz) δ = 166.9, 153.3, 151.4, 150.0, 147.4, 147.0, 136.2, 134.0, 131.5, 128.6, 127.6, 127.4, 126.5, 124.2, 123.2, 122.2, 122.0, 121.9, 118.8, 113.0, 112.8, 112.0, 111.9, 77.3, 77.0, 76.7, 70.6, 70.5, 70.2, 70.1, 69.1, 69.7, 69.1, 68.7, 68.3, 66.3, 61.2, 61.00, 58.3, 52.9, 46.2, 37.5, 37.2, 34.8, 31.4, 26.2, 14.7 ppm; FAB-MS m/z 1218.2 $[\text{M}-\text{PF}_6+\text{H}]^+$, 20%, 1152.6 $[(\text{M}-\text{PF}_6+\text{H})-\text{SO}_2]^+$, 100%; IR (KBr) 3404, 3166, 1719, 1654, 1311, 1106, 843 cm^{-1} . Anal. Calcd for $\text{C}_{66}\text{H}_{86}\text{F}_6\text{FeN}_3\text{O}_{13}\text{PS}(\text{H}_2\text{O})_{1.0}$ C, 58.19; H, 6.36; N, 3.08%. Found C, 57.43; H, 6.43; N, 3.04%.

4.1.11. Synthesis of C_{60} -rotaxane 14a (from 12). To a solution of the axle **6** (21.2 mg, 0.050 mmol) and DB24C8–fullerene conjugate **12** (78 mg, 0.060 mmol) in chloroform (0.3 mL), were added 3,5-dimethylphenyl isocyanate (12.7 μL , 0.09 mmol) and di-*n*-butyltin dilaurate (DBTDL) (4.2 μL , 0.007 mmol). The reaction mixture under Ar atmosphere was stirred at room temperature for 48 h. After the removal of solvent the residue was subjected to preparative HPLC to give the crude product (71 mg). Further purification by preparative HPLC gave the rotaxane **14a** in pure form (62 mg, 66%). ^1H NMR (CDCl_3 , 270 MHz) δ = 7.45 (s, 1H, –NH), 7.37–7.30 (m, 3H, Ar-H of axle), 7.05–6.99 (m, 4H, Ar-H of end-cap and wheel), 6.95–6.83 (m, 6H, Ar-H of wheel), 6.67 (br s, 1H, –NH), 4.60 (m, 4H, CH_2 of axle and wheel), 4.40–3.25 (m, 32H, CH_2 of wheel and axle), 2.43 (s, 3H, CH_3 of wheel), 2.26 (s, 6H, CH_3 of end-cap), 1.76 (br s, CH_2 of axle), 1.21 (s, 18H, *t*-butyl of axle) ppm; ^{13}C NMR (CDCl_3 , 100 MHz) δ = 166.6, 157.4, 157.1, 153.8, 151.4, 149.6, 147.5, 147.5, 147.4, 147.3, 147.1, 146.32, 146.29, 146.1, 146.0, 145.9, 145.8, 145.7, 145.3, 145.0, 144.7, 144.5, 142.9, 142.4, 142.3, 142.0, 141.9, 141.5, 141.4, 141.3, 140.0, 139.8, 138.4, 138.1, 135.9, 135.7, 135.6, 132.3, 131.6, 128.4, 124.9, 124.2, 123.3, 122.0, 121.9, 119.2, 116.6, 113.0, 112.3, 112.0, 77.3, 77.2, 77.0, 76.69, 70.5, 70.2, 70.1, 70.0, 69.9, 69.7, 68.8, 68.3, 68.3, 66.5, 66.2, 60.9, 52.8, 46.9, 46.2, 42.7, 40.7, 34.8, 31.4, 26.21, 21.4, 19.5 ppm; FAB-MS m/z 1716.1 $[\text{M}-\text{PF}_6]^+$; IR (KBr) 3422, 3164, 1719, 1654, 841 cm^{-1} . Anal. Calcd for $\text{C}_{118}\text{H}_{82}\text{F}_6\text{N}_3\text{O}_{11}\text{P}(\text{CHCl}_3)_1(\text{C}_6\text{H}_{14})_1$ C, 72.57; H, 4.73; N, 2.03%. Found C, 72.83; H, 4.51; N, 2.01%.

4.1.12. Synthesis of C_{60} -rotaxane 5a (from 13a). A mixture of **13a** (50 mg, 0.04 mmol) and fullerene (122 mg, 0.17 mmol) in 1,2-dichlorobenzene (30 mL) were heated at 140 °C for 1 h. The reaction mixture was passed through a short column of silica gel. Elution with toluene removes the unreacted fullerene and final elution with 5% MeOH/ CHCl_3 gives the crude product, which was purified by preparative HPLC to afford **14a** (32 mg, 42%).

4.1.13. Synthesis of C_{60} -rotaxane 14b (from 12). To a solution of the axle (**6**) (21 mg, 0.050 mmol) and DB24C8–fullerene conjugate **12** (78 mg, 0.060 mmol) in chloroform (0.3 mL), 4-ferrocenylphenyl isocyanate (27 mg, 0.090 mmol) and di-*n*-butyltin dilaurate (DBTDL) (4.2 μL , 0.0070 mmol). The reaction mixture under Ar atmosphere was stirred at room temperature for 48 h. After the removal of solvent the residue was subjected to HPLC to give the crude product (52 mg). Further purification by preparative HPLC gave the rotaxane (**14b**) in pure form (43 mg, 42%). ^1H NMR (CDCl_3 , 270 MHz) δ = 7.8 (m, 2H, Ar-H of end-cap), 7.62 (br s, 1H, –NH), 7.5–7.36 (m, 8H, Ar-H of end-cap, axle and wheel), 6.91–6.89 (m, 4H, Ar-H of wheel), 6.81 (br s, 1H, –NH), 4.58–3.32 (m, 45H, CH_2 of axle and wheel, $\text{CH}=\text{}$ of end-cap), 2.44 (s, 3H, CH_3 of wheel), 1.75 (br s, 2H, CH_2 of axle), 1.21 (s, 18H, *t*-butyl of axle) ^{13}C NMR (CDCl_3 , 100 MHz) δ = 166.8, 157.4, 157.1, 153.4, 149.7, 147.6, 147.5, 147.5, 147.4, 146.3, 146.2, 146.1, 146.0, 145.9, 145.7, 145.1, 144.7, 142.9, 142.4, 142.1, 142.0, 141.6, 141.4, 141.42, 141.37, 140.0, 139.9, 136.3, 135.9, 135.8, 133.81, 132.3, 131.7, 128.3, 123.3, 122.1, 121.9, 118.9, 113.0, 113.0, 112.6, 112.1, 104.4, 102.2, 85.4, 77.6, 70.3, 70.2, 70.1, 69.9, 69.8, 69.0, 68.3, 66.5, 66.3, 61.0, 56.5, 52.8, 46.9, 46.2, 42.8, 40.6, 29.7, 26.2, 19.6; FAB-MS m/z 1874.1 $[\text{M}-\text{PF}_6]^+$; IR (KBr) 3423, 3166, 1719, 1654, 842 cm^{-1} . Anal. Calcd for $(\text{C}_{126}\text{H}_{86}\text{F}_6\text{FeN}_3\text{O}_{11}\text{P})(\text{CHCl}_3)(\text{C}_6\text{H}_{14})(\text{H}_2\text{O})$ C, 71.81; H, 4.58; N, 1.89%. Found C, 71.20; H, 4.25; N, 1.47%.

4.1.14. Synthesis of C_{60} -rotaxane 14b (from 13b). A mixture of **13b** (50 mg, 0.037 mmol) and fullerene (107 mg, 0.15 mmol) in 1,2-dichlorobenzene (5 mL) were heated at 140 °C for 1 h. The reaction mixture was passed through a short column of SiO_2 . Elution with toluene removed the unreacted fullerene and final elution with 1–5% MeOH/ CHCl_3 gave the crude product, which was purified by preparative HPLC to afford **14b** (22 mg, 22%) as a brownish-red film.

4.1.15. Synthesis of C_{60} -rotaxane 16. To a solution of the axle (**6**) (21.2 mg, 0.05 mmol) and DB24C8–fullerene conjugate **15** (79 mg, 0.06 mmol) in chloroform (0.3 mL), were added 3,5-dimethylphenyl isocyanate (11.1 μL , 0.075 mmol) and di-*n*-butyltin dilaurate (DBTDL) (3 μL , 0.005 mmol). The reaction mixture under Ar atmosphere was stirred at room temperature for 48 h. After the removal of solvent, the residue was subjected to preparative HPLC to give the crude product (32 mg). After repeated purification by preparative HPLC the rotaxane (**16**) was isolated in its pure form (15 mg, 16%) as a dark purple solid. ^1H NMR (CDCl_3 , 270 MHz) δ = 7.31 (s, 2H, Ar-H of axle), 7.24 (s, 1H, Ar-H of axle), 6.98–7.03 (m, 4H, Ar-H of wheel and end-cap), 6.87–6.89 (m, 6H, Ar-H of wheel), 6.65 (br s, 1H, –NH), 4.62 (2H, CH_2 of axle), 4.52 (q, 2H, CH_2 of wheel), 4.22–3.37 (m, 28H, CH_2 of wheel and axle), 2.24 (s, 6H, CH_3 of end cap), 1.82 (m, 2H, CH_2 of axle), 1.4 (t, 3H, CH_3 of wheel), 1.18 (s, 18H *t*-butyl of axle) ppm ^{13}C NMR (CDCl_3 , 400 MHz) δ = 21.4, 26.1, 29.7, 34.8, 46.2, 52.1, 52.8, 61.2, 63.6, 68.4, 68.5, 69.9, 70.5, 71.5, 112.8, 113.9, 116.4, 12.0, 122.9, 123.3, 124.1, 125.1, 128.3, 131.5, 137.2, 138.6, 139.3, 140.8, 140.9, 141.7, 141.9, 142.1, 143.7, 144.4, 144.7, 144.8, 145.0, 145.1, 145.2, 145.3, 147.3, 147.7, 148.15, 151.4, 153.2, 163.4 ppm; FAB-MS (matrix: mNBA) $[\text{M}-\text{PF}_6]^+$ 1735.5; IR (KBr) 3422, 1735, 1685, 1654, 841 cm^{-1} . Anal. Calcd for

C₁₁₇H₇₉F₆N₂O₁₄P C, 74.67; H, 4.23; N, 1.45%. Found C, 74.58; H, 4.51; N, 1.49%.

4.1.16. Synthesis of C₆₀-rotaxane 18. A mixture of **17a** (54 mg, 0.09 mmol), DB24C8 (81 mg, 0.18 mmol) and C₆₀ (97 mg, 0.14 mmol) in dry ODCB (1.0 mL) under argon atmosphere in the dark was slowly heated to 80 °C, and was stirred at 80 °C for 12 h. The reaction mixture was directly chromatographed (SiO₂, eluent: toluene to CHCl₃-methanol (90/10)) to collect a dark brown band (118 mg), a part of which (107 mg) was further purified by preparative GPC (eluent: CHCl₃) to give **18** as a dark brown solid (46 mg, 33%). Mp 180–182 °C. ¹H NMR (400 MHz, CDCl₃, 323 K) δ=8.37 (s, 1H), 8.27 (d, 1H, *J*=6.3 Hz), 7.79 (d, 1H, *J*=7.8 Hz), 7.56 (br, 2H), 7.37–7.35 (m, 4H), 6.88–6.76 (m, 11H), 5.35 (s, 2H), 4.82–4.48 (m, 8H), 4.12–4.09 (m, 8H), 3.82–3.71 (m, 8H), 3.51–3.46 (m, 8H), 2.13 (s, 6H) ppm; IR (NaCl) 2922, 1716, 1504, 1455, 1253, 1210, 1180, 1123, 1102, 1056, 953, 842, 749, 557, 526 cm⁻¹; FAB-MS (matrix: mNBA) *m/z* 1554.5 [M-PF₆]⁺. Anal. Calcd for C₁₁₀H₆₀F₆N₁O₁₀P₁·(CHCl₃)_{0.5}: C, 75.39; H, 3.46; N, 0.80%. Found: C, 75.06; H, 3.56; N, 0.87%.

4.1.17. C₆₀-Rotaxane 20. A dark brown solid. ¹H NMR (400 MHz, CDCl₃, 323 K) δ=8.27 (s, 1H), 8.12 (d, 1H, *J*=7.7 Hz), 7.73 (d, 1H, *J*=7.7 Hz), 7.43–7.21 (m, 4H), 6.87–6.85 (m, 9H), 4.83–4.51 (m, 6H), 4.27–4.08 (m, 8H), 3.88–3.45 (m, 20H), 2.07–2.03 (m, 2H), 1.23–1.16 (s, 18H) ppm; IR (NaCl) 2960, 1719, 1595, 1504, 1454, 1253, 1207, 1123, 1054, 954, 911, 843, 734, 557, 526 cm⁻¹; FAB-MS (matrix: mNBA) *m/z* 1576.6 [M-PF₆]⁺. Anal. Calcd for C₁₁₁H₇₀F₆N₁O₁₀P₁·(CHCl₃)_{0.5}·(H₂O)_{1.5}: C, 74.01; H, 4.09; N, 0.77%. Found: C, 73.91; H, 4.48; N, 0.90%.

4.1.18. C₆₀-Rotaxane 21. A black purple solid. ¹H NMR (400 MHz, CDCl₃, 323 K) δ=9.05 (s, 1H), 8.93–8.80 (m, 8H), 8.22–7.73 (m, 16H), 7.62–7.50 (m, 4H), 7.36–6.72 (m, 12H), 5.28 (br, 2H), 4.65–4.55 (m, 4H), 4.29–3.40 (m, 28H), 2.23 (s, 6H), 1.48 (s, 54H) ppm; IR (NaCl) 2962, 2870, 2357, 1717, 1519, 1506, 1456, 1362, 1265, 1101, 845, 733, 667, 557, 527 cm⁻¹. UV-vis λ_{max} (nm) (ε/M⁻¹ cm⁻¹) (CHCl₃): 433 (320,000), 555 (20,000), 596 (9700); FAB-MS (matrix: mNBA) *m/z* 2609.2 [M-PF₆]⁺. Anal. Calcd for C₁₇₉H₁₃₅-F₆N₆O₁₁PZn·(CHCl₃)_{0.25}: C, 77.27; H, 4.89; N, 3.02%. Found: C, 76.99; H, 5.11; N, 2.90%.

Acknowledgements

This work was financially supported from the Grant-in-Aid for Scientific Research from the Ministry of Education, Science, Sports, Culture, and Technology.

References and notes

- Kadish, K. M.; Ruoff, R. S. *Fullerenes*; Wiley: New York, 2000; p 225.
- (a) Kihara, N.; Takata, T. *J. Synth. Org. Chem. Jpn.* **2001**, *59*, 206. (b) *Molecular Catenanes, Rotaxanes, and Knots*; Sauvage, J.-P., Dietrich-Buchecker, C., Eds.; Wiley-VHC: Weinheim, 1999. (c) Amabilino, D. B.; Stoddart, J. F. *Chem. Rev.* **1995**, *95*, 2725.
- (a) Tachibana, Y.; Kihara, N.; Ohga, Y.; Takata, T. *Chem. Lett.* **2000**, 806–807. (b) Tachibana, Y.; Kihara, N.; Takata, T. *J. Am. Chem. Soc.* **2004**, *126*, 3438–3439. (c) Oku, T.; Furusho, Y.; Takata, T. *Angew. Chem., Int. Ed.* **2004**, *43*, 966–969.
- Ramamurthy, V.; Schanze, K. S. In *Molecular and Supramolecular Photochemistry*, Vol. 7; Marcel Dekker: New York, 2001.
- (a) Watanabe, N.; Kihara, N.; Furusho, Y.; Takata, T.; Araki, Y.; Ito, O. *Angew. Chem., Int. Ed.* **2003**, *42*, 681–683. (b) Sandanayaka, A. S. D.; Watanabe, N.; Ikeshita, K.; Araki, Y.; Kihara, N.; Furusho, Y.; Ito, O.; Takata, T. *J. Phys. Chem. B* **2005**, *109*, 2516–2525.
- Sandanayaka, A. S. D.; Sasabe, H.; Araki, Y.; Furusho, Y.; Ito, O.; Takata, T. *J. Phys. Chem. A* **2004**, *108*, 5145–5155.
- Sandanayaka, A. S. D.; Ikeshita, K.; Watanabe, N.; Araki, Y.; Furusho, Y.; Kihara, N.; Takata, T.; Ito, O. *Bull. Chem. Soc. Jpn.* **2005**, *78*, 1008–1017.
- (a) Diederich, F.; Dietrich-Buchecker, C.; Nierengarten, J.-F.; Sauvage, J.-P. *J. Chem. Soc., Chem. Commun.* **1995**, 781–782. (b) Ashton, P. R.; Diederich, F.; Gómez-López, M.; Nierengarten, J.-F.; Preece, J. A.; Raymo, F. M.; Stoddart, J. F. *Angew. Chem., Int. Ed.* **1997**, *36*, 1448–1451. (c) Nakamura, Y.; Minami, S.; Iizuka, K.; Nishimura, J. *Angew. Chem., Int. Ed.* **2003**, *42*, 3158–3162. (d) Li, K.; Schuster, D. I.; Guldi, D. M.; Herranz, M.Á.; Echegoyen, L. *J. Am. Chem. Soc.* **2004**, *126*, 3388–3389. (e) Li, K.; Bracher, P. J.; Guldi, D. M.; Herranz, M.Á.; Echegoyen, L.; Schuster, D. I. *J. Am. Chem. Soc.* **2004**, *126*, 9156–9157. (f) Ros, T. D.; Guldi, D. M.; Morales, A. F.; Leigh, D. A.; Prato, M.; Turco, R. *Org. Lett.* **2003**, *5*, 689–691.
- Takata, T.; Kihara, N.; Furusho, Y. *Adv. Polym. Sci.* **2004**, *171*, 1.
- Diederich, F.; Isaacs, I.; Philp, D. *Chem. Soc. Rev.* **1994**, 243.
- Furusho, Y.; Sasabe, H.; Natsui, D.; Murakawa, K.; Takata, T.; Harada, T. *Bull. Chem. Soc. Jpn.* **2004**, *77*, 179–185.
- Takata, T.; Kawasaki, H.; Kihara, N.; Furusho, Y. *Macromolecules* **2001**, *34*, 5449–5456.
- Diederich, F.; Echegoyen, L.; Gómez-López, M.; Kessinger, R.; Stoddart, J. F. *J. Chem. Soc., Perkin Trans. 2* **1999**, 1577–1586.
- Sasabe, H.; Kihara, N.; Furusho, Y.; Mizuno, K.; Ogawa, A.; Takata, T. *Org. Lett.* **2004**, *6*, 3957–3960.
- (a) Tashiro, K.; Aida, T.; Zheng, J.-Y.; Kinbara, K.; Saigo, K.; Sakamoto, S.; Yamaguchi, K. *J. Am. Chem. Soc.* **1999**, *121*, 9477–9478. (b) Zheng, J.-Y.; Tashiro, K.; Hirabayashi, Y.; Kinbara, K.; Saigo, K.; Aida, T.; Sakamoto, S.; Yamaguchi, K. *Angew. Chem., Int. Ed.* **2001**, *40*, 1857–1861. (c) Boyd, P. D.; Hodgson, M. C.; Rickard, C. E. F.; Oliver, A. G.; Chaker, L.; Brothers, P. J.; Bolskar, R. D.; Tham, F. S.; Reed, C. A. *J. Am. Chem. Soc.* **1999**, *121*, 10487–10495. (d) Sun, D.; Tham, F. S.; Reed, C. A.; Chaker, L.; Burgess, M.; Boyd, P. D. *J. Am. Chem. Soc.* **2000**, *122*, 10704–10705. (e) Ayabe, M.; Ikeda, A.; Kubo, Y.; Takeuchi, M.; Shinkai, S. *Angew. Chem., Int. Ed.* **2002**, *41*, 2790–2792. (f) Kubo, Y.; Sugasaki, A.; Ikeda, M.; Sugiyasu, K.; Sonoda, K.; Ikeda, A.; Takeuchi, M.; Shinkai, S. *Org. Lett.* **2002**, *4*, 925–928. (g) Wang, Y.-B.; Lin, Z. *J. Am. Chem. Soc.* **2003**, *125*, 6072–6073.

Supramolecular pseudo-rotaxane type complexes from π -extended TTF dimer crown ether and C₆₀

Marta C. Díaz,^a Beatriz M. Illescas,^a Nazario Martín,^{a,*} J. Fraser Stoddart,^b M. Angeles Canales,^c Jesús Jiménez-Barbero,^c Ginka Sarova^d and Dirk M. Guldi^d

^aDepartamento de Química Orgánica, Facultad de Química, Universidad Complutense, E-28040 Madrid, Spain

^bDepartment of Chemistry and Biochemistry, University of California at Los Angeles, 405 Hilgard Avenue, Los Angeles, CA 90095, USA

^cCentro de Investigaciones Biológicas (CSIC), E-28040 Madrid, Spain

^dInstitute for Physical and Theoretical Chemistry, Universität Erlangen, 91058 Erlangen, Germany

Received 22 June 2005; revised 10 July 2005; accepted 12 July 2005

Available online 18 November 2005

Abstract—A new cyclophane-type crown ether endowed with two exTTF units forms supramolecular ensembles with different dibenzylammonium salts with a binding constant of $K_a \sim 50 \text{ M}^{-1}$ determined by ¹H NMR and fluorescence experiments. Cyclic voltammetry studies show the existence of electronic interaction between the exTTF units due to the flexible nature of the crown ether chains.
© 2005 Elsevier Ltd. All rights reserved.

1. Introduction

The well-known π -electron donor features of tetrathiafulvalenes (TTFs) led to myriad applications.¹ Initially, incentives for their preparation involved the development of novel molecular materials. In this context, the discovery of, for example, the first TTF complex with metallic charge-transfer properties (CT),² triggered implementation of TTF in several areas of modern research. During recent years, the utility of TTF (**1**) as a versatile building block in macrocyclic and supramolecular chemistry³ has shown that TTF is far more than a simple component for molecular conductors.^{4–7}

TTF is a non-aromatic 14π -electron molecule, which is reversibly oxidized to the cation radical and dication in an accessible potential window. Substitutions or chemical modification of the TTF framework emerged as powerful means to fine-tune these properties. Such characteristics render TTF an interesting building block for molecular and supramolecular assemblies,^{3,6} including macrocycles, cyclophanes, cage molecules, catenanes, rotaxanes, dendrimers, polymers, etc.

One of the most interesting aspects of TTF chemistry, namely, that of CT interactions in TTF-based cyclophanes

and cage molecules has recently been reviewed.⁸ The incorporation of TTF into cyclophane hosts is expected to amplify the host–guest interaction with a complementary electroactive guest. Such interactions might electrochemically be signaled. Interestingly, some cyclophanes containing two TTF units (i.e., **3**⁹ and **4**,¹⁰ Chart 1) show the presence of intramolecular interactions between the two TTF units, either in their neutral (**4**) or in their monooxidized form (**3**).

Unlike TTF, π -extended TTF **2** (Chart 1), in which the two dithiole moieties are attached to a central benzene ring of an anthracene linker, undergoes a single two-electron oxidation to yield the corresponding dication. Strong steric repulsions, due to the *peri* hydrogen atoms of the adjacent benzene rings, enforce a ‘saddle-type’ conformation in the neutral molecule. Dramatic structural changes accompany the oxidation process.¹¹

Integrating exTTF into macrocyclic and supramolecular systems has yet to be explored. To the best of our knowledge, a limited number of cyclophane type derivatives have been reported.¹² To this end, compound **5** is the only known exTTF based cyclophane derivative, in which, however, no intramolecular interactions between the two exTTF were observed.

Implementation of C₆₀ as a 3-dimensional electron acceptor holds great promise on account of its small reorganization energy in electron transfer reactions and has exerted

Keywords: Crown ether; Tetrathiafulvalene; Supramolecular complexes.

* Corresponding author. Tel.: +34 91 3944227; fax: +34 91 3944103; e-mail: nazmar@quim.ucm.es

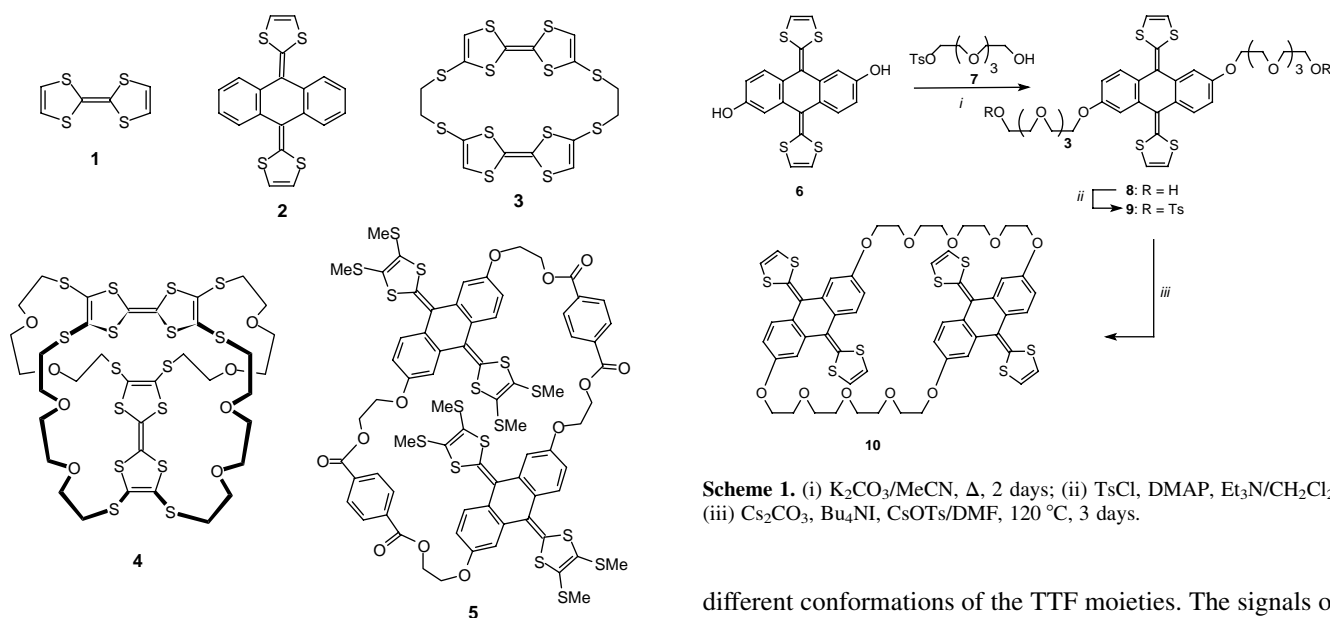


Chart 1.

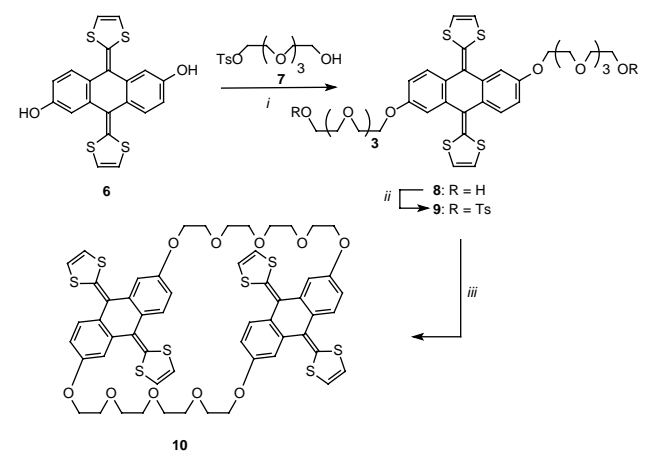
noteworthy impact on the improvement of light-induced charge-separation. The integration of C₆₀ and TTF or exTTF into photosynthetic model system is a particularly promising approach.^{13,14} In particular, photoexcitation of these C₆₀-TTF and C₆₀-exTTF systems generates highly energetic and long-lived charge separated states. Recently, we reported the first example of a supramolecular C₆₀-TTF ensemble, in which the donor and acceptor units were brought together through a complementary guanidinium-carboxylate ion pair.¹⁵

In this work, we wish to report on the synthesis of the first exTTF based crown ether derivative containing two exTTF moieties. The supramolecular interactions between this macrocyclic exTTF derivative and a functionalized C₆₀ bearing a secondary ammonium salt has been tested by a variety of techniques.

2. Results and discussion

The synthesis of the macrocyclic bis- π -extended TTF is summarized in Scheme 1. In particular, dihydroxy exTTF derivative **6** was prepared in a multistep synthetic procedure that was previously reported by our group.^{13f} Next, alkylation of diol **6** with tetraethylglycol monotosylate (**7**) under basic conditions yielded the exTTF derivative **8**, which was then tosylated with tosyl chloride. The cyclization takes place by a nucleophilic substitution between diol **6** and the ditosylated derivative **9**. The cyclic derivative **10** is obtained in 30% yield as a yellow solid. On the other hand, the employ of the corresponding dibromide compound—instead of ditosylate **9**—led to lower yields (18%). The reaction is performed at low solute concentrations in the presence of cesium carbonate¹⁶ to favor the cyclization over oligomerization processes.

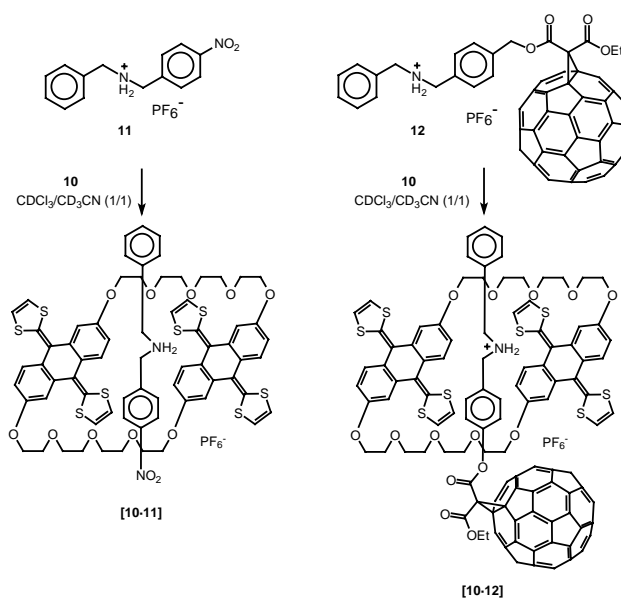
Macrocycle **10** was characterized by FTIR, MS, ¹H and ¹³C NMR. The ¹H NMR spectrum indicates the presence of two



Scheme 1. (i) K₂CO₃/MeCN, Δ , 2 days; (ii) TsCl, DMAP, Et₃N/CH₂Cl₂; (iii) Cs₂CO₃, Bu₄NI, CsOTs/DMF, 120 °C, 3 days.

different conformations of the TTF moieties. The signals of the aromatic protons are observed as two doublets with a coupling constant of $J=8.5$ Hz [$\delta\sim 7.50$ (2H) and $\delta\sim 7.43$ (2H)], two doublets with a small $J=2.1$ Hz [$\delta\sim 7.21$ (2H) and $\delta\sim 7.03$ (2H)], and a multiplet at $\delta\sim 6.7$ (4H), thus appearing as two sets of signals. In the same way, the dithiol ring protons are observed as two different multiplets at $\delta\sim 6.52$ and 6.48 integrating for 4 protons each. Finally, the methylene protons of the polyether chains appear as multiplets at δ values between 4.1 and 3.7.

We tested the cyclic exTTF (**10**) to form supramolecular complexes with secondary amines (Scheme 2) that are endowed with two different acceptors (i.e., a nitro group or a fullerene cage). These salts (**11** and **12**) were prepared by following previously reported procedures.¹⁷ First evidence for complexation was obtained when comparing the ¹H NMR spectra of the free species with the spectrum of a mixture of **10** and the corresponding salt.



Scheme 2.

We have determined the association constant (K_a) for complexing benzyl-*p*-nitrobenzylammonium hexafluorophosphate **11** with crown ether derivative **10**. The K_a value— 50 M^{-1} —was deduced from the complexation-induced changes in the chemical shifts of the aromatic protons of the exTTF cycle in ^1H NMR binding titrations (500 MHz, $\text{CDCl}_3/\text{CD}_3\text{CN}$ 1:1, 298 K).¹⁸

The formation of complexes [**10**·**11**] and [**10**·**12**] was also evidenced by electrospray mass spectrometry, where we have observed the presence of the peaks corresponding to the 1:1 complexes after loss of the counteranion (i.e., 1383 for [**10**·**11**] and 2200 for [**10**·**12**]).

The redox potentials of compounds **10** and **12** were determined by cyclic voltammetry (CV) measurements, carried out in a dichloromethane/acetonitrile solvent mixture at room temperature using glassy carbon (GC) as working electrode, standard Ag/AgCl as reference electrode and with tetrabutylammonium perchlorate (0.1 M) as supporting electrolyte. The data are gathered in Table 1, together with those measured for exTTF **2** under the same experimental conditions.

Table 1

Compound	$E_{\text{pa}}^{1,\text{ox}}$	$E_{\text{pa}}^{2,\text{ox}}$	$E_{\text{pc}}^{\text{ox},a}$	$E_{\text{pc}}^{1,\text{red}}$	$E_{\text{pc}}^{2,\text{red}}$	$E_{\text{pc}}^{3,\text{red}}$	$E_{\text{pc}}^{4,\text{red}}$
2	0.12		0.01				
10	0.01	0.07	-0.03				
12				-0.75	-1.13	-1.63	-2.01

In MeCN- CH_2Cl_2 (1/1), Ag/AgCl versus Pt, scan rate 100 mV s^{-1} .

^a Reduction process from the dication to the neutral molecule.

Unlike the parent TTF, exTTFs exhibit only one, two-electron, quasireversible oxidation wave to form the dication, which has been confirmed by Coulombimetric analysis.¹⁹ The coalescence of the two one-electron processes into one two-electron process reveals that the presence of the quinonoid structure between the two 1,3-dithiole rings leads to unstable, highly distorted, non-planar radical cations.¹¹ For compound **10**—with two exTTF units—two closely-spaced oxidation peaks are observed in the cyclic voltammogram (Fig. 1). These are attributed to consecutive oxidations of the first and second exTTF moieties, respectively (i.e., $\text{D}^0\text{-D}^0 \rightarrow \text{D}^{2+}\text{-D}^0 \rightarrow \text{D}^{2+}\text{-D}^{2+}$). Weak electronic interactions are thought to be responsible for the difference in oxidation potentials between the first and the second exTTF. Consequently, the oxidation of the first moiety shifts the oxidation potential of the second unit to slightly more positive potentials (Table 1). This interaction is made possible by the flexibility of the polyether chains, in contrast with the rigidity of the spacer in **5** (Chart 1), which prevents electronic interaction between the exTTF moieties.

For **12**, four reduction waves were observed, which correspond to the first four reduction steps of the fullerene moiety. As expected, these reduction values are cathodically shifted in comparison with parent C_{60} , as a consequence of the saturation of a double bond of the C_{60} core, which raises the LUMO energy. As previously reported for this compound,¹⁷ the first reduction wave shows a shoulder

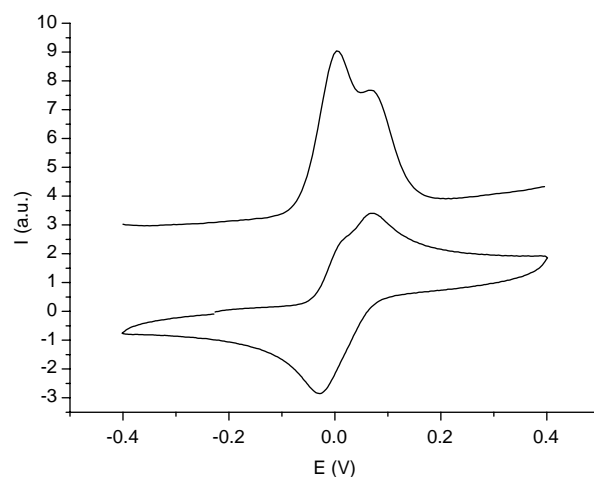


Figure 1. DPV and cyclic voltammogram of **10** in $\text{CH}_3\text{CN}/\text{CH}_2\text{Cl}_2$ 1:1 (Ag/AgCl vs Pt) at 100 mV s^{-1} .

probably due to an irreversible process taking place after the one-electron reduction. The intensity of the cathodic peak of the third reduction wave clearly indicates that other irreversible process accompanies the three-electron reduction of the C_{60} moiety.²⁰

In complementary work the fullerene/macrocycle complexation was tested in fluorescence experiments. The basis for this approach are electron donor–acceptor interactions between C_{60} and exTTF that effect the singlet excited state deactivation of the photoexcited fullerene. In particular, the fullerene (i.e., $2.95 \times 10^{-6} \text{ M}$) fluorescence—photoexcited at 330 nm—was followed in titration experiments, where variable concentrations of the macrocycle (i.e., 3.08×10^{-6} – $3.39 \times 10^{-5} \text{ M}$) were added. An illustration is given in Figure 2, which documents that the fullerene fluorescence decreases in intensity gradually as the macrocycle was added.

In each measurement, the fluorescence was corrected by a background spectrum that was recorded using matching macrocycle concentrations. Then the non-linear quenching of the fullerene fluorescence was used to quantify the fullerene/macrocycle association constant through the following relationship:

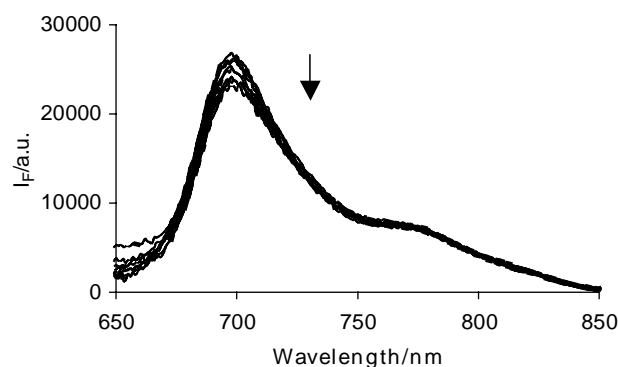


Figure 2. Room temperature fluorescence spectra of fullerene ($2.95 \times 10^{-6} \text{ M}$) in *ortho*-dichlorobenzene upon adding variable concentrations of macrocycle (3.08×10^{-6} – $3.39 \times 10^{-5} \text{ M}$); 330 nm excitation wavelength.

$$I_F = I_0 + \frac{(I_\infty - I_0)}{2c_0} \times \left[\frac{1}{K_S} + c_0 + c_{MC} - \sqrt{\left(\frac{1}{K_S} + c_0 + c_{MC} \right)^2 - 4c_0c_{MC}} \right]$$

Data, as, for example, taken at the 698 nm fluorescence maximum (Fig. 3), were used to determine a K_S value of $55 \pm 5 \text{ M}^{-1}$, which is in excellent agreement with the data based on NMR experiments.

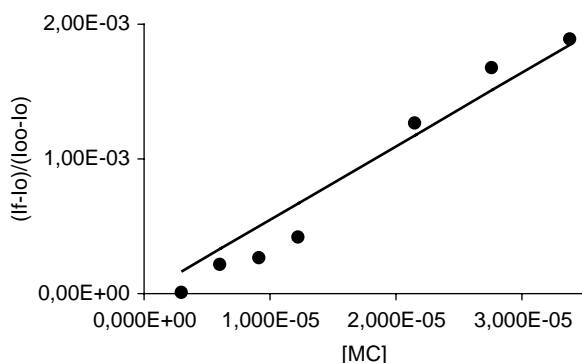


Figure 3. $(I_F - I_0)/(I_\infty - I_0)$ versus macrocycle concentration relationship based on the fluorescence spectrum shown in Figure 2.

3. Conclusions

In summary, we have carried out the synthesis of the first cyclophane-type crown ether (**10**) containing two exTTF units. The flexible oligoether chains connecting the exTTF moieties are responsible for the observed electronic communication existing between them by cyclic voltammetry experiments.

Complexation of crown ether **10** with dibenzylammonium salts bearing electron accepting groups such as *p*-nitrobenzene (**11**) or [60]fullerene²¹ (**12**) afforded new supramolecular ensembles [**10**·**11**] and [**11**·**12**]. The binding constants for complex [**10**·**11**] determined by ¹H NMR (in CDCl₃/CD₃CN) and fluorescence (in *o*-DCB) experiments showed values of $K_a \sim 50 \text{ M}^{-1}$. These findings reveal that these new supramolecular structures are appealing systems for further photoinduced electron transfer studies. Work is in progress to synthesize other different sized macrocycles in order to increase the binding constants of related systems, thus mimicking the natural photosynthetic process.

4. Experimental

4.1. General

4.1.1. 2,6-Bis[2-[2-[2-(2-hydroxyethoxy)ethoxy]ethoxy]ethoxy]-9,10-bis-1,3-dithiol-2-ylidene-9,10-dihydroanthracene (8). To a degassed solution of the monotosylate **7** (1.3 mmol), K₂CO₃ (2.62 mmol) and a catalytic amount of LiBr in MeCN anhydrous (10 mL), the dihydroxy derivative **6** (0.73 mmol) was added under argon. The mixture was heated to reflux for 24 h and then filtered off. The residue was taken up in H₂O (10 mL), and the resulting solution was

extracted with CH₂Cl₂ (2 × 25 mL). The combined organic layers were evaporated in vacuo and the oily residue was taken up in CH₂Cl₂ (50 mL). This solution was carefully washed with a mixture of satd aq NaCl and 10% NaOH aq solution (3:1, 3 × 50 mL). Drying (MgSO₄) and evaporation under reduced pressure followed by column chromatography (SiO₂, CH₂Cl₂) afforded **8** as a yellow solid. Yield: 58%; mp: 251–253 °C (dec); ¹H NMR (CDCl₃, 400 MHz) δ 7.57 (d, 2H, $J_1 = 8.5$ Hz), 7.22 (d, 2H, $J_2 = 2.5$ Hz), 6.83 (dd, 2H, $J_1 = 8.5$ Hz, $J_2 = 2.5$ Hz), 6.28 (s, 4H), 4.20 (t, 4H, $J = 4.5$ Hz), 3.76 (t, 4H, $J = 4.5$ Hz), 3.76–3.59 (m, 24H), 2.60 (s, 2H); ¹³C NMR (100 MHz, CDCl₃) δ 156.7, 137.0, 134.1, 129.1, 128.6, 126.1, 121.8, 117.2, 112.1, 111.0, 72.5, 70.8, 70.6, 70.5, 70.3, 69.7, 67.6, 61.7; FTIR (KBr) ν (cm⁻¹) 3420, 2957, 2938, 2874, 1657, 1597, 1524, 1499, 1456, 1425, 1371, 1309, 1298, 1255, 1158, 1107, 1066, 1021, 950; MS (EI) m/z 888 (M⁺).

4.1.2. 2,6-Bis[2-[2-[2-(2-hydroxyethoxy)ethoxy]ethoxy]ethoxy]-9,10-bis-1,3-dithiol-2-ylidene-9,10-dihydroanthracene ditosylate (9). A solution of **8** (0.4 mmol) was cooled to 0 °C and a catalytic amount of DMAP, TsCl (1 mmol) and Et₃N (2 mmol) were added, keeping the mixture with vigorous stirring. The reaction was allowed to warm to room temperature and let stand overnight. Cool water (100 mL) was added and the mixture was extracted with CH₂Cl₂ (3 × 50 mL). The combined organic layers were dried (MgSO₄) and evaporated to dryness, yielding a residue, which was purified by column chromatography (SiO₂:CH₂Cl₂). Yield: 84%; mp: 265–267 °C (dec); ¹H NMR (400 MHz, CDCl₃) δ 7.77 (d, 4H, $J = 8.2$ Hz), 7.55 (d, 2H, $J_1 = 8.5$ Hz), 7.20 (d, 2H, $J_2 = 2.3$ Hz), 7.30 (d, 4H, $J = 8.2$ Hz), 6.81 (dd, 2H, $J_1 = 8.5$ Hz, $J_2 = 2.3$ Hz), 6.26 (s, 4H), 4.18 (t, 4H, $J = 4.9$ Hz), 4.13 (t, 4H, $J = 4.7$ Hz), 3.86 (t, 4H, $J = 4.9$ Hz), 3.71–3.55 (m, 20H), 2.40 (s, 6H); ¹³C NMR (100 MHz, CDCl₃) δ 158.0, 143.1, 133.2, 131.4, 130.5, 127.5, 126.5, 124.6, 124.1, 113.1, 111.5, 70.7, 70.6, 69.3, 68.7, 21.6; FTIR (KBr) ν (cm⁻¹) 2924, 2851, 1603, 1561, 1542, 1471, 1424, 1370, 1180, 1111, 821, 736, 700; MS (EI) m/z 1073 (M⁺).

4.1.3. Compound 10. To a suspension of Cs₂CO₃ (3.3 mmol) in anhydrous DMF (4 mL) under argon, a solution of diol **6** (0.33 mmol) in DMF (5 mL) was added, and the mixture was heated to 60 °C. After 30 min, CsOTs (0.66 mmol) and Bu₄NI (0.03 mmol) were added. A solution of the ditosylate derivative **9** (0.33 mmol) in anhydrous DMF (5 mL) was slowly added over a period of 2 h and, after addition, temperature was raised to 120 °C. The mixture was kept with stirring and under reflux for 3 days and then was allowed to cool to room temperature. The solution was filtered off and the residue washed with DMF (30 mL). The solvent was removed in vacuo and the residue was taken up in a mixture of toluene (20 mL) and water (10 mL). After separation, the organic phase was dried (CaCl₂) and concentrated under reduced pressure, yielding a residue, which was purified by column chromatography (SiO₂, CH₂Cl₂). The macrocyclic compound **10** was obtained as a yellow solid. Yield: 30%; mp: 273–275 °C (dec); ¹H NMR (500 MHz, DMSO-*d*₆) δ 7.50 (d, 2H, $J = 8.5$ Hz), 7.43 (d, 2H, $J = 8.5$ Hz), 7.21 (d, 2H, $J = 2.1$ Hz), 7.03 (d, 2H, $J = 2.1$ Hz), 6.77–6.70 (m, 4H), 6.52 (m, 4H), 6.48 (m, 4H), 4.14–4.05 (m, 8H), 3.86–3.81

(m, 8H), 3.65 (m, 16H); ^{13}C NMR (125 MHz, DMSO- d_6) δ 158.0, 133.5, 132.9, 126.8, 126.5, 124.5, 124.0, 113.0, 111.5, 70.3, 69.1, 67.7; FTIR (KBr) ν (cm^{-1}) 2925, 2852, 2718, 1601, 1562, 1543, 1508, 1471, 1424, 1226, 1111, 822, 737, 700; MS (EI) m/z 1140 (M^+).

Acknowledgements

Support of this work by MCYT of Spain (BQU-2002-00855) is gratefully acknowledged. M.C. D. is indebted to CAM for financial support (GR/MAT/0633/2004). This work was carried out with partial support from the EU (RTN networks “WONDERFULL” and “CASSIUSCLAYS”), SFB 583, FCI and the Office of Basic Energy Sciences of the US Department of Energy.

References and notes

1. *TTF Chemistry: Fundamentals and Applications of Tetra-thiafulvalene*; Yamada, J., Sugimoto, T., Eds.; Kodansha-Springer, 2004.
2. Ferraris, J. P.; Cowan, D. O.; Walatka, V.; Perlstein, J. H. *J. Am. Chem. Soc.* **1973**, *95*, 948.
3. (a) Lehn, J.-M. *Supramolecular Chemistry*; VCH: Weinheim, Germany, 1995. (b) Atwood, J. L., Davies, J. E. D., MacNicol, D. D., Vögtle, F., Eds.; *Comprehensive Supramolecular Chemistry*; Pergamon: Oxford, UK, 1996; Vols. 1–11.
4. Bryce, M. R. *Adv. Mater.* **1999**, *11*, 11.
5. Nielsen, M. B.; Lomholt, C.; Becher, J. *Chem. Soc. Rev.* **2000**, *29*, 153.
6. Bryce, M. R. *J. Mater. Chem.* **2000**, *10*, 589.
7. Segura, J. L.; Martín, N. *Angew. Chem., Int. Ed.* **2001**, *40*, 1372.
8. Jeppesen, J. O.; Nielsen, M. B.; Becher, J. *Chem. Rev.* **2004**, *104*, 5115.
9. (a) Takimiya, K.; Aso, Y.; Ogura, F.; Otsubo, T. *Chem. Lett.* **1995**, 735. (b) Takimiya, K.; Oharuda, A.; Aso, Y.; Ogura, F.; Otsubo, T. *Chem. Mater.* **2000**, *12*, 2196.
10. Nielsen, M. B.; Thorup, N.; Becher, J. *J. Chem. Soc., Perkin Trans. 1* **1998**, 1305.
11. (a) Martín, N.; Sánchez, L.; Seoane, C.; Ortí, E.; Viruela, P. M.; Viruela, R. *J. Org. Chem.* **1998**, *63*, 1268. (b) For a recent review on quinonoid exTTFs, see: Martín, N.; Ortí, E. In Nalwa, H. S., Ed.; *Handbook of Advanced Electronic Photonic Materials and Devices*; Academic: New York, 2001; Vol. 3; Chapter 6.
12. (a) Godbert, N.; Batsanov, A. S.; Bryce, M. R.; Howard, J. A. K. *J. Org. Chem.* **2001**, *66*, 713. (b) Christensen, C. A.; Batsanov, A. S.; Bryce, M. R.; Howard, J. A. K. *J. Org. Chem.* **2001**, *66*, 3313.
13. (a) Guldi, D. M.; González, S.; Martín, N.; Antón, A.; Garín, J.; Orduna, J. *J. Org. Chem.* **2000**, *65*, 1978. (b) Martín, N.; Sánchez, L.; Herranz, M. A.; Guldi, D. M. *J. Phys. Chem. A* **2000**, *104*, 46–48. (c) Martín, N.; Sánchez, L.; Guldi, D. M. *Chem. Commun.* **2000**, 113. (d) Segura, J. L.; Priego, E. M.; Martín, N.; Luo, C. P.; Guldi, D. M. *Org. Lett.* **2000**, *2*, 4021. (e) Herranz, M. A.; Martín, N.; Ramey, J.; Guldi, D. M. *Chem. Commun.* **2002**, 2968. (f) González, S.; Martín, N.; Guldi, D. M. *J. Org. Chem.* **2003**, *68*, 779–791. (g) González, S.; Martín, N.; Swartz, A.; Guldi, D. M. *Org. Lett.* **2003**, *5*, 557. (h) Sánchez, L.; Pérez, I.; Martín, N.; Guldi, D. M. *Chem. Eur. J.* **2003**, *9*, 2457. (i) Sánchez, L.; Sierra, M.; Martín, N.; Guldi, D. M.; Wienk, M. W.; Janssen, R. A. J. *Org. Lett.* **2005**, *7*, 1691. (j) Guidi, D. M.; Giacalone, F.; de la Torre, G.; Segura, J. L.; Martín, N. *Chem. Eur. J.* **2005**, *11*, 1267. (k) Giacalone, F., Segura, J. L., Martín, N., Ramey, J., Guidi, D. M. *Chem. Eur. J.* **2005**, *11*, 4819.
14. (a) Liddell, P. A.; Kodis, G.; de la Garza, L.; Bahr, J. L.; Moore, A. L.; Moore, T. A.; Gust, D. *Helv. Chim. Acta* **2001**, *84*, 2765. (b) Kreher, D.; Cariou, M.; Liu, S.-G.; Levillain, E.; Veciana, J.; Rovira, C.; Gorgues, A.; Hudhomme, P. *J. Mater. Chem.* **2002**, *12*, 2137 and references therein. (c) Kodis, G.; Liddell, P. A.; de la Garza, L.; Moore, A. L.; Moore, T. A.; Gust, D. *J. Mater. Chem.* **2002**, *12*, 2100.
15. Segura, M.; Sánchez, L.; de Mendoza, J.; Martín, N.; Guldi, D. M. *J. Am. Chem. Soc.* **2003**, *125*, 15093.
16. Balzani, V.; Credi, A.; Mattersteig, G.; Mathews, O. A.; Raymo, F. M.; Stoddart, J. F.; Venturi, M.; White, A. J. P.; Williams, D. J. *J. Org. Chem.* **2000**, *65*, 1924.
17. Diederich, F.; Echegoyen, L.; Gómez-López, M.; Kessinger, R.; Stoddart, J. F. *J. Chem. Soc., Perkin Trans. 2* **1999**, 1577.
18. To perform the ^1H NMR binding studies, the concentration of **10** was kept constant (1 mM) and increasing amounts of **11** were added (from 0.3 to 30 mM). The chemical shifts of the aromatic protons of **10** were observed. The complexation-induced variation of the chemical shift ($\Delta\delta$) was plotted against the concentration of **11**. The K_a value was obtained by a nonlinear regression analysis curve-fitting using SigmaPlot v8.0.
19. Moore, A. J.; Bryce, M. R. *J. Chem. Soc., Perkin Trans. 1* **1991**, 157.
20. The retro-cyclopropanation reaction of methanofullerenes is well documented in the literature: see, for example: (a) Knight, B.; Martín, N.; Ohno, T.; Ortí, E.; Rovira, C.; Veciana, J.; Vidal-Gancedo, J.; Viruela, P.; Viruela, R.; Wudl, F. *J. Am. Chem. Soc.* **1997**, *119*, 9871. (b) Kessinger, R.; Crassous, J.; Herrmann, A.; Rüttimann, M.; Echegoyen, L.; Diederich, F. *Angew. Chem., Int. Ed.* **1998**, *37*, 1919. (c) Boudon, C.; Gisselbrecht, J.-P.; Gross, M.; Herrmann, A.; Rüttimann, M.; Crassous, J.; Cardullo, F.; Echegoyen, L.; Diederich, F. *J. Am. Chem. Soc.* **1998**, *120*, 8545. (d) Beulen, M. W. J.; Echegoyen, L.; Rivera, J. A.; Herranz, M. A.; Martín-Domenech, A.; Martín, N. *Chem. Commun.* **2000**, 917. (e) Beulen, M. W. J.; Rivera, J. A.; Herranz, M. A.; Illescas, B.; Martín, N.; Echegoyen, L. *J. Org. Chem.* **2001**, *66*, 4393. (f) Beulen, M. W. J.; Rivera, J. A.; Herranz, M. A.; Martín-Domenech, A.; Martín, N.; Echegoyen, L. *Chem. Commun.* **2001**, 407. (g) Herranz, M. A.; Beulen, M. W. J.; Rivera, J. A.; Echegoyen, L.; Díaz, M. C.; Illescas, B. M.; Martín, N. *J. Mater. Chem.* **2002**, *12*, 2048.
21. For the first reported fullerene-containing rotaxane and pseudo rotaxane see, respectively: (a) Diederich, F.; Dietrich-Buchecker, Ch.; Nierengarten, J.-F.; Sauvage, J.-P. *J. Chem. Soc., Chem. Commun.* **1995**, 781. (b) Ashton, P. R.; Diederich, F.; Gómez-López, M.; Nierengarten, J.-F.; Preece, J. A.; Raymo, F. M.; Stoddart, J.-F. *Angew. Chem., Int. Ed.* **1997**, *36*, 1448.

Synthesis of a soluble fullerene–rotaxane incorporating a fumamide template

Aurelio Mateo-Alonso and Maurizio Prato*

Dipartimento di Scienze Farmaceutiche, Università degli Studi di Trieste, Piazzale Europa 1, Trieste 34127, Italy

Received 21 June 2005; revised 18 July 2005; accepted 20 July 2005

Available online 14 November 2005

Abstract—The synthesis of a fullerene–rotaxane is described. The thread is constituted by a C₆₀ unit, which acts as a stopper, functionalized with a solubilizing side chain by 1,3 dipolar cycloaddition. The rotaxane is assembled by hydrogen bond-assisted synthesis using a fumamide template.

© 2005 Elsevier Ltd. All rights reserved.

1. Introduction

Rotaxanes have generated a lot of expectations due to their potential technological applications.^{1,2} They can be prepared by means of different intermolecular interactions such as hydrogen bonds,^{3–7} π -stacking,⁸ metal complexation.⁹ The applicability of these systems can be enhanced when using photo- and electroactive units like fullerenes. Owing to the unique photochemical and electrochemical properties of fullerene derivatives,^{10,11} a wide variety of molecular devices can be produced with diverse applicability, including information storage, nanosensing, conversion of light into electric current. C₆₀ has shown a great efficiency as an electron acceptor in donor–acceptor systems.^{10,11} Since photoinduced electron transfer between the donor and C₆₀ can take place through space, they can be connected by means of non-covalent interactions. An example by Schuster and co-workers showed lifetimes up to 32 μ s in ZnP–C₆₀ Sauvage-type rotaxanes.^{12,13} Nevertheless, it has been reported that interlocked ZnP–C₆₀ dyads held together by hydrogen bonds have shown similar lifetimes to their covalently linked analogues.¹⁴ The nature of the linker between the two units controls the distance, the orientation and the electronic coupling between the two units and thus, small structural variations can affect to the lifetime of the charge-separated state. This has been previously documented in covalently linked purpurin–C₆₀ dyads.¹⁵ Therefore, it is worthy to explore different interlocked systems not only to obtain higher lifetimes but also to understand which are the structural factors that control the efficiency of these systems.

In a collaborative work between Leigh's group and our group,³ a fullerene–rotaxane was assembled by clipping a benzylic amide macrocycle around a fullerene thread via hydrogen bond-templated synthesis with a glycyglycine template. C₆₀ acted both as a stopper and an electroactive unit. We decided to establish a straightforward synthetic route to fullerene–rotaxanes containing a fumamide template that should establish the basis for the preparation of supramolecular donor–acceptor systems. Fumaramides have shown to be the best templates for closure of benzylic amide rotaxanes.¹⁶ They can be photochemically isomerized leading to light driven molecular shuttles.^{17–19}

2. Results and discussion

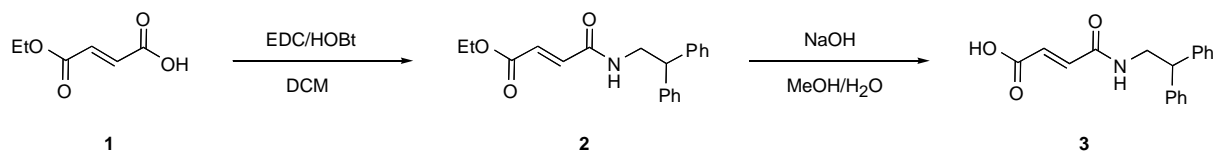
The target thread displayed two stoppers, C₆₀ on one side and a 2,2'-diphenylethyl amide on the opposite side. These stoppers have been shown to cooperate in the stabilization of similar rotaxanes in the solid state by π -stacking.¹⁶ More importantly, a fumamide template was placed in between to direct the ring closure of the macrocycle around the thread.

Our synthetic strategy was based on the preparation of a fumaric acid derivative that contains the non-fullerene stopper. Then, it could be coupled by amidation with a fullerene building block that displays a free amine (Scheme 1). Fumaric acid monoethyl ester **1** was coupled with 2, 2'-diphenylethylamine using the EDC/HOBt couple. The ethyl ester **2** was hydrolyzed in the presence of aqueous sodium hydroxide to yield the corresponding acid **3**.¹⁸

Keywords: Supramolecular; Fullerene; Rotaxane; Hydrogen bond.

* Corresponding author. Fax: +39 040 52572;

e-mail addresses: prato@units.it; prato@univ.trieste.it



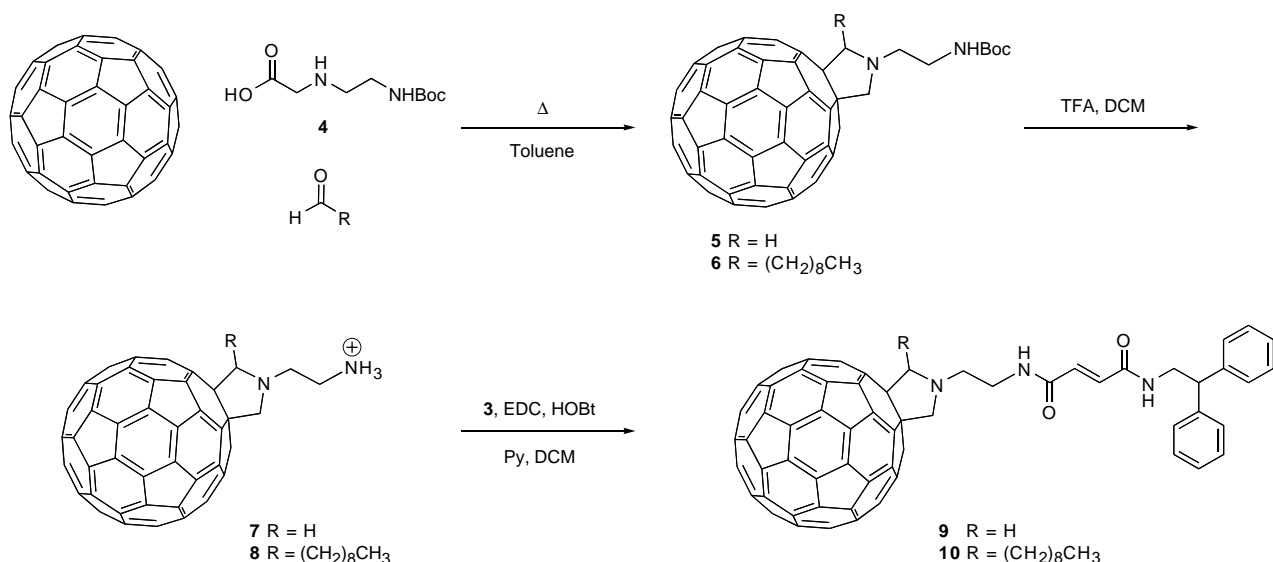
Scheme 1.

C_{60} was functionalized through [3+2] cycloaddition using an azomethine ylide generated in situ by condensation between aminoacid **4** and formaldehyde giving the monoadduct **5**, as previously reported by our group²⁰ (Scheme 2). Then, the amino group was deprotected yielding the ammonium salt **7**. The acid **3** was activated in the presence of EDC and HOBt and coupled with the fullerene salt **7** using pyridine as solvent, leading to the corresponding fullerene thread **9**. The thread **9** showed to be insoluble in chloroform or DMSO and could only be characterized by mass spectroscopy. The solubility of the thread in non-disrupting hydrogen bond solvents, such as chloroform, is one of the most important requirements for the preparation of this type of rotaxanes. However, rotaxane formation was attempted using thread **9** under the previously reported conditions,³ but after the addition of the macrocycle precursors no reaction was observed.

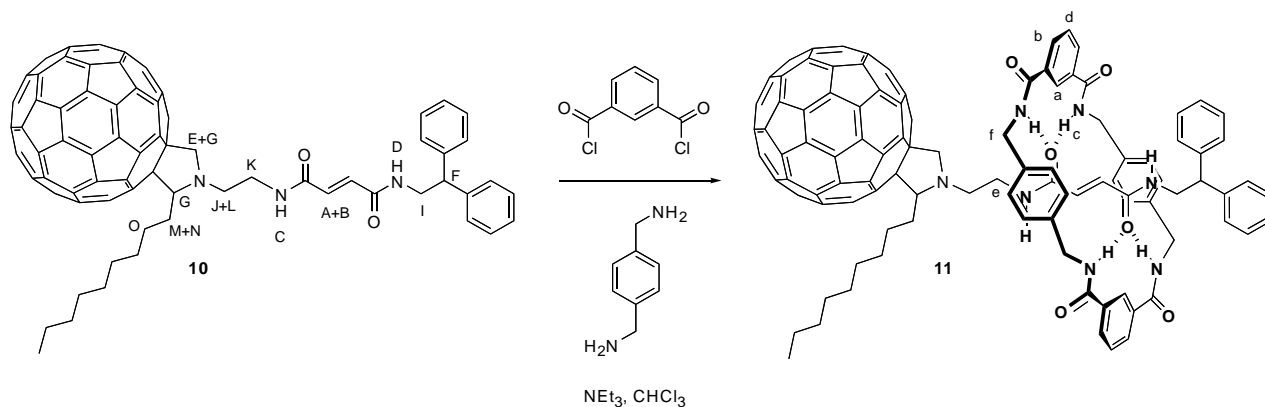
These results clearly show that the combination of fullerenes and fumaramides gave highly insoluble molecules in chlorinated solvents. To overcome this problem, a solubilizing chain was introduced. This was easily achieved by functionalization of C_{60} using 1,3 dipolar cycloaddition (Scheme 2). The cycloaddition was carried out using again aminoacid **4**²⁰ and decanal instead of formaldehyde, introducing a hydrocarbon chain in the fulleropyrrolidine ring. This chain should increase the solubility in chloroform, but also should allow the clipping of the rotaxane since the hydrocarbon chain is pretty flexible. The reaction gave the fullerene building block **6**, which was deprotected using diluted TFA. The ammonium salt **8** was dissolved in pyridine and allowed to react with acid **3**, which was

previously activated using the EDC/HOBt couple. The reaction afforded the desired thread **10**, which was soluble in chloroform and was fully characterized by NMR, MS, IR and UV–vis-NIR. A purity >98% was observed by HPLC using toluene/*i*PrOH 99:1 as eluent. The chromatogram showed a single peak corresponding to thread **10** with a retention time of 31 min.

Rotaxane **11** was assembled by slow addition of isophthaloyl chloride and *p*-xylylenediamine in the presence of NEt_3 (Scheme 3). It was purified by flash chromatography. The formation of the rotaxane **11** was confirmed both by NMR (¹H NMR, COSY) and MS. The purity of rotaxane **11** was checked by HPLC showing a single peak at 29 min and a purity >98%. The ¹H NMR spectrum of rotaxane **11** in CDCl_3 shows an upfield shift of the protons on the fumaramide double bond (from 6.88 to 5.74 ppm), which is more pronounced in pyridine-*d*₅ (from 7.76 to 6.22 ppm) (Figure 1, signals A and B). This effect proved not only the formation of the rotaxane but also that the macrocycle laid on the fumaramide template. The shifting observed is caused by the shielding of the benzylic aromatic rings on the macrocycle over the thread due to anisotropy. The spectrum of rotaxane **11** in CDCl_3 displays a shifting of the amide protons (Figure 1, signals C and D) to the aromatic region. This effect was observed more clearly in pyridine-*d*₅, where the amide protons on the thread **10** appeared more downfield (9.82 and 9.51 ppm) due to hydrogen bonding with the solvent. The spectrum of rotaxane **11** in pyridine-*d*₅ showed the amide protons of the template shifted even more downfield (10.72 and 10.53 ppm).



Scheme 2.



Scheme 3.

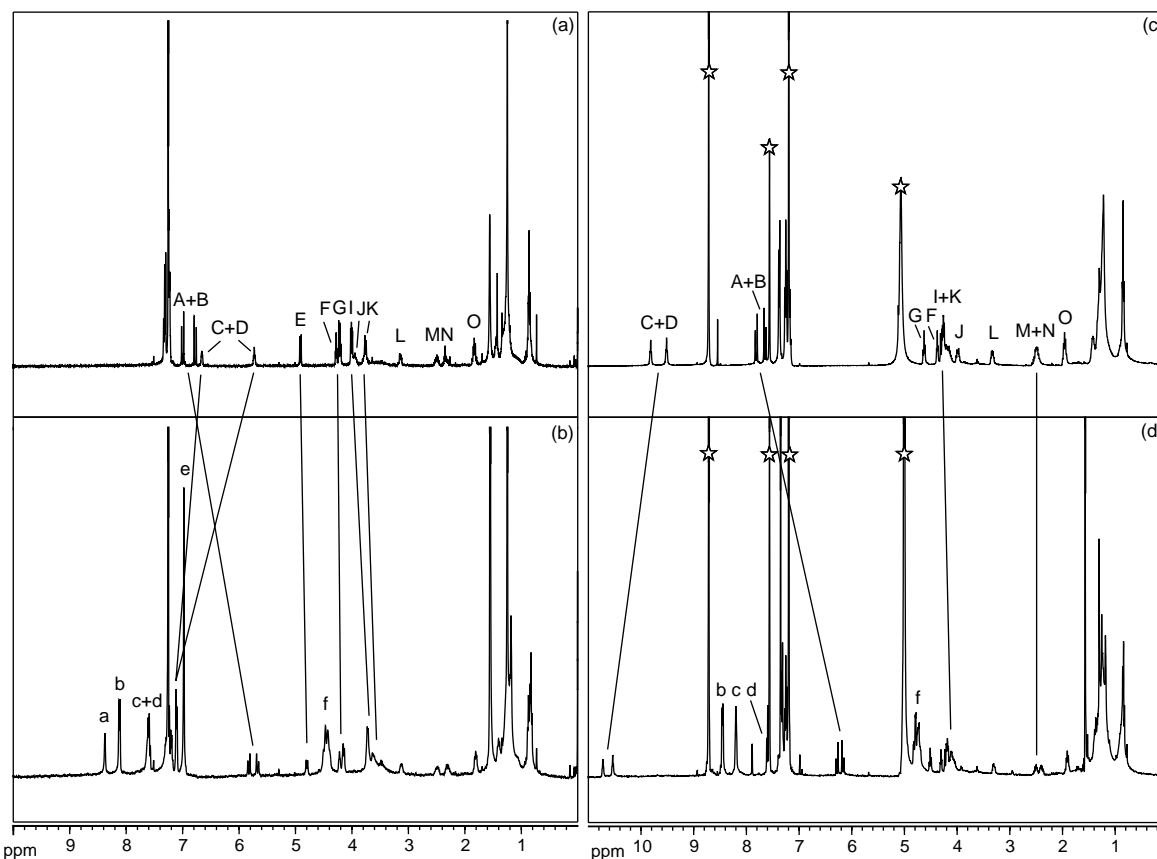


Figure 1. ^1H NMR (400 MHz) of (a) thread **10** in CDCl_3 , (b) rotaxane **11** in CDCl_3 , (c) thread **10** in pyridine- d_5 and (d) rotaxane **11** in pyridine- d_5 . The peaks highlighted correspond to the residual solvent peaks.

On the other hand the UV–vis–NIR spectra of thread **10** and rotaxane **11** did not show any major differences.

3. Conclusions

Fullerene–rotaxane **11** was assembled by hydrogen bond-directed synthesis using a fumaramide template. The insolubility of the fumaramide template together with C_{60} was overcome by the introduction of a solubilizing hydrocarbon chain. This required the preparation of a novel fullerene building block by 1,3-dipolar cycloaddition. The solubilization of the new thread in chloroform allowed the preparation of the rotaxane.

4. Experimental

4.1. General

NMR spectra were recorded on a Varian Gemini-200 (200 MHz) or on a Jeol (400 MHz) at room temperature in CDCl_3 (unless otherwise stated). Chemical shifts reported in ppm are referred to TMS. Infrared spectra were recorded on a Jasco FTIR-200 spectrometer. Mass Spectroscopy: Electrospray (ES-MS) experiments were recorded at Università degli Studi di Trieste on a Perkin-Elmer API1 at 5600 eV. UV–vis–NIR measurements were recorded on a Varian 5000 UV–vis–NIR spectrometer. HPLC experiments were carried out using a semipreparative Phenomenex

Prodigy 5 μm silica 100 \AA column and a Waters 996 photodiode detector. Toluene/*i*PrOH 99:1 was used as the mobile phase. Flow rate gradient 0–1 mL/min (0–3 min), followed by a constant flow rate of 1 mL/min (3–57 min). Commercially available products were used without further purification. Anhydrous CHCl_3 stabilized with amylenes was purchased from Aldrich and used as received.

4.1.1. Fumaric acid mono-2,2'-diphenylethylamide monoethyl ester (2). Fumaric acid monoethyl ester (200 mg, 1.39 mmol), 2,2'-diphenylethylamine (274 mg, 1.39 mmol), HOBt (170 mg, 1.39 mmol) were stirred at room temperature in DCM (10 mL). EDC (275, 1.39 mmol) was added in small portions and the resulting solution was stirred at room temperature for 20 h. The solution was taken up with AcOEt (50 mL) and was washed with aqueous HCl (0.5 N, 50 mL), aqueous NaHCO_3 (saturated, 50 mL) and brine (50 mL). The organic phase was dried over MgSO_4 and the solvent was evaporated under vacuum yielding the desired product (423 mg, 93%).

Mp 111–112 $^\circ\text{C}$ (Mp 112–113 $^\circ\text{C}$). ^1H NMR (200 MHz): 7.34–7.19 (m, 10H, Ar), 6.77 (d, $J=14.4$ Hz, 1H, HC=CH), 6.72 (d, $J=14.4$ Hz, 1H, HC=CH), 5.80–5.65 (m, 1H, NH), 4.30–4.15 (m, 3H, $\text{OCOCH}_2\text{CH}_3$ and CHPh_2), 4.01 (dd, $J=8.0, 5.7$ Hz, OCNHCH_2), 1.31 (t, $J=7.0$ Hz, $\text{OCOCH}_2\text{CH}_3$).

4.1.2. Fullerene thread 9. Fullerene 7^{20} (25 mg, 27 μmol) was dissolved in pyridine (anhydrous, 2.5 mL). Then a solution of acid 3^{18} (16 mg, 54 μmol), EDC (11 mg, 54 μmol), HOBt (7 mg, 54 μmol) in CH_2Cl_2 (5 mL), which was previously stirred for 15 min, was added over the fullerene solution. The resulting solution was stirred at room temperature for 15 min. The solution was washed with aqueous HCl (0.5 N, 50 mL $\times 2$), aqueous NaHCO_3 (saturated, 50 mL $\times 2$) and brine (50 mL). The organic phase was dried over MgSO_4 and the solvent was evaporated under vacuum. The crude was purified by flash chromatography (toluene/*i*PrOH 8:2) and by reprecipitation ($\text{CHCl}_3/\text{MeOH}$ 9:1/ether) yielding the desired product (25 mg, 85%). MS: 1086 (M+H) $^+$.

4.1.3. Fullerene building block 6. A solution of C_{60} (237 mg, 0.312 mmol), aminoacid 4^{20} (50 mg, 0.313 mmol) and decanal (244 mg, 1.560 mmol) were sonicated for 30 min in toluene (240 mL). Then the solution was refluxed for 25 min. The solvent was evaporated by vacuum distillation. The residue was purified by flash chromatography (toluene), unreacted C_{60} was eluted followed by the desired product. This was further purified by reprecipitation using $\text{CHCl}_3/\text{MeOH}$ (120 mg, 37%).

^1H NMR (200 MHz): 5.29 (br s, 1H, NH); 4.96 (d, 1H, $J=10.4$ Hz, $\text{C}_{60}\text{-CH}_2\text{-N}$); 4.34 (d, 1H, $J=5.8$ Hz, $\text{C}_{60}\text{-CHR-N}$); 4.27 (d, 1H, $J=10.4$ Hz, $\text{C}_{60}\text{-CH}_2\text{-N}$); 3.82–3.55 (m, 3H, $\text{NCH}_2\text{CH}_a\text{H}_b\text{N}$); 3.18–3.12 (m, 1H, $\text{NCH}_2\text{CH}_a\text{H}_b\text{N}$); 2.62–2.25 (m, 2H, $\text{C}_{60}\text{-CH-CH}_2$); 2.00–0.85 (m, 26H). ^{13}C NMR (50 MHz): 156.15, 155.98, 154.80, 153.34, 147.04, 147.02, 146.37, 146.35, 146.13, 146.11, 146.03, 145.92, 145.88, 145.85, 145.83, 145.55, 145.53, 145.42, 145.22, 145.16, 145.14, 145.12, 145.05, 144.55, 144.41, 144.30, 144.28, 143.08, 142.97, 142.53,

142.52, 142.49, 142.12, 142.08, 142.06, 142.03, 141.99, 141.96, 141.95, 141.91, 141.69, 141.63, 141.13, 140.09, 139.80, 139.55, 136.78, 136.01, 135.40, 135.32, 77.25, 76.51, 66.48, 51.70, 31.91, 31.48, 30.15, 29.70, 29.58, 29.30, 28.52, 27.60, 22.72, 14.19. IR (NaCl): 3356, 2922, 2849, 1701, 1498, 1461, 1363, 1248, 1168. MS: 1034 (M+H) $^+$.

4.1.4. Fullerene thread 10. Fullerene **6** (120 mg, 0.116 mmol) was dissolved in DCM (3 mL) and TFA (3 mL) was added in small portions. The resulting solution was stirred at room temperature for 3 h. The solvent was evaporated under vacuum. The residue was then dissolved in pyridine (anhydrous, 12 mL). Then a solution of acid 3^{18} (51 mg, 0.172 mmol), EDC (36 mg, 0.172 mmol), HOBt (25 mg, 0.182 mmol) in DCM (12 mL), which was previously stirred for 15 min, was added to the fullerene solution. The resulting solution was stirred at room temperature for 15 min. The solution was washed with aqueous HCl (0.5 N, 50 mL $\times 2$), aqueous NaHCO_3 (saturated, 50 mL $\times 2$) and brine (50 mL). The organic phase was dried over MgSO_4 and the solvent was evaporated under vacuum. The crude was purified by flash chromatography (CHCl_3) yielding the desired product (117 mg, 83%).

^1H NMR (400 MHz, CDCl_3): 7.4–7.2 (m, 10H, Ar); 6.99 (d, 1H, $J=14.82$ Hz, CH=CH); 6.77 (d, 1H, $J=14.82$ Hz, CH=CH); 6.70–6.60 (m, 1H, CONH); 5.73 (t, 1H, $J=5.88$ Hz, CONH); 4.90 (d, 1H, $J=10.25$ Hz, H_E); 4.28 (t, 1H, $J=6.63$ Hz, CH_FPh_2); 4.25–4.15 (m, 2H, H_G); 4.00 (dd, 2H, $J=5.89, 7.76$ Hz, H_I); 3.97–3.90 (m, 1H, H_J); 3.75–3.60 (m, 2H, H_K); 3.20–3.10 (m, 1H, H_L); 2.55–2.45 (m, 1H, H_M); 2.45–2.35 (m, 1H, H_N); 1.83 (q, 2H, $J=7.85$ Hz, H_O); 1.7–0.8 (m, 17H). ^1H NMR (400 MHz, pyridine- d_5): 9.82 (t, 1H, $J=5.59$ Hz, CONH); 9.51 (t, 1H, $J=5.62$ Hz, CONH); 7.88 (d, 1H, $J=14.98$ Hz, CH=CH); 7.64 (d, 1H, $J=14.98$ Hz, CH=CH); 7.50–7.10 (m, 10H, Ar); 4.62 (t, 2H, H_G); 4.38 (t, 1H, $J=5.58$ Hz, CH_FPh_2); 4.30–4.10 (m, 4H, $\text{H}_I + \text{H}_K$); 4.05–3.90 (m, 1H, m, 1H, H_J); 3.40–3.25 (m, 1H, m, 1H, H_L); 2.60–2.40 (m, 2H, $\text{H}_M + \text{H}_N$); 1.96 (q, 2H, $J=7.60$ Hz, H_O); 1.5–0.6 (m, 17H). ^{13}C NMR (50 MHz, pyridine- d_5): 165.74, 165.62, 157.49, 156.04, 154.77, 147.69, 147.66, 147.42, 147.35, 147.07, 146.83, 146.78, 146.73, 146.71, 146.58, 146.55, 146.51, 146.48, 146.34, 146.25, 145.93, 145.89, 145.83, 145.77, 145.73, 145.31, 145.14, 145.04, 145.01, 143.82, 143.66, 143.20, 142.95, 142.92, 142.76, 142.69, 142.65, 142.58, 142.41, 142.35, 140.74, 140.70, 140.46, 140.25, 137.76, 134.93, 134.35, 134.22, 129.42, 129.05, 127.37, 77.50, 72.39, 51.70, 32.65, 30.91, 30.55, 30.39, 30.35, 30.12, 28.14, 23.54, 14.87. IR (NaCl): 3745, 3288, 3079, 2921, 2850, 2360, 1630, 1544, 1456, 1338, 1189, 748. MS: 1212 (M+H) $^+$. UV–vis–NIR (THF, λ_{max}): 255, 292, 320, 431, 704.

4.1.5. Rotaxane 11. A solution of *p*-xylylenediamine (144 mg, 1.050 mmol) in CHCl_3 (anhydrous, 40 mL) and a separate solution of isophthaloyl chloride (213 mg, 1.050 mmol) in CHCl_3 (anhydrous, 40 mL) were added dropwise, simultaneously for 4 h to a stirred solution of the thread **10** (85 mg, 0.070 mmol) in CHCl_3 (anhydrous, 150 mL) containing NEt_3 (153 μL , 2.100 mmol) under argon. After the addition, the reaction mixture was stirred overnight at room temperature. The solution was filtered through Celite, concentrated to dryness and

chromatographed (CHCl_3), giving unreacted thread (33 mg) and rotaxane **11** (30 mg, 25% yield).

^1H NMR (400 MHz, CDCl_3): 8.37 (s, 2H, H_a); 8.11 (d, 4H, $J=8.30$ Hz, H_b); 7.69–7.59 (m, 4H, NH_c); 7.59 (t, 2H, $J=7.94$ Hz, H_d); 7.30–7.20 (m, 10H, Ar); 7.70–7.10 (m, 2H, $\text{H}_c + \text{H}_d$); 6.98 (s, 8H, H_e); 5.82 (d, 1H, $J=14.77$ Hz, $\text{CH}=\text{CH}$); 5.67 (d, 1H, $J=14.77$ Hz, $\text{CH}=\text{CH}$); 4.80 (d, 1H, $J=10.64$ Hz, H_e); 4.55–4.35 (m, 8H, H_f); 4.22 (t, 1H, $J=4.75$ Hz, CH_fPh_2); 4.19–4.10 (m, 5H, $\text{H}_i + \text{H}_j + \text{H}_k$); 3.15–3.05 (m, 1H, H_l); 2.60–2.40 (m, 1H, H_m); 2.40–2.20 (m, 1H, H_n); 1.85–1.75 (m, 2H, H_o); 1.5–0.7 (m, 17H).

^1H NMR (400 MHz, pyridine- d_5): 10.75 (t, 1H, $J=5.15$ Hz, CONH); 10.53 (t, 1H, $J=5.50$ Hz, CONH); 8.45 (dt, 4H, $J=7.76$ and 1.82 Hz, H_b); 8.25–8.15 (m, 4H, H_c); 7.59 (t, 2H, $J=7.76$ Hz, H_d); 7.40–7.15 (m, Ar); 6.28 (d, 1H, $J=14.91$ Hz, $\text{CH}=\text{CH}$); 6.17 (d, 1H, $J=14.91$ Hz, $\text{CH}=\text{CH}$); 4.85–4.60 (m, 8H, H_f); 4.51 (t, 2H, $J=7.94$ Hz, H_g); 4.31 (t, 1H, $J=5.63$ Hz, CH_fPh_2); 4.30–4.00 (m, 5H, $\text{H}_i, \text{H}_k, \text{H}_j$); 3.35–3.25 (m, 1H, H_l); 2.55–2.45 (m, 1H, H_m); 2.45–2.35 (m, 1H, H_n); 1.9 (q, 2H, $J=7.96$ Hz, H_o); 1.4–0.6 (m, 17H). IR (NaCl): 2360, 1639, 1525, 466. MS: 1744 (M+H) $^+$. UV-vis-NIR (THF, λ_{max}): 249, 292, 320, 431, 703.

Acknowledgements

This work has been supported by the EU (RTN EMMMA), Università di Trieste and MIUR (PRIN 2004, prot. 2004035502). We are grateful to Dr. Tatiana Da Ros and Dr. Giovanni Bottari for help and useful comments. We also thank Dr. Fabio Hollan for the mass measurements.

References and notes

- Balzani, V.; Credi, A.; Raymo, F. M.; Stoddart, J. F. *Angew. Chem., Int. Ed.* **2000**, *39*, 3349–3391.
- Balzani, V.; Gomez-Lopez, M.; Stoddart, J. F. *Acc. Chem. Res.* **1998**, *31*, 405–414.
- Da Ros, T.; Guldi, D. M.; Morales, A. F.; Leigh, D. A.; Prato, M.; Turco, R. *Org. Lett.* **2003**, *5*, 689–691.
- Vogtle, F.; Handel, M.; Meier, S.; Ottenshildebrandt, S.; Ott, F.; Schmidt, T. *Liebigs Ann.* **1995**, 739–743.
- Leigh, D. A.; Murphy, A.; Smart, J. P.; Slawin, A. M. Z. *Angew. Chem., Int. Ed.* **1997**, *36*, 728–732.
- Hubner, G. M.; Glaser, J.; Seel, C.; Vogtle, F. *Angew. Chem., Int. Ed.* **1999**, *38*, 383–386.
- Martinez-Diaz, M. V.; Spencer, N.; Stoddart, J. F. *Angew. Chem., Int. Ed.* **1997**, *36*, 1904–1907.
- Anelli, P. L.; Ashton, P. R.; Ballardini, R.; Balzani, V.; Delgado, M.; Gandolfi, M. T.; Goodnow, T. T.; Kaifer, A. E.; Philp, D.; Pietraszkiewicz, M.; Prodi, L.; Reddington, M. V.; Slawin, A. M. Z.; Spencer, N.; Stoddart, J. F.; Vicent, C.; Williams, D. J. *J. Am. Chem. Soc.* **1992**, *114*, 193–218.
- Diederich, F.; Dietrich-Buchecker, C. O.; Nierengarten, J.-F.; Sauvage, J. P. *J. Chem. Soc., Chem. Commun.* **1995**, 781–782.
- Tagmatarchis, N.; Prato, M. Organofullerene materials. In *Fullerene-Based Materials*; Prassides, K., Ed.; Structure and Bonding; Springer Verlag: Berlin, 2004; Vol. 109, pp 1–39.
- Mateo-Alonso, A.; Tagmatarchis, N.; Prato, M. In *Fullerenes and Their Derivatives*; Gogotsi, Y. Ed.; Handbook in Nanomaterials; CRC, 2006, in press.
- Li, K.; Bracher, P. J.; Guldi, D. M.; Herranz, M. A.; Echegoyen, L.; Schuster, D. I. *J. Am. Chem. Soc.* **2004**, *126*, 9156–9157.
- Li, K.; Schuster, D. I.; Guldi, D. M.; Herranz, M. A.; Echegoyen, L. *J. Am. Chem. Soc.* **2004**, *126*, 3388–3389.
- Watanabe, N.; Kihara, N.; Furusho, Y.; Takata, T.; Araki, Y.; Ito, O. *Angew. Chem., Int. Ed.* **2003**, *42*, 681–683.
- Ohkubo, K.; Kotani, H.; Shao, J. G.; Ou, Z. P.; Kadish, K. M.; Li, G. L.; Pandey, R. K.; Fujitsuka, M.; Ito, O.; Imahori, H.; Fukuzumi, S. *Angew. Chem., Int. Ed.* **2004**, *43*, 853–856.
- Gatti, F. G.; Leigh, D. A.; Nepogodiev, S. A.; Slawin, A. M. Z.; Teat, S. J.; Wong, J. K. Y. *J. Am. Chem. Soc.* **2001**, *123*, 5983–5989.
- Altieri, A.; Bottari, G.; Dehez, F.; Leigh, D. A.; Wong, J. K. Y.; Zerbetto, F. *Angew. Chem., Int. Ed.* **2003**, *42*, 2296–2300.
- Bottari, G.; Leigh, D. A.; Perez, E. M. *J. Am. Chem. Soc.* **2003**, *125*, 13360–13361.
- Bottari, G.; Dehez, F.; Leigh, D. A.; Nash, P. J.; Perez, E. M.; Wong, J. K. Y.; Zerbetto, F. *Angew. Chem., Int. Ed.* **2003**, *42*, 5886–5889.
- Kordatos, K.; Da Ros, T.; Bosi, S.; Vázquez, E.; Bergamin, M.; Cusan, C.; Pellarini, F.; Tomberli, V.; Baiti, B.; Pantarotto, D.; Georgakilas, V.; Spalluto, G.; Prato, M. *J. Org. Chem.* **2001**, *66*, 4915–4920.

Inclusion of methano[60]fullerene derivatives in cavitand-based coordination cages

Laura Pirondini,^a Davide Bonifazi,^{b,*} Barbara Cantadori,^a Paolo Braiuca,^b Mara Campagnolo,^c
Rita De Zorzi,^c Silvano Geremia,^c François Diederich^{d,*} and Enrico Dalcanale^{a,*}

^aDipartimento di Chimica Organica e Industriale and INSTM UdR Parma, Università degli Studi di Parma, 43100 Parma, Italy

^bDipartimento di Scienze Farmaceutiche, Università degli Studi di Trieste, 34127 Trieste, Italy

^cDipartimento di Scienze Chimiche, Università degli Studi di Trieste, 34127 Trieste, Italy

^dLaboratorium für Organische Chemie, ETH-Hönggerberg, CH-8093 Zürich, Switzerland

Received 24 May 2005; accepted 7 June 2005

Available online 28 November 2005

Abstract—The X-ray study of self-assembled coordination cage **1**, constituted of two tetrapyrrolyl-substituted resorcin[4]arene cavitands coupled through four square-planar palladium complexes is reported. The coordination cage, embracing an internal cavity of ca. 840 Å³, reveals to have the right size for the inclusion of large molecules such as fullerenes. Cage **1** forms 1:1 complexes with methano[60]fullerene derivatives **3** and **4** bearing a dimethyl and a diethyl malonate addend, respectively. Evidence for inclusion complexation was provided by ¹H NMR spectroscopic studies and ESI-MS investigations, which unambiguously showed the formation of 1:1 fullerene–cage complexes. The association constants (*K_a*) were experimentally determined to be ca. 150 M⁻¹ at 298 K in CD₂Cl₂. In both complexes **1·3** and **1·4**, the malonate residue is threaded through one of the four lateral portals, as clearly shown by docking simulations.

© 2005 Elsevier Ltd. All rights reserved.

1. Introduction

Current materials-oriented science is characterized by the vigorous exploration of new efficient chemical methods for the development of new nano-sized architectures in which functional molecules possessing unique optical and electrochemical properties can be selectively hosted.^{1–3} The ability of the supramolecular approach to confine and stabilize molecular species by specific weak intermolecular interactions in both solid and liquid phase makes it particularly attractive for engineering many potential molecule-based applications ranging from sensors to nanotechnology.^{4,5} Metal-directed self-assembly has been widely employed to engineer two- and three-dimensional structures showing internal cavities capable of trapping molecules.^{6–10} In this respect, cavitand-based coordination cages^{11–16} are increasingly attracting attention as one of the most promising classes of molecular hosts due to the versatile properties of the cavitand scaffold in terms of preorganization, geometry, and synthetic modularity.¹⁷

π-Conjugated molecules such as fullerenes with tunable electronic properties are appealing building blocks for the construction of functional materials possessing exceptional electrochemical and photophysical properties. With the availability of macroscopic quantities of these all-carbon compounds, large efforts have been geared toward discovering rapid and efficient methods for their purification¹⁸ and subsequent inclusion in photosynthetic,^{19,20} photonic,^{21,22} and molecular electronics devices.^{23,24} Numerous examples of fullerene-containing complexes have appeared in the literature, in which the host molecules consist mainly of macrocyclic molecules, such as calixarenes,^{25–28} resorcinarenes,^{29,30} cyclotrimeratrylenes,³¹ cyclodextrins,^{32,33} porphyrins,³⁴ and cyclic [6]paraphenylene-acetylene,³⁵ which spontaneously form complexes in the presence of C₆₀ or C₇₀. Consequently, the preparation of specific preorganized³⁶ receptors containing two or more covalently-linked macrocycles, exploiting a high selectivity toward fullerenes binding, were also explored.³⁷ In this respect, Fukazawa and co-workers prepared the first covalently-linked biscalix[5]arene fullerene receptor, with association constants ranging from 76 to 163 × 10³ M⁻¹ at 298 K in toluene.³⁸ Recently, Saigo, Aida, and co-workers reported a series of cyclophane-type metal-porphyrin dimers that encapsulate fullerenes in organic solvents (with fast host–guest exchange on the NMR time scale)

Keywords: Fullerenes; Cavitands; Self-assembly; Inclusion; Coordination cages.

* Corresponding authors. Fax: +39 521 905472 (E.D.); +39 040 52572 (D.B.); +41 1 632 1109 (F.D.); e-mail addresses: dbonifazi@units.it; diederich@org.chem.ethz.ch; enrico.dalcanale@unipr.it

and in the solid state, showing exceptionally high association constants (ca. $2.4 \times 10^7 \text{ M}^{-1}$ for C_{60} in benzene at 298 K) as a consequence of the strong charge-transfer interaction between the two electron-rich tetrapyrrolic macrocycles and the electron-deficient fullerene sphere. Parallel studies were also reported by Reed, Boyd, and co-workers, who engineered fashionable jaw-like hosts as fullerene binders.^{39,40} Consecutive to these works, several other papers have been reported for the construction of porphyrin-based receptors for fullerenes showing a variety of stimulating features. Thus a dendritic porphyrin receptor with a pronounced allosteric effect in the binding of three C_{60} molecules⁴¹ and a bisporphyrin receptor that can be reversibly switched by complexation with metals were described by Shinkai and co-workers.⁴² However, more rarely the encapsulation of fullerenes in self-assembled cages has been employed.^{43–45} Shinkai *et al.*, reported for the first time a 1:1 complex between a C_{60} molecule and a homooxocalix[3]arene dimer cross-linked by three Pd(II) complexes.^{43,46} Very recently, Claessens and Torres described the encapsulation of C_{60} in an isomeric mixture of C_3 -symmetric coordination cages constituted by two pyridine-bearing subphthalocyanine ligands connected by three metal complexes.⁴⁷

In this work, we describe the self-assembly, crystal structure, and fullerene inclusion properties of cavitand-based coordination cage **1** composed of two tetrapyrridyl-substituted cavitands connected through four square-planar palladium complexes.

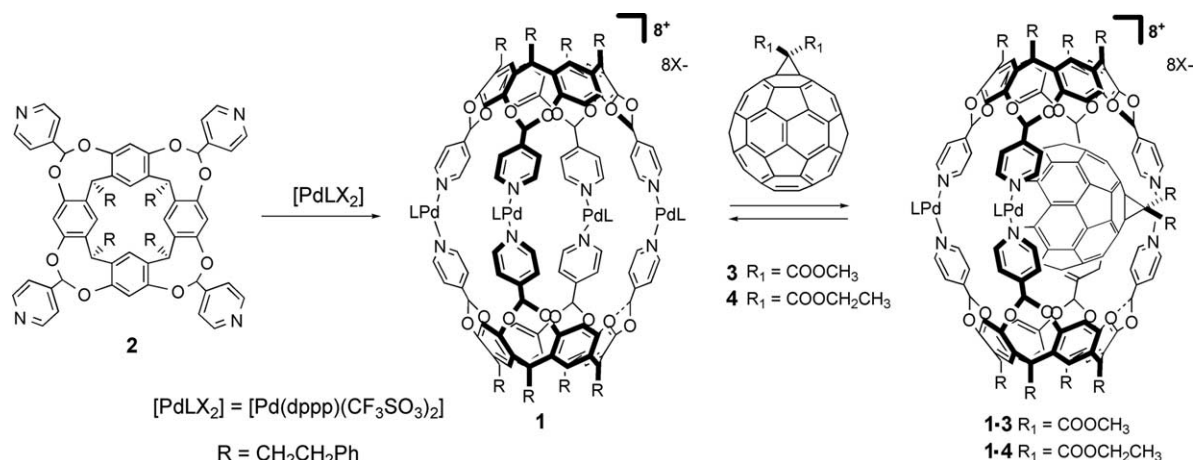
2. Results and discussion

Self-assembly of cavitand ligand **2** into molecular cage **1** was carried out as outlined in Scheme 1, following the protocol reported in the literature.⁴⁸ The typical procedure for the cage preparation is based on the mixing of cavitand ligand **2** with a metal precursor, such as $[\text{Pd}(\text{dppp})(\text{CF}_3\text{SO}_3)_2]$, in a 1:2 molar ratio at room temperature in chlorinated solvents or acetone, affording cage **1** in quantitative yield. The ^1H NMR spectrum showed the formation of a new set of proton resonances, indicative of the presence of a single compound. The downfield shift of the pyridine protons

ortho to the nitrogen is indicative of coordination to the Pd ions, whereas the upfield shift of the OCHO protons, pointing inside the cavity, is diagnostic of the cage formation.⁴⁸ The high symmetry of compound **1** in solution was also confirmed by the ^{31}P NMR spectra, which featured a sharp singlet indicating the equivalence of the eight phosphorous atoms.

A small crystal of coordination cage **1**, suitable for X-ray diffraction, was obtained by slow evaporation of a solution of **1** in acetone. The electron density maps and the refinement of the structure revealed the presence of one octa-cationic coordination cage in the triclinic unit cell, intramolecularly related by a crystallographic symmetry center. The molecular structure, depicted in Figure 1, nicely reveals the presence of four square-planar Pd(II) complexes in the equatorial region connecting two cavitand units (equatorial distance between two successive Pd(II) ions is 12.3 Å). The coordination cage shows a pseudo C_{2h} symmetry in the solid state, which increases to D_{2h} if the terminal (3-phenyl)propyl substituents are excluded.

All Pd(II) metal ions form tetra-coordinated species, with the $\text{N}(\text{Py})\text{--Pd--N}(\text{Py})$ and $\text{P}(\text{dppp})\text{--Pd--P}(\text{dppp})$ angles ranging from 85.9 to 87.5° and from 91.1 to 91.9°, respectively, indicating a small distortion in the square-planar coordination geometry at the Pd(II) metal centers. The positive charges of the four Pd(II) metal centers are counterbalanced by eight CF_3SO_3^- anions, of which four are crystallographically independent. All CF_3SO_3^- ions are disordered at least along two directions. Six CF_3SO_3^- counterions closely surround the cage (Fig. 2a), of which four are in close contact with the Pd(II) metal ions (Pd–O distance 3.0 Å) and two hosted within the two hindered portals between two Pd(II) centers (shortest Pd–O distance = 4.3 Å). Of the two remaining CF_3SO_3^- molecules, one is located outside the cage in a crystallographic center of symmetry and one is confined within the capsule cavity. Both sites are at half occupancy. The latter observation contrasts with the ^{19}F NMR measurements obtained in solution, which clearly showed no permanent inclusion of CF_3SO_3^- anions inside the cage cavity.⁴⁸ The lateral portals are wide enough to allow a fast exchange of the counterions with the bulk solvent.⁴⁹ Eleven acetone molecules (5.5



Scheme 1. Schematic representation of the coordination cage formation and the complexation of **1** with methano[60]fullerene derivatives **3** and **4**. dppp: 1,1'-bis(diphenylphosphino)propane.

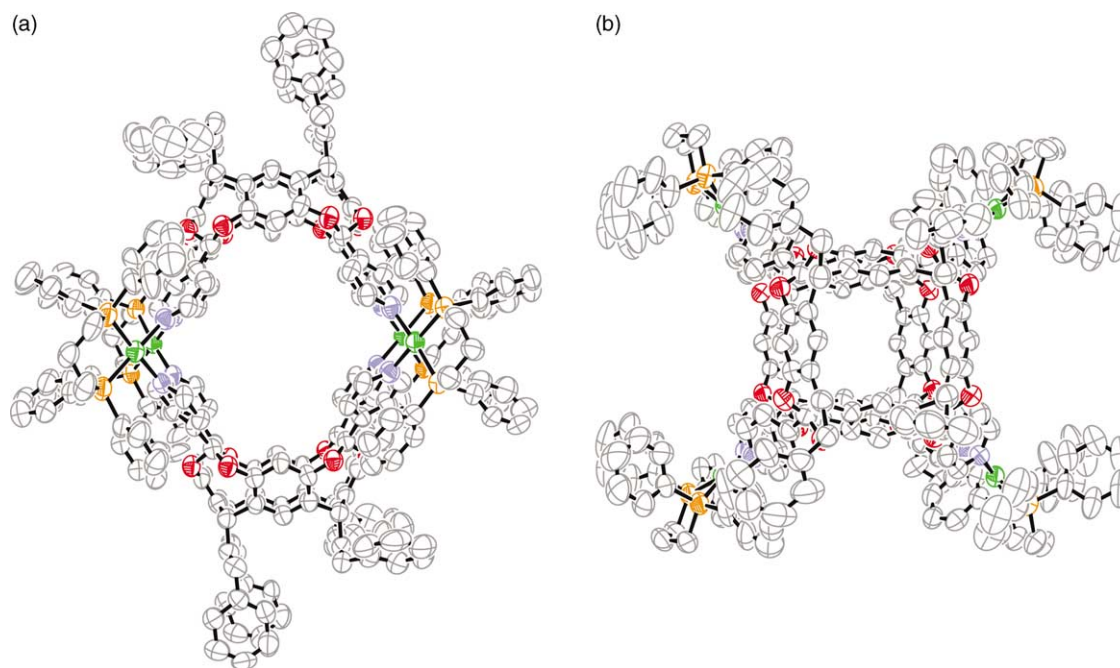


Figure 1. ORTEP representation of cavitaand-based cage **1**. Eleven acetone solvent molecules and eight CF_3SO_3^- anions in the crystal are omitted for clarity. Atomic displacement parameters obtained at 100 K are drawn at the 30% probability level. Atom colors: blue N, red O, green Pd, okra P, grey C.

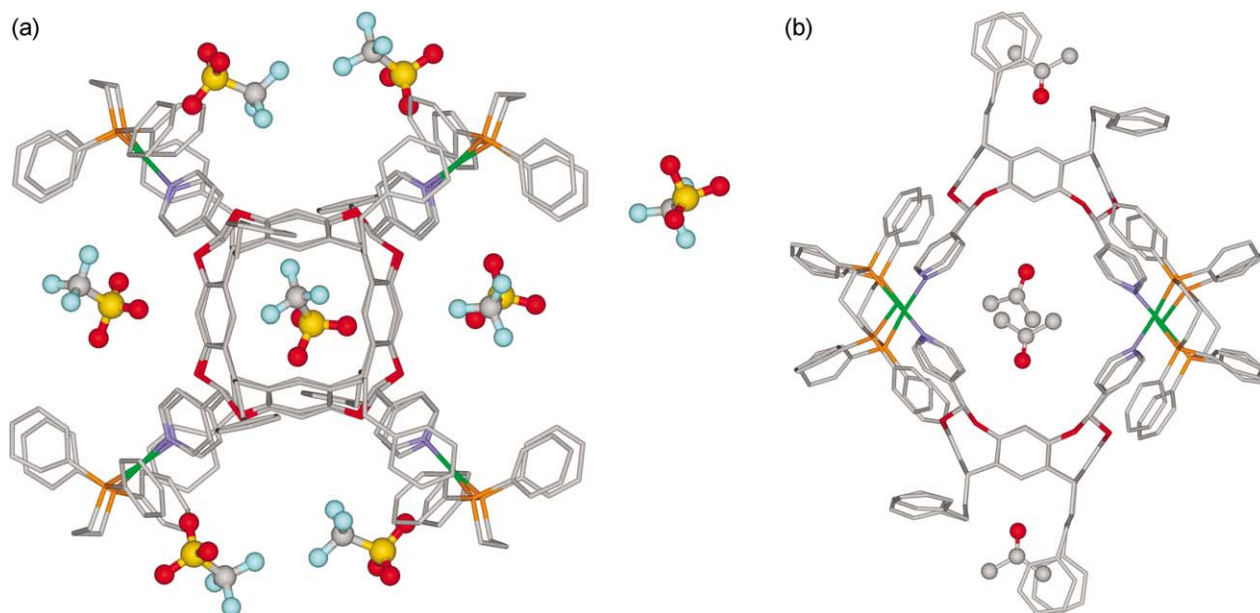


Figure 2. (a) Top view and (b) side view of the crystal structure of coordination cage **1** with eight CF_3SO_3^- anions and four acetone molecules, respectively, showing that three guest molecules have been confined within the cage cavity. Only the acetone molecules close to the cage have been displayed. For the sake of clarity, only one position of the disordered CF_3SO_3^- and acetone molecules is depicted. All H-atoms have been omitted for clarity. Atom colors: blue N, red O, green Pd, okra P, sky-blue F, yellow S, grey C.

molecule per asymmetric unit) were also detected per coordination cage. Among all, only two acetone molecules are confined within the cage cavity disordered along two directions, while the rest is located outside the cavity (Fig. 2b).

Several encapsulation experiments with suitably sized guests such as adamantane, 1,2,4,5-tetramethylbenzene, anthracene, pyrene, sodium picrate, and fullerenes in various solvents were attempted. The complexation

experiments, monitored by ^1H NMR, were performed at 298 K by adding an excess of guest to a solution of cavitaand **2** in CD_2Cl_2 , followed by addition of 2 equiv of the metal precursor $[\text{Pd}(\text{dppp})(\text{CF}_3\text{SO}_3)_2]$ in order to form the cage in the presence of the guest. Adamantane, 1,2,4,5-tetramethylbenzene, anthracene, pyrene, and sodium picrate were not permanently encapsulated in the cage probably due to the rapid exchange with the solvent molecules through the large equatorial portals. On the other hand, the encapsulation experiments using methano[60]fullerene **3** as guest showed

a slow host–guest exchange on the ^1H NMR time scale (298 K). Coordination cage **1** self-assembled in the presence of methano[60]fullerene **3** ($c_1=6.5\times 10^{-1}$ mM and $c_3=5.4$ mM) in CD_2Cl_2 displaying three sets of resonances, which correspond to the two free components (**1** and **3**) and the 1:1 complex **1·3**, respectively (Fig. 3). The singlets at $\delta=4.10$ and 3.57 ppm corresponds to the OCH_3 protons (Fig. 3) of free and complexed methano[60]fullerene **3**, respectively. The upfield shift of the latter signal is a good indication for the formation of the cage–fullerene complex **1·3**. Integration of the resonance signals for the free and complexed methano[60]fullerene species affords the association constant $K_a\approx 150\text{ M}^{-1}$. The complexation between cavitand **2** and methano[60]fullerene **3** in the absence of the metal precursor $[\text{Pd}(\text{dppp})(\text{CF}_3\text{SO}_3)_2]$ was also investigated. As expected, the ^1H NMR spectrum of a 1:2 mixture of fullerene **3** and cavitand **2** shows no changes in the fullerene- and cavitand-centered proton resonances, thus indicating that tetrapyriddy-substituted molecule **2** alone does not form any supramolecular complex with the methano[60]fullerene guest.

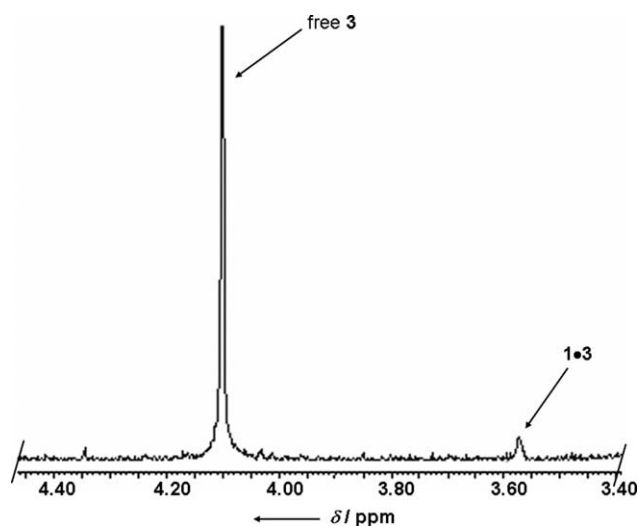


Figure 3. Excerpt of the 300-MHz ^1H NMR spectrum of cage–fullerene complex **1·3** (CD_2Cl_2 , 298 K).

Next, the complexation of methano[60]fullerene derivative **4** with capsule **1** was also investigated. The ^1H NMR spectrum (300 MHz, CD_2Cl_2 , 298 K) of cage **1** self-assembled in the presence of fullerene **4** ($c_1=6.5\times 10^{-1}$ mM and $c_4=5.4$ mM) shows two sets of resonances, one for the free and one for the encapsulated fullerene **4**, in agreement with slow host–guest exchange. The ^1H NMR spectrum resembles the one recorded for the mixture of **1** and **3**, displaying the diagnostic signals for the OCH_2CH_3 and OCH_2CH_3 protons of methano[60]fullerene derivative **4** as quadruplet (Fig. 4) and triplet, respectively, in their free and encapsulated forms. The multiplets centered at $\delta=4.56$ and 1.49 ppm correspond to the OCH_2CH_3 proton resonances of free guest, whereas those at $\delta=4.58$ and 1.51 ppm are assigned to the methano[60]fullerene species embraced within the cage. The K_a value for the formed 1:1 cage–fullerene complex **1·4** in CD_2Cl_2 revealed to be, within the experimental errors, the same as that reported for complex **1·3**. Encapsulation experiments with pristine C_{60} in $\text{CD}_3\text{C}_6\text{D}_5$ were also performed ($c_1=6.5\times 10^{-1}$ mM and

$c_{\text{C}_{60}}=5.4$ mM). However, no fullerene-centered resonances were observed for the complexed species in the ^{13}C NMR spectrum, probably because the anisotropic ring current effects of the interior of the cage do hardly affect the ^{13}C NMR resonances of the carbon sphere. Similarly, complexation of **3** and **4** could not be detected by ^{13}C NMR spectroscopy.

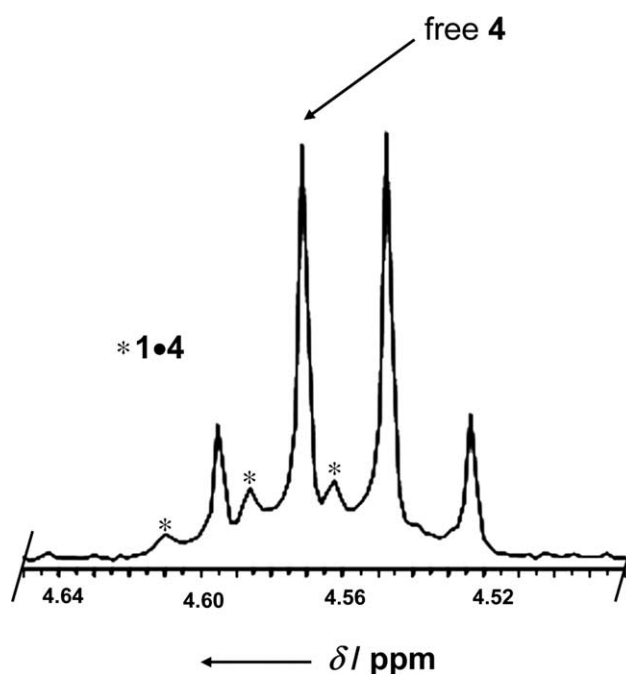


Figure 4. Excerpt of the 300-MHz ^1H NMR spectrum of cage–fullerene complex **1·4** (CD_2Cl_2 , 298 K).

The formation of complexes **1·3** and **1·4** was also evidenced by electrospray ionization (ESI) mass spectrometry in the positive ion mode. The mass spectrum recorded from a 1:8 mixture of coordination cage **1** and methano[60]fullerene **3** (solvent: $\text{CH}_2\text{Cl}_2/\text{MeOH}$ 9:1) displayed a set of peaks belonging to the M^{2+} and M^{3+} ions of both **1** and **1·3** species (Table 1). The base peak detected at m/z 1780.5 corresponds to the triply-charged ion $[\mathbf{1}\cdot\mathbf{3}\cdot\mathbf{3}\times\text{CF}_3\text{SO}_3]^{3+}$, while the corresponding $[\mathbf{1}\cdot\mathbf{3}\cdot\mathbf{3}\times\text{CF}_3\text{SO}_3]^{3+}$ ion is observed at m/z 2064.9. Under the same conditions, the M^{3+} and M^{4+} ions of complex **1·4** were also detected, albeit with lower abundance (Table 1).

Table 1. m/z Values and relative intensities of the peaks observed in mass spectra from samples (solvent: $\text{CH}_2\text{Cl}_2/\text{MeOH}$ 9:1) containing cage–fullerene complexes **1·3** or **1·4**.

Observed ion	Experimental mass (m/z)	Calculated mass (m/z)	Relative intensity (%)
Complex 1·3			
$[\mathbf{1}\cdot\mathbf{3}\cdot\mathbf{2}\times\text{CF}_3\text{SO}_3]^{2+}$	3172.0	3171.80	5
$[\mathbf{1}\cdot\mathbf{2}\times\text{CF}_3\text{SO}_3]^{2+}$	2746.5	2746.42	70
$[\mathbf{1}\cdot\mathbf{3}\cdot\mathbf{3}\times\text{CF}_3\text{SO}_3]^{3+}$	2064.9	2064.84	35
$[\mathbf{1}\cdot\mathbf{3}\times\text{CF}_3\text{SO}_3]^{3+}$	1780.5	1781.26	100
Complex 1·4			
$[\mathbf{1}\cdot\mathbf{2}\times\text{CF}_3\text{SO}_3]^{2+}$	2745.7	2746.42	20
$[\mathbf{1}\cdot\mathbf{4}\cdot\mathbf{3}\times\text{CF}_3\text{SO}_3]^{3+}$	2075.2	2074.20	20
$[\mathbf{1}\cdot\mathbf{4}\cdot\mathbf{4}\times\text{CF}_3\text{SO}_3]^{4+}$	1518.0	1518.38	15
$[\mathbf{1}\cdot\mathbf{4}\times\text{CF}_3\text{SO}_3]^{4+}$	1298.4	1298.68	55

Docking simulations (carried out using the MMFF94× force field as implemented in MOE, see Section 4) performed on cage **1** encapsulating C₆₀ or methano[60]fullerenes **3** and **4**, indicate that all fullerenes species are well accommodated within the cage cavity (Fig. 5). The energy minimized geometry of complex **1**·C₆₀ (not shown) showed

that the fullerene sphere is positioned in the geometrical center of the cavity with the distance between the fullerene sphere and the pyridine ring planes ranging from 3.0 to 3.7 Å, suggesting fullerene–pyridine π-stacking interactions. Although complexes **1**·**3** and **1**·**4** maintain the same geometry as compound **1**·C₆₀, the fullerene sphere is

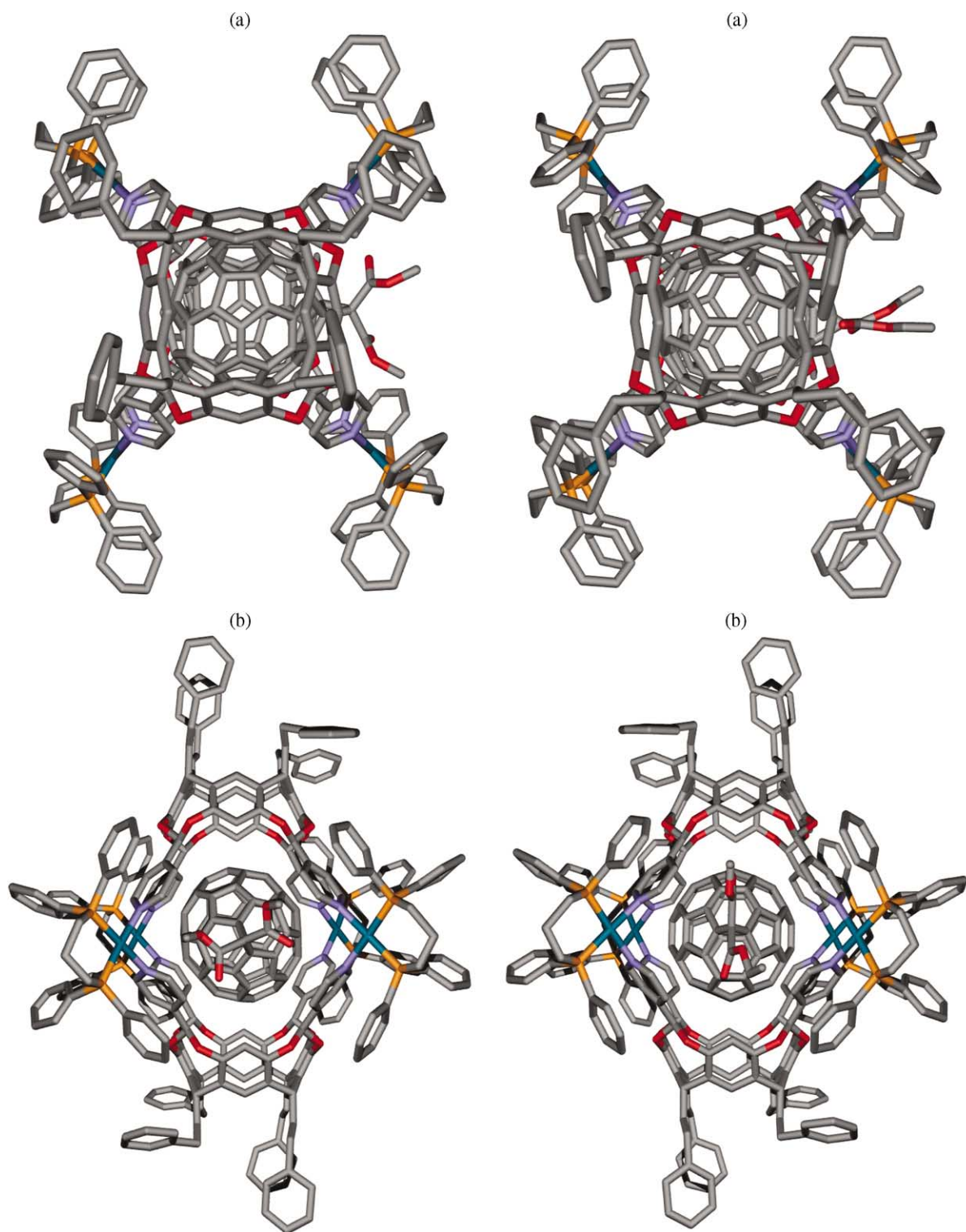


Figure 5. Energy minimized structures (MMFF94×-based docking calculation as implemented in MOE) of cage–fullerene complexes (left) **1**·**3** and (right) **1**·**4**. Top (a) and side (b) view. All H-atoms have been omitted for clarity. Atom colors: blue N, red O, green Pd, okra P, grey C.

slightly shifted toward one portal by ca. 0.1–0.2 Å with respect to the cavity centers because of the presence of the malonate addend. Specifically, in both **1·3** and **1·4** complexes, the malonate residue is threaded through one of the four lateral portals (Fig. 5a). Notably, under the geometrical constrictions applied for these calculations, only two of the four lateral portals are sterically suitable for accommodating the malonate substituents (calculated difference in energy for malonate placement in favorable vs unfavorable portals: $\Delta\Delta E \approx 6.6 \text{ kcal mol}^{-1}$). The volume of the internal cavity of **1** has been estimated in 840 \AA^3 and the four lateral portals have an approximate diameter of 6 Å at the van-der-Waals limits.⁴⁸ The van-der-Waals volume of C_{60} has been calculated in the range 450–549 Å³ with an intermediate value of about 500 \AA^3 .⁵⁰ The resulting packing coefficient of C_{60} within the cavity of **1** is ca. 0.59, which is very close to the optimal value of 0.55 predicted for effective volume-optimized cavity inclusion.⁵¹ Although the geometrical requisites of the preorganized cavity of cage **1** are ideal for the inclusion of C_{60} and its derivatives, no specific interactions, that is, charge-transfer, accounting for high association constants have been identified.

3. Conclusion

Cavitand-based coordination cage **1** features a molecular recognition geometry suitable for the construction of novel supramolecular architectures hosting spherically sized guests, such as fullerenes, as determined by the crystal structure. In chlorinated solvents, the coordination cage forms a 1:1 complex with methano[60]fullerene derivatives **3** and **4**. The inclusion of fullerene derivatives is not related to specific host–guest interactions, but is driven by dispersion forces and π -stacking contacts between the guest and the inner surface of the host. For this reason, the correct match between cavity size, guest shape, and volume is pivotal for effective inclusion, both in terms of packing coefficient and guest confinement (i.e., no guest escape from the lateral portals). The kinetic stability of cavitand-based coordination cages,⁵² is sufficient to observe fullerene inclusion via NMR under slow exchange conditions and in perspective, to exploit some of the peculiar properties of fullerenes in confined environment. Besides, the surface-

directed self-assembly of this class of coordination cages on gold provides an opportunity for the direct formation of these supramolecular complexes on surfaces.⁵³

4. Experimental

4.1. General

Reagents and solvents were purchased reagent grade and used without further purification. Cavitand **2**⁴⁸ and methano[60]fullerene derivatives **3**⁵⁴ and **4**⁵⁴ were synthesized according to the protocols reported in literature. ¹H NMR spectra were recorded on a Bruker Avance 300 MHz spectrometer at 300 K, and all chemical shifts were reported in ppm relative to the proton resonances resulting from incomplete deuteration of the NMR solvents. ESI-MS experiments were performed on a Waters ZMD spectrometer equipped with an electrospray interface.

4.2. Determination of the association constants

The association constants (K_a) were obtained by means of single-point measurements of the concentration of the complexed and uncomplexed species from the ¹H NMR spectra at 298 K by the relationship $K_a = [\text{cage} \cdot \text{fullerene}] / [\text{cage}][\text{fullerene}]$.

4.3. Geometry optimization

The geometries of supramolecular complexes **1·C**₆₀, **1·3**, and **1·4** have been calculated by molecular docking simulations. The spatial coordinates of cage **1** have been derived from the X-ray crystallographic structure, while those for C_{60} and methano[60]fullerenes **3** and **4** have been obtained from their energy minimized structure (calculated via a truncated Newton algorithm⁵⁵ and MMFF94x force field⁵⁶ as implemented in MOE). The force field method has been applied for 50 runs of a 6-cycles simulation annealing protocol, by means of the function DOCK as implemented in the molecular operating environment (MOE) package (Chemical Computing Inc., Montreal, 2004) version 2004.03, starting from 50 random conformations/positions and from a

Table 2. Crystal and refinement data

Formula	(C ₂₇₆ H ₂₅₀ N ₈ O ₁₆ P ₄ Pd ₄) 8 × (CF ₃ SO ₃) 11 × (C ₃ H ₆ O)	$\lambda/2 \sin \theta_{\max}$ (Å)	0.94
F_w	6429.5	Reflns measured	29390
T (K)	100 (2)	Reflns unique	18707
λ (Å)	1.000	Params	1934
Cryst system, space group	Triclinic, <i>P</i> -1	Restraints	1494
a, b, c (Å)	21.5179(8) 21.7484(8) 22.6496(7)	Reflns $I > 2.0\sigma(I)$	17329
α, β, γ (deg)	93.854(2) 116.314(2) 106.929(2)	R_{merge}	0.026 (0.077, in shell 0.97–0.94 Å)
V (Å ³)	8848.1(5)	Gof	1.81
Z, D_{calcd}	1, 1.199 mg/m ³	$R [I > 2\sigma(I)]$	$R_1 = 0.116, wR_2 = 0.354$
μ (mm ⁻¹)	0.843	R (all data)	$R_1 = 0.119, wR_2 = 0.361$
$F(000)$	3320		

simulation temperature of 1000 K. All calculations have been performed on an Intel Xeon 3.0 GHz bi-processor workstation, running Red Hat 9 Linux OS.

4.4. X-ray crystal structure determination

Crystals of coordination cage **1** were grown by slow evaporation of a solution of **1** in acetone. The X-ray structure of a small crystal was obtained using synchrotron radiation under cryogenic control. Data collection was performed at the X-ray diffraction beamline of Elettra Synchrotron, Trieste (Italy) (monochromatic wavelength $\lambda = 1.0000 \text{ \AA}$) using a Mar CCD detector with the rotating crystal method. The crystal soaked with an aqueous solution of PEG 1500 (50% g/ml) was mounted in a loop and flash frozen to 100 K with a nitrogen stream. The diffraction data were indexed and integrated using DENZO⁵⁷ and scaled with SCALEPACK.⁵⁷ The structure was solved by direct methods using SHELXS⁵⁸ and Fourier analyses and refined by the full-matrix least-squares based on F^2 using SHELXL-97.⁵⁹ The refinement was performed using geometrical constraints for the CF_3SO_3^- ions and the acetone molecules. To further optimize the content of the cavities, the SQUEEZE function of the program PLATON⁶⁰ was used. A residual electron density of 23 electrons/cell was found in the remaining voids (11% of cell volume). A refinement using reflections modified by the SQUEEZE program fit well and the R -factor was substantially reduced from 0.123 to 0.119. The 23-electrons count per cell was not included in the calculated density and in $F(000)$. In the final refinement, all non-hydrogen atoms (except those of the disordered CF_3SO_3^- anions and the acetone molecules) were treated anisotropically (using the card SIMU to restrain the anisotropic thermal parameters) and the hydrogen atoms were included at calculated positions with isotropic U factors = $1.2U_{\text{eq}}$. Essential crystal and refinement data are given in Table 2. Crystallographic data (excluding structure factors) for the structures reported in this paper have been deposited with the Cambridge Crystallographic Data Centre (CCDC) as supplementary publication no. CCDC 267407. Copies of the data can be obtained, free of charge, on application to the CCDC, 12 union Road, Cambridge CB2 1EZ UK (fax: +44 1223 336 033; e-mail:deposit@ccdc.cam.ac.uk).

Acknowledgements

F.D. and D.B. acknowledge the financial support by the Swiss National Science Foundation and the NCCR 'Nanoscience'. E.D. and L.P. acknowledge the financial support by MURST through FIRB 'Nanoorganization of materials with magnetic and optical properties'. Use was made of instrumental facilities at the Centro Interfacoltà di Misure G. Casnati of the University of Parma. S.G. thanks Italian MIUR, FIRB RBAU01HAAA, for generous financial support.

Supplementary data

Supplementary data associated with this article can be found, in the online version, at doi:10.1016/j.tet.2005.06.122.

References and notes

- Lehn, J.-M. *Science* **2002**, *295*, 2400–2403.
- Reinholdt, D. N.; Crego-Calama, M. *Science* **2002**, *295*, 2403–2407.
- Whitesides, G. M.; Grzybowski, B. *Science* **2002**, *295*, 2418–2421.
- Jasat, A.; Sherman, J. C. *Chem. Rev.* **1999**, *99*, 931–967.
- Hof, F.; Craig, S. L.; Nuckolls, C.; Rebek, J. *Angew. Chem., Int. Ed.* **2002**, *41*, 1488–1508.
- (a) Yoshizawa, M.; Nakagawa, J.; Kurnazawa, K.; Nagao, M.; Kawano, M.; Ozeki, T.; Fujita, M. *Angew. Chem., Int. Ed.* **2005**, *44*, 1810–1813. (b) Fujita, M.; Ogura, G. *Bull. Chem. Soc. Jpn.* **1996**, *69*, 1471–1482. (c) Chand, D. K.; Biradha, K.; Fujita, M. *Chem. Commun.* **2001**, 1652–1653. (d) Fujita, M. *Chem. Soc. Rev.* **1998**, *27*, 417–425. (e) Fujita, M.; Fujita, N.; Ogura, K.; Yamaguchi, K. *Nature* **1999**, *400*, 52–55.
- (a) Saalfrank, R. W.; Deutscher, C.; Sperner, S.; Nakajima, T.; Ako, A. M.; Uller, E.; Hampel, F.; Heinemann, F. W. *Inorg. Chem.* **2004**, *43*, 4372–4382. (b) Saalfrank, R. W.; Deutscher, C.; Maid, H.; Ako, A. M.; Sperner, S.; Nakajima, T.; Bauer, W.; Hampel, F.; Hess, B. A.; Hommes, N.; Puchta, R.; Heinemann, F. W. *Chem. Eur. J.* **2004**, *10*, 1899–1905. (c) Saalfrank, R. W.; Reimann, U.; Goritz, M.; Hampel, F.; Scheurer, A.; Heinemann, F. W.; Buschel, M.; Daub, J.; Schunemann, V.; Trautwein, A. X. *Chem. Eur. J.* **2002**, *8*, 3614–3619.
- (a) Brumaghim, J. L.; Michels, M.; Raymond, K. N. *Eur. J. Org. Chem.* **2004**, 4552–4559. (b) Brumaghim, J. L.; Michels, M.; Pagliero, D.; Raymond, K. N. *Eur. J. Org. Chem.* **2004**, 5115–5118.
- (a) Fiedler, D.; Pagliero, D.; Brumaghim, J. L.; Bergman, R. G.; Raymond, K. N. *Inorg. Chem.* **2004**, *43*, 846–848. (b) Leung, D. H.; Fiedler, D.; Bergman, R. G.; Raymond, K. N. *Angew. Chem., Int. Ed.* **2004**, *43*, 963–966.
- (a) Fiedler, D.; Bergman, R. G.; Raymond, K. N. *Angew. Chem., Int. Ed.* **2004**, *43*, 6748–6751. (b) Fiedler, D.; Leung, D. H.; Bergman, R. G.; Raymond, K. N. *Acc. Chem. Res.* **2005**, *38*, 349–358.
- Jacopozzi, P.; Dalcanale, E. *Angew. Chem., Int. Ed.* **1997**, *36*, 613–615.
- Fox, O. D.; Dalley, N. K.; Harrison, R. G. *J. Am. Chem. Soc.* **1998**, *120*, 7111–7112.
- Fox, O. D.; Drew, M. G. B.; Beer, P. D. *Angew. Chem., Int. Ed.* **2000**, *39*, 136–140.
- Park, S. J.; Lee, J. W.; Sakamoto, S.; Yamaguchi, K.; Hong, J.-I. *Chem. Eur. J.* **2003**, *9*, 1768–1774.
- Pinalli, R.; Cristini, V.; Sottili, V.; Geremia, S.; Campagnolo, M.; Caneschi, A.; Dalcanale, E. *J. Am. Chem. Soc.* **2004**, *126*, 6516–6517.
- Kobayashi, K.; Yamada, Y.; Yamanaka, M.; Sei, Y.; Yamaguchi, K. *J. Am. Chem. Soc.* **2004**, *126*, 13896–13897.
- Cram, D. J.; Cram, J. M. *Container Molecules and Their Guests*; Royal Society of Chemistry: Cambridge, 1994.
- Xiao, J.; Meyerhoff, M. E. *J. Chromatogr. A* **1995**, *715*, 19–29.
- Armaroli, N.; Boudon, C.; Felder, D.; Gisselbrecht, J. P.; Gross, M.; Marconi, G.; Nicoud, J. F.; Nierengarten, J. F.; Vicinelli, V. *Angew. Chem., Int. Ed.* **1999**, *38*, 3730–3733.
- Gust, D.; Moore, T. A.; Moore, A. L. *Acc. Chem. Res.* **2001**, *34*, 40.
- Hatano, T.; Ikeda, A.; Akiyama, T.; Yamada, S.; Sano, M.; Kanekiyo, Y.; Shinkai, S. *J. Chem. Soc., Perkin Trans. 2* **2000**, 909–912.

22. Hatano, T.; Bae, A. H.; Sugiyasu, K.; Fujita, N.; Takeuchi, M.; Ikeda, A.; Shinkai, S. *Org. Biomol. Chem.* **2003**, *1*, 2343–2347.
23. Metzger, R. M.; Baldwin, J. W.; Shumate, W. J.; Peterson, I. R.; Mani, P.; Mankey, G. J.; Morris, T.; Szulcowski, G.; Bosi, S.; Prato, M.; Comito, A.; Rubin, Y. *J. Phys. Chem. B* **2003**, *107*, 1021–1027.
24. Bonifazi, D.; Salomon, A.; Enger, O.; Cahen, D.; Diederich, F. *Adv. Mat.* **2002**, *14*, 802–805.
25. Mizyed, S.; Ashram, M.; Miller, D. O.; Georghiou, P. E. *J. Chem. Soc., Perkin Trans. 2* **2001**, 1916–1919.
26. Atwood, J. L.; Barbour, L. J.; Heaven, M. W.; Raston, C. L. *Chem. Commun.* **2003**, *9*, 2270–2271.
27. Atwood, J. L.; Koutsantonis, G. A.; Raston, C. L. *Nature* **1994**, *368*, 229–231.
28. Ikeda, A.; Kawaguchi, M.; Suzuki, Y.; Hatano, T.; Numata, M.; Shinkai, S.; Ohta, A.; Aratono, M. *J. Incl. Phenom. Macrocycl. Chem.* **2000**, *38*, 163–170.
29. Martínez García, M.; Velazquez Launizar, C.; Lara Ochoa, F.; Toscano, A.; Chen, G. J.; Cruz-Almanza, R. *Supramol. Chem.* **2000**, *11*, 255–261.
30. Martínez García, M.; Teran Cabañas, R.; Tlapanco Ochoa, A.; Toscano, A.; Cruz-Almanza, R. *Fullerene Sci. Technol.* **2000**, *8*, 475–482.
31. Nierengarten, J.-F.; Oswald, L.; Eckert, J.-F.; Nicoud, J.-F.; Armaroli, N. *Tetrahedron Lett.* **1999**, *40*, 5681–5684.
32. Yoshida, Z. I.; Takekuma, H.; Takekuma, S. I.; Matsubara, Y. *Angew. Chem., Int. Ed.* **1994**, *33*, 1597–1599.
33. Andersson, T.; Nilsson, K.; Sundahl, M.; Westman, G.; Wennerstrom, O. *J. Chem. Soc., Chem. Commun.* **1992**, 604–606.
34. (a) Sun, D.; Tham, F. S.; Reed, C. A.; Chaker, L.; Boyd, P. D. W. *J. Am. Chem. Soc.* **2002**, *124*, 6604–6612. (b) Sun, Y. P.; Drovetskaya, T.; Bolskar, R. D.; Bau, R.; Boyd, P. D. W.; Reed, C. A. *J. Org. Chem.* **1997**, *62*, 3642–3649.
35. (a) Kawase, T.; Tanaka, K.; Fujiwara, N.; Darabi, H. R.; Oda, M. *Angew. Chem., Int. Ed.* **2003**, *42*, 1624–1628. (b) Kawase, T.; Tanaka, K.; Seirai, Y.; Shiono, N.; Oda, M. *Angew. Chem., Int. Ed.* **2003**, *42*, 5597–5600. (c) Kawase, T.; Fujiwara, N.; Tsutumi, M.; Oda, M.; Maeda, Y.; Wakahara, T.; Akasaka, T. *Angew. Chem., Int. Ed.* **2004**, *43*, 5060–5062.
36. Ikeda, A.; Yoshimura, M.; Shinkai, S. *Tetrahedron Lett.* **1997**, *38*, 2107–2110.
37. Diederich, F.; Gómez-Lopez, M. *Chem. Soc. Rev.* **1999**, *28*, 263–277.
38. Haino, T.; Yanase, M.; Fukazawa, Y. *Angew. Chem., Int. Ed.* **1998**, *37*, 997–998.
39. Sun, D. Y.; Tham, F. S.; Reed, C. A.; Chaker, L.; Boyd, P. D. W. *J. Am. Chem. Soc.* **2002**, *124*, 6604–6612.
40. Sun, D. Y.; Tham, F. S.; Reed, C. A.; Chaker, L.; Burgess, M.; Boyd, P. D. W. *J. Am. Chem. Soc.* **2000**, *122*, 10704–10705.
41. Ayabe, M.; Ikeda, A.; Kubo, Y.; Takeuchi, M.; Shinkai, S. *Angew. Chem., Int. Ed.* **2002**, *41*, 2790–2792.
42. Ayabe, M.; Ikeda, A.; Shinkai, S.; Sakamoto, S.; Yamaguchi, K. *Chem. Commun.* **2002**, *8*, 1032–1033.
43. Ikeda, A.; Yoshimura, M.; Udzu, H.; Fukuhara, C.; Shinkai, S. *J. Am. Chem. Soc.* **1999**, *121*, 4296–4297.
44. Yanase, M.; Haino, T.; Fukazawa, Y. *Tetrahedron Lett.* **1999**, *40*, 2781–2784.
45. Haino, T.; Araki, H.; Yamanaka, Y.; Fukazawa, Y. *Tetrahedron Lett.* **2001**, *42*, 3203–3206.
46. Ikeda, A.; Udzu, H.; Yoshimura, M.; Shinkai, S. *Tetrahedron* **2000**, *56*, 1825–1832.
47. Claessens, C. G.; Torres, T. *Chem. Commun.* **2004**, 1298–1299.
48. Pirondini, L.; Bertolini, L.; Cantadori, B.; Ugozzoli, F.; Massera, C.; Dalcanale, E. *Proc. Natl. Acad. Sci. U.S.A.* **2002**, *99*, 4911–4915.
49. For an example where a CF_3SO_3^- anion is trapped in the cage interior see: Fochi, F.; Jacopozzi, P.; Wegelius, E.; Rissanen, K.; Cozzini, P.; Marastoni, E.; Fiscaro, E.; Manini, P.; Fokkens, R.; Dalcanale, E. *J. Am. Chem. Soc.* **2001**, *123*, 7539–7552.
50. Adams, G. B.; O’Keeffe, M.; Ruoff, R. S. *J. Phys. Chem.* **1994**, *98*, 9465–9469.
51. Mecozzi, S.; Rebek, J. *Chem. Eur. J.* **1998**, *4*, 1016–1022.
52. Zuccaccia, D.; Pirondini, L.; Pinalli, R.; Dalcanale, E.; Macchioni, A. *J. Am. Chem. Soc.* **2005**, *127*, 7025–7032.
53. Menozzi, E.; Pinalli, R.; Speets, E. A.; Ravoo, B. J.; Dalcanale, E.; Reinhoudt, D. N. *Chem. Eur. J.* **2004**, *10*, 2199–2206.
54. Cardullo, F.; Seiler, P.; Isaacs, L.; Nierengarten, J.-F.; Haldimann, R. F.; Diederich, F.; Mordasini Denti, T.; Thiel, W.; Boudon, C.; Gisselbrecht, J.-P.; Gross, M. *Helv. Chim. Acta* **1997**, *80*, 343–371.
55. Dembo, P. S.; Steihaug, T. *Math. Program* **1983**, *26*, 190–212.
56. Halgren, T. A. *J. Comput. Chem.* **1999**, *20*, 720–729.
57. Otwinowski, Z.; Minor, W. *Meth. Enzym.* **1997**, *276*, 307–326.
58. Sheldrick, G. M. *Acta Crystallogr., Sect. A* **1990**, *46*, 467–473.
59. Scheldrick, G. M. *SHELXL-97 Program for the Refinement of Crystal Structures*, University of Göttingen: Germany, 1997.
60. Spek, A. L. *Acta Crystallogr. Sect. A* **1990**, *46*, C-34.

Molecular programming of organogelators which can accept [60]fullerene by encapsulation

Michihiro Shirakawa, Norifumi Fujita, Hisashi Shimakoshi, Yoshio Hisaeda and Seiji Shinkai*

Department of Chemistry and Biochemistry, Graduate School of Engineering, Kyushu University, 744 Moto-oka, Nishi-ku, Fukuoka 819-0395, Japan

Received 10 May 2005; accepted 20 July 2005

Available online 6 December 2005

Abstract—New porphyrin-based gelators bearing eight hydrogen-bond-forming amide groups at their periphery were synthesized. They acted as versatile gelators for aromatic solvents. SEM and TEM observations and X-ray crystallographic analysis established that they tend to aggregate into a two-dimensional sheet-like structure utilizing the intermolecular hydrogen-bonding interaction. In this structure the porphyrin–porphyrin π – π stacking interaction is not involved because of the energetically-predominant hydrogen-bonding interactions, keeping the space distance of 12.9 Å. Very interestingly, when C_{60} was added, the morphology was transformed to a one-dimensional fibrous structure, which can enjoy a porphyrin– C_{60} –porphyrin interaction. This multicapsular structure having porphyrin-based compartments for hosting C_{60} was further characterized by XRD, EPR of a Cu(II) analogue, and the theoretical calculation. Thus, this paper presents a new concept, ‘molecular recognition in gel’, which is effective for the weak host–guest interaction.

© 2005 Elsevier Ltd. All rights reserved.

1. Introduction

Molecular design of [60]fullerene (C_{60}) receptors has been of much concern because they enable us to immobilize or deposit C_{60} in the desired positions without damaging its ample π -conjugate system by the introduction of substituents. Among the receptors developed thus far,^{1–8} it is known that the large binding constants are obtained from a cyclic bisporphyrin system.⁷ More recently, we found that a porphyrin-appended cholesterol-based gelator can solubilize a high concentration of C_{60} into the organogel phase.⁹ Surprisingly, this organogel system afforded a strict 1:2 C_{60} /porphyrin stoichiometry in a sandwiched fashion in the superstructure.⁹ This novel information stimulated us to design a new porphyrin-appended gelator, in which the hydrogen-bonding sites are programmed so that the resultant assembly can accept C_{60} , creating a cavity complementary to C_{60} in its superstructure. A potential hint for this molecular design is obtained from calixarene-based molecular capsules demonstrated by Rebek’s group: that is, two ligand (calixarene) moieties are connected by complementary hydrogen-bonding array, adjusting a distance between the two ligand moieties.¹⁰ Previously, we synthesized amide-appended porphyrins **1a**, **1b**, and **2a** to design a new organogel system in which the π – π stacking interaction among the porphyrin moieties and the hydrogen-

bonding interaction among the amide moieties can operate cooperatively (Fig. 1).¹¹ UV–vis absorption spectral analysis and X-ray analysis of the single crystals show that porphyrins in **1a** and **1b** adopt the H aggregation mode, whereas those in **2a** adopt the J aggregation mode.¹¹

We noticed on the basis of the computational modeling studies that when **2a** dimerizes into a capsular molecule by the hydrogen-bonding interaction, four amide groups in one porphyrin moiety and another four amide groups in another porphyrin moiety can form a circular hydrogen-bonding array according to the β -sheet motif and the inner space is exactly comparable with the size of C_{60} (Fig. 2).¹⁴ This result strongly suggests that **2a** should assemble, in the presence of C_{60} , into the one-dimensional array, because four amide groups on the one side are used for the capsule formation and those on the another side are used for the ‘intercapsular’ interaction (Scheme 1).¹⁵

If this is the case, a stoichiometry between C_{60} and **2a** should become 1:2. With these objects in mind, we examined the influence of added C_{60} on the aggregation properties of **2a** in the gel phase. Very interestingly, we found that added C_{60} induces a striking morphological change, forming a 1:2 C_{60} /**2a** complex. By taking these results into account, we further investigated on the molecular arrangement using an EPR-active compounds. The designed Cu(II) porphyrin gelator (**2b**) is structurally equivalent to **2a** and the Cu(II) ion bound to the porphyrin

* Corresponding author. Fax: +81 92 802 2820; e-mail: seijitcm@mbox.nc.kyushu-u.ac.jp

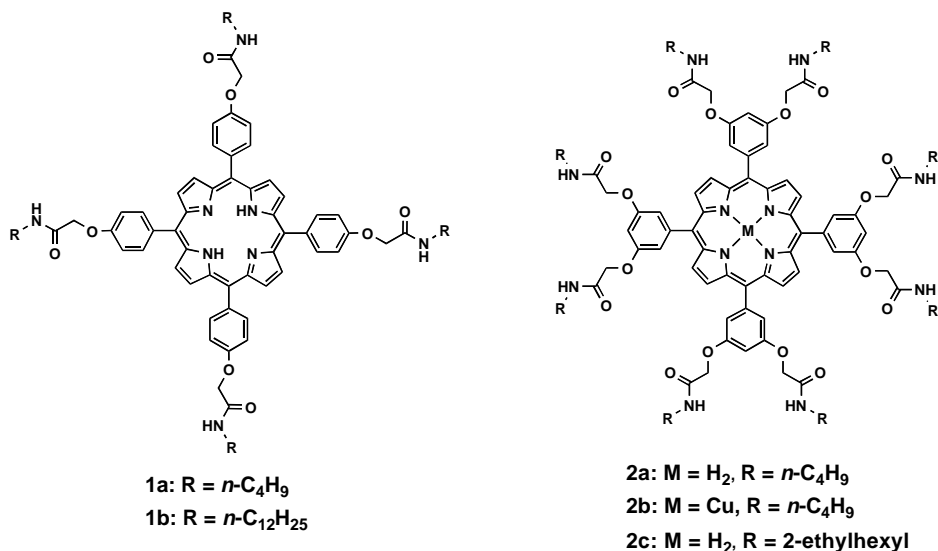


Figure 1. Molecular structures of **1a**, **1b**, **2a**, **2b**, and **2c**.

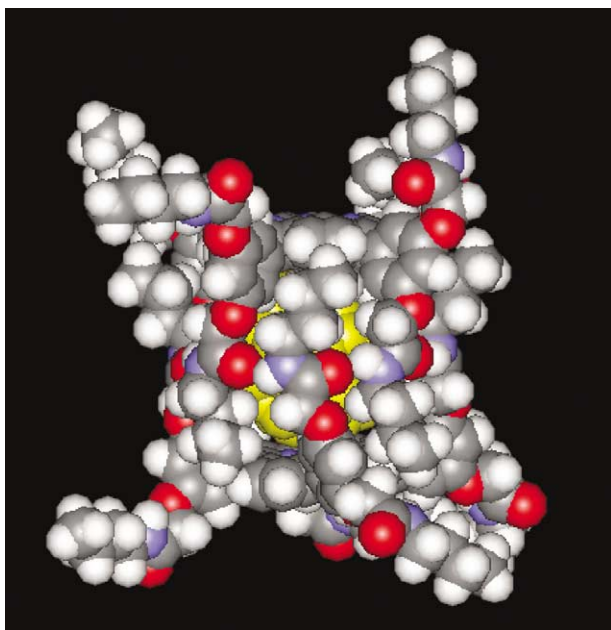


Figure 2. Side view of energy-minimized $(\text{C}_{60}) \cdot (\mathbf{2a})_2$ complex with Discover 3/Insight II 98.0.

center can act as an EPR probe to estimate Cu–Cu distance, giving the structural insight of the porphyrin arrangement in the multicapsular 1:2 $\text{C}_{60}/\mathbf{2}$ complex.

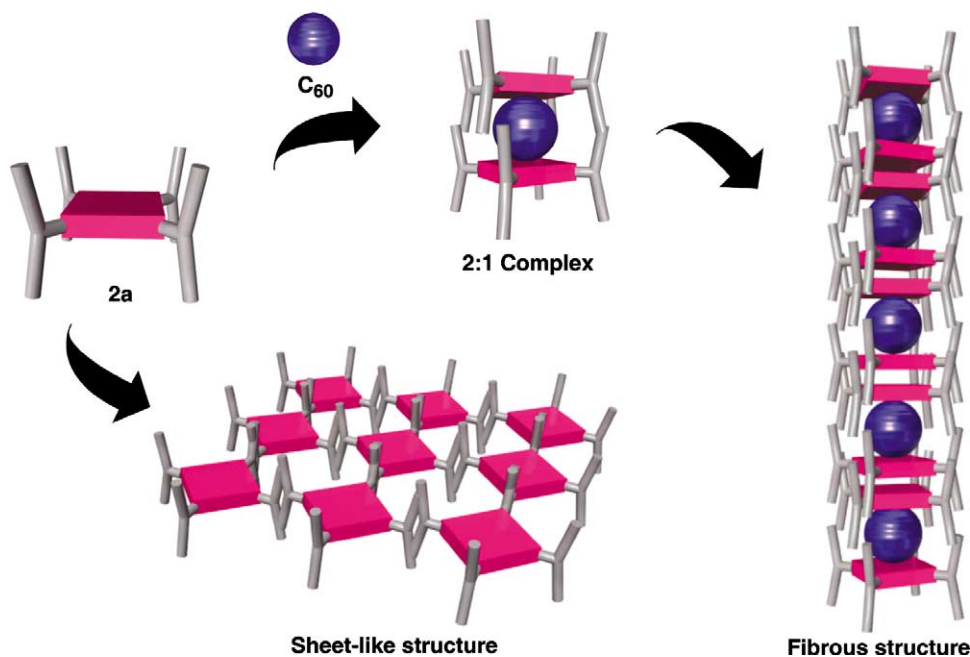
We also noticed that in the molecular programming on **2**, the bulkiness of the alkyl tethers as well as an appropriate design of the amide–amide hydrogen-bonding network and porphyrin– C_{60} interaction may play crucial roles for successful formation of the 1:2 $\text{C}_{60}/\mathbf{2}$ molecular capsule. Accordingly, we prepared the reference compounds having 2-ethylhexyl groups at the alkyl tethers (**2c**), which are too bulky to accommodate a C_{60} molecule inside the dimerized porphyrins (Scheme 2).

2. Results and discussion

Here, we report that a novel porphyrin-based organogelator having rationally positioned hydrogen-bonding sites at the porphyrin periphery for C_{60} encapsulation. Furthermore, the rationality of our molecular programming on this issue is further confirmed by the reference compound **2c** and the structural insight of the molecular arrangement of **2** is clearly revealed by the EPR measurement using an EPR active copper porphyrin gelator (**2b**).

The gelation properties have been tested for 7 selected solvents, which can dissolve C_{60} . The gelation test was carried out as follows: the gelator was mixed in a capped test tube with the appropriate amount of solvent and the mixture was heated until the solid was dissolved. By this procedure the solvent boiling point can become higher than that under standard atmospheric pressure. The sample vial was cooled in air to 25 °C, left for 1 h at this temperature and then turned upside down. When the gelator formed a clear or slightly opaque gel by immobilizing the solvent at this stage, it was denoted by a ‘G’ mark in Table 1. It is known that when **2a** (10 mg/mL) is dissolved in refluxing solvent and then the solution is cooled to 25 °C, benzene, toluene, and chlorobenzene give the gel whereas *o*-xylene, *p*-xylene, and anisole give the precipitate.¹¹ When C_{60} (0.5 equiv to **2a**) was added, all 7 selected aromatic solvents gave the gel.

In addition, the gel-to-sol phase-transition temperature (T_{gel}) for the benzene gel (79 °C in the absence of C_{60}) was enhanced up to 120 °C by the addition of C_{60} . These findings support the view that added C_{60} efficiently improves the gel stability, probably by changing the morphology of the **2a** aggregate formed in the benzene gel. Gelation properties of **2b** are also improved by the addition of C_{60} in case of toluene, *p*-xylene, anisole, and *o*-dichlorobenzene under the same conditions, implying that **2b** possesses a versatile gelation ability compellable with that of **2a**. Interestingly, the strong red fluorescence observed for the solution containing **2a** and C_{60} at high temperature is completely quenched in the gel phase after



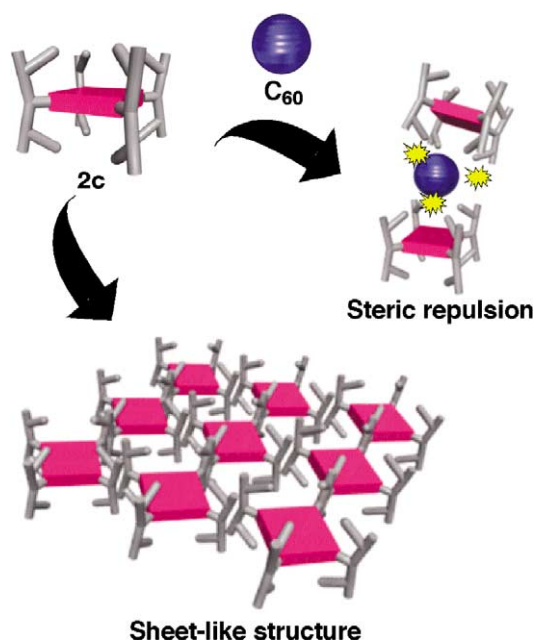
Scheme 1. Aggregation mode of **2a** in the presence and the absence of C_{60} .

cooling of the solution (Fig. 3). The finding implies that the one-dimensional superstructure consisting of porphyrins and C_{60} s would show very novel electron-transfer phenomena in the gel phase. In contrast, **2c** having the bulky substituents on the alkyl tethers on the porphyrin periphery does not change its gelation properties upon C_{60} addition. As seen in the molecular modeling of a 1:2 $C_{60}/2c$ complex, the bulky ethylhexyl groups avoid formation of a capsular structure because of the steric repulsion between the bulky groups and C_{60} .

J and H assembling modes of the porphyrin aggregate are clearly discriminated by UV spectroscopic analyses. As shown in Figure 4, the Soret band observed for the **2a** or **2b** + benzene gel (5.0 g/mL) is red-shifted by 7 and 5 nm, respectively, in comparison with the solution of **2a** and **2b**. This shift is due to the J aggregation nature of the **2a** and **2b**. On the other hand, the Soret band of the **2a** and **2b** gels after adding 0.5 equiv of C_{60} was scarcely shifted from that in the dilute benzene solutions of **2a** and **2b**, indicating that the aggregation mode is neither H aggregate nor J aggregate. This problem will be discussed more in the later part of this paper.

The reference compound **2c** again shows the contrastive results that the Soret band of **2c** + benzene gel (5.0 g/mL) is red-shifted by 5 nm in comparison with the solution of **2c**. This shift is due to the J aggregation nature of the **2c** and that of **2c** gel. Even after adding 0.5 equiv of C_{60} , this system still showed the red-shifted absorption indicating that the aggregation mode of **2c** is scarcely affected by C_{60} addition. These results again indicate that aggregation modes of **2a** and **2b** are affected by the addition of C_{60} and that of **2c** is not affected because C_{60} may not interact with **2c** due to the steric repulsion of the alkyl groups in **2c**.

The complementary results are obtained from the transmission and scanning microscopic analyses. SEM images of



Scheme 2. Possible aggregation mode of **2c**.

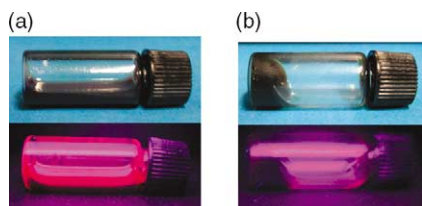
the xerogels prepared from the **2a** or **2b** + benzene gel are shown in Figure 5. The assemblies in the absence of C_{60} feature sheet-like structures.¹¹ Addition of 0.50 equiv C_{60} dramatically changes the sheets to the fibers, which are characteristic of the low-molecular-weight organogel system. TEM pictures taken without a staining reagent are also shown in Figure 5. In the absence of C_{60} , one can only recognize the low contrast sheet-like structures (Fig. 5c). Addition of C_{60} changes the morphology into the fibrous structure, and the fibrils show the strong contrast due to the absorption of electron beam by C_{60} (Fig. 5d). These SEM and TEM observations clearly support the view that added C_{60} changes the two-dimensional aggregation mode into the one-dimensional one. In contrast, SEM pictures of

Table 1. Gelatin properties of **2a**, **2b**, and **2c** in the absence or in the presence of C₆₀ in aromatic solvents^a

Solvent	2a		2b		2c	
	Only	+C ₆₀ ^b	Only	+C ₆₀ ^b	Only	+C ₆₀ ^b
Benzene	G	G	G	G	G	G
Toluene	G	G	P	G	G	G
<i>o</i> -Xylene	P	G	P	P	G	G
<i>p</i> -Xylene	P	G	P	G	G	G
Anisole	P	G	P	G	P	P
Chlorobenzene	G	G	G	G	P	P
<i>o</i> -Dichlorobenzene	P	G	P	G	P	P

^a The solution was warmed until a gelator was dissolved and then cooled to 25 °C grow the gel: G=gel, P=precipitate.

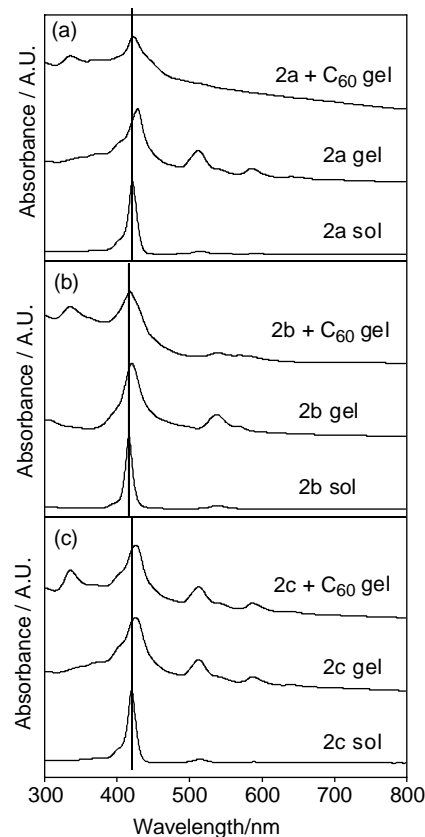
^b [Gelator]=10.0 mg/mL, [C₆₀]=[gelator]/2.

**Figure 3.** Pictures of (a) **2a** + anisole solution in the presence of 0.50 equiv of C₆₀ heated at 90 °C under UV light (365 nm) irradiation and (b) gel obtained by cooling (a) solution to 25 °C.

the **2c** + benzene gel before and after addition of C₆₀ show the same sheet-like structure, indicating that assemblies of **2c** in the gel phase adopt the sheet-like two-dimensional structure and the macroscopic morphology is not affected by C₆₀ addition.

To obtain direct evidence on the molecular arrangement of **2a** in the absence of C₆₀, we conducted an X-ray crystallographic analysis. In general, gelator molecules tend to pile up or accumulate in a one- or two-dimensional direction and result in needle-like or thin crystals. This growth mode makes it difficult to obtain a single crystal suitable for X-ray crystallographic analysis. Previously, we succeeded in growth of the single crystal from **2a** when it was recrystallized from acetone–hexane mixed solvent. The crystal structure of **2a** thus obtained is shown in Figure 6¹¹. The porphyrin rings are arranged two-dimensionally in an *a*–*b* plane to form a layer structure coplanar to the porphyrin rings, and the amide groups are used to connect them within the layer.

One hydrogen-bonding network that runs in parallel to the layer consists of four amide groups supplied from four different porphyrins. The layer–layer distance along the *c*-axis is 12.858 Å, which is too far for porphyrins to enjoy the π – π stacking interaction. Instead, the layer–layer space is filled with the alkyl groups of the amide groups and the solvated molecules. One can thus conclude that the crystal packing mode of porphyrin rings in **2a** has a two-dimensional character without the direct porphyrin–porphyrin interaction. That is because one *meso*-phenyl group has two amide groups at the 3- and 5-positions and the hydrogen-bonding force plays a decisive role to determine the structure.

**Figure 4.** UV–vis absorption spectra in the sol phase (lower) and in the gel phase without C₆₀ (center) or with 0.50 equiv of C₆₀ (upper); (a) **2a**, (b) **2b**, and (c) **2c**.

The XRD spectrum of xerogels obtained from **2a** + benzene gel is shown in Figure 7a. The ‘theoretical’ XRD spectrum can be illustrated using the X-ray crystallographic data as shown in Figure 7b. In Figure 7a, one can recognize a strong peak at $2\theta=6.87^\circ$ ($d=12.9$ Å), which is ascribed to the refraction from the (001) plane constructed by the porphyrin layers. The same peak is also observable in Figure 7b, indicating that the xerogel also has the (001) plane. The foregoing findings support the view that in the present porphyrin-based organogel system, the packing mode of the molecular assemblies constructed in the organogels is very similar to that grown in the single crystals.

Considering these lines of information, **2a**, **2b**, and **2c** adopt the similar hydrogen-bonding pattern extending two-dimensionally through the amide–amide interaction, leading to the formation of macroscopic sheet-like morphologies. In the XRD diagrams of the xerogel sample of **2a** gel with C₆₀ (Fig. 8), however, a $2\theta=7.14^\circ$ ($d=1.24$ nm) peak, which was ascribed to the refraction from the (001) plane constructed by two-dimensional porphyrin layers,¹¹ disappeared and a $2\theta=4.90^\circ$ ($d=1.80$ nm) peak newly appeared,¹⁴ which would be ascribable to the columnar diameter in the one-dimensional (C₆₀)_n·(**2a**)_{2n} aggregate.

The foregoing findings consistently support the view that **2a** has a latent capability to create a one-dimensional multicapsular structure in the presence of C₆₀, although it is assembled into a two-dimensional sheet-like structure in

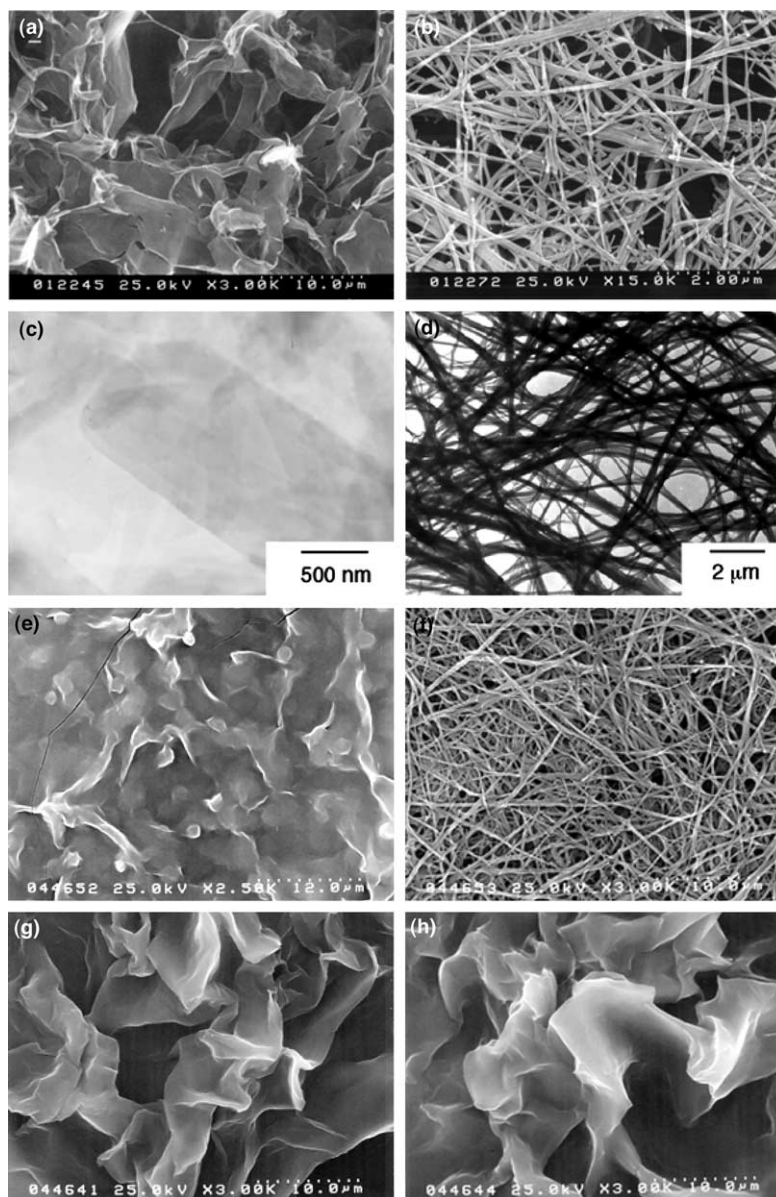


Figure 5. SEM (first, third, and fourth line) and TEM (second line) pictures of the xerogels prepared from (a), (c); **2a** (1.52 mM)+benzene gel, (b), (d); **2a** (1.52 mM) with 0.50 equiv C_{60} +benzene gel, (e) **2b** (2.92 mM)+benzene gel, (f) **2b** (2.92 mM) with 0.50 equiv C_{60} +benzene gel, (g) **2c** (4.77 mM)+benzene gel, and (h) **2c** (4.77 mM) with 0.50 equiv of C_{60} +benzene gel.

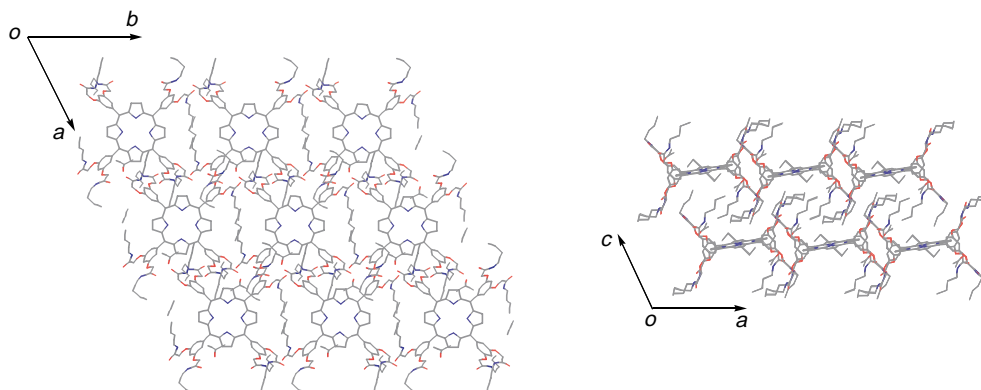


Figure 6. Crystal structure of **2a**.

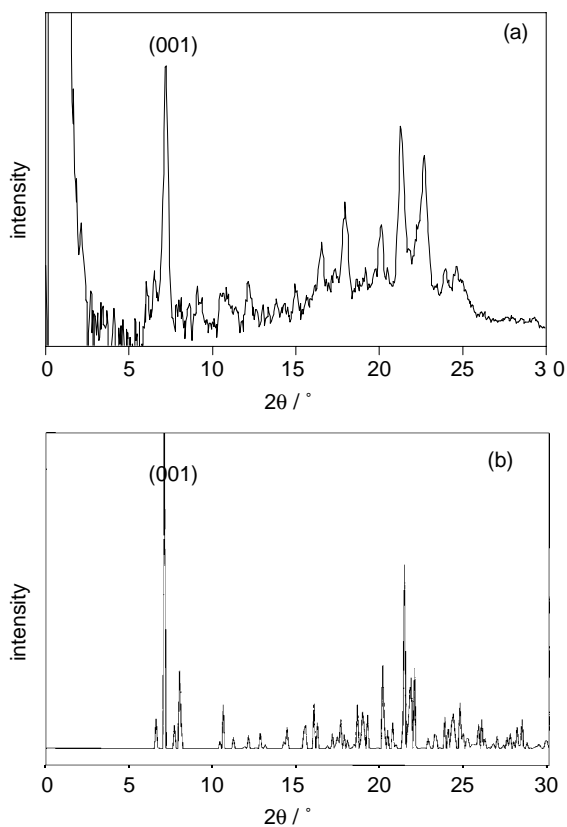


Figure 7. Powder X-ray diffraction diagrams of **2a**: (a) the xerogel prepared from benzene and (b) theoretical profile illustrated using the X-ray crystallographic data.

the absence of C_{60} . These novel C_{60} -induced morphological changes are due to a strong porphyrin– C_{60} interaction as well as skillfully programmed hydrogen-bonding sites.

The foregoing various analyses confirmed that **2b** can be regarded to be structurally equivalent to **2a** in the aggregation mode and the EPR analyses on the **2b** xerogel may give us the detailed structural information on the one-dimensional $(C_{60})_n \cdot (2a)_{2n}$ aggregate based on the spin–spin interaction between the Cu(II) ions in the porphyrin cores. We conducted the EPR analyses on the xerogel prepared from **2b** + benzene gel in the absence of C_{60} . The obtained EPR data on the **2b** xerogel (Fig. 9a) show a characteristic pattern assignable to the Cu(II) in the porphyrin core without any spin–spin interaction. This EPR result is well consistent with that of the crystallographic analysis on the **2a** xerogel, that is, the distance between Cu(II) ions on the porphyrin cores of **2b** is about 12 Å, which does not allow the spin–spin interaction between Cu(II) ions. However, the EPR analysis of the xerogel prepared from **2b** + benzene gel in the presence of C_{60} gives a totally different pattern as shown Figure 9b. The EPR pattern appears at around 1500 G assignable to the spin–spin interaction between Cu(II) ions, characteristic of the forbidden transition. This observation reveals that the two Cu(II) ions exist in the proximity and gives us information on the distance between the Cu(II) ions. From the given $D_2 = 0.0428$ and $g_2 = 2.19$, r can be calculated to be 4.18 nm, which is an adequate center to center distance for very slightly slipped porphyrins.¹²

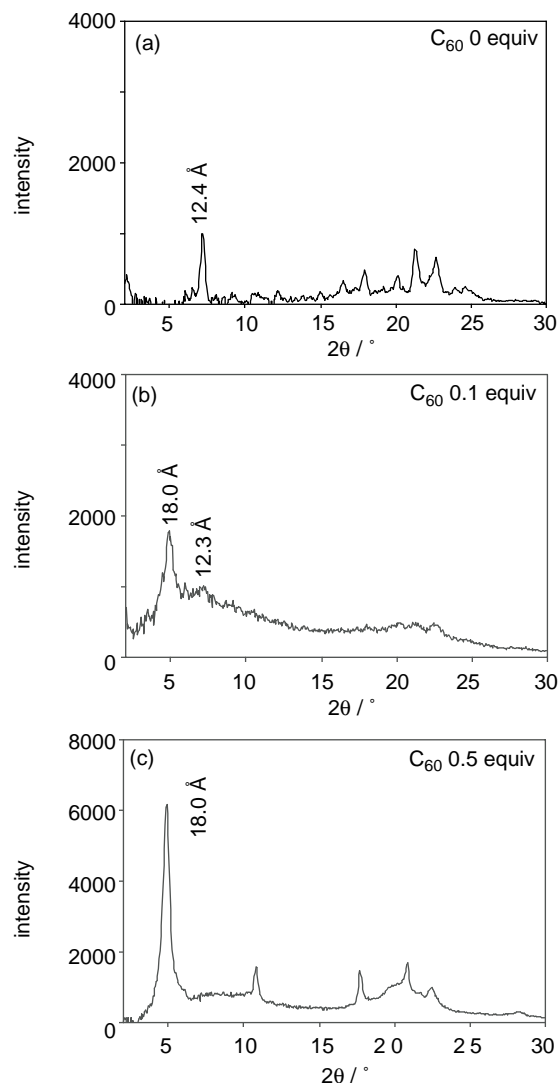


Figure 8. Powder X-ray diffraction diagrams of the xerogels prepared from (a) the **2a** + benzene gel, (b) the **2a** with 0.10 equiv C_{60} + benzene gel, and (c) the **2a** with 0.50 equiv C_{60} + benzene gel.

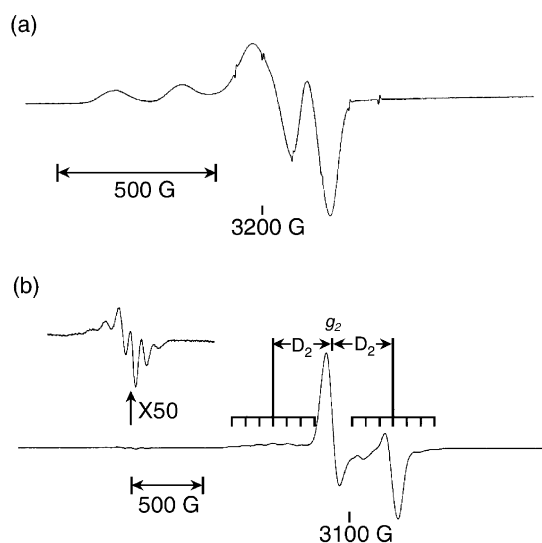


Figure 9. EPR spectra of the xerogel prepared from (a) the **2b** + benzene gel at rt and (b) the **2b** with 0.50 equiv C_{60} + benzene gel at 77 K.

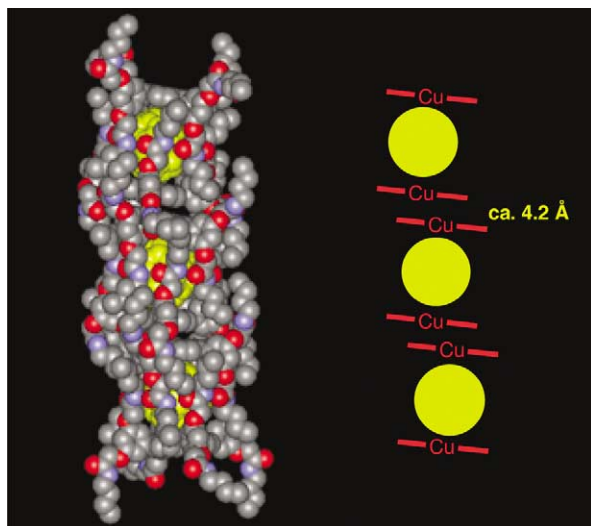


Figure 10. Energy-minimized structure of $(C_{60})_3 \cdot (2b)_6$ complex with Discover 3/Insight II 98.0; (a) side view, (b) top view.

With the above information in hand, we recalculated the molecular modeling on the capsular aggregate, assuming that 1:2 $C_{60}/2b$ (1 capsule) is a one unit and the distance between the Cu(II) porphyrins is 4.2 Å. The resultant energy-minimized structure is shown in Figure 10: C_{60} -accommodated capsules are assembled through the strong π - π stacking as well as the amide–amide hydrogen-bondings.

3. Conclusion

In summary, we have designed novel porphyrin-based organogelators having appropriately positioned hydrogen-bonding sites at the porphyrin periphery for C_{60} encapsulation. For such purposes, one of the structural prerequisites on the molecular programming is proved to be the bulkiness of the alkyl tethers in the amide substituents. When the appropriate substituents are attached to the tethers, the designed porphyrin-based organogelators such as **2a** and **2b** can transform their aggregation mode from a two-dimensional sheet structure to a one-dimensional multicapsular structure upon addition of C_{60} where two porphyrin cores sandwich one C_{60} molecule. On the other hand, if the alkyl substituents are bulky such as ethylhexyl groups in **2**, the porphyrin-based organogelator cannot accept C_{60} as a guest, leading to the formation of the two-dimensional sheet structure in the absence or even in the presence of C_{60} molecules. Our appropriate design and structural analyses on the porphyrin gelator have enabled us to create the one-dimensional fullerene deposition with strict positioning (center–center distance is ca. 1.6 nm) through gelation accompanied with molecular recognition processes. This new concept, ‘molecular recognition in gel’, is found to be effective especially for the weak host–guest interaction, which may be difficult in the dynamic solution phase. We expect that thus established concept spreads the field of molecular recognition, nanoscale assemblies, π -conjugate system, and functional polymer chemistry as well as material chemistry for the future advanced nanotechnologies.

4. Experimental

4.1. General

All starting materials and solvents were purchased from Tokyo Kasei Organic Chemicals, Wako Organic Chemicals, or Aldrich and used as received. The 1H NMR spectra were recorded on a Bruker AC 250 (250 MHz) spectrometer. Chemical shifts are reported in ppm downfield from tetramethylsilane (TMS) as the internal standard. Mass spectral data were obtained using a Perseptive Voyager RP matrix assisted laser desorption/ionization-time-of flight (MALDI-TOF) mass spectrometer and/or a JEOL JMS HX110A high-resolution magnetic sector fast atom bombardment (FAB) mass spectrometer. UV–vis spectra were recorded with a Shimadzu UV-2500 PC spectrophotometer.

4.2. Gelation tests

The gelator and the solvent were put in a septum-capped test tube and heated until the solid was dissolved. The sample vial was cooled in air to 25 °C, then left for 1 h at this temperature. The state of the materials was evaluated by the ‘stable-to-inversion of a test tube’ method.

4.3. Powder X-ray diffraction

The gel was prepared in a sample tube and frozen by liquid nitrogen. The frozen specimen was evaporated by a vacuum pump for 1 day at rt. The obtained xerogel was put into a glass capillary ($\Phi=2.0$ mm). An X-ray diffractogram was recorded on an imaging plate using Cu radiation ($\lambda=1.54178$ Å at a distance of 15 cm).

4.4. SEM observation

A piece of the gel was placed on a carbon coated copper grid and removed after 10 s, leaving some small patches of the gel on the grid. Obtained sample was shielded by Pt and examined with a Hitachi S-5500 scanning electron microscope. The accelerating voltage of SEM was 25 or 10 kV.

4.5. TEM observation

A carbon coated copper grid was immersed in the gel and dried for 12 h under reduced pressure. The grid was examined with a Hitachi H-600 transmission electron microscope.

4.6. FT-IR measurement of xerogels and solids

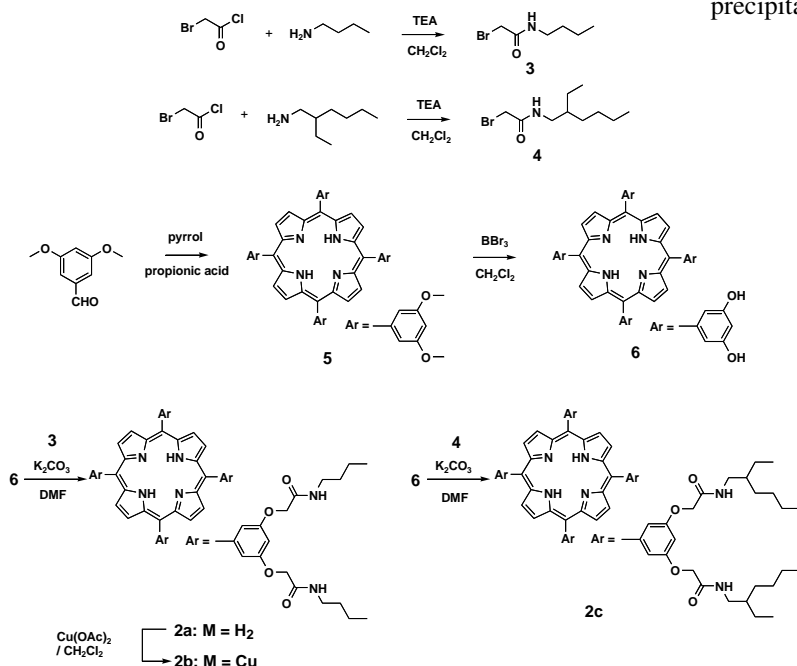
All FT-IR measurements of xerogels and solids were performed in attenuated total reflection (ATR) with a Perkin Elmer Spectrum One.

4.7. EPR measurement

ESR spectra of the xerogels were measured on a JEOL JES-FE1G X-band spectrometer equipped with an Advantest TR-5213 microwave counter and an Echo Electronics EFM-200 NMR field meter. For the low temperature measurement, the sample was cooled to 77 K in liquid nitrogen.

4.8. Materials

4.8.1. Synthetic scheme.



Each step in the synthetic scheme has been done according to the method previously reported. 5,10,15,20-Tetrakis(3',5'-dihydroxyphenyl)porphine (**6**) was obtained by demethylation reaction of 5,10,15,20-tetrakis(3',5'-dimethoxyphenyl)porphine (**5**), which was synthesized by Adler method.¹³ *N*-Butylbromoacetamide (**3**) and *N*-2-ethylhexylbromoacetamide (**4**) were prepared by Schotten–Baumann reaction¹⁴ from bromoacetylchloride with butylamine or 2-ethylhexylamine, respectively.

4.8.2. 5,10,15,20-Tetrakis[3',5'-bis(*N*-butylamidemethoxy)phenyl]porphine (2a**).** A mixture of 5,10,15,20-tetrakis(3',5'-dihydroxyphenyl)porphine (300 mg, 0.40 mmol), *N*-butylbromoacetamide (1.25 g, 6.5 mmol), and well pulverized K₂CO₃ (893 mg, 6.5 mmol) in 20 mL of dry DMF was warmed at 60 °C for 2 days. The solvent was evaporated under reduced pressure and the residue was extracted with chloroform. The organic layer was washed with 0.01 M hydrochloric acid, aqueous 5% NaHCO₃, and water and then was dried over Na₂SO₄. After the solvent was evaporated under reduced pressure, the solid residue was further purified through chromatography [silica gel, CHCl₃/MeOH = 100:1 (v/v)] to give **1** in 46% (306 mg); mp 194–195 °C; ¹H NMR (250 MHz, CDCl₃, TMS, rt) δ -2.88 (s, 2H), 0.91 (t, *J* = 7.2 Hz, 24H), 1.29 (m, 16H), 1.51 (m, 16H), 3.35 (q, *J* = 6.7 Hz, 16H), 4.67 (s, 16H), 6.76 (t, *J* = 5.8 Hz, 8H), 6.97 (s, 4H), 7.49 (s, 8H), 8.86 (s, 8H); MS (MALDI-TOF, dithranol) *m/z*: calculated: 1647.9 for M+H⁺, found: 1648.9; IR (ATR): 3318, 2930, 1663, 1588, 1172 cm⁻¹; UV–vis (CHCl₃) λ_{max}: 421, 515, 549, 591, 650 nm; Elemental analysis: calculated for C₉₂H₁₁₈N₁₂O₁₆·1.5H₂O: C, 67.05; H, 7.22; N, 10.20; found: C, 66.92; H, 7.21; N, 10.14.

4.8.3. 5,10,15,20-Tetrakis[3',5'-bis(*N*-butylamidemethoxy)phenyl]porphinatocopper (2b**).** To a solution of **1** (100 mg, 61 μmol) in chloroform (5 mL) was added

a suspension of Cu(OAc)₂ (22 mg, 0.12 mmol) in methanol (5 mL), and stirred at rt for 5 h. The reaction mixture was poured into methanol (100 mL), and filtration of the precipitate gave **2b** as a red solid (100 mg, 96%); mp

210–212 °C; IR (ATR): 3307, 2956, 2931, 2871, 1663, 1594, 1537, 1430, 1355, 1163, 772 cm⁻¹; MS (MALDI-TOF, dithranol) *m/z*: calculated: 1708.80 for [M+H⁺], found 1709.20; UV–vis (CHCl₃) λ_{max}: 416, 539, 570 (shoulder) nm; Elemental analysis: calculated for C₉₂H₁₁₆·CuN₁₂O₁₆·1.5H₂O: C, 63.63; H, 6.91; N, 9.68; found: C, 63.41; H, 6.78; N, 9.66.

4.8.4. 5,10,15,20-Tetrakis[3',5'-bis(*N*-2-ethylhexylamidemethoxy)phenyl]porphine (2c**).** Compound **2c** was obtained as purple solid in 55% yield by the method similar to the synthesis of compound **2a** from 5,10,15,20-tetrakis(3',5'-dihydroxyphenyl)porphine and *N*-ethylhexylbromoacetamide; mp 143–145 °C; ¹H NMR (250 MHz, CDCl₃, TMS, rt) δ -2.88 (s, 2H), 0.91 (t, *J* = 7.3 Hz, 24H), 0.88 (t, *J* = 7.3 Hz, 24H), 1.25–1.40 (m, 64H), 1.41–1.60 (m, 8H), 3.32 (t, *J* = 6.0 Hz, 16H), 4.70 (s, 16H), 6.64 (t, *J* = 5.9 Hz, 8H), 6.97 (t, *J* = 1.8 Hz, 4H), 7.49 (d, *J* = 1.8 Hz, 8H), 8.86 (s, 8H); MS (MALDI-TOF, dithranol) *m/z*: calculated: 2096.4 for [M+H⁺], found: 2097.6; IR (ATR): 3317, 2957, 2927, 2859, 1663, 1592, 1537, 1163 cm⁻¹; UV–vis (CHCl₃) λ_{max}: 420, 515, 548, 589, 645 nm; Elemental analysis: calculated for C₁₂₄H₁₈₂N₁₂O₁₆·1.5H₂O: C, 70.12; H, 8.78; N, 7.91; found: C, 70.02; H, 8.78; N, 7.85.

Acknowledgements

This work was partially supported by Grant-in-Aid for Young Scientists (B) (No. 16750122) and the 21st Century COE Program, 'Functional Innovation of Molecular Informatics' from the Ministry of Education, Culture, Science, Sports and Technology of Japan and JSPS fellowship (for M.S.) Authors would like to thank Ms. Okasaki of Kyushu University for FAB-MS (HR) measurements.

References and notes

1. Anderson, T.; Nilsson, K.; Sundahl, M.; Westman, G.; Wennerström, O. *J. Chem. Soc., Chem. Commun.* **1992**, 604–606.
2. Ikeda, A.; Yoshimura, M.; Udzu, H.; Fukuhara, C.; Shinkai, S. *J. Am. Chem. Soc.* **1999**, *121*, 4296–4297.
3. Haino, T.; Yanase, M.; Fukazawa, Y. *Angew. Chem., Int. Ed.* **1997**, *36*, 259–260.
4. Komatsu, K.; Fujiwara, K.; Murata, Y.; Brann, T. *J. Chem. Soc., Perkin Trans. 1* **1999**, 2963–2966.
5. Kawase, T.; Tanaka, K.; Fujiwaka, N.; Darabi, H. R.; Oda, M. *Angew. Chem., Int. Ed.* **2003**, *42*, 1624–1628.
6. (a) Sun, D.; Tham, F. S.; Reed, C. A.; Chaker, L.; Burgess, M.; Boyd, P. D. W. *J. Am. Chem. Soc.* **2000**, *122*, 10704–10705. (b) Sun, D.; Tham, F. S.; Reed, C. A.; Chaker, L.; Boyd, P. D. W. *J. Am. Chem. Soc.* **2002**, *124*, 6604–6612.
7. Zheng, J.-H.; Tashiro, K.; Hirabayashi, Y.; Kinbara, K.; Saigo, K.; Aida, T.; Sakamoto, S.; Yamaguchi, K. *Angew. Chem., Int. Ed.* **2001**, *41*, 1858–1861.
8. Kubo, Y.; Sugasaki, A.; Ikeda, M.; Sugiyasu, K.; Sonoda, K.; Ikeda, A.; Takeuchi, M.; Shinkai, S. *Org. Lett.* **2002**, *4*, 925–928.
9. Ishi-i, T.; Iguchi, R.; Snip, E.; Ikeda, M.; Shinkai, S. *Langmuir* **2001**, *17*, 5825–5833.
10. Hof, F.; Craig, S. L.; Nuckolls, C.; Rebek, J., Jr. *Angew. Chem., Int. Ed.* **2002**, *41*, 1488–1508 and references therein.
11. Shirakawa, M.; Kawano, S.-i.; Fujita, N.; Sada, K.; Shinkai, S. *J. Org. Chem.* **2003**, *68*, 5037–5044.
12. (a) Belford, R. L.; Chasteen, N. D.; So, H.; Tapscott, R. E. *J. Am. Chem. Soc.* **1969**, *91*, 4675–4680. (b) Chikira, M.; Kon, H.; Hawley, R. A.; Smith, K. M. *J. Chem. Soc., Dalton Trans.* **1979**, 245–249. (c) Eaton, S. S.; Eaton, G. R.; Chang, C. K. *J. Am. Chem. Soc.* **1985**, *107*, 3177–3184.
13. Adlar, A. D. *J. Org. Chem.* **1967**, *32*, 476.
14. (a) Schotten, C. *Ber.* **1884**, *17*, 2554. (b) Baumann, E. *Ber.* **1886**, *19*, 3218.
15. Preliminary communication: Shirakawa, M.; Fujita, N.; Shinkai, S. *J. Am. Chem. Soc.* **2003**, *125*, 9902–9903.

Fullerene encapsulation with calix[5]arenes

Takeharu Haino,* Manabu Yanase, Chigusa Fukunaga and Yoshimasa Fukazawa*

Department of Chemistry, Graduate School of Science, Hiroshima University, 1-3-1 Kagamiyama, Higashi-Hiroshima 7398526, Japan

Received 22 April 2005; revised 6 September 2005; accepted 11 September 2005

Available online 11 November 2005

Abstract—This paper presents the synthesis of the fullerene hosts based on the calix[5]arenes and their binding properties. Calix[5]arenes **1a**, **2**, **3a** bind C₆₀ or C₇₀ in organic solvents. The solvent effect of the fullerene complexation was clearly observed; the association constant decreases in a solvent with high solubility for C₆₀. Covalently linked double-calix[5]arenes **4–6** were also investigated on their binding properties for fullerenes in organic solvents. Their binding abilities for both C₆₀ and C₇₀ are extremely high in toluene solution. Higher binding selectivity toward C₇₀ is observed by all the double-calix[5]arenes. The selectivity of **5a** toward C₇₀/C₆₀ is highest in toluene with a value of 10. The structures of the supramolecular complexes of the calix[5]arene hosts and C₆₀ or C₇₀ were investigated by using ¹H and ¹³C NMR studies. The molecular mechanics calculation and X-ray structure reveal that the interior of the calix[5]arene is complementary to the exterior of C₆₀ molecule. In contrast, the host–guest complexes of C₇₀ with the simple calix[5]arenes take many conformational options due to its less symmetric shape. The molecular mechanics calculation and our chemical shift simulation nicely worked to estimate the reliable structures; the calix[5]arene cavity takes up C₇₀ molecule, and the C₇₀ molecule tilts significantly from the C5 axis of the calix[5]arene. In the case of the host–guest complex of C₇₀ with the double-calix[5]arene, the molecular dynamics simulation of the host–guest complex represented the realistic movement of the bound C₇₀ inside the cavity. The combination of the molecular dynamics simulation and the chemical shift simulation of the host–guest complex suggested that the C₇₀ molecule rapidly moves inside the cavity.

© 2005 Elsevier Ltd. All rights reserved.

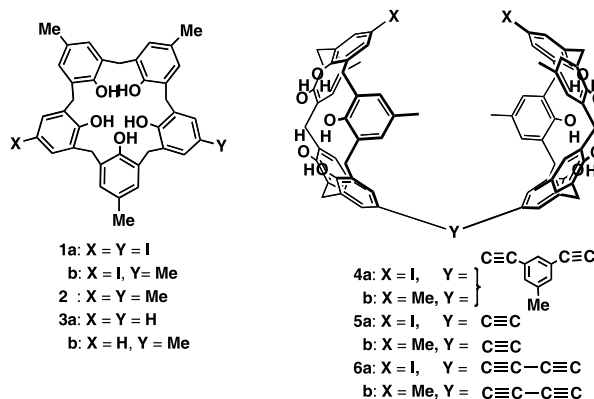
1. Introduction

C₆₀ and its family represent an intriguing class of molecules due to their unique physical and chemical properties. Their applications have been directed to many research areas such as chemistry, material science, biology, etc.¹ Developing specific containers for fullerenes is of great interest in constructing fullerene-based functional materials. Pioneering works focused on its hydrophobic nature and spheroidal shape, and resulted in the inclusion of C₆₀ within water-soluble cyclodextrins² and calixarenes,³ having the concave cavities complementary to the exterior of C₆₀.

Since the epochal finding of the selective precipitation of C₆₀/calix[8]arene complex from a mixture of fullerenes in carbon soot in toluene,⁴ recent focuses for fullerene encapsulation have shifted in organic solvents. The development of host molecules capable of encapsulating C₆₀ in organic solvent is one of the challenging tasks. The design of host molecules is mainly based on complementary concept. The effective contact between the convex surface of C₆₀ and the interior of concave hosts can be achieved with van der Waals, π–π stacking, and charge transfer interactions. Calix[6]arene,⁵ homoaxacalix[3]arene,⁶

cyclotrimeratrylene,⁷ macrocyclic paraphnylenes,⁸ and aza-calixarene⁹ are the class of host molecules, and showed the effective complexation with C₆₀ and/or C₇₀. Recently, planar π surfaces of porphyrins and metalloporphyrins have been found to interact with the convex π surface of fullerenes.¹⁰ Porphyrin or metalloporphyrin clefts are the other type of fullerene hosts, showing high binding abilities in organic solvents.¹¹

For the past decade, we have been interested in developing fullerene hosts,¹² and have found that calix[5]arenes and covalently linked double-calix[5]arenes are excellent hosts for C₆₀ and C₇₀.¹³ In this paper, we report a full account of the fullerene encapsulation of calix[5]arenes **1–3** and covalently linked double-calix[5]arenes **4–6**.



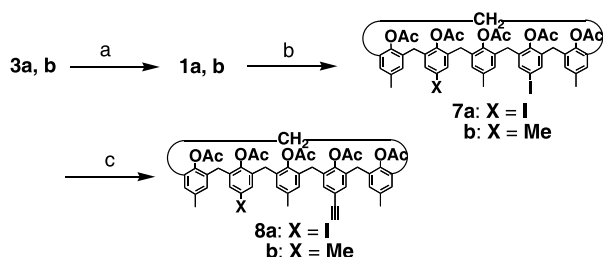
Keywords: Encapsulation; Host–guest complex; Complexation induced shift; Fullerene; Calix[5]arene.

* Corresponding authors. Tel.: +81 82 424 7403; fax: +81 82 424 0724; e-mail addresses: haino@sci.hiroshima-u.ac.jp; fukazawa@sci.hiroshima-u.ac.jp

2. Results and discussion

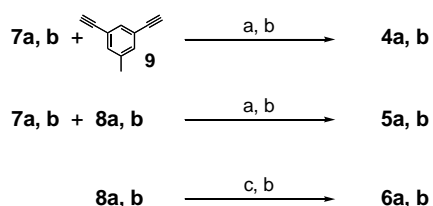
2.1. Synthesis of calix[5]arene hosts

The syntheses of the calix[5]arene hosts were started from known calix[5]arenes **3**.¹⁴ Iodination at the unsubstituted para positions by benzyltrimethylammonium dichloroiodide in methanol and methylene chloride in the presence of calcium carbonate afforded calix[5]arenes **1** in good yield. The five phenolic hydroxyl groups of **1** were acetylated with acetic anhydride to provide **7**. Trimethylsilylethynyl group was introduced onto calix[5]arenes **7** via Sonogashira coupling of **7** and trimethylsilylacetylene, followed by removal of the trimethylsilyl group to give **8** (scheme 1).



Scheme 1. Reagents and conditions: (a) BTMAICl₂, CaCO₃, CH₂Cl₂–MeOH; (b) Ac₂O, pyridine; (c) TMSCCl, CuI, Pd(PPh₃)₄, *n*-BuNH₂, THF; (d) KF, MeOH.

Covalently linked double-calix[5]arenes **4**–**6** were synthesized according to Scheme 2. Sonogashira coupling reaction of **7** with 0.5 equiv of diethynyltoluene **9**, followed by deprotection of the acetyl groups smoothly proceeded to give desired double calix[5]arenes **4**. Coupling of **7** and **8** via palladium (0) catalysis, followed by deprotection of the acetyl groups afforded ethynyl-linked double-calix[5]arenes **5**. Oxidative coupling of **8** with copper (II) acetate, followed by deprotection furnished **6**.



Scheme 2. Reagents and conditions: (a) CuI, Pd(PPh₃)₄, *n*-BuNH₂, THF; (b) K₂O₃, MeOH; (c) Cu(OAc)₂, Pyridine.

2.2. Complexation studies for calix[5]arenes 1–3

A toluene solution of C₆₀ shows beautiful magenta color. The host–guest interaction of calix[5]arene hosts **1a**, **2**, **3a** and C₆₀ can be visually monitored by a color change of the solution to pale yellow upon the addition of the hosts. The binding study of the host and fullerene was carried out by absorption spectra in a variety of organic solvents. Figure 1 shows the spectral change of C₆₀ during the addition of **1a** in carbon disulfide solution.

The intensity of the absorption spectra of C₆₀ in the 400–470 nm region increased, whereas that of the longer wavelength region decreased as the concentration of **1a** was

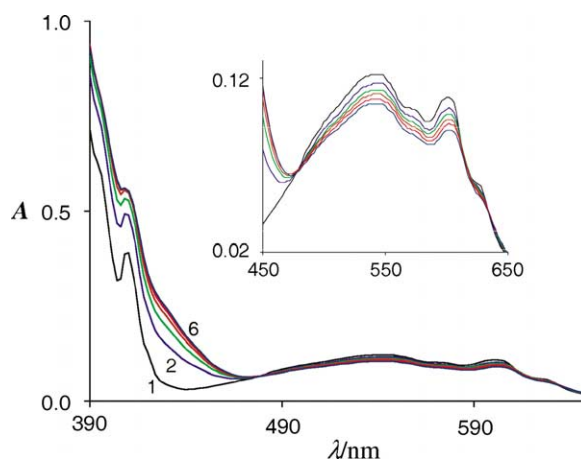


Figure 1. Absorption spectra of C₆₀ (1.07×10^{-4} mol/L) in the presence of **1a** in CS₂. The concentrations of **1a** are from the bottom (curves (1)–(6)), 0.0, 1.12, 2.23, 3.35, 4.46, 5.58, ($\times 10^{-3}$ mol/L). The inset is the expanded spectra in the region from 450 to 650 nm.

increased. These characteristic spectral changes as well as the isosbestic point at 478 nm support the formation of the host–guest complex between a C₆₀ molecule and **1a** in a ratio of 1:1. These findings were commonly observed when each of the host was added to a C₆₀ solution.

The binding behavior of a host for C₇₀ was also investigated. A color change of the C₇₀ toluene solution was not detected upon the addition of the host, but a slight change of the absorption spectra of C₇₀ was observed upon the addition of **1a** in CS₂ (Fig. 2). The intensity of the band in 460 nm region decreased upon the addition of **1a**. The isosbestic point was found at 426 nm, indicating the 1:1 host–guest stoichiometry of **1a** and C₇₀.

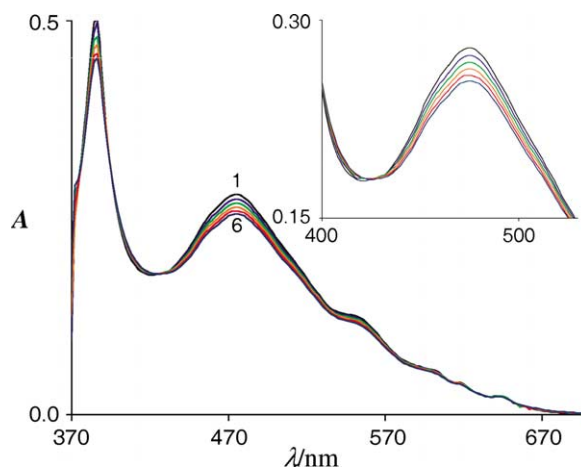


Figure 2. Absorption spectra of C₇₀ (1.33×10^{-5} mol/L) in the presence of **1a** in CS₂, the concentration of **1a** from the top (curves (1)–(6)), 0.0, 1.85, 3.70, 5.55, 7.41, 9.26 ($\times 10^{-3}$ mol/L). The inset is the expanded spectra in the region from 400 to 530 nm.

The association constants of the host–guest complexes for C₆₀ and C₇₀ were determined by Benesi–Hildebrand method¹⁵ in a variety of organic solvents (Tables 1 and 2). The calix[5]arenes show effective binding both for C₆₀ and C₇₀ molecules in the organic solvents. One of the interesting findings is that the calix[5]arenes bind C₆₀ more preferentially than C₇₀ in every solvents. The results suggest that the

Table 1. Association constants K_a (M^{-1}) of hosts **1a**, **2**, and **3a** with C_{60} at 298 K

	Toluene	Carbon disulfide	Tetralin	ODCB
1a	2100 ± 100	660 ± 30	750 ± 90	310 ± 40
2	1670 ± 70	600 ± 3	570 ± 80	280 ± 10
3a	590 ± 70	280 ± 70	270 ± 90	210 ± 10

Table 2. Association constants K_a (M^{-1}) of hosts **1a**, **2**, and **3a** with C_{70} at 298 K

	Toluene	Carbon disulfide	Tetralin	ODCB
1a	520 ± 60	260 ± 60	210 ± 20	240 ± 40
2	380 ± 30	280 ± 30	90 ± 10	230 ± 20
3a	310 ± 30	160 ± 10	80 ± 20	190 ± 20

calix[5]arene cavity is more complementary to the exterior of C_{60} than C_{70} .

Substitution of some of the methyl groups of upper rim of the calix[5]arene by an atom with high polarizability enhances the association of fullerenes: the host carrying two iodine groups on its upper rim provide the largest binding constant, suggesting that dispersion force play an important role in the complex formation between the host and the guest. Some earlier works suggested that charge transfer interaction results in the large stabilization of C_{60} and hosts since C_{60} is a good electron acceptor.^{2,5} C_{70} is better electron acceptor than C_{60} since C_{70} has lower LUMO level.¹⁶ The calix[5]arene hosts show high binding affinities for C_{60} over C_{70} , indicating the charge transfer does not mainly operate in the host–guest associations. In our cases, van der Waals interaction given by the effective contact between the host cavity and the exterior of C_{60} or C_{70} most probably presents the large stabilization of the host–guest complexes.

2.3. Solvent effect

Obviously the association constant is solvent dependent. The association constants decrease in the order of toluene, carbon disulfide, tetralin, and *o*-dichlorobenzene (ODCB). The solubility of C_{60} increases in this order. Apparently, solubility of C_{60} in these solvents plays an important role in the binding process. Plot of the free energies of the C_{60} complexation versus solubilities of C_{60} in the aromatic solvents gives a good linear relationship (correlation coefficient r^2 : 0.99 for **1a**, 0.99 for **2**, 0.95 for **3a**) (Fig. 3).

The aromatic solvent molecules, such as toluene, tetralin, and ODCB, can contact onto the molecular surface of a C_{60} molecule in a face-to-face fashion, surrounding around the dissolved C_{60} molecule. This type of solvation should be mainly caused via van der Waals interactions between the solvents and the C_{60} molecule. ODCB has two highly polarizable chlorine atoms, which create large van der Waals interaction to the C_{60} molecule. The largest solubility of C_{60} in ODCB most probably reflects the largest solvent–guest van der Waals interaction. The regression analysis clearly indicates that the complexation competes against the solvation of C_{60} in the aromatic solvents.¹⁷

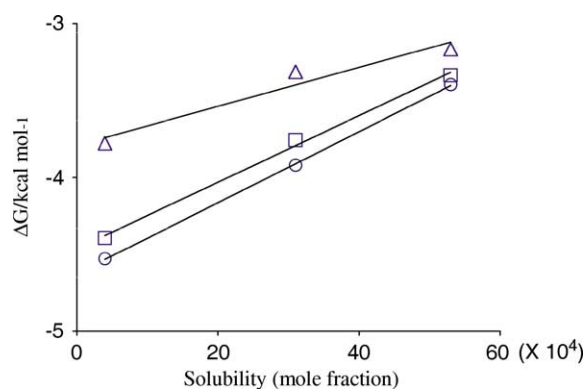


Figure 3. Regression analysis of the free energies of the complexation versus solubilities of C_{60} : 4.0×10^4 in toluene, 31×10^4 in tetralin, 53×10^4 in ODCB (Ruoff, R. S.; Tse, D. S.; Malhotra, R.; Lorents, D. C. *J. Phys. Chem.* 1993, 93, 3379–3383). Characters, \circ , \square , and \triangle indicate **1a**, **2**, and **3a**.

2.4. Complexation studies for double-calix[5]arenes

Covalently linked double-calix[5]arenes **4–6** are also good hosts for C_{60} and C_{70} . The spectral changes of C_{60} upon the addition of **4a** in carbon disulfide are similar to those when **1a** was added (Fig. 4). The presence of the isosbestic points and Job's plot supports the 1:1 host–guest complex formation. The C_{70} complexation to **4a** gave more prominent changes than to **1a**: the shoulder intensity of the absorption band in 400–440 nm region increased while that of the broad absorption band in the 450–560 nm region decrease. The isosbestic points are observed, and Job's plot confirmed the 1:1 complex formation with C_{70} . The association constants for both C_{60} and C_{70} with each host molecule were obtained by a non-linear curve fitting analysis of the titration curves (Fig. 5).

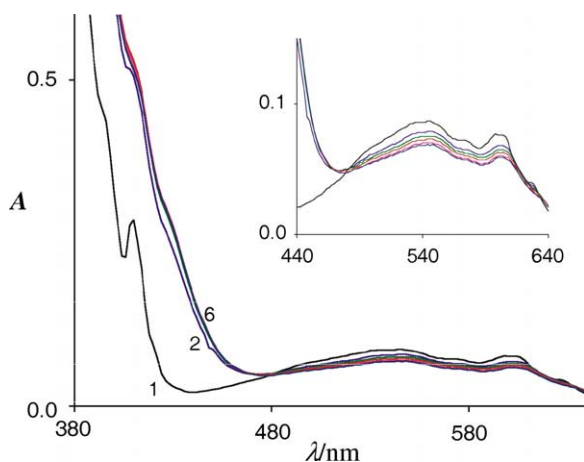


Figure 4. Absorption spectra of C_{60} (0.90×10^{-4} mol/L) in the presence of **4a** in CS_2 . The concentrations of **4a** are from the bottom (curves (1)–(6)), 0.0, 0.84, 1.68, 2.52, 3.36, 4.20 ($\times 10^{-3}$ mol/L). The inset is the expanded spectra in the region from 440 to 640 nm.

The binding constant of **4a** for C_{60} is $76,000 M^{-1}$ in toluene, more than 36 times higher than the corresponding value of C_{60} and **1a**. This dramatic increase of the binding ability of **4a** to C_{60} clearly indicates an effective cooperation of the two calix[5]arene cavities for the C_{60} encapsulation. The bridging units between the two calix[5]arene core are

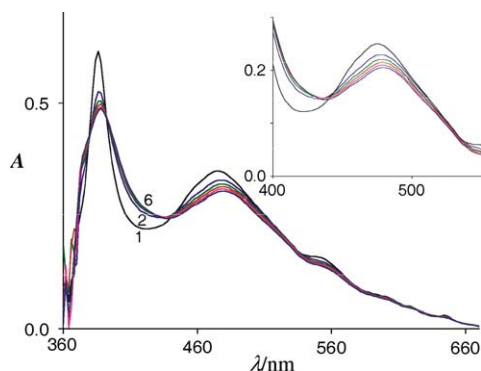


Figure 5. Absorption spectra of C_{70} (1.57×10^{-5} mol/L) in the presence of **4a** in CS_2 . The concentration of **4a** from the top (curves (1)–(6)), 0.0, 2.10, 4.20, 6.30, 8.40, $10.5 (\times 10^{-3})$ mol/L. The inset is the expanded spectra in the region from 400 to 550 nm.

obviously play an important role in the binding abilities for C_{60} . The association constants for the binding of C_{60} and the double calix[5]arenes decrease in the order of **4** > **5** > **6**. This trend is valid in all the solvents. Apparently, the binding ability of the host is dependent on the shape complementarity of its cavity interior. The binding ability of the double calix[5]arene host toward C_{60} is again solvent dependent. The same trend as was found in the simple calix[5]arene hosts (**1**–**3**) was also seen in these bridged hosts.

Most calixarene-based simple fullerene hosts have stronger binding ability to C_{60} than to C_{70} .^{5–8} Surprisingly, the binding preference of double-calix[5]arenes **4**–**6** is completely opposite to that of the simple calix[5]arenes. Compound **4a** showed highest association constant ($163,000 \pm 16,000 M^{-1}$) for C_{70} in toluene, two times as high as that for C_{60} in the same solvent. The highest selectivity for C_{70} over C_{60} was achieved by **5a** in toluene: the association constant for C_{70} is 10 times as high as that for C_{60} . The selectivities and binding abilities are again solvent dependent. The selectivity of C_{70}/C_{60} for **5a** is highest in toluene, but decreased in carbon disulfide and ODCB. The same trend was observed in other double-calix[5]arenes (Table 3).

In the simple calix[5]arene hosts **1**–**3**, enhancement of the guest binding was observed when some of the upper rim methyl groups were replaced by iodine atoms. However, the enhancement of the guest binding was not observed by such replacement in the double calix[5]arenes.

2.5. Structures of host–guest complexes of simple calix[5]arenes in solution

The investigation of the solution structure of the host–guest complex is informative for understanding the details of the fullerene-calix[5]arene interactions. Since the five phenols of a calix[5]arene creates the cyclic hydrogen bonds, the calix[5]arene has large aromatic cavity, which provides the magnetically shielded environment due to the five aromatic rings. Thus, the complexation induced shift (CIS) of the ^{13}C resonance of C_{60} gives an insight into the solution structure of the host–guest complex. The ^{13}C NMR resonance of C_{60} in 20% CD_2Cl_2 – CS_2 appeared at 143.55 ppm (Fig. 6a). Upon the addition of the equimolar amount of **1a**, the resonance shifted to 143.20 ppm (Fig. 6b). Judging from the association constant, 48% of the guest is bound by the host; thus, the CIS value of the host–guest complex is estimated to be -0.73 ppm. Accordingly, the high field shift of the ^{13}C resonance of C_{60} clearly indicates that the C_{60} molecule is taken up inside the cavity of calix[5]arene **1a**.

The structure of the complex of calix[5]arene and C_{60} is given by X-ray crystallographic analysis.¹⁸ The structure of C_{60} and **2** in the crystalline state is shown in Figure 7. The host–guest complex of **2** and the C_{60} has C_{5v} symmetry; thus, the five-fold rotation axes of the host coincides with one of the five-fold rotation axis of the guest, and a five-membered ring of the guest adopts parallel arrangement to the mean plane composed of the five phenolic oxygens of the host. As seen in the crystal structure, a half of the C_{60} carbons stay inside the cavity, and is shielded by the five aromatic rings. In this structure, all the C_{60} carbons experienced the considerable magnetic shielding, so that the structure nicely explains the large CIS value of the complexed C_{60} , and suggested that the structure in solution is similar to the structure in the crystalline state.

The ^{13}C NMR spectra of C_{70} were also measured in the presence and the absence of host **2** in 20% CD_2Cl_2 – CS_2 solution. A C_{70} has the five sets of nonequivalent carbons, due to its D_{5h} symmetry: each set of the carbons is assigned to a, b, c, d, and e from the polar end to the equatorial plane. All the carbons shifted upfield (a: -0.886 , b: -0.886 , c: -0.770 , d: -0.712 , e: -0.705 ppm) when host **2** was added (Fig. 8).

At the condition, a ratio of the bound C_{70} molecule is 73% based on the association constant ($K_a = 385 \pm 27 M^{-1}$) of **2** in 20% CD_2Cl_2 – CS_2 . The CIS values of the carbons for the host–guest complex **2**/ C_{70} were estimated, and listed in Table 4. The upfield shifts of the C_{70} clearly indicate that

Table 3. Association constants K_a (M^{-1}) of hosts **4**–**6** with C_{60} or C_{70} at 298 K

	C_{60}			C_{70}		
	Toluene	Carbon disulfide	ODCB	Toluene	Carbon disulfide	ODCB
4a	$76,000 \pm 5000$	5400 ± 800	3000 ± 200	$163,000 \pm 16,000$	9600 ± 300	4100 ± 100
4b	$68,000 \pm 5000$	2530 ± 60		$118,000 \pm 12,000$	4600 ± 100	
5a	8300 ± 200	1500 ± 100	1200 ± 100	$85,000 \pm 13,000$	6600 ± 200	1900 ± 20
5b	9000 ± 200	1380 ± 60		$91,000 \pm 9000$	3500 ± 300	
6a	2700 ± 100	370 ± 10	440 ± 50	5500 ± 200	1000 ± 100	490 ± 20
6b	4100 ± 100	720 ± 80		7300 ± 800	1100 ± 100	

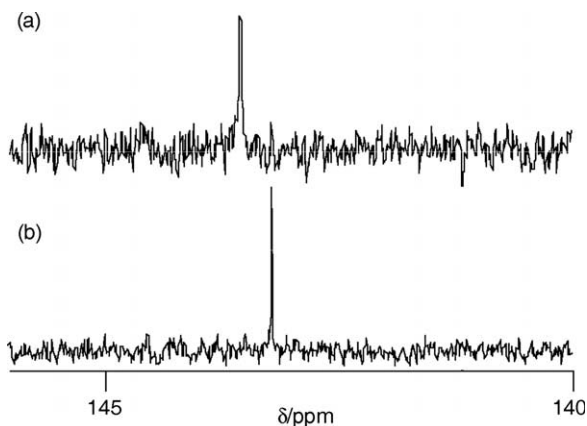


Figure 6. ¹³C NMR spectra of (a) C₆₀ (1.75 × 10⁻³ mol/L) and (b) in the presence of the equimolar amount of host **1a** in 20% CD₂Cl₂-CS₂.

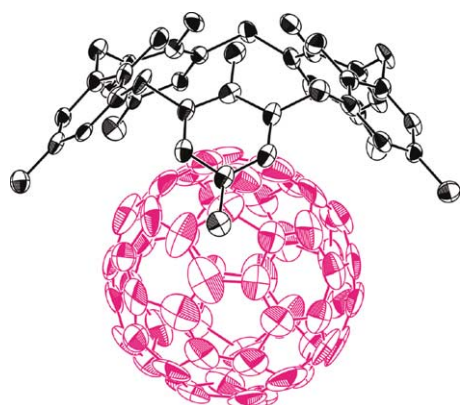


Figure 7. Crystal structure of C₆₀ and **2**.

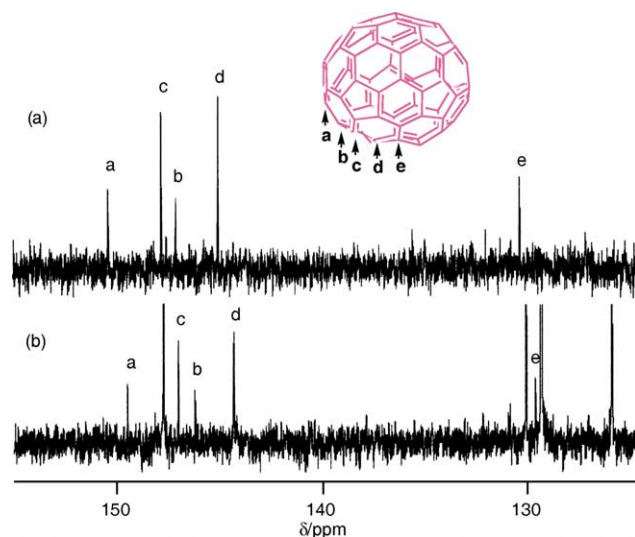


Figure 8. ¹³C NMR spectra of (a) C₇₀ (7.9 × 10⁻⁴ mol/L), and (b) in the presence of **2** (7.8 × 10⁻³ mol/L) in 20% CD₂Cl₂-CS₂.

C₇₀ is encapsulated within the host cavity. C₇₀ is less symmetric than C₆₀, giving rise to many plausible structures for the host–guest complex. The induced shifts decreased from the polar end (a) to the equatorial carbon (e), suggesting that the polar end seems to stay deeply inside the cavity.

Table 4. The complexation induced shifts Δδ (CIS) of the average five carbons for the calculated structure of the complex **2**/C₇₀

No.	a	b	c	d	e
1	-1.168	-1.087	-0.998	-1.129	-1.166
17	-1.490	-1.167	-1.086	-0.978	-0.900
78	-1.609	-1.360	-1.139	-0.832	-0.729
Averaged ^a	-1.337	-1.151	-1.040	-1.014	-0.997
Observed ^b	-0.886	-0.886	-0.770	-0.712	-0.705
Estimated ^c	-1.214	-1.214	-1.055	-0.975	-0.966

^a The values were obtained by the simple average of the CIS values of each carbon atoms for the 160 structures.

^b Observed CIS values when 73% of C₇₀ bound to **2**.

^c The CIS values of 1:1 complex estimated from the observed values.

To gain the precise structural information of the host–guest complexes, the structure of the complex of **2**/C₇₀ was calculated by the molecular modeling study with the aid of MacroModel V.6.5.¹⁹ The low mode search algorithm was applied for the conformational search of the host–guest complex with amber* force field. Total 160 unique structures were obtained in the energy window of 5.0 kJ/mol from the most stable one. The most stable structure of the host–guest complex has oblique arrangement of the principal axis of the guest with respect to that of the host (cant angle θ: 56°) (Fig. 9a).

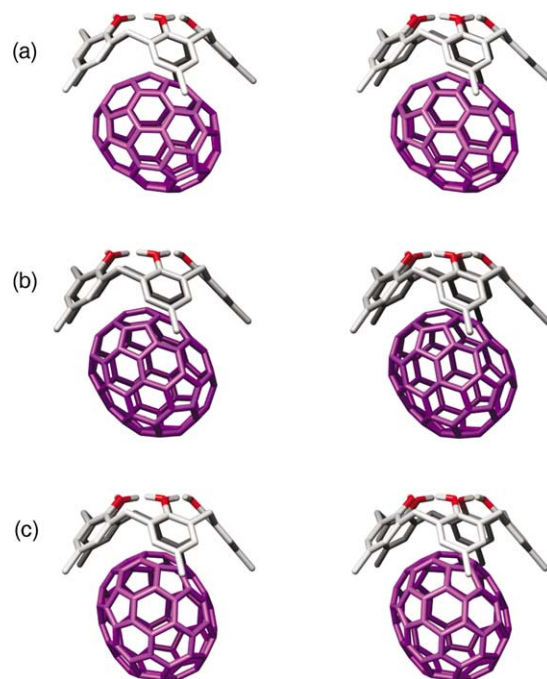


Figure 9. Stereo drawings of the three typical calculated structures of the complex C₇₀ and **2**: (a) the most stable, (b) 17th, and 78th structures.

Raston and Atwood have recently reported that a similar tilt of the C₇₀ molecule occurs when complexed by the calix[5]arene in the solid state.²⁰ The cant angle decreases with the increase of the steric energy, and the 139th structure has the angle of less than 20 degree (Fig. 10). The local anisotropic effect of the five benzene rings of the calix[5]arene upon the C₇₀ carbons can be estimated by our chemical shift simulation method.²¹ The magnetic

environment of the bound C_{70} has nine nonequivalent carbons if the C_5 fold symmetry is taken into account even in the host cavity. The complexation induced shifts of the nine carbons for the most stable structure were estimated to be a: -2.025 , b: -1.803 , c: -1.514 , d: -1.495 , e: -1.166 , d': -0.763 , c': -0.482 , b': -0.370 , and a': -0.310 ppm.

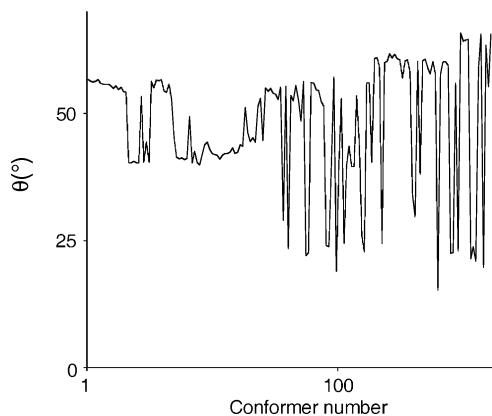


Figure 10. Plot of cant angle θ versus conformer number.

Carbon a is the polar end of them, facing the cavity wall. The values decrease from a to the other polar end of the carbon a', pointing outside of the cavity. Since the rapid association–dissociation equilibrium of the C_{70} molecule bring about the magnetic environment of the C_{70} molecule to be D_{5h} symmetry. Thus, the calculated complexation induced values were averaged to give rise to the five induced shifts (Table 4). The CIS values are sensitive to the cant angle of the C_{70} molecule: the values of carbon a increase, whereas those of carbon e decrease with the decrease of the guest cant angle.

The calculated CIS values obtained by the simple average of the 160 structures, nicely reproduce the observed values, suggesting that the C_{70} molecule mainly adopts the tilted arrangement to the calix[5]arene C_5 axis (average cant angle of 160 structures, 47.9°) although there are many conformational options in the host–guest complex.

2.6. Structures of host–guest complexes of double-calix[5]arenes in solution

The double calix[5]arenes showed extremely high binding abilities for both C_{60} and C_{70} , and bind more preferentially to C_{70} than to C_{60} . The 1H and ^{13}C NMR spectroscopies gave structural insights of the host–guest complexes. In free host **4b**, a ring flipping process of the calix[5]arene core occurs rapidly at room temperature to give a broad singlet of the bridge methylene resonance.

An AB-quartet like resonance of the bridge methylene appeared upon the addition of C_{60} , indicating that the energetic barrier to the ring flipping is increased by the complexation with the C_{60} guest (Fig. 11). In other word, the attractive van der Waals interactions are produced by the effective face-to-face contacts of the calix[5]arene aromatic rings to a molecular surface of C_{60} .

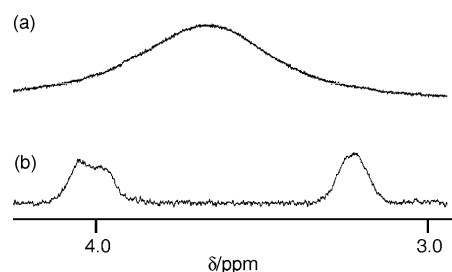


Figure 11. 1H NMR spectra of (a) **4b** (6.0×10^{-4} mol/L) and (b) in the presence of C_{60} (1.0×10^{-3} mol/L) in toluene- d_8 at 298 K.

The ^{13}C NMR spectra of C_{60} were measured in the presence and absence of host **4a** in 20% CD_2Cl_2 – CS_2 and toluene- d_8 (Fig. 12). The ^{13}C resonance of C_{60} moved upfield with a CIS value of -0.743 ppm upon the addition of the equimolar amount of **4a**. The similar upfield shifts of ^{13}C resonance of C_{60} were observed in the case of **5a** and **6a** (Table 5). Based on the binding ratio of C_{60} , the theoretical complexation induced shifts of the fully entrapped guest are calculated (Table 5). These values are 1.6–2.1 times as large as that of the complex **1a**/ C_{60} , indicating that the two calix[5]arene units of the hosts work together to cover up a C_{60} molecule. The similarity of these values suggests that the structure of supramolecular complex is not dependent on the solvent.

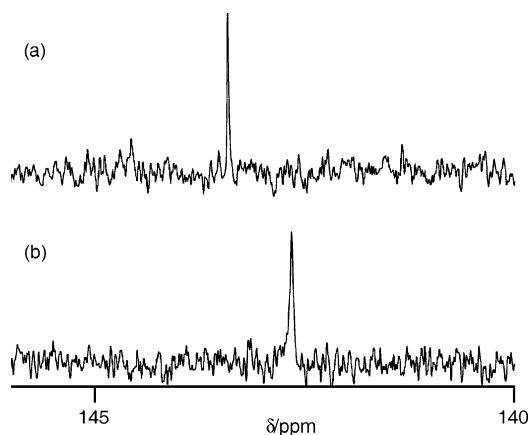


Figure 12. ^{13}C NMR spectra of (a) C_{60} (1.25×10^{-3} mol/L) and (b) in the presence of the equimolar amount of host **4a** in 20% CD_2Cl_2 – CS_2 .

Table 5. The observed complexation induced shifts $\Delta\delta$ (CIS) of C_{60} with the double-calix[5]arene hosts

Solvent	4a	5a	6a
20% CD_2Cl_2 – CS_2	-0.743 (62%) ^a	-0.643 (42%) ^a	-0.318 (28%) ^a
Estimated ^b	-1.198	-1.531	-1.136
Toluene- d_8	-1.304 (98%) ^a	-1.152 (91%) ^a	-1.055 (82%) ^a
Estimated ^b	-1.331	-1.152	-1.286

^a Ratio of C_{60} bound with the host molecule was estimated by the association constant.

^b The CIS values of the host–guest complexes were estimated by the ratio of the bound C_{60} .

The molecular mechanics calculations were carried out to gain an insight into the structure of the host–guest complex of C_{60} with the double calix[5]arenes. Figure 13 shows the

most stable structures of the complexes for **4b–6b**. The two calix[5]arene units cover up a C_{60} molecule in every complex. C_{60} is placed in the highly shielded environment by the 10 phenolic rings. These calculated structures rationalize the large complexation induced shifts.

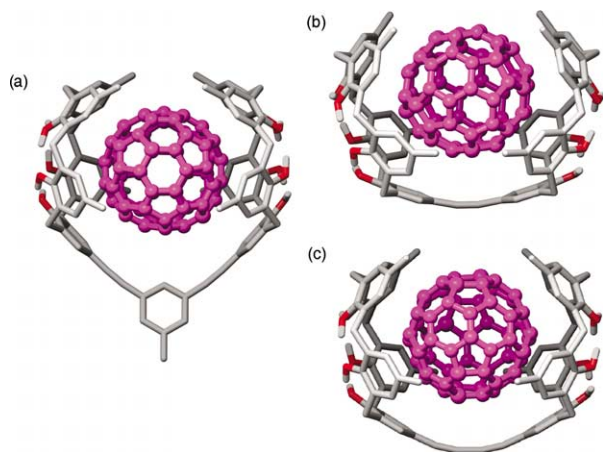


Figure 13. The calculated structures of the host–guest complex of C_{60} with (a) **4b**, (b) **5b**, and (c) **6b**.

The ^{13}C NMR spectra of C_{70} were also measured in the presence and absence of the double calix[5]arene host (Fig. 14). Every carbon resonance was shifted upfield, indicating that the C_{70} molecule situates in the shielding environment of the two calix[5]arene units. The complexation induced shifts of the five sets of the C_{70} carbons were 1.77, 1.55, 1.16, 0.81, and 0.69 ppm for a, b, c, d, and e carbons. Since the association constant of the complex formation in benzene is quite large, almost all the C_{70} molecules in solution were entrapped in the host cavity in the NMR measurement condition. The carbon a gives the large upfield shift, and the values decrease gradually to carbon e. This means that the polar ends of the C_{70} molecule stay deeply inside the calix[5]arene cavities.

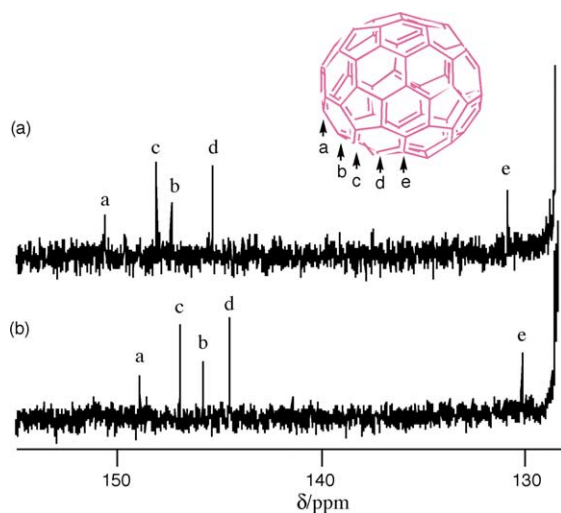


Figure 14. ^{13}C NMR spectra of (a) C_{70} (7.70×10^{-4} mol/L), and (b) in the presence of **4a** (1.52×10^{-3} mol/L) in benzene- d_6 .

The structure of the complex of **4a**/ C_{70} were calculated by the molecular modeling study with the aid of MacroModel V.6.5.¹⁹ During the conformational search, many conformational options exist in the complex. These should dynamically equilibrate to each other. In order to take into account of the dynamic movement of the host and the bound guest, a molecular dynamics simulation was carried out with a stochastic dynamic treatment at 300 K with amber* force field.²² Although we cannot include explicit solvent molecules, the stochastic dynamic treatment sometimes gives random forces, which correspond the solvent collisions. The molecular dynamics simulation of the host–guest complex **4a**/ C_{70} was started from the global minimum structure (Fig. 15), performed for 2000 ps.

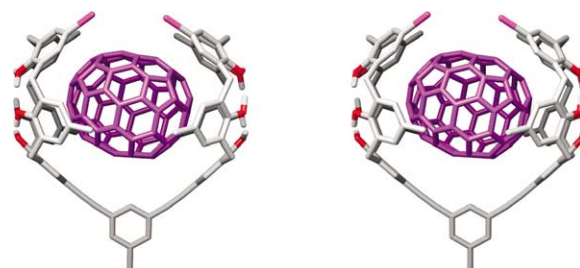


Figure 15. Stereo drawing of the most stable complex structure of **4a**/ C_{70} .

During the simulation, the 2000 structures were sampled at every 1 ps. The movements of the C_{70} molecule in the host cavity was monitored by the time dependent torsion angle ϕ , which is defined as connecting the centroid of the five phenol oxygens of the one calix[5]arene unit of the host, to the two terminals of the principal axis of the C_{70} molecule and to the other centroid of the five phenol oxygens. The molecular dynamic calculation of the complex simulates dynamic motions of the C_{70} molecule inside the host cavity (Fig. 16).

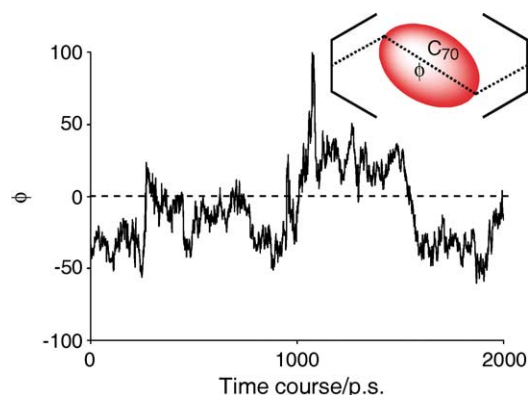


Figure 16. Trajectory of the torsion angle ϕ between the principal axis of C_{70} and the line connecting the each center of the five phenol oxygens in the calix[5]arene moiety of **4a**.

During the simulation, the C_{70} molecule moves rapidly inside the cavity, including partial rotation of the C_{70} in the host cavity. The time averaged value of the dihedral angle is -7.3° , indicating that the average structure of the complex

4a/C₇₀ has parallel arrangement of the C₇₀ principal axis to the line connecting two terminal centroids of the host. The time averaged complexation induced shifts of the C₇₀ carbons were estimated using 500 structures extracted at every 4 ps interval during the simulation. The calculated induced shifts have high correlation coefficient ($r^2=0.984$) to the observed (Fig. 17). Accordingly, the molecular dynamics simulation represents the reliable motion of the bound C₇₀ molecule within the host cavity.

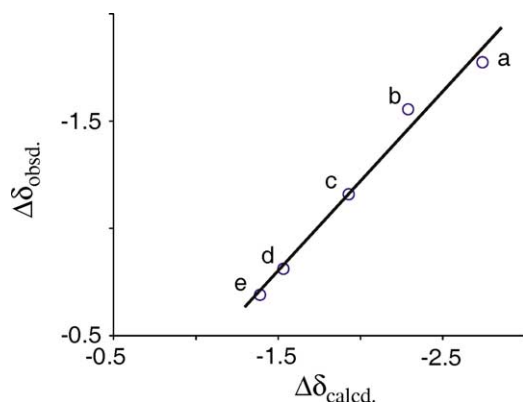


Figure 17. Correlation plot of the calculated versus observed CIS values of the C₇₀ carbons (a–e).

3. Conclusions

In this paper, we demonstrated that the calix[5]arenes and the covalently linked double-calix[5]arenes are good hosts for both C₆₀ and C₇₀ with extremely high binding constants in organic solvents. These high binding abilities of the calix[5]arenes are mainly derived from the strong van der Waals interactions, coming from the shape complementarity of the host cavities to the exterior of the fullerenes. The solvent effect for the fullerene complexations was clearly observed: the fullerene complexation competes against the solvation of fullerene in aromatic solvents. The aromatic solvents can have the face-to-face type interaction on the large surface of the fullerenes, reducing the fullerene–host interactions due to the contribution of the desolvation. The solution structures of the host–guest complexes were discussed. The exterior of a C₆₀ molecule just fits to the calix[5]arene cavity. In solid and in solution, C₆₀ was nicely taken up within the calix[5]arene cavities. Less symmetric C₇₀ has many conformational options in the host–guest complex; accordingly, estimating the plausible structure of the host–guest complex by simple molecular models is risky business. The combination of our chemical shift simulation and molecular mechanics calculation or molecular dynamics simulation estimated the reliable structures. The method can be one of the good ways to determine structures of a host–guest complex in solution.

4. Experimental

4.1. General

¹H NMR spectra were measured with a JEOL EX-270, a JEOL Lambda 500, or a Varian Mercury 300 spectrometer

using Me₄Si as internal standard. ¹³C NMR spectra were taken with JEOL Lambda 500, JEOL JNM-EX400, or a Varian Mercury 300 spectrometer. ¹³C NMR chemical shifts (δ) are given in ppm downfield internal Me₄Si, or from internal chloroform-*d* ($\delta=77.0$), and carbon disulfide ($\delta=192.8$). All NMR spectra were recorded in CDCl₃ unless otherwise indicated. IR spectra were measured on a Hitachi 260-10S or a JASCO FT/IR-420S spectrometer. Mass spectra were reported with a JEOL JMX-SX 102 mass spectrometer. Elemental analyses were performed on a Perkin Elmer 2400CHN elemental analyzer. Melting points were measured with a Yanagimoto micro melting point apparatus and are uncorrected. UV spectra were measured on a JASCO V-560 spectrometer.

All reaction was carried out under an argon atmosphere unless otherwise noted. THF, Et₂O, toluene, and dioxane were freshly distilled from Na-benzophenone. Dichloromethane and pyridine were freshly distilled from CaH₂. MeOH and EtOH were freshly distilled from activated magnesium. Column chromatography was performed using Merck silica gel (70–230 mesh).

Molecular mechanics and molecular dynamics calculations were carried out by MacroModel V 6.5 program package running on SGI O2. Low mode search option was used for the initial geometry generation, and the given geometries were optimized by a conjugate gradient energy minimization using amber* force field. Molecular dynamics simulation was carried out from the most stable structure obtained by the above method. The simulation took stochastic dynamics option with SHAKE using amber* force field.

4.1.1. 5,11,17,23-Tetramethyl-31,32,33,34,35-pentahydroxy calix[5]arene 3b. To a solution of 6.6 g (10 mmol) of 5-*tert*-butyl-11,17,23,29-tetramethyl-31,32,33,34,35-pentahydroxy calix[5]arene and 4 g (43 mmol) of phenol in 200 ml of toluene was added 8 g (60 mmol) of AlCl₃. The reaction mixture was stirred at room temperature for 6 h and was quenched by addition of 1 N HCl. The resulting solution was extracted with AcOEt, and the organic solution was dried (Na₂SO₄) and concentrated under reduced pressure. The residue was purified by column chromatography on silica gel (40:60 hexane/benzene) to give 3.3 g (14.8 mmol) of **3b** (56%). Mp 260 °C; ¹H NMR 7.16 (d, 2H, $J=7.2$ Hz), 6.97 (s, 8H), 6.82 (t, 1H, $J=7.2$ Hz), 3.78 (br s, 10H), 2.22 (s, 6H), 2.21 (s, 6H); ¹³C NMR 150.12, 147.86, 147.79, 130.58, 130.55, 129.61, 129.58, 129.10, 126.79, 126.49, 126.46, 126.44, 126.36, 121.40, 31.36, 31.34, 20.42, 20.40; IR (KBr) 3100–3500, 1484, 1223 cm⁻¹. Anal. Calcd for C₃₉H₃₈O₅·C₆H₆: C, 81.29; H, 6.67. Found: C, 80.80; H, 6.85.

4.1.2. 5,17-Diiodo-11,23,29-trimethyl-31,32,33,34,35-pentahydroxy-calix[5]arene 1a. A solution consisting of 4.2 g (7.1 mmol) of **3a**, 11.0 g (31.5 mmol) of BTMA-ICl₂, and 1.0 g (10 mmol) of CaCO₃ in 100 ml of CH₂Cl₂–MeOH (7/3 v/v) was stirred at room temperature for 4 h. Excess CaCO₃ was filtered and the filtrate was concentrated; then, to the obtained residue was added a NaHSO₃ solution. The mixture was extracted with CHCl₃. The organic solution was dried (Na₂SO₄) and concentrated under reduced

pressure. The residue was purified by column chromatography on silica gel (100% benzene) to give 4.67 g (81%) of **1**. Mp 280 °C (dec); ^1H NMR 7.48 (s, 2H), 7.05–6.94 (m, 8H), 3.75 (s, 10H), 2.25 (s, 9H); ^{13}C NMR 150.36, 147.65, 147.58, 137.63, 137.59, 130.00, 129.72, 129.67, 129.43, 129.29, 126.45, 125.63, 125.47, 83.67, 30.98, 20.42; IR (KBr) 3100–3500, 2940, 1620, 1500, 1390 cm^{-1} ; FAB-MS 825 (M+H). Anal. Calcd for $\text{C}_{38}\text{H}_{34}\text{O}_5\text{I}_2$: C, 55.36; H, 4.16. Found: C, 55.34; H, 4.19.

4.1.3. 5-Iode-11,17,23,29-tetramethyl-31,32,33,34,35-pentahydroxy-calix[5]arene 1b. A solution consisting of 15.0 g (26.0 mmol) of **3b**, 13.0 g (37.0 mmol) of BTMA- ICl_2 , and 1.2 g (12 mmol) of CaCO_3 in 300 ml of CH_2Cl_2 –MeOH (7/3 v/v) was stirred at room temperature for 4 h. Excess CaCO_3 was filtered and the filtrate was concentrated; then, to the obtained residue was added a NaHSO_3 solution. The mixture was extracted with CHCl_3 . The organic layers were dried (Na_2SO_4) and concentrated under reduced pressure. The residue was purified by column chromatography on silica gel (100% benzene) to give 13.3 g (72%) of **1b**. Mp 260 °C (dec); ^1H NMR 7.46 (s, 2H), 6.97 (s, 6H), 6.91 (s, 2H), 3.75 (s, 10H), 2.22 (s, 6H), 2.21 (s, 6H); ^{13}C NMR 150.36, 147.75, 147.65, 137.48, 130.80, 130.58, 129.91, 129.64, 129.59, 129.41, 126.55, 126.41, 126.27, 125.43, 83.62, 31.29, 30.97, 20.41, 20.39; IR (KBr) 3100–3500, 1483, 1453, 1221, 684 cm^{-1} . Anal. Calcd for $\text{C}_{39}\text{H}_{37}\text{O}_5\text{I}$: C, 65.73; H, 5.23. Found: C, 65.84; H, 5.25.

4.1.4. 11,23-Diiodo-5,17,29-trimethyl-31,32,33,34,35-pentaacetoxy calix[5]arene 7a. To a solution of 4.67 g (5.67 mmol) of **1a** in 80 ml of pyridine was added 30 ml of Ac_2O . The reaction mixture was stirred at room temperature for 12 h and was quenched by the addition of 1 N HCl (300 ml). The resulting solution was extracted with CHCl_3 , and the organic solution was dried (Na_2SO_4) and concentrated under reduced pressure. The residue was purified by column chromatography on silica gel (20:80 AcOEt/benzene) to give 4.81 g (82%) of **7a**. Mp >300 °C; IR (KBr) 1740, 1450, 1360 cm^{-1} ; FAB-MS 1035 (M+H); Anal. Calcd for $\text{C}_{48}\text{H}_{44}\text{O}_{10}\text{I}_2$: C, 55.71; H, 4.29. Found: C, 55.59; H, 4.34.

4.1.5. 5-Iode-11,17,23,29-tetramethyl-31,32,33,34,35-pentaacetoxy-calix[5]arene 7b. To a solution of 15.0 g (21.0 mmol) of **1b** in 180 ml of pyridine was added 90 ml of Ac_2O . The reaction mixture was stirred at room temperature for 12 h and was quenched by the addition of 1 N HCl (500 ml). The resulting solution was extracted with CHCl_3 , and the organic solution was dried (Na_2SO_4) and concentrated under reduced pressure. The residue was purified by column chromatography on silica gel (20:80 AcOEt/benzene) to give 10.0 g (52%) of **7b**. Mp >300 °C; IR (KBr) 1759, 1369, 1216, 1191 cm^{-1} . Anal. Calcd for $\text{C}_{49}\text{H}_{47}\text{O}_{10}\text{I}$: C, 63.78; H, 5.13. Found: C, 63.79; H, 4.96.

4.1.6. 5-Iode-17-ethynyl-11,23,29-trimethyl-31,32,33,34,35-pentaacetoxy-calix[5]arene 8a. To a suspension of 1.0 g (0.97 mmol) of **7a** and 0.03 g (0.16 mmol) of CuI in 30 ml of THF was added 1.0 ml (10 mmol) of *n*-butyl amine, 0.1 ml (0.7 mmol) of TMS–acetylene, and 0.2 g (0.17 mmol) of $\text{Pd}(\text{PPh}_3)_4$ in 10 ml of THF under Ar. The reaction mixture was stirred at room temperature for 12 h

and was diluted with CHCl_3 (300 ml), washed with saturated NaHCO_3 . The organic layers were dried (Na_2SO_4) and concentrated under reduced pressure. The residue was purified by column chromatography on silica gel (20:80 AcOEt/benzene) and GPC to give 0.2 g of the trimethylsilylethynylated product. A suspension of 0.2 g (0.21 mmol) of the product and 2 g (34.5 mmol) of KF in 30 ml of CH_2Cl_2 –MeOH (1/2 v/v) was stirred at room temperature for 12 h. The reaction mixture was diluted with CHCl_3 (200 ml), and the organic solution was washed with H_2O , dried (Na_2SO_4) and concentrated under reduced pressure. The residue was purified by column chromatography on silica gel (20:80 AcOEt/benzene) to give 0.16 g (25%) of **8a**. IR (KBr) 2920, 2080, 1740, 1600, 1450, 1360 cm^{-1} .

4.1.7. 5-Ethynyl-11,17,23,29-tetramethyl-31,32,33,34,35-pentaacetoxy-calix[5]arene 8b. To a suspension of 1.0 g (0.97 mmol) of **7b** and 0.03 g (0.16 mmol) of CuI in 30 ml of THF was added 1.0 ml (10 mmol) of *n*-butyl amine, 0.1 ml (0.7 mmol) of TMS–acetylene, and 0.2 g (0.17 mmol) of $\text{Pd}(\text{PPh}_3)_4$ in 10 ml of THF under Ar. The reaction mixture was stirred at room temperature for 12 h and was diluted with CHCl_3 (300 ml), washed with saturated NaHCO_3 . The organic solution was dried (Na_2SO_4) and concentrated under reduced pressure. The residue was purified by column chromatography on silica gel (20:80 AcOEt/benzene) and GPC to give 0.2 g of the trimethylsilylethynylated product. A suspension of 0.2 g (0.21 mmol) of the product and 2 g (34.5 mmol) of KF in 30 ml of CH_2Cl_2 –MeOH (1/2 v/v) was stirred at room temperature for 12 h. The reaction mixture was diluted with CHCl_3 (200 ml), washed with H_2O , dried (Na_2SO_4) and concentrated under reduced pressure. The residue was purified by column chromatography on silica gel (20:80 AcOEt/benzene) to give 0.16 g (25%) of **7b**. IR (KBr) 2920, 2080, 1740, 1600, 1450, 1360 cm^{-1} .

4.1.8. Double-calix[5]arene 4a. To a suspension of 1.2 g (1.16 mmol) of **7a** and 0.03 g (0.16 mmol) of CuI in 30 ml of THF was added 1.0 ml (10 mmol) of *n*-butyl amine, 0.05 g (0.36 mmol) of **9** in 10 ml of THF, and 0.12 g (0.1 mmol) of $\text{Pd}(\text{PPh}_3)_4$ in 10 ml of THF under Ar. The reaction mixture was stirred at room temperature for 12 h and was diluted with CHCl_3 (300 ml), washed with saturated NaHCO_3 . The organic solution was dried (Na_2SO_4) and concentrated under reduced pressure. The residue was purified by column chromatography on silica gel (20:80 AcOEt/benzene) and GPC to give 0.25 g of the protected double-calix[5]arene. A suspension of 0.1 g (0.05 mmol) of the product and 0.36 g (2.6 mmol) of K_2CO_3 in 30 ml of THF–MeOH (1/2 v/v) was stirred at room temperature for 2 h. The reaction mixture was diluted with CHCl_3 (200 ml), and the organic solution was washed with 1 N HCl (100 ml), dried (Na_2SO_4) and concentrated under reduced pressure. The residue was purified by column chromatography on silica gel (40:60 hexane/benzene) and GPC to give 0.04 g (19%) of **4a**. Mp 280 °C (dec); ^1H NMR 7.52 (s, 1), 7.48 (s, 4), 7.39 (s, 4), 7.29 (s, 2), 6.94–7.07 (m, 12), 3.77 (br s, 20), 2.34 (s, 3), 2.25 (s, 18); ^{13}C NMR 150.78, 150.39, 147.68, 147.62, 147.53, 138.18, 137.61, 132.62, 132.60, 131.65, 131.18, 130.96, 130.02, 129.87, 129.75, 129.69, 129.43, 129.36, 127.15, 127.01, 126.51,

126.41, 125.89, 125.74, 125.57, 125.46, 123.56, 115.98, 89.48, 87.55, 83.65, 31.30, 31.16, 30.99, 30.94, 21.04, 20.42; IR (KBr) 3100–3650, 2920, 2210, 1580, 1480, 1385 cm^{-1} ; FAB-MS 1533 (M+H). Anal. Calcd for $\text{C}_{87}\text{H}_{74}\text{O}_{10}\text{I}_2$: C, 68.14; H, 4.86. Found: C, 67.92; H, 4.69.

4.1.9. Double-calix[5]arene 4b. To a suspension of 1.29 g (1.40 mmol) of **7b** and 0.03 g (0.16 mmol) of CuI in 30 ml of THF was added 1.0 ml (10 mmol) of *n*-butyl amine, 0.096 g (0.68 mmol) of **9** in 10 ml of THF, and 0.12 g (0.1 mmol) of Pd(PPh₃)₄ in 10 ml of THF under Ar. The reaction mixture was stirred at room temperature for 12 h and was diluted with CHCl₃ (300 ml), washed with saturated NaHCO₃. The organic layers were dried (Na₂SO₄) and concentrated under reduced pressure. The residue was purified by column chromatography on silica gel (20:80 AcOEt/benzene) and GPC to give 0.90 g of the protected double-calix[5]arene. A suspension of the product and 0.70 g (5.2 mmol) of K₂CO₃ in 30 ml of THF–MeOH (1/2 v/v) was stirred at room temperature for 2 h. The reaction mixture was diluted with CHCl₃ (200 ml), washed with 1 N HCl (100 ml), and the organic solution was dried (Na₂SO₄) and concentrated under reduced pressure. The residue was purified by column chromatography on silica gel (40:60 hexane/benzene) and GPC to give 0.33 g (36%) of **4b**. Mp 254 °C (dec); ¹H NMR 7.51 (s, 1H), 7.39 (s, 4H), 7.29 (s, 2H), 7.00 (s, 8H), 6.99 (s, 8H), 3.77 (s, 20H), 2.33 (s, 3H), 2.24 (s, 24H); ¹³C NMR 150.86, 147.82, 147.67, 132.57, 131.61, 130.84, 130.64, 129.83, 129.66, 127.16, 126.56, 126.46, 126.36, 126.22, 125.75, 123.57, 115.82, 110.73, 89.33, 87.48, 31.34, 31.22, 20.43; IR (KBr) 3100–3500, 2208, 1482, 1228 cm^{-1} . FAB-MS 1309 (M+H); Anal. Calcd for $\text{C}_{89}\text{H}_{80}\text{O}_{10} \cdot 2\text{H}_2\text{O}$: C, 79.43; H, 6.29. Found: C, 79.20; H, 6.19.

4.1.10. Double-calix[5]arene 5a. To a suspension of 0.17 g (0.18 mmol) of **8a**, 0.37 g (0.36 mmol) of **7a**, and 0.02 g (0.10 mmol) of CuI in 10 ml of THF was added 0.2 ml (2 mmol) of *n*-butyl amine and 0.1 g (0.085 mmol) of Pd(PPh₃)₄ in 10 ml of THF under Ar. The reaction mixture was stirred at room temperature for 12 h and was diluted with CHCl₃ (300 ml), washed with saturated NaHCO₃. The organic layers were dried (Na₂SO₄) and concentrated under reduced pressure. The residue was purified by column chromatography on silica gel (30:70 AcOEt/benzene) and GPC to give 0.17 g of the protected double-calix[5]arene. A suspension of 0.17 g (0.092 mmol) of the product and 1 g (7.2 mmol) of K₂CO₃ in 30 ml of THF–MeOH (1/2 v/v) was stirred at room temperature for 2 h. The reaction mixture was diluted with CHCl₃ (200 ml), washed with 1 N HCl (100 ml), and the organic solution was dried (Na₂SO₄) and concentrated under reduced pressure. The residue was purified by column chromatography on silica gel (40:60 hexane/benzene) and GPC to give 0.052 g (20%) of **5a**. Mp 280 °C (dec); ¹H NMR 7.48 (s, 4H), 7.41 (s, 4H), 7.01 (m, 8H), 6.95 (s, 4H), 3.76 (br s, 20H), 2.24 (s, 18H); ¹³C NMR 150.56, 150.39, 147.69, 147.62, 147.53, 137.60, 132.51, 131.15, 130.97, 130.92, 130.08, 130.02, 129.84, 129.69, 129.44, 129.35, 127.10, 126.97, 126.52, 126.40, 125.91, 125.76, 125.56, 125.47, 116.21, 87.93, 83.65, 31.28, 31.26, 31.20, 31.00, 30.93, 20.42; IR (KBr) 3100–3650, 2920, 1605, 1480, 1370 cm^{-1} ; FAB-MS 1419 (M+H). Anal.

Calcd for $\text{C}_{78}\text{H}_{68}\text{O}_{10}\text{I}_2$: C, 66.00; H, 4.83. Found: C, 66.32; H, 4.89.

4.1.11. Double-calix[5]arene 5b. To a suspension of 0.68 g (0.83 mmol) of **8b**, 1.50 g (1.69 mmol) of **7b**, and 0.07 g (0.34 mmol) of CuI in 10 ml of THF was added 1.0 ml (10 mmol) of *n*-butyl amine and 0.2 g (0.17 mmol) of Pd(PPh₃)₄ in 10 ml of THF under Ar. The reaction mixture was stirred at room temperature for 12 h and was diluted with CHCl₃ (300 ml), washed with saturated NaHCO₃. The organic solution was dried (Na₂SO₄) and concentrated under reduced pressure. The residue was purified by column chromatography on silica gel (30:70 AcOEt/benzene) and GPC to give 0.96 g of the protected double-calix[5]arene. A suspension of 0.96 g (0.58 mmol) of the product and 2 g (14.4 mmol) of K₂CO₃ in 30 ml of THF–MeOH (1/2 v/v) was stirred at room temperature for 2 h. The reaction mixture was diluted with CHCl₃ (200 ml), washed with 1 N HCl (100 ml), and the organic solution was dried (Na₂SO₄) and concentrated under reduced pressure. The residue was purified by column chromatography on silica gel (40:60 hexane/benzene) and GPC to give 0.40 g (36%) of **5b**. Mp 254 °C (dec); ¹H NMR 7.18 (s, 4H), 6.92–6.93 (s, 16H), 3.76 (s, 20H), 2.26 (s, 24H); ¹³C NMR 150.61, 147.82, 147.66, 132.45, 130.81, 130.63, 129.80, 129.73, 129.65, 127.10, 126.55, 126.46, 126.37, 125.78, 116.11, 87.93, 31.34, 31.25, 20.43; IR (KBr) 3100–3500, 2919, 1483 cm^{-1} ; FAB-MS 1195 (M+H); Anal. Calcd for $\text{C}_{80}\text{H}_{74}\text{O}_{10} \cdot 2\text{H}_2\text{O}$: C, 78.02; H, 6.38. Found: C, 78.27; H, 6.23.

4.1.12. Double-calix[5]arene 6a. To a solution of 2 g (10 mmol) of Cu(OAc)₂ in 20 ml of pyridine was added dropwise 0.68 g (0.73 mmol) of **8a** in 30 ml of pyridine. The reaction mixture was stirred at 45 °C for 3 h and was quenched by addition of 1 N HCl (200 ml). The resulting solution was extracted with CHCl₃, and the organic solution was dried (Na₂SO₄) and concentrated under reduced pressure. The residue was purified by column chromatography on silica gel (10:90 AcOEt/benzene) to give 0.51 g of the protected double-calix[5]arene. A suspension of 0.12 g (0.064 mmol) of the product and 1 g (7.2 mmol) of K₂CO₃ in 30 ml of THF–MeOH (1/2 v/v) was stirred at room temperature for 2 h. The reaction mixture was diluted with CHCl₃ (200 ml), washed with 1 N HCl (100 ml), and the organic solution was dried (Na₂SO₄) and concentrated under reduced pressure. The residue was purified by column chromatography on silica gel (40:60 hexane/benzene) and GPC to give 0.07 g (56%) of **6a**. Mp 280 °C (dec); ¹H NMR 7.48 (s, 4H), 7.38 (s, 4H), 6.92–7.03 (m, 12H), 3.75 (s, 20H), 2.24 (s, 18H); ¹³C NMR 151.47, 150.36, 147.66, 147.55, 147.47, 137.63, 137.59, 133.47, 133.43, 131.26, 131.04, 130.99, 130.00, 129.92, 129.68, 129.42, 129.28, 127.33, 127.20, 126.59, 126.48, 126.33, 125.71, 125.58, 125.45, 114.58, 83.66, 81.34, 72.88, 31.30, 31.23, 31.01, 30.95, 29.69, 20.35; IR (KBr) 3100–3650, 2920, 2150, 1600, 1480, 1380 cm^{-1} . FAB-MS 1443 (M+H). Anal. Calcd for $\text{C}_{80}\text{H}_{68}\text{O}_{10}\text{I}_2$: C, 66.57; H, 4.75. Found: C, 66.63; H, 4.53.

4.1.13. Double-calix[5]arene 6b. To a solution of 2 g (10 mmol) of Cu(OAc)₂ in 20 ml of pyridine was added dropwise 0.40 g (0.49 mmol) of **8b** in 30 ml of pyridine. The reaction mixture was stirred at 45 °C for 3 h and was quenched by addition of 1 N HCl (200 ml). The resulting

solution was extracted with CHCl_3 , and the organic solution was dried (Na_2SO_4) and concentrated under reduced pressure. The residue was purified by column chromatography on silica gel (10:90 AcOEt/benzene) to give 0.28 g of the protected double-calix[5]arene. A suspension of 0.28 g (0.17 mmol) of the product and 1 g (7.2 mmol) of K_2CO_3 in 30 ml of THF–MeOH (1/2 v/v) was stirred at room temperature for 2 h. The reaction mixture was diluted with CHCl_3 (200 ml), washed with 1 N HCl (100 ml), and the organic solution was dried (Na_2SO_4) and concentrated under reduced pressure. The residue was purified by column chromatography on silica gel (40:60 hexane/benzene) and GPC to give 0.120 g (41%) of **6b**. Mp 252 °C (dec); ^1H NMR 7.25 (s, 4H), 6.99 (s, 12H), 6.96 (s, 4H), 3.76 (s, 20H), 2.23 (s, 24H); ^{13}C NMR 151.54, 147.79, 147.59, 133.40, 130.92, 130.64, 129.87, 129.66, 129.64, 129.59, 127.33, 126.57, 126.43, 126.30, 125.57, 114.46, 81.37, 72.82, 31.31, 31.07, 20.43, 20.40; IR (KBr) 3100–3500, 2141, 1482, 1229 cm^{-1} ; FAB-MS 1219 (M+H). Anal. Calcd for $\text{C}_{82}\text{H}_{74}\text{O}_{10}$: C, 80.76; H, 6.12. Found: C, 80.47; H, 6.29.

References and notes

- (a) Dresselhaus, M. S.; Dresselhaus, G.; Eklund, P. C. *Science of Fullerenes and Carbon Nanotubes*; Academic: San Diego, 1996. (b) Guldi, D. M.; Martín, N. *J. Mater. Chem.* **2002**, *12*, 1978–1992. (c) Schön, J. H.; Kloc, C.; Batlogg, B. *Nature* **2000**, *408*, 549–552. (d) Schön, J. H.; Kloc, C.; Batlogg, B. *Science* **2001**, *293*, 2432–2434. (e) Nakamura, E.; Isobe, H.; Tomita, N.; Sawamura, M.; Jinno, S.; Okayama, H. *Angew. Chem., Int. Ed.* **2000**, *39*, 4254–4257. (f) Bernstein, R.; Prat, F.; Foote, C. S. *J. Am. Chem. Soc.* **1999**, *121*, 464–465. (g) Wada, Y.; Tsukada, M.; Fujihara, M.; Matsushige, K.; Ogawa, T.; Haga, M.; Tanaka, S. *Jpn. J. Appl. Phys.* **2000**, *39*, 3835–3849.
- (a) Andersson, T.; Nilsson, K.; Sundahl, M.; Westman, G.; Wennerström, O. *Chem. Commun.* **1992**, 604–606. (b) Yoshida, Z.; Takekuma, H.; Takekuma, S.; Matsubara, Y. *Angew. Chem., Int. Ed. Engl.* **1994**, *33*, 1597–1599. (c) Komatsu, K.; Fujiwara, K.; Murata, Y.; Braun, T. *J. Chem. Soc., Perkin Trans. 1* **1999**, 2963–2966.
- (a) Williams, R. M.; Verhoeven, J. W. *Recl. Trav. Chim. Pays-Bas* **1992**, *111*, 531–532. (b) Ikeda, A.; Hatano, T.; Kawaguchi, M.; Suenaga, H.; Shinakai, S. *Chem. Commun.* **1999**, 1403–1404.
- (a) Atwood, J. L.; Koutsantnis, G. A.; Raston, C. L. *Nature* **1994**, *368*, 229. (b) Suzuki, T.; Nakashima, K.; Shinkai, S. *Chem. Lett.* **1994**, 699.
- (a) Araki, K.; Akao, K.; Ikeda, A.; Suzuki, T.; Shinkai, S. *Tetrahedron Lett.* **1996**, *37*, 73–76. (b) Bhattacharya, S.; Nayak, S. K.; Semwal, A.; Banerjee, M. *Spectrochim. Acta, Part A* **2005**, *61*, 595–606.
- (a) Ikeda, A.; Hatano, T.; Shinkai, S.; Akiyama, T.; Yamada, S. *J. Am. Chem. Soc.* **2001**, *123*, 4855–4856. (b) Tsubaki, K.; Tanaka, K.; Fuji, K.; Tanaka, K.; Kinoshita, T. *Chem. Commun.* **1998**, 895–896.
- (a) Matsubara, H.; Hasegawa, A.; Shiwaku, K.; Asano, K.; Uno, M.; Takahashi, S.; Yamamoto, K. *Chem. Lett.* **1998**, 923–924. (b) Matsubara, H.; Shimura, T.; Hasegawa, A.; Semba, M.; Asano, K.; Yamamoto, K. *Chem. Lett.* **1998**, 1099–1100.
- Kawase, T.; Tanaka, K.; Fujiwara, N.; Darabi, H. R.; Oda, M. *Angew. Chem., Int. Ed.* **2003**, *42*, 1624–1628.
- Wang, M.-X.; Zhang, X.-H.; Zheng, Q.-Y. *Angew. Chem., Int. Ed.* **2004**, *43*, 838–842.
- (a) Boyd, P. D. W.; Hodgson, M. C.; Rickard, C. E. F.; Oliver, A. G.; Chaker, L.; Brothers, P. J.; Bolskar, R. D.; Tham, F. S.; Reed, C. A. *J. Am. Chem. Soc.* **1999**, *121*, 10487–10495. (b) Olmstead, M. M.; Costa, D. A.; Maitra, K.; Noll, B. C.; Phillips, S. L.; Van Calcar, P. M.; Balch, A. L. *J. Am. Chem. Soc.* **1999**, *121*, 7090–7097.
- (a) Sun, D.; Tam, F. S.; Reed, C. A.; Chaker, L.; Burgess, M.; Boyd, P. D. W. *J. Am. Chem. Soc.* **2000**, *122*, 10704–10705. (b) Tashiro, K.; Aida, T.; Zheng, J.-Y.; Kinbara, K.; Saigo, K.; Sakamoto, S.; Yamaguchi, K. *J. Am. Chem. Soc.* **1999**, *121*, 9477–9478. (c) Zheng, J.-Y.; Tashiro, K.; Hirabayashi, Y.; Kinbara, K.; Saigo, K.; Aida, T.; Sakamoto, S.; Yamaguchi, K. *Angew. Chem., Int. Ed.* **2001**, *40*, 1858–1861. (d) Iwamoto, H.; Yamaguchi, M.; Hiura, S.; Fukazawa, Y. *Heterocycles* **2004**, *63*, 2005–2011.
- (a) Haino, T.; Araki, H.; Fujiwara, Y.; Tanimoto, Y.; Fukazawa, Y. *Chem. Commun.* **2002**, 2148–2149. (b) Haino, T.; Yamanaka, Y.; Araki, H.; Fukazawa, Y. *Chem. Commun.* **2002**, 402–403. (c) Haino, T.; Araki, H.; Yamanaka, Y.; Fukazawa, Y. *Tetrahedron Lett.* **2001**, *42*, 3203–3206. (d) Yanase, M.; Haino, T.; Fukazawa, Y. *Tetrahedron Lett.* **1999**, *40*, 2781–2784.
- (a) Haino, T.; Yanase, M.; Fukazawa, Y. *Angew. Chem., Int. Ed.* **1998**, *37*, 997–998. (b) Haino, T.; Yanase, M.; Fukazawa, Y. *Angew. Chem., Int. Ed.* **1997**, *36*, 259–260.
- (a) Böhmer, V. *Angew. Chem., Int. Ed. Engl.* **1995**, *34*, 713–745. (b) No, K.; Kwon, K. M. *Synthesis* **1996**, 1293–1295. (c) Haino, T.; Harano, T.; Matsumura, K.; Fukazawa, Y. *Tetrahedron Lett.* **1995**, *36*, 5793–5796. (d) Haino, T.; Matsumura, K.; Harano, T.; Yamada, K.; Saijyo, Y.; Fukazawa, Y. *Tetrahedron* **1998**, *54*, 12185–12196.
- Connors, K. A. *Binding Constants*; Wiley: New York, 1987.
- Yang, Y.; Arias, F.; Echegoyen, L.; Chibante, L. P. F.; Flanagan, S.; Robertson, A.; Wilson, L. J. *J. Am. Chem. Soc.* **1995**, *117*, 7801–7804.
- Yanase, M.; Matsuoka, M.; Tatsumi, Y.; Suzuki, M.; Iwamoto, H.; Haino, T.; Fukazawa, Y. *Tetrahedron Lett.* **2000**, *41*, 493–496.
- Haino, T.; Yanase, M.; Fukazawa, Y. *Tetrahedron Lett.* **1997**, *38*, 3739–3742.
- Mohamadi, F.; Richards, N. G. J.; Guida, W. C.; Liskamp, R.; Lipton, M.; Caufield, C.; Chang, G.; Hendrickson, T.; Still, W. C. *J. Comp. Chem.* **1990**, *11*, 440–467.
- Atwood, J. L.; Barbour, L. J.; Heaven, M. W.; Raston, C. L. *Chem. Commun.* **2003**, 2270–2271.
- (a) Fukazawa, Y.; Ogata, K.; Usui, S. *J. Am. Chem. Soc.* **1988**, *110*, 8692–8693. (b) Fukazawa, Y.; Deyama, K.; Usui, S. *Tetrahedron Lett.* **1992**, *33*, 5803–5806. (c) Fukazawa, Y.; Usui, S.; Tanimoto, K.; Hirai, Y. *J. Am. Chem. Soc.* **1994**, *116*, 8169–8175. (d) Fukazawa, Y.; Hayashibara, T.; Yang, Y.; Usui, S. *Tetrahedron Lett.* **1995**, *36*, 3349–3352.
- Van Gunsteren, W. F.; Berendsen, J. C. J. *Comput. Aided Mol. Des.* **1987**, *1*, 173–176.

Supramolecular complexation studies of [60]fullerene with calix[4]naphthalenes—a reinvestigation

Paris E. Georghiou,* Anh Huu Tran, Skylar S. Stroud and David W. Thompson*

Department of Chemistry, Memorial University of Newfoundland, St. John's, Newfoundland and Labrador A1B 3X7, Canada

Received 27 June 2005; revised 16 September 2005; accepted 19 September 2005

Available online 15 December 2005

Abstract—Estimations of equilibrium or association constant (K_{ASSOC}) values reported by many other groups for the supramolecular complexation between [60]fullerene ('C₆₀') with different macrocyclic hosts, in solvents such as toluene or carbon disulfide, for example, is often conducted by UV–vis absorption and/or ¹H NMR spectroscopy. In this paper, the complexation behaviour of two calix[4]naphthalene hosts with C₆₀ in toluene and carbon disulfide has been re-examined, using both of these methods. An analysis is presented of the data newly obtained, in light of recent advances and understanding published by others of the limitations of, in particular, the absorption spectroscopic methods. The discussion presented is also intended to aid those who may be unfamiliar with the nuances and limitations of the analytic models involving C₆₀ supramolecular complexation. Also presented is a general mechanism for C₆₀ supramolecular complexation studies, which lay the groundwork for further experiments.

© 2005 Elsevier Ltd. All rights reserved.

1. Introduction

In 1999 Diederich and Gomez-Lopez¹ reviewed advances on supramolecular fullerene chemistry which had taken place during the previous decade and pointed out the importance of inclusion complexes of [60]fullerene ('C₆₀') with various macrocyclic host molecules. Prominent among those host molecules reviewed were the calixarenes, for example, **1**, (Fig. 1), a class of molecules whose unusual and varied properties continue to be subjects of extensive study.²

In 1992 Williams and Verhoeven showed that the water-soluble calix[8]arene derivative (**2**) was capable of extracting C₆₀ into an aqueous phase.³ Later, Atwood⁴ and coincidentally, Shinkai,⁵ discovered that in toluene solution, *p*-*tert*-butylcalix[8]arene (**3**) could selectively sequester C₆₀ from a mixture containing both C₆₀ and C₇₀, by forming a precipitate of a 1:1 complex with C₆₀. An attempt to crystallize this precipitate from chloroform resulted instead in de-complexation, leading to the production of pure C₆₀. This finding among others, led to extensive studies of

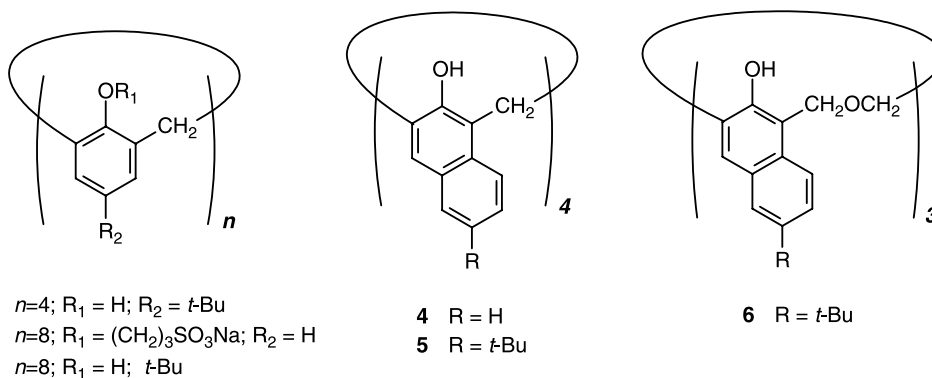


Figure 1. Structures of compounds 1–6.

Keywords: Supramolecular complexation; [60]Fullerene; Calixarenes; Calixnaphthalenes; Association constants; Binding constants; Contact-pair transitions.

* Corresponding authors. Tel.: +1 709 737 8517; fax: +1 709 737 3702 (P.E.G.); tel.: +1 709 737 8046; fax: +1 709 737 3702 (D.W.T.); e-mail addresses: parisg@mun.ca; dthompso@mun.ca

fullerenes with various other calixarenes and calixarene derivatives, many of which were more recently reviewed in 2001 by Shinkai et al.⁶

In 1999 we reported⁷ that calix[4]naphthalenes, for example, **4** and **5**, a class of naphthalene-ring based calixarenes,⁸ also formed supramolecular complexes with C₆₀. At the time, we had reasoned that the deeper, more electron-rich cavities formed by the naphthalene subunits would facilitate binding with the electron-deficient fullerenes, as a result of the extra π - π^* interactions⁹ possible when compared with the corresponding calix[4]arenes, which do not bind with C₆₀. Our initial results were consistent with this hypothesis. Those findings were based upon the observation that the pale yellow solutions of *p*-*tert*-butylcalix[4]naphthalene (**5**) in toluene, turned to red-brown upon the addition of C₆₀. UV–vis absorption spectroscopic studies conducted at the time were strongly suggestive of 1:1 supramolecular complexation between C₆₀ and, for example, **5**, in all three solvents which were used, namely, toluene, benzene and CS₂, affording binding, or apparent association constants (K_{ASSOC}) of 676 ± 28 , 295 ± 13 , and $6920 \pm 330 \text{ M}^{-1}$, respectively. These binding constants were determined by measuring the changes of the absorbances at $\lambda = 430 \text{ nm}$ of solutions into which microlitre aliquots of solutions (e.g., $2\text{--}10 \times 10^{-4} \text{ M}$) of the host molecule, in the same solvent, were added to a fullerene solution (approximately $1 \times 10^{-4} \text{ M}$). The $\lambda = 430 \text{ nm}$ region is that upon which studies were basing their evidence for complex formation with similar systems,^{6,7,10–14} and as discussed below, could be misleading.

Toluene, benzene or CS₂ are solvents commonly used for such spectrophotometric-based supramolecular complexation studies with fullerenes. The solubilities¹⁵ of C₆₀ at 298 K, in benzene ($1.22\text{--}2.58 \times 10^{-3} \text{ M}$), toluene ($2.99\text{--}4.44 \times 10^{-3} \text{ M}$) or CS₂ ($7.17\text{--}16.4 \times 10^{-3} \text{ M}$) are sufficient enough to conveniently allow the determination of association (formation) constants for the complexation of various macrocyclic hosts with C₆₀ in these solvents, using either absorption spectroscopy or, ¹H NMR spectroscopy.¹⁶ For the ¹H NMR studies, the deuterated analogues, benzene-*d*₆ or toluene-*d*₈ are used, but for CS₂, an external deuterium atom-containing lock is required. In several examples reported more recently by Mukerjee's group,^{17,18} however, the use of tetrachloromethane, surprisingly, has also been used in complexation studies of various calixarenes with C₆₀ using both absorption and NMR studies, even though the solubility of C₆₀ in this solvent is lower (i.e., $1.4\text{--}6.2 \times 10^{-4} \text{ M}$),¹⁵ than those of the other solvents described above.

Although ruby-red rod-like crystals of a 1:1 complex of C₆₀ and **5** (as confirmed by +FAB MS data) were produced from the slow evaporation of a toluene solution that was equimolar with respect to both C₆₀ and **5**, we were unable at the time to obtain suitable single-crystal X-ray diffraction data from these crystals. During the collection of the diffraction data, the solvent diffused out from the crystal lattice resulting in the observation of only very low angle peaks. Later, however, we successfully obtained a single-crystal X-ray structure of the related *p*-*tert*-butylhexahomotrioxacalix[3]naphthalene **6**,¹⁹ which revealed it to be a 2:1 'capsule-like'⁶ structure in which a C₆₀ molecule is

encapsulated by two molecules of **6**. The *tert*-butyl groups of each molecule of **6** surround the fullerene in a pincer-like embrace, in support with the hypothesis that π -CH₃ interactions are dominant ones. The binding, or association constants in this study were determined in both toluene-*d*₈ and benzene-*d*₆, by measuring ¹H NMR shift changes in **6** as a function of added C₆₀.

Since our initial 1999 studies with **4** and **5** were undertaken using UV–vis absorption spectroscopy only, we decided to reinvestigate their complexation properties. We have now found that while the ¹H NMR spectra of solutions of **5** in toluene-*d*₈ to which aliquots of C₆₀ were added, showed clear, reasonably sizeable chemical shift changes, and afforded reproducible K_{ASSOC} values, we could find no comparable evidence for any complexation of either **4** or **5** in CS₂ solution. In this paper, we describe the results from a reinvestigation of the supramolecular complexation properties of **4** and **5** using both ¹H NMR and absorption spectroscopy, in light of more recent research findings by us, and by other researchers, in particular, with respect to the behaviour of C₆₀ in various solvents.

2. Methods and materials

2.1. General methods

Carbon disulfide (redistilled, industrial hygiene analysis grade), toluene (spectrograde) and C₆₀ were used as purchased, without further purification. Calixnaphthalenes **4** and **5** were prepared as described previously.²⁰

UV–vis absorption spectroscopy. All UV–vis absorption data were conducted on a HP 8452A diode array spectrophotometer with thermostated cell compartments. Temperatures were recorded to $\pm 0.1 \text{ }^\circ\text{C}$ with a thermocouple. All mass determinations were conducted on a CAHN 27 microbalance. Aliquots of solid portions of C₆₀ were added to 2.50 mL of solutions, which were approximately $1.00\text{--}2.00 \times 10^{-3} \text{ M}$, of the respective calixnaphthalene, in screw-capped 1.00 cm-pathlength quartz glass cuvettes. After each addition, solutions were sonicated for 10 min and the cuvettes were placed into the thermostated cell compartment, and the resulting spectra were recorded relative to air blanks.

¹H NMR spectroscopy. All of the ¹H NMR spectra were conducted in toluene-*d*₈ or CS₂, with TMS as internal standard, and in the case of CS₂, with a DMSO-*d*₆ external lock. Unless otherwise indicated, spectra were recorded on a Bruker Avance 500 spectrometer in pulse mode at 298 K at 500 MHz, using a 16 K data table for a 10.0 ppm sweep width having a digital resolution of 0.321 Hz. Chemical shifts in the ¹H NMR spectra were measured relative to TMS shifts (0.000 ppm). The DMSO-*d*₆ external lock was made by injecting a sample of DMSO-*d*₆ with 5% TMS into a closed-end capillary tube, and sealing the open end. For each measurement, the same capillary tube containing the DMSO-*d*₆ was inserted into the NMR tube using a specially-designed commercially available Teflon[®] insert. In a typical experiment, aliquots of a stock solution of the host calixnaphthalene (1.00 mL, of approximately

1.00–2.00 $\times 10^{-3}$ M solutions) were added to NMR tubes, and in the case of the CS₂ determinations, a sealed capillary tube containing the DMSO-*d*₆ external lock, was inserted into the sample, and the reference signals of pure host were recorded. The calculated amounts of solid C₆₀ were then added in small portions to the host solutions in the NMR tubes. After each addition, the solutions were sonicated for approximately 10 min. ¹H NMR measurements were recorded at 298 K at 500 MHz, unless otherwise noted.

2.2. Data analysis

(a) Complexation studies using absorption spectroscopy.

The complexation studies of **4**, and **5** in toluene or CS₂ solution, with C₆₀ which were conducted by UV–vis spectroscopy were analyzed using a form of the Benesi–Hildebrand equation (Eq. 1):^{21,22} where [H] is the molar concentration of host (**4** or **5**), [C₆₀] is the molar concentration of C₆₀; A is the absorption of the solutions (measured against the blank), and $\Delta\epsilon_C$ = the difference in the molar extinction coefficient between the C₆₀:H complex and that of uncomplexed host. A plot of 1/[C₆₀] versus 1/A (or [C₆₀]/A), known as a double-reciprocal plot, gives a straight line whose intercept on the y-axis divided by the slope gives K_{ASSOC} . Extrapolation, using least-squares linear regression analysis gives the value for the intercept.

$$\frac{[H]}{A} = \left\{ \frac{1}{(K_{ASSOC}\Delta\epsilon_C[C_{60}])} \right\} + \frac{1}{\Delta\epsilon_C} \quad (1)$$

(b) Association constant (K_{ASSOC}) determinations by ¹H NMR spectroscopy.

The association constants were determined by ¹H NMR spectroscopy, and also by absorption spectroscopy. For the NMR spectra, changes in the chemical shifts ($\Delta\delta$) of the signals showing the largest change as a function of added C₆₀ were measured. K_{ASSOC} values were determined using Eq. 2 by plotting 1/ $\Delta\delta$ versus 1/[C₆₀];

$$\frac{1}{\Delta\delta} = \left\{ \frac{1}{(\Delta\delta K_{ASSOC}[C_{60}])} \right\} + \frac{1}{\Delta\delta_0} \quad (2)$$

and by the Foster–Fyfe modification (Eq. 3),^{16,23} by plotting $\Delta\delta/[C_{60}]$ versus $\Delta\delta$:

$$\frac{\Delta\delta}{[C_{60}]} = -\Delta\delta K_{ASSOC} + \Delta\delta_0 K_{ASSOC} \quad (3)$$

Data were analyzed by linear least-squares regression analyses using Excel and were validated according to criteria described by both Hirose²⁴ and Fielding.¹⁶ Eq. 2 is a form of the Benesi–Hildebrand formula for the NMR method, where $\Delta\delta = (\delta_{observed} - \delta_{free})$. In the titration experiments, which were conducted, changes in chemical shift, $\Delta\delta$, of the *tert*-butyl signals in the ¹H NMR spectra of the calixnaphthalene were measured after aliquots of C₆₀ powder were added directly into the solutions in the NMR tubes and the resulting solutions sonicated before recording the spectra, as described in Section 2. $\Delta\delta_0 = (\delta_{complex} - \delta_{free})$ cannot be determined directly when the exchange, or equilibrium between host and guest, and host–guest complex, is rapid; [C₆₀] = equilibrium concentration of the

free or uncomplexed guest (C₆₀), that is, [C₆₀] = [C_{60o}] – [H:C₆₀] (where [C_{60o}] = initial concentration of guest, and [H:C₆₀] = concentration of the host–guest complex at equilibrium. However, a plot of 1/ $\Delta\delta$ versus 1/[C₆₀] will give a straight line whose slope = 1/($\Delta\delta_0 \times K_{ASSOC}$) and slope = 1/($\Delta\delta_0$), therefore, dividing the intercept by the slope will give a value for K_{ASSOC} (note: $\Delta\delta_0$ is also referred to as $\Delta\delta_{max}$ or δ_∞ by other authors). Alternatively, in order to avoid an extrapolation to obtain the value for the intercept, the Foster–Fyfe equation (Eq. 3) can be used. A plot of $\Delta\delta/[C_{60}]$ versus $\Delta\delta$ gives $-K_{ASSOC}$ directly from the slope, thus not requiring a value for the intercept, which is potentially subject to large errors.²¹ However, with limited amounts of host or guest compounds available to allow for a more intensive study, the two methods do not differ significantly. Similar treatments can be employed with the absorption spectroscopic titration method, as well. Since [C₆₀] is difficult to measure, the above equations can be simplified by the assumption that [C₆₀] = [C_{60o}]. This assumption is valid when $K_{ASSOC} \times [C_{60}] \ll 1$, that is, when complexation is weak, and so, using [C_{60o}] instead of [C₆₀] can be used to obtain K_{ASSOC} . There are other treatments, which could be employed but as long as the method used is described and validated according Hirose²⁴ and/or Fielding¹⁶ the results obtained can be considered to be reliable. In the present study both validation protocols were used for the data obtained using the Foster–Fyfe equation.

3. Results and discussion

Electronic absorption spectroscopy. The UV–vis absorption spectra of C₆₀ and **5** in toluene solution are shown in Figure 2. The assignment of electronic transitions and the solvent dependence of the transitions found in C₆₀ shown in Figure 2a have been published elsewhere.²⁵ The highly structured band envelope found between $\lambda = 400$ nm (25,000 cm⁻¹) to 650 nm (15,400 cm⁻¹) have been assigned to symmetry-forbidden electronic transitions and the symmetry-allowed vibronic transitions.²⁶ Following the nomenclature of Gallagher et al.,²⁶ the A₀ band at $\lambda = 405$ nm (24,690 cm⁻¹) and C band at $\lambda = 330$ nm (30,300 cm⁻¹) in hexane solvent are assigned to symmetry-allowed $1^1T_{1u} \rightarrow 1^1A_{1g}$ and $3^1T_{1u} \rightarrow 1^1A_{1g}$ transitions,

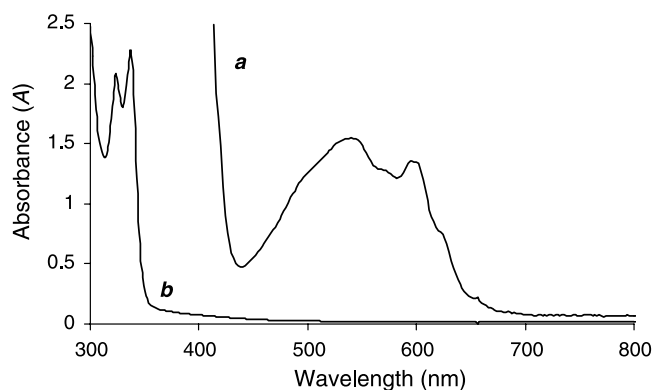


Figure 2. UV–vis absorption curves (a) of C₆₀; and (b) of **5**, in toluene solutions.

respectively. The A₀ and C transitions are solvatochromic, and are stabilized by polar solvents and aromatic solvents which may interact with C₆₀ via π interactions. The bands between $\lambda=400$ – 650 nm have well-defined peaks in aliphatic solvents; however, in aromatic solvents there is extensive broadening and changes in the intensity of these transitions.

The UV–vis absorption spectrum of **5** in toluene solution shown in Figure 2b, is dominated by transitions at $\lambda=327$ nm ($30,580$ cm⁻¹) and 337 nm ($29,670$ cm⁻¹), which tail out to 420 nm. The structured band centered at $\lambda=332$ nm has been assigned to an ¹A_g→¹L_b transition to generate a singlet excited state, which is polarized along the long axis based on comparison of the transitions found in 2-hydroxynaphthalene.²⁷ The molar absorptivity of **5** is approximately four times that found for 2-hydroxynaphthalene itself, and the band envelopes have a similar shape, indicating that there is only very weak ground-state electronic coupling between the 2-hydroxynaphthyl units in **5**.

The complexation of C₆₀ and the determinations of the association constants with a range of host molecules using UV–vis spectroscopy have been reported in many studies.^{6,7,10–14,17,18} However, the successful determination of the association constants from UV–vis spectra, relies on a clear spectroscopic signal, which is attributable to complex formation. Complexation of C₆₀ with various hosts gives rise to enhanced absorptivities between $\lambda=400$ – 470 nm, which have been assigned to resonant inter-fullerene molecular transitions, associated with aggregates of C₆₀^{3,28} or in some cases, to charge-transfer (CT) bands.^{17,18} It should be noted in the context of this manuscript, that CT bands are defined as being photo-induced electron-transfer transitions where the electron is transferred from the electron-rich naphthyl moieties to the electron-deficient C₆₀. It is difficult to predict a priori what spectral changes would occur upon complexation of C₆₀ with **4**, or with **5**. Therefore, a solvent-dependent study was undertaken in which C₆₀ was dissolved in three different, neat 1-substituted naphthyl solvents, to attempt to model the expected spectral changes that would accrue upon complexation of C₆₀ with **4**, or with **5**.²⁹

Dissolution of C₆₀ in these neat naphthalene solvents all afforded purplish-red solutions. The extinction coefficients

for C₆₀ in 1-chloronaphthalene, 1-bromonaphthalene and 1-methylnaphthalene are summarized in Table 1. Data for C₆₀ in *n*-hexane, toluene, chlorobenzene, and methoxybenzene, are included in this table, for comparative purposes. It is known that ϵ_{\max} at $\lambda=600$ nm for C₆₀ ranges from 570 M⁻¹ cm⁻¹ in *n*-hexane to 788 M⁻¹ cm⁻¹ in toluene solution. Values of ϵ_{\max} ($\lambda=600$ nm) for C₆₀ in chlorobenzene ($\epsilon_{\max}=794$ M⁻¹ cm⁻¹) and methoxybenzene ($\epsilon_{\max}=769$ M⁻¹ cm⁻¹) are similar in magnitude to that found in toluene solution and are slightly higher than those found in *n*-hexane. The values of ϵ_{\max} ($\lambda=410$ nm) for C₆₀ increase in the order of *n*-hexane ($\epsilon_{\max}=490$ M⁻¹ cm⁻¹) < chlorobenzene ($\epsilon_{\max}=2313$ M⁻¹ cm⁻¹) < toluene ($\epsilon_{\max}=2561$ M⁻¹ cm⁻¹) < methoxybenzene ($\epsilon_{\max}=5744$ M⁻¹ cm⁻¹), while the values of ϵ_{\max} ($\lambda=470$ – 600 nm) are relatively constant for the four solvents. These solvents do not form CT complexes and the observed enhanced absorptivities are due to resonant inter-fullerene molecular transitions as described previously.^{3,28} A different pattern of relative ϵ_{\max} values are apparent for C₆₀ in the naphthalene ring-containing solvents. There is enhanced absorptivity in the $\lambda=400$ – 520 nm range for C₆₀ in these solvents, while there is less absorptivity at 580 nm relative to the substituted benzene solvents. There are also distinct differences between the band shape envelopes of C₆₀ in the benzene ring-based solvents, relative to those of C₆₀ in 1-bromo-, 1-chloro- and 1-methylnaphthalene. The dramatic increase in absorbance in the $\lambda=400$ – 520 nm range for C₆₀ in the naphthalene ring-containing solvents points to the appearance of a new transition, reasonably assigned as a contact-pair CT transition, based also on the findings of Berberan-Santos,²⁷ and Ogilby.³⁰ While the present study was underway, a detailed analysis of the spectra of C₆₀ with potential electron donors, such as the substituted naphthalenes described above, in toluene was published recently.²⁷ In that work, Berberan-Santos derived a model for the absorption spectra and the pseudo-equilibria for contact complexes. They found that there was no temperature-dependence for the equilibrium constant of the 1-methylnaphthalene:C₆₀ contact CT pair in toluene, and also that the association constants were typically small (0.5 – 2 M⁻¹).

In the present study, magenta solutions of C₆₀ in toluene produced reddish-brown solutions with **5**, consistent with complex formation between C₆₀ with **5**. UV–vis spectroscopic measurements for the titration of **5** in toluene (approximately 2.00×10^{-3} M) with increasing amounts of

Table 1. Relative extinction coefficients and molar extinction coefficients ϵ (M⁻¹ cm⁻¹) of C₆₀ in different solvents at 298 (+/-3) K

Solvent	Relative ϵ ($\epsilon(\text{M}^{-1} \text{cm}^{-1}))^a$				
	ϵ_{410}	ϵ_{470}	ϵ_{520}	ϵ_{580}	ϵ_{600}
<i>n</i> -Hexane ^b	0.860 (490)	0.600 (205)	1.00 (570)	0.830 (473)	1.00 (570)
Toluene ^{b,c}	3.25 (2561)	0.556 (438)	1.05 (826)	0.860 (678)	1.00 (788)
Chlorobenzene ^c	2.91 (2313)	0.560 (444)	1.06 (843)	0.833 (662)	1.00 (794)
Methoxybenzene ^c	7.45 (5744)	0.550 (423)	1.01 (773)	0.899 (691)	1.00 (769)
1-Chloronaphthalene ^d	8.16 (6315)	1.08 (842)	1.25 (975)	0.667 (514)	1.00 (780)
1-Bromonaphthalene ^d	8.20 (6400)	1.10 (858)	1.25 (975)	0.670 (522)	1.00 (780)
1-Methylnaphthalene ^d	9.17 (7150)	3.33 (2597)	1.33 (1037)	0.667 (522)	1.00 (780)

^a Relative extinction coefficients were determined by the equation $I(\lambda_{\max}^i)/I(\lambda_{\max}^{600 \text{ nm}})$ where I is the intensity at λ_{\max}^i and $I(\lambda_{\max}^{600 \text{ nm}})$ is the reference wavelength.

^b Ref. 25.

^c Ref. 35.

^d This work. The values of ϵ indicated in brackets were calculated assuming $\epsilon_{600}=780$ M⁻¹ cm⁻¹.

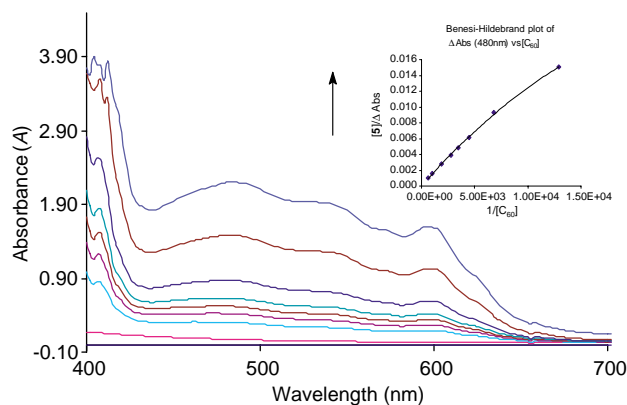


Figure 3. UV-vis titration curves showing the changes in absorption of **5** in toluene solution as a function of increasing $[C_{60}]$. Insert: double-reciprocal plot for the titration at $\lambda=430$ nm.

C_{60} are shown in Figure 3. The spectral data at $\lambda=430$ nm were subjected to the Benesi–Hildebrand analysis outlined in Section 2. Linear least-squares regression analysis of the double-reciprocal plot gave estimates of both the $\Delta\epsilon$ and the K_{ASSOC} values. Following the arguments of Berberan-Santos and the well-known difficulties of extracting $\Delta\epsilon$ and K_{ASSOC} values from double-reciprocal plots, our data were re-plotted according to the following equation (Eq. 4, in which $[H] = [5]$), which is the non-linear form from which the Benesi–Hildebrand equation was derived:

$$\Delta A = \frac{\Delta\epsilon_C K_{ASSOC} [5][C_{60}]}{1 + K_{ASSOC} [C_{60}]} \quad (4)$$

The values for $\Delta\epsilon_C$ ($1.32 \times 10^{-6} \text{ cm}^{-1} \text{ M}^{-1}$ at $\lambda=430$ nm) and K_{ASSOC} ($176 \pm 21 \text{ M}^{-1}$) estimated from the fits to the Benesi–Hildebrand equation, were used in this non-linear form to validate and ensure that the parameters made were not an artifact of extracting $\Delta\epsilon_{CT}$ and the K_{ASSOC} values solely from the fits to the double-reciprocal plots. The experimental data shown in Figure 4 and the resulting fit are in excellent agreement thereby validating the experimental data. Under similar conditions in CS_2 solution, however, as will be elaborated upon below, analysis of the data obtained

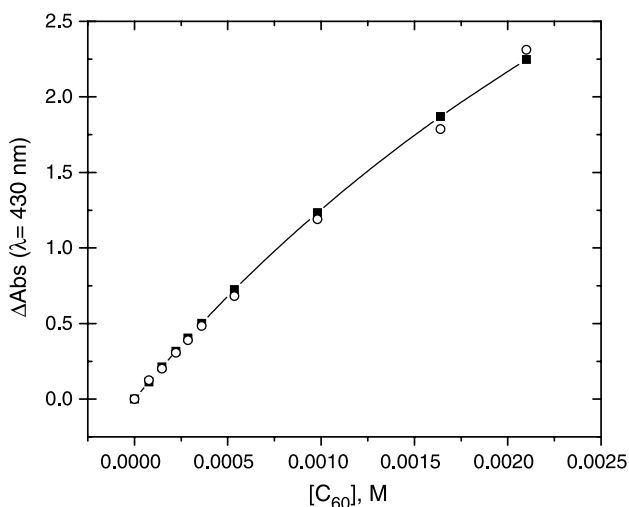


Figure 4. Plots of ΔA versus $[C_{60}]$: open circles = from observed data (from Fig. 3); filled squares = calculated from non-linear form of the Benesi–Hildebrand equation.

from the UV-vis titrations between C_{60} with **5** did not provide unequivocal evidence for complexation.

1H NMR spectroscopy. The titration experiments in which aliquots of C_{60} were added to solutions of **5** in toluene- d_8 , revealed that the chemical shifts of all of the proton signals were affected to some extent. The signals for the *tert*-butyl methyl groups, and the H-5 protons³¹ showed the largest relative changes, and were almost identical in magnitude (Fig. 5).

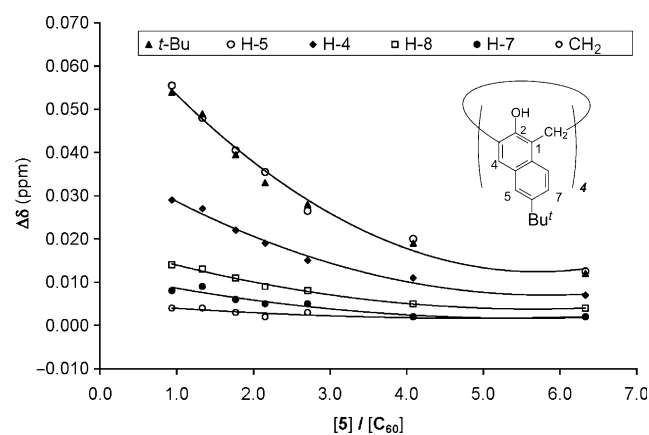


Figure 5. Plots of chemical shift changes ($\Delta\delta$) for protons on **5** in toluene- d_8 solution versus added C_{60} . Insert: formula of **5** showing the numbering of positions on the naphthyl ring sub-units.

Molecular mechanics³² modeling indicates that the fullerene is nestled deeply into the cavity formed by the naphthalene rings in **5** (Fig. 6). The *tert*-butyl groups tightly embrace the C_{60} molecule, with the closest average distances between a proton on a *tert*-butyl group, and a carbon atom of the fullerene being 3.21 Å. Furthermore, the naphthalene rings are tilted inwards towards the fullerene, with the H-5 protons being closer to the fullerene, than the other, H-7 protons, which are *ortho* to the *tert*-butyl groups. The closest average distances of the H-5 and H-7 protons to a carbon atom on the fullerene are 3.66 versus 4.37 Å, respectively. Therefore, the deshielding of the H-5 protons by the fullerene would be expected to be larger, and thus could account for the observed trends for these protons in the NMR data.

We previously reported similar observations from the complexation studies of C_{60} with **6**.¹⁹ Molecular mechanics modeling on the complex formed between C_{60} with **6** are in agreement with the actual X-ray structure of this complex,¹⁹ and show the close contacts between the *tert*-butyl methyl protons and the fullerene. The closest average distance from such protons to a carbon atom on the fullerene is 3.18 Å. An analysis by Shinkai et al.⁶ of other calixarene supramolecular complexes with C_{60} suggested that the presence of *tert*-butyl groups on such hosts appear to be one of the necessary prerequisites, confirming the importance of π - CH_3 interactions in these systems.

Based upon the largest $\Delta\delta$ values measured, which were those from the protons of the *tert*-butyl groups, the mean K_{ASSOC} value from duplicate determinations, for the complexation of C_{60} with **5** in toluene- d_8 at 298 K, was

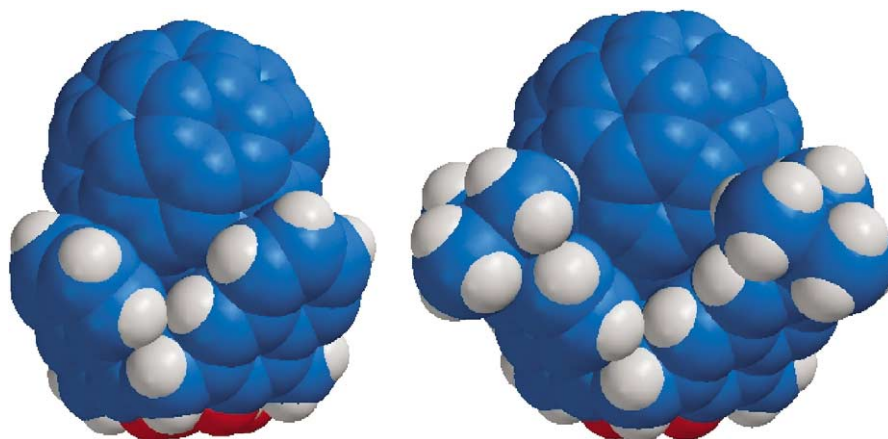


Figure 6. Computer-generated 1:1 supramolecular complexes of C₆₀ with **4** (left) and **5** (right).³²

Table 2. Association constants for the complexation behaviour of **5** with C₆₀ using the Foster–Fyfe treatment of the ¹H NMR data, as a function of temperature

Expt. #	K_{assoc}	r^2	T	$1/T(\times 10^3)$	$\log K_{\text{assoc}}$	$\ln K_{\text{assoc}}$
1	194.21	0.977	278	3.597	2.29	5.27
1	205.52	0.886	288	3.472	2.31	5.32
1	215.62	0.859	298	3.356	2.33	5.37
2	219.26	0.959	298	3.356	2.34	5.39
2	279.47	0.921	318	3.145	2.45	5.63
2	72.118	0.110	338	2.959	1.86	4.28
2	39.127	0.031	358	2.793	1.59	3.66

$217 \pm 44 \text{ M}^{-1}$. This value is in reasonable agreement with the corresponding K_{ASSOC} value obtained from the UV–vis absorption determinations ($176 \pm 21 \text{ M}^{-1}$ see above) obtained during this reinvestigation. Variable-temperature (VT) ¹H NMR spectra were determined in the same solvent and the results are summarized in Table 2. Figure 7 shows the temperature-dependence of the chemical shifts of the *tert*-butyl group protons of **5**. Analysis of the data using the Foster–Fyfe method described in Section 2 gave a direct measure of K_{ASSOC} for each of the temperatures indicated in Table 2. However, for the higher temperatures examined the fits using either the Benesi–Hildebrand, or Foster–Fyfe treatments are very poor. At higher temperatures it was observed that a dark red-brown precipitate formed over the course of the experiment. Therefore, the K_{ASSOC} values determined above 338 K should be viewed as lower, imprecise estimates of the true association constants.

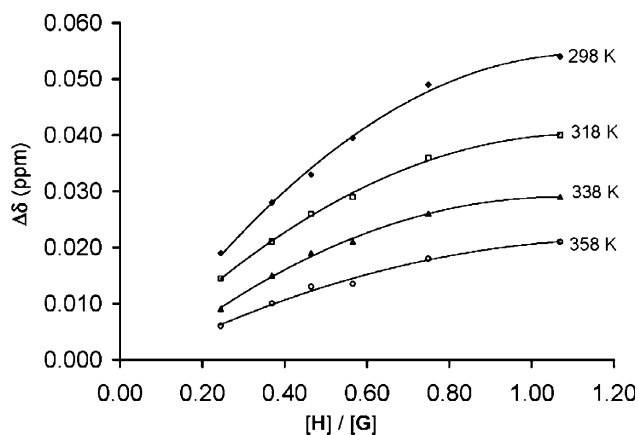


Figure 7. Changes in the chemical shifts of the *tert*-butyl group protons in **5** as a function of temperature.

The determination of the K_{ASSOC} values allows a direct measurement of the Gibbs free energy for complexation using $\Delta G^\circ = -RT \ln K_{\text{ASSOC}}$. The free energy of complexation as a function of temperature determined by ¹H NMR in this study are shown in Figure 8.

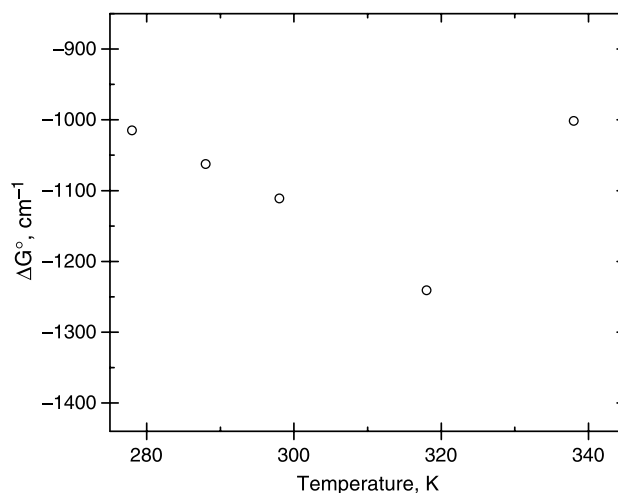


Figure 8. Scatter diagram showing ΔG° free energy of complexation of **5** with C₆₀ as a function of temperature determined by ¹H NMR in toluene-*d*₈.

As indicated previously, there was no unequivocal evidence for complexation between C₆₀ and **5** in CS₂ from UV–vis absorption determinations. Also, in contrast to the results obtained in toluene-*d*₈ solutions, addition of C₆₀ to solutions of **5** in CS₂ also did not reveal any discernable changes in the chemical shifts of any of its protons in the ¹H NMR titration experiments. A possible explanation for the lack of observed $\Delta\delta$ changes in the ¹H NMR titration experiment for **5** with C₆₀ in CS₂ may be that the aggregates of C₆₀,

which are known to form in this solvent may be too large to fit, or complex within the relatively small cavity of **5**. It should be noted, however, that in other cases, with different macrocyclic hosts, $\Delta\delta$ changes may be observed in both CS_2 and toluene- d_8 and that the phenomenon described in the present work is not necessarily a general one, for example, in complexation studies between C_{60} with some concave pentathio-substituted corannulene hosts recently reported by us, K_{ASSOC} values could be determined in both solvents.³³

Molecular mechanics modeling (Fig. 6) also suggested that 1:1 complexation between **4** and C_{60} was conceivable,³⁴ with the closest average distances of the H-5 and H-7 protons to a carbon atom on the fullerene in the C_{60} :**4** complex being very similar to those determined for the C_{60} :**5** complex, (i.e., 3.51 vs 3.66 Å, and 4.21 vs 4.37 Å, respectively), and the closest average distances of the H-6 protons being only approximately 3.74 Å. However, the titration experiments in either toluene- d_8 or CS_2 solution, revealed no discernable changes in the chemical shifts of any of its protons. Since **4** has no *tert*-butyl groups, these results support the contention that the π - CH_3 interactions are important for effective complexation with C_{60} . Another factor, which could account for the observed lack of complexation with **4** is suggested by its X-ray structure. We previously reported,²⁰ that the X-ray structure obtained from crystals of **4** formed from toluene solution, revealed that the unit cell contains two molecules of **4** packed in such a way that a naphthalene ring of one molecule is situated within the hydrophobic cavity of the other. Each of the molecules in this unit cell are in pinched-cone conformations, and three molecules of toluene surround the ‘supramolecular dimer’ in the solid state. Also, we have recently found that **4** shows excimer emission properties in toluene solution, which is evidence to suggest that such dimeric structures might also exist in solution,³⁵ which could be more competitive than complexation of C_{60} within the cavities of **4**.

Proposed mechanism of complexation. It should be noted that several factors must be taken into account when cross-comparing spectroscopic techniques for the determination of association constants. The chemical behaviour of the complexes under study and their temperature-dependence often play an important role. In the most straightforward case, where the complexes are soluble over the entire temperature range being examined, and where the spectroscopic probes used to evaluate the association constants are probing the same chemical process, the analysis of the temperature-dependent data is simple and should yield comparable results, within experimental error. In this study, this is clearly not the case, and a detailed analysis of all temperature-dependent processes and chemical properties must be undertaken. In the analysis outlined below, the properties of the compounds examined in this study, as a function of temperature, will be examined and the chemical dynamics, which are often ignored and that could be occurring with this, and similar systems, will be presented. Scheme 1 outlines a possible kinetic scheme for processes that accrue prior to and during, the 1:1 supramolecular complexation.

The proposed mechanism is comprised of at least seven identifiable chemical processes, each governed by 2 rate constants and an equilibrium constant. Therefore, each process displays its own temperature-dependence, and consequently the spectroscopic signatures of complexation will be temperature-dependent. In the kinetic limit where aggregation of C_{60} is minimal, and the solvation of conformational isomers, their interconversion, and the desolvation of their cavities are kinetically fast, complexation becomes the rate determining step. In such a case, the extraction of supramolecular binding constants from UV-vis data and ^1H NMR data should agree within experimental error. In many instances, this is not the case. On the other-hand, the ^1H NMR determination for supramolecular complexation is specific for only one of these processes, namely process ‘(vi)’ where

	Process	Equilibrium	Equilibrium constant
(i)	Solvation of C_{60}	$\text{C}_{60} + n\text{S} \xrightleftharpoons[k_{-1}]{k_1} \text{C}_{60}(\text{S})_n$	$K_1 = \frac{k_1}{k_{-1}} = \frac{[\text{C}_{60}\text{S}_n]}{[\text{C}_{60}][\text{S}]^n}$
(ii)	Aggregation	$n\text{C}_{60} \xrightleftharpoons[k_a^r]{k_a^f} (\text{C}_{60})_n$	$K_{\text{agg}} = \frac{k_a^f}{k_a^r} = \frac{[(\text{C}_{60})_n]}{[\text{C}_{60}]^n}$
(iii)	Solvation of conformational isomers	$5^i + n\text{S} \xrightleftharpoons[k_{-2}]{k_2} 5^i(\text{S})_n$	$K_2 = \frac{k_2}{k_{-2}} = \frac{[5^i\text{S}_n]}{[5^i][\text{S}]^n}$
(iv)	Interconversion of isomers	$5^i(\text{S})_n \xrightleftharpoons[k_i^r]{k_i^f} 5^c(\text{S})_x + (n-x)\text{S}$	$K_{\text{int}} = \frac{k_i^f}{k_i^r} = \frac{[5^c\text{S}_x][\text{S}]^{n-x}}{[5^i\text{S}_n]}$
(v)	Desolvation of cavity	$5^c(\text{S})_x \xrightleftharpoons[k_{+s}]{k_{-s}} 5^c + x\text{S}$	$K_s = \frac{k_{-s}}{k_{+s}} = \frac{[5^c][\text{S}]^x}{[5^c\text{S}_x]}$
(vi)	Complexation of C_{60}	$5^c + \text{C}_{60} \xrightleftharpoons[k_c^r]{k_c^f} \{5^c//\text{C}_{60}\}$	$K_{\text{assoc}} = \frac{k_c^f}{k_c^r} = \frac{[\{5^c//\text{C}_{60}\}]}{[5^c][\text{C}_{60}]}$
(vii)	Precipitation	$\{5^c//\text{C}_{60}\} \xrightleftharpoons{K_{\text{sp}}} \{5^c//\text{C}_{60}\}_{\text{ppt}}$	

Scheme 1. Kinetics and thermodynamics for supramolecular complexation of, for example, **5** and its conformational isomers, 5^i with C_{60} in a solvent (S).

chemical shift differences due to complexes can be discerned. Conversely, steady-state UV–vis spectroscopic methods are sensitive to all of the processes outlined in Scheme 1 except for the interconversion of the conformational isomers and desolvation of their cavities, which would require time-resolved spectroscopic methods to discern. The work of Berberan-Santos²⁹ and Catalan³⁶ showed that the solvation environment around C₆₀ has a profound visible spectroscopic effect in the $\lambda=400\text{--}520$ nm range, wavelengths which are often used to extract absorption changes used to determine binding constants. Great care must be taken to ascertain the absorption spectroscopic behaviour of C₆₀ to ensure that the spectral changes are indeed attributable to complexation, and are not due to some of the other processes, which may be occurring. For example, C₆₀ is known to aggregate in CS₂ giving rise to increased absorptivity that has nothing to do with host–guest types of complexation. In fact, aggregation may compete with host–guest complexation and the magnitude of the apparent binding constant will be governed by the equilibrium constant of aggregation as well as by the K_{ASSOC} for the host–guest complexation.²⁸ Furthermore, precipitation of the host–guest adduct is also particularly problematic because the precipitate may not be too perceptible to the human eye but will result in light scattering, whose contribution to the absorption spectrum increases with decreasing wavelength. This results in a sloping baseline, which cannot often be detected underneath the complex absorption band manifolds that are produced during a titration experiment, in particular with respect to C₆₀ in CS₂.³⁷

4. Summary and conclusions

The fact that we had previously concluded that calixnaphthalene **4** did show simple 1:1 complexation behaviour as determined by absorption spectroscopy, perhaps could be due several factors, including the conditions employed, and a misinterpretation that the absorbance changes at 430 nm were only due to complex formation. This will require further evaluation and we are seeking to address this question in due course. It should be noted for example, that Tucci et al. in their 1999 paper¹⁴ also found a discordance between their absorption data based upon absorbance changes at 430 nm, and ¹H NMR data for one of their deep-cavitand molecules with C₆₀ in toluene solution.

Acknowledgements

The authors thank the Natural Sciences and Engineering Research Council of Canada (NSERC) and Memorial University of Newfoundland (M.U.N.). The authors also thank Adam Bishop (M.U.N.) for his contributions in the analysis of spectral data.

References and notes

- Diederich, F.; Gomez-Lopez, M. *Chem. Soc. Rev.* **1999**, *28*, 263–277.
- For recent monographs see: (a) Gutsche, C. D. In *Calixarenes Revisited*; Stoddard, J. F., Ed.; Monographs in Supramolecular Chemistry; Royal Society of Chemistry: Cambridge, 1998. (b) *Calixarenes in Action*; Mandolini, L., Ungaro, R., Eds.; Imperial College: London, England, 2000. (c) *Calixarenes 2001*; Asfari, Z., Böhmer, V., Harrowfield, J., Eds.; Kluwer Academic: Dordrecht, 2001.
- Williams, R. M.; Verhoeven, J. W. *Recl. Trav. Chim. Pays-Bas* **1992**, *111*, 531–532.
- Atwood, J. L.; Koutsoantonis, G. A.; Raston, C. L. *Nature* **1994**, *368*, 229.
- Suzuki, T.; Nakashima, K.; Shinkai, S. *Chem. Lett.* **1994**, 699–702.
- Zhong, Z.-L.; Ikeda, A.; Shinkai, S. In *Calixarenes 2001*; Asfari, Z., Böhmer, V., Harrowfield, J., Vicens, J., Eds.; Kluwer Academic: Dordrecht, 2001; Chapter 26, pp 476–495.
- Georghiou, P. E.; Mizyed, S.; Chowdhury, S. *Tetrahedron Lett.* **1999**, *40*, 611–614.
- Georghiou, P. E.; Miller, D. O.; Tran, A. H.; Al-Saraierh, H.; Li, Z.; Ashram, M.; Chowdhury, S.; Mizyed, S. *Synlett* **2005**, *6*, 879–891.
- For an insightful discussion on $\pi\text{--}\pi^*$ interactions, see: Hunter, C. A.; Saunders, J. K. M. *J. Am. Chem. Soc.* **1990**, *112*, 5525–5534.
- Haino, T.; Yanase, M.; Fukazawa, Y. *Angew. Chem., Int. Ed.* **1997**, *36*, 259–260.
- Haino, T.; Yanase, M.; Fukazawa, Y. *Angew. Chem., Int. Ed.* **1998**, *37*, 997–998.
- Tsubaki, K.; Tanaka, K.; Kinoshita, T.; Fuji, K. *Chem. Commun.* **1998**, *37*, 895–896.
- Ikeda, A.; Yoshimura, M.; Shinkai, S. *Tetrahedron Lett.* **1997**, *38*, 2107–2110.
- Tucci, F. C.; Rudkevitch, D. M.; Rebek, J. *J. Org. Chem.* **1999**, *64*, 4555–4559.
- Korobov, M. V.; Smith, A. L. In *Fullerene: Chemistry, Physics and Technology*; Kadish, K. M., Ruoff, R. S., Eds.; Wiley: New York, 2000; pp 55–56.
- Fielding, L. *Tetrahedron* **2000**, *56*, 6151–6170.
- Bhattacharya, S.; Nayak, S. K.; Chattopadhyay, S.; Banerjee, M.; Mukherjee, A. K. *J. Chem. Soc., Perkin Trans. 2* **2001**, 2292–2297 and references therein.
- Bhattacharya, S.; Nayak, S. K.; Chattopadhyay, S.; Banerjee, M.; Mukherjee, A. K. *J. Phys. Chem. B* **2003**, *107*, 11830–11834 and references therein.
- Mizyed, S.; Ashram, M.; Miller, D. O.; Georghiou, P. E. *J. Chem. Soc., Perkin Trans. 2* **2001**, 1916–1919.
- Georghiou, P. E.; Ashram, M.; Clase, H. J.; Bridson, J. N. *J. Org. Chem.* **1998**, *63*, 1819–1826.
- (a) Benesi, H. A.; Hildebrand, J. H. *J. Am. Chem. Soc.* **1949**, *71*, 2703–2707. (b) Traylor, T. J.; Tsuchiya, S.; Campbell, D.; Mitchell, M.; Stynes, D.; Koga, N. *J. Am. Chem. Soc.* **1985**, *107*, 604–614.
- (a) Tsubake, H.; Furuta, H.; Odani, A.; Takeda, Y.; Kudo, Y.; Liu, Y.; Sakamoto, H.; Kimura, K. In Davies, J. E. D., Ripmeester, J. A., Eds.; *Comprehensive Supramolecular Chemistry*; Elsevier Science: Oxford, 1996; Vol. 8, pp 425–482. (b) Connors, K. A. *Binding Constants*; Wiley: New York, 1987.
- Foster, R.; Fyfe, C. A. *J. Chem. Soc., Chem. Commun.* **1965**, 642. For a discussion of the relative advantages of employing the Foster–Fyfe modification to the Benesi–Hildebrand treatment of complexation data obtained from ¹H NMR studies see Ref. 16.
- Hirose, K. *J. Inc. Phenom.* **2001**, *39*, 193–209.
- Leach, R.S.; Tse, D. S.; Despres, A.; Breheret, E.; Hare, J. P.; Dennis, T. J.; Kroto, H. W.; Taylor, R.; Walton, D. R. M. *Chem. Phys.* **1992**, *160*, 451.

26. Gallagher, S. H.; Armstrong, R. S.; Lay, R. A.; Reed, C. A. *J. Phys. Chem.* **1995**, *99*, 5817–5825.
27. Tolbert, L. M.; Solntsev, K. M. *Acc. Chem. Res.* **2002**, *35*, 19–27.
28. Atwood, J. L.; Barnes, M. J.; Gardiner, M. G.; Raston, C. L. *Chem. Commun.* **1996**, 1449–1450.
29. During the course of this study, similar findings were reported by Sarova, G.; Berberan-Santos, M. N. *J. Phys. Chem. B.* **2004**, *108*, 17261–17268.
30. Scurlock, R. D.; Ogilby, P. R. *J. Photochem. Photobiol., A* **1995**, *91*, 21–25.
31. The numbering for the protons are based upon the naphthalene ring numbering system.
32. Molecular modeling was conducted using Spartan'04 Windows version 1.0.3 Molecular Modeling Software from Wavefunction Inc., Irvine, CA, USA. Molecular mechanics (MMFF94) calculations were conducted on the optimized geometry of the host and/or complexes.
33. (a) Mizyed, S.; Georghiou, P. E.; Bancu, M.; Cuadra, B.; Rai, A. K.; Cheng, P.; Scott, L. T. *J. Am. Chem. Soc.* **2001**, *123*, 12770–12774. (b) Georghiou, P. E.; Tran, A. H.; Mizyed, S.; Bancu, M.; Scott, L. T. *J. Org. Chem.* **2005**, *70*, 6158–6163.
34. For a similar absence of experimental evidence for complexation behaviour with C₆₀ for a different naphthalene-ring based molecular receptor lacking *tert*-butyl substituents, which we have recently studied, see: Tran, A. H.; Miller, D. O.; Georghiou, P. E. *J. Org. Chem.* **2005**, *70*, 1115–1121.
35. Thompson, D. W.; Bishop, A.; El-Dali, A. Unpublished observations.
36. Catalan, J.; Saiz, J. L.; Laynez, J. L.; Jagerovic, N.; Elguero, J. *Angew. Chem., Int. Ed. Engl.* **1995**, *34*, 105–107.
37. Bokare, A. D.; Patnaik, A. *J. Phys. Chem. B* **2003**, *107*, 6079–6086.

Synthesis of water-soluble 2-alkylcyclodextrin–C₆₀ conjugates and their inclusion complexation in aqueous solution

Yong Chen,^a Yali Wang,^a André Rassat,^{a,†} Pierre Sinay,^a Yu Zhao^b and Yongmin Zhang^{a,b,*}

^aEcole Normale Supérieure, Département de Chimie, associé au CNRS, 24 rue Lhomond, 75231 Paris Cedex 05, France

^bZJU-ENS Joint Laboratory of Medicinal Chemistry, Zhejiang University, Hangzhou 310031, China

Received 14 June 2005; revised 2 September 2005; accepted 4 September 2005

Available online 2 December 2005

Abstract—Two β -cyclodextrin–C₆₀ conjugates (**3** and **4**) with a flexible linker at the secondary face of cyclodextrin are synthesized by a single reaction of 2-(ω -azidoundecanyl)-2-*O*-heptakis (2,3,6-tri-*O*-methyl)- β -cyclodextrin (**2**) and C₆₀, both of which display satisfactory water solubility. Structural analyses show that **3** is a closed [5,6] aziridinofullerene, whereas **4** is a bis-adduct derivative. Using rhodamine B (RhB) as a guest molecule, the inclusion complexation behavior of **3** was investigated in aqueous solution.

© 2005 Elsevier Ltd. All rights reserved.

1. Introduction

Water-soluble fullerenes have recently become an important topic because of their potential biological applications,¹ such as the DNA-cleaving ability and anti-HIV activity.² In particular, a number of water-soluble cyclodextrin–fullerene conjugates have been synthesized.^{3,4} We recently prepared novel 2:1 cyclodextrin–fullerene conjugates, which were highly water-soluble.^{5,6} In order to see the influence of the number of cyclodextrin on solubility, we have searched for a 1:1 cyclodextrin–fullerene conjugate using the aziridinofullerene approach.^{7,8}

2. Results and discussion

The cyclodextrin linker, 2-(ω -azidoundecanyl)-2-*O*-heptakis (2,3,6-tri-*O*-methyl)- β -cyclodextrin **2**,⁶ readily prepared from permethylated β -cyclodextrin **1**, was reacted with C₆₀ under standard conditions.⁷ Two products were isolated: **3** and **4** with 31 and 15% yield, respectively (Scheme 1). According to MALDI-TOF MS, **3** was a monoadduct (peak at 2325 [M+Na⁺]) and **4** a bis-adduct (peak at 3906 [M+Na⁺]).

In principle, four isomers could be formed by monoaddition of alkyl azide on C₆₀, the bridge nitrogen spanning over either a 5,6-ring or a 6,6-ring junction, each giving either ‘closed’ or ‘open’ adducts. ¹³C NMR spectra provide

additional information: the C_s symmetry of [5,6] adducts should divide the 60 carbons into 32 different types, while the C_{2v} symmetry of [6,6] adducts reduces this number to 17.⁹ In the present case, the ¹³C NMR spectra of **3** and **4** both show more than 30 signals within the range of δ 130–150 ppm, thus indicating a symmetry lower than C_{2v}.

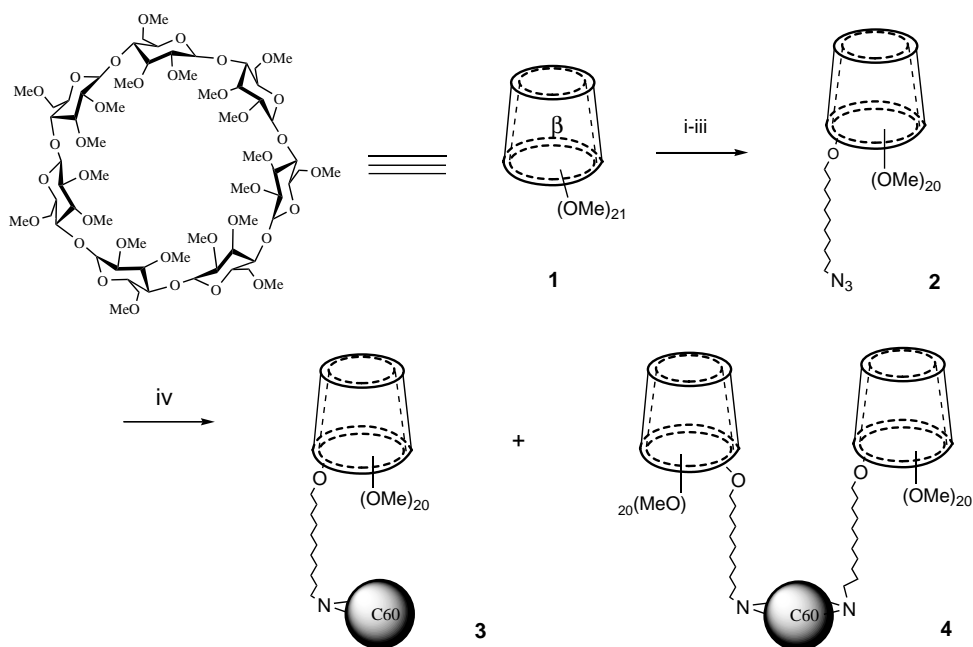
The ¹³C NMR (DEPT) of **3** displays a signal at δ 70.90 ppm, that can be assigned to sp³ carbons, and indicating a ‘closed’ conformation of the C₆₀ sphere. Compound **3** is thus a closed [5,6] adduct. This was contrary to our expectation: it is well established in the literature that addition of alkyl azide yields the (open) [5,6] fulleroid and the (closed) [6,6] fullerene adduct.⁸

To our knowledge, there are only two bona fide reports in the literature (both from Sinyashin’s group),^{10,11} on the formation of closed [5,6] adducts. The authors studied the addition to C₆₀ of isocyanuratoalkyl azides with different methylene chains and found that ‘the type of monoadducts...is determined by not only the reaction temperature but also the number of methylene units in the alkyl groups in the azide’: by reacting isocyanuratoalkyl azides with 3–6 methylene units, at 100 °C, closed [5,6] adducts were obtained. In our case, the addition reaction was performed in refluxing chlorobenzene at 131 °C, and there were 11 methylene groups in the azidocompound, thus extending Sinyashin et al. results. In order to confirm the influence of the chain length, we studied the addition to C₆₀ of 11-azidoundecanyl tosylate **5** under the same conditions. This reaction gave two compounds: **6** (12%) and **7** (9%), as shown in Scheme 2.

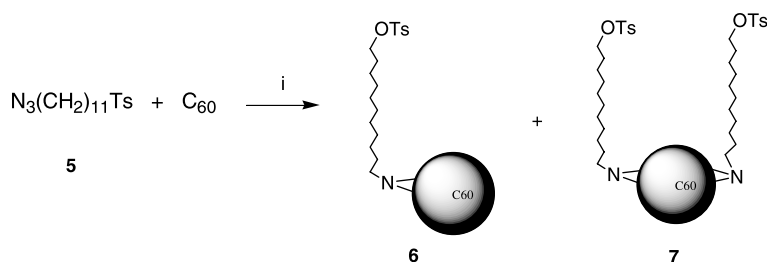
Keywords: Fullerene; C₆₀; Cyclodextrin; Conjugate; Rhodamine B.

* Corresponding author. Tel.: +33 1 44323335; fax: +33 1 44323397; e-mail: yongmin.zhang@ens.fr

† Deceased July 16, 2005.



Scheme 1. Reagents and conditions: (i) DIBAL, toluene, 0 °C, 18 h (56%); (ii) $\text{N}_3(\text{CH}_2)_{11}\text{OTs}$, NaH, DMF, 80 °C, 15 h (71%); (iii) CH_3I , NaH, THF, 66 °C, 5 h (70%); (iv) C_{60} , chlorobenzene, 131 °C, 48 h: **3** (31%), **4** (15%).



Scheme 2. Reagent and condition: (i) Chlorobenzene, 131 °C, 23 h: **6** (12%), **7** (9%).

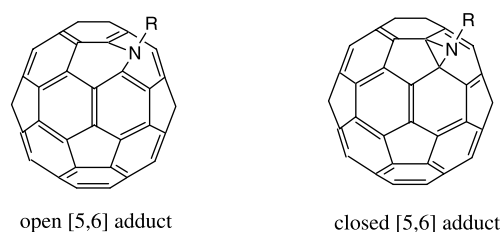
The MALDI-TOF MS showed peaks at 1060 $[\text{M}+\text{H}^+]$, 1082 $[\text{M}+\text{Na}^+]$ for **6**, indicating a monoadduct, whereas peaks at 1399 $[\text{M}+\text{H}^+]$ and 1421 $[\text{M}+\text{Na}^+]$ for **7**, indicating a bis-adduct.

The ^{13}C NMR spectrum of **6** shows more than 30 signals within the range of δ 130–150 ppm, thus indicating a symmetry lower than C_{2v} , and a signal at δ 70.68 ppm, assigned to sp^3 carbons, indicating again a ‘closed’ conformation of the C_{60} sphere.

Thus, these results show at 131 °C addition of azides with $(\text{CH}_2)_{11}$ chain yield closed [5,6] adduct (Scheme 3).

On the other hand, the structures of bis-adducts **4** and **7** have not been determined: the ^{13}C NMR spectrum of **4** and **7** both show more than 30 signals within the range of δ 130–150 ppm, thus indicating a symmetry lower than C_2 , and two signals at 164.59 and 70.86 for **4** and at 164.56 and 70.68 for **7**, respectively. This indicates the presence of both an open and a closed adducts, but the symmetry does not give further information.

The cyclodextrin–fullerene conjugates are soluble in water: clear solution were obtained after dissolving in water



Scheme 3. Two types of [5,6] adduct.

(100 μL) 1 mg of **3** and 12 mg for **4**, giving solubilities of 10 and 120 mg/mL, respectively. This last value is comparable with those of the previously reported 2:1 cyclodextrin–fullerene conjugates,^{5,6} but the 1:1 conjugate is much less soluble.

Following Yuan et al.,⁹ we studied the association of RhB with **3** in aqueous buffer solution (pH 7.20) using fluorescence spectroscopy. These authors used a related cyclodextrin–fullerene conjugate, the main differences being a very short linker, an open [5,6] structure and a peracetyl cyclodextrin moiety. They found that when gradually adding the cyclodextrin– C_{60} conjugate to a RhB

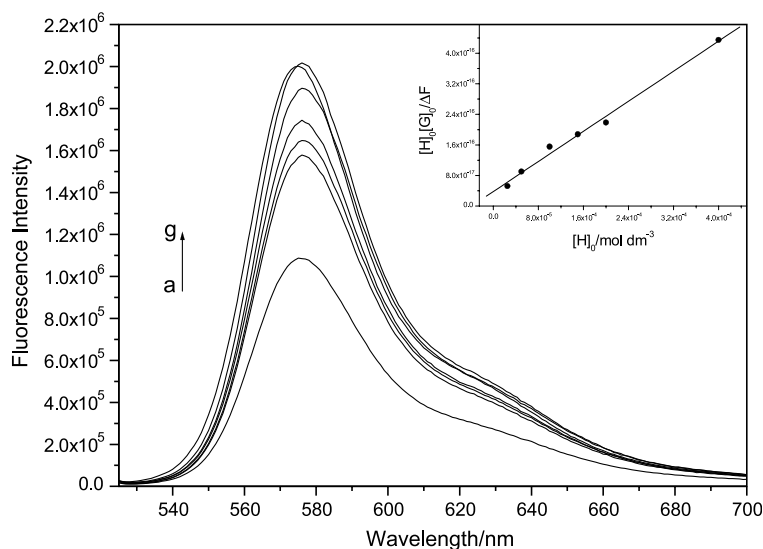


Figure 1. Fluorescence spectra of RhB (1.0×10^{-6} M) in the presence of (a) 0, (b) 25, (c) 50, (d) 100, (e) 150, (f) 200 and (g) 400 equiv of **3**. The inset represents the linear analysis to calculate the complex stability constants.

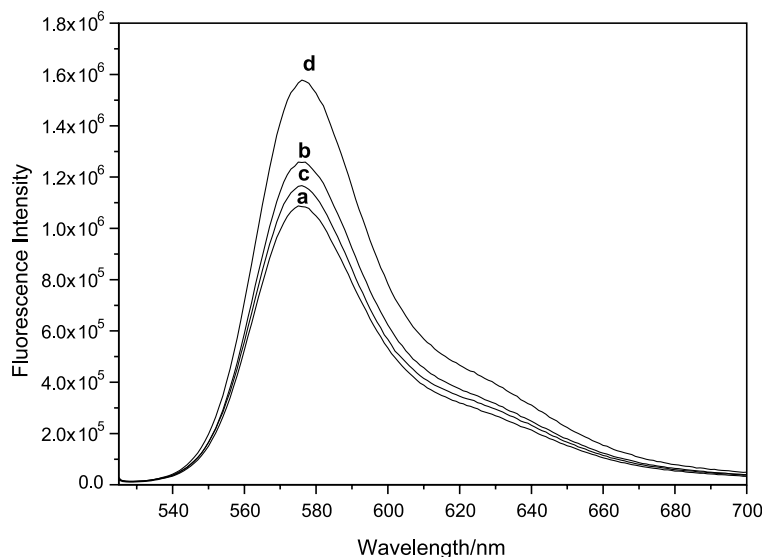


Figure 2. Fluorescence spectra of RhB (1.0×10^{-6} M) in aqueous buffer solution, in the absence (a) and in the presence of 25 equiv of (b) **1**, (c) **2** and (d) **3**.

solution, the fluorescence of RhB decreases. In our case, as illustrated in Figure 1, the fluorescence is enhanced when the concentration of **3** increases.

Furthermore, the fluorescence enhancement in presence of **3** is much stronger than with **1** and **2** (Fig. 2). Since it is generally agreed that the fluorescence of RhB is quenched by the hydrogen bonds of water,¹¹ this increase of fluorescence may be attributed to an efficient shielding induced by **3**.

Different tentative interpretations are possible. If a 1:1 complexation model is assumed, the association constant (K_s) of this equilibrium can be determined by spectral titration. A K_s value of 25700 M^{-1} is obtained. It is fairly larger (by a factor of > 4) than those for **1** (6010 M^{-1}) and **2** (1470 M^{-1}), and for the complexation of Yuan's compound with RhB, for which a much lower K_s (2800 M^{-1}) is reported.⁹ This suggests a special type of complexation,

possibly a cooperative effect involving C_{60} . However, another interpretation can be put forward: because of its structure, **3** could easily form micelle in water solution, and as the concentration of **3** increases, RhB is more 'buried' in the hydrophobic pocket of the micelle. The presence of C_{60} could also play a role. Further work is necessary for a definitive interpretation.

3. Conclusion

We have synthesized a new CD- C_{60} conjugate **3** with the following features: a closed [5,6] aziridino structure, and a connection through a C_{11} methylene chain to the secondary rim of CD. The unexpected occurrence of the closed [5,6] structure confirms the results of Sinyashin et al. This new conjugate is water soluble, but less than related bis-adducts, such as **4**. The fluorescence properties of the complex **3** with RhB need further investigation.

4. Experimental

4.1. General procedures

Optical rotations were measured at 20 ± 2 °C with a Perkin Elmer Model 241 digital polarimeter, using a 10 cm, 1 mL cell. MALDI-TOF Mass spectra were recorded with a perSeptive Biosystems Voyager Elite (Framingham MA-USA) time of flight mass spectrometer. This instrument was equipped with a nitrogen laser (337 nm), a delayed extraction, and a reflector. PEG Standards were used to calibrate the mass scale with the two-points calibration software 3.07.1 from Sigma (France) and used without further purification. Elemental analyses were performed by Service de Microanalyse de l'Université Pierre et Marie Curie, 4 Place Jussieu, 75005 Paris, France. NMR spectra were recorded on a Bruker DRX 400 spectrometer at ambient temperature. ^1H NMR chemical shifts are referenced to residual protic solvent (CDCl_3 , $\delta_{\text{H}} = 7.30$) or the internal standard TMS ($\delta_{\text{H}} = 0.00$). ^{13}C NMR chemical shifts are referenced to the solvent signal ($\delta_{\text{C}} = 77.0$ for the central line of CDCl_3). Reactions were monitored by thin-layer chromatography (TLC) on a pre-coated silica gel 60 F₂₅₄ plate (layer thickness 0.2 mm; Merck, Darmstadt, Germany) and detection by charring with sulphuric acid. Flash column chromatography was performed on silica gel 60 (230–400 mesh, Merck).

4.1.1. CD-C₆₀ conjugates 3 and 4. 2-(ω -Azidoundecanyl)-2-*O*-heptakis(2,3,6-tri-*O*-methyl)- β -cyclodextrin **2** (157 mg, 0.096 mmol) and C₆₀ (46.8 mg, 0.065 mmol, 0.67 equiv) were dissolved in chlorobenzene (36 mL), and the reaction mixture was refluxed in the dark under argon until the increase of product ceased (48 h), as monitored by TLC. After removing the solvent in vacuum, the residue was chromatographed on a silica gel column. The column was first eluted with toluene to give un-reacted C₆₀, and then with cyclohexane–acetone (3/2, v/v) to afford the CD-C₆₀ conjugates **3** and **4** in 31 and 15% yield, respectively.

Analytical data for 3. R_f 0.57 for TLC (cyclohexane/acetone, 3:2); $[\alpha]_{\text{D}}^{23} + 4$ (c 1.0 in CHCl_3); UV–vis (CH_2Cl_2): λ_{max} (ϵ) = 262 nm ($2.24 \times 10^5 \text{ mol}^{-1} \text{ dm}^3 \text{ cm}^{-1}$), 326 nm ($6.92 \times 10^4 \text{ mol}^{-1} \text{ dm}^3 \text{ cm}^{-1}$); MALDI-TOF MS m/z 2325 ($\text{M} + \text{Na}^+$); ^1H NMR (400 MHz, CDCl_3 , TMS) δ 1.28–1.40 (m, 18H), 3.21–3.98 (m, 106H), 5.09 (d, $J = 3.42$ Hz, $1 \times \text{H}_1$), 5.15 (2d, $J = 3.57$ Hz, $2 \times \text{H}_1$), 5.17–5.20 (m, $4 \times \text{H}_1$); ^{13}C NMR (100 MHz, CDCl_3 , TMS) δ 25.93, 27.27, 29.46, 29.50, 29.61, 29.73, 30.01 ($9 \times \text{CH}_2$), 51.64 ($1 \times \text{CH}_2\text{N}$), 58.31, 58.37, 58.47, 58.56, 58.58, 58.61, 58.88, 58.91, 61.30, 61.36, 61.46, 61.61 ($20 \times \text{OCH}_3$), 70.72, 70.79, 70.86, 70.88, 70.99 ($7 \times \text{C}_5$), 70.90 ($2 \times \text{sp}^3 \text{ C}$), 71.14, 71.22, 71.24, 71.32, 71.40, 71.46, 71.49 ($7 \times \text{C}_6$), 79.79, 79.90, 79.98, 80.02, 80.07, 80.14, 80.35, 80.37, 80.85, 81.52, 81.59, 81.62, 81.65, 81.73, 81.75, 81.89, 81.92, 82.01 ($7 \times \text{C}_2$, $7 \times \text{C}_3$, $7 \times \text{C}_4$), 98.82, 98.84, 98.91 ($7 \times \text{C}_1$), 133.62, 135.73, 136.08, 137.09, 137.22, 137.72, 137.89, 138.39, 139.08, 140.62, 141.34, 142.52, 142.70, 142.79, 142.92, 142.99, 143.09, 143.43, 143.54, 143.74, 144.05, 144.07, 144.17, 144.23, 144.35, 144.45, 144.64, 144.96, 145.33, 147.01, 147.74 (C₆₀). Anal. Calcd for C₁₃₃H₁₃₁O₃₅N·3H₂O: C, 67.50; H, 5.88; N, 0.59. Found: C, 67.84; H, 6.54; N, 0.54.

Analytical data for 4. R_f 0.40 for TLC (cyclohexane/acetone, 3:2); $[\alpha]_{\text{D}}^{23} + 5$ (c 1.0 in CHCl_3); UV–vis (CH_2Cl_2): λ_{max} (ϵ) = 262 nm ($2.38 \times 10^5 \text{ mol}^{-1} \text{ dm}^3 \text{ cm}^{-1}$), 326 nm ($7.37 \times 10^4 \text{ mol}^{-1} \text{ dm}^3 \text{ cm}^{-1}$); MALDI-TOF MS m/z 3906 ($\text{M} + \text{Na}^+$); ^1H NMR (400 MHz, CDCl_3 , TMS) δ 1.28–1.45 (m, 36H), 3.20–4.09 (m, 106H), 5.09 (2d, $J = 3.32$ Hz, $2 \times \text{H}_1$), 5.15 (4d, $J = 3.5$ Hz, $4 \times \text{H}_1$), 5.17–5.19 (m, $8 \times \text{H}_1$); ^{13}C NMR (100 MHz, CDCl_3 , TMS) δ 25.98, 27.32, 29.47, 29.54, 29.57, 29.64, 29.66, 29.69, 30.05 ($18 \times \text{CH}_2$), 51.69 ($2 \times \text{CH}_2\text{N}$), 58.36, 58.41, 58.53, 58.62, 58.64, 58.93, 58.96, 61.35, 61.39, 61.50, 61.52, 61.67 ($40 \times \text{OCH}_3$), 70.76, 70.83, 70.91, 70.92, 71.03 ($14 \times \text{C}_5$), 71.17, 71.26, 71.28, 71.36, 71.42, 71.44 ($14 \times \text{C}_6$), 79.83, 79.94, 80.02, 80.11, 80.18, 80.22, 80.40, 80.42, 80.91, 81.51, 81.62, 81.66, 81.69, 81.77, 81.79, 81.92, 81.96, 82.05 ($14 \times \text{C}_2$, $14 \times \text{C}_3$, $14 \times \text{C}_4$), 98.88, 98.90, 98.97 ($14 \times \text{C}_1$), 130.51, 131.91, 132.98, 134.51, 135.11, 137.16, 138.79, 138.91, 139.25, 139.49, 141.49, 141.59, 141.95, 142.66, 143.26, 143.52, 143.66, 143.90, 143.93, 143.97, 144.03, 144.07, 144.13, 144.49, 144.55, 144.83, 144.91, 145.05, 145.38, 145.45, 146.84, 147.62 (C₆₀). Anal. Calcd for C₂₀₆H₂₆₂O₇₀N₂·3H₂O: C, 62.79; H, 6.85; N, 0.71. Found: C, 62.76; H, 7.09; N, 0.51.

4.1.2. Tosylate-C₆₀ conjugates 6 and 7. 11-Azidoundecanyl tosylate **5** (90 mg, 0.24 mmol) and C₆₀ (114 mg, 0.16 mmol, 0.67 equiv) were dissolved in chlorobenzene (60 mL), and the reaction mixture was refluxed in the dark under argon until the increase of product ceased (23 h), as monitored by TLC. After removing the solvent in vacuum, the residue was chromatographed on a silica gel column. The column was eluted with cyclohexane–dichloromethane (1/1, v/v) to afford the **6** and **7** in 12 and 9% yield, respectively.

Analytical data for 6. R_f 0.40 for TLC (cyclohexane/dichloromethane, 1:1); $[\alpha]_{\text{D}}^{23} - 7$ (c 1.2 in CHCl_3); UV–vis (CH_2Cl_2): λ_{max} (ϵ) = 260 nm ($4.5 \times 10^5 \text{ mol}^{-1} \text{ dm}^3 \text{ cm}^{-1}$), 330 nm ($1.2 \times 10^5 \text{ mol}^{-1} \text{ dm}^3 \text{ cm}^{-1}$); MALDI-TOF MS m/z 1060.20 ($\text{M} + \text{H}^+$), 1082.17 ($\text{M} + \text{Na}^+$); ^1H NMR (400 MHz, CDCl_3): δ 1.28–1.45 (m, 18H, $9 \times \text{CH}_2$), 2.49 (s, 3H, CH_3), 3.84 (t, 2H, $J = 7.2$ Hz, N-CH_2), 4.07 (t, 2H, $J = 6.4$ Hz, O-CH_2), 7.38 (d, 2H, $J = 8.1$ Hz, arom.H), 7.83 (d, 2H, $J = 8.2$ Hz, arom.H); ^{13}C NMR (100 MHz, CDCl_3): δ 21.65 (CH_3), 25.34, 27.27, 28.83, 28.94, 29.38, 29.42, 29.45, 29.53, 29.58, 29.68 (9C , $9 \times \text{CH}_2$), 51.68 (N-CH_2), 70.68 ($\text{SO}_2\text{-CH}_2$), 127.87 (2C, arom.C), 129.78 (2C, arom.C), 133.25, 133.71, 135.82, 136.17, 137.20, 137.27, 137.81, 137.98, 138.48, 139.17, 140.71, 141.41, 142.60, 142.70, 142.78, 142.88, 143.08, 143.19, 143.37, 143.63, 143.82, 144.14, 144.27, 144.31, 144.44, 144.54, 144.58, 144.72, 145.03, 147.05, 147.81 (C₆₀).

Analytical data for 7. R_f 0.08 for TLC (cyclohexane/dichloromethane, 1:1), 0.36 for TLC (cyclohexane/dichloromethane, 1:2); $[\alpha]_{\text{D}}^{23} - 4$ (c 0.8 in CHCl_3); UV–vis (CH_2Cl_2): λ_{max} (ϵ) = 260 nm ($8.4 \times 10^5 \text{ mol}^{-1} \text{ dm}^3 \text{ cm}^{-1}$), 330 nm ($2.9 \times 10^5 \text{ mol}^{-1} \text{ dm}^3 \text{ cm}^{-1}$); MALDI-TOF MS m/z 1399.46 ($\text{M} + \text{H}^+$), 1421.56 ($\text{M} + \text{Na}^+$); ^1H NMR (400 MHz, CDCl_3): δ 1.25–1.45 (m, 36H, $18 \times \text{CH}_2$), 2.50 (s, 6H, $2 \times \text{CH}_3$), 4.04–4.10 (m, 8H, $2 \times \text{N-CH}_2$, $2 \times \text{O-CH}_2$), 7.38 (d, 4H, $J = 8.2$ Hz, arom.H), 7.83 (d, 4H, $J = 8.2$ Hz, arom.H); ^{13}C NMR (100 MHz, CDCl_3):

δ 21.65 ($2 \times \text{CH}_3$), 25.36, 27.32, 28.85, 28.98, 29.41, 29.49, 29.50, 29.59 (18C , $18 \times \text{CH}_2$), 51.70 ($2 \times \text{N}-\text{CH}_2$), 70.67 ($2 \times \text{SO}_2-\text{CH}_2$), 127.86 (4C, arom.C), 129.79 (4C, arom.C), 130.54, 131.97, 132.99, 133.23, 134.54, 135.15, 137.18, 138.81, 138.94, 139.28, 139.52, 141.50, 141.53, 141.61, 141.98, 142.68, 143.30, 143.55, 143.70, 143.93, 144.00, 144.07, 144.10, 144.16, 144.53, 144.58, 144.86, 144.94, 145.08, 145.42, 146.85, 147.63 (C_{60}).

Acknowledgements

We thank Cyclolab (Hungary) for a generous supply of starting material (Permethylated β -CD). Y. Chen thanks the French Ministry of Research and Technology for post-doctoral fellowship. Financial support from the CNRS and the ENS is gratefully acknowledged.

References and notes

- (a) Ungurenasu, C.; Airinei, A. *J. Med. Chem.* **2000**, *43*, 3186–3188. (b) Samal, S.; Geckeler, K. E. *Chem. Commun.* **2000**, 1101–1102. (c) Gonzalez, K. A.; Wilson, L. J.; Wu, W. J.; Nancollas, G. H. *Bioorg. Med. Chem.* **2002**, *10*, 1991–1997. (d) Bosi, S.; Da Ros, T.; Spalluto, G.; Prato, M. *Eur. J. Med. Chem.* **2003**, *38*, 913–923. (e) Sayes, C. M.; Fortner, J. D.; Guo, W.; Lyon, D.; Boyd, A. M.; Ausman, K. D.; Tao, Y. J.; Sitharaman, B.; Wilson, L. J.; Hughes, J. B.; West, J. L.; Colvin, V. L. *Nano Lett.* **2004**, *4*, 1881–1887.
- (a) Sijbesma, R.; Srdanov, G.; Wudl, F.; Castoro, J. A.; Wilkins, C.; Friedman, S. H.; DeCamp, D. L.; Kenjon, G. L. *J. Am. Chem. Soc.* **1993**, *115*, 6510–6512. (b) Friedman, S. H.; DeCamp, D. L.; Sijbesma, R.; Srdanov, G.; Wudl, F.; Kenjon, G. L. *J. Am. Chem. Soc.* **1993**, *115*, 6506–6509.
- (a) Anderson, T.; Nilsson, K.; Sundahl, M.; Westman, G.; Wennerstorm, O. *Chem. Commun.* **1992**, 604–606. (b) Priyadarsini, K. I.; Mohan, H.; Tyagi, A. K.; Mittal, J. P. *J. Phys. Chem.* **1994**, *98*, 4756–4759. (c) Kanazawa, K.; Nakanishi, H.; Ishizuka, Y.; Nakamura, T.; Matsumoto, M. *Fullerene Sci. Technol.* **1994**, *2*, 189–194.
- (a) Murthy, C. N.; Geckeler, K. E. *Chem. Commun.* **2001**, 1194–1195. (b) Samal, S.; Choi, B. J.; Geckeler, K. E. *Chem. Commun.* **2000**, 1373–1374.
- (a) Filippone, S.; Rassat, A. *C. R. Chimie* **2003**, *6*, 83–86. (b) Filippone, S.; Heimann, F.; Rassat, A. *Chem. Commun.* **2002**, 1508–1509.
- Yang, J.; Wang, Y.; Rassat, A.; Zhang, Y.; Sinaÿ, P. *Tetrahedron* **2004**, *60*, 12163–12168.
- Prato, M.; Li, Q. C.; Wudl, F.; Lucchini, V. *J. Am. Chem. Soc.* **1993**, *115*, 1148–1150.
- Grösser, T.; Prato, M.; Lucchini, V.; Hirsch, A.; Wudl, F. *Angew. Chem., Int. Ed. Engl.* **1995**, *34*, 1343–1345.
- Yuan, D.-Q.; Koga, K.; Kourogi, Y.; Fujita, K. *Tetrahedron Lett.* **2001**, *42*, 6727–6729.
- Sinyashin, O. G.; Romanova, I. P.; Yusupova, G. G.; Nafikova, A. A.; Kovalenko, V. I.; Azancheev, N. M.; Fattakhov, S. G.; Reznik, V. S. *Russ. Chem. Bull., Int. Ed.* **2001**, *50*, 2162–2171.
- Sinyashin, O. G.; Romanova, I. P.; Yusupova, G. G.; Kovalenko, V. I.; Yanilkin, V. V.; Azancheev, N. M. *Mendeleev Commun.* **2000**, 96–98.



Hierarchical self-assembly of all-organic photovoltaic devices

Chih-Hao Huang,^a Nathan D. McClenaghan,^a Alexander Kuhn,^b
Georges Bravic^c and Dario M. Bassani^{a,*}

^a*LCOO/CNRS UMR 5802, Centre de Recherche en Chimie Moléculaire, Université Bordeaux I, 33405 Talence, France*

^b*LACReM, ENSCPB Université Bordeaux I, 33607 Pessac, France*

^c*Institut de Chimie de la Matière Condensée de Bordeaux-CNRS, Université Bordeaux I,
87 Avenue du Dr. Schweitzer, F-33608 Pessac, France*

Received 14 June 2005; revised 22 September 2005; accepted 24 September 2005

Available online 16 November 2005

Abstract—Photovoltaic devices built by a hierarchical self-assembly process using hydrogen-bonding terminated self-assembled monolayers (SAMs) on gold and the combination of a hydrogen-bonding barbituric acid appended fullerene and a complementary melamine terminated π -conjugated thiophene-based oligomer are presented. The incorporation of these electron donor (oligomer) and electron acceptor (methanofullerene) assemblies into simple photovoltaic (PV) devices as thin films leads to a 2.5 fold-enhancement in photocurrent compared to analogous systems comprising non-hydrogen-bonding C_{60} -oligomer systems, which is ascribed to higher molecular-level ordering. The modification of the gold electrode surface with self-assembled monolayers bearing hydrogen-bonding molecular recognition endgroups was seen to further enhance the PV response of the corresponding functional supramolecular device. This superposition of two types of self-assembly facilitates the generation of binary supramolecular fullerene-containing architectures. Importantly, all functional materials are accessible in a direct fashion.

© 2005 Elsevier Ltd. All rights reserved.

1. Introduction

Silicon-based photovoltaic devices have played a major role in the development of light energy-to-electrical energy conversion, and multi-junction solar cells have been reported with efficiencies of 31%.¹ Portability, durability (lack of moving parts), and zero emission during operation are attractive features that are countered only by their relatively high manufacturing costs and fragility. For these reasons, as well as concerns about the use of rare-earth heavy metals in the active layers, hybrid inorganic/organic and all-organic polymer alternatives have been actively pursued in recent years as viable alternatives amenable to large-scale deployment.² Based on current organic polymer technology and of additional interest for the construction of *o*-LED and *o*-FET devices, the polymer approach has benefited from increased interest since the report by Sariciftci and co-workers demonstrating that a substantial improvement in the photovoltaic properties of such materials could be obtained by blending a small amount of C_{60} into the polymer mixture.³ In such composite devices, it has been

proposed that the fullerene component acts as the electron transport material, increasing the efficiency of charge separation and transport. However, the introduction of high proportions of C_{60} results in phase separation, creating unwanted heterogeneous domains, which adversely affect the photovoltaic response.⁴ A successful strategy to enhance compatibility between the organic polymer and fullerene components involves appending solubilizing groups to the latter. This allows a higher fullerene loading to be used, which results in improved performance (up to 3%) and increased device stability.⁵ At the same time, the synthesis and photophysical investigation of covalently-linked fullerene π -conjugated oligomer dyads, triads, and more complex dendritic assemblies has led to important breakthroughs in the comprehension of the fundamental energy and electron transfer processes leading to the generation of long-lived charge separated states. Thus, through covalent modification of C_{60} , introduction of a plethora of electron-rich oligomers, including oligo(*p*-phenylene vinylene)s,⁶ oligo(thiophenes)⁷ and others⁸ has been achieved and used to construct increasingly complex covalent architectures, including several doubly fullerene-terminated oligomer ‘dumbbells’.⁹ The construction of solid-state devices based on these covalent adducts is underway and bodes well for future applications.¹⁰

Keywords: Oligomer; Fullerene; Electron donor; Hydrogen-bonding; Photovoltaic; Self-assembly.

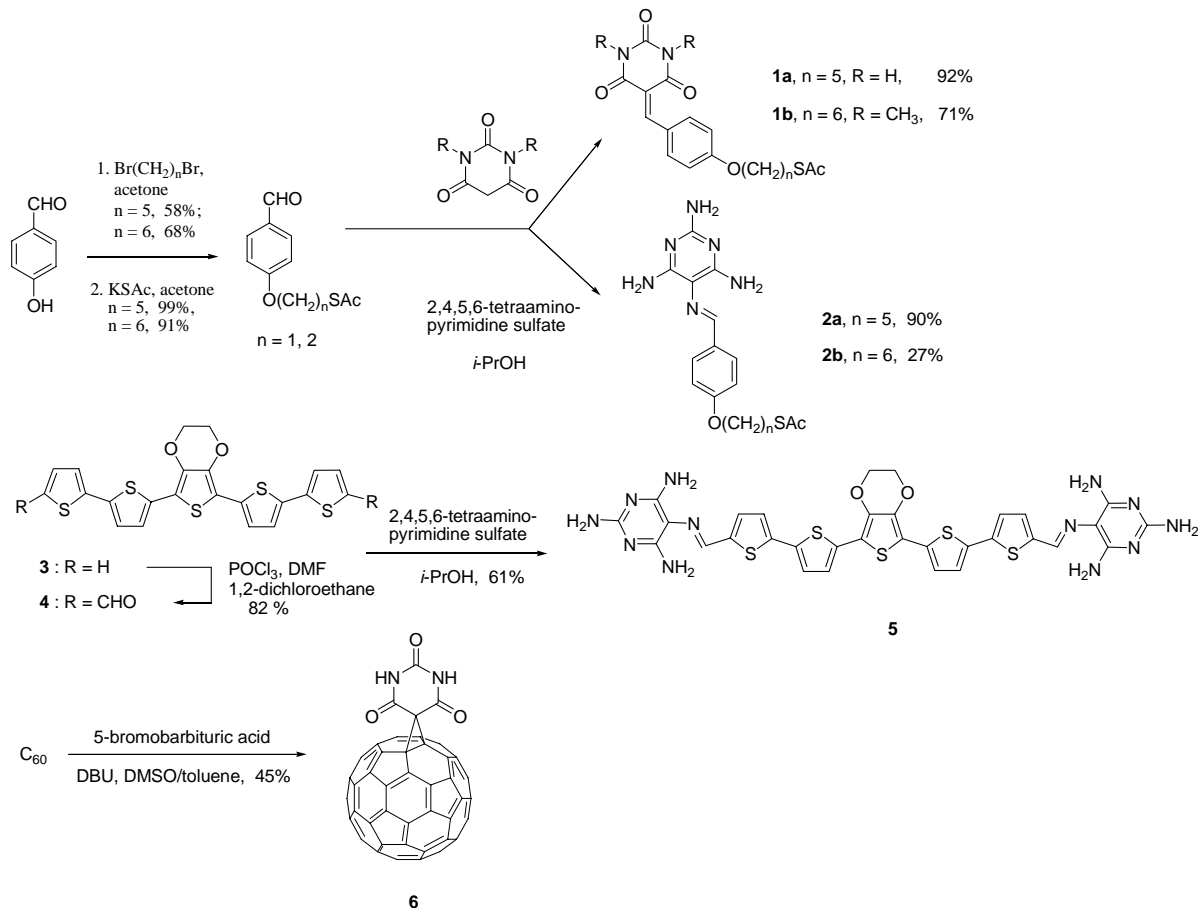
* Corresponding author. Tel.: +335 4000 2827; fax: +335 4000 6158; e-mail: d.bassani@lcoo.u-bordeaux1.fr

Photoinduced charge separation in composite devices takes place at a heterojunction between the electron donor and electron acceptor materials. However, highly ordered materials are required for efficient charge transport, and the conciliation of these apparently contradictory requirements is a major challenge.¹¹ The effect of ordering on charge mobility was recently illustrated with sexithiophene whose charge carrier mobility increases on passing from an amorphous film ($10^{-5} \text{ cm}^2 \text{ V}^{-1} \text{ s}^{-1}$) to a partially organized film ($2 \times 10^{-3} \text{ cm}^2 \text{ V}^{-1} \text{ s}^{-1}$) to the single crystal ($10^{-1} \text{ cm}^2 \text{ V}^{-1} \text{ s}^{-1}$).¹² Although covalent tethering surmounts the phase separation problem, a high degree of long-range ordering conducive to charge transport is more difficult to obtain. For these reasons, the induction of long-range ordering through self-assembly, using non-covalent supramolecular interactions, is particularly appealing. Hydrogen-bonding systems offer the possibility to generate preordained structures in which the binding strength can be modulated and the relative geometry between active units controlled.¹³ Additionally, in certain cases hydrogen-bonding has been shown to promote photoinduced electron transfer processes.¹⁴

Several examples of hydrogen-bonding systems combining fullerenes and π -conjugated oligomers have recently appeared in the literature, for example using ammonium groups and crown ethers,¹⁵ or self-complementary ureidopyrimidinone units.¹⁶ However, the recently described fullerene–barbituric acid dyad **6**¹⁷ (see Scheme 1) presents a unique

combination of features compatible with the construction of functional self-assembled devices: (i) the hydrogen-bonding motif, capable of forming up to six hydrogen bonds, is non-self-complementary and can be introduced in a single synthetic step; (ii) the symmetry of **6**, which presents two identical edges, is conducive with the formation of extended arrays in the presence of conjugated oligomers bearing complementary hydrogen-bonding units; (iii) its compact nature is adapted to promote close inter-fullerene approach in a binary system where the other component is a melamine-like unit. The first two features are important to assure programmed extended bicontinuous photo-/electroactive molecular tapes and efficient photoinduced electron transfer, while the latter two points are prerequisites for charge movement following the primary electron transfer act.

Molecule **6** was recently reported to form supramolecular assemblies in solution¹⁷ with simple melamine units, in a manner related to unfunctionalized barbituric acid,¹⁸ and to play the role of an electron acceptor in ultra-fast photoinduced electron transfer processes with oligothiophenevinylene electron donors in discrete 1:1 supramolecular complexes.¹⁹ Clearly, the presence of barbituric acid does not adversely affect the electronic properties of the fullerene cage, and the fullerene–grafted barbiturate is capable of forming hydrogen-bonded structures, even if a degree of distortion appears to be present on the barbiturate unit due to non-bonding interactions between the carbonyl groups and the fullerene cage.^{16,20} Molecule **6** was therefore deemed a



Scheme 1. Synthesis and structural formulae of **1–6**.

good candidate for the pursuit of functional supramolecular devices.

To be of interest for future development, the electron donor (oligomer) and acceptor (fullerene) components should be easily accessible in high yields with direct synthetic approaches (Scheme 1). The functionalized fullerene is obtained in one step,¹⁷ while the oligomer can be functionalized with hydrogen-bonding molecular recognition units, either melamine or barbituric acid, starting from the same dialdehyde also in one step.²¹ These strategies in themselves constitute a widely applicable methodology to introduce complementary molecular recognition motifs, which is currently lacking. Thus the possibility to incorporate complementary, yet non-self-complementary hydrogen-bonding motifs onto conjugated oligomers (potentially different oligomers) opens the door to the construction of molecular fabrics and libraries of mixed chromophore layers, where the judicious choice of suitably-decorated chromophores assures a better matching of absorption properties with the solar spectrum.

In the current study, the focus is directed at the combination of a melamine-appended oligothiophene **5** with the complementary barbiturate-appended fullerene **6**, and the development of self-assembled optoelectronic devices based on the resulting assemblies. Different microscopic hydrogen-bonding structures may be anticipated using these molecular building blocks bearing complementary units, in line with findings on simpler binary melamine:barbiturate structures described previously, which are shown schematically in Figure 1.¹⁸ Although rosettes, crinkled tapes, and linear tapes are possible, only the linear tape architectures can satisfy all the hydrogen-bonding sites present in the complementary components and their formation is expected to be thermodynamically favored.¹⁸ Preliminary photovoltaic measurements have been reported,²¹ and we now report the effect of elaborating the gold electrode surface with the appropriate bifunctional hydrogen-bonding motif and thiol-terminated species. The terminal thiol-group interacts with the gold surface resulting in the formation of self-assembled monolayers (SAMs) that are proposed to better accommodate the subsequent formation of the photo-/electroactive fullerene-containing thin films due to complementary hydrogen-bonding interactions. Several interesting all-organic systems have been recently reported in the context of photovoltaic devices, including examples based on photoactive SAMs²² and chromophore-appended nanotubes,²³ as well as fullerene-oligomer dyads/triads.¹⁰ The incorporation of hydrogen-bonding motifs giving photo-/electroactive molecules programmed to assemble into hierarchical extended photovoltaic arrays has received less attention.

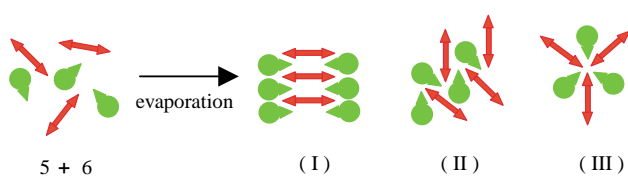


Figure 1. Possible hydrogen-bonding architectures formed with components **5** (red) and **6** (green). Compared to the crinkled tape (II) and rosette (III), only the hydrogen-bonded tape structure (I) satisfies all the hydrogen-bonding requirements of both components.

2. Results and discussion

2.1. Synthesis

Pertinent synthetic procedures and structural formulae of the molecules used in this study are shown in Scheme 1. Fullerene–barbituric acid dyad **6** was prepared by a Bingel reaction between 5-bromobarbituric and C₆₀ in a toluene:DMSO mixture.^{17,24} The synthesis of the oligomers and introduction of molecular recognition motifs was recently reported.²¹ Briefly, the 5T chromophore (**3**; a symmetric linear pentathiophene oligomer with a central EDOT unit) was obtained via Suzuki cross-coupling reaction between the boron ester of dithiophene and 2,5-dibromo-EDOT. This parent unit was subsequently functionalized by a double Vilsmeier-Haack formylation giving dialdehyde **4**, which can be considered as a versatile starting point for the introduction of terminal molecular recognition motifs.

Introduction of the melamine unit was achieved using a Schiff base reaction to give **5**. As Schiff base formation is an equilibrium process, good yields of the most stable adduct can be obtained on reaction with an excess of 2,4,5,6-tetraaminopyrimidine. Equally, the symmetric complementary barbituric acid-terminated oligomer (not shown) could be prepared in one step in similarly high yield by a Knoevenagel reaction with barbituric acid. The alkylthioacetate terminated barbituric acid or cyanurate were prepared by adapting the above methodologies.²⁵ Structurally-related barbiturate species were previously reported by Ringsdorf, albeit in lower yields.²⁶ 4-Hydroxybenzaldehyde was alkylated with the appropriate α,ω -dibromoalkane²⁷ followed by condensation with potassium thioacetate²⁸ giving an intermediate, which could be subsequently condensed with either barbituric acid or tetraaminopyrimidine to give **1** or **2**, respectively.

2.2. X-ray crystal structure of **3**

Conjugation—and hence electron–hole pair delocalization—over adjacent heterocycles in oligo- and polythiophene derivatives is highest when the structure adopts a planar geometry maximizing π -overlap. This is indeed the case in most oligothiophenes (with the exception of some 3,4-disubstituted thiophene-containing derivatives), for which a large number of solid-state structures have been reported.¹² Substitution in the thiophene C-3 and C-4 position generally introduces sufficient steric repulsion to induce a deviation from planarity. Although only a few crystal structures of EDOT-containing oligothiophenes have been reported, these do not indicate that the EDOT moiety introduces a substantial deviation from planarity. To investigate whether this is the case in **3**, its solid-state structure was determined by X-ray diffraction. Single crystals were grown from THF solution, crystallizing in a monoclinic $p21/n$ unit cell.[†] The structure of **3**, shown in

[†] Crystallographic data (excluding structure factors) for the structures in this paper have been deposited with the Cambridge Crystallographic Data Centre as supplementary publication numbers CCDC 275009. Copies of the data can be obtained, free of charge, on application to CCDC, 12 Union Road, Cambridge CB2 1EZ, UK [fax: +44 1223 336033 or e-mail: deposit@ccdc.cam.ac.uk].

Figure 2, indicates that the planarity of the pentameric oligomer is indeed retained even upon introduction of the functionalized central unit, although one of the terminal thiophenes shows a torsion angle of 24.7° in the S(11)–C(15)–C(22)–(S21) plane, presumably due to crystal packing forces. The extended crystal packing structure is a herringbone type as observed with related oligothiophene species.¹²

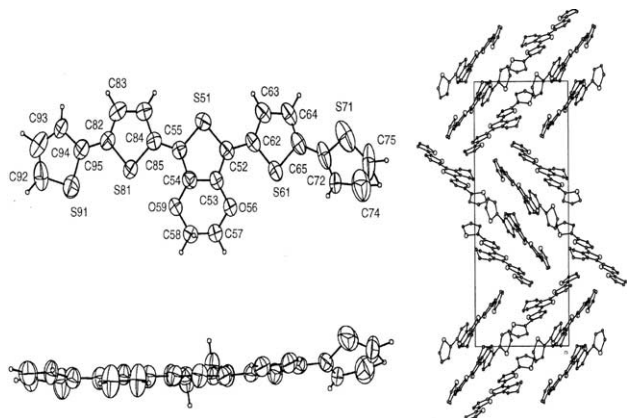


Figure 2. X-ray crystal structure of **3** and crystal packing.

2.3. Thin films comprising photo-/electroactive oligomer and fullerene units

2.3.1. Fluorescence microscopy of thin films. Blends of π -conjugated oligomers and fullerenes have the tendency to undergo phase separation, and high-speed spin-coating of these species onto the appropriate substrate from volatile solvents is often used to overcome this process. In the current study, drop-casting of thin films from solution (0.5 mM **5** in DMSO or DMSO/THF solutions) onto a solid substrate followed by slow evaporation of the solvent is anticipated to favor the formation of thermodynamically equilibrated non-covalent architectures (see Fig. 1). As a preliminary test to see if homogeneous films would result from this drop-casting technique, mixtures of the pertinent species were separately deposited on microscope slides in order to visualize the residual fluorescence from the films. Bearing in mind that the oligomer fluorescence will be quenched in the presence of fullerene (either via energy or electron transfer), an estimation of bulk homogeneity can be made by examining the intensity and distribution of the residual fluorescent areas. The fluorescence microscopy images of three different thin films are shown in Figure 3. In the first case, the intense fluorescence of oligomer **5** can be clearly seen. In the second case (b), **5** and C_{60} were co-deposited in a 1:2 stoichiometry from DMSO solution. Though a portion of the intrinsic oligomer fluorescence is quenched by the presence of C_{60} , localized regions of fluorescence are visible showing that the film exhibits considerable heterogeneity, presumably due to phase separation during the deposition process. In the third case (c), films of **5** and **6** (in a 1:2 stoichiometry) were deposited. Here, the oligomer fluorescence is comprehensively quenched, indicating that the fullerene and oligomer components are more homogeneously dispersed than in (b). While these results per se do not provide irrefutable evidence as to the formation of the hydrogen-bonding

architectures proposed above, they do indicate that the compatibility between inherently incompatible compounds such as oligothiophenes and C_{60} can be significantly enhanced by the presence of complementary molecular recognition groups. In practical terms, this implies that the electron-rich oligomers are mostly located in the vicinity of a fullerene moiety, which can translate into enhanced charge separation efficiency.

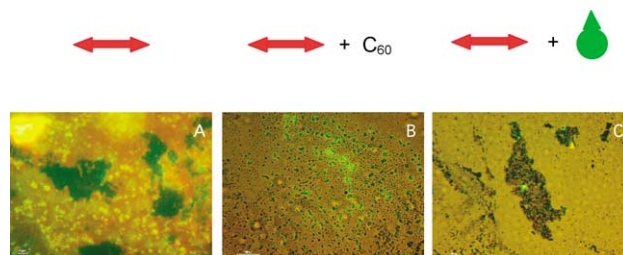


Figure 3. Representative fluorescence microscopy images of thin films of oligomer **5** (left); **5** + C_{60} , 1:2 equiv (center); and **5** + **6**, 1:2 equiv (right).

2.3.2. Electrochemical and photoelectrochemical studies of thin films on a gold surface.

Thin films analogous to those described above were subsequently deposited from solution onto a gold electrode and introduced into a standard three-electrode photoelectrochemical cell, with methylviologen in water acting as an electron carrier, sodium sulfate as the supporting electrolyte and a platinum wire counter electrode.²¹ Irradiation was performed using a high-pressure mercury lamp equipped with a band-pass filter (400–500 nm; intensity = 150 mW cm^{-2}).²⁹ In line with the idea of higher organization and better compatibility of the two different electron donor and acceptor materials giving the highest photocurrent, the best performance was measured for a mixture of **5** and **6**, which was anticipated to be the most organized thin film comprising the hydrogen-bonding fullerene and the complementary π -conjugated oligomer.²¹ This response was 2.5 times higher than that obtained on combining **5** with unsubstituted C_{60} , while the lowest conversion was obtained for the film of oligomer **5** alone with a value, which was half that obtained with **5**: C_{60} .

From the I/V graph of photocurrent generated versus applied potential, the open-circuit voltage conversion efficiency $\Phi(V_{oc})$, and short-circuit quantum conversion efficiency $\Phi(I_{sc})$ of the photovoltaic device could be estimated. Respectively, these values express the fraction of light energy that is converted into voltage, and the number of photoelectrons generated for every photon of light that is absorbed³⁰ (film thickness was estimated at ca. 200 nm using AFM, which also showed that the films were even and reproducible).

$$\Phi(V_{oc}) = V_{oc}/E_{00} \quad (1)$$

$$\Phi(I_{sc}) = (dn_e/dt)/(dn_{hv}/dt) \quad (2)$$

where n_e and n_{hv} are the number of photoelectrons and number of photons absorbed, respectively, while E_{00} is the energy of the $S_1 \leftarrow S_0$ transition in eV. The incident light intensity of 150 mW cm^{-2} corresponds to an average photon flux of 5.6×10^{-8} Einstein (at 450 nm). Considering

the device comprising an oligomer film without fullerene, it is estimated that ca. 2.7% of incident light is absorbed (based on the measured thickness of the film). From Eqs. 1 and 2 above and values of $V_{oc}=0.39$ V and $I_{sc}=6.8$ μ A, one can estimate the efficiency of open-circuit voltage conversion, $\Phi(V_{oc})=0.14$, and the quantum conversion efficiency, $\Phi(I_{sc})=0.05$. These values are comparable to other photovoltaic devices based on similar technology (although experimental error, associated mainly with the determination of film thickness, must be taken into consideration). Thus, comparing the relative photocurrents generated for the thin films, the quantum conversion efficiencies were estimated at 5% for **5** alone; 9% for **5**:C₆₀; 1:2 stoichiometry, and ca. 25% for **5**:**6**; 1:2 stoichiometry. This latter value compares favorably with recent photovoltaic devices based on the layer-by-layer construction of conjugated polymers and C₆₀ and with IPCE values of 15%.³¹ In all cases it can be assumed that absorption of light is effected almost exclusively by the oligomer, as fullerene derivatives possess low molar absorptivities above 400 nm. Therefore, despite uncertainties in the absolute values for the efficiency of these simple devices, these results show that the films comprising two complementary hydrogen-bonding electroactive units are more performant. An additional factor that became immediately apparent during this initial testing phase of the devices is their inherent stability towards air and moisture. Indeed, the photovoltaic cell set-up uses an aerated aqueous solution of methylviologen as the electron transport agent. The response of **5** alone is stable over time, whereas device B (**5** + pristine C₆₀) exhibits a slow (ca. 10% loss) of efficiency over a period of 1 h. During this same period, no measurable decrease in efficiency was detected for the device prepared with **5** + **6**.

2.3.3. Thin films on a hydrogen-bonding SAM modified gold surface. To obtain photoactive fullerene-containing architectures directed by a hierarchical combination of supramolecular self-assembly processes, gold–thiol interactions can be employed in addition to hydrogen-bonding. The self-assembly of different nanoparticles (gold and CdS) was recently demonstrated using nanoparticles whose surface was decorated with thiol-terminated melamines and barbiturates, respectively.²⁵ The gold electrode surface was first modified by reaction with a barbiturate or melamine unit bearing a thiol-terminated alkyl chain, thus generating a self-assembled monolayer with the capacity to bind electroactive units using non-covalent interactions. In the current case, the choice of hydrogen-bonding building blocks used to decorate the SAMs would be anticipated to dictate the chemical nature of the layer adjacent to the surface self-assembled monolayer. These anticipated second layers would be a π -conjugated melamine-bearing oligomer (**5**) with a barbiturate-decorated surface, and a barbituric acid bearing fullerene (**6**) with a melamine-decorated surface. In other words, the SAM may serve as a homogeneous starting point for subsequent deposition of the photoactive binary thin film.

Hydrogen-bonding SAMs were obtained by dipping the gold-substrate into a solution of the appropriate thiol **1**–**2**, see Scheme 1 for structural formulae. The surface coverage was subsequently evaluated by electrochemical and surface

ellipsometry measurements. In the first case, the determination of surface coverage can be obtained by electrochemistry while the thickness of the monolayer can be determined by ellipsometry, and the surface coverage estimated by rastering the surface with the incident laser beam.

The surface coverage by self-assembled monolayers of the gold electrode can readily be evaluated by electrochemistry when the chemisorbed molecules serve as a barrier to block a redox process involving a species in solution at the electrode surface.³² In the current case the reduction of Fe³⁺ (as the potassium hexacyanoferrate (III) salt) to Fe²⁺ was employed to check for defects in the SAM. For the surface coated with **1a**, a highly uniform close packing monolayer layer was formed. As shown in Figure 4, essentially no Fe^{III} reduction could be measured upon modification of the gold surface with the barbiturate-terminated alkane-thiol, compared with the electrochemical response for bare gold. The situation was somewhat different when the experiment was repeated with the corresponding melamine-terminated alkane-thiol (Fig. 4). A much poorer blocking effect was observed with **2a** suggesting a less ordered SAM. This result was rationalized by considering the experimentally determined ‘odd–even’ effect reported for simple alkanethiol SAMs where the number of repeat units (odd /or even) influences close-packing of the molecules.³³ The experiment was thus repeated with molecule **2b**, which is identical with **2a** except for the incorporation of an additional methylene repeat unit in the alkyl chain. This simple structural modification resulted in a much better passivation of the

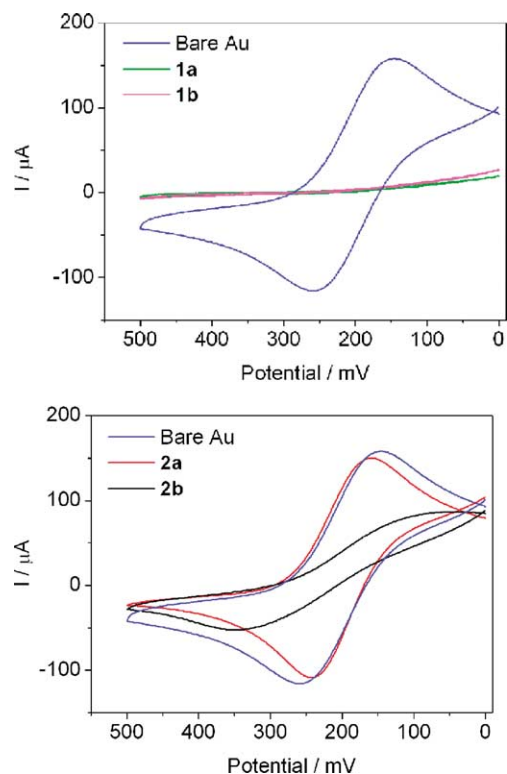


Figure 4. Cyclic voltammograms of the reduction of aqueous K₃[Fe(CN)₆] using gold electrodes whose surfaces were modified with **1a** or **1b** (top) and **2a** or **2b** (below).

electrode surface. This result is consistent with the formation of a better monolayer, as shown in Figure 4. A similar behavior was observed upon investigation of the *N*-methylated derivative of **1a**, for which compact SAMs took several days to form (data not shown). Again, incrementing the pentamethylene linker by one $-\text{CH}_2-$ unit (compound **1b**) significantly improved the self-assembly of compact monolayers, which were formed overnight.

Ellipsometry measurements of surfaces modified with **1a** and **2b** are shown in Figure 5, which correspond to the closest packing SAMs as estimated by electrochemistry, formed with thiol-terminated barbiturates and melamines, respectively. Rastering the modified surface gave infor-

mation on the coverage, and a homogeneous layer, in terms of height is obtained (Fig. 5a). Using this height profile (Fig. 5b), an estimation of the geometry adopted can be obtained and this is represented in Figure 5c for both **1a** and **2b**. The measured height corresponds well to the dimensions obtained using molecular modeling. In the case of **1a** the measured height was 1.50 nm while the calculated value was 1.42 nm. For **2b** the measured height was 1.83 nm with a calculated value of 1.90 nm.

Photoelectronic devices similar to those reported in Section 2.3.2 were prepared using gold electrodes modified with SAMs prepared from compounds **1a**, **1b**, and **2b**. Comparison of the response obtained from electrodes modified with **2b** versus **1a** provides an indication as to the effect of the

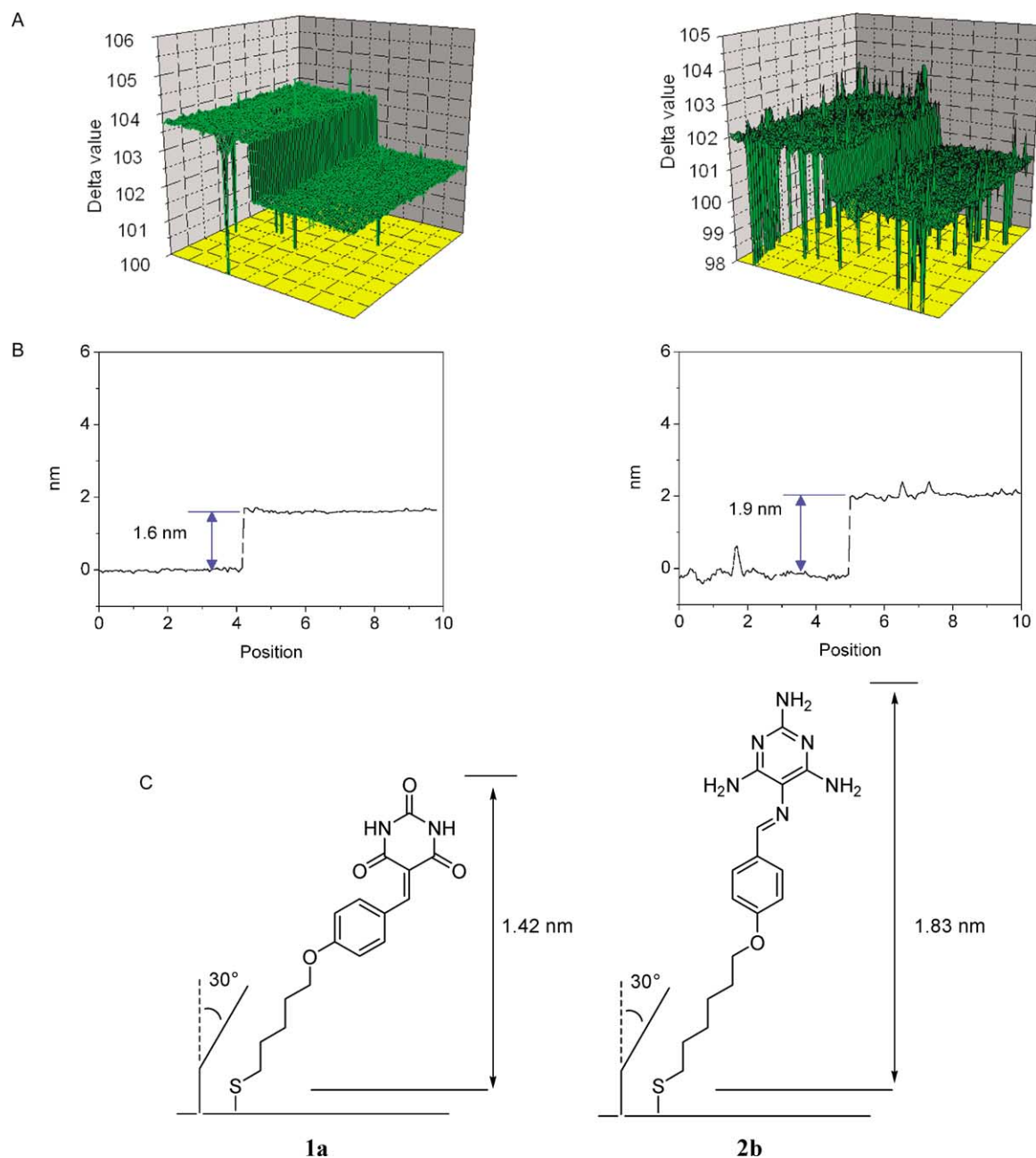


Figure 5. Characterization of SAMs obtained for **1a** (left) and **2b** (right) modified gold surfaces using ellipsometry: (a) topology of surface; (b) height profile and (c) calculated height assuming close-packing of the molecules.

hydrogen-bonding endgroup, whereas the use of **1b** serves as a control in which hydrogen-bonding is blocked. Since it was shown that incorporating the barbiturate-appended fullerene **6** resulted in thin films giving greater photocurrent than pristine C₆₀, only devices based on **5** and **6** (in a 1:2 stoichiometry) are considered in this section. The different photocurrent response for each of the four different devices is shown in Figure 6, where device A is the film deposited on the bare gold; device B is the thin film deposited on the surface decorated with melamine **2b**; device C is the film deposited on the surface decorated with **1b**; and device D is the film deposited on the surface decorated with the alkanethiol–barbiturate **1a**. It was immediately clear that device A is the least performant device when compared to the devices incorporating SAM-decorated surfaces, all of which gave a higher photocurrent.

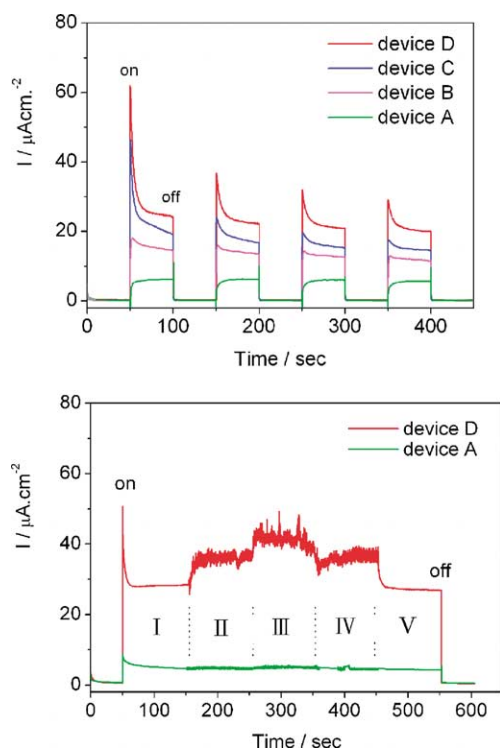


Figure 6. Top: Photocurrent generated with thin films of **5**+**6**, 1:2 equiv deposited on: bare gold (device A); Au/**2b** (melamine endgroup, device B); Au/**1b** (*N,N'*-dimethylbarbiturate endgroup, device C); Au/**1a** (barbiturate endgroup, device D). Bottom: Effect of stirring on the photocurrent of devices A and D; with stirring off (I and V), slow stirring (II and IV) and fast stirring (III).

The behavior of device D is intriguing, displaying a rapid decrease in the photogenerated current upon each illumination cycle. We attribute this reproducible behavior to extension of the diffusion layer due to depletion of the MV²⁺ in the vicinity of the electrode. To confirm this, we proceeded to monitor the photovoltaic response of device D upon mechanical stirring of the solution. The results are presented in Figure 6, in which it is quite clear that the photovoltaic response of D increases substantially upon stirring, in a way that is proportional to the rate of stirring. Therefore, in the case of device D the observed performance is limited by the rate of diffusion of the electron-carrying species in solution rather than the charge carrier mobility in the material. This is not the case for the other devices, for

which the effect of stirring the solution is much lower or absent, as in the case of device A. Device D also displayed exceptional stability, no deterioration in its response being observed after two week storage under ambient conditions.

3. Conclusions

The formation of SAMs appended with suitable recognition motifs is shown to be advantageous in the construction of supramolecular all-organic photovoltaic devices. Based on the formation of hydrogen-bonded networks, the molecular constituents in these devices are programmed to self-assemble into molecular-level heterojunctions. Thus two levels of self-assembly can be employed to generate multi-component functional fullerene-containing supramolecular architectures. Although direct measurement of the degree of order instilled by the presence of complementary hydrogen-bonding donor–acceptor sites is difficult, considerable differences in efficiency and behavior are noted. The improvement of the photovoltaic response when using the SAM modified surfaces may in part originate from either the variations in the surface properties (the increased hydrophobicity of the SAM-covered surface results in lower contact angles when exposed to organic solvents) and/or inhibition of the phonon quenching of the excited states generated in close proximity of the gold surface.³⁴ However, this reasoning alone is insufficient to explain the difference in behavior between devices B, C, and D. In the latter device, it can be anticipated that the presence of a barbituric acid-appended SAM may induce the preferential deposition of the complementary melamine-containing oligothiophene unit **5**. In contrast, the use of the melamine-based SAM (device B) would lead to the selective deposition of fullerene derivative **6**. Due to the electrical bias applied during the photovoltaic measurements, it is expected that the latter construction should be less efficient as the presence of the fullerene proximal to the gold electrode would induce an energy barrier to the transport of holes towards the cathode. Work is in progress to further elucidate the morphologies of these films and to test their photovoltaic response in solid-state devices.

4. Experimental

4.1. General

¹H and ¹³C NMR spectra were recorded at room temperature on a Bruker DPS-200 FT, AC-250 FT or DPX-300 FT spectrometer using residual solvent proton peaks as internal references unless otherwise indicated. Chemical shifts are given in ppm (δ) with respect to tetramethylsilane. Abbreviations used are s=singlet, d=doublet, t=triplet, q=quartet, and br=broad. Mass spectra were recorded on a VG Autospec-Q by EI (70 eV); *m/z* (%). High resolution mass spectra were recorded on a FTICR mass spectrometer Bruker 4.7T BioApex II. The elemental analysis was carried out by the Service Centrale d'Analyse at Vernaison (CNRS-France). Merck silica gel 60 (70–230 mesh) was used for flash chromatography. Electronic absorption spectra were obtained using a Hitachi U-3300 spectrophotometer. Fluorescence spectra were recorded on

a Hitachi F-4500 fluorescence spectrophotometer. Fluorescence microscopy images were taken on a Nikon Eclipse E600 FN instrument equipped with a 365 nm excitation filter.

4.1.1. Materials. Commercially available starting materials and anhydrous DMSO and DMF (Fluka) were used as received. The preparation of compound **5** was recently described.²¹ Tetrahydrofuran (THF) was distilled over sodium/benzophenone immediately before use. All reactions were carried out under a nitrogen atmosphere. The polycrystalline gold electrodes (nickel (80 Å), chromium (20 Å) and gold (3900 Å) on 1.0 mm glass) were purchased from ACM France. 4-(5-Bromopentyloxy)benzaldehyde and 4-(6-bromohexyloxy)benzaldehyde were prepared following a procedure described in the literature.²⁷

4.1.2. Cleaning of substrates and preparation of monolayers and devices. The gold electrodes were cut into slides (ca. 2.5 cm × 1.0 cm) and were cleaned by immersion in 'piranha' solution (H₂SO₄/30% H₂O₂, 7:3 (v/v); Caution: 'Piranha' is an extremely dangerous oxidizing agent and should be handled with care using appropriate shielding) for 30 min, and were then rinsed with deionized water and absolute ethanol and dried with a stream of argon. For SAM-based devices, the clean gold slides were immersed in anhydrous THF–ethanol (1/5) mixed-solutions of alkylthioacetate terminated **1a**, **1b**, **2a**, or **2b** (1 mM) overnight. To remove any solution-deposited material, the slides were then rinsed with ca. 5 mL of anhydrous ethanol, followed by immersing in an ethanol solution for 5 min, and dried with a stream of argon. In all devices, deposition was carried out by drop-casting 20 μL of 2.0 × 10⁻⁵ M DMSO solutions of **5** with 2.0 equiv of **6**. The slow evaporation of the solvent under reduced pressure left a thin film of material on a well-defined area (2.50 cm²) of the gold electrode. The modified slide was then dried with a stream of argon and before use in photoelectrochemical measurements.

4.1.3. Experimental conditions. All photoelectrochemical studies were performed as previously described.²¹ The cyclic voltammograms were recorded in 1 mM K₃[Fe(CN)₆] aqueous solution with 0.1 M KNO₃ as the supporting electrolyte. The working electrode was a modified gold slide, the counter electrode was a platinum wire, and an Ag/AgCl (saturated KCl) reference electrode was used. The Fe³⁺/Fe²⁺ redox potential was obtained with a scan speed of 50 mV s⁻¹. The ellipsometer (Jelli2000, Nanofilm Technologie GmbH, Germany) equipped with a frequency doubled Nd-Yag laser (λ = 532 nm, P_{max} = 50 mW), was used for the thickness measurements, and the obtained data were analyzed with the furnished software. The incident angle was set to 65°. A refractive index of 1.50 was assumed for all films in the calculation of the thickness.

4.2. Synthesis

4.2.1. 5-(4'-Formylphenoxy)pentyl thioacetate.²⁸ 4-(5-Bromopentyloxy)benzaldehyde (1.00 g, 3.68 mmol) and potassium thioacetate (0.43 g, 3.68 mmol) in acetone (20 mL) were stirred at room temperature overnight. The

resulting white precipitate was filtered off and the filtrate was concentrated under reduced pressure to give a white solid (0.97 g, yield = 99%). ¹H NMR (200 MHz, CDCl₃) δ 9.87 (s, 1H, CHO), 7.82 (d, 2H, *J* = 8.7 Hz, ArH), 6.98 (d, 2H, *J* = 8.7 Hz, ArH), 4.03 (t, 2H, *J* = 6.3 Hz, OCH₂), 2.90 (t, 2H, *J* = 7.0 Hz, S–CH₂), 2.33 (s, 3H, CH₃), 1.87–1.77 (m, 2H), 1.67–1.50 (m, 4H); ¹³C NMR (50 MHz, CDCl₃) δ 195.2, 190.8, 164.1, 132.0, 129.8, 114.7, 104.5, 68.0, 30.6, 29.3, 28.9, 28.5, 25.2.

4.2.2. 6-(4'-Formylphenoxy)hexyl thioacetate.²⁸ 4-(6-Bromohexyloxy)benzaldehyde (7.78 g, 27.28 mmol) and potassium thioacetate (3.18 g, 27.28 mmol) in acetone (20 mL) were stirred at room temperature overnight. The resulting white precipitate was filtered off and the filtrate was concentrated under reduced pressure to give a white solid (6.98 g, yield = 91%). ¹H NMR (200 MHz, CDCl₃) δ 9.87 (s, 1H, CHO), 7.82 (d, 2H, *J* = 8.7 Hz, ArH), 6.98 (d, 2H, *J* = 8.7 Hz, ArH), 4.03 (t, 2H, *J* = 6.3 Hz, OCH₂), 2.87 (t, 2H, *J* = 7.1 Hz, S–CH₂), 2.32 (s, 3H, CH₃), 1.82–1.76 (m, 2H), 1.67–1.55 (m, 2H), 1.54–1.43 (m, 4H); ¹³C NMR (50 MHz, CDCl₃) δ 195.5, 190.4, 163.9, 131.7, 129.5, 114.4, 104.5, 67.9, 30.3, 29.2, 28.7, 28.6, 28.1, 25.2.

4.2.3. 5-[4-[(Tetrahydro-2,4,6-trioxo-5(2H)-pyrimidinyl)liene)methyl]phenoxy]pentyl thioacetate (1a). 5-(4'-Formylphenoxy)pentyl thioacetate (0.67 g, 2.52 mmol), and barbituric acid (0.33 g, 2.52 mmol) in ethanol:water (14 mL, 5:2; v/v), was stirred under reflux for 10 min, and then at room temperature overnight. The resulting yellow suspension was filtered, washed with EtOH (10 mL) and dried under reduced pressure to give a yellow solid (0.87 g, yield = 92%). ¹H NMR (200 MHz, *d*₆-DMSO) δ 11.29 (s, 1H, NH), 11.18 (s, 1H, NH), 8.36 (d, 2H, *J* = 9.0 Hz, ArH), 8.24 (s, 1H, CH=C), 7.05 (d, 2H, *J* = 9.0 Hz, ArH), 4.09 (t, 2H, *J* = 6.4 Hz, OCH₂), 2.86 (t, 2H, *J* = 6.9 Hz, S–CH₂), 2.31 (s, 3H, CH₃), 1.80–1.70 (m, 2H), 1.61–1.43 (m, 4H); ¹³C NMR (50 MHz, *d*₆-DMSO) δ 195.3, 163.9, 162.9, 162.2, 154.9, 150.2, 137.5, 125.0, 115.4, 114.3, 67.8, 30.6, 28.9, 28.2, 27.9, 24.6. APCI-MS *m/z* (%) 377 (M+1, 100); 376 (M, 75). HRMS 376.1088, M⁺; Calcd 376.1093. Anal. Calcd for C₁₈H₂₀N₂O₅S: C 57.43, H 5.36, N 7.44. Found: C 57.28, H 5.40, N 7.43.

4.2.4. 6-{4-[(1,3-Dimethyl-tetrahydro-2,4,6-trioxo-5(2H)-pyrimidinyl)liene)methyl]phenoxy}hexyl thioacetate (1b). 6-(4'-Formylphenoxy)hexyl thioacetate (1.55 g, 5.54 mmol), and *N,N'*-dimethylbarbituric acid (0.88 g, 5.54 mmol) in benzene (100 mL) were stirred under reflux for 4 h using Dean-Stark apparatus. After cooling to room temperature, the solvent was removed, and the residue was dissolved in CHCl₃ (100 mL), extracted with saturated aqueous NaHCO₃ solution (50 mL), dried over MgSO₄, and concentrated under reduced pressure to give a yellow solid (1.65 g, yield = 71%). ¹H NMR (200 MHz, CDCl₃) δ 8.51 (s, 1H, CH=C), 8.32 (d, 2H, *J* = 9.0 Hz, ArH), 6.95 (d, 2H, *J* = 9.0 Hz, ArH), 4.06 (t, 2H, *J* = 6.4 Hz, OCH₂), 3.41 (s, 3H, N–CH₃), 3.39 (s, 3H, N–CH₃), 2.88 (t, 2H, *J* = 7.1 Hz, S–CH₂), 2.33 (s, 3H, CH₃), 1.87–1.77 (m, 2H), 1.65–1.42 (m, 6H); ¹³C NMR (50 MHz, CDCl₃) δ 196.0, 164.0, 163.2, 161.0, 159.0, 151.4, 138.1, 125.3, 114.1, 114.0, 68.2, 30.6, 29.4, 29.0, 28.9, 28.8, 28.4, 28.3, 25.5. HRMS 419.1634, M⁺; Calcd 419.1640.

4.2.5. 5-{4-[(2,4,6-Triamino-N5-pyrimidinyl)liene-methyl]phenoxy}pentyl thioacetate (2a). 2,4,5,6-Tetraaminopyrimidine sulfate (3.21 g, 13.06 mmol), potassium carbonate (1.79 g, 13.06 mmol), and 5-(4'-formylphenoxy)pentyl thioacetate (0.87 g, 3.27 mmol) in 2-propanol (15 mL) were stirred under reflux overnight. After cooling to room temperature, water (30 mL) was added to the reaction. The brown suspension solution was filtered, washed with water (10 mL), EtOH (10 mL), and diethyl ether (10 mL), then dried under reduced pressure to give a deep-yellow solid (1.31 g, yield=90%). ¹H NMR (200 MHz, *d*₆-DMSO) δ 8.49 (s, 1H, N=CH), 7.79 (d, 2H, *J*=8.6 Hz, ArH), 6.97 (d, 2H, *J*=8.7 Hz, ArH), 5.95 (s, 4H, NH₂), 5.65 (s, 2H, NH₂), 4.00 (t, 2H, *J*=6.3 Hz, OCH₂), 2.86 (t, 2H, *J*=6.9 Hz, S-CH₂), 2.32 (s, 3H, CH₃), 1.80–1.67 (m, 2H), 1.65–1.43 (m, 4H); ¹³C NMR (50 MHz, *d*₆-DMSO) δ 195.4, 160.0, 159.2, 157.1, 152.9, 130.8, 129.0, 114.3, 102.0, 67.4, 30.6, 28.9, 28.3, 28.1, 24.7. ESI-MS *m/z* (M⁺, 387.7). HRMS 388.1680, M⁺; Calcd 388.1681.

4.2.6. 6-{4-[(2,4,6-Triamino-N5-pyrimidinyl)liene-methyl]phenoxy}hexyl thioacetate (2b). 2,4,5,6-Tetraaminopyrimidine sulfate (8.51 g, 34.65 mmol), potassium carbonate (4.78 g, 34.65 mmol), and 6-(4'-formylphenoxy)hexyl thioacetate (2.43 g, 8.66 mmol) in 2-propanol (25 mL) was stirred under reflux overnight. After cooling to room temperature, water (150 mL) was added to the reaction. The brown suspension solution was filtered, washed with water (100 mL), and CH₂Cl₂ (20 mL), then dried under reduced pressure to give a deep-yellow solid (0.92 g, yield=27%). ¹H NMR (200 MHz, *d*₆-DMSO) δ 8.49 (s, 1H, N=CH), 7.78 (d, 2H, *J*=8.6 Hz, ArH), 6.96 (d, 2H, *J*=8.6 Hz, ArH), 5.90 (s, 4H, NH₂), 5.57 (s, 2H, NH₂), 4.00 (t, 2H, *J*=6.4 Hz, OCH₂), 2.84 (t, 2H, *J*=7.0 Hz, S-CH₂), 2.32 (s, 3H, CH₃), 1.80–1.60 (m, 2H), 1.60–1.30 (m, 6H); ¹³C NMR (50 MHz, *d*₆-DMSO) δ 195.3, 159.9, 159.8, 157.4, 152.4, 130.9, 128.9, 114.3, 102.2, 67.4, 30.6, 29.1, 28.5, 28.3, 27.9, 25.0. APCI-MS *m/z* (%) 404 (M+1, 100); 403 (M, 30). HRMS 403.1904, M⁺; Calcd 403.1916.

Acknowledgements

We thank Dr. B. Desbats for assistance with ellipsometry measurements and Dr. R. Oda for access to fluorescence microscope instrumentation. Financial support from the CNRS and French Ministry of Research (AC Nanosciences-Nanotechnologies) is gratefully acknowledged.

References and notes

1. Takamoto, T.; Agui, T.; Ikeda, E.; Kurita, H. *Proc. of the 28th IEEE Photovoltaic Specialists Conf.*, 2000, p 976.
2. Brabec, C. J.; Sariciftci, N. S.; Hummelen, J. C. *Adv. Funct. Mater.* **2001**, *11*, 15–26. Brabec, C. J. *Sol. Energy Mater. Sol. Cells* **2004**, *83*, 273–292.
3. Shaheen, S.; Brabec, C.; Fromherz, T.; Padinger, F.; Sariciftci, S.; Gloetzel, E. Patent WO0184645, Nov 8, 2001, published.

4. Yu, G. T.; Gao, Y.; Hummelen, J. C.; Wudl, F.; Heeger, A. J. *Science* **1995**, *270*, 1789–1791. Matsumoto, K.; Fujitsuka, M.; Sato, T.; Onodera, S.; Ito, O. *J. Phys. Chem. B* **2000**, *104*, 11632–11638.
5. Al-Ibrahim, M.; Ambacher, O.; Sensfuss, S.; Gobsch, G. *Appl. Phys. Lett.* **2005**, *86*, 201120/1–201120/3.
6. Nierengarten, J.-F.; Eckert, J.-F.; Nicoud, J.-F.; Ouali, L.; Krasnikov, V.; Hadziioannou, G. *Chem. Commun.* **1999**, 617–618. Peeters, E.; van Hal, P. A.; Knol, J.; Brabec, C. J.; Sariciftci, N. S.; Hummelen, J. C.; Janssen, R. A. J. *J. Phys. Chem. B* **2000**, *104*, 10174–10190. Eckert, J.-F.; Nicoud, J.-F.; Nierengarten, J.-F.; Liu, S.-G.; Echegoyen, L.; Armaroli, N.; Barigeletti, F.; Ouali, L.; Krasnikov, V.; Hadziioannou, G. *J. Am. Chem. Soc.* **2000**, *122*, 7467–7479.
7. Yamashiro, T.; Aso, Y.; Otsubo, T.; Tang, H.; Harima, Y.; Yamashita, K. *Chem. Lett.* **1999**, 443–444. Hirayama, D.; Yamashiro, T.; Takimiya, K.; Aso, Y.; Otsubo, T.; Norieda, H.; Imahori, H.; Sakata, Y. *Chem. Lett.* **2000**, 570–571. Sánchez, L.; Rispen, M. T.; Hummelen, J. C. *Angew. Chem., Int. Ed.* **2002**, *41*, 838–840.
8. Gu, T.; Nierengarten, J.-F. *Tetrahedron Lett.* **2001**, *42*, 3175–3178. Martineau, C.; Blanchard, P.; Rondeau, D.; Delaunay, J.; Roncali, J. *Adv. Mater.* **2002**, *14*, 283–287. Apperloo, J. J.; Martineau, C.; van Hal, P. A.; Roncali, J.; Janssen, R. A. J. *J. Phys. Chem. A* **2002**, *106*, 21–31. Obara, Y.; Takimiya, K.; Aso, Y.; Otsubo, T. *Tetrahedron Lett.* **2001**, *42*, 6877–6881.
9. See examples: van Hal, P. A.; Knol, J.; Lamgeveld-Voss, B. H. W.; Meskers, S. C. J.; Hummelen, J. C.; Janssen, R. A. J. *J. Phys. Chem. A* **2000**, *104*, 5974–5988. Segura, J. L.; Martín, N. *Tetrahedron Lett.* **1999**, *40*, 3239–3242. Guldi, D. M.; Luo, C.; Swartz, A.; Gomez, R.; Segura, J. L.; Martín, N. *J. Phys. Chem. A* **2004**, *108*, 455–467. van Hal, P. A.; Beckers, E. H. A.; Meskers, S. C. J.; Janssen, R. A. J.; Jousselme, B.; Blanchard, P.; Roncali, J. *Chem. Eur. J.* **2002**, *8*, 5415–5429. Dhanabalan, A.; Knol, J.; Hummelen, J. C.; Janssen, R. A. J. *Synth. Met.* **2001**, *119*, 519–522.
10. Guldi, D. M.; Luo, C.; Swartz, A.; Gómez, R.; Segura, J. L.; Martín, N.; Brabec, C.; Sariciftci, N. S. *J. Org. Chem.* **2002**, *67*, 1141–1152. Negishi, N.; Takimiya, K.; Otsubo, T.; Harima, Y.; Aso, Y. *Chem. Lett.* **2004**, *33*, 654–655.
11. Brédas, J.-L.; Beljonne, D.; Coropceanu, V.; Cornil, J. *Chem. Rev.* **2004**, *104*, 4971–5003. Fox, M. A. *Acc. Chem. Res.* **1999**, *32*, 201–207.
12. Servet, B.; Horowitz, G.; Ries, S.; Lagorse, O.; Alnot, P.; Yassar, A.; Deloffre, F.; Srivastava, P.; Hajlaoui, R.; Lang, P.; Garnier, F. *Chem. Mater.* **1994**, *6*, 1809–1815. Horowitz, G.; Garnier, F.; Yassar, A.; Hajlaoui, R.; Kouki, F. *Adv. Mater.* **1996**, *8*, 52–54. Garnier, F. *Philos. Trans. R. Soc. London, Ser. A: Math. Phys. Eng. Sci.* **1997**, *355*, 815–827.
13. For a recent review on hydrogen-bonding fullerenes, see: Sánchez, L.; Martín, N.; Guldi, D. M. *Angew. Chem., Int. Ed.* **2005**, *44*, 5374–5382.
14. De Rege, P. J. F.; Williams, S. A.; Therien, M. J. *Science* **1995**, *269*, 1409–1413.
15. Guttierrez-Nava, M.; Nierengarten, H.; Masson, P.; Van Dorsselaer, A.; Nierengarten, J.-F. *Tetrahedron Lett.* **2003**, *44*, 3043–3046.
16. Beckers, E. H. A.; Schenning, A. P. H. J.; Van Hal, P. A.; El-Ghayoury, A.; Sanchez, L.; Hummelen, J. C.; Meijer, E. W.; Janssen, R. A. J. *Chem. Commun.* **2002**, 2888–2889.

17. McClenaghan, N. D.; Absalon, C.; Bassani, D. M. *J. Am. Chem. Soc.* **2003**, *125*, 13004–13005. McClenaghan, N. D.; Bassani, D. M. *Int. J. Photoenergy* **2004**, *6*, 185–192.
18. Whitesides, G. M.; Simanek, E. E.; Mathias, J. P.; Seto, C. T.; Chin, D.; Mammen, M.; Gordon, D. M. *Acc. Chem. Res.* **1995**, *28*, 37–44. Simanek, E. E.; Li, X.; Choi, I. S.; Whitesides, G. M. In Lehn, J. M., Ed.; *Comprehensive Supramolecular Chemistry*; Pergamon: New York, 1996; Vol. 9; Chapter 17.
19. McClenaghan, N. D.; Grote, Z.; Darriet, K.; Zimine, M.; Williams, R. M.; De Cola, L.; Bassani, D. M. *Org. Lett.* **2005**, *7*, 807–810.
20. Robinson, A. P. G.; Palmer, R. E.; Tada, T.; Kanayama, T.; Preece, J. A.; Philp, D.; Jonas, U.; Diederich, F. *Chem. Phys. Lett.* **1998**, *289*, 586–590. Lamparth, I.; Schick, G.; Hirsch, A. *Liebigs Ann. Recl.* **1997**, 253–258.
21. Huang, C.-H.; McClenaghan, N. D.; Kuhn, A.; Hofstraat, J. W.; Bassani, D. M. *Org. Lett.* **2005**, *7*, 3409–3412.
22. Cho, Y.-J.; Ahn, T. K.; Song, H.; Kim, K. S.; Lee, C. Y.; Se, W. S.; Lee, K.; Kwangyeol, K.; Seong, K.; Kim, D.; Park, J. T. *J. Am. Chem. Soc.* **2005**, *127*, 2380–2381. Kim, K.-S.; Kang, M. S.; Ma, H.; Jen, A. K.-Y. *Chem. Mater.* **2004**, *16*, 5058–5062.
23. Guldi, D. M.; Rahman, G. M. A.; Prato, M.; Jux, N.; Qin, S.; Ford, W. *Angew. Chem., Int. Ed.* **2005**, *44*, 2015–2018.
24. Bingel, C. *Chem. Ber.* **1993**, *126*, 1957–1959.
25. Baron, R.; Huang, C.-H.; Bassani, D. M.; Onopriyenko, A.; Zayats, M.; Willner, I. *Angew. Chem., Int. Ed.* **2005**, *44*, 4010–4015.
26. Steinbeck, M.; Ringsdorf, H. *Chem. Commun.* **1996**, 1193–1194.
27. Sudeep, P. K.; Ipe, B. I.; Thomas, K. G.; Gerore, M. V.; Barazzouk, S.; Hotchandani, S.; Kama, P. V. *Nano Lett.* **2002**, *2*, 29–35.
28. Nicolaou, K. C.; Cho, S. Y.; Hughes, R.; Winssinger, N.; Smethurst, C.; Labischinski, H.; Endermann, R. *Chem. Eur. J.* **2001**, *7*, 3798–3823.
29. Compare with: Hirayama, D.; Takimiya, K.; Aso, Y.; Otsubo, T.; Hasobe, T.; Yamada, H.; Imahori, H.; Fukuzumi, S.; Sakata, Y. *J. Am. Chem. Soc.* **2002**, *124*, 532–533. Imahori, H.; Liu, J.-C.; Hosomizu, K.; Sato, T.; Mori, Y.; Hotta, H.; Matano, Y.; Araki, Y.; Ito, O.; Maruyama, N.; Fujita, S. *Chem. Commun.* **2004**, 2066–2067.
30. Lahav, M.; Heleg-Shabtai, V.; Wasserman, J.; Katz, E.; Willner, I.; Dürr, H.; Hu, Y.-Z.; Bossmann, S. H. *J. Am. Chem. Soc.* **2000**, *122*, 11480–11487. Imahori, H.; Norieda, H.; Yamada, H.; Nishimura, Y.; Yamazaki, I.; Sakata, Y.; Fukuzumi, S. *J. Am. Chem. Soc.* **2001**, *123*, 100–110.
31. Brabec, C. J.; Padinger, F.; Hummelen, J. C.; Janssen, R. A. J.; Sariciftci, N. S. *Synth. Met.* **1999**, *102*, 861–864.
32. Porter, M. D.; Bright, T. B.; Allara, D. L.; Chidsey, C. E. D. *J. Am. Chem. Soc.* **1987**, *109*, 3559–3568.
33. Ulman, A. *Chem. Rev.* **1996**, *96*, 1533–1554. Love, J. C.; Estroff, L. A.; Kriebel, J. K.; Nuzzo, R. G.; Whitesides, G. M. *Chem. Rev.* **2005**, *105*, 1103–1169. Rong, H.-T.; Frey, S.; Yang, Y.-J.; Zharnikov, M.; Buck, M.; Wühn, M.; Wöll, C.; Helmchen, G. *Langmuir* **2001**, *17*, 1582–1593. Cyganik, P.; Buck, M. *J. Am. Chem. Soc.* **2004**, *126*, 5960–5961.
34. Ekgasit, S.; Yu, F.; Knoll, W. *Langmuir* **2005**, *21*, 4077–4082.

Synthesis of fullerohelicates and fine tuning of the photoinduced processes by changing the number of addends on the fullerene subunits

Michel Holler,^a François Cardinali,^a Hind Mamlouk,^a Jean-François Nierengarten,^{a,b,*}
Jean-Paul Gisselbrecht,^c Maurice Gross,^c Yannick Rio,^d Francesco Barigelletti^d
and Nicola Armaroli^{d,*}

^aGroupe de Chimie des Fullerènes et des Systèmes Conjugués, Ecole Européenne de Chimie, Polymères et Matériaux, Université Louis Pasteur et CNRS, 25 rue Becquerel, 67087 Strasbourg Cedex 2, France

^bGroupe de Chimie des Fullerènes et des Systèmes Conjugués, Laboratoire de Chimie de Coordination du CNRS, 205 route de Narbonne, 31077 Toulouse Cedex 4, France

^cLaboratoire d'Electrochimie et de Chimie Physique du Corps Solide, Université Louis Pasteur et CNRS, 4 rue Blaise Pascal, 67070 Strasbourg Cedex, France

^dIstituto per la Sintesi Organica e la Fotoreattività, Molecular Photoscience Group, Consiglio Nazionale delle Ricerche, via Gobetti 101, 40129 Bologna, Italy

Received 10 June 2005; revised 5 July 2005; accepted 8 July 2005

Available online 2 December 2005

Abstract—Two fullerene-substituted *m*-phenylene-bis-phenanthroline ligands have been prepared. The synthesis of the first derivative (**L1**) is based on an esterification reaction between a C₅ symmetrical *cis*-2 fullerene bis-adduct bearing a carboxylic acid function and a bis-phenanthroline alcohol (**5**). The second ligand (**L2**) has been obtained by reaction of a bis-phenanthroline malonate (**9**) and C₆₀ under Bingel conditions. The copper(I) complexes of **L1** and **L2** have been prepared by treatment with a slight excess of Cu(CH₃CN)₄BF₄. NMR spectroscopy and mass spectrometry analysis have unambiguously shown that these complexes are bis-copper(I) helicates substituted with two fullerene moieties. The photophysical properties of the copper(I) complexes Cu₂(**L1**)₂ and Cu₂(**L2**)₂ have been investigated. In both systems photoinduced electron transfer from the central metal-complexed unit to the external fullerenes may occur, in principle, by excitation of both moieties. However, this is found to be the case only for the methanofullerene system Cu₂(**L2**)₂. Unexpectedly, for Cu₂(**L1**)₂, photoexcitation of the peripheral carbon spheres is followed by regular internal deactivation. Possible reasons for this behavior are examined in light of current theories for photoinduced energy and electron transfer.

© 2006 Elsevier Ltd. All rights reserved.

1. Introduction

Transition metals have been widely used for the construction of spectacular two- and three-dimensional supramolecular structures.^{1–10} Among these self-assembled systems, polymetallic helical coordination compounds have generated significant research efforts in the last two decades.^{11–13} Such supramolecular arrays, named helicates by Lehn,¹⁴ have been intensively studied to understand metal-directed self-assembly processes.¹⁵ Furthermore, the structural features of helicates have been beautifully exploited by Sauvage and Dietrich-Buchecker as templates

for the synthesis of topologically non-trivial compounds such as molecular knots^{16,17} and doubly-interlocked [2]catenanes.¹⁸ In recent years, this field has moved towards the creation of functional systems with increased attention to potential applications. For example, it has been shown by Ziessel and co-workers that a helicate core can behave as a mesogenic unit, thus providing an original chiral scaffold for the preparation of new liquid crystals.¹⁹ As part of this research, we have recently shown that helicates can be incorporated in photoactive supramolecular functional devices.²⁰ Specifically, a bis-copper(I) helicate substituted with two fullerene moieties has been prepared. Photophysical measurements have revealed that photoinduced electron transfer occurs from the photoexcited Cu(I)-complexed unit to the C₆₀ acceptor thus showing that such helicate-acceptor arrays are potentially interesting candidates for the preparation of solar cells. In this paper,

Keywords: Copper(I) complexes; Electron transfer; Fullerene; Phenanthroline ligands; Photophysical properties.

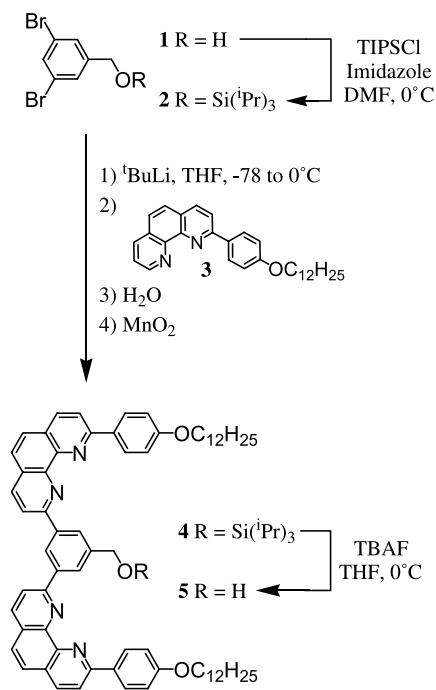
* Corresponding authors. Tel.: +33 561 33 31 00; fax: +33 561 55 30 03 (J.-F.N.); Tel.: +39 051 639 9820; fax: +39 051 639 9844 (N.A.); e-mail addresses: jfnierengarten@lcc-toulouse.fr; armaroli@isof.cnr.it

we now give a full account on the synthesis and the electronic properties of these fullerene-substituted helicates, that is, fullerohelicates.

2. Results and discussion

2.1. Preparation of the bis-phenanthroline ligands

In the design of these compounds, we have selected a *m*-phenylene-bis-phenanthroline core known to form a double-stranded helicate upon complexation to copper(I).²¹ This ligand was actually functionalized with a hydroxy group to allow the attachment of the two fullerene subunits at the end of the synthesis. The synthesis of the bis-phenanthroline precursor is depicted in Scheme 1. Reaction of 3,5-dibromobenzyl alcohol (**1**) with triisopropylsilyl chloride (TIPSCl) in DMF in the presence of imidazole gave the protected alcohol **2** in 83% yield. Treatment of **2** with an excess of ^tBuLi at –78 °C followed successively by reaction of the resulting organolithium derivative with mono-substituted phenanthroline **3**²² (0.5 equiv), hydrolysis and rearomatization with MnO₂ afforded **4** in 31% yield. This moderate yield is mainly associated to the difficulties encountered during the purification of compound **4**. Indeed, ligand **4** has a high affinity for lithium²³ and even by washing extensively the crude material with water, an important part of the fractions of **4** obtained upon column chromatography on SiO₂ are polluted with traces of Li complexes of **4**. Finally, treatment of TIPS-protected derivative **4** with tetra-*n*-butylammonium fluoride (TBAF) in THF at 0 °C then gave compound **5** in 88% yield.



Scheme 1. Preparation of bis-phenanthroline **5**.

The preparation of the first C₆₀-substituted bis-phenanthroline ligand (**L1**) is based on an esterification reaction between a fullerene derivative bearing a carboxylic acid function and

alcohol **5** (Scheme 2). To this end, compound **6** was prepared first. This C_s symmetrical *cis*-2 fullerene bis-adduct was obtained in ten steps according to a previously reported procedure.²⁴ Treatment of *t*-butyl ester **6** with CF₃CO₂H in CH₂Cl₂ gave the corresponding carboxylic acid derivative **7** in a quantitative yield. Subsequent reaction with benzylic alcohol **5** under esterification conditions using *N,N'*-dicyclohexylcarbodiimide (DCC), 4-dimethylaminopyridine (DMAP) and 1-hydroxybenzotriazole (HOBT) led to ligand **L1** in 24% yield.

The synthesis of the second C₆₀-substituted bis-phenanthroline ligand relies upon Bingel type chemistry²⁵ and is shown in Scheme 3. DCC-mediated esterification of benzylic alcohol **5** with carboxylic acid **8**²⁴ yielded malonate **9**. The reaction of C₆₀ with compound **9**, iodine and 1,8-diazabicyclo[5.4.0]undec-7-ene (DBU) under Bingel conditions then gave methanofullerene **L2** in 22% yield.

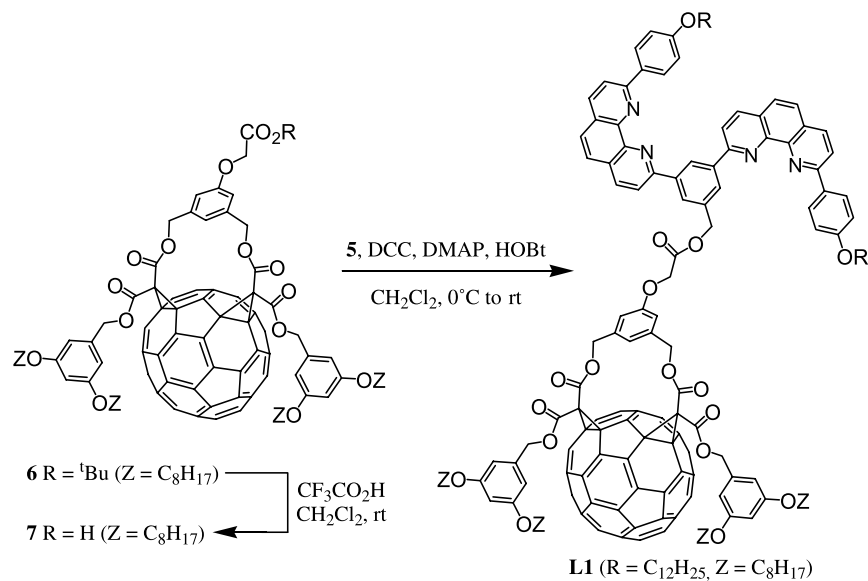
Ligands **L1** and **L2** were characterized by ¹H- and ¹³C NMR, UV–vis and IR spectroscopies. The ¹H NMR spectra of both compounds show the signals of the *m*-phenylene-bis-arylphenanthroline core. Effectively, both spectra are characterized by three sets of AB quartets in the aromatic region in a typical pattern for a disymmetrically 2,9-disubstituted-1,10-phenanthroline derivative, an AA'XX' system for the aromatic protons of the 4-didodecyloxyphenyl unit and an A₂X system for the aromatic protons of the central phenyl ring. In the case of compound **L2**, the ¹H NMR spectrum reveals also two singlets at δ 5.96 and 5.48 ppm corresponding to the resonances of the two different benzylic CH₂ groups, an A₂X system for the aromatic protons of the 3,5-dioctyloxyphenyl moiety as well as the diagnostic signals of the alkyloxy groups. The ¹H NMR spectrum of **L1** shows all the characteristic features of the C_s symmetrical 1,3-phenylenebis(methylene)-tethered fullerene *cis*-2 bis-adduct substituent.²⁶ Effectively, in addition to the signals arising from the 3,5-dioctyloxyphenyl moieties, an AB quartet and a singlet are observed for the diastereotopic benzylic CH₂ groups and an AX₂ system is revealed for the aromatic protons of the 1,3,5-trisubstituted bridging phenyl ring. Finally, the ¹³C NMR spectra of **L1** and **L2** are typical of C_s symmetric fullerene derivatives in full accordance with the proposed molecular structures.

In addition, methanofullerene **11** used as reference compound for the photophysical studies was prepared in two steps from malonic acid **8** (Scheme 4). DCC-mediated esterification of **8** with EtOH afforded **10** in 73% yield. Subsequent treatment with C₆₀ in the presence of I₂ and DBU yielded compound **11** in 31% yield.

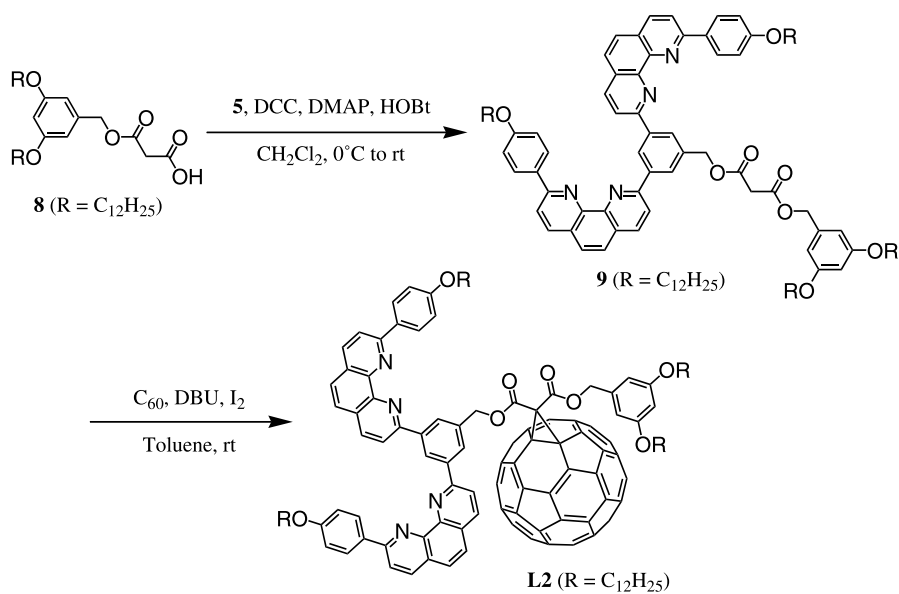
2.2. Preparation of the copper(I) helicates

The copper(I) complexes Cu₂(**4**)₂, Cu₂(**L1**)₂ and Cu₂(**L2**)₂ (Fig. 1) were obtained by treatment of the corresponding ligands with a slight excess of Cu(CH₃CN)₄BF₄ in CH₂Cl₂/CH₃CN at room temperature.

Cu₂(**4**)₂ was thus formed in a good yield; however, due to difficulties encountered during its purification, the isolated yield was quite low (22%). Actually, a part of the product stuck all along the SiO₂ (or Al₂O₃) column (this could be easily observed because of the compound's dark red color)



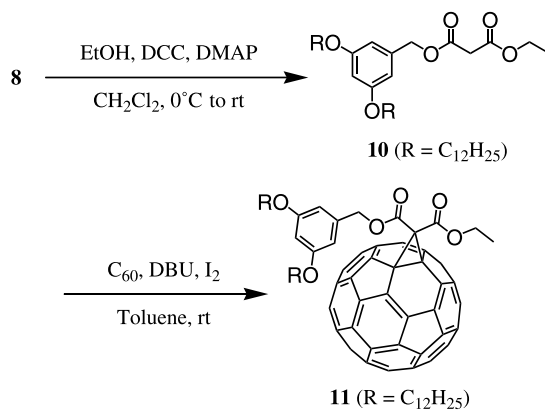
Scheme 2. Preparation of ligand L1.



Scheme 3. Preparation of ligand L2.

and could not be eluted any more. In order to prevent this problem, the copper(I) complexes obtained from ligands L1 and L2 were not purified by column chromatography on SiO₂ or Al₂O₃. Indeed, we found that gel permeation chromatography (Biorads, Biobeads SX-1, CH₂Cl₂) was an efficient tool to obtain both compounds in a pure form without significant loss of material. Cu₂(L1)₂ and Cu₂(L2)₂ were thus isolated in 75 and 52% yield, respectively.

The ¹H NMR spectra of ligand 4 and complex Cu₂(4)₂ are depicted in Figure 2. Upon complexation to copper(I), dramatic changes are observed for the chemical shift of the signals corresponding to the protons belonging to the bis-phenanthroline moiety due to the stacking of the aromatic subunits in the helicate. As a result of the ring current effect of the aromatic units of one *m*-phenylene-bis-aryphenanthroline moiety on the second ligand in



Scheme 4. Preparation of model compound 11.

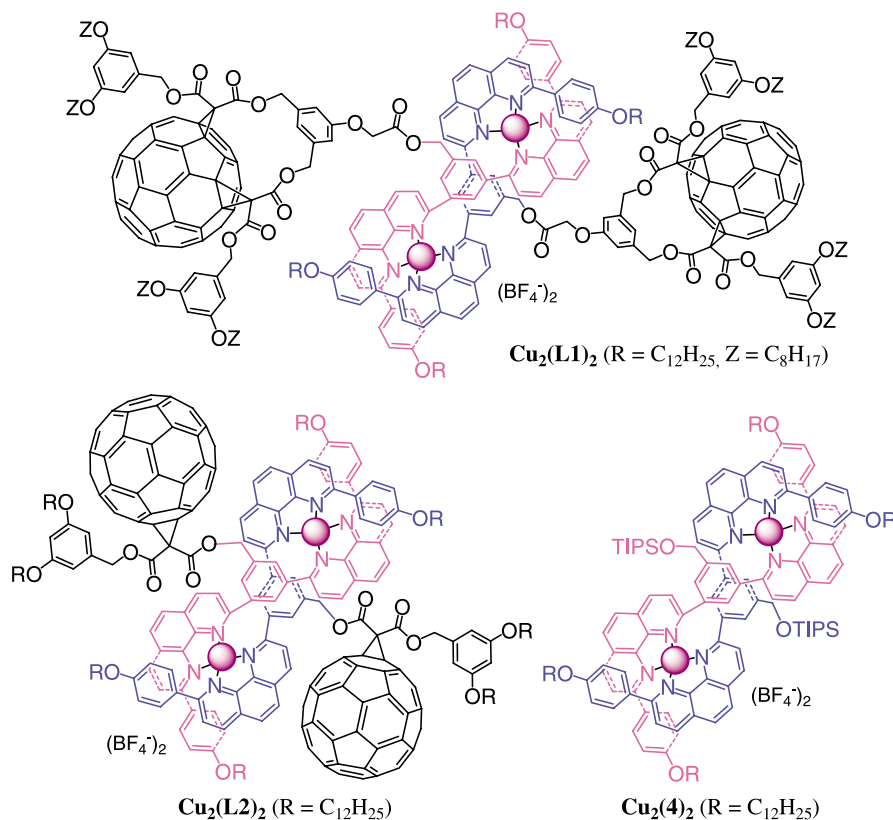


Figure 1. Helicates $\text{Cu}_2(\mathbf{4})_2$, $\text{Cu}_2(\text{L1})_2$ and $\text{Cu}_2(\text{L2})_2$.

the complex, the signals of the aromatic protons are shielded by about 0.2–2.0 ppm in $\text{Cu}_2(\mathbf{4})_2$ when compared to the corresponding signals in ligand **4**. The shielding effect is particularly dramatic for protons H_b , H_c , H_d , H_3 and H_4 as one could expect by a simple inspection of the calculated

structure of $\text{Cu}_2(\mathbf{4})_2$ (Fig. 2). Importantly, the ^1H NMR spectrum provide clear evidence for the formation of a chiral complex, that is, a helical system. In particular, the methylenic protons that were enantiotopic in ligand **4** are not equivalent any longer in complex $\text{Cu}_2(\mathbf{4})_2$ and give rise

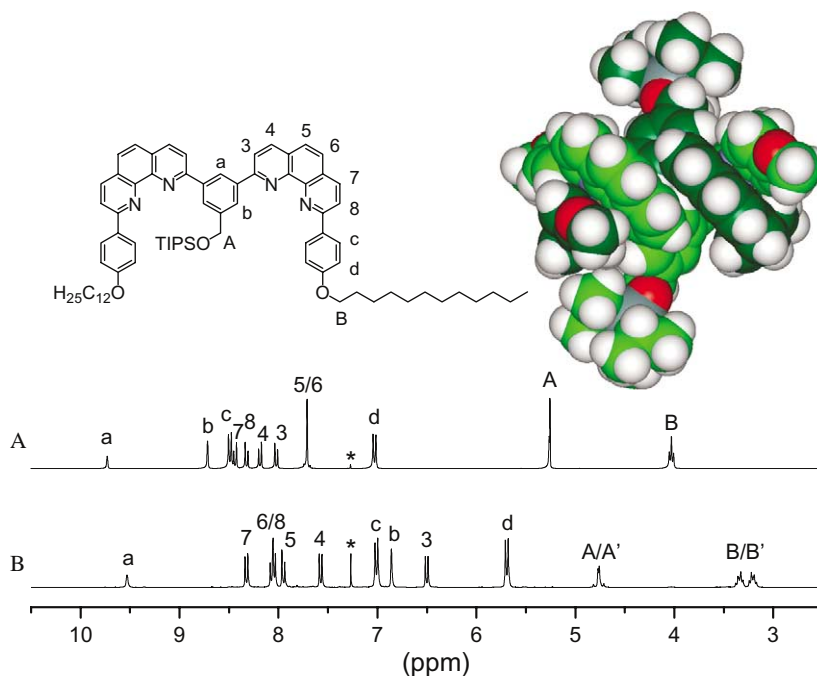


Figure 2. (A) ^1H NMR spectrum (CDCl_3 , 300 MHz, *: solvent peak) of ligand **4**. (B) ^1H NMR spectrum (CDCl_3 , 300 MHz, *: solvent peak) of helicate $\text{Cu}_2(\mathbf{4})_2$. Top: calculated structure of $\text{Cu}_2(\mathbf{4})_2$ (the four dodecyloxy groups have been replaced by methoxy units for clarity).

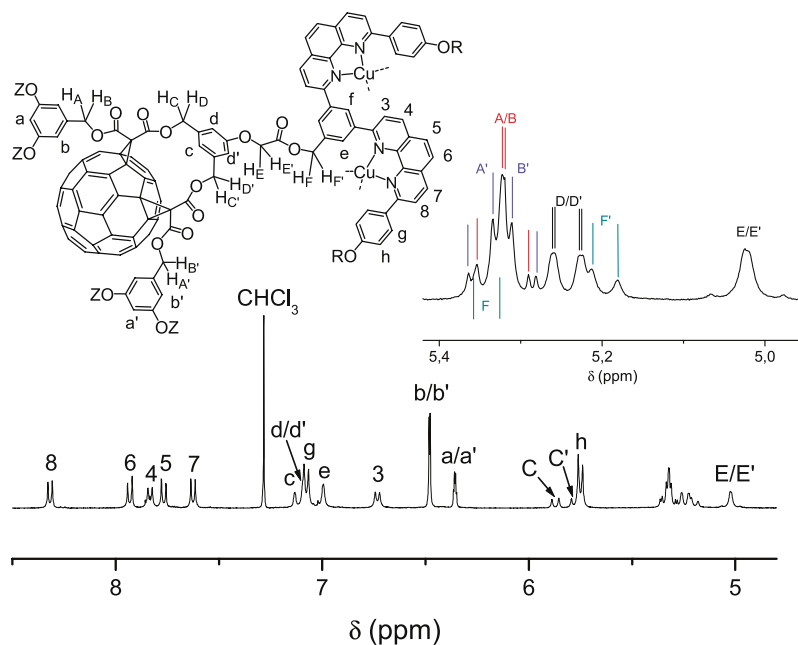


Figure 3. ^1H NMR spectrum (CDCl_3 , 400 MHz) of fullerohelicate $\text{Cu}_2(\text{L1})_2$. The six AB quartets corresponding to the resonances of the six different diastereotopic CH_2 groups provide definitive evidence for the helical structure. Unambiguous assignment was achieved on the basis of 2D-COSY and NOESY spectra recorded at room temperature in CDCl_3 .

to more complicated sets of signals. For example, the benzylic protons of the CH_2OTIPS unit are observed as a singlet at δ 5.25 ppm in **4** while they appear as an AB quartet at δ 4.77 ppm in the corresponding copper(I) complex. Indeed, these protons are enantiotopic in **4** and diastereotopic in the chiral complex $\text{Cu}_2(\text{4})_2$.

As observed for $\text{Cu}_2(\text{4})_2$, dramatic changes in chemical shift are seen for the resonances of the aromatic protons of the bis-phenanthroline subunit in the ^1H NMR spectra of $\text{Cu}_2(\text{L1})_2$ and $\text{Cu}_2(\text{L2})_2$ when compared to the corresponding signals in the spectrum of **L1** and **L2**. Owing to the chirality of both $\text{Cu}_2(\text{L1})_2$ and $\text{Cu}_2(\text{L2})_2$, the 2 equiv fullerene moieties have lost their plane of symmetry. For this reason, some of the protons that were equivalent in the ligands are not equivalent any longer in the complex. This is illustrated with the ^1H NMR spectra of $\text{Cu}_2(\text{L1})_2$ (Fig. 3). In particular, the six AB quartets corresponding to the resonances of the six different diastereotopic CH_2 groups provide definitive evidence for the helical structure. The structure of $\text{Cu}_2(\text{L1})_2$ was also confirmed by mass spectrometry. The FAB-MS of $\text{Cu}_2(\text{L1})_2$ is characterized by a singly charged peak at m/z 5734.0 and a doubly charged ion peak at m/z 2824.7, which can be assigned to $\text{Cu}_2(\text{L1})_2$ after loss of one and two tetrafluoroborate counteranions, respectively.

2.3. Electrochemical properties

The electrochemical properties of **6**, **11**, $\text{Cu}_2(\text{4})_2$, $\text{Cu}_2(\text{L1})_2$ and $\text{Cu}_2(\text{L2})_2$ were investigated by cyclic voltammetry (CV) in $\text{CH}_2\text{Cl}_2 + 0.1 \text{ M } n\text{Bu}_4\text{NPF}_6$ solutions. The results are summarized in Table 1. As a typical example, the cyclic voltammogram recorded for $\text{Cu}_2(\text{L1})_2$ is depicted in Figure 4.

Table 1. Reduction and oxidation characteristics of **6**, **11**, $\text{Cu}_2(\text{4})_2$, $\text{Cu}_2(\text{L1})_2$ and $\text{Cu}_2(\text{L2})_2$ observed by CV on a glassy C electrode in $\text{CH}_2\text{Cl}_2 + 0.1 \text{ M } \text{Bu}_4\text{NPF}_6^a$

Compound	Oxidation		Reduction	
	E_2	E_1	E_1	E_2
6			−1.07 (45) ^b	−1.45 ^{b,c}
11			−1.03 (80)	−1.41 (80)
$\text{Cu}_2(\text{4})_2$	+0.46 (75)	+0.35 (100)	−1.83 (95)	−2.23 ^c
$\text{Cu}_2(\text{L1})_2$	+0.57 (75)	+0.37 (75)	−1.07 (100) ^d	−1.44 ^c
$\text{Cu}_2(\text{L2})_2$	+0.61 (75)	+0.41 (80)	−0.96 (80) ^d	−1.42 (90) ^d

^a Values for $(E_{\text{pa}} + E_{\text{pc}})/2$ (V vs Fc/Fc^+) and ΔE_{pc} (mV, in parenthesis) at a scan rate of 0.1 V s^{-1} .

^b From Ref. 29.

^c Peak potential values at a scan rate of 0.1 V s^{-1} , irreversible process.

^d Dielectronic process.

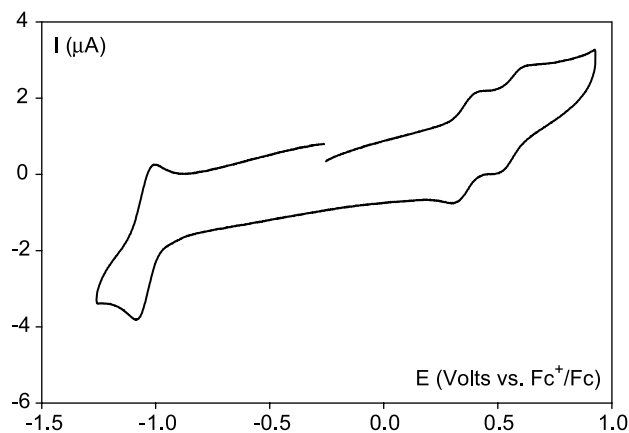


Figure 4. Cyclic voltammetry of fullerohelicate $\text{Cu}_2(\text{L1})_2$ on a glassy carbon electrode at $v=0.1 \text{ V s}^{-1}$ in $\text{CH}_2\text{Cl}_2 + 0.1 \text{ M } \text{Bu}_4\text{NPF}_6$.

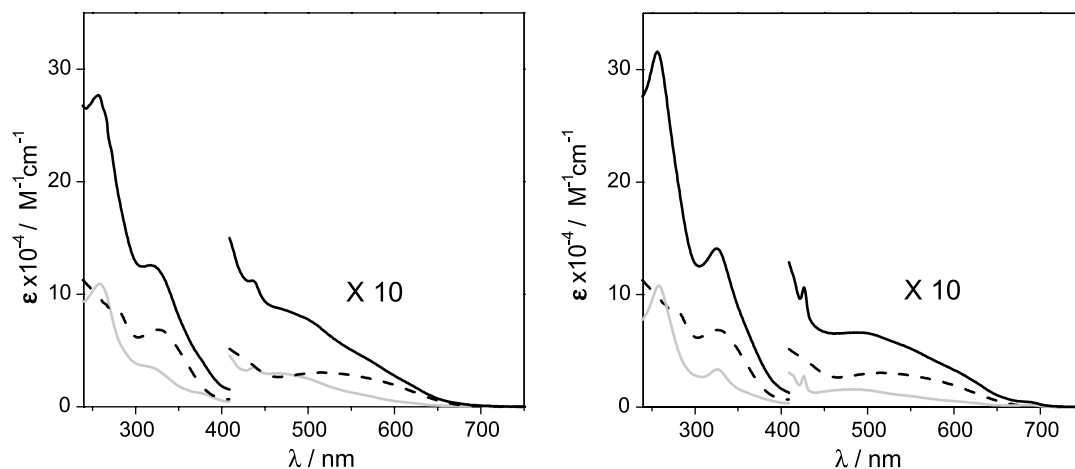


Figure 5. Left: absorption spectra of **6** (grey full line), $\text{Cu}_2(\mathbf{4})_2$ (black dashed line) and $\text{Cu}_2(\mathbf{L1})_2$ (black full line) in CH_2Cl_2 . Right: absorption spectra of **11** (grey full line), $\text{Cu}_2(\mathbf{4})_2$ (black dashed line) and $\text{Cu}_2(\mathbf{L2})_2$ (black full line) in CH_2Cl_2 .

As already reported for related copper(I) helicates,^{20,27,28} a strong electronic interaction between both copper atoms in $\text{Cu}_2(\mathbf{4})_2$, $\text{Cu}_2(\mathbf{L1})_2$ and $\text{Cu}_2(\mathbf{L2})_2$ is evidenced by the electrochemical measurements. Effectively, the anodic region of their cyclic voltammograms is characterized by two distinct waves for the Cu-centered oxidations. In other words, the second oxidation process occurs at a higher potential, indicating the influence of the first Cu(II) center, which renders oxidation of the second metal more difficult. Comparison of the oxidation potentials of $\text{Cu}_2(\mathbf{L1})_2$ and $\text{Cu}_2(\mathbf{L2})_2$ with those of the corresponding model compound $\text{Cu}_2(\mathbf{4})_2$ shows a small but evident trend. The two oxidation potentials of both $\text{Cu}_2(\mathbf{L1})_2$ and $\text{Cu}_2(\mathbf{L2})_2$ are slightly shifted to more positive values by 20–110 and 60–150 mV, respectively. These shifts could be a consequence of small electronic interactions between the dinuclear copper(I) core and the C_{60} units, resulting in a more difficult oxidation for the metallic centers. However, the photophysical studies revealed no particular electronic interactions between the fullerene moieties and the helicate core (see below). In addition, the different subunits are separated by rather long spacers. Therefore, it appears more reasonable to ascribe the observed potential shift to solvation effects resulting from the presence of the surrounding apolar fullerene groups.

As far as the reduction potentials are concerned, the two fullerene subunits behave as independent redox centers in both $\text{Cu}_2(\mathbf{L1})_2$ and $\text{Cu}_2(\mathbf{L2})_2$. Compounds **11** and $\text{Cu}_2(\mathbf{L2})_2$ show a similar behavior totally consistent with previously reported data for methanofullerenes.^{29,30} Fullerene *cis*-2 bis-adducts $\text{Cu}_2(\mathbf{L1})_2$ and **6** essentially retain the cathodic electrochemical pattern of methanofullerenes but the reduction potentials are shifted to more negative values when compared to those of $\text{Cu}_2(\mathbf{L2})_2$ and **11**. Indeed, this small shift results from the saturation of an additional double bond on the C_{60} surfaces, which causes a partial loss of ‘conjugation’ when going from mono- to bis-adducts.

2.4. Photophysical properties

Reference compounds. The photophysical properties of methanofullerenes and bis-methanofullerenes have already been investigated in detail.^{29,31,32} They exhibit a broad absorption throughout the UV–vis region and a weak fluorescence centered at about 700 nm. For the sake of comparison with the corresponding helicates the absorption and fluorescence spectra of **6** and **11** in CH_2Cl_2 are depicted in Figures 5 and 6, whereas in Table 2 fluorescence quantum yields and singlet lifetimes are reported.

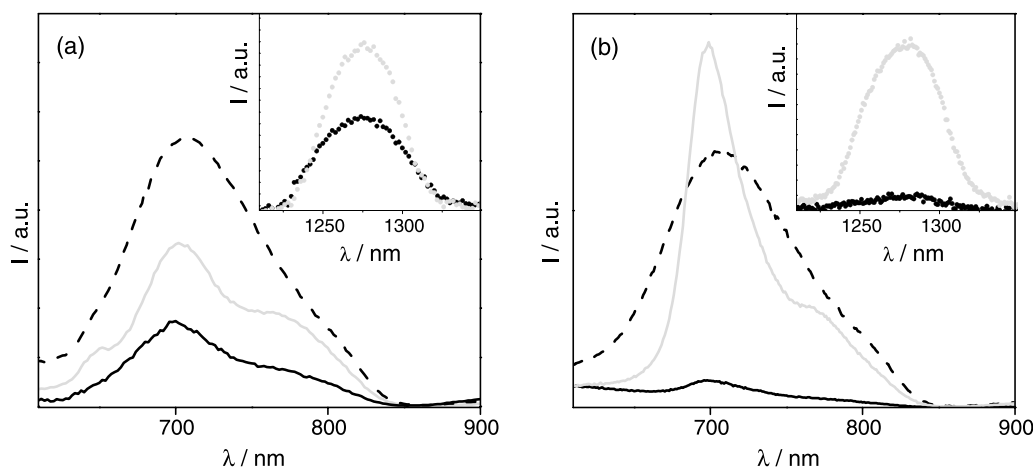


Figure 6. (a) Emission spectra of **6** (grey full line), $\text{Cu}_2(\mathbf{4})_2$ (black dashed line) and $\text{Cu}_2(\mathbf{L1})_2$ (black full line) in CH_2Cl_2 . (b) Emission spectra of **11** (grey full line), $\text{Cu}_2(\mathbf{4})_2$ (black dashed line) and $\text{Cu}_2(\mathbf{L2})_2$ (black full line) in CH_2Cl_2 . Inset: sensitized singlet oxygen luminescence spectra of reference fullerenes (grey) and multicomponent arrays (black). In all cases $\lambda_{\text{ex}} = 540$ (a) and 500 nm (b) where light partitioning Cu/ C_{60} is 1/1. Absorbance = 0.30, uncorrected spectra.

Table 2. Photophysical properties in CH₂Cl₂ at 298 K

	C ₆₀ fluorescence			MLCT band		
	λ_{max} (nm) ^a	τ (ns)	$\phi \times 10^4$	λ_{max} (nm) ^a	τ (ns)	$\phi \times 10^4$
Cu₂(4)₂	—	—	—	707 (741)	<0.2, 130	6.9
6	702 (704)	1.4	3.0	—	—	—
Cu₂(L1)₂	702 (704) ^b	1.4	3.0	—	—	—
11	698 (698)	1.4	4.5	—	—	—
Cu₂(L2)₂	702 (704)	^c	0.7	—	^d	—

^a In brackets are reported the emission maxima from spectra corrected for the photomultiplier response.

^b The uncorrected emission spectrum published earlier (see Ref. 20) was obtained with a different, near-IR sensitive photomultiplier tube.

^c Non detectable due to signal weakness.

^d Only the short-lived component ($\tau < 0.2$ ns) is detected.

The absorption and luminescence properties of **Cu₂(4)₂**, to be used as reference for the helicate core, are in line with analogous Cu(I) complexes of 2,9-diphenyl-phenanthroline ligands and the typical metal-to-ligand-charge-transfer (MLCT) emission band around 700 nm is recorded.^{33–37} Notably, the luminescence decay trace is biexponential with $\tau_1 < 0.5$ ns and $\tau_2 = 130$ ns (oxygen free CH₂Cl₂, Fig. 7). Since excitation is addressed selectively to the low energy side of the MLCT bands ($\lambda_{\text{exc}} = 637$ nm), one can exclude excitation of the free phenanthroline ligand or its protonated form.^{38–40}

The formation of the long-lived MLCT emitting state in copper(I)-phenanthrolines is preceded by extensive structural rearrangements, namely (i) flattening distortion of the initial pseudo-tetrahedral Franck-Condon geometry and (ii) expansion of the coordination number.^{41,42} These processes occur in the tens of picosecond timescale.⁴³ The short-lived component observed for **Cu₂(4)₂**, whose lifetime is shorter than our instrumental resolution (200 ps), might be associated with excited states that have not yet undergone structural rearrangements. The long-lived component is attributed to ‘relaxed’ excited states and stems from ¹MLCT and ³MLCT levels in thermal equilibrium and separated by an energy gap of about 1500 cm⁻¹.^{44,45}

Fullerohelicate Cu₂(L1)₂. The electronic absorption spectrum of the bismethanofullerene **Cu₂(L1)₂** in CH₂Cl₂ is reported in Figure 5 and corresponds well to the sum of the absorption spectra of its component units (**6** and **Cu₂(4)₂**). This is in contrast with what was observed for a Cu(I)-bisphenanthroline complex sandwiched between two fullerenes, where the absorption spectrum indicates electronic interactions among the subunits.⁴⁶ In **Cu₂(L1)₂** a spacer is inserted between the inorganic core and the organic units. Thus, although the system is relatively flexible, the interchromophoric distance is long enough to prevent electronic interactions observable in the absorption spectra.

Since excitation cannot be selectively addressed to a specific subunit of **Cu₂(L1)₂**, we chose to excite at 540 nm where the light partitioning among the Cu(I) chromophores and carbon spheres in **Cu₂(L1)₂** is identical.⁴⁶ Under these conditions the quenching of the long-lived MLCT luminescence band is complete and only a fluorescence band attributable to the C₆₀ moiety is detected, which exhibits the same lifetime and a 50% intensity decrease relative to the reference molecule **6** (Table 2 and Fig. 6). A 50% decrease of the fullerene triplet yield is also measured, by means of the intensity of the sensitized singlet oxygen emission band (Fig. 6).⁴⁷ From the above results it is possible to conclude that (i) the metal complexed core of **Cu₂(L1)₂** undergoes photoinduced quenching not attributable to energy transfer because no sensitization of the fullerene singlet and triplet states occur; (ii) following light excitation, the fullerene moieties of **Cu₂(1)₂** behave in the same way as the reference molecule **6**.²⁰

Fullerohelicate Cu₂(L2)₂. The absorption spectrum of **Cu₂(L2)₂** corresponds to the sum of the spectra of its component units (**Cu₂(4)₂** + **11** × 2), indicating negligible electronic interactions among the organic and the inorganic fragments. The most important difference that characterizes the methanofullerene **Cu₂(L2)₂** versus the bis-methanofullerene **Cu₂(L1)₂** helicate is the fact that in the former, at any excitation wavelengths, both the MLCT emission and the fullerene fluorescence are dramatically quenched (Fig. 6). Interestingly the only signal detected in the lifetime

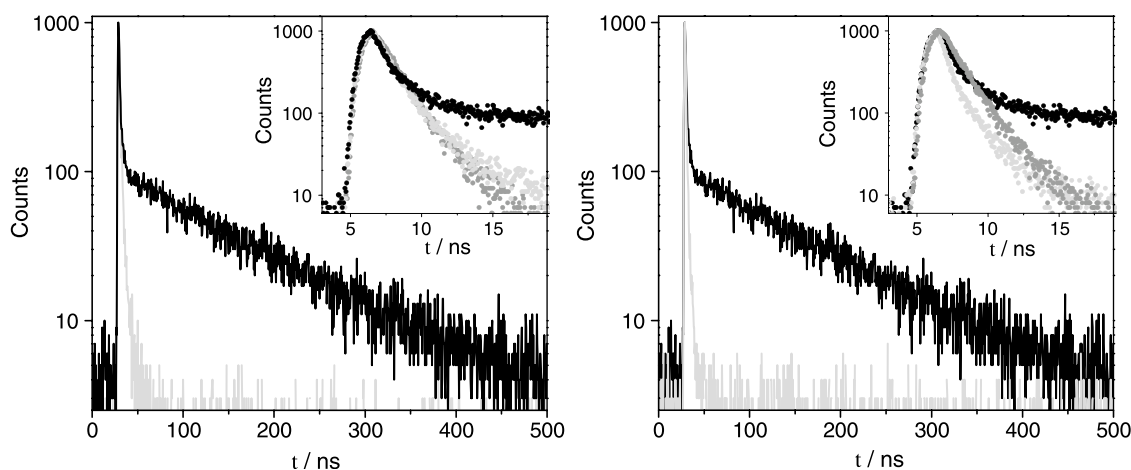


Figure 7. Left: time profile of luminescence of **6** (grey), **Cu₂(4)₂** (black) and **Cu₂(L1)₂** (light grey) in CH₂Cl₂. Right: time profile of luminescence of **11** (grey), **Cu₂(4)₂** (black) and **Cu₂(L2)₂** (light grey) in CH₂Cl₂.

experiments of $\text{Cu}_2(\text{L}2)_2$ is the ultrashort-lived component of the MLCT emission (Fig. 7, right). This indicates that the intercomponent process related to the quenching of the MLCT emission band is slower than the molecular rearrangements, which follow photoexcitation (see above). A negligible amount of fullerene triplet is evidenced by the sensitized singlet oxygen experiments (Fig. 6) and transient absorption spectra.

Energy diagrams and rationale. The energy level diagrams reporting the lowest electronic levels of $\text{Cu}_2(\text{L}1)_2$ and $\text{Cu}_2(\text{L}2)_2$ are depicted in Figure 8; they facilitate the rationalization of the above described light induced processes, which are different for the two helicates.

The energy level of the $^3\text{MLCT}$ state (1.59 eV) and of the fullerene singlet were determined by 77 K emission spectra, whereas the $^1\text{MLCT}$ state is positioned taking into account a gap of about 1500 cm^{-1} relative to $^3\text{MLCT}$.³⁵ The energy of the fullerene lowest triplets cannot be determined experimentally due to the lack of phosphorescence emission and was estimated by theoretical calculations.^{29,32} Finally, the charge separated states are estimated from the one-electron redox potential,⁴⁸ without considering coulombic interactions. This approximation is acceptable since no electronic interactions are evidenced in the ground state for these helicates and, in addition, the coulombic contribution has been shown to be negligible in fullerene multicomponent systems.⁴⁹ Apart from the different location of the fullerene triplet states, which probably do not actively participate in photoinduced processes and are likely to be positioned with scarce precision from theoretical methods a relevant, albeit small, difference in the diagrams of the two helicates seems to be the energy of the charge separated states.

In the case of the bis-methano fullerene system $\text{Cu}_2(\text{L}1)_2$ quenching by electron transfer of the $^3\text{MLCT}$ state is the only possibility, because no sensitization of the fullerene levels is observed, ruling out the possibility of energy transfer.²⁰ By contrast, direct excitation of the fullerene moieties ends up into unmodified deactivation of the carbon sphere relative to the model compounds.

From the energy diagram in Figure 8 it is evident, for $\text{Cu}_2(\text{L}1)_2$, that electron transfer from either Cu^{-1}F

(fullerene singlet) or $^3\text{Cu}_{\text{MLCT}}\text{-F}$ ($^3\text{MLCT}$, Cu-complexed moiety) are both moderately exergonic ($\Delta G^0 = -0.31$ and -0.15 eV, respectively). In both cases electron transfer can be reasonably located in the normal region of the Marcus parabola;⁴⁸ thus, in principle, the fullerene singlet should promote a faster electron transfer than $^3\text{MLCT}$ due to the larger reaction exoergonicity. However, the experimental trend is the opposite. As discussed previously with a similar system⁴⁶ we attribute this ‘asymmetric’ behavior (i.e., electron transfer originated only upon excitation of the central core, despite similar thermodynamics when the peripheral C_{60} 's are stimulated) to the different nature of the involved excited states, that is, charge transfer versus localized. In particular, formation of a metal-to-ligand-charge-transfer state, which occurs prior to $\text{Cu} \rightarrow \text{C}_{60}$ electron transfer, lowers both external and internal reorganization energies related to the process and abates the kinetic activation barrier.⁴⁶ The external contribution is related to the solvent repolarization around the newly formed charged species while the internal reorganization energy has to do with the molecular internal rearrangements that accompany electron transfer processes. These events, which facilitates electron transfer, occur to some extent when the lowest MLCT state(s) of Cu(I)-phenanthrolines are formed, whereas do not take place upon formation of a localized $\pi\pi^*$ state (i.e., C_{60} singlet). In addition to these arguments it must also be emphasized that the formation of a MLCT state prior to the final charge separation may contribute to yield a better electronic interaction between the two chromophores since it causes redistribution of negative charge on the phenyl-phenanthroline ligand,⁵⁰ that is, in the direction of the attached C_{60} electron acceptor, according to the helicate structures. This makes the donor-acceptor distance effectively smaller, likely favoring the reaction kinetics. Similar electronic effects on the rate of photoinduced electron transfer have been recently observed for organic⁵¹ and hybrid⁵² donor-acceptor arrays.

In the case of the methanofullerene system $\text{Cu}_2(\text{L}2)_2$ the quenching of the $^3\text{MLCT}$ state may occur, in principle, via electron transfer to the lower lying charge separated state ($\Delta G^0 = -0.22$ eV) or via energy transfer to fullerene triplet level (ΔG^0 ca. -0.10 eV), followed by charge separation (ΔG^0 ca. -0.12 eV). All these processes occur at a faster rate than the resolution of

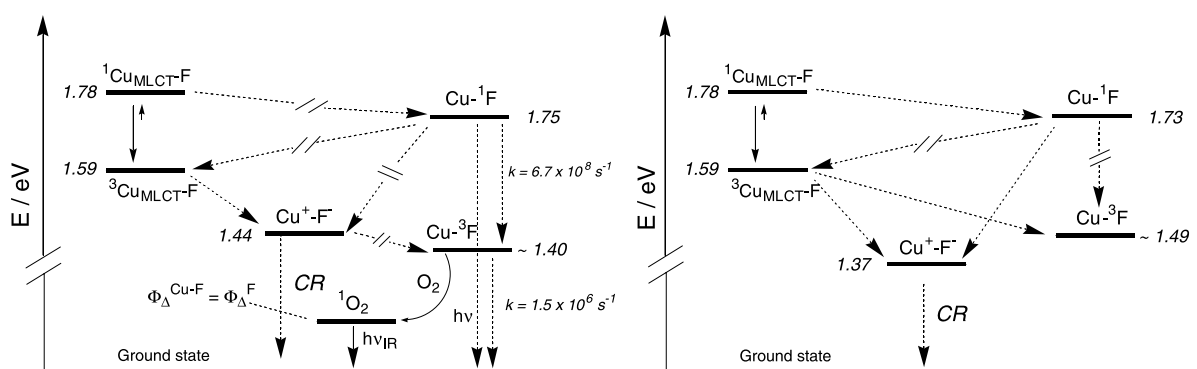


Figure 8. Energy level diagrams of $\text{Cu}_2(\text{L}1)_2$ (left) and $\text{Cu}_2(\text{L}2)_2$ (right) with the related photoinduced processes upon excitation of both chromophores. In the shorthand notations, where Cu-F stands for the fullerohelicates $\text{Cu}_2(\text{L}1)_2$ or $\text{Cu}_2(\text{L}2)_2$, only one fullerene (F) unit is indicated because under our experimental conditions, that is, light intensity, only one C_{60} unit can be excited.

our flash photolysis apparatus (20 ns) and, whatever the deactivation path, the final sink of photoinduced processes is the charge separated level, since spectroscopic fingerprints of fullerene singlet and triplet levels are not found in $\text{Cu}_2(\text{L2})_2$ either via fluorescence or transient absorption spectroscopy.

A more interesting issue is the quenching of the fullerene singlet level, which is observed for the methanofullerene system $\text{Cu}_2(\text{L2})_2$ but not for the bismethanofullerene array $\text{Cu}_2(\text{L1})_2$. At this stage it is important to point out that this result confirms a trend observed earlier in Cu(I)–phenanthroline/ C_{60} arrays having topologies ranging from rotaxanes,³² to dendrimers,²⁹ to sandwich-type triads,⁴⁶ in which the metal complexed unit is always the central core of the molecular architecture. In fact we have found previously that quenching of the fullerene moiety occurs in a rotaxane having methanofullerenes as terminal units, whereas in bismethanofullerene dendrimers and sandwich-type complexes the carbon sphere is never quenched. In other words, considering all the systems investigated so far, in Cu(I)–phenanthroline/ C_{60} arrays the fullerene units are always quenched by the metal-complexed unit when methanofullerenes are involved whereas quenching is never found for bismethanofullerene arrays.

These results do not depend upon the separation of the two chromophores, which in both cases has been estimated to be 8–12 Å, based on molecular modeling. The basic factor that seems to affect the final outcome is the structure of the fullerene, that is, methano versus bismethanofullerene.

From the energy diagram of Figure 8 one can derive that in $\text{Cu}_2(\text{L2})_2$ the quenching of the fullerene singlet can occur in principle (i) via energy transfer to $^3\text{MLCT}$ level or (ii) via electron transfer to yield the Cu(I)–phenanthroline \rightarrow C_{60} charge separated state. From the residual fullerene fluorescence (about 15% compared to the reference molecule **11**), one can estimate an upper limit for the quenching rate constant of $4 \times 10^9 \text{ s}^{-1}$ by means

of Eq. 1:

$$k_{\text{EnT}} = \frac{(\frac{\Phi_{\text{ref}}}{\Phi} - 1)}{\tau_{\text{ref}}} \quad (1)$$

where Φ and Φ_{ref} are the C_{60} fluorescence quantum yield of the $\text{Cu}_2(\text{L2})_2$ helicate and of the reference compound **11**, whereas τ_{ref} is the singlet lifetime of the latter.

Using the available photophysical data, it is possible to calculate the $\text{C}_{60} \rightarrow$ Cu(I)–phenanthroline energy transfer rate according to the dipole–dipole Förster mechanism,⁵³ which turns out to be $4 \times 10^8 \text{ s}^{-1}$, that is, one order of magnitude smaller than the experimental value. Thus, this mechanism can be ruled out. Model calculations to estimate the energy transfer rate according to the electron exchange model (Dexter-type mechanism) are not easily amenable. However, on the basis of experimental data it is possible to evaluate the overlap integral according to Dexter, which turns out to be virtually identical for $\text{Cu}_2(\text{L1})_2$ and $\text{Cu}_2(\text{L2})_2$. Thus, given the completely different behavior of the two helicates, it is unlikely that energy transfer plays a major role in the quenching of the fullerene singlet, pointing to an electron transfer process.

The most relevant difference in the photophysical parameters of the reference methano- and bismethanofullerenes **6** and **11** is the shape of the corrected emission spectra (see Table 2 and Fig. 9). Having this in mind we carried out a spectral analysis of such profiles in order to get more insight into the tendency of the two functionalized carbon spheres to undergo electron transfer from the lowest singlet excited states. In particular, the analysis provides the internal reorganization energy for deactivation of the fluorescent level in the two cases. The results are collected in Table 3 and illustrated in Figure 9 (see Section 4 for more details). As one can see, along the vibrational mode corresponding to a typical C–C vibration ($\hbar\omega_m$ in the range $1350\text{--}1400 \text{ cm}^{-1}$)^{54,55} the fluorescent state of the bismethanofullerene **6** is more distorted than that of the methanofullerene **11** (the displacement parameter S_m amounts to 1.79 and 0.79, respectively). This results in different values for the internal reorganization

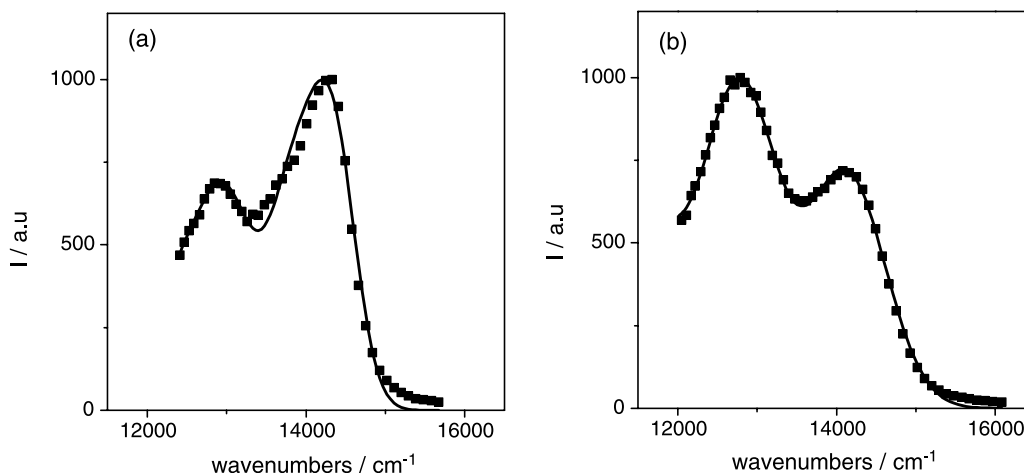


Figure 9. Vibronic analysis of the corrected fluorescence profiles (experimental points, squares; fits, full lines) for methanofullerene **11** (a) and bismethanofullerene **6** (b); see text for further details.

Table 3. Data from vibronic analysis of the fluorescence spectra^a

Compound	E_0 (cm ⁻¹)	S_m ^b	$\hbar\omega_m$ (cm ⁻¹) ^b	λ_i (eV) ^c
11	14330	0.79	1380	0.14
6	14350	1.79	1350	0.30

^a According to Eq. 3 (see Section 4), CH₂Cl₂, 298 K; excitation performed at 430 nm.

^b Parameters for the high frequency mode (corresponding to aromatic C–C vibrations);^{54,55,57,58} the low frequency mode, $\hbar\omega_l$ was 500 cm⁻¹ yielding $S_l=0.68$ and 0.78 for **11** and **6**, respectively, and $\Delta\bar{\nu}_{1/2}=680$ and 930 cm⁻¹, respectively.

^c Internal reorganization energy along the prominent high frequency mode, $\lambda_i=S_m\times\hbar\omega_m$, see text.

energy for deactivation of the fluorescent level in the two cases, $\lambda_i=0.30$ and 0.14 eV, for **6** and **11**, respectively. As a consequence, the nuclear factor (NF) for the electron transfer, Eq. 2, turns out to be 0.29 and 0.05, respectively, as evaluated by assuming $\lambda=\lambda_o+\lambda_i$, with a solvent reorganization energy $\lambda_o=0.5$ eV in both cases.⁵⁶

$$NF = \exp\left[-\frac{(\lambda + \Delta G^0)^2}{4\lambda k_B T}\right] \quad (2)$$

These results suggest that the singlet excited states of methanofullerenes are more prone to undergo electron transfer than those of bismethanofullerenes, thanks to the associated smaller internal reorganization energy. In addition methanofullerenes are slightly easier to reduce than bismethanofullerenes (Table 1), also giving a thermodynamic advantage for electron transfer in multicomponent arrays containing the monofunctionalized derivative. The combined effect of the above discussed kinetic and thermodynamic factors can explain the different and somehow unexpected trend in photoprocesses of multicomponent arrays containing Cu(I)–phenanthrolines linked to methanofullerenes versus bismethanofullerenes, which has been invariably found in a variety of molecular architectures.^{29,32,46}

3. Conclusions

Bisphenanthroline ligands bearing a fullerene subunit have been prepared. The corresponding copper(I) complexes have been obtained by treatment with a cuprous salt. NMR spectroscopy and mass spectrometry analysis have unambiguously shown that these complexes are bis-copper(I) helicate substituted with two fullerene moieties. The fullerohelicates **Cu₂(L1)₂** and **Cu₂(L2)₂** do not exhibit ground state electronic interactions but undergo light induced intercomponent processes upon light excitation. In both systems photoinduced electron transfer from the central metal-complexed unit to the external fullerenes may occur, in principle, by excitation of both moieties. However, this is found to be the case for only the methanofullerene system **Cu₂(L2)₂**. Unexpectedly, for **Cu₂(L1)₂**, photoexcitation of the peripheral carbon spheres is followed by regular internal deactivation. This ‘asymmetric’ behavior has been interpreted on the basis of the different character of the involved excited states, that is, charge transfer (Cu–phenanthroline excitation), versus, localized (C₆₀ excitation). In the former case the impact on external and internal reorganization energy contributes to reduce the

kinetic barrier on the way to the complete Cu(I)–phenanthroline → C₆₀ charge separation. A vibronic analysis of the fluorescence spectra of the functionalized C₆₀'s **6** and **11**, sheds light into the different ability of methano- and bismethanofullerenes to undergo electron transfer in arrays containing Cu(I)–phenanthrolines. Both kinetic and thermodynamic factors (related to internal reorganization energies and reduction potentials) are likely to disfavor electron transfer regardless of the fullerene singlet level to the metal complex in the case of bismethanofullerenes, regardless the molecular architecture.

4. Experimental

4.1. General

Reagents and solvents were purchased as reagent grade and used without further purification. THF was distilled over sodium benzophenone ketyl. Compounds **3**,¹⁷ **6**,⁴⁷ **7**⁴⁷ and **8**⁴⁷ were prepared as previously reported. All reactions were performed in standard glassware under an inert Ar atmosphere. Evaporation and concentration were done at water aspirator pressure and drying in vacuo at 10⁻² Torr. Column chromatography: silica gel 60 (230–400 mesh, 0.040–0.063 mm) was purchased from E. Merck. Thin-Layer Chromatography (TLC) was performed on glass sheets coated with silica gel 60 F₂₅₄ purchased from E. Merck, visualization by UV light. UV–vis spectra were recorded on a Hitachi U-3000 spectrophotometer. NMR spectra were recorded on a Bruker AC 300 or a Bruker AM 400 with solvent peaks as reference. FAB-mass spectra (*m/z*; % relative intensity) were taken on a ZA HF instrument with 4-nitrobenzyl alcohol as matrix. Elemental analyses were performed by the analytical service at the Institut Charles Sadron, Strasbourg.

4.1.1. Compound 2. To a solution of 3,5-dibromobenzyl alcohol **1** (6.11 g, 23 mmol) in DMF (40 mL) at 0 °C was added TIPSCl (6.17 mL, 28 mmol) and imidazole (3.75 g, 55 mmol). After 24 h the solvent was removed under vacuum and the residue dissolved in ether. The organic layer was washed with water, brine, dried over MgSO₄ and filtered. After removal of the solvent under reduced pressure, purification by column chromatography (SiO₂, CH₂Cl₂/hexane 1:9), afforded compound **2** (8.0 g, 19 mmol) as a colorless oil in an 83% yield. ¹H NMR (CDCl₃, 200 MHz): δ 1.10 (m, 21H), 4.78 (s, 2H), 7.43 (s, 2H), 7.54 (s, 1H).

4.1.2. Compound 4. A solution of *t*BuLi (6.1 mL, 10.4 mmol) in pentane was added to a solution of **2** (1.0 g, 2.4 mmol) in THF (4 mL) under argon at –78 °C. After 1 h, the temperature was allowed to raise to 0 °C, and then the mixture was cooled again to –78 °C. This mixture was added to a solution of **3** (1.98 g, 4.5 mmol) in THF (10 mL) under argon at 0 °C. After 2 h at 0 °C, the solution was allowed to raise slowly to room temperature and then water was added. The solvent was removed under reduced pressure. The residue was dissolved in CH₂Cl₂ and washed with water. The organic layer was dried over MgSO₄ (10 g), and MnO₂ (30 g, 0.35 mol) was added in three times. After 30 min, the suspension was filtered over Celite and washed

with CH_2Cl_2 (1 L). The solvent was removed and the residue purified by column chromatography (SiO_2 , $\text{CH}_2\text{Cl}_2/\text{MeOH}$ 99.8:0.2). Compound **4** (0.84 g, 0.73 mmol) was obtained as a yellow solid in a 31% yield. ^1H NMR (CDCl_3 , 300 MHz): δ 0.91 (t, $J=7$ Hz, 6H), 1.27 (s, 57H), 1.87 (m, 4H), 4.03 (t, $J=7$ Hz, 4H), 5.25 (s, 2H), 7.02 (d, $J=9$ Hz, 4H), 7.71 (AB, $J=9$ Hz, 4H), 8.02 (d, $J=8.5$ Hz, 2H), 8.18 (d, $J=8.5$ Hz, 2H), 8.32 (d, $J=8.5$ Hz, 2H), 8.44 (d, $J=8.5$ Hz, 2H), 8.49 (d, $J=9$ Hz, 4H), 8.71 (broad s, 2H), 9.73 (broad s, 1H).

4.1.3. $\text{Cu}_2(\mathbf{4})_2$ complex. Copper(I) salt $\text{Cu}(\text{CH}_3\text{CN})_4\text{BF}_4$ (44 mg, 0.14 mmol) and **4** (160 mg, 0.14 mmol) were dissolved in CH_2Cl_2 (20 mL). After 2 h the solvent was removed under reduced pressure and the residue purified by column chromatography (SiO_2 , $\text{CH}_2\text{Cl}_2/\text{MeOH}$ 99:1 in presence of NaBF_4 and then Al_2O_3 , $\text{CH}_2\text{Cl}_2/\text{MeOH}$ 99:1). The $\text{Cu}_2(\mathbf{4})_2$ complex (40 mg, 0.015 mmol) was obtained as a glassy red solid in a 22% yield. ^1H NMR (CDCl_3 , 300 MHz): δ 0.87 (t, $J=7$ Hz, 12H), 1.32 (m, 114H), 1.55 (m, 8H), 3.20 (m, 4H), 3.34 (m, 4H), 4.77 (AB, $J=14$ Hz, 4H), 5.69 (d, $J=8.5$ Hz, 8H), 6.50 (d, $J=8.5$ Hz, 4H), 6.86 (broad s, 4H), 7.01 (d, $J=8.5$ Hz, 8H), 7.57 (d, $J=8.5$ Hz, 4H), 7.95 (d, $J=8.5$ Hz, 4H), 8.05 (d, $J=8.5$ Hz, 4H), 8.07 (d, $J=8.5$ Hz, 4H), 8.32 (d, $J=8$ Hz, 4H), 9.53 (broad s, 2H). Elemental analysis calculated for $\text{C}_{152}\text{H}_{192}\text{O}_6\text{N}_8\text{Si}_2\text{-Cu}_2\text{B}_2\text{F}_8$ C 70.65%, H 7.49%, N 4.34%, found C 70.84%, H 7.70%, N 4.01%.

4.1.4. Compound 5. A 1 M TBAF solution (0.7 mL, 0.7 mmol) in THF was added to a solution of **4** (0.675 g, 0.6 mmol) in THF (20 mL) at 0 °C. After 30 min at the same temperature, an aqueous solution of NH_4Cl (30 mL) was added. The THF was removed under reduced pressure and the aqueous layer extracted with CH_2Cl_2 . The organic layer was dried over MgSO_4 , filtered and the solvent removed under reduced pressure. The residue was purified by column chromatography (SiO_2 , $\text{CH}_2\text{Cl}_2/\text{MeOH}$ 98:2) and afforded compound **5** (0.583 g, 0.6 mmol) as a yellow solid in an 88% yield. ^1H NMR (CDCl_3 , 300 MHz): δ 0.91 (t, $J=7$ Hz, 6H), 1.37 (m, 36H), 1.83 (m, 4H), 3.96 (t, $J=7$ Hz, 4H), 4.84 (s, 2H), 7.01 (d, $J=9$ Hz, 4H), 7.56 (AB, $J=9$ Hz, 4H), 7.98 (d, $J=8.5$ Hz, 2H), 8.02 (d, $J=8.5$ Hz, 2H), 8.12 (d, $J=8.5$ Hz, 2H), 8.23 (d, $J=8.5$ Hz, 2H), 8.41 (d, $J=9$ Hz, 4H), 8.45 (d, $J=1.5$ Hz, 2H), 9.44 (broad s, 1H).

4.1.5. Compound L1. DCC (32 mg, 0.16 mmol) and DMAP (8 mg, 0.07 mmol) were added to a solution of alcohol **5** (150 mg, 0.15 mmol) and acid **7** (282 mg, 0.16 mmol) in CH_2Cl_2 stabilized in amylene (50 mL) at 0 °C under argon. After 1 h, the cooling bath was removed and a catalytic amount of HOBt was added. The mixture was allowed to slowly warm to room temperature. After 40 h the mixture was filtered and the solvent removed under reduced. Purification by column chromatography (SiO_2 , $\text{CH}_2\text{Cl}_2/\text{MeOH}$ 99.3:0.7) afforded **L1** (100 mg, 0.04 mmol) as a red glassy product in a 24% yield. IR (KBr): 1750 (C=O). ^1H NMR (CDCl_3 , 300 MHz): δ 0.89 (m, 18H), 1.27 (m, 76H), 1.67 (m, 8H), 1.83 (m, 4H), 3.82 (t, $J=6.5$ Hz, 8H), 4.03 (t, $J=6.5$ Hz, 4H), 4.83 (s, 2H), 4.93 (d, $J=13.5$ Hz, 2H), 5.25 (s, 4H), 5.63 (d, $J=13.5$ Hz, 2H), 5.64 (s, 2H), 6.33 (t, $J=2$ Hz, 2H), 6.43 (d, $J=2$ Hz, 4H), 6.78 (s, 2H), 7.02 (s, 4H), 7.04 (s, 1H), 7.81 (s, 4H), 8.18 (AB, $J=8.5$ Hz, 4H), 8.43 (m, 8H), 8.70 (s, 2H), 9.73

(s, 1H). ^{13}C NMR (CDCl_3 , 75 MHz): δ 14.10, 22.65, 22.67, 26.06, 26.12, 29.22, 29.24, 29.35, 29.49, 29.65, 29.69, 31.79, 31.91, 48.96, 65.57, 66.81, 67.01, 67.31, 68.03, 68.08, 68.61, 70.52, 101.56, 107.03, 112.59, 114.58, 116.07, 119.50, 119.85, 125.49, 126.27, 127.05, 127.44, 128.16, 128.44, 128.99, 129.23, 131.61, 134.37, 135.71, 136.04, 136.22, 136.49, 136.62, 136.83, 136.99, 137.73, 138.28, 139.97, 140.13, 141.00, 141.07, 142.21, 142.68, 143.10, 143.52, 143.66, 143.89, 144.10, 144.25, 144.52, 144.88, 144.92, 145.10, 145.28, 145.53, 145.64, 145.69, 145.42, 145.80, 146.00, 147.26, 147.41, 148.57, 155.48, 156.42, 157.80, 160.33, 160.55, 162.44, 162.51, 168.54.

4.1.6. Compound $\text{Cu}_2(\mathbf{L1})_2$. Copper(I) salt $\text{Cu}(\text{CH}_3\text{CN})_4\text{BF}_4$ (13 mg, 0.036 mmol) and compound **L1** (100 mg, 0.036 mmol) were dissolved in a mixture of $\text{CH}_2\text{Cl}_2/\text{acetonitrile}$ (10 mL). After 3 h the solvents were removed under reduced pressure and the residue dissolved in CH_2Cl_2 . The organic layer was washed with water and dried over MgSO_4 . After removal of the solvent under reduced pressure the residue was purified by gel permeation chromatography (Biorad, Biobeads SX-1, CH_2Cl_2). $\text{Cu}_2(\mathbf{L1})_2$ was obtained (79 mg, 0.014 mmol) as a red glassy product in a 75% yield. UV-vis (CH_2Cl_2): 437 (850), 313 (10,150), 258 (25,600). IR (KBr): 1748 (C=O). ^1H NMR (CDCl_3 , 400 MHz): δ 0.90 (m, 36H), 1.31 (m, 152H), 1.57 (m, 8H), 1.72 (m, 16H), 3.29 (m, 4H), 3.43 (m, 4H), 3.85 (m, 16H), 5.02 (AB, $J=12.5$ Hz, 4H), 5.27 (AB, $J=9$ Hz, 4H), 5.23 (d, $J=10$ Hz, 2H), 5.24 (d, $J=10$ Hz, 2H), 5.32 (AB, $J=9$ Hz, 4H), 5.33 (AB, $J=9$ Hz, 4H), 5.75 (d, $J=8.5$ Hz, 8H), 5.76 (d, $J=13.5$ Hz, 2H), 5.88 (d, $J=13.5$ Hz, 2H), 6.36 (m, 4H), 6.48 (m, 8H), 6.73 (d, $J=8.5$ Hz, 4H), 7.00 (s, 4H), 7.08 (d, $J=8.5$ Hz, 8H), 7.09 (s, 4H), 7.11 (s, 2H), 7.63 (d, $J=9$ Hz, 4H), 7.77 (d, $J=8.5$ Hz, 4H), 7.83 (d, $J=8.5$ Hz, 4H), 7.93 (d, $J=8.5$ Hz, 4H), 8.32 (d, $J=9$ Hz, 4H), 9.61 (s, 2H). ^{13}C NMR (CDCl_3 , 75 MHz): δ 14.12, 14.15, 17.32, 21.83, 22.68, 22.71, 26.05, 26.10, 29.00, 29.26, 29.40, 29.62, 29.71, 31.83, 31.95, 49.06, 66.84, 67.84, 68.08, 68.78, 70.61, 101.66, 107.18, 112.62, 121.57, 124.42, 125.67, 126.70, 126.93, 127.36, 127.63, 129.02, 130.24, 135.74, 136.04, 136.52, 137.16, 137.63, 138.88, 139.88, 141.08, 142.25, 142.49, 142.73, 143.17, 143.59, 144.15, 144.54, 144.95, 145.23, 145.56, 145.70, 145.92, 147.47, 148.68, 151.05, 152.49, 156.59, 157.98, 159.80, 160.37, 162.53, 168.70. FAB-MS: 5734.0 ($[\text{M}-\text{BF}_4]^+$), 2824.7 ($[\text{M}-2\text{BF}_4]^{2+}$).

4.1.7. Compound 9. DCC (50 mg, 0.24 mmol) and DMAP (10 mg, 0.08 mmol) were added to a solution of alcohol **5** (200 mg, 0.20 mmol) and malonic acid **8** (137 mg, 0.24 mmol) in CH_2Cl_2 stabilized with amylene (40 mL) at 0 °C under argon. After 1 h, the cooling bath was removed and a catalytic amount of HOBt was added. The mixture was allowed to slowly warm to room temperature. After 40 h the mixture was filtered and the solvent removed under reduced pressure. Column chromatography (SiO_2 , $\text{CH}_2\text{Cl}_2/\text{MeOH}$ 99.9:0.1) afforded compound **9** (300 mg, 0.20 mol) partially purified as a glassy brown solid. ^1H NMR (CDCl_3 , 300 MHz): δ 0.89 (m, 12H), 1.29 (m, 72H), 1.86 (m, 8H), 3.84 (t, $J=7$ Hz, 4H), 3.92 (t, $J=7$ Hz, 4H), 4.60 (s, 2H), 5.13 (s, 2H), 5.60 (s, 2H), 6.36 (s, 1H), 6.47 (d, $J=2$ Hz, 2H), 7.06 (d, $J=9$ Hz, 4H), 7.79 (s, 4H), 8.10 (d, $J=8.5$ Hz, 2H), 8.27 (d, $J=8.5$ Hz,

2H), 8.37 (d, $J=8.5$ Hz, 2H), 8.45 (d, $J=8.5$ Hz, 2H), 8.49 (d, $J=9$ Hz, 4H), 8.70 (s, 2H), 9.76 (s, 1H).

4.1.8. Compound L2. DBU (0.25 mL, 1.63 mmol) was added to a solution of C₆₀ (146 mg, 0.20 mmol), compound **9** (311 mg, 0.20 mmol) and iodine (155 mg, 0.61 mmol) in toluene (150 mL) under argon. After 20 h the mixture was filtered on SiO₂ (CH₂Cl₂ then CH₂Cl₂/MeOH 95:5) and the solvent was removed under reduced pressure. Purification by column chromatography (SiO₂, CH₂Cl₂/MeOH 99.8:0.2) afforded **L2** (100 mg, 0.04 mmol) as a red glassy product in a 22% yield. UV-vis (CH₂Cl₂): 478 (1800), 426 (2900), 323 (86,600), 260 (170,700). IR (KBr): 1746 (C=O). ¹H NMR (CDCl₃, 300 MHz): δ 0.89 (m, 12H), 1.26 (m, 68H), 1.53 (m, 4H), 1.65 (m, 4H), 1.86 (m, 4H), 3.75 (t, $J=6.5$ Hz, 4H), 4.07 (t, $J=6.5$ Hz, 4H), 5.48 (s, 2H), 5.96 (s, 2H), 6.30 (broad s, 1H), 6.45 (d, $J=2$ Hz, 2H), 7.12 (d, $J=9$ Hz, 4H), 7.79 (s, 4H), 8.17 (AB, $J=8$ Hz, 4H), 8.40 (AB, $J=8$ Hz, 4H), 8.51 (d, $J=9$ Hz, 4H), 8.86 (s, 2H), 9.71 (s, 1H). ¹³C NMR (CDCl₃, 75 MHz): δ 14.11, 22.67, 22.69, 26.08, 26.15, 29.25, 29.34, 29.37, 29.43, 29.53, 29.63, 29.66, 29.71, 31.90, 31.91, 52.00, 67.99, 68.12, 68.78, 71.44, 101.60, 106.55, 114.70, 119.33, 119.72, 125.37, 126.29, 126.83, 127.42, 128.17, 128.92, 129.08, 131.82, 135.95, 136.62, 136.73, 136.82, 138.83, 138.99, 140.11, 140.49, 140.59, 141.67, 141.98, 142.20, 142.65, 142.72, 143.40, 143.62, 143.96, 144.26, 144.43, 144.65, 144.82, 144.87, 144.94, 145.00, 145.03, 146.01, 155.35, 156.50, 160.33, 160.57, 163.40, 163.54.

4.1.9. Compound Cu₂(L2)₂. Copper(I) salt Cu(CH₃CN)₄BF₄ (15 mg, 0.048 mmol) and compound **L2** (90 mg, 0.04 mmol) were dissolved in a mixture of CH₂Cl₂/acetonitrile (20 mL). After 1 h the solvents were removed under reduced pressure and the residue dissolved in CH₂Cl₂. The organic layer was washed with water and dried over MgSO₄. After removal of the solvent under reduced pressure the residue was purified by gel permeation chromatography (Biorad, Biobeads SX-1, CH₂Cl₂). Cu₂(L2)₂ was obtained (50 mg, 0.01 mmol) as a red glassy product in a 52% yield. IR (KBr): 1747 (C=O). ¹H NMR (CDCl₃, 300 MHz): δ 0.89 (m, 24H), 1.27 (m, 144H), 1.52 (m, 8H), 1.73 (m, 8H), 3.23 (m, 4H), 3.37 (m, 4H), 3.89 (t, $J=6.5$ Hz, 8H), 5.65 (AB, $J=12$ Hz, 4H), 5.67 (AB, $J=12$ Hz, 4H), 5.78 (d, $J=9$ Hz, 8H), 6.39 (broad s, 2H), 6.48 (d, $J=8.5$ Hz, 4H), 6.70 (d, $J=2$ Hz, 4H), 7.10 (broad s, 4H), 7.20 (d, $J=9$ Hz, 8H), 7.67 (d, $J=8.5$ Hz, 4H), 7.74 (d, $J=8.5$ Hz, 4H), 7.78 (d, $J=8.5$ Hz, 4H), 7.91 (d, $J=8.5$ Hz, 4H), 8.50 (d, $J=8.5$ Hz, 4H), 9.62 (s, 2H). ¹³C NMR (CDCl₃, 75 MHz): δ 14.13, 14.16, 22.69, 22.73, 26.07, 26.16, 29.05, 29.30, 29.37, 29.41, 29.47, 29.65, 29.70, 29.74, 31.92, 31.96, 52.64, 67.82, 68.20, 69.64, 71.47, 71.68, 101.98, 107.76, 112.58, 121.30, 124.66, 125.50, 126.83, 127.45, 127.63, 129.29, 130.18, 135.33, 136.01, 136.54, 136.92, 137.64, 137.82, 138.26, 139.86, 140.36, 140.80, 141.12, 141.75, 141.85, 142.08, 142.22, 142.29, 142.39, 143.08, 143.13, 143.24, 143.77, 143.85, 143.97, 144.08, 144.40, 144.49, 144.69, 144.84, 144.92, 145.08, 145.28, 145.37, 145.48, 152.38, 156.58, 159.90, 160.54, 163.56, 163.83. MALDI-TOF MS: 4711.5 ([M-BF₄]⁺).

4.1.10. Compound 10. DCC (0.97 g, 4.75 mmol) and DMAP (0.193 g, 1.58 mmol) were added to a solution of

ethanol (10 mL, 170 mmol) and malonic acid **8** (1.78 g, 3.17 mmol) in CH₂Cl₂ stabilized with amylene (40 mL) at 0 °C under argon. After 1 h, the cooling bath was removed and the mixture allowed to slowly warm to room temperature. After 40 h the mixture was filtered and the solvent removed under reduced pressure. Purification by column chromatography (SiO₂, CH₂Cl₂/MeOH 99.5:0.5) afforded compound **10** (1.36 g, 2.31 mmol) as a colorless oil in a 73% yield. ¹H NMR (CDCl₃, 200 MHz): δ 0.89 (t, $J=7$ Hz, 6.5H), 1.28 (m, 39H), 1.76 (m, 4H), 3.41 (s, 2H), 3.91 (t, $J=6$ Hz, 4H), 4.19 (q, $J=7$ Hz, 2H), 5.09 (s, 2H), 6.40 (broad s, 1H), 6.47 (broad s, 2H).

4.1.11. Compound 11. DBU (0.26 mL, 1.66 mmol) was added to a solution of C₆₀ (300 mg, 0.42 mmol), compound **10** (246 mg, 0.42 mmol) and iodine (317 mg, 1.25 mmol) in toluene (300 mL) under argon. After 20 h the mixture was filtered on SiO₂ (CH₂Cl₂ then CH₂Cl₂/MeOH 95:5) and the solvent was removed under reduced pressure. Purification by column chromatography (SiO₂, CH₂Cl₂) afforded **11** (173 mg, 1.3 mmol) as a red glassy product in a 31% yield. ¹H NMR (CDCl₃, 300 MHz): δ 0.90 (t, $J=7$ Hz, 6H), 1.28 (m, 39H), 1.74 (m, 4H), 3.92 (t, $J=6.5$ Hz, 4H), 4.54 (q, $J=7$ Hz, 2H), 5.45 (s, 2H), 6.43 (t, $J=2$ Hz, 1H), 6.62 (d, $J=2$ Hz, 2H). ¹³C NMR (CDCl₃, 75 MHz): δ 14.13, 22.70, 26.13, 26.90, 29.29, 29.37, 29.45, 29.63, 29.66, 29.71, 30.19, 31.93, 43.47, 52.08, 63.51, 68.17, 68.90, 71.57, 101.70, 107.26, 136.61, 138.61, 139.47, 140.88, 140.93, 141.88, 141.94, 142.19, 142.21, 142.94, 143.01, 143.84, 143.89, 144.48, 144.56, 144.61, 144.69, 144.88, 145.04, 145.07, 145.16, 145.17, 145.22, 145.25, 160.54, 163.47.

4.2. Electrochemistry

The electrochemical studies were carried out in CH₂Cl₂ (Fluka-spectroscopic grade used without further purification) containing 0.1 M Bu₄NPF₆ (Merck-electrochemical grade) as supporting electrolyte. A classical three electrode cell was connected to a computerized electrochemical device Autolab (Eco Chemie B.V. Utrecht, Holland) driven by a GPSE software running on a personal computer. The working electrode was a glassy carbon disk (3 mm in diameter), the auxiliary electrode a platinum wire and the reference electrode an aqueous Ag/AgCl reference electrode. All potentials are given versus Fc/Fc⁺ used as internal standard.

4.3. Photophysical measurements

Absorption spectra were recorded with a Perkin-Elmer λ 40 spectrophotometer. Emission spectra were obtained with an Edinburgh FLS920 spectrometer (continuous 450 W Xe lamp), equipped with a peltier-cooled Hamamatsu R928 photomultiplier tube (185–850 nm) or a Hamamatsu R5509-72 supercooled photomultiplier tube (193 K, 800–1700 nm range for singlet oxygen luminescence spectra). Corrected spectra were obtained via a calibration curve supplied with the instrument. Emission lifetimes were determined with the time correlated single photon counting technique using the Edinburgh FLS920 spectrometer equipped with a laser diode head as excitation source (1 MHz repetition rate, λ_{exc} = 407 or 637 nm, 200 ps time

resolution upon deconvolution) and the above mentioned Hamamatsu R928 PMT as detector. Nanosecond transient absorption spectroscopy was carried out with an apparatus described earlier.⁴⁶

4.4. Spectral analysis

The vibronic band profiles of the corrected luminescence spectra, $I(E)$, on an energy scale (E , cm^{-1}) were fitted by using Eq. 3, allowing a two-mode analysis of the Frank-Condon envelop.^{54,55}

$$I(E) = \sum_m \sum_l \left(\frac{E_0 - m\hbar\omega_m - l\hbar\omega_l}{E_0} \right)^3 \frac{S_m^m S_l^l}{m! l!} \times \exp \left[-4(\ln 2) \left(\frac{E - E_0 + m\hbar\omega_m + l\hbar\omega_l}{\Delta\bar{\nu}_{1/2}} \right)^2 \right] \quad (3)$$

with and $S_j = \lambda_j / \hbar\omega_j$ ($j = m$ and l)

In this equation, E_0 is the energy of the 0–0 transition (the energy gap between the 0–0 vibrational levels in the excited and ground states), m and l are vibrational quantum numbers for high-frequency and low-frequency modes, $\hbar\omega_m$ and $\hbar\omega_l$ (in practice upper limits m and $l=5$ are employed), $\Delta\bar{\nu}_{1/2}$ is the width at half maximum of the vibronic band, λ and S are the reorganization energy and the displacement parameter along those modes, and k_B is the Boltzmann constant. High values for S_m (typically, in the range 0.7–1 and more)⁵⁷ indicate that the excited state is significantly distorted along the concerned vibrational mode because of electronic localization effects. On the contrary, when the excited state undergoes extended electronic delocalization, low S_m values are obtained (typically, in the range 0.2–0.6)⁵⁸ indicating that the electronic curve for the excited level is not much displaced relative to that for the ground state.

Acknowledgements

This work was supported by the CNRS, the French Ministry of Research (ACI Jeunes Chercheurs to J.-F.N.) the CNR (commissa PM-P03-ISTM-C4/PM-P03-ISOF-M5, Componenti Molecolari e Supramolecolari o Macromolecolari con Proprietà Fotoniche ed Optoelettroniche) and the EU for the RTN contract no HPRN-CT-2002-00171 (FAMOUS). F.C. thanks the Région Alsace and the CNRS for a PhD fellowship. We further thank M. Schmitt for high field NMR spectra and J.-M. Strub for MS measurements.

References and notes

- Lehn, J. M. *Supramolecular chemistry: concepts and perspectives: a personal account built upon the George Fisher Baker non-resident lectureship in chemistry at Cornell University and the Lezione Lincee, Accademia nazionale dei Lincei, Roma*; VCH: Weinheim, New York, 1995.
- Marquis-Rigault, A.; Dupont-Gervais, A.; Van Dorsselaer, A.; Lehn, J.-M. *Chem. Eur. J.* **1996**, *2*, 1395–1398.
- Fujita, M. *Chem. Soc. Rev.* **1998**, *27*, 417–425.
- Fujita, M. *Acc. Chem. Res.* **1999**, *32*, 53–61.
- Fujita, M.; Tominaga, M.; Hori, A.; Therrien, B. *Acc. Chem. Res.* **2005**, *38*, 369–378.
- Stang, P. J.; Olenyuk, B. *Acc. Chem. Res.* **1997**, *30*, 502–518.
- Stang, P. J. *Chem. Eur. J.* **1998**, *4*, 19–27.
- Leininger, S.; Olenyuk, B.; Stang, P. J. *Chem. Rev.* **2000**, *100*, 853–907.
- Seidel, S. R.; Stang, P. J. *Acc. Chem. Res.* **2002**, *35*, 972–983.
- Schmittel, M.; Kalsani, V. *Top. Curr. Chem.* **2005**, *245*, 1–53.
- Constable, E. C. *Tetrahedron* **1992**, *48*, 10013.
- Piguet, C.; Bernardinelli, G.; Hopfgartner, G. *Chem. Rev.* **1997**, *97*, 2005–2062.
- Albrecht, M. *Chem. Rev.* **2001**, *101*, 3457–3497.
- Lehn, J.-M.; Rigault, A.; Siegel, J.; Harrowfield, J.; Chevrier, B.; Moras, D. *Proc. Natl. Acad. Sci. U.S.A.* **1987**, *84*, 2565.
- Dietrich-Buchecker, C. O.; Sauvage, J. P. *Angew. Chem., Int. Ed.* **1989**, *28*, 189.
- Dietrich-Buchecker, C. O.; Nierengarten, J. F.; Sauvage, J. P.; Armaroli, N.; Balzani, V.; De Cola, L. *J. Am. Chem. Soc.* **1993**, *115*, 11237–11244.
- Dietrich-Buchecker, C. O.; Sauvage, J. P.; Armaroli, N.; Ceroni, P.; Balzani, V. *Angew. Chem. Int., Ed.* **1996**, *35*, 1119–1121.
- Nierengarten, J. F.; Dietrich-Buchecker, C. O.; Sauvage, J. P. *J. Am. Chem. Soc.* **1994**, *116*, 375–376.
- El-ghayoury, A.; Douce, L.; Skoulios, A.; Ziessel, R. *Angew. Chem., Int. Ed.* **1998**, *37*, 2205–2208.
- Cardinali, F.; Mamlouk, H.; Rio, Y.; Armaroli, N.; Nierengarten, J. F. *Chem. Commun.* **2004**, 1582–1583.
- Dietrich-Buchecker, C. O.; Sauvage, J. P.; De Cian, A.; Fischer, J. *Chem. Commun.* **1994**, 2231.
- Armaroli, N.; Accorsi, G.; Gisselbrecht, J. P.; Gross, M.; Eckert, J. F.; Nierengarten, J. F. *New J. Chem.* **2003**, *27*, 1470–1478.
- Dietrich-Buchecker, C. O.; Hwang, N. G.; Sauvage, J. P. *New J. Chem.* **1999**, *23*, 911–914.
- Felder, D.; Nava, M. G.; Carreon, M. D.; Eckert, J. F.; Luccisano, M.; Schall, C.; Masson, P.; Gallani, J. L.; Heinrich, B.; Guillon, D.; Nierengarten, J. F. *Helv. Chim. Acta* **2002**, *85*, 288–319.
- Bingel, C. *Chem. Ber.* **1993**, *126*, 1957.
- Zhang, S.; Rio, Y.; Cardinali, F.; Bourgoigne, C.; Gallani, J. L.; Nierengarten, J. F. *J. Org. Chem.* **2003**, *68*, 9787–9797.
- El-Ghayoury, A.; Harriman, A.; De Cian, A.; Fischer, J.; Ziessel, R. *J. Am. Chem. Soc.* **1998**, *120*, 9973–9974.
- Gisselbrecht, J. P.; Gross, M.; Lehn, J. M.; Sauvage, J. P.; Ziessel, R.; Piccini Leopardi, C.; Anieta, J. M.; Germain, G.; Van Meersche, M. *Nouv. J. Chimie* **1984**, *8*, 661–667.
- Armaroli, N.; Boudon, C.; Felder, D.; Gisselbrecht, J. P.; Gross, M.; Marconi, G.; Nicoud, J. F.; Nierengarten, J. F.; Vicinelli, V. *Angew. Chem., Int. Ed.* **1999**, *38*, 3730–3733.
- Felder, D.; Nierengarten, H.; Gisselbrecht, J. P.; Boudon, C.; Leize, E.; Nicoud, J. F.; Gross, M.; Van Dorsselaer, A.; Nierengarten, J. F. *New J. Chem.* **2000**, *24*, 687–695.
- Bensasson, R. V.; Bienvenue, E.; Fabre, C.; Janot, J. M.; Land, E. J.; Leach, S.; Leboulair, V.; Rassat, A.; Roux, S.; Seta, P. *Chem. Eur. J.* **1998**, *4*, 270–278.
- Armaroli, N.; Diederich, F.; Dietrich-Buchecker, C. O.; Flamigni, L.; Marconi, G.; Nierengarten, J. F.; Sauvage, J. P. *Chem. Eur. J.* **1998**, *4*, 406–416.

33. Armaroli, N. *Chem. Soc. Rev.* **2001**, *30*, 113–124.
34. Scaltrito, D. V.; Thompson, D. W.; O'Callaghan, J. A.; Meyer, G. J. *Coord. Chem. Rev.* **2000**, *208*, 243–266.
35. Miller, M. T.; Gantzel, P. K.; Karpishin, T. B. *Inorg. Chem.* **1999**, *38*, 3414–3422.
36. McMillin, D. R.; McNett, K. M. *Chem. Rev.* **1998**, *98*, 1201–1219.
37. Gushurst, A. K. I.; McMillin, D. R.; Dietrich-Buchecker, C. O.; Sauvage, J. P. *Inorg. Chem.* **1989**, *28*, 4070–4072.
38. Armaroli, N.; De Cola, L.; Balzani, V.; Sauvage, J. P.; Dietrich-Buchecker, C. O.; Kern, J. M. *J. Chem. Soc., Faraday Trans.* **1992**, *88*, 553–556.
39. Armaroli, N.; Balzani, V.; De Cola, L.; Hemmert, C.; Sauvage, J. P. *New J. Chem.* **1994**, *18*, 775–782.
40. Armaroli, N.; Ceroni, P.; Balzani, V.; Kern, J. M.; Sauvage, J. P.; Weidmann, J. L. *J. Chem. Soc., Faraday Trans.* **1997**, *93*, 4145–4150.
41. Chen, L. X.; Shaw, G. B.; Novozhilova, I.; Liu, T.; Jennings, G.; Attenkofer, K.; Meyer, G. J.; Coppens, P. *J. Am. Chem. Soc.* **2003**, *125*, 7022–7034.
42. Chen, L. X.; Jennings, G.; Liu, T.; Gosztola, D. J.; Hessler, J. P.; Scaltrito, D. V.; Meyer, G. J. *J. Am. Chem. Soc.* **2002**, *124*, 10861–10867.
43. Gunaratne, T.; Rodgers, M. A. J.; Felder, D.; Nierengarten, J. F.; Accorsi, G.; Armaroli, N. *Chem. Commun.* **2003**, 3010–3011.
44. Kirchhoff, J. R.; Gamache, R. E.; Blaskie, M. W.; Del Paggio, A. A.; Lengel, R. K.; McMillin, D. R. *Inorg. Chem.* **1983**, *22*, 2380–2384.
45. Felder, D.; Nierengarten, J. F.; Barigelletti, F.; Ventura, B.; Armaroli, N. *J. Am. Chem. Soc.* **2001**, *123*, 6291–6299.
46. Rio, Y.; Enderlin, G.; Bourgoigne, C.; Nierengarten, J. F.; Gisselbrecht, J. P.; Gross, M.; Accorsi, G.; Armaroli, N. *Inorg. Chem.* **2003**, *42*, 8783–8793.
47. Armaroli, N.; Accorsi, G.; Felder, D.; Nierengarten, J. F. *Chem. Eur. J.* **2002**, *8*, 2314–2323.
48. Balzani, V.; Scandola, F. *Supramolecular Photochemistry*; Ellis Horwood: Chichester, UK, 1991.
49. Armaroli, N.; Accorsi, G.; Song, F. Y.; Palkar, A.; Echegoyen, L.; Bonifazi, D.; Diederich, F. *ChemPhysChem* **2005**, *6*, 732–743.
50. Gordon, C. K.; McGarvey, J. J. *Inorg. Chem.* **1991**, *30*, 2986–2989.
51. Lukas, A. S.; Zhao, Y. Y.; Miller, S. E.; Wasielewski, M. R. *J. Phys. Chem. B* **2002**, *106*, 1299–1306.
52. Flamigni, L.; Marconi, G.; Dixon, I. M.; Collin, J. P.; Sauvage, J. P. *J. Phys. Chem. B* **2002**, *106*, 6663–6671.
53. Eckert, J. F.; Nicoud, J. F.; Nierengarten, J. F.; Liu, S. G.; Echegoyen, L.; Barigelletti, F.; Armaroli, N.; Ouali, L.; Krasnikov, V.; Hadziioannou, G. *J. Am. Chem. Soc.* **2000**, *122*, 7467–7479.
54. Barqawi, K. R.; Murtaza, Z.; Meyer, T. J. *J. Phys. Chem.* **1991**, *95*, 47–50.
55. Claude, J. P.; Meyer, T. J. *J. Phys. Chem.* **1995**, *99*, 51–54.
56. Peeters, E.; van Hal, P. A.; Knol, J.; Brabec, C. J.; Sariciftci, N. S.; Hummelen, J. C.; Janssen, R. A. J. *J. Phys. Chem. B* **2000**, *104*, 10174–10190.
57. Goze, C.; Chambron, J. C.; Heitz, V.; Pomeranc, D.; Salom-Roig, X. J.; Sauvage, J. P.; Morales, A. F.; Barigelletti, F. *Eur. J. Inorg. Chem.* **2003**, 3752–3758.
58. Hammarström, L.; Barigelletti, F.; Flamigni, L.; Armaroli, N.; Sour, A.; Collin, J. P.; Sauvage, J. P. *J. Am. Chem. Soc.* **1996**, *118*, 11972–11973.



Artificial photosynthetic reaction centers with carotenoid antennas

Stephanie L. Gould, Gerdenis Kodis, Paul A. Liddell, Rodrigo E. Palacios, Alicia Brune, Devens Gust,* Thomas A. Moore* and Ana L. Moore*

Department of Chemistry and Biochemistry, Center for the Study of Early Events in Photosynthesis, Arizona State University, Tempe, AZ 85287-1604, USA

Received 2 June 2005; revised 28 June 2005; accepted 30 June 2005

Available online 20 December 2005

Abstract—Two reaction center-antenna models based on a purpurin macrocycle linked to a C_{60} and to a carotenoid polyene have been synthesized. In these systems the C_{60} moiety is the primary electron acceptor, the purpurin is the primary electron donor and the carotenoid moiety acts both as an antenna and secondary electron donor. Formation of the initial charge separated state, $C-Pur^{+}-C_{60}^{-}$, following excitation with light absorbed by either the purpurin or C_{60} takes place on the 10 ps time scale. The final charge separated state, $C^{+}-Pur-C_{60}^{-}$, is formed in one of the compounds with a quantum yield of 32% based upon light absorbed by the carotenoid. In order to function as an antenna, the carotenoid pigment must be electronically coupled to the purpurin. The purpurin C ring provides an excellent framework for locating a carotenoid polyene in partial conjugation with the macrocycle, leading to a relatively strong electronic communication between the chromophores; functionalization of a *meso* position of the purpurin provides a site for the covalent attachment of C_{60} .

© 2005 Elsevier Ltd. All rights reserved.

1. Introduction

Over the last 30 years, a great deal of research effort has been invested in the study of artificial constructs that mimic the photoinduced electron transfer lying at the heart of photosynthetic solar energy conversion. In the 11 years since the first report of photoinduced electron transfer in a porphyrin–fullerene dyad,¹ fullerenes have been found to be excellent electron acceptors for incorporation into artificial reaction centers.^{2–4} Their relatively negative reduction potentials, low solvent and internal reorganization energies, low susceptibility to solvent stabilization of the radical anion, and potential ability to act as electron accumulators are qualities that enhance their performance in this capacity.^{2,5–7} Recently, researchers have begun incorporating into artificial photosynthetic constructs not only photoinduced charge separation, but also antenna function.^{8–10} Natural and artificial photosynthetic antennas gather light and transfer the resulting excitation energy to the site of charge separation.

Antenna complexes in photosynthetic organisms usually consist of elaborate protein matrices that bind pigments such as chlorophylls and carotenoids in well-defined architectures that promote efficient light absorption and singlet energy transfer.^{11–13} The carotenoids in these assemblies absorb light in the blue-green region of the spectrum (where chlorophyll has a low extinction coefficient) and transfer excitation energy to chlorophylls situated nearby—usually in van der Waals contact. This small separation between energy donors and acceptors is a requirement dictated by the extremely short excited state lifetimes of the carotenoids.¹³ In other words, energy transfer must be very rapid in order to compete with decay of the excited states by other pathways. The energy transfer process culminates with the arrival of the excitation energy at the reaction center where energy transduction takes place.

The inclusion of carotenoids as artificial antennas also requires strong electronic communication between the chromophores. The C ring of a purpurin provides an excellent framework for locating a carotenoid polyene in partial conjugation with the macrocycle of the tetrapyrrole.¹⁴ Also, proper functionalization of a *meso* position of the purpurin allows covalent linking of C_{60} , which serves to accept an electron from the excited state of the purpurin.

Keywords: Purpurin; Carotenoid; Porphyrin; Pyrroles; Antenna; Energy transfer; Photoinduced electron transfer; C_{60} as primary electron acceptor.

* Corresponding authors. Tel.: +1 480 965 2953; fax: +1 480 965 2747; e-mail addresses: gust@asu.edu; tmoore@asu.edu; amoore@asu.edu; ana.moore@asu.edu

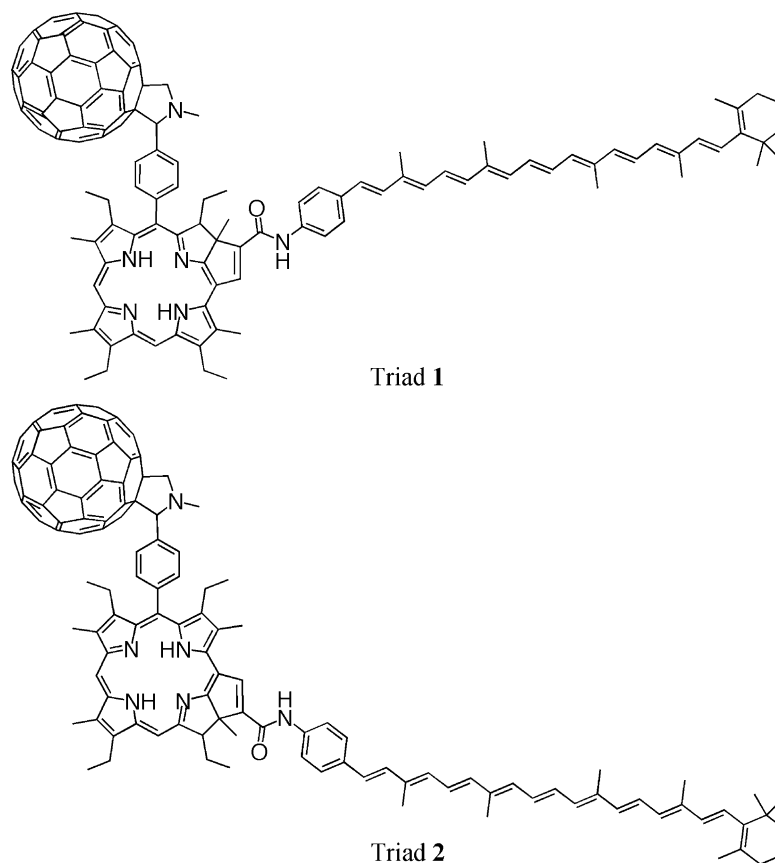


Figure 1. Structures of triads 1 and 2.

In this work, we describe two closely related artificial antenna-reaction center systems, triads **1** and **2** (Fig. 1), where the carotenoid moiety is attached to the C ring of a purpurin by an amide linkage, allowing fast and relatively efficient energy transfer (<100 fs) from the carotenoid to the purpurin. In these assemblies the charge-separation process can be initiated by light absorbed by the carotenoid antenna.

2. Results and discussion

2.1. Synthesis

The purpurin components of **1** and **2**, derived from the same porphyrin, were synthesized according to Scheme 1. The approach is an adaptation of one employed by Robinson and co-workers,^{15–17} and began with 5-(4-carbomethoxyphenyl)-3,7,13,17-tetraethyl-2,8,12,18-tetramethylporphyrin (**6**), which was prepared via a McDonald condensation¹⁸ of two different dipyrromethanes, **7** and **8**.

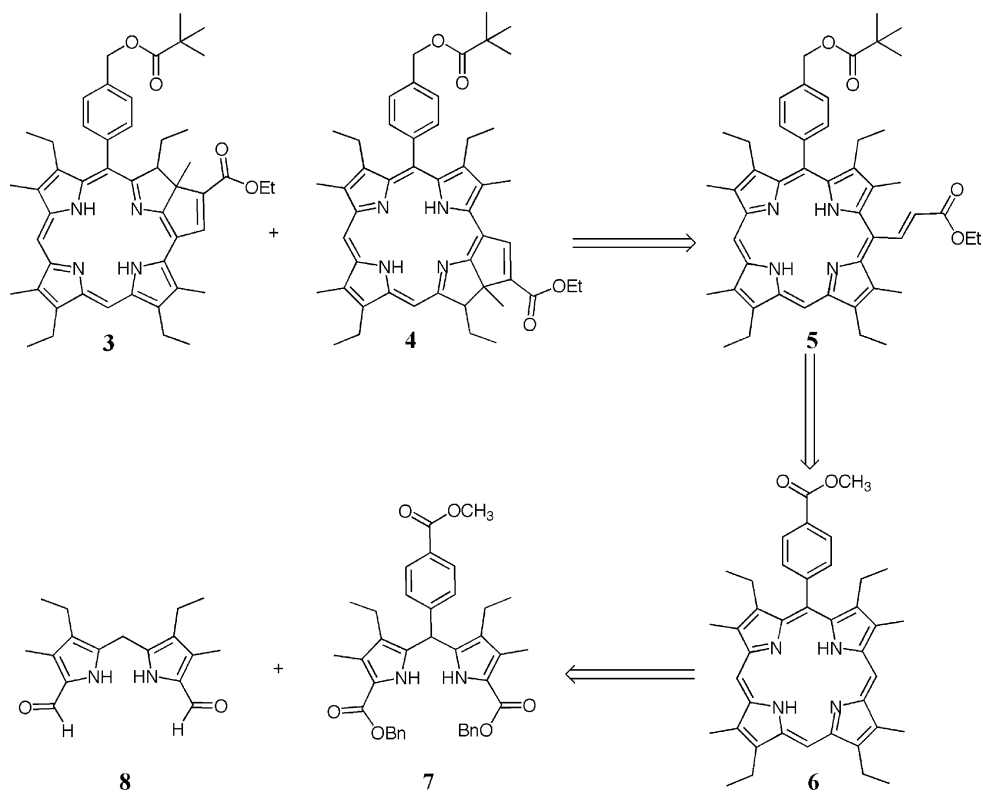
The synthesis of dipyrromethane **7** is outlined Scheme 2. Pyrrole **9** was converted to **10** by treating it with sulfonyl chloride and hydrolyzing the tri-chloride intermediate to **10** (92% yield).¹⁹ Iododecarboxylation by heating **10** with NaHCO₃ and I₂ resulted in pyrrole **11** (94% yield). Mild hydrogenation gave **12** (94% yield). Transesterification by distillation at reduced pressure replaced the

ethyl ester with a benzyl ester protecting group at position 2 (**13**, 87% yield). Dipyrromethane **7** was prepared in 88% yield, by treating **13** with methyl 4-formylbenzoate **14**.

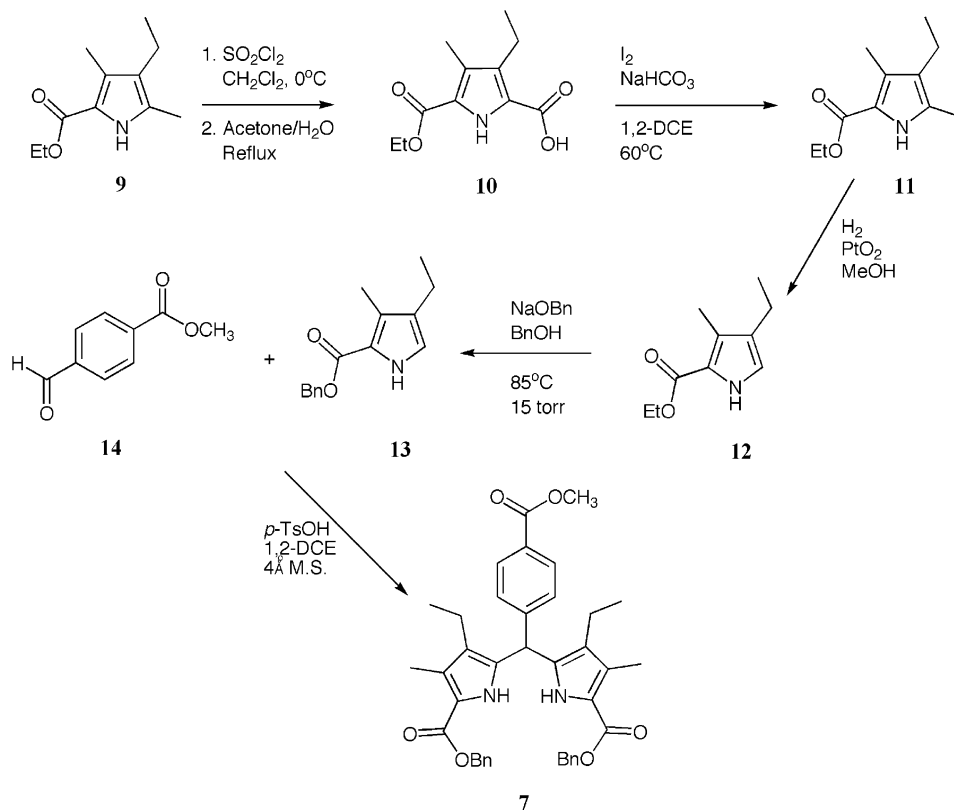
Scheme 3 illustrates the formation of **6**. Dipyrromethane **7** was hydrogenated to give **15** in 99% yield. Condensation of **15** with 3,7-diethyl-2,8-dimethyl-1,9-diformyldipyrromethane²⁰ **8** afforded **6** (51% yield).

The methyl ester of **6** was reduced to the benzyl alcohol with lithium aluminum hydride, giving porphyrin **16** (99% yield, Scheme 4). Protection of the benzyl alcohol with pivaloyl chloride resulted in **17** (87% yield). Nickel was inserted into **17** in 95% yield, using nickel(II) acetylacetonate to give **18**. The Vilsmeier reaction of **18** resulted in formylation at both positions 10 and 15 to give **19** (88% yield) and **20** (11% yield).

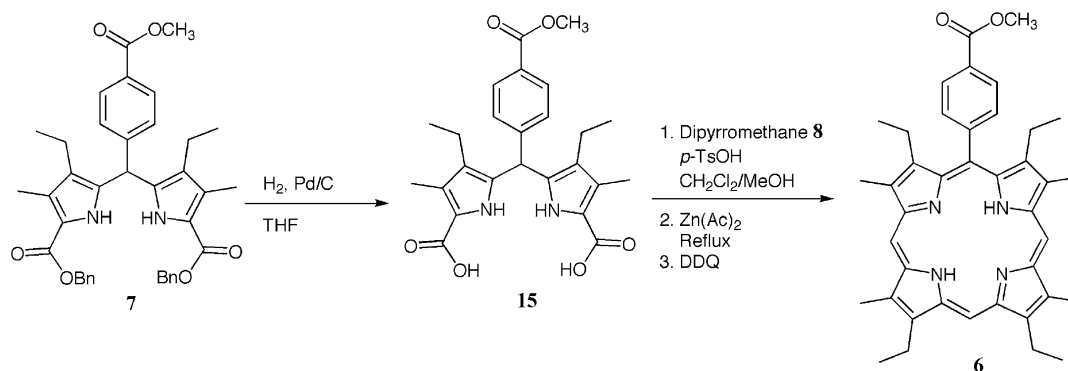
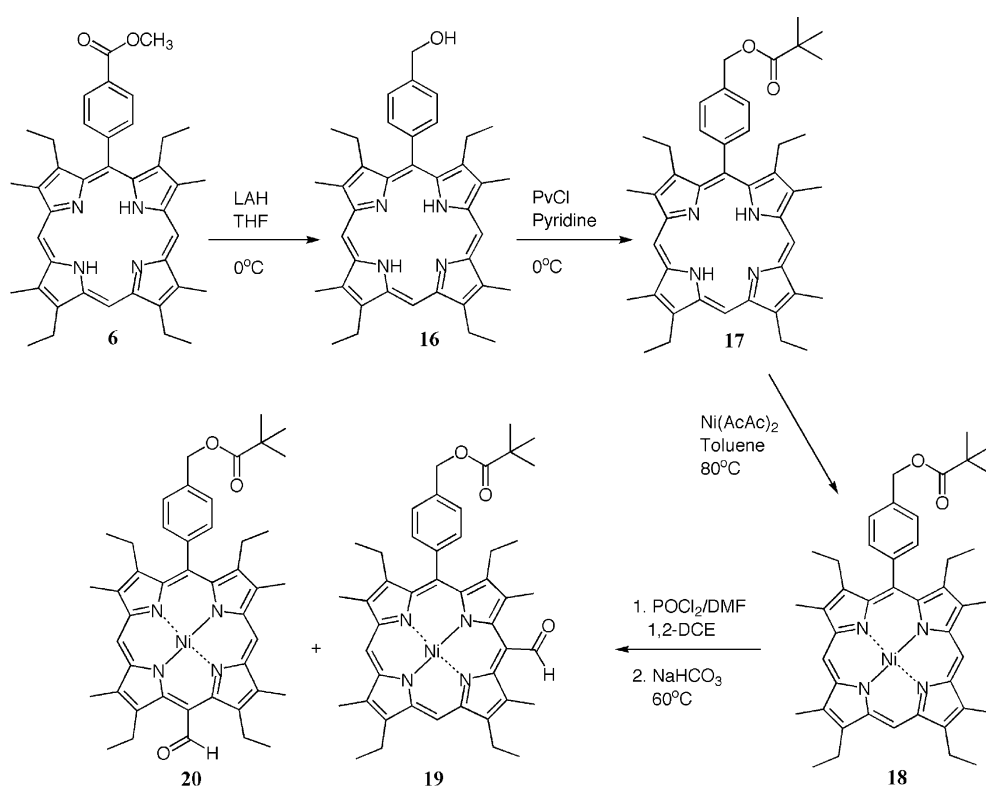
Purpurins **3** and **4** were synthesized from porphyrin **19**, shown in Scheme 5. A Wittig-type reaction using a large excess of (carbethoxymethylene)triphenyl phosphorane resulted in **21** (95% yield). Removal of nickel was accomplished with trifluoroacetic acid, during which time some cyclization also occurred. Immediate treatment of the crude product with 1,8-diazabicyclo[5.4.0]undec-7-ene (DBU) in toluene was used to complete the cyclization of **22** into purpurins **3** (53% yield) and **4** (33% yield).



Scheme 1. Retro-synthetic design of purpurins.



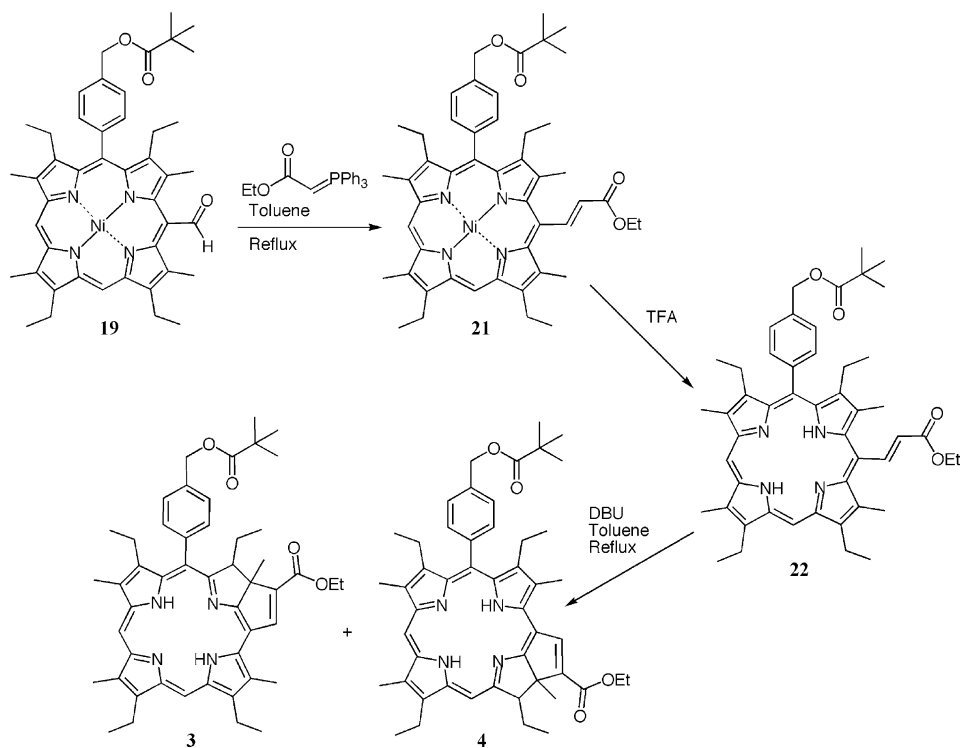
Scheme 2. Synthesis of dipyrromethane **7**.

Scheme 3. Synthesis of porphyrin **6**.Scheme 4. Synthesis of formyl porphyrins **19** and **20**.

Purpurin **3** was synthetically modified to permit coupling to a carotenoid moiety and a fullerene to form triad **1**. Although **3** was separated from regio-isomer **4**, NMR evidence indicated that it consisted of a mixture of stereoisomers. The reactions used to modify **3** are illustrated Scheme 6. Deprotection of the pivaloyl ester without affecting the ethyl ester was accomplished with potassium hydroxide in tetrahydrofuran and methanol at room temperature, resulting in purpurin **23** in 99% yield. Oxidation of the benzyl alcohol to the aldehyde was done with manganese (IV) dioxide. Following chromatography, **24** was obtained in 81% yield. Using the same potassium hydroxide treatment, but heating the reaction at 40 °C for 7 days, the ethyl ester of **24** was hydrolyzed to carboxylic acid **25** in 90% yield. Finally a *tert*-

butyldiphenylsilyl ester (TBDPSi) protecting group was formed by treatment of **25** with *tert*-butyldiphenylsilylchloride (88% yield).

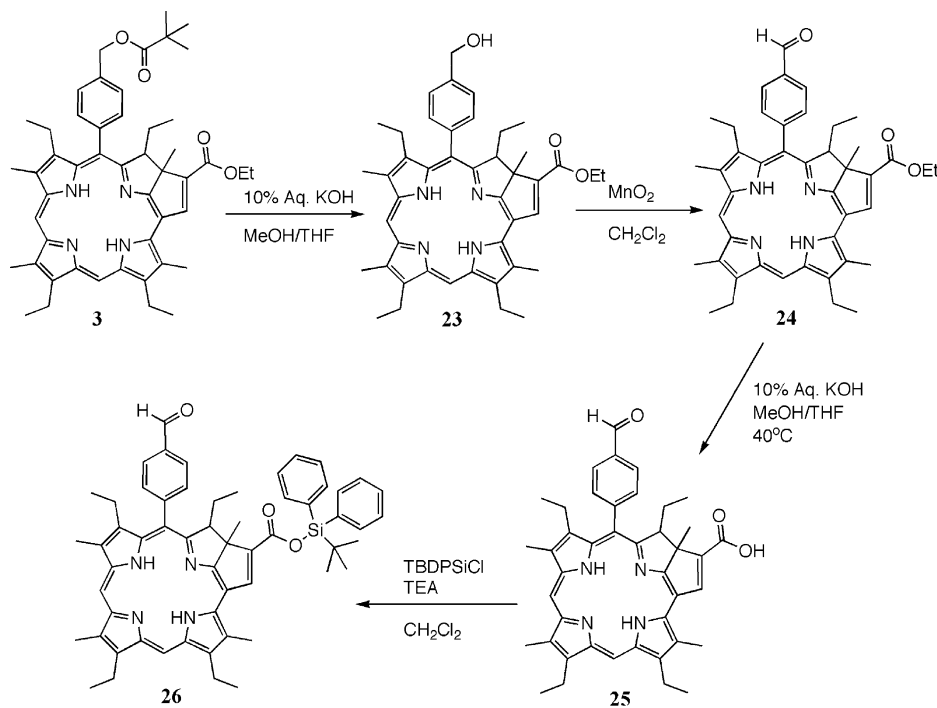
Scheme 7 shows the coupling of all three components to give triad **1**. Dyad **27** was prepared via a Prato reaction²¹ by refluxing **26**, C₆₀ and sarcosine in toluene overnight. Two isomeric compounds were isolated by column chromatography. The more polar product was produced in slightly higher yield, and used in subsequent spectroscopic studies. The carboxylic acid group of **27** was deprotected to give **28** in 82% yield. Because dyad **28** was not soluble in any solvents tested, neither purification of the by column chromatography nor NMR characterization was done. The crude **28** was washed extensively with



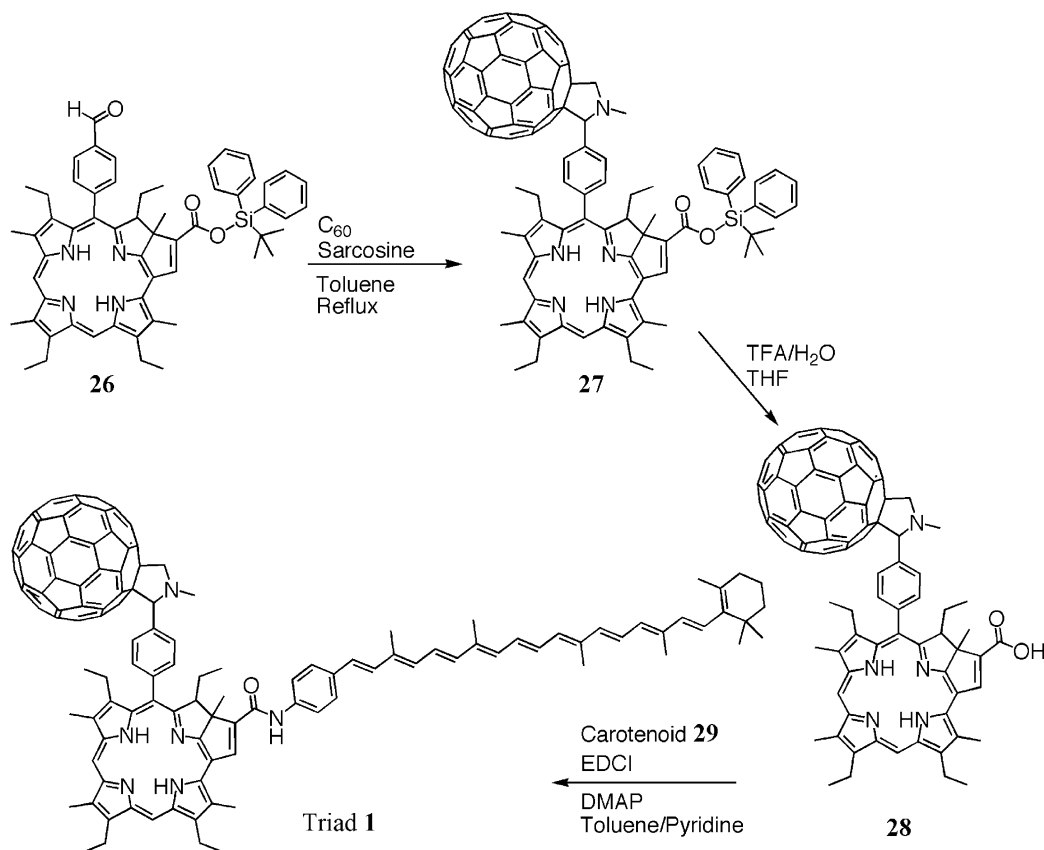
Scheme 5. Synthesis of purpurins **3** and **4**.

methanol to remove any *tert*-butyldiphenylsilyl alcohol produced during the deprotection. Attachment of **29**, 7'-apo-7'-(4-aminophenyl)- β -carotene, Figure 2, was accomplished with *N*-ethyl-*N'*-(3-dimethylaminopropyl)carbodiimide (31% yield).

Several model compounds were necessary to fully elucidate the photochemistry of triad **1**. Dyad **28** was coupled to a *trans,trans*-farnesol moiety to give **30** (38% yield) in order to increase solubility and prevent aggregation without significantly modifying the photophysical properties (Scheme 8).



Scheme 6. Modification of purpurin **3**.



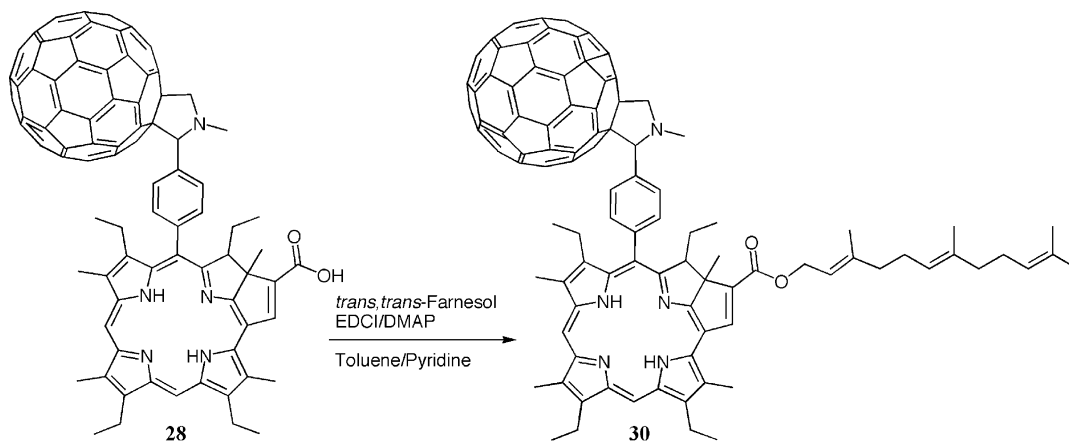
Scheme 7. Synthesis of triad 1.

Another necessary model compound was purpurin–carotene dyad **33** (Scheme 9). Purpurin **23** was protected with a methoxymethyl (MOM) group to give **31** in 56% yield. Purpurin **31** was then deprotected to the free carboxylic acid **32** under basic conditions (87% yield). Coupling of carotenoid **29** and **32** occurred in 88% yield to give **33**.

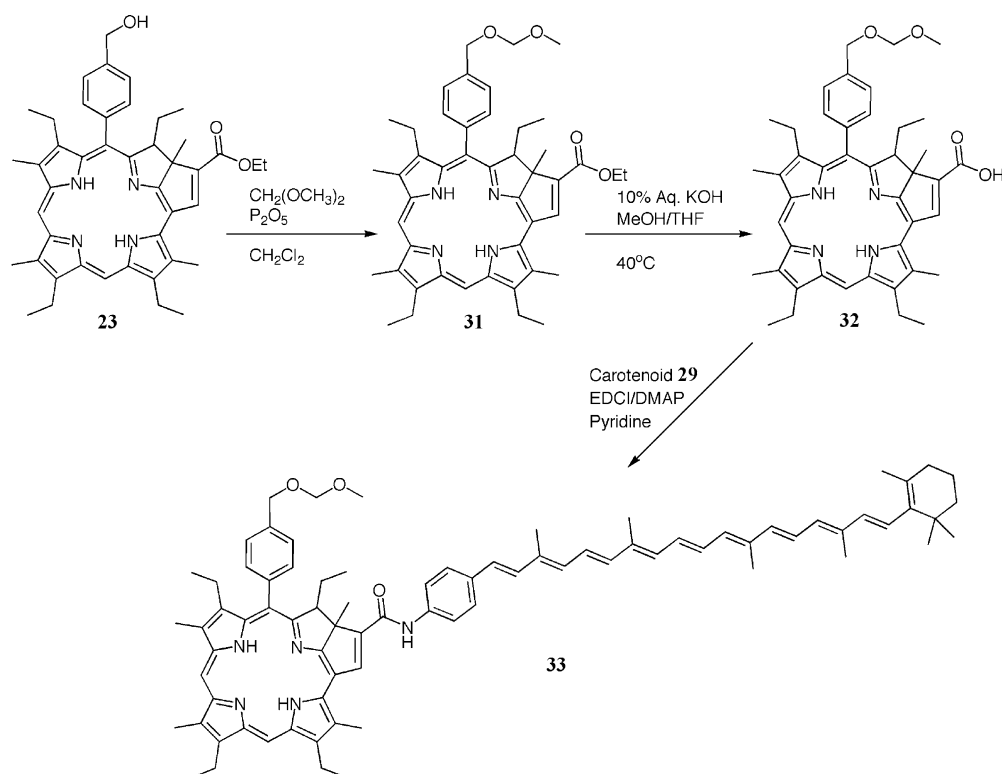
The synthesis of triad **2** began with the hydrolysis of purpurin **4** with potassium hydroxide in tetrahydrofuran and methanol to give the corresponding benzyl alcohol

purpurin **34** (95% yield, Scheme 10). Oxidation of **34** to **35** (71% yield) was followed by deprotection of the ethyl ester by base-promoted hydrolysis to give **36** in 88% yield. Protection of the carboxylic acid as a *tert*-butyldiphenylsilyl ester was accomplished in 88% yield using *tert*-butyldiphenylsilyl chloride and triethylamine in dichloromethane.

A Prato reaction (Scheme 11) of **37** with fullerene (C_{60}) and sarcosine resulted in dyad **38** (36% yield). Dyad **38** was deprotected with trifluoroacetic acid to give the insoluble



Scheme 8. Synthesis of model dyad **30**.

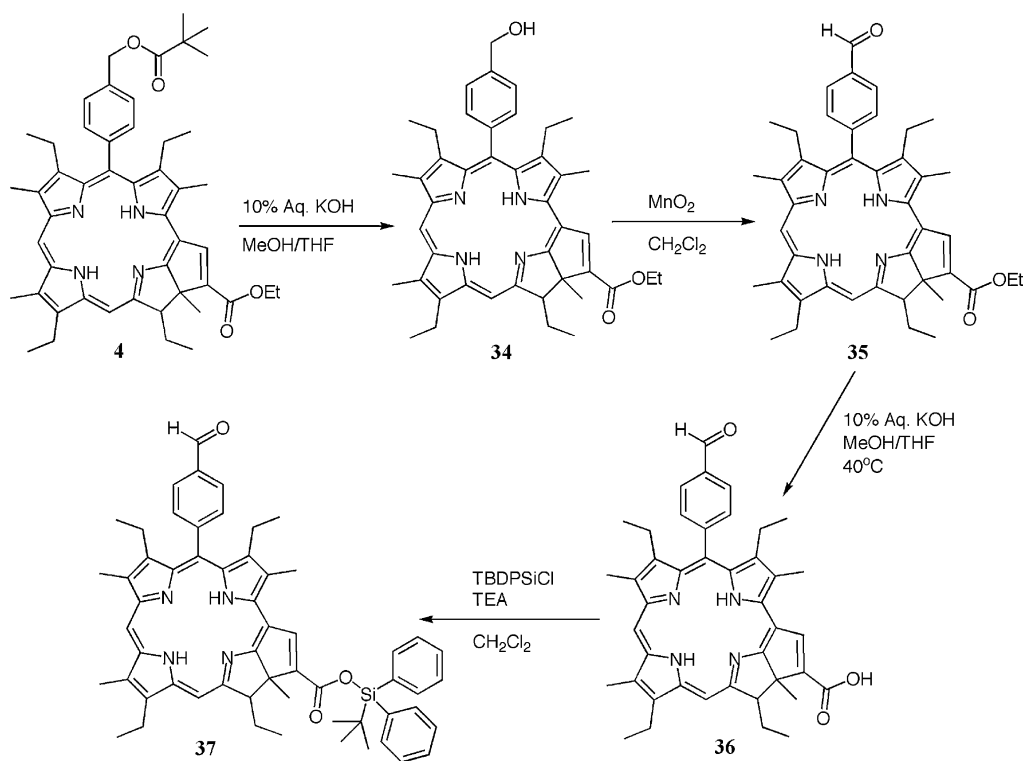


Scheme 9. Synthesis of dyad **33**.

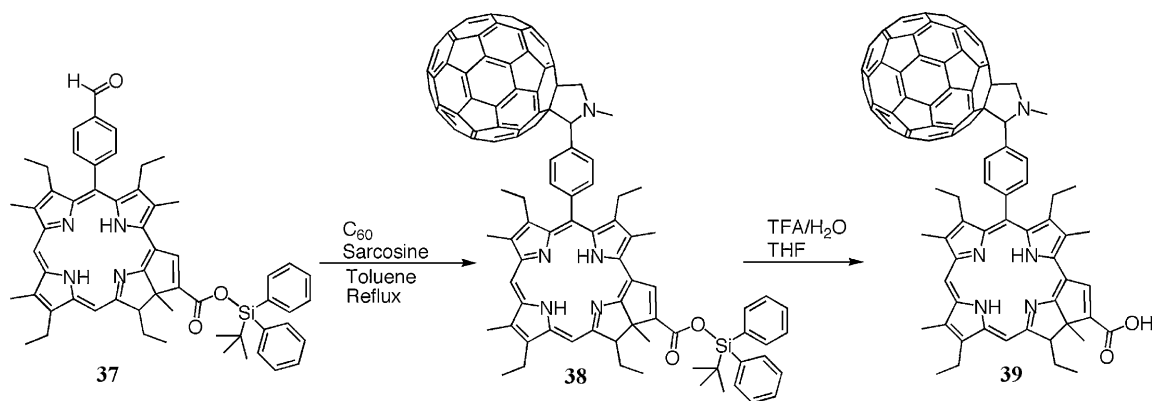
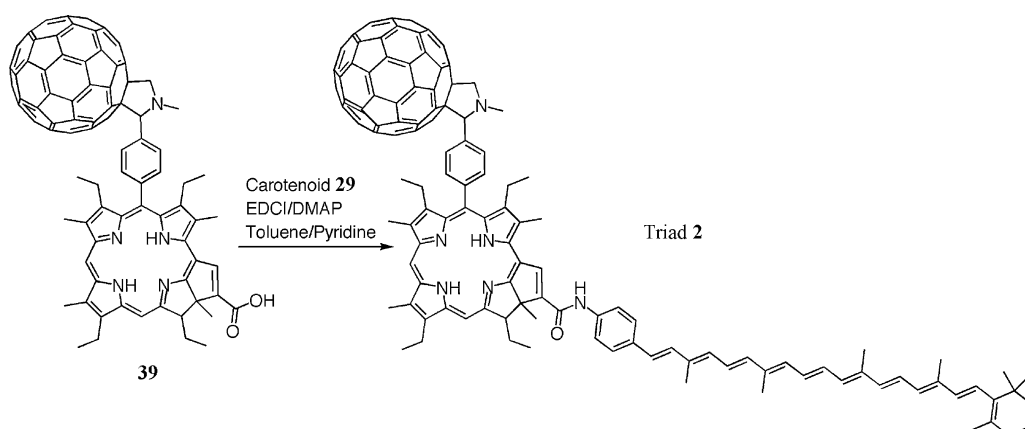
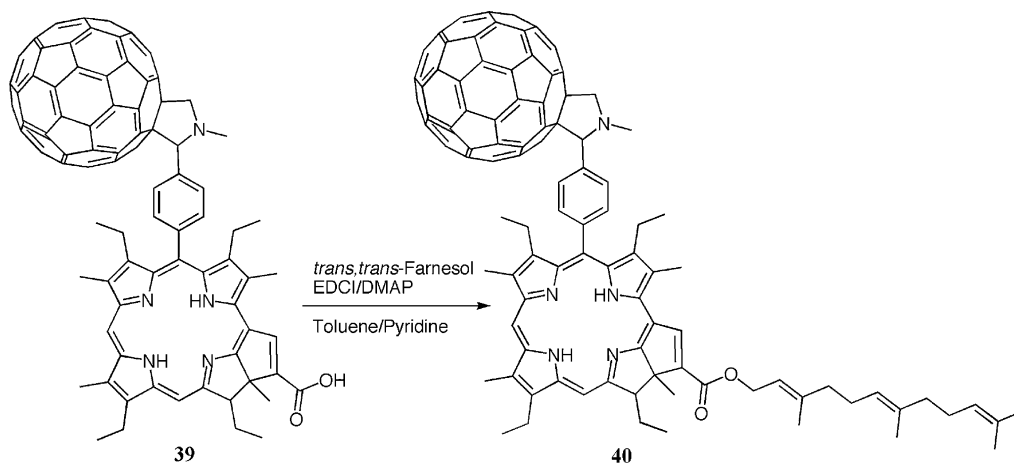
39. The crude acid was washed with methanol to remove any *tert*-butyldiphenylsilyl alcohol formed during the reaction.

Final coupling of **39** to carotenoid **29** resulted in triad **2**

(82% yield, **Scheme 12**). For this reaction, dyad **39** was stirred in toluene/pyridine with 4-(dimethylamino)pyridine until the solid residue had dissolved. The coupling reagent and carotenoid were then added to the solution. Following purification by column chromatography, the final



Scheme 10. Modification of purpurin **4**.

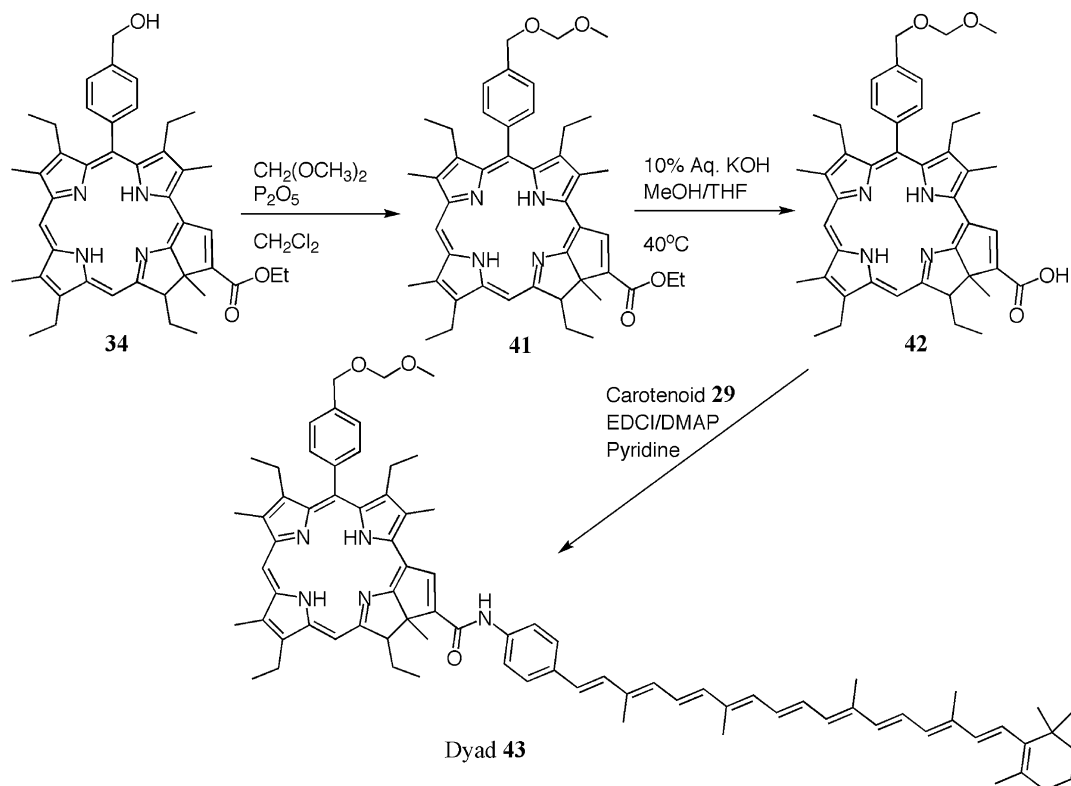
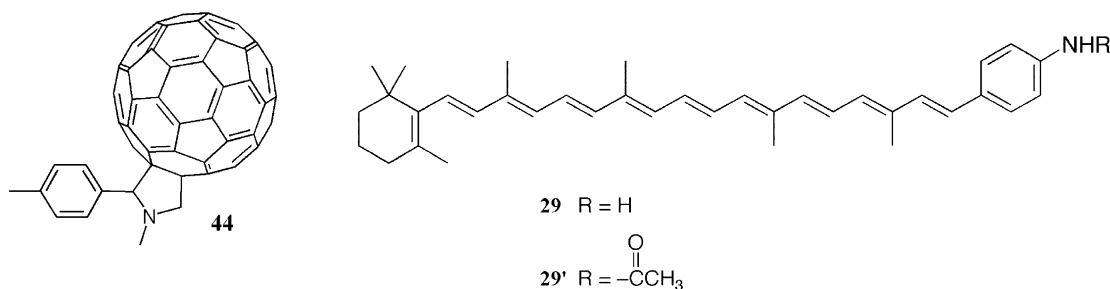
Scheme 11. Synthesis of dyad **39**.Scheme 12. Synthesis of triad **2**.Scheme 13. Synthesis of model dyad **40**.

purification was done by normal phase high-pressure column chromatography (HPLC).

Model compounds similar to those needed for triad **1** were also necessary for triad **2**. Dyad **39** was coupled to *trans,trans*-farnesol to give dyad **40** (Scheme 13). Dyad **43**

(Scheme 14) was prepared by a method similar to that used to synthesize **33**.

Fullerene reference compound **44** (Fig. 2) was prepared by the Prato reaction of *p*-tolualdehyde with sarcosine and C₆₀.²²

Scheme 14. Synthesis of dyad **43**.Figure 2. Model fullerene **44** and carotenoids **29** and **29'**.

2.2. Spectroscopic studies

2.2.1. Steady-state absorption spectra. The absorption spectra of triad **1**, dyad **30**, reference purpurin **3** (normalized to the spectrum of **1** at the Q_y absorption maximum, 697 nm), model fullerene **44**, and carotenoid model **29'** (7'-apo-7'-(acetamidophenyl)- β -carotene, arbitrary scaling) in benzonitrile are shown in Figure 3a. The absorption spectra of triad **2**, dyad **40**, reference purpurin **4** (normalized to **2** at the Q_y absorption maximum, 695 nm), model fullerene **44**, and carotenoid model **29'** (arbitrary scaling) in benzonitrile are shown in Figure 3b.

Triad **1** has a Soret maximum at 434 nm and Q-bands at 576, 642, and 697 nm. Triad **2** has a Soret maximum at 441 nm and Q-bands at 581, 638, and 695 nm. The broad bands with maxima at 489 and \sim 520 nm correspond to the absorption of the carotenoid. Fullerene **44** has a very weak maximum at 704 nm, and absorbs at all shorter wavelengths throughout

the visible and near-UV regions. The spectra of dyads **30** and **40** show a change in relative intensity (more pronounced in **40**) and a red shift (\sim 2 nm) of all the bands compared to reference purpurins **3** and **4**. In addition, it is clear that there is a change in relative intensity and a red shift (\sim 5 nm) of the Q_x bands (around 580 nm) in **1** and **2** compared to reference purpurins **3** and **4**. After subtraction of the underlying carotenoid absorption, the Soret bands of triads **1** and **2** were also found to display a small bathochromic shift compared to **3** and **4**, in addition to some broadening and a change in relative intensity. Similarly, the carotenoid absorption bands of **1** and **2** show red shifts of \sim 5 nm and a substantial loss of fine structure between 470 and 530 nm relative to model **29'**. The origin of the perturbations observed is most likely interchromophore interactions arising from the partial conjugation between them. However, it is important to note that the transient absorption and emission spectra of the triads and dyads remain similar to those of the model

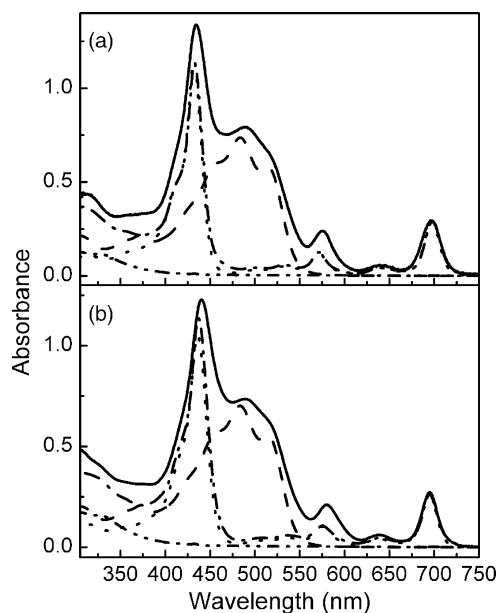


Figure 3. (a) Absorption spectra of triad **1** (—), dyad **30** (---), purpurin **3** (···), fullerene **44** (-·-·-·-), and carotenoid **29'** (---) in benzonitrile. (b) Absorption spectra of triad **2** (—), dyad **40** (---), purpurin **4** (···), fullerene **44** (-·-·-·-), and carotenoid **29'** (---) in benzonitrile.

systems, indicating that the coupling is not so strong that the spectral identity of the excited singlet states of the individual chromophores is lost.

2.2.2. Steady-state fluorescence. The steady-state fluorescence emission spectra of the purpurin and fullerene moieties in **1**, **2**, **30**, **40**, **33**, and **43** (not shown) are similar in shape and are typical of porphyrin/purpurin-like macrocycles and fullerenes. In benzonitrile, **3** has fluorescence emission maxima at 706 and ~ 768 nm, **4** at 702 and ~ 766 nm, and fullerene **44** at 715 and ~ 800 nm. The emission of the purpurin and fullerene moieties in **1**, **2**, **30**, **40**, **33**, and **43** is strongly quenched compared to that of reference purpurins **3** and **4** and fullerene **44**. We ascribe the quenching of the purpurin emission to singlet energy and/or electron transfer involving the carotenoid and/or fullerene moieties.

Fluorescence excitation measurements of dyads **33** and **43** were performed to investigate the possibility of singlet-singlet energy transfer from the carotenoid to the purpurin (Fig. 4). Transfer was indeed observed. In toluene, the average quantum yield of energy transfer in the 460–520 nm range is 0.58 ± 0.08 for dyad **33** and 0.57 ± 0.09 for dyad **43**, although a small increase in the ratio with increasing wavelength is apparent. These yields are similar to that measured for a previously-studied carotene-purpurin dyad (0.67 ± 0.04).¹⁴

2.2.3. Time-resolved fluorescence studies. The lifetime of the S_1 state of the purpurin was determined for **1**, **2**, **30**, **40**, **33**, **43**, **3** and **4**. Benzonitrile solutions of the compounds were excited with ~ 9 ps laser pulses at 590 nm, and the fluorescence decay was measured using the time-correlated single photon counting technique in the 690–820 nm range. The fluorescence lifetimes of purpurins **3** and **4** were 2.84 ns ($\chi^2=1.03$) and 2.45 ns ($\chi^2=1.01$), respectively (minor

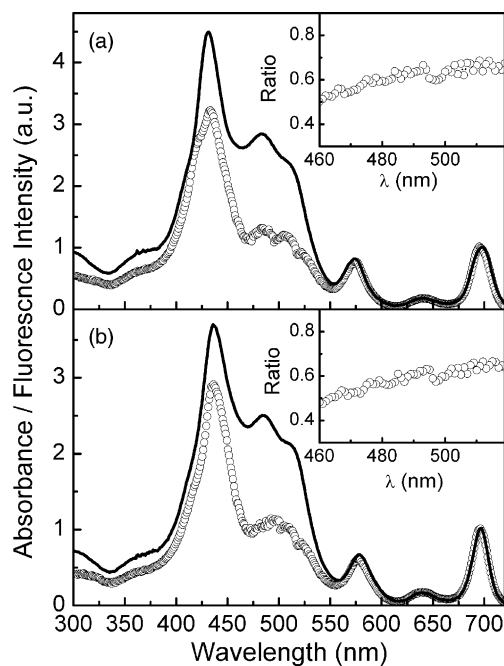


Figure 4. (a) Absorption spectrum of dyad **33** (—) in toluene. The corrected fluorescence excitation spectrum of a $\sim 6 \times 10^{-7}$ M solution of **33** in toluene (oooo), normalized to the absorption spectrum at the purpurin Q bands, is also shown. The fluorescence excitation spectrum was corrected in the range 350–700 nm using a file generated from the absorption and fluorescence excitation spectra of purpurin **3**. The inset shows the ratio of the normalized fluorescence excitation intensity to the absorbance of dyad **33**, after first subtracting the absorbance of **3** from both spectra. (b) Absorption spectra of dyad **43** (—) in toluene. The corrected fluorescence excitation spectrum of a $\sim 6 \times 10^{-7}$ M solution of **43** in toluene (ooooo), normalized to the absorption spectrum at the purpurin Q bands, is also shown. The fluorescence excitation spectrum was corrected in the range 350–700 nm using a file generated from the absorption and fluorescence excitation spectra of purpurin **4**. The inset shows the ratio of the normalized fluorescence excitation intensity to the absorbance of dyad **43**, after first subtracting the absorbance of **4** from both spectra.

components, $< 10\%$, were also required in order to fit the data). Model fullerene **44** showed a single-exponential decay of 1.38 ns ($\chi^2=1.09$). Triads **1** and **2** and dyads **30** and **40** showed a ~ 15 ps major ($\sim 90\%$) decay component, which is at the lower limit of the spectrometer time resolution. Carotenopurpurin dyad **33** featured 265 ps (78%) and 660 ps (20%) decays in benzonitrile, and lifetimes of 1.8 ns (60%) and 2.5 ns (40%) in *n*-hexane. The fluorescence decay of isomeric dyad **43** in benzonitrile was fit with major decay components of 200 ps (78%) and 390 ps (20%). Similar lifetimes were previously reported for a similar dyad containing the same carotenoid and a related purpurin moiety.¹⁴

The fluorescence quenching observed for **33** and **43**, relative to **3** and **4**, has been seen in other covalently linked dyads of this general type. The lifetime of the S_1 state of the purpurin moiety of **33** decreases with increasing solvent polarity. This solvent sensitivity suggests that a possible mechanism for the quenching is electron transfer from the carotenoid to the purpurin S_1 state, resulting in the charge separated state $C^{\cdot+}-Pur^{\cdot-}$, as has been observed in related systems.^{23,24} However, other mechanisms, including singlet energy transfer from the macrocycle to the S_1 state of the carotenoid, could also explain the quenching.²⁴ The

fluorescence decays of **33** and **43** were biexponential in all the solvents examined. The presence of two isomeric populations, possibly due to differences in the locations of the central hydrogen atoms on the macrocycle, diastereoisomerism resulting from the two adjacent chiral centers, or restricted rotation about the linkage bonds, are possible explanations for this observation.

2.2.4. Time-resolved absorption studies. Solutions of **1**, **2**, **30**, **40**, **33**, **43** were excited with ~ 100 fs laser pulses at 695 nm and the transient absorptions were recorded using the pump-probe method. The spectra were measured in the 930–1070 nm and 450–770 nm regions. A total of 70 and 155 kinetic traces were recorded over those wavelength regions, respectively, at times ranging from -50 to 4500 ps relative to the laser flash. The data were fitted globally using singular value decomposition.

To determine whether the S_1 singlet excited state of the carotenoid acts as a donor of singlet excitation energy to the macrocycle of dyads **33** and **43**, transient absorption measurements in toluene with excitation at 480 nm were made (not shown). The lifetimes of S_1 were found to be 7.9 and 7.7 ps for dyads **33** and **43**, respectively. Model carotenoid **29'** had a 7.8 ps singlet state lifetime in toluene. Within experimental error, these S_1 lifetimes are all the same, indicating that energy transfer from the S_1 state of the carotenoid to the purpurin is negligible. Thus, the observed energy transfer is ascribed to the S_2 state of the carotenoid.

Verification of the formation of a $\text{Pur}^{\cdot+}-\text{C}_{60}^{\cdot-}$ charge separated state comes from the spectroscopic investigation of dyads **30** and **40** in benzonitrile with excitation at 695 nm, where most of the light absorption is by the purpurin. Figure 5 shows the decay-associated spectra of **30** obtained by a global analysis of the data. The best fit was achieved with two components having lifetimes of 12 and 70 ps. The 12 ps component has characteristic purpurin ground state bleaching bands around 580, 640, 700 nm and stimulated emission bands around 700 and 770 nm. The amplitudes are consistent with decay of a singlet excited state of the purpurin and formation of the $\text{Pur}^{\cdot+}-\text{C}_{60}^{\cdot-}$ charge separated state. The 70 ps component shows spectral characteristics of the purpurin radical cation around 850 nm and fullerene radical anion around 1010 nm, and is indicative of the decay of the charge separated state. The

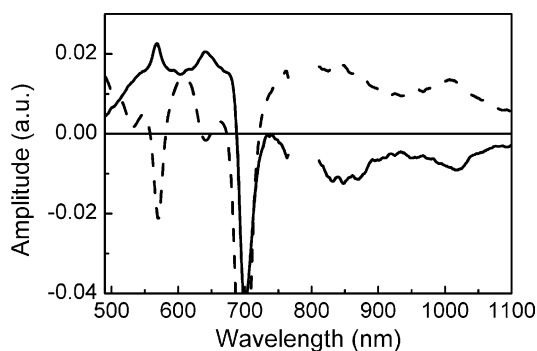


Figure 5. Decay-associated transient absorption spectra for dyad **30** in benzonitrile obtained from a global analysis of transient absorption data taken after excitation at 695 nm with a ~ 100 fs laser pulse. The lifetimes of the components are 12 ps (—) and 70 ps (---).

decay-associated spectrum of dyad **40** is very similar (not shown). In this case, the best fit was achieved with two components having lifetimes of 7 and 35 ps.

Figure 6 shows the decay-associated spectra of triad **1** obtained by global analysis of the data obtained with excitation at 695 nm in benzonitrile. The best fit was achieved with five components having lifetimes of 10, 30, 260, and 1600 ps and a component that did not decay on the 5 ns time scale. The 10 ps component corresponds to the decay of the purpurin excited singlet state and formation of $\text{C}-\text{Pur}^{\cdot+}-\text{C}_{60}^{\cdot-}$. This component also has features characteristic of the decay of the $\text{C}^{\cdot+}-\text{Pur}^{\cdot-}-\text{C}_{60}$ charge separated state, which forms with a time constant of 260 ps. The 30 ps component has characteristic purpurin ground state bleaching bands around 580, 640 and 700 nm and no stimulated emission around 770; instead, there is induced absorption due to the purpurin radical cation and a negative band around 980 nm due to the growing-in of carotenoid radical cation absorption. Thus, the 30 ps component represents the decay of $\text{C}-\text{Pur}^{\cdot+}-\text{C}_{60}^{\cdot-}$ and concurrent formation of $\text{C}^{\cdot+}-\text{Pur}-\text{C}_{60}^{\cdot-}$ by a charge shift reaction. The 1600 ps component does not have characteristic purpurin ground state bleaching bands, but does show ground state bleaching around 500 nm due to carotenoid moiety, and induced absorption around 1000 nm due to the carotenoid radical cation and fullerene radical anion. Thus, this component represents the decay of $\text{C}^{\cdot+}-\text{Pur}-\text{C}_{60}^{\cdot-}$. The non-decaying component has some features characteristic of the carotenoid triplet state: ground state bleaching around 500 nm and induced absorption at 540 nm. The decay-associated spectra of triad **2** are similar (not shown). The best fit for **2** was achieved with five components having lifetimes of 6, 30, 200, 1200 ps, and non-decaying on the 5 ns time scale.

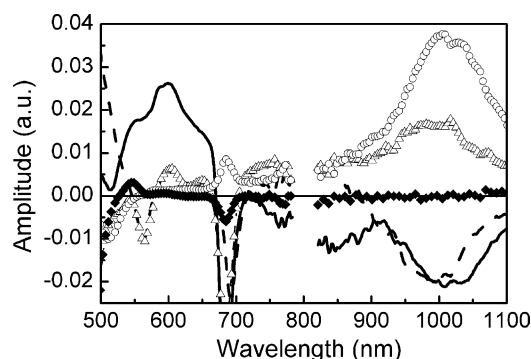


Figure 6. Decay-associated transient absorption spectra for triad **1** in benzonitrile obtained from a global analysis of transient absorption data taken after excitation at 695 nm with a ~ 100 fs laser pulse. The lifetimes of the components are 10 ps (—), 30 ps (---), 260 ps (triangles), 1600 ps (circles) and a non-decaying component on this time scale (diamonds).

The formation of the $\text{C}^{\cdot+}-\text{Pur}^{\cdot-}$ charge separated state as a quenching mechanism for the corresponding purpurin excited singlet state was investigated in model dyads **33** and **43** in benzonitrile. The rise of induced absorption around 980 nm with a 6 ps lifetime was found, as was a decay with a time constant of 265 and 200 ps for **33** and **43**, respectively, (data not shown). The fluorescence lifetime of **33** (265 ps) unambiguously associates the 265 ps component with the rise of the $\text{C}^{\cdot+}-\text{Pur}^{\cdot-}$ state. Therefore,

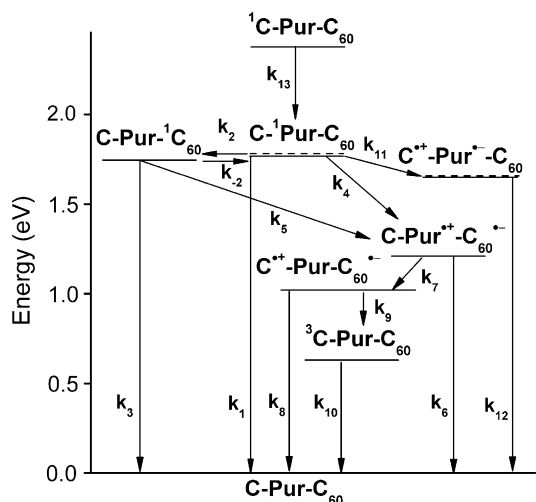


Figure 7. Transient states of triads **1** (—), **2** (---) and relevant interconversion pathways. The carotenoid excited state is assumed to be analogous to 1B_u (often referred as S_2).

the 6 ps component is the $C^{\cdot+}-Pur^{\cdot-}$ lifetime and the kinetics observed in the time-resolved absorption studies are inverted. Similar behavior was observed in the case of **43**.

Excitation of deoxygenated samples of **1** and **2** in benzonitrile with a ~ 5 ns laser pulse at 590 nm permitted further investigations of the long-lived states (not shown). The induced absorption band at 540 nm associated with the carotenoid triplet state was found to decay with a 4 μ s lifetime.

2.2.5. Analysis of the kinetic data. The model chosen for the interpretation of the kinetic and spectroscopic data dealing with single energy and electron transfer in triads **1** and **2** is shown in Figure 7, which indicates the relevant high-energy states and kinetic pathways. The rate constants for the various reactions in Figure 7, obtained experimentally from the transient spectroscopic measurements on the triads and model compounds or estimated as described below, are reported in Table 1. The energies of the various spectroscopic states were determined from the wavenumber average of the longest-wavelength absorption and shortest-wavelength emission maxima of **1**, **2** and appropriate model compounds. The purpurin first excited singlet state lies at 1.77 and 1.78 eV in **1** and **2**, respectively, whereas the energy of $C-Pur^{-1}C_{60}$ is 1.75 eV above the ground state. The energies of the charge separated states were estimated from cyclic voltammetric data on the individual components. The first reduction potential for a C_{60} model (-0.55 V vs SCE) and the first oxidation potential for a carotenoid model (0.47 V) have been previously

reported.^{22,25} The first reduction potential of purpurins **3** and **4** were determined experimentally to be -1.18 and -1.19 V, respectively; the first oxidation potential obtained for **3** and **4** was 0.66 V. From these data, the energies of the charge separated states were estimated as 1.21 eV for $C-Pur^{\cdot+}-C_{60}^{\cdot-}$, 1.65 and 1.66 eV for $C^{\cdot+}-Pur^{\cdot-}-C_{60}$ of **1** and **2**, respectively, and 1.02 eV for $C^{\cdot+}-Pur-C_{60}^{\cdot-}$. The energy of the triplet state $^3C-Pur-C_{60}$ of **1** and **2** is not known, but the energy of the lowest triplet state of a closely related carotenoid has been estimated to be 0.63 eV.²⁶

The values for k_1 were obtained from the fluorescence lifetimes of purpurins **3** and **4**, while k_3 came from the fluorescence lifetime of **44**. Because it was not possible to excite exclusively the C_{60} or the purpurin moiety, the values for k_4 and k_5 could not be measured independently. Molecular orbital calculations (Hartree-Fock/STO-G3, Gaussian 98) were used to compare the amplitudes of the HOMO (for hole transfer, step 4) and LUMO (for electron transfer, step 5) orbitals of the purpurin moiety at the *meso* positions linking Pur to C_{60} . Qualitatively, the amplitudes are similar. In the absence of additional information, we assumed that the electronic coupling is comparable for both reactions. This, together with the fact that there is only a very small difference in thermodynamic driving force for reactions 4 and 5, suggests that the approximation $k_4=k_5$ is reasonable. The values reported for these rates constants in Table 1 were obtained from the transient absorption data (10 and 6 ps components in the case of **1** and **2**, respectively).

The rate constants for charge recombination of the initial charge separated state $C-Pur^{\cdot+}-C_{60}^{\cdot-}$ to the ground state (k_6) was estimated from the 70 and 35 ps components of the transient absorption data for Pur- C_{60} dyads **30** and **40**, respectively. The shorter lifetime of $Pur^{\cdot+}-C_{60}^{\cdot-}$ for **40** explains the reduced quantum yield of the final charge separation in this compound compared with **1** (see below). The charge shift rate constant (k_7) was obtained from the lifetime of $C-Pur^{\cdot+}-C_{60}^{\cdot-}$ obtained by the transient absorption measurements with the triads ($(30\text{ ps})^{-1} - k_6$). The measured lifetime of the final charge separated states $C^{\cdot+}-Pur-C_{60}^{\cdot-}$ can be used to determine k_8 , $(1600\text{ ps})^{-1}$ and $(1200\text{ ps})^{-1}$, for **1** and **2**, respectively. In both cases it is assumed that $k_8 \gg k_9$. The lifetime of the carotenoid triplet in the absence of oxygen (4 μ s) was used to calculate k_{10} . The rate constant for the formation of $C^{\cdot+}-Pur^{\cdot-}-C_{60}$ from the purpurin first excited singlet state, k_{11} , was estimated from the transient absorption measurements on caroteno-purpurin dyads **33** and **43**. The values for k_{11} were estimated as $\approx (265\text{ ps})^{-1} - k_1$ in the case of **1** and $\approx (200\text{ ps})^{-1} - k_1$ in the case of **2**. The $C^{\cdot+}-Pur^{\cdot-}-C_{60}$ undergoes very rapid decay ($k_{12} \approx (6\text{ ps})^{-1}$) in both dyads. In the triads, there is no experimental evidence that this state evolves into the

Table 1. Rate constants for the relevant interconversion pathways between the transient states of CPurC₆₀ (triad **1**) and CPurC₆₀ (triad **2**) in benzonitrile^a

k_1	k_2	k_2	k_3	k_4	k_5	k_6	k_7	k_8	k_9	k_{10}	k_{11}	k_{12}	k_{13}
Triad 1													
0.35	$\ll k_4, k_5$	$\ll k_4, k_5$	0.72	100	~ 100	14.29	19.04	~ 0.63	$\ll k_8$	0.00025	~ 3.42	166.7	~ 9206
Triad 2													
0.41	$\ll k_4, k_5$	$\ll k_4, k_5$	0.72	166.7	~ 166.7	28.57	4.76	~ 0.83	$\ll k_8$	0.00025	~ 4.59	166.7	~ 8837

^a Expressed in $(\text{ns})^{-1}$.

final charge separated state $C^+-Pur-C_{60}^-$. The value for k_{13} , energy transfer from an upper excited state of the carotenoid to the purpurin, is $\Phi/[(1-\Phi)\tau_{S_2}]$, where Φ is the quantum yield of energy transfer from the carotenoid to the purpurin and τ_{S_2} is the lifetime of the S_2 state of the carotenoid model measured by fluorescence upconversion (150 fs).¹⁴

Because of rapid photoinduced electron transfer due to strong coupling between the fullerene and purpurin moieties and a large driving force ($-\Delta G^0 \sim 0.56$ eV), the equilibrium between singlet excited states in **1** and **2**, as well as in the corresponding model dyads, was not observed experimentally, and rates k_2 and k_{-2} are unknown.

The quantum yields of the states shown in Figure 7 may be determined by simulation of the kinetic pathways displayed therein using the rate constants given above. The simulations were done using the Chemical Kinetics Simulator (IBM, version 1.01). Quantum yields of 0.55 and 0.13 were obtained for the final charge separated state $C^+-Pur-C_{60}^-$ for **1** and **2**, respectively. Quantum yields of 0.04 and 0.05 were calculated for $C^+-Pu^+-C_{60}^-$ in the case of **1** and **2**, respectively. The quantum yield of the carotenoid triplet was determined using the comparative method as 0.02 in the case of **1** with benzonitrile as solvent.^{27,28}

3. Conclusions

Two reaction center-antenna models based on a purpurin macrocycle have been successfully synthesized. In these systems, the carotenoid moiety acts as a reasonably efficient antenna and covers a range of the solar spectrum between 460–540 nm where solar irradiance is high and where the purpurin moiety does not absorb strongly. Energy transfer from the excited state of the carotenoid to the macrocyclic purpurin moiety with approximately 60% efficiency is observed for both triads. Because of the optically forbidden nature of the S_1 singlet excited state of the carotenoid, absorption of light initially populates only the second excited state (S_2). In spite of its extremely short lifetime (~ 150 fs), the S_2 state is an effective energy donor, whereas the longer-lived S_1 is not. Energy transfer on the fs time scale is facilitated by the partial conjugation provided by the C-ring double bond of the purpurin and the amide bond that links the polyene and the purpurin.

Once the excitation has been transferred to the macrocycle, photoinduced electron transfer to the primary electron acceptor, C_{60} , dominates the decay of the purpurin excited state. Because of the considerable electronic coupling between the purpurin and the C_{60} moieties and the large driving force for the formation of the initial charge separated state, $C^+-Pur^+-C_{60}^-$, the electron transfer reaction takes place on the ≤ 10 picosecond time scale.

The time constant for recombination of the initial charge separated state $C^+-Pur^+-C_{60}^-$ is extremely small (30 and 70 ps for **1** and **2**, respectively) compared to those for the

same reaction in related porphyrin- C_{60} systems having a similar linkage between the chromophores. This fast recombination may be due in part to the relatively low energy of $(C^+-Pur^+-C_{60}^-)$, which locates the charge recombination process near the maximum of the Marcus–Hush relationship of rate constant and free energy change.^{29–32}

The quantum yield of $C^+-Pur-C_{60}^-$ based upon light absorbed by the purpurin is 0.55 in **1** and 0.13 in **2**. Taking into consideration the $\sim 60\%$ quantum yield for the energy transfer from the carotenoid to the purpurin in both cases, the quantum yield of formation of the final charge separated state based upon light absorbed by the carotenoid moiety can be estimated as 32% for **1** and just 7% for **2**. The relatively short lifetime for the final charge separated state, 1600 ps, may be traced in part to the relatively strong electronic coupling between the purpurin and carotenoid, which enhances the rate of charge recombination but was required to achieve significant carotenoid antenna function. This suggests that if the same carotenes are to be used as both antennas and secondary electron donors in artificial assemblies for solar energy harvesting, at least one of the radical ions resulting from photoinduced electron transfer must be moved rapidly to another site in order to use the electrochemical potential energy effectively.

4. Experimental

4.1. Synthesis

The 1H NMR spectra were recorded on Varian spectrometers at 300 or 500 MHz. Unless otherwise specified, samples were dissolved in deuteriochloroform with tetramethylsilane as internal reference. Mass spectra were obtained with a matrix-assisted laser desorption/ionization time-of-flight spectrometer (MALDI-TOF). HPLC purification was done with a Shimadzu SIL-6B HPLC instrument equipped with a Linear UV-vis-206 multi-wavelength detector and a Phenomenex Spherisorb 5-Silica (250 \times 10 mm) SP/1022C column.

All chemicals were purchased from Aldrich, Acros or Lancaster. Fullerene C_{60} , was purchased from materials and electrochemical research (MER) Corporation. Carotenoids **29** and **29'** were prepared using literature procedures.¹ Solvents were obtained from EM Science. Tetrahydrofuran was distilled from sodium metal and benzophenone in a nitrogen atmosphere immediately prior to use. Toluene was distilled from CaH_2 and dichloromethane was distilled from potassium carbonate. All solvents were stored over the appropriate molecular sieves prior to use. Thin-layer chromatography (TLC) was done with silica gel coated glass plates from Analtech. Column chromatography was carried out using EM Science silica gel 60 with 230–400 mesh. All reactions with purpurin molecules were carried out with an argon atmosphere, while all the other reactions were carried out under a nitrogen atmosphere.

4.1.1. 5-Carboxy-2-carboxy-3-ethyl-4-methylpyrrole (10). The title compound was prepared by adding 25.7 mL

(317 mmol) of sulfonyl chloride drop wise, over 15 min, to a cooled (0 °C) solution of 20 g (102 mmol) of 2-carbomethoxy-4-ethyl-3,5-dimethylpyrrole, **9**, in 600 mL of dry dichloromethane. Gas evolved during vigorous stirring at room temperature over the course of 1.5 h. The solvent was removed under reduced pressure after N₂ had been bubbled through the mixture for 5 min. A portion of toluene (300 mL) was added and removed under reduced pressure, to ensure all sulfonyl chloride was removed before the oily residue was dried under a high vacuum for 2 h. Acetone (80 mL) was added followed by the addition of 80 mL of water drop wise. The oily suspension was refluxed for 2 h. The solution was cooled overnight in a refrigerator, during which time the product precipitated. After filtering, the solid was suspended in 300 mL of saturated NaHCO₃ (aqueous) and heated to 70 °C until all of the solid had dissolved (~2 h). After cooling, the aqueous layer was washed with diethyl ether and then acidified to pH 2 with concentrated hydrochloric acid. The resulting solid was filtered and dried to give 21 g (92% yield) of pyrrole **10**. ¹H NMR (300 MHz, CDCl₃) δ 1.13 (3H, t, *J* = 8 Hz, 3-CH₂CH₃), 1.39 (3H, t, *J* = 7 Hz, -OCH₂CH₃), 2.30 (3H, s, 4-CH₃), 2.78 (2H, q, *J* = 8 Hz, 3-CH₂CH₃), 4.36 (2H, q, *J* = 7 Hz, -OCH₂CH₃), 9.42 (1H, br s, pyrrole-NH); MALDI-TOF-MS *m/z* 224.09 (C₁₁H₁₅NO₄⁺, calcd 224.09).

4.1.2. 2-Carbomethoxy-4-ethyl-5-iodo-3-methylpyrrole (11). Pyrrole **10** (20 g, 89 mmol) and 14.9 g (178 mmol) of solid NaHCO₃ were heated to 60 °C in 200 mL of water until the entire solid had dissolved. After the addition of 165 mL of dry 1,2 dichloroethane, 14.9 g (178 mmol) of I₂ was added to the cloudy solution in portions over 3–4 min during which carbon dioxide evolved. The red/purple solution was refluxed for 45 min. After cooling, excess sodium sulfite was added to remove any unreacted I₂. The two phases were separated; the aqueous layer was extracted with dichloromethane (2×). The organic layers were combined and backwashed with brine (3×), dried with Na₂SO₄ and concentrated to yield 25.64 g (94%) of **11**. ¹H NMR (300 MHz, CDCl₃) δ 1.05 (3H, t, *J* = 7 Hz, 4-CH₂CH₃), 1.35 (3H, t, *J* = 7 Hz, -OCH₂CH₃), 2.32 (3H, s, 3-CH₃), 2.38 (2H, q, *J* = 7 Hz, 4-CH₂CH₃), 4.31 (2H, q, *J* = 7 Hz, -OCH₂CH₃), 8.83 (1H, br s, pyrrole-NH); MALDI-TOF-MS *m/z* 307.87 (C₁₀H₁₄INO₂⁺, calcd 308.01).

4.1.3. 2-Carbomethoxy-4-ethyl-3-methylpyrrole (12). Pyrrole **11** (25.6 g, 83.5 mmol) was hydrogenated by evacuating and flushing a flask containing the pyrrole, 330 mL of methanol, and 66 mg (0.29 mmol) of PtO₂, with H₂, followed by vigorous stirring overnight under a balloon pressure of H₂. The solvent was removed and the solid residue partitioned between water and dichloromethane. The aqueous layer was extracted with dichloromethane (2×). The combined organic layers were washed with saturated NaHCO₃ (aqueous) and brine (2×), dried over Na₂SO₄ and concentrated to yield 14.8 g (98%) of **12**. ¹H NMR (300 MHz, CDCl₃) δ 1.17 (3H, t, *J* = 8 Hz, 4-CH₂CH₃), 1.35 (3H, t, *J* = 7 Hz, -OCH₂CH₃), 2.29 (3H, s, 3-CH₃), 2.43 (2H, q, *J* = 8 Hz, 4-CH₂CH₃), 4.31 (2H, q, *J* = 7 Hz, -OCH₂CH₃), 6.66 (1H, d, *J* = 3 Hz, 5-H), 8.75 (1H, br s, pyrrole-NH); MALDI-TOF-MS *m/z* 180.1 (C₁₀H₁₅NO₂⁺-H, calcd 180.1).

4.1.4. 2-Carbomethoxy-4-ethyl-3-methylpyrrole (13). The title compound was prepared by dissolving 14.7 g (81.1 mmol) of substituted pyrrole **12** in 200 mL of benzyl alcohol. In a separate flask 0.19 g of sodium metal was reacted with 100 mL of benzyl alcohol. Following complete reaction of the sodium metal, this solution was added to the pyrrole solution. Stirring was continued for 48 h at 85 °C under reduced pressure, ~15 Torr. Excess benzyl alcohol was removed by evaporation under reduced pressure. Column chromatography (silica gel, 1:9 ethyl acetate/hexanes) resulted in 17.2 g (87% yield) of pyrrole **13**. ¹H NMR (300 MHz, CDCl₃) δ 1.16 (3H, t, *J* = 8 Hz, 4-CH₂CH₃), 2.30 (3H, s, 3-CH₃), 2.43 (2H, q, *J* = 8 Hz, 4-CH₂CH₃), 5.30, (2H, s, -CH₂Ar), 6.67 (1H, d, *J* = 3 Hz, 5-H), 7.30–7.44 (5H, m, Ar-H), 8.70 (1H, br s, pyrrole-NH); MALDI-TOF-MS *m/z* 266.12 (C₁₅H₁₇NO₂Na⁺, sodium adduct, calcd 266.12).

4.1.5. 1,9-Dicarbomethoxy-5-(4-carbomethoxyphenyl)-3,7-diethyl-2,8-dimethyl-dipyrromethane (7). The title compound was prepared by stirring 4 g (16 mmol) of pyrrole **13**, 1.35 g (8.22 mmol) of methyl 4-formylbenzoate (**14**), 40 mL of dry 1,2-dichloroethane, 1.56 g (8.22 mmol) of *p*-toluenesulfonic acid and 2 g of 4 Å molecular sieves at room temperature for 19 h. Molecular sieves were removed by filtration through a pad of Celite, which was subsequently washed with dichloromethane. The organic layer was concentrated and purified by column chromatography (silica gel, 1:4 ethyl acetate/hexanes) to give 4.5 g (88% yield) of **7**. ¹H NMR (300 MHz, CDCl₃) δ 0.89 (6H, t, *J* = 8 Hz, 3,7-CH₂CH₃), 2.27 (6H, s, 2,8-CH₃), 2.31 (4H, q, *J* = 8 Hz, 3,7-CH₂CH₃), 3.91 (3H, s, -CO₂CH₃), 5.21 (4H, d, *J* = 2 Hz, 1,9-CH₂Ar), 5.60 (1H, s, 5-H), 7.14 (2H, d, *J* = 8 Hz, 5-Ar-H), 7.26–7.35 (10H, m, 1,9-Ar-H), 7.94 (2H, d, *J* = 8 Hz, 5-Ar-H), 8.58 (2H, br s, pyrrole-NH); MALDI-TOF-MS *m/z* 655.3 (C₃₉H₄₀N₂O₆Na⁺, sodium adduct, calcd 655.3).

4.1.6. 5-(4-Carbomethoxyphenyl)-3,7-diethyl-2,8-dimethyl-1,9-dicarboxydipyrromethane (15). Hydrogenation of **7** (4.5 g, 7.1 mmol) with 0.5 g of 5% Pd/C in 100 mL freshly distilled tetrahydrofuran occurred at balloon pressure by H₂ with vigorous stirring overnight. Pd/C was removed by filtration through a pad of Celite. The filtration pad was washed with methanol. The eluent was condensed to yield 3.2 g (99% yield) of compound **15**. ¹H NMR (300 MHz, CDCl₃) δ 0.95 (6H, t, *J* = 7 Hz, 3,7-CH₂CH₃), 2.27 (6H, s, 2,8-CH₃), 2.40 (4H, q, *J* = 7 Hz, 3,7-CH₂CH₃), 3.90 (3H, s, -CO₂CH₃), 5.61 (1H, s, 5-H), 7.06 (2H, d, *J* = 8 Hz, 5-Ar-H), 7.87 (2H, d, *J* = 8 Hz, 5-Ar-H), 9.47 (2H, br s, pyrrole-NH); MALDI-TOF-MS *m/z* 475.20 (C₂₅H₂₈N₂O₆Na⁺, sodium adduct, calcd 475.18).

4.1.7. 5-(4-Carbomethoxyphenyl)-3,7,13,17-tetraethyl-2,8,12,18-tetramethylporphyrin (6). The title compound was prepared by adding 21 g (110 mmol) of *p*-toluenesulfonic acid, previously azeotroped with toluene (3×), in 75 mL of dry methanol drop wise over 15 min to a solution of 3.2 g (7.0 mmol) of phenyl dipyrromethane, **15**, 2.0 g (7.0 mmol) of 3,7-diethyl-1,9-diformyl-2,8-dimethyldipyrromethane, **8**, and 600 mL of distilled dichloromethane. The solution was stirred in the dark for 24 h followed by the addition of 90 mL of freshly prepared saturated methanolic

zinc(II) acetate dihydrate solution. The reaction mixture was refluxed for 2 h. After cooling, 3 g (14 mmol) of 2,3-dichloro-5,6-dicyano-1,4-benzoquinone was added and the stirring continued at room temperature for 24 h. The organic layer was washed with saturated aqueous NaHCO_3 (3 \times), dried over Na_2SO_4 and concentrated. The product was purified by column chromatography (silica gel, dichloromethane) to give two products: the zinc metalated porphyrin and the free-base porphyrin, **6**. The metalated porphyrin and any mixed fractions were condensed and re-dissolved in 100 mL of trifluoroacetic acid. After stirring for 4 h, TLC indicated no zinc porphyrin remained. The solution was poured into 10% methanol/dichloromethane and neutralized with NaHCO_3 (aqueous). The organic layer was separated and washed with water (3 \times), dried over Na_2SO_4 , concentrated and combined with the free-base porphyrin from the separation above. The combined fractions of porphyrin, **6**, were re-crystallized with dichloromethane/methanol to give 2.19 g (51% yield). ^1H NMR (300 MHz, CDCl_3) δ -3.21 (1H, br s, pyrrole-NH), -3.08 (1H, br s, pyrrole-NH), 1.14 (6H, t, $J=8$ Hz, 3,7- CH_2CH_3), 1.88 (6H, t, $J=8$ Hz, 13,17- CH_2CH_3), 2.72 (4H, q, $J=8$ Hz, 3,7- CH_2CH_3), 3.55 (6H, s, 2,8- CH_3), 3.64 (6H, s, 12,18- CH_3), 4.06 (4H, q, $J=8$ Hz, 13,17- CH_2CH_3), 4.14 (3H, s, 5-Ar- CO_2CH_3), 8.31 (2H, d, $J=9$ Hz, 5-Ar-H), 8.37 (2H, d, $J=9$ Hz, 5-Ar-H), 9.93 (1H, s, 15-H), 10.18 (2H, s, 10,20-H); MALDI-TOF-MS m/z 612.4 ($\text{C}_{40}\text{H}_{44}\text{N}_4\text{O}_2^+$, calcd 612.4); UV-vis (CH_2Cl_2) 403, 503, 535, 575, 645 nm.

4.1.8. 3,7,13,17-Tetraethyl-5-(4-hydroxymethylphenyl)-2,8,12,18-tetramethylporphyrin (16). In a 2 L round-bottomed flask 1.0 g (1.6 mmol) of porphyrin **6** was dissolved in 800 mL of freshly distilled tetrahydrofuran and cooled to 0 °C. Lithium aluminum hydride (80 mg) was added slowly to the cloudy solution. Stirring was continued at 0 °C and the progress of the reaction was monitored by TLC. Upon complete reduction, approximately 6 h, the excess lithium aluminum hydride was deactivated with ice. The solution was filtered through a pad of Celite. The Celite was washed with dichloromethane, and the eluent concentrated. The residue was dissolved in 300 mL of dichloromethane and washed with water (3 \times), dried with Na_2SO_4 and concentrated to give 948 mg (99% yield) of **16**. ^1H NMR (300 MHz, CDCl_3) δ -3.20 (1H, br s, pyrrole-NH), -3.07 (1H, br s, pyrrole-NH), 1.14 (6H, t, $J=8$ Hz, 3,7- CH_2CH_3), 1.87 (6H, t, $J=8$ Hz, 13,17- CH_2CH_3), 2.75 (4H, q, $J=8$ Hz, 3,7- CH_2CH_3), 3.55 (6H, s, 2,8- CH_3), 3.63 (6H, s, 12,18- CH_3), 4.06 (4H, q, $J=8$ Hz, 13,17- CH_2CH_3), 5.10 (2H, s, 5- CH_2Ar), 7.67 (2H, d, $J=8$ Hz, 5-Ar-H), 8.19 (2H, d, $J=8$ Hz, 5-Ar-H), 9.92 (1H, s, 15-H), 10.17 (2H, s, 10,20-H); MALDI-TOF-MS m/z 584.3 ($\text{C}_{39}\text{H}_{44}\text{N}_4\text{O}^+$, calcd 584.4); UV-vis (CH_2Cl_2) 403, 502, 537, 571, 625 nm.

4.1.9. 3,7,13,17-Tetraethyl-2,8,12,18-tetramethyl-5-[4-(1',1',1'-trimethylacetylmethyl)phenyl]porphyrin (17). Porphyrin **16** (940 mg, 1.6 mmol) was esterified in 200 mL of dry pyridine; following cooling to 0 °C 0.6 mL (7 mmol) of pivaloyl chloride was added. After approximately 5 h the reaction was completed, as indicated by TLC. The mixture was poured into 400 mL of dichloromethane and washed with water (3 \times). The organic layer was dried

over Na_2SO_4 and concentrated. Porphyrin **17** was purified by column chromatography (silica gel, 1:20 methanol/dichloromethane) to give 940 mg (87% yield). ^1H NMR (300 MHz, CDCl_3) δ -3.21 (1H, br s, pyrrole-NH), -3.08 (1H, br s, pyrrole-NH), 1.13 (6H, t, $J=8$ Hz, 3,7- CH_2CH_3), 1.38 (9H, s, 5-Ar- $\text{C}(\text{CH}_3)_3$), 1.87 (6H, t, $J=8$ Hz, 13,17- CH_2CH_3), 2.73 (4H, q, $J=8$ Hz, 3,7- CH_2CH_3), 3.55 (6H, s, 2,8- CH_3), 3.63 (6H, s, 12,18- CH_3), 4.06 (4H, q, $J=8$ Hz, 13,17- CH_2CH_3), 5.49 (2H, s, 5- CH_2Ar), 7.66 (2H, d, $J=8$ Hz, 5-Ar-H), 8.19 (2H, d, $J=8$ Hz, 5-Ar-H), 9.92 (1H, s, 15-H), 10.17 (2H, s, 10,20-H); MALDI-TOF-MS m/z 668.4 ($\text{C}_{44}\text{H}_{52}\text{N}_4\text{O}_2^+$, calcd 668.4); UV-vis (CH_2Cl_2) 403, 502, 536, 572, 625 nm.

4.1.10. Nickel 3,7,13,17-tetraethyl-2,8,12,18-tetramethyl-5-[4-(1',1',1'-trimethylacetylmethyl)phenyl]porphyrin (18). The title compound was prepared by heating 940 mg (1.4 mmol) of porphyrin **17** and 2.4 g (9.3 mmol) of nickel(II) acetylacetonate in 400 mL dry toluene to 80 °C overnight. After cooling, the toluene was removed under reduced pressure and the residue re-dissolved in chloroform. The organic layer was washed consecutively with water, saturated NaHCO_3 (aqueous) and water, then dried over Na_2SO_4 and concentrated. Porphyrin **18** was re-crystallized with dichloromethane/methanol to give 968 mg (95% yield). ^1H NMR (300 MHz, CDCl_3) δ 0.90 (6H, t, $J=7$ Hz, 3,7- CH_2CH_3), 1.34 (9H, s, 5-Ar- $\text{C}(\text{CH}_3)_3$), 1.73 (6H, t, $J=8$ Hz, 13,17- CH_2CH_3), 2.57 (4H, q, $J=7$ Hz, 3,7- CH_2CH_3), 3.31 (6H, s, 2,8- CH_3), 3.40 (6H, s, 12,18- CH_3), 3.84 (4H, q, $J=8$ Hz, 13,17- CH_2CH_3), 5.42 (2H, s, 5- CH_2Ar), 7.56 (2H, d, $J=8$ Hz, 5-Ar-H), 7.97 (2H, d, $J=8$ Hz, 5-Ar-H), 9.50 (1H, s, 15-H), 9.58 (2H, s, 10,20-H); MALDI-TOF-MS m/z 724.4 ($\text{C}_{44}\text{H}_{50}\text{N}_4\text{O}_2\text{Ni}^+$, calcd 724.3); UV-vis (CH_2Cl_2) 399, 522, 558 nm.

4.1.11. Nickel 2,8,12,18-tetraethyl-5-formyl-3,8,13,18-tetramethyl-10-[4-(1',1',1'-trimethylacetylmethyl)phenyl]porphyrin (19) and nickel 3,7,13,17-tetraethyl-5-formyl-2,8,12,18-tetramethyl-15-[4-(1',1',1'-trimethylacetylmethyl)phenyl]porphyrin (20). Porphyrin **18** (1.02 g, 1.41 mmol) was cooled to 0 °C in 600 mL of distilled 1,2-dichloroethane. In a separate flask 10 mL of phosphorous oxychloride was added drop wise to 20 mL of cooled (0 °C) dimethylformamide. After the addition of the phosphorous oxychloride, the solution was stirred at room temperature for 20 min prior to being added drop wise to the porphyrin suspension. The porphyrin solution was stirred at room temperature for 4 h, during which time the solution turned green. Saturated aqueous NaHCO_3 (600 mL) was added and the pH was adjusted to 8 with additional solid NaHCO_3 . The two-phase solution was stirred at 60 °C overnight. After cooling, the two phases were separated; the aqueous phase was extracted with dichloromethane. The combined organic layers were washed with water (3 \times), dried over Na_2SO_4 and concentrated. Purification was obtained by column chromatography (silica gel, 1:99 ethyl acetate/toluene) to give both porphyrin **19** (970 mg, 88% yield) and porphyrin **20** (120 mg, 11% yield). Porphyrin **19**: ^1H NMR (500 MHz, CDCl_3) δ 0.72 (3H, t, $J=7$ Hz, 8- CH_2CH_3), 0.95 (3H, t, $J=7$ Hz, 12- CH_2CH_3), 1.33 (9H, s, 10-Ar- $\text{C}(\text{CH}_3)_3$), 1.61 (3H, t, $J=8$ Hz, 18- CH_2CH_3), 1.66 (3H, t, $J=8$ Hz, 2- CH_2CH_3), 2.30–2.37 (4H, m, 8,12- CH_2CH_3), 3.07 (3H, s, 13- CH_3),

3.12 (3H, s, 7-CH₃), 3.18 (3H, s, 17-CH₃), 3.34 (3H, s, 3-CH₃), 3.59–3.64 (4H, m, 2,18-CH₂CH₃), 5.38 (2H, s, 10-CH₂Ar), 7.55 (2H, d, *J* = 8 Hz, 10-Ar-H), 7.84 (2H, d, *J* = 8 Hz, 10-Ar-H), 8.97 (1H, s, 20-H), 9.14 (1H, s, 15-H), 11.54 (1H, s, 5-CHO); MALDI-TOF-MS *m/z* 752.3 (C₄₅H₅₀N₄O₃Ni⁺, calcd 752.3); UV-vis (CH₂Cl₂) 432, 659 (b) nm. Porphyrin **20**: ¹H NMR (500 MHz, CDCl₃) δ 0.88 (6H, t, *J* = 7 Hz, 13,17-CH₂CH₃), 1.32 (9H, s, 15-Ar-C(CH₃)₃), 1.71 (6H, t, *J* = 8 Hz, 3,7-CH₂CH₃), 2.44 (4H, q, *J* = 7 Hz, 13,17-CH₂CH₃), 3.11 (6H, s, 12,18-CH₃), 3.17 (6H, s, 2,8-CH₃), 3.72 (4H, q, *J* = 8 Hz, 3,7-CH₂CH₃), 5.38 (2H, s, 15-CH₂Ar), 7.54 (2H, d, *J* = 8 Hz, 15-Ar-H), 7.84 (2H, d, *J* = 8 Hz, 15-Ar-H), 9.10 (2H, s, 10,20-H), 11.58 (1H, s, 5-CHO); MALDI-TOF-MS *m/z* 752.3 (C₄₅H₅₀N₄O₃Ni⁺, calcd 752.3); UV-vis (CH₂Cl₂) 432, 649(b) nm.

4.1.12. Nickel 10-(3-carbethoxypropenyl)-3,7,13,17-tetraethyl-2,8,12,18-tetramethyl-5-[4-(1',1',1'-trimethylacetylmethyl)phenyl]porphyrin (21). Porphyrin **19** (950 mg, 1.26 mmol) and 3.5 g (10 mmol) of (carbethoxymethylene)triphenyl phosphorane in 400 mL of dry toluene were refluxed overnight in the dark. An additional 3.5 g (10 mmol) of phosphorane was added and the refluxing was continued over a second night. After cooling, the solution was reduced to 10% of the original volume and purified by column chromatography (silica gel, 1:24 ethyl acetate/toluene). Pure porphyrin **21** (987 mg, 95% yield) was obtained. ¹H NMR (300 MHz, CDCl₃) δ 0.68 (3H, t, *J* = 8 Hz, 7-CH₂CH₃), 1.01 (3H, t, *J* = 8 Hz, 3-CH₂CH₃), 1.33–1.38 (12H, m, 5-Ar-C(CH₃)₃, 10-CO₂CH₂CH₃), 1.61–1.73 (6H, m, 13,17-CH₂CH₃), 2.34–2.52 (4H, m, 3,7-CH₂CH₃), 3.02 (3H, s, 2-CH₃), 3.17 (3H, s, 8-CH₃), 3.28 (3H, s, 18-CH₃), 3.38 (3H, s, 12-CH₃), 3.67–3.75 (4H, m, 13,17-CH₂CH₃), 4.31 (2H, q, *J* = 7 Hz, 10-CO₂CH₂CH₃), 5.40 (1H, d, *J* = 16 Hz, 10-(2'-CH₂-)), 5.42 (2H, s, 5-CH₂Ar), 7.58 (2H, d, *J* = 8 Hz, 5-Ar-H), 7.93 (2H, d, *J* = 8 Hz, 5-Ar-H), 9.14 (1H, s, 15-H), 9.27 (1H, s, 20-H), 9.77 (1H, d, *J* = 16 Hz, 10-(1'-CH₂-)); MALDI-TOF-MS *m/z* 822.38 (C₄₉H₅₆N₄O₄Ni⁺, calcd 822.37); UV-vis (CH₂Cl₂) 422, 545, 578 nm.

4.1.13. 20-Carbethoxy-4,8,14,18-tetraethyl-3,9,13,19-tetramethyl-16-[4-(1',1',1'-trimethylacetylmethyl)phenyl]purpurin (3) and 20-carbethoxy-4,8,14,18-tetraethyl-3,9,13,19-tetramethyl-6-[4-(1',1',1'-trimethylacetylmethyl)phenyl]purpurin (4). A solution of porphyrin **21** (1.0 g, 1.2 mmol) and 150 mL of trifluoroacetic acid was stirred at room temperature for 3 days. The solution was poured into dichloromethane and neutralized with NaHCO₃ (aqueous). The organic layer was washed with water (3×), dried over Na₂SO₄ and concentrated. The crude product, porphyrin **22**, was dissolved in 200 mL of dry toluene and refluxed with 1 mL of 1,8-diazabicyclo[5.4.0]undec-7-ene (DBU) for 6 h. The solvent was removed and the product purified by column chromatography (silica gel, 1:24 ethyl acetate/toluene) to give purpurins **3** and **4**. Each was re-crystallized from dichloromethane and methanol, to give 438 mg (53% yield) of purpurin **3** and 274 mg (33% yield) of purpurin **4**. 1D (¹H) and 2D (COSY, ROESY, HMBC and HMQC) NMR techniques were used to characterize both purpurins. Purpurin **3**: ¹H NMR (500 MHz, CDCl₃) δ -0.64 (1H, s, pyrrole-NH), 0.14 (1H, s, pyrrole-NH), 0.56

(3H, t, *J* = 7 Hz, 18-CH₂CH₃), 1.04 (3H, t, *J* = 8 Hz, 14-CH₂CH₃), 1.24 (3H, s, 19-CH₃), 1.31 (9H, s, 16-Ar-C(CH₃)₃), 1.50 (3H, t, *J* = 7 Hz, 20-CO₂CH₂CH₃), 1.68 (3H, t, *J* = 8 Hz, 8-CH₂CH₃), 1.71 (3H, t, *J* = 8 Hz, 4-CH₂CH₃), 2.22–2.28 (1H, m, 14-CH₂CH₃), 2.36–2.41 (1H, m, 18-CH₂CH₃), 2.61–2.69 (1H, m, 14-CH₂CH₃), 2.69–2.75 (1H, m, 18-CH₂CH₃), 3.307 (3H, s, 9-CH₃), 3.309 (3H, s, 13-CH₃), 3.51 (3H, s, 3-CH₃), 3.73 (2H, q, *J* = 8 Hz, 8-CH₂CH₃), 3.87 (2H, q, *J* = 8 Hz, 4-CH₂CH₃), 3.98 (1H, t, *J* = 4 Hz, 18-H), 4.43–4.50 (2H, m, 20-CO₂CH₂CH₃), 5.35 (2H, s, 16-CH₂Ar), 7.12 (1H, d, *J* = 8 Hz, 16-Ar-H), 7.40 (1H, d, *J* = 8 Hz, 16-Ar-H), 7.72 (1H, d, *J* = 8 Hz, 16-Ar-H), 8.51 (1H, s, *J* = 8 Hz, 16-Ar-H), 9.33 (1H, s, 6-H), 9.49 (1H, s, 21-H), 9.56 (1H, s, 11-H); MALDI-TOF-MS *m/z* 766.4 (C₄₉H₅₈N₄O₄⁺, calcd 766.5); UV-vis (CH₂Cl₂) 428, 498, 529, 569, 636, 696 nm. Purpurin **4**: ¹H NMR (500 MHz, CDCl₃) δ -0.39 (1H, s, pyrrole-NH), 0.36 (1H, s, pyrrole-NH), 0.90 (3H, t, *J* = 8 Hz, 8-CH₂CH₃), 0.96 (3H, t, *J* = 8 Hz, 4-CH₂CH₃), 1.16 (3H, s, 19-CH₃), 1.35 (9H, s, 6-Ar-C(CH₃)₃), 1.57 (3H, t, *J* = 7 Hz, 20-CO₂CH₂CH₃), 1.69 (3H, t, *J* = 8 Hz, 14-CH₂CH₃), 1.78 (3H, t, *J* = 8 Hz, 18-CH₂CH₃), 2.02–2.07 (1H, m, 8-CH₂CH₃), 2.37–2.42 (1H, m, 4-CH₂CH₃), 2.57–2.67 (2H, m, 4,8-CH₂CH₃), 2.96–3.03 (1H, m, 18-CH₂CH₃), 3.16 (3H, s, 9-CH₃), 3.23–3.26 (1H, m, 18-CH₂CH₃), 3.36 (3H, s, 3-CH₃), 3.39 (3H, s, 13-CH₃), 3.66–3.76 (2H, m, 14-CH₂CH₃), 4.02–4.04 (1H, dd, *J* = 9 Hz, 3 Hz, 18-H), 4.51–4.56 (2H, m, 20-CO₂CH₂CH₃), 5.44 (2H, s, 6-CH₂Ar), 7.56 (1H, d, *J* = 8 Hz, 6-Ar-H), 7.65 (1H, d, *J* = 8 Hz, 6-Ar-H), 7.84 (1H, d, *J* = 8 Hz, 6-Ar-H), 8.21 (1H, d, *J* = 8 Hz, 6-Ar-H), 8.62 (1H, s, 16-H), 9.48 (1H, s, 11-H), 9.50 (1H, s, 21-H); MALDI-TOF-MS *m/z* 766.4 (C₄₉H₅₈N₄O₄⁺, calcd 766.5); UV-vis (CH₂Cl₂) 433, 499, 536, 574, 634, 693 nm.

4.1.14. 20-Carbethoxy-4,8,14,18-tetraethyl-16-(4-hydroxymethylphenyl)-3,9,13,19-tetramethylpurpurin (23). Purpurin **3** (100 mg, 0.130 mmol) was dissolved in 80 mL of freshly distilled tetrahydrofuran and 20 mL of methanol. To this solution, 4 mL of 10% aqueous potassium hydroxide was added and the stirring continued for 17 h. The reaction mixture was poured into dichloromethane and washed with dilute citric acid and water (4×). The organic layer was dried over Na₂SO₄ and concentrated to give 88 mg of product (99% yield). ¹H NMR (300 MHz, CDCl₃) δ -0.64 (1H, s, pyrrole-NH), 0.17 (1H, s, pyrrole-NH), 0.63 (3H, t, *J* = 7 Hz, 18-CH₂CH₃), 1.04 (3H, t, *J* = 7 Hz, 14-CH₂CH₃), 1.25 (3H, s, 19-CH₃), 1.50 (3H, t, *J* = 7 Hz, 20-CO₂CH₂CH₃), 1.67 (3H, t, *J* = 8 Hz, 8-CH₂CH₃), 1.72 (3H, t, *J* = 8 Hz, 4-CH₂CH₃), 2.28–2.38 (2H, m, 14,18-CH₂CH₃), 2.61–2.71 (2H, m, 14,18-CH₂CH₃), 3.30 (3H, s, 9-CH₃), 3.31 (3H, s, 13-CH₃), 3.51 (3H, s, 3-CH₃), 3.69–3.77 (2H, m, 8-CH₂CH₃), 3.86 (2H, q, *J* = 8 Hz, 4-CH₂CH₃), 3.99–4.09 (1H, m, 18-H), 4.44–4.50 (2H, m, 20-CO₂CH₂CH₃), 4.96 (2H, s, 16-Ar-CH₂OH), 7.15–7.18 (1H, m, 16-Ar-H), 7.38–7.42 (1H, m, 16-Ar-H), 7.64–7.72 (1H, m, 16-Ar-H), 8.44–8.52 (1H, m, 16-Ar-H), 9.34 (1H, s, 6-H), 9.47 (1H, s, 21-H), 9.56 (1H, s, 11-H); MALDI-TOF-MS *m/z* 668.4 (C₄₃H₄₈N₄O₃⁺, calcd 668.4); UV-vis (CH₂Cl₂) 428, 530, 569, 600, 641, 696 nm.

4.1.15. 20-Carbethoxy-4,8,14,18-tetraethyl-16-(4-formylphenyl)-3,9,13,19-tetramethylpurpurin (24). Purpurin **23** (88 mg, 0.13 mmol) was dissolved in 20 mL of

dichloromethane. To this solution, portions of manganese (IV) dioxide (10 mg each) was added every 10 min until TLC indicated complete oxidation. The suspension was filtered through a pad of Celite and the residue was washed with 800 mL of a 10% methanol/dichloromethane solution. The solvent was removed under reduced pressure and the resulting residue was purified by column chromatography (silica gel, 1:99 methanol/dichloromethane) to give 70 mg (81% yield) of purpurin **24**. $^1\text{H NMR}$ (300 MHz, CDCl_3) δ -0.54 (1H, s, pyrrole-NH), 0.24 (1H, s, pyrrole-NH), 0.60 (3H, t, $J=7$ Hz, $18\text{-CH}_2\text{CH}_3$), 1.02 (3H, t, $J=7$ Hz, $14\text{-CH}_2\text{CH}_3$), 1.26 (3H, s, 19-CH_3), 1.49 (3H, t, $J=7$ Hz, $20\text{-CO}_2\text{CH}_2\text{CH}_3$), 1.69 (3H, t, $J=8$ Hz, $8\text{-CH}_2\text{CH}_3$), 1.72 (3H, t, $J=8$ Hz, $4\text{-CH}_2\text{CH}_3$), $2.21\text{--}2.32$ (2H, m, $14,18\text{-CH}_2\text{CH}_3$), $2.59\text{--}2.72$ (2H, m, $14,18\text{-CH}_2\text{CH}_3$), 3.30 (3H, s, 9-CH_3), 3.31 (3H, s, 13-CH_3), 3.50 (3H, s, 3-CH_3), 3.72 (2H, q, $J=8$ Hz, $8\text{-CH}_2\text{CH}_3$), 3.36 (2H, q, $J=8$ Hz, $4\text{-CH}_2\text{CH}_3$), $4.01\text{--}4.04$ (1H, m, 18-H), $4.43\text{--}4.49$ (2H, m, $20\text{-CO}_2\text{CH}_2\text{CH}_3$), $7.45\text{--}7.53$ (1H, m, 16-Ar-H), $7.90\text{--}8.30$ (2H, m, 16-Ar-H), $8.60\text{--}8.80$ (1H, m, 16-Ar-H), 9.33 (1H, s, 6-H), 9.46 (1H, s, 21-H), 9.57 (1H, s, 11-H), 10.27 (1H, s, 16-Ar-CHO); MALDI-TOF-MS m/z 680.4 ($\text{C}_{44}\text{H}_{48}\text{N}_4\text{O}_3^+$, calcd 680.4); UV-vis (CH_2Cl_2) 428 , 502 , 530 , 569 , 637 , 696 nm.

4.1.16. 20-Carboxy-4,8,14,18-tetraethyl-16-(4-formylphenyl)-3,9,13,19-tetramethylpurpurin (25). The title compound was prepared by stirring 70 mg (0.10 mmol) of purpurin **24** in 80 mL of freshly distilled tetrahydrofuran and 40 mL of methanol with 4 mL of 10% aqueous potassium hydroxide at 40°C for 7 days. The reaction mixture was poured into 100 mL of dichloromethane and immediately washed with dilute aqueous citric acid ($1\times$) and then water ($4\times$). The organic layer was dried over Na_2SO_4 and concentrated to yield 60 mg (90% yield) of purpurin **25**. $^1\text{H NMR}$ (300 MHz, CDCl_3) δ -0.50 (1H, s, pyrrole-NH), 0.37 (1H, s, pyrrole-NH), 0.65 (3H, t, $J=7$ Hz, $18\text{-CH}_2\text{CH}_3$), 1.03 (3H, t, $J=8$ Hz, $14\text{-CH}_2\text{CH}_3$), 1.26 (3H, s, 19-CH_3), $1.61\text{--}1.76$ (6H, m, $4,8\text{-CH}_2\text{CH}_3$), $2.24\text{--}2.33$ (2H, m, $14,18\text{-CH}_2\text{CH}_3$), $2.62\text{--}2.72$ (2H, m, $14,18\text{-CH}_2\text{CH}_3$), 3.30 (3H, s, 9-CH_3), 3.31 (3H, s, 13-CH_3), 3.51 (3H, s, 3-CH_3), $3.70\text{--}3.78$ (2H, m, $8\text{-CH}_2\text{CH}_3$), $3.78\text{--}3.88$ (2H, m, $4\text{-CH}_2\text{CH}_3$), $4.01\text{--}4.03$ (1H, m, 18-H), $7.30\text{--}7.36$ (1H, m, 16-Ar-H), $7.90\text{--}8.00$ (1H, m, 16-Ar-H), $8.05\text{--}8.30$ (1H, m, 16-Ar-H), $8.61\text{--}8.75$ (1H, m, 16-Ar-H), 9.34 (1H, s, 6-H), 9.57 (1H, s, 21-H), 9.64 (1H, s, 11-H), 10.27 (1H, s, 16-Ar-CHO); MALDI-TOF-MS m/z 652.4 ($\text{C}_{42}\text{H}_{44}\text{N}_4\text{O}_3^+$, calcd 652.3); UV-vis (CH_2Cl_2) 429 , 498 , 569 , 596 , 637 , 697 nm.

4.1.17. 20-Carbo(tert-butyl)diphenylsiloxy)-16-(4-formylphenyl)-4,8,14,18-tetraethyl-3,9,13,19-tetramethylpurpurin (26). Purpurin **25** (30 mg, 0.046 mmol) was dissolved in 20 mL of dichloromethane. To this solution $10\ \mu\text{L}$ (0.069 mmol) of triethylamine and $14\ \mu\text{L}$ (0.055 mmol) of *tert*-butyldiphenylsilylchloride was added. After 1.5 h, the solvent was removed under reduced pressure and the mixture was separated by column chromatography (silica gel, 1:19 ethyl acetate/toluene) to give purpurin **26** (35 mg, 88% yield). $^1\text{H NMR}$ (300 MHz, CDCl_3) δ -0.50 (1H, s, pyrrole-NH), 0.31 (1H, s, pyrrole-NH), 0.50 (3H, t, $J=7$ Hz, $18\text{-CH}_2\text{CH}_3$), $1.01\text{--}1.33$ (15H, m, $14\text{-CH}_2\text{CH}_3$, 19-CH_3 , $20\text{-SiC}(\text{CH}_3)_3$), 1.71 (3H, t, $J=8$ Hz, $8\text{-CH}_2\text{CH}_3$), 1.74 (3H, t, $J=8$ Hz, $4\text{-CH}_2\text{CH}_3$),

$2.07\text{--}2.17$ (1H, m, $14\text{-CH}_2\text{CH}_3$), $2.22\text{--}2.33$ (1H, m, $18\text{-CH}_2\text{CH}_3$), $2.59\text{--}2.70$ (2H, m, $14,18\text{-CH}_2\text{CH}_3$), 3.32 (6H, s, $9,13\text{-CH}_3$), 3.53 (3H, s, 3-CH_3), 3.74 (2H, t, $J=8$ Hz, $8\text{-CH}_2\text{CH}_3$), $3.85\text{--}3.95$ (3H, m, $4\text{-CH}_2\text{CH}_3$, 18-H), $7.41\text{--}7.47$ (5H, m, 16-Ar-H , $20\text{-Si}(\text{Ph})_2$), $7.75\text{--}7.78$ (3H, m, 16-Ar-H , $20\text{-Si}(\text{Ph})_2$), $7.89\text{--}7.92$ (4H, m, $20\text{-Si}(\text{Ph})_2$), $8.01\text{--}8.20$ (1H, m, 16-Ar-H), $8.50\text{--}8.62$ (1H, m, 16-Ar-H), 9.36 (1H, s, 6-H), 9.59 (1H, s, 21-H), 9.71 (1H, s, 11-H), 10.26 (1H, s, 16-Ar-CHO); MALDI-TOF-MS m/z 890.5 ($\text{C}_{58}\text{H}_{62}\text{N}_4\text{O}_3\text{Si}^+$, calcd 890.4); UV-vis (CH_2Cl_2) 430 , 501 , 534 , 571 , 639 , 699 nm.

4.1.18. Dyad 27. Purpurin **26** (30 mg, 0.034 mmol) was refluxed in 20 mL of toluene with 57 mg (0.079 mmol) of fullerene (C_{60}) and 38 mg (0.42 mmol) of sarcosine overnight. The solvent was removed under reduced pressure and the products isolated by column chromatography (silica gel, 0.5:0.5:99 ethyl acetate/carbon disulfide/toluene). Two products **27-F1** and **27-F2**, were isolated and determined to be the isomers. Dyad **27-F1** (10 mg, 18% yield): $^1\text{H NMR}$ (500 MHz, 50:50 $\text{CDCl}_3/\text{CS}_2$) δ -0.57 (1H, s, pyrrole-NH), 0.07 (9H, s, $20\text{-SiC}(\text{CH}_3)_3$), 0.14 (1H, s, pyrrole-NH), $0.80\text{--}0.95$ (6H, m, $14,18\text{-CH}_2\text{CH}_3$), 1.24 (3H, s, 19-CH_3), 1.70 (3H, t, $J=8$ Hz, $8\text{-CH}_2\text{CH}_3$), 1.75 (3H, t, $J=8$ Hz, $4\text{-CH}_2\text{CH}_3$), $2.18\text{--}2.26$ (2H, m, $14,18\text{-CH}_2\text{CH}_3$), $2.30\text{--}2.38$ (2H, m, $14,18\text{-CH}_2\text{CH}_3$), 2.85 (3H, s, pyrrolidine- CH_3), 3.22 (3H, s, 9-CH_3), 3.30 (3H, s, 13-CH_3), 3.54 (3H, s, 3-CH_3), 3.73 (2H, q, $J=8$ Hz, $8\text{-CH}_2\text{CH}_3$), $3.88\text{--}3.91$ (2H, m, $4\text{-CH}_2\text{CH}_3$), $4.16\text{--}4.20$ (1H, m, pyrrolidine-H), $4.27\text{--}4.34$ (1H, m, 18-H), $4.93\text{--}4.95$ (2H, m, pyrrolidine-H), $7.30\text{--}7.32$ (1H, m, 16-Ar-H), $7.40\text{--}7.50$ (3H, m, $20\text{-Si}(\text{Ph})_2$), $7.54\text{--}7.55$ (2H, m, $20\text{-Si}(\text{Ph})_2$), $7.66\text{--}7.72$ (3H, m, $20\text{-Si}(\text{Ph})_2$), $7.90\text{--}7.95$ (3H, m, 16-Ar-H , $20\text{-Si}(\text{Ph})_2$), $7.98\text{--}7.99$ (1H, m, 16-Ar-H), $8.42\text{--}8.44$ (1H, m, 16-Ar-H), 9.31 (1H, s, 6-H), 9.49 (1H, s, 21-H), 9.73 (1H, s, 11-H); MALDI-TOF-MS m/z 1638.5 ($\text{C}_{120}\text{H}_{67}\text{N}_5\text{O}_2\text{Si}^+$, calcd 1638.5); UV-vis (toluene) 329 , 431 , 501 , 534 , 571 , 646 , 699 , 750 nm. **27-F2** (12 mg, 22% yield): $^1\text{H NMR}$ (500 MHz, 50:50 $\text{CDCl}_3/\text{CS}_2$) δ -0.56 (1H, s, pyrrole-NH), 0.07 (9H, s, $20\text{-SiC}(\text{CH}_3)_3$), 0.23 (1H, s, pyrrole-NH), $0.74\text{--}0.92$ (6H, m, $14,18\text{-CH}_2\text{CH}_3$), 1.24 (3H, s, 19-CH_3), 1.71 (3H, t, $J=8$ Hz, $8\text{-CH}_2\text{CH}_3$), 1.79 (3H, t, $J=8$ Hz, $4\text{-CH}_2\text{CH}_3$), $2.20\text{--}2.30$ (4H, m, $14,18\text{-CH}_2\text{CH}_3$), 2.74 (3H, s, pyrrolidine- CH_3), 3.20 (3H, s, 9-CH_3), 3.32 (3H, s, 13-CH_3), 3.58 (3H, s, 3-CH_3), $3.71\text{--}3.78$ (2H, m, $8\text{-CH}_2\text{CH}_3$), $3.86\text{--}3.92$ (2H, m, $4\text{-CH}_2\text{CH}_3$), $4.18\text{--}4.22$ (1H, m, pyrrolidine-H), $4.56\text{--}4.60$ (2H, m, pyrrolidine-H), $7.19\text{--}7.21$ (1H, m, 16-Ar-H), $7.47\text{--}7.50$ (7H, m, 16-Ar-H , $20\text{-Si}(\text{Ph})_2$), $7.87\text{--}7.94$ (4H, m, $20\text{-Si}(\text{Ph})_2$), $8.11\text{--}8.13$ (1H, m, 16-Ar-H), $8.49\text{--}8.50$ (1H, m, 16-Ar-H), 9.31 (1H, s, 6-H), 9.50 (1H, s, 21-H), 9.72 (1H, m, 11-H); MALDI-TOF-MS m/z 1638.5 ($\text{C}_{120}\text{H}_{67}\text{N}_5\text{O}_2\text{Si}^+$, calcd 1638.5); UV-vis (toluene) 320 , 431 , 502 , 530 , 572 , 638 , 699 , 750 nm.

Dyad **28** was prepared by dissolving 10 mg (0.006 mmol) of dyad **27-F2** in 5 mL of tetrahydrofuran. To this solution, 0.75 mL of trifluoroacetic acid and 0.5 mL of water were added. The green solution was stirred at room temperature for 3 h, at which time an additional 0.75 mL of trifluoroacetic acid and 0.5 mL of water were added. After a total of 7 h of stirring, the solution was poured into toluene and washed consecutively with water ($1\times$), saturated aqueous NaHCO_3 ($2\times$) and water ($2\times$). The organic layer was dried

and concentrated. The residue was washed (3×) with methanol. After each washing the solution was centrifuged, the solvent was decanted and the solid retained. The final residue (7 mg, 82% yield) was placed under high vacuum for 8 h prior to use in the following reaction. NMR was not obtained due to the limited solubility of the final product. MALDI-TOF-MS m/z 1400.4 ($C_{104}H_{49}N_5O_2^+$, calcd 1400.4); UV-vis (toluene) 314, 431, 530, 572, 640, 699 nm.

4.1.19. Triad 1. Dyad **28** (7 mg, 0.005 mmol) and 0.1 mg (0.001 mmol) of 4-(dimethylamino)pyridine were stirred in 5 mL of pyridine until all of the solutes had dissolved. To this solution, 7 mg (0.01 mmol) of carotenoid **29** and 2 mg (0.01 mmol) *N*-ethyl-*N'*-(3-dimethylaminopropyl)carbodiimide was added and the stirring continued for 36 h. The solution was poured into dichloromethane and washed with water (3×). The organic layer was dried over Na_2SO_4 and concentrated. Purification was done by column chromatography (silica gel, 1:0.1:99 ethyl acetate/triethylamine/toluene). Triad **1** (4 mg) was obtained in 31% yield. 1H NMR (500 MHz, 50:50 $CDCl_3/CS_2$) δ -0.78 (1H, br s, pur pyrrole-NH), -0.12 (1H, br s, pur pyrrole-NH), 0.80–0.95 (6H, m, pur 14,18- CH_2CH_3), 1.04 (6H, s, car 16,17- CH_3), 1.26 (3H, s, pur 19- CH_3), 1.42–1.44 (2H, m, pur 14- CH_2CH_3), 1.48–1.50 (2H, m, car 2- CH_2 -), 1.62–1.74 (13H, m, pur 4,8- CH_2CH_3 , pur 18- CH_2CH_3 , car 3- CH_2 -, car 18- CH_3), 1.98–2.05 (14H, m, car 4- CH_2 -, car 19,20,19',20'- CH_3), 2.37 (3H, s, pyrrolidine- CH_3), 3.30 (3H, s, pur 9- CH_3), 3.39 (3H, s, pur 13- CH_3), 3.50 (3H, s, pur 3- CH_3), 3.72–3.89 (4H, m, pur 4,8- CH_2CH_3), 4.11–4.14 (1H, m, pyrrolidine-H), 4.27–4.32 (1H, m, pur 18-H), 4.88–4.92 (1H, m, pyrrolidine-H), 5.05–5.09 (1H, m, pyrrolidine-H), 6.08–6.90 (14H, m, car =CH-), 7.43–7.48 (1H, m, pur 16-Ar-H), 7.53–7.55 (2H, m, car H-1', H-5'), 7.60–7.65 (1H, m, pur 16-Ar-H), 7.68–7.71 (2H, m, car H-2', H-4'), 7.90–7.96 (1H, m, pur 16-Ar-H), 8.48–8.50 (1H, m, pur 16-Ar-H), 9.27–9.42 (3H, m, pur 6,11,21-H); MALDI-TOF-MS m/z 1887.8 ($C_{141}H_{94}N_6O^+$, calcd 1887.8); UV-vis (toluene) 320, 433, 483, 512, 574, 643, 689 nm.

4.1.20. Dyad 30. Dyad **30** was prepared by stirring 7 mg (0.005 mmol) of dyad **28**, 2 μ L (0.007 mmol) of *trans,trans*-farnesol and 0.1 mg (0.001 mmol) of 4-(dimethylamino)pyridine in 1.5 mL pyridine and 1.5 mL toluene until all of the solid had dissolved. To this solution, 1.3 mg (0.007 mmol) of *N*-ethyl-*N'*-(3-dimethylaminopropyl)carbodiimide was added and the stirring continued at room temperature for 48 h. At this time TLC indicated that dyad **28** was still present, therefore, an additional 1.3 mg (0.007 mmol) of *N*-ethyl-*N'*-(3-dimethylaminopropyl)carbodiimide was added and the stirring was continued for 24 h. The reaction was quenched with water, diluted with toluene and washed with water (3×). The organic layer was dried over Na_2SO_4 and concentrated. The product was purified by column chromatography (silica gel, 1:1:98–5:1:94 ethyl acetate/carbon disulfide/toluene) to give 5 mg (38% yield) of dyad **30**. 1H NMR (500 MHz, 50:50 $CDCl_3/CS_2$) δ -0.62 (1H, br s, pur pyrrole-NH), 0.15 (1H, br s, pur pyrrole-NH), 0.78–0.96 (14H, m, pur 14,18- CH_2CH_3 , far 4,5,8,9- CH_2 -), 1.30–1.38 (15H, m, pur 19- CH_3 , far 3,7,11,12- CH_3), 1.66–1.76 (6H, m, pur 4,8- CH_2CH_3), 2.05–2.30 (4H, m, pur 14,18- CH_2CH_3), 2.62 (3H, s, pyrrolidine- CH_3), 2.98 (2H, s, far 1- CH_2 -),

3.25 (3H, s, pur 9- CH_3), 3.29 (3H, s, pur 13- CH_3), 3.52 (3H, s, pur 3- CH_3), 3.71 (2H, q, $J=7$ Hz, pur 8- CH_2CH_3), 3.88 (2H, q, $J=8$ Hz, pur 4- CH_2CH_3), 3.95–3.99 (1H, m, pyrrolidine-H), 4.27–4.32 (1H, m, pur 18-H), 4.85–4.99 (2H, m, pyrrolidine-H), 5.00–5.10 (2H, m, far 6,10-CH=), 5.60–5.62 (1H, m, far 2-CH=), 7.29–7.37 (1H, m, pur 16-Ar-H), 7.82–7.85 (1H, m, pur 16-Ar-H), 8.23–8.39 (1H, m, pur 16-Ar-H), 8.60–8.64 (1H, m, pur 16-Ar-H), 9.27 (1H, s, pur 6-H), 9.45 (1H, s, pur 21-H), 9.48 (1H, s, pur 11-H); MALDI-TOF-MS m/z 1604.5 ($C_{119}H_{73}N_5O_2^+$, calcd 1604.6); UV-vis (toluene) 314, 431, 533, 571, 641, 700 nm.

4.1.21. 20-Carboethoxy-4,8,14,18-tetraethyl-16-[4-(methoxymethoxy)methylphenyl]-3,9,13,19-tetramethylpurpurin (31). A portion of phosphorous pentoxide (13 mg, 0.089 mmol) was added to a solution of purpurin **23** (40 mg, 0.059 mmol) in 2 mL of dichloromethane and 1 mL of dimethoxymethane. After 1 h, an additional 13 mg (0.089 mmol) of phosphorous pentoxide was added and the stirring was continued for 3 h. The reaction was quenched by pouring the solution into cold saturated $NaHCO_3$ (aqueous). The product was extracted with dichloromethane (3×). The combined organic layers were backwashed with saturated aqueous NaCl (2×), dried over Na_2SO_4 and concentrated. Purpurin **31** (24 mg, 56% yield) was isolated by column chromatography (silica gel, 1:99 methanol/dichloromethane). 1H NMR (300 MHz, $CDCl_3$) δ -0.57 (1H, s, pyrrole-NH), 0.19 (1H, s, pyrrole-NH), 0.64 (3H, t, $J=7$ Hz, 18- CH_2CH_3), 1.04 (3H, t, $J=8$ Hz, 14- CH_2CH_3), 1.27 (3H, s, 19- CH_3), 1.50 (3H, t, $J=7$ Hz, 20-CO $_2CH_2CH_3$), 1.69 (3H, t, $J=8$ Hz, 8- CH_2CH_3), 1.73 (3H, t, $J=8$ Hz, 4- CH_2CH_3), 2.29–2.41 (2H, m, 14,18- CH_2CH_3), 2.62–2.72 (2H, m, 14,18- CH_2CH_3), 3.30 (3H, s, 9- CH_3), 3.31 (3H, s, 13- CH_3), 3.51 (3H, s, 3- CH_3), 3.54 (3H, s, 16-Ar-OCH $_3$), 3.73 (2H, q, $J=8$ Hz, 8- CH_2CH_3), 3.86 (2H, q, $J=8$ Hz, 4- CH_2CH_3), 3.97–3.99 (1H, m, 18-H), 4.43–4.52 (2H, m, 20-CO $_2CH_2CH_3$), 4.85 (2H, s, 16-Ar-OCH $_2O$ -), 4.87 (2H, s, 16-Ar-CH $_2O$ -), 7.12–7.19 (1H, m, 16-Ar-H), 7.39–7.42 (1H, m, 16-Ar-H), 7.69–7.72 (1H, m, 16-Ar-H), 8.44–8.50 (1H, m, 16-Ar-H), 9.33 (1H, s, 6-H), 9.50 (1H, s, 21-H), 9.56 (1H, s, 11-H); MALDI-TOF-MS m/z 726.4 ($C_{46}H_{54}N_4O_4^+$, calcd 726.4); UV-vis (CH_2Cl_2) 429, 499, 530, 569, 639, 696 nm.

4.1.22. 20-Carboxy-4,8,14,18-tetraethyl-16-[4-(methoxymethoxy)methylphenyl]-3,9,13,19-tetramethylpurpurin (32). The title compound was prepared by stirring 24 mg (0.033 mmol) of purpurin **31** in 20 mL of tetrahydrofuran, 5 mL of methanol and 1 mL of 10% aqueous potassium hydroxide at 40 °C for 7 days. After cooling, the reaction mixture was poured into dichloromethane and washed with dilute citric acid (1×) and water (4×). The organic layer was dried with Na_2SO_4 and concentrated to give 20 mg (87% yield) of purpurin **32**. 1H NMR (300 MHz, $CDCl_3$) δ -0.57 (1H, s, pyrrole-NH), 0.10 (1H, s, pyrrole-NH), 0.60 (3H, t, $J=7$ Hz, 18- CH_2CH_3), 0.96 (3H, t, $J=8$ Hz, 14- CH_2CH_3), 1.22 (3H, s, 19- CH_3), 1.52–1.61 (3H, m, 8- CH_2CH_3), 1.80–1.83 (3H, m, 4- CH_2CH_3), 2.23–2.32 (2H, m, 14,18- CH_2CH_3), 2.62–2.72 (2H, m, 14,18- CH_2CH_3), 3.21 (6H, s, 9,13- CH_3), 3.42 (3H, s, 3- CH_3), 3.45 (3H, s, 16-Ar-OCH $_3$), 3.74–3.82 (2H, m, 8- CH_2CH_3), 3.88–3.93 (2H, m, 4- CH_2CH_3), 3.97–3.99 (1H, m, 18-H), 4.76 (2H, s, 16-Ar-OCH $_2O$ -), 4.79 (2H, s, 16-Ar-CH $_2O$ -), 7.07–7.12

(1H, m, 16-Ar-H), 7.32–7.39 (1H, m, 16-Ar-H), 7.62–7.70 (1H, m, 16-Ar-H), 8.38–8.44 (1H, m, 16-Ar-H), 9.29 (1H, s, 6-H), 9.42 (1H, s, 21-H), 9.51 (1H, s, 11-H); MALDI-TOF-MS m/z 698.4 ($C_{44}H_{50}N_4O_4^+$, calcd 698.4); UV-vis (CH_2Cl_2) 429, 499, 530, 569, 643, 698 nm.

4.1.23. Dyad 33. Purpurin **32** (20 mg, 0.029 mmol) was dissolved in 5 mL of dry pyridine. To this solution, 22 mg (0.044 mmol) of carotenoid **29**, 7 mg (0.035 mmol) of *N*-ethyl-*N'*-(3-dimethylaminopropyl)carbodiimide, and 2 mg (0.003 mmol) of 4-(dimethylamino)pyridine were added and the stirring continued for 2 days. The solution was poured into dichloromethane and washed with water (3×). The organic layer was dried over Na_2SO_4 and concentrated. Pure dyad **33** (30 mg, 88% yield) was obtained by column chromatography (silica gel, 1:19 ethyl acetate/toluene). 1H NMR (300 MHz, $CDCl_3$) δ -0.72 (1H, s, pur pyrrole-NH), 0.07 (1H, s, pur pyrrole-NH), 0.78 (3H, t, $J=7$ Hz, pur 18- CH_2CH_3), 0.83–0.88 (3H, m, pur 14- CH_2CH_3), 1.03 (6H, s, car 16,17- CH_3), 1.26 (3H, s, pur 19- CH_3), 1.44–1.49 (2H, m, car 2- CH_2 -), 1.59–1.66 (2H, m, car 3- CH_2 -), 1.67–1.76 (9H, m, pur 4,8- CH_2CH_3 , car 18- CH_3), 1.98–2.01 (14H, car 4,- CH_2 -), car 19,20,19',20'- CH_3), 2.29–2.45 (2H, m, pur 14,18- CH_2CH_3), 2.64–2.69 (2H, m, pur 14,18- CH_2CH_3), 3.32 (6H, s, pur 9,13- CH_3), 3.52 (6H, s, pur 3- CH_3 , 16-Ar-O CH_3), 3.69–3.75 (2H, m, pur 8- CH_2CH_3), 3.86–3.89 (2H, m, 4- CH_2CH_3), 4.10–4.13 (1H, m, pur 18-H), 4.83 (3H, s, pur 16-Ar-O CH_2O -), 4.84 (3H, s, pur 16-Ar- CH_2O -), 6.15–6.92 (14H, m, car = CH -), 7.12–7.19 (1H, m, pur 16-Ar-H), 7.39–7.42 (1H, m, pur 16-Ar-H), 7.49 (2H, d, $J=8$ Hz, car H-1', H-5'), 7.73 (2H, d, $J=8$ Hz, car H-2', H-4'), 7.73–7.79 (1H, m, pur 16-Ar-H), 8.44–8.50 (1H, m, pur 16-Ar-H), 9.19 (1H, s, pur 6-H), 9.35 (1H, s, pur 21-H), 9.56 (1H, s, pur 11-H); MALDI-TOF-MS m/z 1186.7 ($C_{81}H_{95}N_5O_3^+$, calcd 1185.7); UV-vis (CH_2Cl_2) 429, 480, 495, 572, 637, 694 nm.

4.1.24. 20-Carbethoxy-4,8,14,18-tetraethyl-6-(4-hydroxymethylphenyl)-3,9,13,19-tetramethylpurpurin (34). Purpurin **4** (105 mg, 0.137 mmol) was dissolved in 80 mL of tetrahydrofuran and 20 mL of methanol. To this solution, 4 mL of a 10% aqueous potassium hydroxide solution was added and the stirring continued at room temperature overnight. The reaction mixture was poured into dichloromethane and immediately washed with dilute citric acid (1×) and water (4×). The organic layer was dried over Na_2SO_4 and concentrated to give 88 mg (95% yield) purpurin **34**. 1H NMR (300 MHz, $CDCl_3$) δ -0.39 (1H, s, pyrrole-NH), 0.42 (1H, s, pyrrole-NH), 0.91 (3H, t, $J=8$ Hz, 8- CH_2CH_3), 0.97 (3H, t, $J=8$ Hz, 4- CH_2CH_3), 1.17 (3H, s, 19- CH_3), 1.56 (3H, t, $J=7$ Hz, 20-CO $_2CH_2CH_3$), 1.69 (3H, t, $J=8$ Hz, 14- CH_2CH_3), 1.78 (3H, t, $J=8$ Hz, 18- CH_2CH_3), 2.05–2.20 (1H, m, 8- CH_2CH_3), 2.36–2.46 (1H, m, 4- CH_2CH_3), 2.57–2.70 (2H, m, 4,8- CH_2CH_3), 2.96–3.06 (1H, m, 18- CH_2CH_3), 3.15 (3H, s, 9- CH_3), 3.19–3.29 (1H, m, 18- CH_2CH_3), 3.35 (3H, s, 3- CH_3), 3.37 (3H, s, 13- CH_3), 3.64–3.77 (2H, m, 14- CH_2CH_3), 4.01–4.04 (1H, m, 18-H), 4.53 (2H, q, $J=7$ Hz, 20-CO $_2CH_2CH_3$), 5.04 (2H, s, 6-Ar- CH_2OH), 7.57 (1H, d, $J=8$ Hz, 6-Ar-H), 7.65 (1H, d, $J=8$ Hz, 6-Ar-H), 7.84 (1H, d, $J=7$ Hz, 6-Ar-H), 8.20 (1H, d, $J=7$ Hz, 6-Ar-H), 8.61 (1H, s, 16-H), 9.47 (1H, s, 11-H), 9.49 (1H, s, 21-H);

MALDI-TOF-MS m/z 682.4 ($C_{44}H_{50}N_4O_3^+$, calcd 682.4); UV-vis (CH_2Cl_2) 433, 537, 573, 634, 693 nm.

4.1.25. 20-Carbethoxy-4,8,14,18-tetraethyl-6-(4-formylphenyl)-3,9,13,19-tetramethylpurpurin (35). The title compound was prepared by dissolving 85 mg (0.12 mmol) purpurin **34** in 30 mL dichloromethane. To this solution, small portions (5–10 mg) of manganese (IV) dioxide were added every 10 min while monitoring the reaction by TLC. After 1.5 h, TLC indicated that the reaction was complete; the suspension was filtered through a pad of Celite to remove the manganese (IV) dioxide. An additional 800 mL of 10% methanol/dichloromethane was used to wash the Celite. The eluent was condensed and the resulting residue was purified by column chromatography (silica gel, 1:49 methanol/dichloromethane) to give 60 mg (71% yield) purpurin **35**. 1H NMR (300 MHz, $CDCl_3$) δ -0.39 (1H, s, pyrrole-NH), 0.35 (1H, s, pyrrole-NH), 0.88–0.99 (6H, m, 4,8- CH_2CH_3), 1.18 (3H, s, 19- CH_3), 1.55–1.60 (3H, m, 20-CO $_2CH_2CH_3$), 1.67–1.73 (3H, m, 14- CH_2CH_3), 1.78 (3H, t, $J=8$ Hz, 18- CH_2CH_3), 2.00–2.08 (1H, m, 8- CH_2CH_3), 2.36–2.42 (1H, m, 4- CH_2CH_3), 2.55–2.66 (2H, m, 4,8- CH_2CH_3), 2.98–3.08 (1H, m, 18- CH_2CH_3), 3.15 (3H, s, 9- CH_3), 3.18–3.26 (1H, m, 18- CH_2CH_3), 3.36 (3H, s, 3- CH_3), 3.39 (3H, s, 13- CH_3), 3.69–3.76 (2H, m, 14- CH_2CH_3), 4.01–4.06 (1H, m, 18-H), 4.50–4.58 (2H, m, 20-CO $_2CH_2CH_3$), 8.07–8.12 (2H, m, 6-Ar-H), 8.18–8.21 (1H, m, 6-Ar-H), 8.40–8.44 (1H, m, 6-Ar-H), 8.64 (1H, s, 6-H), 9.48 (1H, s, 11-H), 9.49 (1H, s, 21-H), 10.35 (1H, s, 6-Ar-CHO); MALDI-TOF-MS m/z 680.4 ($C_{44}H_{48}N_4O_3^+$, calcd 680.4); UV-vis (CH_2Cl_2) 437, 539, 574, 644, 695 nm.

4.1.26. 20-Carboxy-4,8,14,18-tetraethyl-6-(4-formylphenyl)-3,9,13,19-tetramethylpurpurin (36). A solution of 60 mg (0.089 mmol) purpurin **35** in 60 mL of tetrahydrofuran and 15 mL of methanol was degassed by bubbling with argon for 10 min. After 3 mL of a 10% aqueous potassium hydroxide solution was added, the mixture was stirred at 40 °C for 4 days. Upon cooling, the solution was poured into dichloromethane and washed immediately with dilute citric acid (1×) and water (4×). The organic layer was dried over Na_2SO_4 and concentrated to yield 50 mg (88%) of purpurin **36**. 1H NMR (300 MHz, $CDCl_3$) δ -0.39 (1H, s, pyrrole-NH), 0.47 (1H, s, pyrrole-NH), 0.85–0.92 (3H, m, 8- CH_2CH_3), 0.95–0.99 (3H, m, 4- CH_2CH_3), 1.25 (3H, s, 19- CH_3), 1.68–1.73 (3H, m, 14- CH_2CH_3), 1.82–1.87 (3H, m, 18- CH_2CH_3), 1.99–2.07 (1H, m, 8- CH_2CH_3), 2.39–2.50 (1H, m, 4- CH_2CH_3), 2.53–2.68 (2H, m, 4,8- CH_2CH_3), 2.98–3.08 (1H, m, 18- CH_2CH_3), 3.15 (3H, s, 9- CH_3), 3.18–3.26 (1H, m, 18- CH_2CH_3), 3.39 (6H, s, 3,13- CH_3), 3.72–3.77 (2H, m, 14- CH_2CH_3), 4.06–4.09 (1H, m, 18-H), 8.11–8.13 (2H, m, 6-Ar-H), 8.19–8.22 (1H, m, 6-Ar-H), 8.42–8.44 (1H, m, 6-Ar-H), 8.66 (1H, s, 16-H), 9.48 (1H, s, 11-H), 9.49 (1H, s, 21-H), 10.35 (1H, s, 6-Ar-CHO); MALDI-TOF-MS m/z 652.3 ($C_{42}H_{44}N_4O_3^+$, calcd 652.3); UV-vis (CH_2Cl_2) 437, 536, 574, 645, 696 nm.

4.1.27. 20-Carbo(*tert*-butyldiphenylsiloxy)-6-(4-formylphenyl)-4,8,14,18-tetraethyl-3,9,13,19-tetramethylpurpurin (37). Purpurin **36** (50 mg, 0.077 mmol), 16 μ L (0.12 mmol) of triethylamine, and 23 μ L (0.088 mmol) of *tert*-butyldiphenylsilylchloride were stirred at room

temperature in 30 mL of dry dichloromethane for 1.5 h. The solvent was removed under reduced pressure and the product purified by column chromatography (silica gel, 1:19 ethyl acetate/toluene) to give 60 mg (88% yield) of **37**. ^1H NMR (300 MHz, CDCl_3) δ -0.39 (1H, s, pyrrole-NH), 0.43 (1H, s, pyrrole-NH), 0.74–0.97 (6H, m, 4,8- CH_2CH_3), 1.06 (9H, s, 20-C(CH_3) $_3$), 1.34 (3H, s, 19- CH_3), 1.56–1.72 (6H, m, 14,18- CH_2CH_3), 1.99–2.36 (2H, m, 4,8- CH_2CH_3), 2.50–2.65 (2H, m, 4,8- CH_2CH_3), 2.92–2.94 (1H, m, 18- CH_2CH_3), 3.15 (3H, s, 9- CH_3), 3.18–3.27 (1H, m, 18- CH_2CH_3), 3.37 (6H, s, 3,13- CH_3), 3.67–3.71 (2H, m, 14- CH_2CH_3), 3.98–4.02 (1H, m, 18-H), 7.34–7.40 (6H, m, 20-Si(Ph) $_2$), 7.69–7.73 (4H, m, 20-Si(Ph) $_2$), 8.06–8.08 (2H, m, 6-Ar-H), 8.16–8.19 (1H, m, 6-Ar-H), 8.39–8.43 (1H, m, 6-Ar-H), 8.60 (1H, s, 16-H), 9.47 (1H, s, 11-H), 9.48 (1H, s, 21-H), 10.30 (1H, s, 6-Ar-CHO); MALDI-TOF-MS m/z 890.5 ($\text{C}_{58}\text{H}_{62}\text{N}_4\text{O}_3\text{Si}^+$, calcd 890.5); UV-vis (CH_2Cl_2) 441, 544, 577, 650, 699 nm.

4.1.28. Dyad 38. Purpurin **37** (60 mg, 0.067 mmol), 94 mg (0.13 mmol) of fullerene (C_{60}) and 60 mg (0.67 mmol) of sarcosine were refluxed in 30 mL of toluene overnight. The solvent was removed under reduced pressure and dyad **38** (40 mg, 36% yield) was purified by column chromatography (silica gel, 1:1:98 ethyl acetate/carbon disulfide/toluene). ^1H NMR (500 MHz, 50:50 $\text{CDCl}_3/\text{CS}_2$) δ -0.30 (1H, s, pyrrole-NH), 0.41 (1H, s, pyrrole-NH), 0.45–0.59 (3H, m, 8- CH_2CH_3), 0.62–0.73 (3H, m, 4- CH_2CH_3), 1.08 (9H, s, 20-Si(CH_3) $_3$), 1.23–1.40 (3H, m, 19- CH_3), 1.60–1.75 (6H, m, 14,18- CH_2CH_3), 2.13–2.37 (2H, m, 4,8- CH_2CH_3), 2.53–2.68 (2H, m, 4,8- CH_2CH_3), 2.83–2.93 (4H, m, 18- CH_2CH_3 , pyrrolidine- CH_3), 3.11 (3H, s, 9- CH_3), 3.15–3.27 (1H, m, 18- CH_2CH_3), 3.37 (6H, s, 3,13- CH_3), 3.66–3.77 (2H, m, 14- CH_2CH_3), 3.90–3.99 (1H, m, 18-H), 4.29–4.43 (1H, m, pyrrolidine-H), 4.58–4.69 (2H, m, pyrrolidine-H), 7.34–7.40 (6H, m, 20-Si(Ph) $_2$), 7.69–7.73 (4H, m, 20-Si(Ph) $_2$), 7.90–8.03 (2H, m, 6-Ar-H), 8.27–8.33 (1H, m, 6-Ar-H), 8.55–8.57 (1H, m, 6-Ar-H), 8.77 (1H, s, 16-H), 9.52 (1H, s, 11-H), 9.62 (1H, s, 21-H); MALDI-TOF-MS: m/z 1638.5 ($\text{C}_{120}\text{H}_{67}\text{N}_5\text{O}_2\text{Si}^+$, calcd 1638.5); UV-vis (toluene) 321, 440, 537, 578, 649, 699, 720 (sh) nm.

4.1.29. Dyad 39. A portion of trifluoroacetic acid (2 mL) and water (1.5 mL) was added to a solution of 40 mg (0.024 mmol) of dyad **38** in 20 mL of tetrahydrofuran. After 3 h, the solution was diluted with toluene and washed consecutively with water (1 \times), saturated aqueous NaHCO_3 (2 \times) and water (2 \times). The organic layer was dried over Na_2SO_4 and concentrated. The residue was washed with methanol (3 \times). After each washing, the solution was centrifuged, saving the solid. The combined solids (30 mg, 88% yield) were dried under vacuum for 8 h prior to use in the next reaction. An NMR spectrum was not obtained due to the limited solubility of dyad **39**. MALDI-TOF-MS m/z 1400.4 ($\text{C}_{104}\text{H}_{49}\text{N}_5\text{O}_2^+$, calcd 1400.4); UV-vis (toluene) 320, 438, 541, 576, 646, 699, 720 (sh) nm.

4.1.30. Triad 2. Dyad **39** (10 mg, 0.007 mmol) and 0.1 mg (0.001 mmol) of 4-(dimethylamino)pyridine were stirred in 2 mL of pyridine and 2 mL of toluene until all solid had dissolved. To this solution, 9 mg (0.017 mmol) of carotenoid **29** and 3 mg (0.017 mmol) of *N*-ethyl-*N'*-(3-dimethylamino-propyl)carbodiimide were added. After 3 days of stirring at room temperature, an additional portion of *N*-ethyl-*N'*-(3-

dimethylaminopropyl)carbodiimide (3 mg, 0.017 mmol) was added. After an additional day, the solution was quenched with water. The solution was poured into toluene and washed with water (3 \times). The organic layer was dried with Na_2SO_4 and concentrated. Triad **2** (11 mg, 82% yield) was purified by column chromatography (silica gel, eluent 3:97–5:95 ethyl acetate/toluene). The presence of stereoisomers was evidenced by HPLC and the ^1H NMR spectrum of the mixture: (500 MHz, 50:50 $\text{CDCl}_3/\text{CS}_2$) δ -0.5 to -0.36 (1H, m, pur pyrrole-NH), 0.20–0.27 (1H, m, pur pyrrole-NH), 0.83–0.89 (6H, m, pur 4,8- CH_2CH_3), 1.02 (6H, s, car 16,17- CH_3), 1.24 (3H, s, pur 19- CH_3), 1.45–1.47 (2H, m, car 2- CH_2 -), 1.60–1.62 (2H, m, car 3- CH_2 -), 1.66–1.74 (6H, br s, pur 14- CH_2CH_3 , car 18- CH_3), 1.78 (3H, t, $J=7.5$ Hz, pur 18- CH_2CH_3), 1.96 (3H, s, car 19- CH_3), 1.98 (3H, s, car 20- CH_3), 2.00 (3H, s, car 20'- CH_3), 2.07 (3H, s, car 19'- CH_3), 2.16–2.30 (2H, m, pur 4,8- CH_2CH_3), 2.50–2.66 (2H, m, pur 4,8- CH_2CH_3), 2.90–2.30 (1H, m, pur 18- CH_2CH_3), 3.01 (3H, s, pur 9- CH_3), 3.07 (3H, s, pyrrolidine- CH_3), 3.2–3.3 (1H, m, pur 18- CH_2CH_3), 3.40 (6H, s, pur 3,13- CH_3), 3.72–3.76 (2H, m, pur 14- CH_2CH_3), 4.05 (1H, m, pur 18-H), 4.10–4.30 (1H, m, pyrrolidine-H), 4.80–5.20 (2H, m, pyrrolidine-H), 6.05–6.96 (14H, m, car =CH-), 7.49 (2H, br s, car H-1', H-5'), 7.75 (3H, m, pur 6-Ar-H, car H-2', H-4'), 8.02 (2H, br s, NH, pur 6-Ar-H), 8.10–8.40 (2H, m, pur 6-Ar-H), 8.61(0.5H, s, pur-16-H), 8.85(0.5H, s, pur 16-Ar-H), 9.05–9.20 (1H, m, pur 11-H), 9.45 (1H, m, pur 21-H). A solvent consisting of 1:99 ethyl acetate/toluene was used to separate the isomers by HPLC. The fractions were identified by mass spectroscopy and UV-vis, but insufficient quantities were collected for NMR analysis. MALDI-TOF-MS: m/z 1887.7 ($\text{C}_{141}\text{H}_{94}\text{N}_6\text{O}^+$, calcd 1887.7); UV-vis (toluene) 320, 438, 480, 512, 579, 646, 697 nm.

4.1.31. Dyad 40. Dyad **39** (15 mg, 0.012 mmol) and 0.1 mg (0.001 mmol) of 4-(dimethylamino)pyridine were stirred in 1 mL of pyridine and 1 mL of toluene until all solid had dissolved. *trans,trans*-Farnesol (5 μL , 0.024 mmol) and 5 mg (0.024 mmol) of *N*-ethyl-*N'*-(3-dimethylamino-propyl)carbodiimide were added. The reaction was quenched with water after 2 days of stirring at room temperature. The solution was poured into toluene and washed with water (3 \times). The organic layer was dried over Na_2SO_4 and concentrated. Dyad **40** (5 mg, 29% yield) was purified by column chromatography (silica gel, 1:99–5:95 ethyl acetate/toluene). Similarly to triad **2**, NMR spectroscopy indicated the presence of isomers, confirmed by UV-vis spectroscopy. HPLC purification (eluent: 0.9:99 ethyl acetate/toluene) was used to prepare dyad **40** for the spectroscopic studies. MALDI-TOF-MS m/z 1604.5 ($\text{C}_{119}\text{H}_{73}\text{N}_5\text{O}_2^+$, calcd 1604.6); UV-vis (toluene) 318, 437, 510, 541, 576, 645, 697 nm.

4.1.32. 20-Carboethoxy-4,8,14,18-tetraethyl-6-[4-(methoxymethoxy)methylphenyl]-3,9,13,19-tetramethylpupurin (41). Purpurin **34** (90 mg, 0.13 mmol) was dissolved in 5 mL of dry dichloromethane. To this solution, 3 mL (29 mmol) of dimethoxymethane and 600 mg (4.4 mmol) of phosphorous pentoxide were added. After stirring at room temperature for 2 h, an additional 300 mg (2.2 mmol) of phosphorous pentoxide was added. The stirring continued for 2 h, then the reaction was poured into dichloromethane and washed with saturated NaHCO_3 (aqueous) and saturated aqueous

NaCl (2×). The organic layer was dried over Na₂SO₄ and concentrated. Purification was done by column chromatography (silica gel, 1:49 methanol/dichloromethane). The final product, purpurin **41** was obtained in 42% yield (40 mg). ¹H NMR (300 MHz, CDCl₃) δ -0.31 (1H, s, pyrrole-NH), 0.42 (1H, s, pyrrole-NH), 0.92 (3H, t, *J*=8 Hz, 8-CH₂CH₃), 0.97 (3H, t, *J*=8 Hz, 4-CH₂CH₃), 1.18 (3H, s, 19-CH₃), 1.54–1.59 (3H, m, 20-CO₂CH₂CH₃), 1.69 (3H, t, *J*=8 Hz, 14-CH₂CH₃), 1.78 (3H, t, *J*=7 Hz, 18-CH₂CH₃), 2.05–2.14 (1H, m, 8-CH₂CH₃), 2.40–2.50 (1H, m, 4-CH₂CH₃), 2.55–2.71 (2H, m, 4,8-CH₂CH₃), 2.96–3.09 (1H, m, 18-CH₂CH₃), 3.19 (3H, s, 9-CH₃), 3.18–3.39 (1H, m, 18-CH₂CH₃), 3.35 (3H, s, 3-CH₃), 3.38 (3H, s, 13-CH₃), 3.57 (3H, s, 6-Ar-OCH₃), 3.67–3.73 (2H, m, 14-CH₂CH₃), 4.00–4.04 (1H, m, 18-H), 4.54 (2H, q, *J*=7 Hz, 20-CO₂CH₂CH₃), 4.89 (2H, s, 6-Ar-OCH₂O-), 4.94 (2H, s, 6-Ar-CH₂O-), 7.57 (1H, d, *J*=8 Hz, 6-Ar-H), 7.64 (1H, d, *J*=8 Hz, 6-Ar-H), 7.84 (1H, d, *J*=8 Hz, 6-Ar-H), 8.19 (1H, d, *J*=8 Hz, 6-Ar-H), 8.61 (1H, s, 16-H), 9.47 (1H, s, 11-H), 9.49 (1H, s, 21-H); MALDI-TOF-MS *m/z* 726.4 (C₄₆H₅₄N₄O₄⁺, calcd 726.4); UV–vis (CH₂Cl₂) 433, 533, 574, 636, 693 nm.

4.1.33. 20-Carboxy-4,8,14,18-tetraethyl-6-[4-(methoxymethoxy)methylphenyl]-3,9,13,19-tetramethylpurpurin (42). Purpurin **41** (40 mg, 0.060 mmol) in 40 mL of tetrahydrofuran and 10 mL of methanol were degassed with argon for 10 min. A portion (2 mL) of a 10% aqueous potassium hydroxide solution was added and the stirring continued at 40 °C for 5 days. After cooling, the solution was poured into dichloromethane and washed immediately with dilute citric acid (1×), saturated aqueous NaHCO₃ (1×), water (3×), saturated aqueous NaCl (1×). The organic layer was dried and concentrated to give 35 mg (92% yield). ¹H NMR (300 MHz, CDCl₃) δ -0.39 (1H, s, pyrrole-NH), 0.59 (1H, s, pyrrole-NH), 0.84–1.00 (6H, m, 4,8-CH₂CH₃), 1.26 (3H, s, 19-CH₃), 1.71 (3H, t, *J*=8 Hz, 14-CH₂CH₃), 1.82–1.88 (3H, m, 18-CH₂CH₃), 2.08–2.15 (1H, m, 8-CH₂CH₃), 2.42–2.50 (1H, m, 4-CH₂CH₃), 2.58–2.73 (2H, m, 4,8-CH₂CH₃), 3.02–3.10 (1H, m, 18-CH₂CH₃), 3.16 (3H, s, 9-CH₃), 3.27–3.33 (1H, m, 18-CH₂CH₃), 3.38 (3H, s, 3-CH₃), 3.40 (3H, s, 13-CH₃), 3.58 (3H, s, 6-Ar-OCH₃), 3.66–3.78 (2H, m, 14-CH₂CH₃), 4.06–4.11 (1H, m, 18-H), 4.91 (2H, s, 6-Ar-OCH₂-), 4.95 (2H, s, 6-Ar-CH₂O-), 7.58 (1H, d, *J*=8 Hz, 6-Ar-H), 7.66 (1H, d, *J*=8 Hz, 6-Ar-H), 7.86 (1H, d, *J*=8 Hz, 6-Ar-H), 8.21 (1H, d, *J*=8 Hz, 6-Ar-H), 8.63 (1H, s, 16-H), 9.47 (1H, s, 11-H), 9.72 (1H, s, 21-H); MALDI-TOF-MS *m/z* 698.4 (C₄₄H₅₀N₄O₄⁺, calcd 698.4); UV–vis (CH₂Cl₂) 433, 535, 575, 638, 695 nm.

Dyad **43** was prepared by stirring 35 mg (0.050 mmol) of purpurin **42**, 51 mg (0.10 mmol) of carotenoid **29**, 19 mg (0.10 mmol) of *N*-ethyl-*N'*-(3-dimethylaminopropyl)carbodiimide and 1 mg (0.008 mmol) of 4-(dimethylamino)pyridine in 7 mL of pyridine at room temperature for 2 days. An additional 19 mg (0.10 mmol) of *N*-ethyl-*N'*-(3-dimethylaminopropyl)carbodiimide was added and the stirring was continued for 1 day. The reaction mixture was poured into dichloromethane and washed with water (3×). The organic layer was dried over Na₂SO₄ and concentrated. Dyad **43** (20 mg, 34% yield) was purified by column chromatography (silica gel, 5:95–8:92 ethyl acetate/toluene). ¹H NMR

(500 MHz, CDCl₃) δ -0.44 (1H, s, pyrrole-NH), 0.29 (1H, s, pyrrole-NH), 0.92 (3H, t, *J*=8 Hz, pur 8-CH₂CH₃), 0.98 (3H, t, *J*=8 Hz, pur 4-CH₂CH₃), 1.03 (6H, s, car 16,17-CH₃), 1.29 (3H, s, pur 19-CH₃), 1.44–1.50 (2H, m, car 2-CH₂-), 1.59–1.64 (2H, m, car 3-CH₂-), 1.70 (3H, t, *J*=8 Hz, pur 14-CH₂CH₃), 1.73 (3H, s, car 18-CH₃), 1.80 (3H, t, *J*=8 Hz, pur 18-CH₂CH₃), 1.99–2.10 (15H, m, pur 8-CH₂CH₃, car 4-CH₂-, car 19,20,19',20'-CH₃), 2.38–2.48 (1H, m, pur 4-CH₂CH₃), 2.59–2.72 (2H, m, pur 4,8-CH₂CH₃), 3.04–3.09 (1H, m, pur 18-CH₂CH₃), 3.17 (3H, s, 9-CH₃), 3.26–3.30 (1H, m, pur 18-CH₂CH₃), 3.39 (6H, s, pur 3,13-CH₃), 3.58 (3H, s, pur 6-Ar-OCH₃), 3.68–3.74 (2H, m, pur 14-CH₂CH₃), 4.11–4.13 (1H, m, 18-H), 4.91 (2H, s, pur 6-Ar-OCH₂-), 4.95 (2H, s, pur 6-Ar-CH₂O-), 6.12–6.93 (14H, m, car =CH-), 7.53 (2H, d, *J*=9 Hz, car H-1', H-5'), 7.58 (1H, d, *J*=8 Hz, pur 6-Ar-H), 7.66 (1H, d, *J*=8 Hz, pur 6-Ar-H), 7.78 (2H, d, *J*=9 Hz, car H-2', H-4'), 7.86 (1H, d, *J*=8 Hz, pur 6-Ar-H), 8.21 (1H, d, *J*=8 Hz, 6-Ar-H), 8.63 (1H, s, pur 16-H), 9.21 (1H, s, pur 11-H), 9.50 (1H, s, pur 21-H); MALDI-TOF-MS *m/z* 1185.7 (C₈₁H₉₅N₅O₃⁺, calcd 1185.7); UV–vis (toluene) 437, 483, 509, 579, 640, 697 nm.

5. Spectroscopic techniques

5.1. Steady-state absorption and fluorescence

UV–vis ground state absorption spectra were measured on a Shimadzu UV2100U UV–vis spectrometer. Steady state fluorescence emission spectra were measured using a Photon Technology International MP-1 spectrofluorimeter and corrected. Excitation was produced by a 75 W xenon lamp and a single-grating monochromator. Fluorescence was detected at 90° to the excitation beam via a single-grating monochromator and an R928 photomultiplier tube having S-20 spectral response and operating in the single-photon-counting mode.

5.2. Time-resolved emission

Fluorescence decay measurements were performed on ~1×10⁻⁵ M solutions by the time-correlated single photon counting method. The excitation source was a cavity-dumped Coherent 700 dye laser pumped by a frequency-doubled Coherent Antares 76s Nd:YAG laser. Fluorescence emission was detected at a magic angle using a single grating monochromator and microchannel plate photomultiplier (Hamamatsu R2809U-11). The instrument response time was ca. 60–90 ps, as verified by scattering from Ludox AS-40. The spectrometer was controlled by software based on a LabView program from National Instruments.

5.3. Time-resolved absorption

Nanosecond transient absorption measurements were made with excitation from an Opotek optical parametric oscillator pumped by the third harmonic of a Continuum Surelight Nd:YAG laser. The pulse width was ~5 ns, and the repetition rate was 5 Hz. The detection portion of the spectrometer has been described.² The femtosecond transient absorption apparatus consists of a kilohertz pulsed laser source and a pump-probe optical setup. The laser pulse

train was provided by a Ti: Sapphire regenerative amplifier (Clark-MXR, Model CPA-1000) pumped by a diode-pumped CW solid state laser (Spectra Physics, Model Millennia V). The typical laser pulse was 100 fs at 790 nm, with a pulse energy of 0.9 mJ at a repetition rate of 1 KHz. Most of the laser energy (85%) was used to pump an optical parametric amplifier (IR-OPA, Clark-MXR). The excitation pulse was sent through a computer-controlled optical delay line. The remaining laser output (15%) was focused into a 1 cm flowing water cell to generate a white light continuum. The continuum beam was further split into two identical parts and used as the probe and reference beams, respectively. The probe and reference signals were focused onto two separated optical fiber bundles coupled to a spectrograph (Acton Research, Model SP275). The spectra were acquired on a dual diode array detector (Princeton Instruments, Model DPDA-1024).³

5.4. Data analysis

To determine the number of significant components in the transient absorption data, singular value decomposition analysis^{4,5} was carried out using locally-written software based on the MatLab 5.0 program (MathWorks, Inc.). Decay-associated spectra were then obtained by fitting the transient absorption change curves over a selected wavelength region simultaneously as described by Eq. 1,

$$\Delta A(\lambda, t) = \sum_{i=1}^n A_i(\lambda) \exp(-t/\tau_i) \quad (1)$$

where $\Delta A(\lambda, t)$ is the observed absorption change at a given wavelength at time delay t and n is the number of kinetic components used in the fitting. A plot of $A_i(\lambda)$ versus wavelength is called a decay-associated spectrum, and represents the amplitude spectrum of the i th kinetic component, which has a lifetime of τ_i . Random errors associated with the reported lifetimes obtained from fluorescence and transient absorption measurements were typically $\leq 5\%$. Simulations of the kinetic pathways were performed with the Chemical Kinetics Simulator, Version 1.01, created by IBM (www.almaden.ibm.com/st/computational_science/ck/msim/index.shtml).

6. Electrochemical measurements

Reduction and oxidation potentials were measured by cyclic voltammetry in a two compartment glass cell, with a glassy carbon electrode as the working electrode, a Pt wire as counter electrode and Ag/AgNO₃ as a reference electrode. Electrode potentials are expressed versus SCE using ferrocene as an internal standard (ferrocene/ferrocenium potential vs SCE: 0.458 V). The electrolyte solution was 0.1 M tetra-*n*-butyl ammonium hexafluorophosphate in benzonitrile. Solutions were purged with nitrogen or argon prior to measurements and an inert atmosphere was maintained thereafter. Cyclic voltammograms, at scan rates from 10–500 mV/s, were obtained with a PAR 173 potentiostat, a PAR 175 universal programmer, and a computer with LabView software.

Acknowledgements

This work was supported by a grant from by the US Department of Energy (DE-FG02-03ER15393). This is publication 645 from the ASU center for the Study of early Events in Photosynthesis.

Supplementary data

Supplementary data associated with this article can be found in the online version, at doi:10.1016/j.tet.2005.06.121.

References and notes

- Liddell, P. A.; Sumida, J. P.; Macpherson, A. N.; Noss, L.; Seely, G. R.; Clark, K. N.; Moore, A. L.; Moore, T. A.; Gust, D. *Photochem. Photobiol.* **1994**, *60*, 537–541.
- Guldi, D. M. *Chem. Soc. Rev.* **2002**, *31*, 22–36.
- Liddell, P. A.; Kuciauskas, D.; Sumida, J. P.; Nash, B.; Nguyen, D.; Moore, A. L.; Moore, T. A.; Gust, D. *J. Am. Chem. Soc.* **1997**, *119*, 1400–1405.
- Gust, D.; Moore, T. A. In *The Porphyrin Handbook* Kadish, K. M., Smith, K. M., Guillard, R., Eds.; Academic: New York, 1999; vol. 8, pp 153–190.
- Imahori, H.; Yamada, H.; Guldi, D. M.; Endo, Y.; Shimomura, A.; Kundu, S.; Yamada, K.; Okada, T.; Sakata, Y.; Fukuzumi, S. *Angew. Chem., Int. Ed.* **2002**, *41*, 2344–2347.
- Imahori, H.; Hagiwara, K.; Akiyama, T.; Aoki, M.; Taniguchi, S.; Okada, T.; Shirakawa, M.; Sakata, Y. *Chem. Phys. Lett.* **1996**, *263*, 545–550.
- Segura, J. L.; Martin, N.; Guldi, D. M. *Chem. Soc. Rev.* **2005**, *34*, 31–47.
- Kuciauskas, D.; Liddell, P. A.; Lin, S.; Johnson, T. E.; Weghorn, S. J.; Lindsey, J. S.; Moore, A. L.; Moore, T. A.; Gust, D. *J. Am. Chem. Soc.* **1999**, *121*, 8604–8614.
- Kodis, G.; Liddell, P. A.; de la Garza, L.; Clausen, P. C.; Lindsey, J. S.; Moore, A. L.; Moore, T. A.; Gust, D. *J. Phys. Chem. A* **2002**, *106*, 2036–2048.
- Imahori, H. *J. Phys. Chem. B* **2004**, *108*, 6130–6143.
- McDermott, G.; Prince, S. M.; Freer, A. A.; Hawthornthwaite-Lawless, A. M.; Papiz, M. Z.; Cogdell, R. J.; Isaacs, N. W. *Nature* **1995**, *374*, 517–521.
- Rozsak, A. W.; Howard, T. D.; Southall, J.; Gardiner, A. T.; Law, C. J.; Isaacs, N. W.; Cogdell, R. J. *Science* **2003**, *302*, 1969–1972.
- Frank, H. A.; Cogdell, R. J. *Photochem. Photobiol.* **1996**, *63*, 257–264.
- Macpherson, A. N.; Liddell, P. A.; Kuciauskas, D.; Tatman, D.; Gillbro, T.; Gust, D.; Moore, T. A.; Moore, A. L. *J. Phys. Chem. B* **2002**, *106*, 9424–9433.
- Gunter, M. J.; Robinson, B. C. *Tetrahedron Lett.* **1990**, *31*, 285–288.
- Robinson, B. C. *Tetrahedron* **2000**, *56*, 6005–6014.
- Gunter, M. J.; Robinson, B. C. *Aust. J. Chem.* **1990**, *43*, 1839–1860.

18. Shanmugathasan, S.; Edwards, C.; Boyle, R. W. *Tetrahedron* **2000**, *56*, 1025–1046.
19. Morgan, B.; Dolphin, D. *J. Org. Chem.* **1987**, *52*, 5364–5374.
20. Liddell, P. A.; Zarate, X.; Moore, A. L.; Moore, T. A.; Gust, D. *Tetrahedron Lett.* **2000**, *41*, 9661–9665.
21. Prato, M.; Maggini, M. *Acc. Chem. Res.* **1998**, *31*, 519–526.
22. Kuciauskas, D.; Liddell, P. A.; Lin, S.; Stone, S. G.; Moore, A. L.; Moore, T. A.; Gust, D. *J. Phys. Chem. B* **2000**, *104*, 4307–4321.
23. Hermant, R. M.; Liddell, P. A.; Lin, S.; Alden, R. G.; Kang, H. K.; Moore, A. L.; Moore, T. A.; Gust, D. *J. Am. Chem. Soc.* **1993**, *115*, 2080–2081.
24. Kodis, G.; Herrero, C.; Palacios, R.; Marino-Ochoa, E.; Gould, S.; de la Garza, L.; van Grondelle, R.; Gust, D.; Moore, T. A.; Moore, A. L.; Kennis, J. T. M. *J. Phys. Chem. B* **2004**, *108*, 414–425.
25. Imahori, H.; Cardoso, S.; Tatman, D.; Lin, S.; Noss, L.; Seely, G. R.; Sereno, L.; de Silber, J. J.; Moore, T. A.; Moore, A. L.; Gust, D. *Photochem. Photobiol.* **1995**, *62*, 1009–1014.
26. Lewis, J. E.; Moore, T. A.; Benin, D.; Gust, D.; Nicodem, D.; Nonell, S. *Photochem. Photobiol.* **1994**, *59*, 35S.
27. Bensasson, R. V.; Land, E. J.; Truscott, T. G. *Flash Photolysis and Pulse Radiolysis. Contribution to the Chemistry of Biology and Medicine*; Pergamon: New York, 1983.
28. Bonnett, R.; McGarvey, D. J.; Harriman, A.; Land, E. J.; Truscott, T. G.; Winfield, U.-J. *Photochem. Photobiol.* **1988**, *48*, 271–276.
29. Marcus, R. A. *J. Chem. Phys.* **1956**, *24*, 966–978.
30. Hush, N. S. *J. Chem. Phys.* **1958**, *28*, 962–972.
31. Marcus, R. A. *Can. J. Chem.* **1959**, *37*, 155–163.
32. Hush, N. S. *Trans. Faraday Soc.* **1961**, *57*, 557–580.

Synthesis and photophysical characterization of a titanium(IV) phthalocyanine–C₆₀ supramolecular dyad

Beatriz Ballesteros,^a Gema de la Torre,^a Tomás Torres,^{a,*} Gordon L. Hug,^b
G. M. Aminur Rahman^c and Dirk M. Guldi^{c,*}

^aUniversidad Autónoma de Madrid, Departamento de Química Orgánica, Campus de Cantoblanco, 28049 Madrid, Spain

^bUniversity of Notre Dame, Radiation Laboratory, Notre Dame, IN 46566, USA

^cUniversität Erlangen, Institute for Physical and Theoretical Chemistry, Egerlandstr. 3, 91058 Erlangen, Germany

Received 2 July 2005; revised 4 August 2005; accepted 8 August 2005

Available online 28 November 2005

Abstract—An axially substituted titanium(IV) phthalocyanine–fullerene donor–acceptor supramolecular dyad has been prepared by two different approaches, one of them representing a convenient convergent strategy. The dyad system exhibits photoinduced electron transfer upon irradiation with visible light to produce a microsecond lived charge separated state.
© 2005 Elsevier Ltd. All rights reserved.

1. Introduction

The unique electronic features of phthalocyanines (Pcs)¹ together with their unique stability and broad versatility has elicited a lot of interest in several fields of materials science, for example, as nonlinear optical media.² On the other hand, the combination of the light-harvesting and electron donor (or acceptor) characteristics of phthalocyanines³ together with the electron accepting properties of fullerenes^{4,5,6} is expected to give rise—ultimately—to efficient solar energy conversion.⁷

Metal-directed self-assembly has recently become a major tool by which coordination chemists can prepare large and elaborate complexes from relatively simple components, as it provides the opportunity to control the properties of a material at the molecular level. In these cases the resulting metallo-supramolecular species are characterized by the large energies associated with metal–ligand bond formation.⁸

Among the different metals that are coordinated by the centre of the Pc macrocycle, some of them, like titanium, bear axial ligands. The ability of axial coordination has been exploited by us to introduce an element of asymmetry to the Pc-molecule, thus preparing compounds with second order

nonlinear optical (NLO)⁹ and photoinduced electron transfer properties.^{5b}

Catechol ligands are known building-blocks for metallo-supramolecular chemistry using Ti(IV).^{8m,n} Particularly, in the field of second harmonic generation,² we have recently studied a series of axially substituted titanium(IV) tetra-*tert*-butylphthalocyanines.⁹ The introduction of a substituent in the axial position does affect dramatically the NLO response of phthalocyanines, since it breaks the centrosymmetry of the macrocycle, with the concomitant appearance of a dipole moment, and adds to the molecule a non-negligible octupolar character. Combination of dipole and octupolar features¹⁰ within the same molecule has already yielded some other fairly interesting nonlinear optical properties in, for example, the field of axially-substituted subphthalocyanines.¹¹ In addition, axial substitution with bulky groups such as substituted catecholates helps to prevent aggregation of macrocycles.¹²

In fact, phthalocyanines emerged as promising sensitiser materials for dye sensitised solar cells (DSSC)¹³ as well as other photovoltaic systems,⁷ but their applications in this field have been limited, in large, by problems associated with aggregation of the dye on the metal oxide surface. In this context, we have recently shown that anchoring a novel titanium phthalocyanine to nanocrystalline TiO₂ films occurs with inappreciable aggregation.¹² The observation of state selective electron injection from the titanium phthalocyanine to the TiO₂ with efficient charge separation prompted us to prepare titanium phthalocyanine-based

Keywords: Phthalocyanine; Fullerene; Titanium(IV); Electron transfer.

* Corresponding authors. Tel.: +34 91 397 5097; fax: +34 91 397 3966 (T.T.); tel: +49 9131 8527340; fax: +49 9131 8528307 (D.M.G.); e-mail addresses: tomas.torres@uam.es; dirk.guldi@chemie.uni-erlangen.de

dyads containing fullerene as acceptor units. We have recently described the preparation of strongly coupled ZnPc–C₆₀ dyads^{5,7} and related systems,¹⁴ which form long-lived and highly emissive charge-separated states. In this connection, induction of self-organization between ZnPc and C₆₀ moieties in an amphiphilic ZnPc–C₆₀ salt, resulted in uniformly nanostructured 1-D nanotubes¹⁵ exhibiting charge transfer features typically found in thin solid films of donor–acceptor composites.

In this paper, we wish to describe the synthesis of a titanium phthalocyanine–fullerene supramolecular dyad **1** (Figure 1)¹⁶ and its photophysical properties.

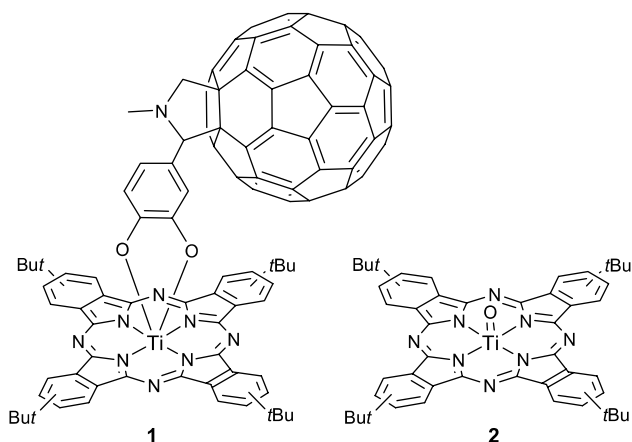
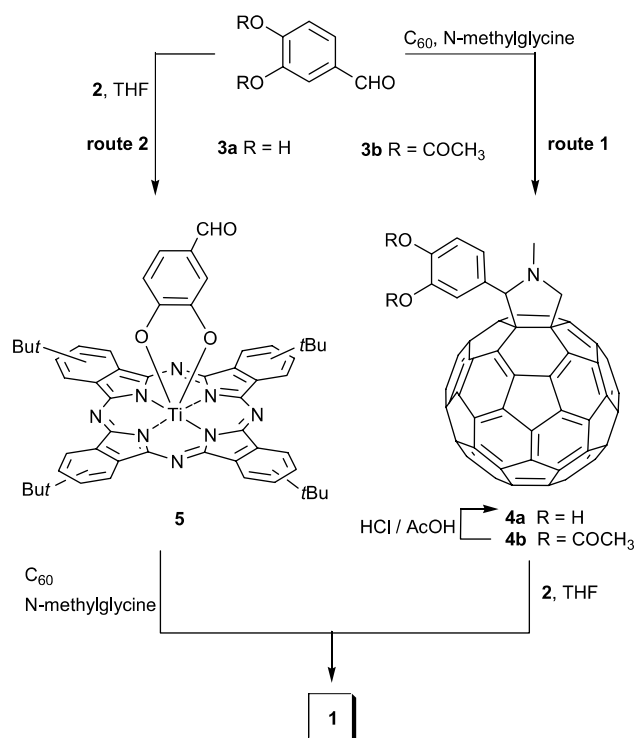


Figure 1. Titanium phthalocyanine–C₆₀ dyad and its precursor.

2. Results and discussion

We have followed efficient synthetic procedures obtaining axially substituted titanium phthalocyanines¹⁷ through reaction of an appropriately substituted titanium oxide phthalocyanine (PcTiO, **2**) (Figure 1) and a catechol-type reagent. The most convenient and convergent route for the synthesis of dyad **1** involves preparation of a catechol subunit bearing C₆₀ (**4a**). This initial step is then followed by displacing the oxygen atom of the (tBu)₄PcTiO **2** to give the fullerene-containing axially substituted dyad **1** (Scheme 1, route 1). The main advantage of this convergent route is its versatility: it enables, for example, the straightforward preparation of other Pc–C₆₀ dyads via reacting fullerene-containing catechol **4a** with appropriately substituted titanium oxide phthalocyanines.

Therefore, we undertook the synthesis of **4a** through 1,3-dipolar cycloaddition of an azamethine ylide, formed in situ by reaction of 3,4-dihydroxybenzaldehyde (**3a**) and *N*-methylglycine, to C₆₀ under standard conditions (Prato reaction). However, this approach led to a complex mixture of mono- and bisadducts, which—owing to the poor solubility of the material—are difficult to separate. This necessitated to perform the Prato reaction with a catechol reagent that is protected as 3,4-diacetoxybenzaldehyde **3b** (commercially available). The corresponding 1,3-dipolar cycloaddition gives rise to the corresponding monoadduct **4b** in 32% yield. Further deprotection in acidic media (AcOH/HCl mixture) yields the fullerene-containing ligand **4a** in 65% yield. Finally, the reaction between tBu₄PcTiO **2**



Scheme 1. Synthetic routes to dyad **1**.

and the chelating agent **4a** proceeded in THF at reflux temperature in 62% yield.

For comparative purposes, we decided to tackle the synthesis of dyad **1** as depicted in Scheme 1, route 2. This path involves a former reaction between 3,4-dihydroxybenzaldehyde (**3a**) and compound **2** to give phthalocyanine **5**, which can be reacted with C₆₀ and *N*-methylglycine in a subsequent step. The synthesis of (4-formylcatechol)-2,3-(tetra-tert-butylphthalocyaninato)titanium(IV) **5** had previously been described by Hanack to proceed in 86% yield.^{17d} This product was shown to react with C₆₀ and *N*-methylglycine affording dyad **1** in 40% yield after purification by column chromatography.

The most remarkable feature in the ¹H NMR spectrum of dyad **1** is the strong shielding of the aromatic protons of the chelating moiety with regard to the chemical shifts of the aromatic protons of compound **4b**. This shielding is a consequence of the ring-current effect of the phthalocyanine core. The pyrrolidine signature appears between $\delta = 4.6$ and 3.5 ppm as two doublets and one singlet—see Figure 2.

The relative intensity of all the signals proves that dyad **1** is present as the major compound, but plausibly a minor amount of the titanium(IV) oxide phthalocyanine **2** remains as a by-product. The broad signals at 6.0, 4.9 and 4.4 ppm that get sharper at higher temperature were assigned to the three protons belonging to the catechol unit—see Figure 3.

The absorption spectrum of **1** in THF exhibits typical bands for C₆₀ and phthalocyanine and nearly represents a linear combination of the spectra of phthalocyanine **2** and the fullerene-containing catechol ligand **4a**—see Figure 4.

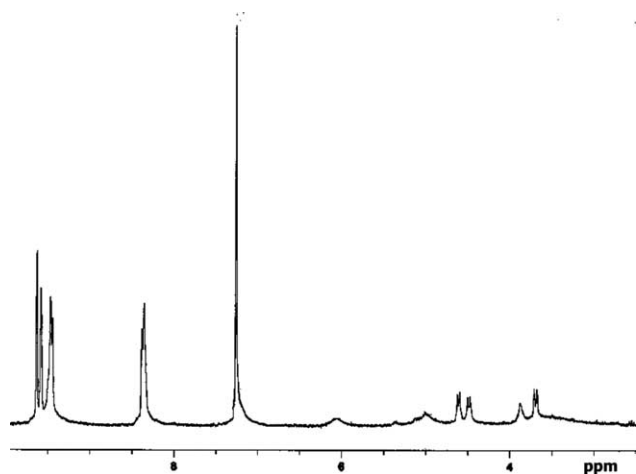


Figure 2. ^1H NMR (CDCl_3 , 300 MHz, 298 K) spectrum of compound **1**.

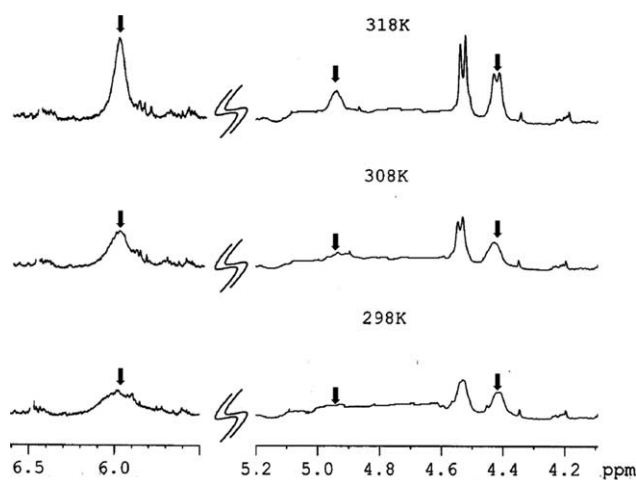


Figure 3. ^1H NMR (CDCl_3 , 500 MHz) spectrum of compound **1** at different temperatures.

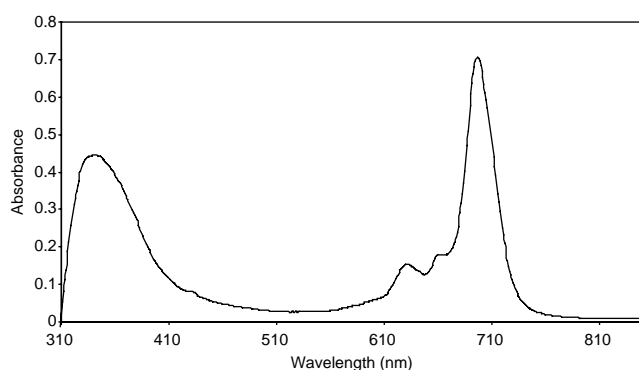


Figure 4. UV/vis (THF , 8.9×10^{-6} mol L^{-1}) spectrum of compound **1**.

MS analyses confirms all structures and the homogeneity of the samples.¹⁶ The MALDI-TOF spectrum—Figure 5—shows the molecular peak (M^+ and $[\text{M}+\text{H}]^+$) at $m/z = 1668.2$ and 1669.2 . In addition, peaks are found that correspond to a loss of C_{60} $[\text{M}-\text{C}_{60}]^+$ at $m/z = 947.3$ and that of titanium(IV) oxide phthalocyanine $[\text{PcTiO}]^+$ at $m/z = 800.4$. It is likely that the latter represents a minor impurity or arise from fragmentation and/or oxidation processes taking place during the MS experiment.

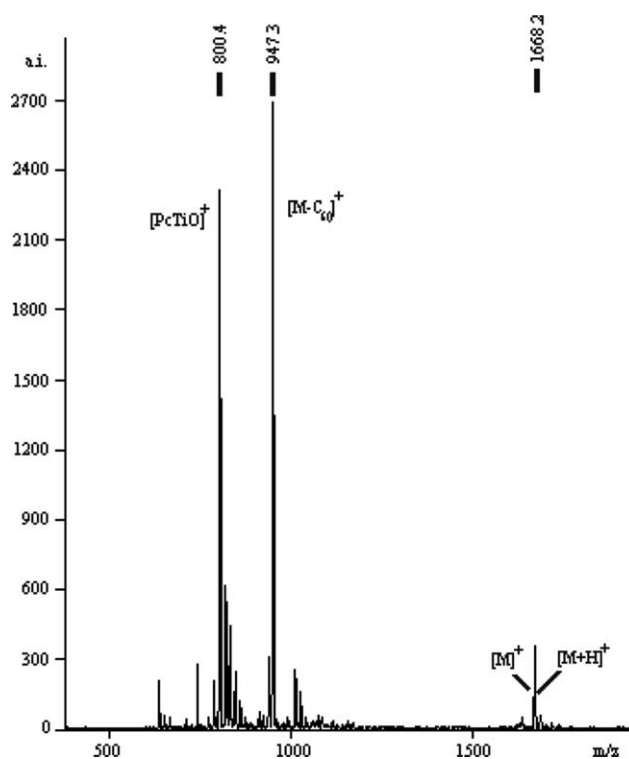


Figure 5. MALDI-TOF mass spectrum of compound **1**.

Our work was complemented by photophysical measurements, in which the photoexcited states of PcTi in **1**, **2**, and **5** were probed by fluorescence (i.e., Fig. 6) and transient absorption (i.e., Fig. 7) techniques. Relatively to PcH_2 (unsubstituted non-metallated Pc) employed as internal reference, the fluorescence quantum yields decreased in the overall order PcH_2 (0.67) > **2** (0.16) > **5** (0.12) > **1** (0.06)—all values were determined in THF . Obviously, insertion of a titanium central metal and, subsequently, replacing the axially-coordinated oxygen in **2** with a catechol-type ligand in **5** leaves already appreciable impact on the fluorescence quantum yields. Due to the redox-inactivity of catechol the observed quenching must, however, be based on energy dissipation with the surrounding solvent environment. On the contrary, in **1** the presence of the electron accepting

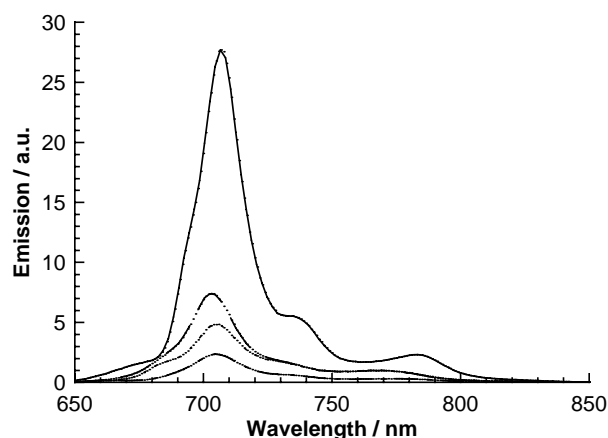


Figure 6. Room temperature fluorescence spectra of PcH_2 (solid line), **2** (dashed line), **5** (dotted line), and **1** (dashed-dotted line) in THF recorded with solutions that exhibit optical absorptions at the 631 nm excitation wavelength of 0.2.

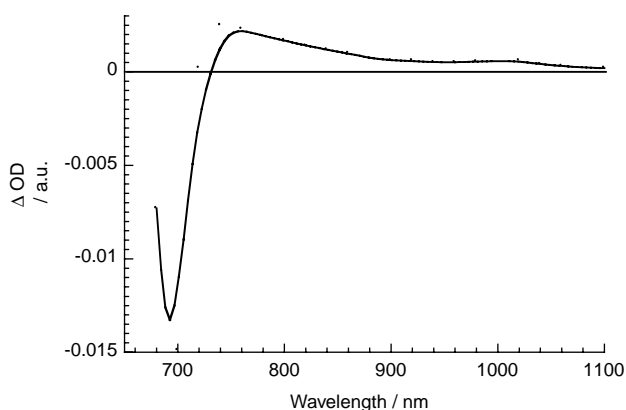


Figure 7. Differential absorption spectrum (visible and near-infrared) obtained upon nanosecond flash photolysis (355 nm) of **1** in nitrogen saturated THF with a 50 ns time delay at room temperature.

C_{60} is likely to result in an intramolecular electron transfer—*vide infra*. Still, when comparing the PcTi fluorescence of **5** and **1** only small differences (i.e., factor of approximately 2) are noted throughout the solvents. This indicates slow electron transfer deactivation due to weak electronic coupling between the electron donating macrocycle and the electron accepting C_{60} .

Conclusive information about the photoproducts came from transient absorption spectroscopy. In particular, with the help of femtosecond and nanosecond laser pulses at 387 and 355 nm, respectively, the fate of the PcTi singlet excited states was probed. Regarding the femtosecond transient absorption measurements of **1**, immediately, after the laser excitation, the strong singlet–singlet absorptions of the PcTi start to grow in. This confirms, despite the presence of C_{60} , the successful formation of the PcTi singlet excited states. Instead of seeing, however, slow ISC dynamics, as the singlet–singlet absorptions decay in the presence of the electron accepting C_{60} with accelerated dynamics (i.e., $1.9 \pm 0.5 \times 10^9 \text{ s}^{-1}$). Spectroscopically, the transient absorption changes, taken after the singlet decay, bear no resemblance with any known triplet excited state (i.e., PcTi and C_{60}).

For example, transient absorption changes were recorded that correspond to the radical ion pair features. The one-electron reduced C_{60} radical ion is identified by its NIR fingerprint at 1000 nm, while the one-electron oxidized PcTi exhibits bleaching of the ground state absorption at 700 nm and new transient absorption in the 740–840 nm region.¹⁸

Analysis of the metastable radical ion pair features revealed charge separation lifetimes in deoxygenated THF and dichloromethane of 1740 ns (i.e., $5.7 \times 10^5 \text{ s}^{-1}$) and 1230 ns (i.e., $8.1 \times 10^5 \text{ s}^{-1}$), respectively.¹⁹ Beneficial for the long radical ion pair lifetime are dynamics that are located in the inverted region of the Marcus parabola and weak donor–acceptor couplings.

3. Conclusion

In conclusion, a novel donor–acceptor ensemble was devised incorporating a PcTi and C_{60} . Once photoexcited

with visible light, an energetically low lying (i.e., $\sim 1.0 \text{ eV}$) and long-lived (i.e., up to 1740 ns) charge-separated state is generated via a rapid intramolecular electron transfer process.

4. Experimental

4.1. General

UV/vis spectra were recorded with a Hewlett-Packard 8453 instrument. MALDI-TOF MS were recorded with a Bruker Reflex III spectrometer. NMR spectra were recorded with a BRUKER AC-300 instrument and a BRUKER DRX-500 instrument. Column chromatographies were carried out on silica gel Merck-60 (230–400 mesh, 60 Å), and TLC on aluminum sheets precoated with silica gel 60 F_{254} (Merck). Chemicals were purchased from Aldrich Chemical Co. and used as received without further purification.

4.1.1. Protected catechol- C_{60} **4b.** A mixture of 3, 4-diacetoxybenzaldehyde **3b** (0.23 g, 1.01 mmol), C_{60} (0.8 g, 1.11 mmol) and *N*-methylglycine (0.45 g, 5.1 mmol) in 1,2-dichlorobenzene (50 mL) was heated at 140 °C under an argon atmosphere for 2 h. After cooling to room temperature, a solid was precipitated by addition of hexane, filtered and purified by column chromatography on a silica gel using toluene–tetrahydrofuran (9/1) as eluent to yield the monoadduct derivative **4b** in the form of a brown solid (0.3 g, 32%). UV/vis (THF, $3.9 \times 10^{-6} \text{ mol L}^{-1}$) λ_{max} [nm] (ϵ in $\text{M}^{-1} \text{ cm}^{-1}$): 213 (2.4×10^5), 255 (2.0×10^5), 312 (6.7×10^4), 330 (6.3×10^4); $^1\text{H NMR}$ (300 MHz, CDCl_3 , 298 K): δ (ppm) = 7.85–7.6 (br, 3H, Ar), 5.02 (d, 1H, $J = 9.45 \text{ Hz}$, CH_2 pyr), 4.98 (s, 1H, CH pyr), 4.32 (d, 1H, $J = 9.45 \text{ Hz}$, CH_2 pyr), 2.89 (s, 3H, CH_3N), 2.32 (s, 6H, CH_3COO); MALDI-TOF MS: $m/z = 970.0$ [$\text{M} + \text{H}$] $^+$, calcd for $\text{C}_{73}\text{H}_{16}\text{NO}_4$: 970.1.

4.1.2. Catechol- C_{60} **4a.** The monoadduct **4b** (0.3 g, 0.34 mmol) was added to a mixture of acetic acid (4.1 mL) and hydrochloric acid (2.2 mL) in 1,2-dichlorobenzene (8 mL) and refluxed for 72 h. Subsequently, the solvent was removed in vacuo and the resulting solid was purified by column chromatography on a silica gel using toluene–tetrahydrofuran (9/1) as eluent to yield **4a** as a brown solid (0.18 g, 65%). UV/vis (THF) λ_{max} [nm] (ϵ in $\text{M}^{-1} \text{ cm}^{-1}$): 213 (2.4×10^5), 255 (2.0×10^5), 312 (6.7×10^4), 330 (6.3×10^4); MALDI-TOF MS: $m/z = 885.2$ [M] $^+$, $m/z = 886.2$ [$\text{M} + \text{H}$] $^+$, calcd for $\text{C}_{69}\text{H}_{12}\text{NO}_2$: 886.1.

4.1.3. PcTiO- C_{60} dyad **1. Route 1.** A mixture of **4a** (22 mg, 0.025 mmol) and **2** (20 mg, 0.025 mmol) in tetrahydrofuran (10 mL) was refluxed under an argon atmosphere for 2 h. Subsequently, the solvent was removed in vacuo and the crude material was purified by column chromatography on a silica gel using chloroform as eluent, to obtain **1** in the form of a green solid (26 mg, 62%).

Route 2. A mixture of **5** (10 mg, 0.011 mmol), C_{60} (8.6 mg, 0.012 mmol) and *N*-methylglycine (4.8 mg, 0.054 mmol) in 1, 2-dichlorobenzene (8 mL) was heated at 140 °C under an argon atmosphere for 3 h. Subsequently, the solvent was removed in vacuo and the resulting solid was purified by

column chromatography on a silica gel using toluene as eluent to obtain **1** as a green solid (40%).

UV/vis (THF, 8.9×10^{-6} mol L⁻¹) λ_{\max} [nm] (ϵ in M⁻¹ cm⁻¹): 341 (5.0×10^4), 631 (1.6×10^4), 697 (7.9×10^4); ¹H NMR (300 MHz, CDCl₃, 298 K): δ (ppm) = 9.63–9.44 (m, 8H), 8.38–8.36 (m, 4H), 6.21–5.99 (br, 1H, H_a), 5.11–4.87 (br, 1H, H_b), 4.61 (d, $J=9.15$ Hz, 1H, CH₂ pyr), 4.49 (d, $J=8.0$ Hz, 1H, H_c), 3.89–3.86 (br, CH pyr), 3.69 (d, $J=9.15$ Hz, 1H, CH₂ pyr), 2.11 (s, 3H, CH₃N), 1.86 (s, 36H, C(CH₃)₃); MALDI-TOF MS: $m/z=1668.2$ [M]⁺, $m/z=1669.2$ [M+H]⁺, calcd for C₁₁₇H₅₈N₉O₂Ti: 1669.4.

Acknowledgements

This work was supported by Ministerio de Educación y Ciencia (Spain), Comunidad de Madrid (Spain) and the Office of Basic Energy Sciences of the U.S. Department of Energy (NDRL 4653), through grants CTQ-2005-08933-BQU, GR/MAT/0513/2004 and SFB 583, respectively. We would also like to thank Christian G. Claessens for useful discussions.

References and notes

- (a) Leznoff, C. C.; Lever, A. B. P. In *Phthalocyanines: Properties and Applications, Vols. 1–4*; VCH: Weinheim, 1989, 1993, 1996. (b) McKeown, N. B. *Phthalocyanine Materials: Synthesis, Structure and Function*; Cambridge University Press: Cambridge, 1998. (c) Kadish, K. M.; Smith, K. M.; Guillard, R. In *The Porphyrin Handbook, Vols. 15–20*; Academic: San Diego, 2003.
- (a) de la Torre, G.; Vázquez, P.; Agulló-López, F.; Torres, T. *J. Mater. Chem.* **1998**, *8*, 1671. (b) de la Torre, G.; Vázquez, P.; Agulló-López, F.; Torres, T. *Chem. Rev.* **2004**, *104*, 3723.
- (a) González, A.; Vázquez, P.; Torres, T. *Tetrahedron Lett.* **1999**, *40*, 3263. (b) Gouloumis, A.; Liu, S.-G.; Vázquez, P.; Echegoyen, L.; Torres, T. *Chem. Commun.* **2001**, 399. (c) González, A.; Vázquez, P.; Torres, T.; Guldi, D. M. *J. Org. Chem.* **2003**, *68*, 8635.
- (a) El-Khouly, M. E.; Ito, O.; Smith, P. M.; D' Souza, F. *J. Photochem. Photobiol. C: Photochem. Rev.* **2004**, *5*, 79. (b) Gust, D.; Moore, T. A.; Moore, A. L. *J. Photochem. Photobiol. B: Photochem. Rev.* **2000**, *58*, 63.
- (a) Guldi, D. M.; Gouloumis, A.; Vázquez, P.; Torres, T. *Chem. Commun.* **2002**, 2056. (b) Guldi, D. M.; Ramey, J.; Martínez-Díaz, M. V.; de la Escosura, A.; Torres, T.; Da Ros, T.; Prato, M. *Chem. Commun.* **2002**, 2774. (c) Guldi, D. M.; Zilbermann, I.; Gouloumis, A.; Vázquez, P.; Torres, T. *J. Phys. Chem. B* **2004**, *108*, 18485.
- (a) Imahori, H.; Tamaki, K.; Guldi, D. M.; Luo, C.; Fujitsuka, M.; Ito, O.; Sakata, Y.; Fukuzumi, S. *J. Am. Chem. Soc.* **2001**, *123*, 2607. (b) Imahori, H.; Tkachenko, V.; Vehmanen, V.; Tamaki, K.; Lemmetyinen, H.; Sakata, Y.; Fukuzumi, S. *J. Phys. Chem. A* **2001**, *105*, 1750. (c) Guldi, D. M.; Martin, N. *J. Mat. Chem.* **2002**, *12*, 1978. (d) Guldi, D. M. *Chem. Soc. Rev.* **2002**, *31*, 22. (e) Imahori, H.; Sakata, Y. *Eur. J. Org. Chem.* **1999**, 2445.
- (a) Loi, M. A.; Denk, P.; Hoppe, H.; Neugebauer, H.; Winder, C.; Meissner, D.; Brabec, C. J.; Sariciftci, N. S.; Gouloumis, A.; Vázquez, P.; Torres, T. *J. Mat. Chem.* **2003**, *13*, 700. (b) Neugebauer, H.; Loi, M. A.; Winder, C.; Sariciftci, N. S.; Gerullo, C.; Gouloumis, A.; Vázquez, P.; Torres, T. *Sol. Energy Mater. Sol. Cells* **2004**, *83*, 201.
- (a) Lehn, J.-M. *Supramolecular Chemistry-Concepts and Perspectives*; VCH: Weinheim, 1995. (b) Constable, E. C. *Prog. Inorg. Chem.* **1994**, *42*, 67. (c) Piguet, C.; Bernardinelli, G.; Hopfgartner, G. *Chem. Rev.* **1997**, *97*, 2005. (d) Saalfrank, R. W.; Bernt, I. *Curr. Opin. Solid State Mater. Sci.* **1998**, *3*, 407. (e) Williams, A. F. *Pure Appl. Chem.* **1996**, *68*, 1285. (f) Dietrich-Buchecker, C.; Rapenne, G.; Sauvage, J. P. *Coord. Chem. Rev.* **1999**, *186*, 167. (g) Fujita, M. *Acc. Chem. Res.* **1999**, *32*, 53. (h) Olenyuk, B.; Fechtenkötter, A.; Stang, P. J. *J. Chem. Soc. Dalton Trans.* **1998**, 1707. (i) Caulder, D. L.; Raymond, K. N. *Acc. Chem. Res.* **1999**, *32*, 975. (j) Hannon, M. J.; Painting, C. L.; Plummer, E. A.; Childs, L. J.; Alcock, N. W. *Chem. Eur. J.* **2002**, *8*, 2225. (k) Claessens, C. G.; Torres, T. *J. Am. Chem. Soc.* **2002**, *124*, 14522. (l) Claessens, C.; Torres, T. *Chem. Commun.* **2004**, 1298. (m) Albrecht, M. *Chem. Soc. Rev.* **1998**, *27*, 281. (n) Albrecht, M.; Janser, I.; Runsink, J.; Raabe, G.; Weis, P.; Fröhlich, R. *Angew. Chem., Int. Ed.* **2004**, *43*, 6662.
- Claessens, C. G.; Gouloumis, A.; Barthel, M.; Chen, Y.; Martin, G.; Agulló-López, F.; Ledoux-Rak, I.; Zyss, J.; Hanack, M.; Torres, T. *J. Porphyrins Phthalocyanines* **2003**, *7*, 291.
- Zyss, J.; Ledoux, I. *Chem. Rev.* **1994**, *94*, 77.
- Claessens, C. G.; González-Rodríguez, D.; Torres, T. *Chem. Rev.* **2002**, *102*, 835.
- Palomares, E.; Martínez-Díaz, M. V.; Haque, S. A.; Torres, T.; Durrant, J. R. *Chem. Commun.* **2004**, 2112.
- Nazeeruddin, Md. K.; Humbphry-Baker, R.; Grätzel, M.; Murrer, B. A. *Chem. Commun.* **1998**, 719.
- (a) González-Rodríguez, D.; Torres, T.; Guldi, D. M.; Rivera, J.; Herranz, M. A.; Echegoyen, L. *J. Am. Chem. Soc.* **2004**, *126*, 6301. (b) Iglesias, R. S.; Claessens, C. G.; Torres, T.; Aminur Rahman, G. M.; Guldi, D. M. *Chem. Commun.* **2005**, *16*, 2113.
- Guldi, D. M.; Gouloumis, A.; Vázquez, P.; Torres, T.; Georgaliskas, V.; Prato, M. *J. Am. Chem. Soc.* **2005**, *127*, 5811.
- After completion of this work, a communication on the preparation of **1** following one of the two procedures described here by us (the non-convergent one, see Scheme 1, route 2) has been reported (Chen, Y.; El-Khouly, M. E.; Sasaki, M.; Araki, Y.; Ito, O. *Org. Lett.* **2005**, *7*, 1613). The data given there for compound **1** do not fully fit our own data, particularly MS and NMR data. The simplest explanation is that the compound reported there is not pure enough, probably, according to our experience, as a consequence of impurities already present in the starting (tBu)₄PcTiO. Indeed, looking carefully at the MS-spectrum reported in the mentioned communication (Fig. 2, supporting information), additional peaks not belonging to compound **1** (compare with our Fig. 5) can be observed at m/z 1434 and 1634, which we have identified as typical by-products produced in the preparation of (tBu)₄PcTiO.
- (a) Goedken, V. L.; Dessy, G.; Ercolani, C.; Fares, V.; Gastaldi, L. *Inorg. Chem.* **1985**, *24*, 991. (b) Kobayashi, N.; Muranaka, A.; Ishii, K. *Inorg. Chem.* **2000**, *39*, 2256. (c) Kobayashi, N.; Muranaka, A. *Chem. Commun.* **2000**, 1855. (d) Barthel, M.; Hanack, M. *J. Porphyrins Phthalocyanines* **2000**, *4*, 635. (e) Barthel, M.; Dini, D.; Vagin, S.; Hanack, M. *Eur. J. Org. Chem.* **2002**, *22*, 3756.
- Guldi, D. M.; Prato, M. *Acc. Chem. Res.* **2000**, *33*, 695.
- Due to the competitive singlet excited state decay, that is, intersystem crossing and electron transfer, the nanosecond spectrum contains some contributions of the PcTi triplet excited state.

Synthesis and characterization of new trinitrofluorene–fullerene dyads as photosensitizers in photorefractive polymer materials. Redox behavior and charge-transfer properties

Luis Martín-Gomis,^a Javier Ortiz,^a Fernando Fernández-Lázaro,^a Ángela Sastre-Santos,^{a,*} Bevan Elliott^b and Luis Echegoyen^{b,*}

^a*División de Química Orgánica, Instituto de Bioingeniería, Universidad Miguel Hernández, Elche 03202 (Alicante), Spain*

^b*Department of Chemistry, Clemson University, 219 Hunter Laboratories, Clemson, SC 29634, USA*

Received 21 June 2005; revised 20 July 2005; accepted 22 July 2005

Available online 1 December 2005

Abstract—Novel trinitrofluorene–C₆₀ dyads bearing a flexible polyether chain have been synthesized and characterized. UV–vis spectroscopy and cyclic voltammetric results indicate that there is no interaction in their ground states. NMR and electrochemical studies of dyads **2** and **3** in solution indicate the existence of a charge-transfer complex between the trinitrofluorene moieties and *N*-ethylcarbazol. Preliminary results of the photorefractive performance of these compounds as sensitizers in polymer composites based on poly(*N*-vinylcarbazole) are similar to that of C₆₀, but with shorter response times and slightly lower gain coefficients.

© 2006 Elsevier Ltd. All rights reserved.

1. Introduction

The photorefractive (PR) effect can be defined as a spatial modulation of the index of refraction induced by a light intensity pattern.¹ In order to display this effect, the material must show both photoconductivity and a high nonlinear response and/or birefringence. Under these conditions, an internal redistribution of charges takes place, which induces the variation on the refraction index. This effect was first observed in 1966 in an inorganic crystal of LiNbO₃.² To name a few, other examples of inorganic materials in which the PR effect has been examined are BaTiO₃, KNbO₃, Bi₁₂SiO₂₀ (BSO), GaAs.³ The applications of these materials have been limited by the difficulty in crystal growing and sample preparation. Organic PR materials, however, exhibit refractive index modulations and gain coefficients which are superior compared to their inorganic counterparts, and due to their versatility, lower cost and easier fabrication and processability are becoming promising candidates for applications in optical holographic data storage, real-time image processing, and phase conjugation.⁴

The PR effect was observed for the first time in organic crystals in 1990 by Sutter and Günter.⁵ Just one year later, in 1991, Ducharme et al. demonstrated PR effect in a polymeric composite.⁶ Since then, several research groups have focused experimental efforts on the development of PR polymers.⁷

The physical phenomena necessary to achieve photorefractivity are photoinduced charge generation, charge transport, trapping, and electrooptical nonlinearity. One of the major approximations to achieve PR effect in organic materials, and the most widely spread indeed, is the use of functional polymers (which are responsible of one or two of the functional properties needed to originate PR effect) doped with molecules responsible for the rest of the functional properties.⁸ The use of polymeric compositions has led to materials with high gain coefficients (*I*), in the order of 200 cm⁻¹, and with diffraction efficiencies (*η*) of 100%.⁹ However, the most important drawback of organic polymers is the low speed of grating formation, that is, the high response time (*τ*), although some compositions are described having speeds in the range of 10 ms. Research has been focused in the design of improved nonlinear optical chromophores,¹⁰ in order to increase *I* while maintaining high values of *η*, but little effort has been paid to increase the photorefractive speed. Moerner and Twieg demonstrated that, at least in certain cases, speed is limited by photoconductivity (*σ_{ph}*) rather than by chromophore orientation.¹¹ Due to the fact that photoconductivity

Keywords: Fullerene; Trinitrofluorene; Electrochemistry; Charge-transfer complexes.

* Corresponding authors. Tel.: +34 96 6658408; fax: +34 96 6658351 (A.S.); tel.: +1 864 6565017; fax: +1 864 6566613 (L.E.); e-mail addresses: asastre@umh.es; luis@clemson.edu

depends on charge generation efficiency, the improvement of the latter should enhance the performance of the material. This leads to the need of a better photosensitizer.

Charge photogeneration efficiency is governed by a competition between recombination of a charge carrier with its parent countercharge, termed geminate recombination, and electron–hole pair dissociation.¹² In order to favor the second possibility, a fast electron transfer from another molecule must take place, that is, an adequate relationship between HOMO and LUMO orbitals of photosensitizer and charge transporting molecule must be achieved. The best performance is obtained by optimizing the charge-transfer (CT) properties between a given sensitizer (an acceptor-like molecule or moiety) and its parent transport molecule (a donor-like molecule or moiety). To date, the most successful class of sensitizers incorporated into photoconductor polymers have been C₆₀ and 2,4,7-trinitro-9-fluorenone (TNF).

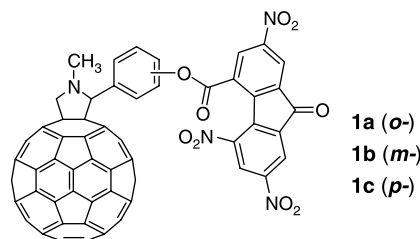
C₆₀ is a unique molecule with a vast array of interesting properties. Among them, it is an outstanding photosensitizer due to its long-lived triplet state, high absorption, the presence of various stable oxidation states and the low degree of charge recombination.¹³ It has been found that the photogeneration efficiency of poly(*N*-vinylcarbazole) (PVK) based composites sensitized with C₆₀ is higher than when other sensitizers are used.¹⁴ On the other hand, the synthesis of functionalized C₆₀ is becoming more and more interesting due to their remarkable optoelectronic properties.¹⁵ C₆₀ derivative [6,6]-phenyl-C₆₁-butyric acid methyl ester ([6,6]-PCBM) has been used as photosensitizer in different photoconducting polymer-based composites presenting a poor charge-carrier generation efficiency.¹⁶

On the other hand, TNF is a strong electron acceptor, even better than C₆₀, a characteristic which allows the formation of robust CT complexes with charge transporting molecules of the carbazol series.¹⁷ Thus, the covalent linking of C₆₀ and trinitrofluorenone would render a photosensitizer combining the exceptional properties of each moiety, and is expected to optimize the charge-transfer properties with PVK increasing the charge generation efficiency.

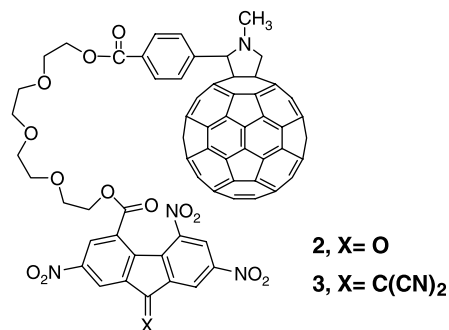
Another point of interest related to the photosensitizer is the laser wavelength needed for the photoexcitation. The election depends on the absorption profiles of the photosensitizer and the nonlinear chromophore. In fact, absorption due to the chromophore should be avoided to reduce losses, while the photosensitizer should show enough absorption to allow charge generation, but not enough to minimize losses. Therefore, photosensitizers in the near infrared domain are interesting. Moreover, sensitizing in this region allows to use commercially-available, cheap lasers, which is a major consideration if these materials are to be used in technologically useful devices. While C₆₀ and TNF are irradiated at 633 nm, 2,4,7-trinitro-9-dicyanomethylenfluorene (TNDCF)^{18–20} operates at 830 nm. [6,6]-PCBM was also utilized as a near infrared photosensitizer in photorefractive polymer composites.²¹

With all these considerations in mind, we decided to synthesize dyads containing C₆₀ and TNF moieties

covalently linked in order to benefit of a synergic collaboration between them. Thus, C₆₀–TNF dyads **1a–c** were synthesized in which the distance between the two subunits was regulated by the position of the phenyl substitution from *ortho* to *meta* to *para*. The photorefractive properties of their compositions with PVK and 4-piperidindicyanostyrene (PDCST) were determined and compared with those of the corresponding compositions bearing C₆₀. While the composite with C₆₀ showed a slightly higher gain coefficient, the compositions with **1a–c**, proved to be 2–3 times faster in grating formation, that is, they had a response time 2–3 times lower when high electric fields were applied.²²



This very positive result prompted us to redesign our photosensitizers. Here we present the synthesis, characterization and electrochemical study of dyads **2** and **3** bearing a flexible polyether chain to enhance the solubility in organic solvents, to avoid phase segregation, to allow a better interaction between the moieties, to introduce the possibility of ion complexation, and prepared to work in the near infrared region.

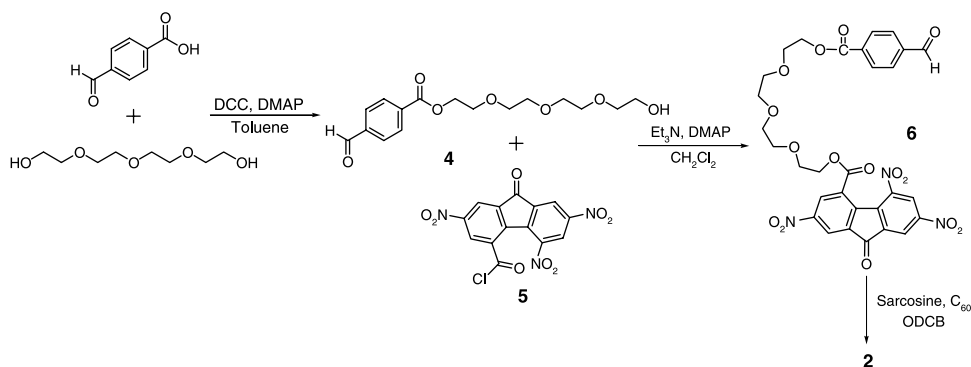


2. Results and discussion

2.1. Synthesis of 2,5,7-trinitrofluorenone–C₆₀ (TNF–C₆₀) and 2,5,7-trinitro-9-dicyanomethylenfluorene–C₆₀ (TNDCF–C₆₀) dyads

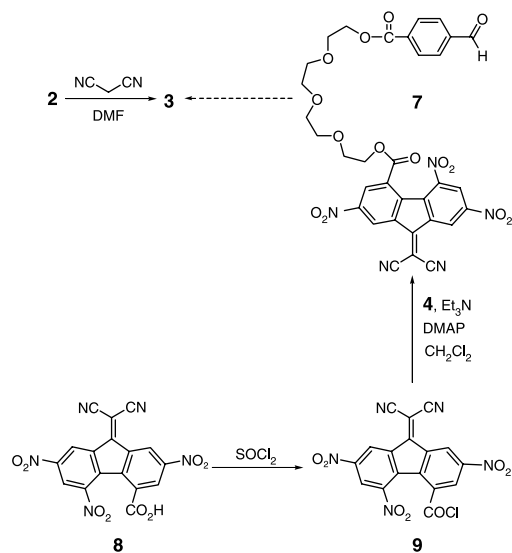
The hydroxyformyl derivative **4** was prepared by esterification of 4-formylbenzoic acid with tetraethylene glycol using *N,N*-dicyclohexylcarbodiimide (DCC) and 4-(dimethylamino)pyridine (DMAP). The reaction of **4** with 2,5,7-trinitrofluorenone-4-carboxylic acid chloride (**5**)²³ in CH₂Cl₂ in the presence of DMAP and triethylamine afforded the corresponding trinitrofluorenone derivative **6**.

Finally, the synthesis of C₆₀–TNF derivative **2** was accomplished by Prato's reaction²⁴ from aldehyde **6** with sarcosine and C₆₀ (Scheme 1).



Scheme 1.

The synthesis of the 2,5,7-trinitro-9-dicyanomethylenfluorene- C_{60} dyad **3** was envisaged by two different ways (Scheme 2): (a) Knoevenagel reaction of TNF- C_{60} derivative **2** and malononitrile, and (b) Prato reaction between the trinitrodicyanomethylenfluorene aldehyde derivative **7**, sarcosine and C_{60} . Thus, reaction of TNF- C_{60} derivative **2** with an excess of malononitrile in DMF at room temperature over a long duration afforded the adduct TNDCF- C_{60} **3** in a good (64%) yield.

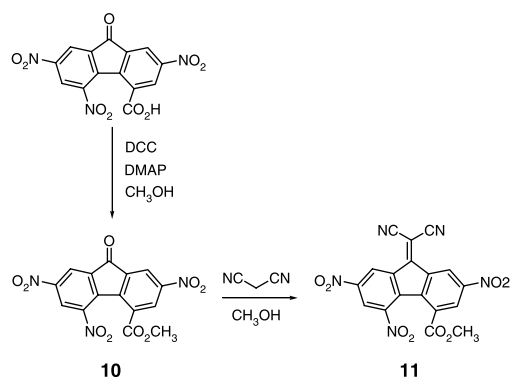


Scheme 2.

The synthesis of 2,5,7-trinitro-9-dicyanomethylenfluorene-4-carboxylic acid chloride (**9**) from 2,5,7-trinitro-9-dicyanomethylenfluorene-4-carboxylic acid (**8**) and $SOCl_2$, followed by the condensation with the hydroxyaldehyde **4** to obtain the formyldicyanomethylenfluorene derivative **7** in a one pot reaction (Scheme 2), gave rise to a mixture of aldehydes **6** and **7** difficult to separate by column chromatography. This hydrolysis of the dicyanomethylenfluorene aldehyde **7** to the fluorenone aldehyde **6** could be attributed to the presence of acidic conditions while generating the acid chloride derivative.

For comparison purposes, methyl 2,5,7-trinitrofluorenone-4-carboxylate (**10**, MTNFC) and methyl 2,5,7-trinitrodicyanomethylenfluorene-4-carboxylate (**11**, MTNDM) were prepared in a good yield from 2,5,7-trinitrofluorenone-4-carboxylic acid in methanol using DCC and DMAP,

following a modification of a previously reported procedure (Scheme 3).



Scheme 3.

The new dyads TNF- C_{60} were fully characterized by 1H , ^{13}C NMR, MALDI-TOF mass spectrometry and elemental analysis.

2.2. Spectroscopic studies

Figure 1 shows the UV-vis spectra of **2** and **3**, together with that of C_{60} for comparison in toluene. The UV-vis spectra of **2** and **3** display strong absorptions due to both the TNF and the fullerene moieties. Both compounds show a typical 1,2-methanofullerene UV-vis spectrum, with a sharp absorption at 430 nm and a broader band at around 700 nm^{24b} showing

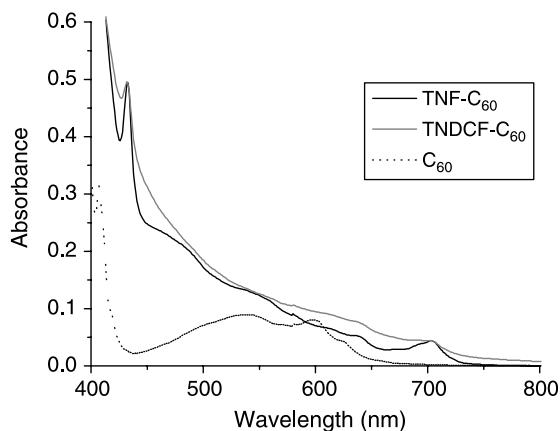


Figure 1. UV-vis spectra of compounds TNF- C_{60} **2** and TNDCF- C_{60} **3** (solid line) and C_{60} (dotted line) in toluene as solvent.

that both the TNF and the C₆₀ moieties have little or no electronic influence on each other in the ground state. It is noteworthy that compound **3** has a stronger absorption in the near IR than compound **2**, because as a consequence, the former could have application as near infrared photosensitizer.

In the presence of an excess of alkaline metal cations (Na⁺, K⁺ and Rb⁺) the UV–vis spectra of dyads **2** and **3** do not show any shift in the absorption bands. A similar result was observed in ¹H NMR. Both observations suggest the absence of a ground state interaction between the two chromophores although the complex was formed.

We also studied the ability of the TNF–C₆₀ dyads **2** and **3** to form intermolecular CT complexes with donors in solution using *N*-ethylcarbazole (ECZ) as the π-donor. The appearance of additional bands in the visible region was not detected maybe due to the overlapping with the signals corresponding to the C₆₀ derivative. However, addition of different amounts of ECZ to a solution of dyads **2** and **3** in CDCl₃ produced pronounced changes both in chemical shifts and splitting patterns for protons within the fluorene ring moiety as observed by ¹H NMR (Figs. 2 and 3).

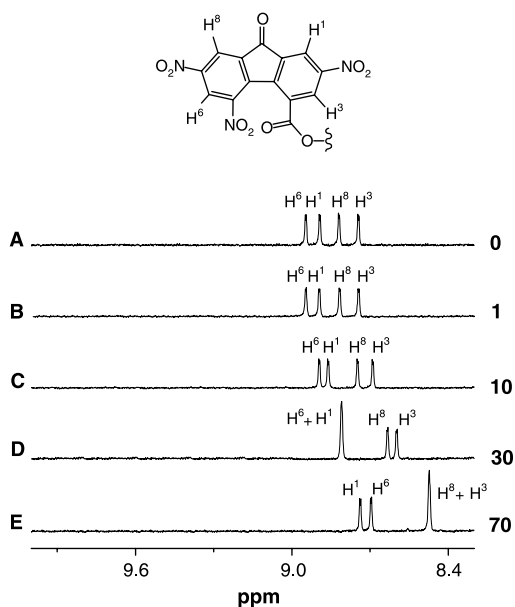


Figure 2. ¹H NMR spectra (CDCl₃, 500 MHz, 298 K) of the TNF–C₆₀ dyad **2** (A), a 1:1 mixture of **2**:ECZ (B), a 1:10 mixture of **2**:ECZ (C), a 1:30 mixture of **2**:ECZ (D) and a 1:70 mixture of **2**:ECZ (E).

Upon addition of the same excess of ECZ larger chemical shifts were observed for the aromatic fluorene protons in compound **3** than in compound **2**. For example, addition of 70 equiv of ECZ give rise to a $\Delta\delta H^8 = 1.03$ ppm for TNDCF–C₆₀ dyad **3** and to a $\Delta\delta H^8 = 0.36$ ppm for TNF–C₆₀ dyad **2**. These observations agree with the higher electron withdrawing character of the TNDCF moiety versus the TNF, leading to a better interaction with ECZ.

Interestingly, no change could be detected by ¹H NMR in the signals corresponding to the fulleropyrrolidine moiety in both dyads **2** and **3** upon addition of ECZ, even to a 100-fold

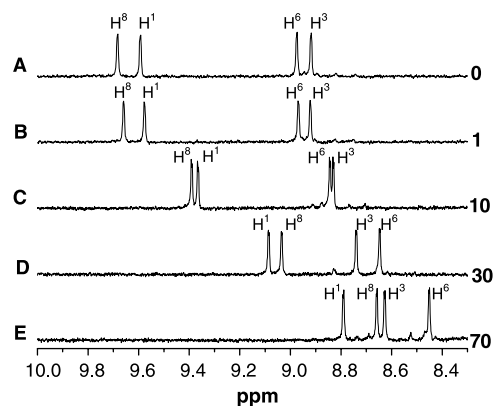
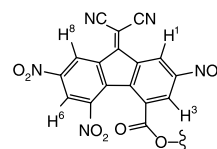


Figure 3. ¹H NMR spectra (CDCl₃, 500 MHz, 298 K) of the TNDCF–C₆₀ dyad **3** (A), a 1:1 mixture of **3**:ECZ (B), a 1:10 mixture of **3**:ECZ (C), a 1:30 mixture of **3**:ECZ (D) and a 1:70 mixture of **3**:ECZ (E).

excess. This result is attributable either to an interaction of the ECZ with another fragment of the ball or to the absence of any interaction at all between ECZ and the ball. To provide insight into this question, we performed ¹³C NMR in CDCl₃ at room temperature of dyads **2** and **3** each in the presence of a 100-fold excess of ECZ. As already pointed out for ¹H NMR, a dramatic effect on the chemical shifts of the signals corresponding to the fluorene moieties was observed ($\Delta\delta \approx 1.5$ and $\Delta\delta \approx 4$ ppm for complexes **2**:ECZ and **3**:ECZ, respectively), while only minor changes could be detected in the signals corresponding to the fulleropyrrolidine moiety ($\Delta\delta \approx 0.4$ ppm). For the rest of atoms of the ball, the displacement was so small, if any, that the close proximity of such a number of signals precluded any assignment. Thus, it seems that the ECZ interacts only with the fluorene moiety.

The association constants of the TNF–C₆₀:ECZ and TNDCF–C₆₀:ECZ complexes were determined at room temperature from the dependence of the δH_{obs}^8 on the

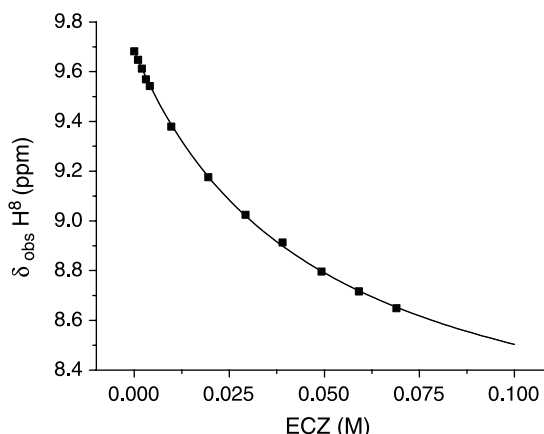


Figure 4. Plot of $\delta_{\text{obs}} H^8$ of compound **3** as a function of the concentration of *N*-ethylcarbazole, where $[3]_0 = 0.83 \times 10^{-3}$ M. Iterative fitting (solid line) affords $\Delta\delta_{\text{max}} = 1.73$ and the association constant $K_a = 21.3 \pm 0.6 \text{ M}^{-1}$.

concentration of ECZ at a constant concentration of 10^{-3} M of dyads **2** and **3** by the use of an iterative nonlinear regression analysis (Fig. 4). The maximum complexation-induced shifts $\Delta\delta_{\max}$ and the association constants K_a (Table 1) were determined by the use of ^1H NMR titration experiments as described in the Section 4.

Table 1. Comparison of $\Delta\delta_{\max}$ and K_a (M^{-1}) for the formation of the complexes between TNF- C_{60} :ECZ and TND CF- C_{60} :ECZ in CDCl_3 at 25°C

	$\Delta\delta_{\max}$	K_a (M^{-1})
TNF- C_{60}	0.59 (H^1)	5.1 ± 0.9
	1.14 (H^3)	
	0.98 (H^6)	
	1.36 (H^8)	
TND CF- C_{60}	1.36 (H^1)	21.3 ± 0.6
	0.50 (H^3)	
	0.93 (H^6)	
	1.73 (H^8)	

Job plot analyses were performed to determine the stoichiometry of the complexes **2**:ECZ and **3**:ECZ. In the case of the **3**:ECZ complex, the plot of the mole fraction χ ($\chi = [\text{ECZ}]_0 / ([\mathbf{3}]_0 + [\text{ECZ}]_0)$) versus the mole fraction multiplied by the complexation-induced ^1H NMR shift of ECZ, $\chi\Delta\delta_{\text{obs}}$, shows a maximum at $\chi = 0.5$, which equates to a 1:1 stoichiometry for the complex (Fig. 5).

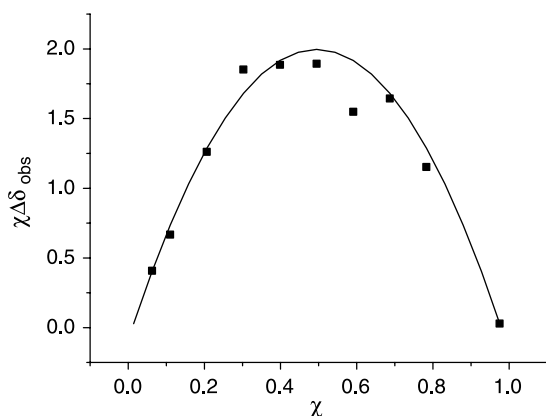


Figure 5. The job plot of the complex TND CF- C_{60} :ECZ (proton H^8 of **3** is reported). The fitting line is calculated with the parameters: $\Delta\delta_{\max} = 1.73$ and $K_a = 21.3 \pm 0.6 \text{ M}^{-1}$.

2.3. Square wave voltammetric studies

Electrochemical Osteryoung square wave voltammetric (OSWV) studies of compounds **2** and **3**, and their respective reference compounds **10** and **11**, showed reduction waves corresponding to both the TNF and *N*-methylfulleropyrrolidine moieties (see Table 2, Figs. 6 and 7). In both cases, the first reduction was slightly shifted anodically, suggesting only a very small interaction between the

Table 2. Electrochemical reduction data for fluorene derivatives

	Reduction (V) versus Fc				
	$E_{1/2}(\text{I})$	$E_{1/2}(\text{II})$	$E_{1/2}(\text{III})$	$E_{1/2}(\text{IV})$	$E_{1/2}(\text{V})$
2	-0.80	-1.01	-1.13	-1.56	-1.94
10	-0.82	-1.17	-2		
3	-0.45	-1.02	-1.56	-1.78	
11	-0.46	-1.03	-1.81		

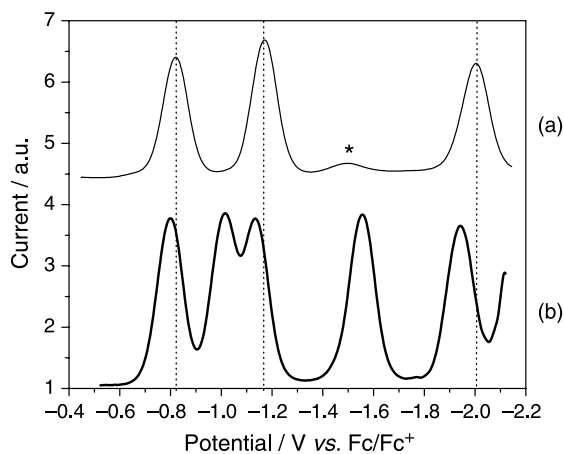


Figure 6. OSWV of (a) compound **10** and (b) compound **2** (impurity designated by *).

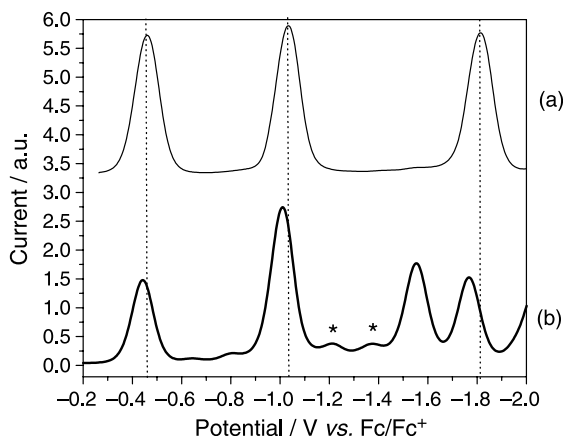


Figure 7. OSWV of (a) compound **11** and (b) compound **3** (impurities designated by *).

fullerene and the substituent. For compound **3**, the second TNF-based reduction overlapped with the first fullerene-based reduction, resulting in a 2-electron wave.

The sequential addition of *N*-ethylcarbazole, up to a 100-fold excess, to the solution of compound **2** (Fig. 8) caused a cathodic shift in the first TNF-based reduction of

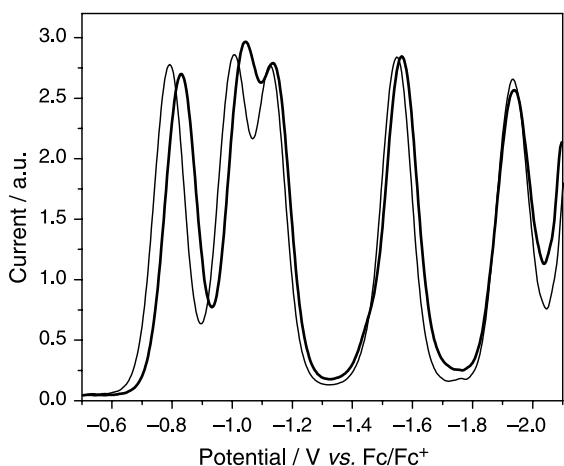


Figure 8. OSWV of compound **2** before (thin line) and after (thick line) addition of 100 equiv of *N*-ethylcarbazole.

38 mV, thus confirming the NMR results suggesting that the π -donor formed a complex with **2**, which increased the electron density on the TNF moiety. The first fullerene-based reduction was also shifted by a comparable amount, which is reasonable since C_{60} is also known to be a good electron acceptor. As a result, the already reduced fluorenone moiety would exhibit a strongly decreased ability to interact with ECZ. In the case of compound **3**, after addition of 100 equiv of *N*-ethylcarbazole (Fig. 9), the first TNF-based reduction was shifted cathodically by 70 mV, while the fullerene-based first reduction did not shift. This observation can be rationalized on the basis of the increased electron-accepting ability due to the two cyano groups on the TNF moiety, which increases dramatically its electron-accepting ability as compared to that of compound **2** to such an extent, that the reduced fluorene moiety still interacts stronger with ECZ than the fullerene one does.

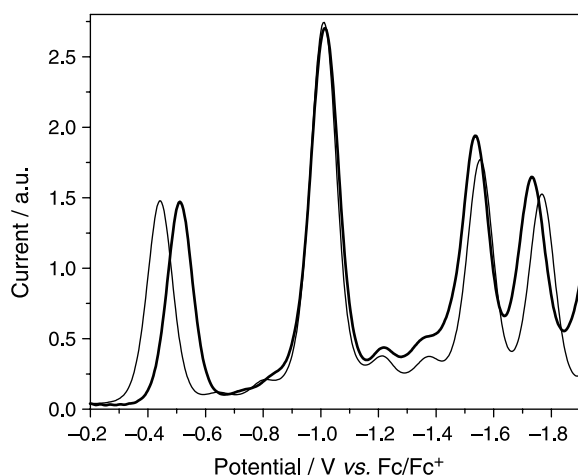


Figure 9. OSWV of compound **3** before (thin line) and after (thick line) addition of 100 equiv of *N*-ethylcarbazole.

Preliminary results of the photorefractive performance of these compounds as sensitizers in polymer composites based on poly(*N*-vinylcarbazole) are similar to that of C_{60} , but with shorter response times and slightly lower gain coefficients. A more detailed study of these experiments is out of the scope of this article and will be published elsewhere.

3. Conclusion

We have prepared and characterized the new C_{60} -fluorene adducts **2** and **3** bearing a flexible chain. UV–vis and electrochemical studies indicate the absence of interaction between both moieties in the ground state. However, addition of an excess of the π -donor ECZ to solutions of compounds **2** and **3** affords complexes in which the carbazole interacts with the fluorene moiety, as detected by NMR and OSWV.

4. Experimental

4.1. General

The chemical reagents were purchased reagent-grade from Aldrich Corporation and were used without further

purification unless otherwise stated. All solvents were purified using standard procedures. Column Chromatography: SiO_2 (40–63 μ m). TLC plates coated with SiO_2 60F254 were visualized by UV light. UV–vis spectra were recorded with a Helios Gamma spectrophotometer and IR spectra with a Nicolet Impact 400D spectrophotometer. NMR spectra were measured with a Bruker AC 300 and with a Bruker AVANCE DRX-500. Mass spectra were obtained from a Bruker Reflex III matrix-assisted laser desorption/ionization time of flight (MALDI-TOF) spectrometer. Elemental analysis were performed on a Thermo Finnigan Flash 1112 CHN elemental analyzer.

The electrochemical measurements of compounds **2** and **3** including the model compounds methyl 2,5,7-trinitrofluorenone-4-carboxylate (**10**, MTNFC) and methyl 2,5,7-trinitrodicyanomethylenfluorene-4-carboxylate (**11**, MTNDCM), were performed in a one-compartment electrochemical cell in oxygen-free tetrahydrofuran (THF) using a CHI 660A electrochemical workstation. For all experiments, a 0.7 mM sample concentration was analyzed. A platinum disk (1 mm) was used as the working electrode and a platinum wire as the counter electrode. A silver wire immersed in the solvent mixture with 0.1 M supporting electrolyte and 0.01 M $AgNO_3$ separated from the bulk of the solution by a Vycor glass served as the pseudo-reference electrode. The supporting electrolyte used was tetrabutylammonium hexafluorophosphate, TBAPF₆ (0.1 M, Fluka, >99%). Ferrocene was added as an internal standard, and all redox waves are referenced to the Fc/Fc^+ redox couple.

4.1.1. Synthesis of 11-hydroxy-3,6,9-trioxaundecyl *p*-formylbenzoate (4**).** A mixture of 4-formylbenzoic acid (1.97 g, 13.1 mmol), tetraethylene glycol (13.47 g, 69.4 mmol), *N,N*-dicyclohexylcarbodiimide (2.79 g, 13.5 mmol), 4-(dimethylamino)pyridine (160 mg, 1.3 mmol) and dry toluene (50 ml) was stirred at 65 °C under argon atmosphere for 5 h. The reaction mixture was cooled and a white solid was filtered off. The organic solution obtained was washed several times with water, dried, concentrated under vacuum, and the crude material was purified by column chromatography (eluent CH_2Cl_2/CH_3OH 15:1) to afford the product as a colourless oil (2.54 g, 59%). FT-IR (Ge-ATR) ν_{max} 3457, 1738, 1367, 1216, 1102 cm^{-1} . 1H NMR (300 MHz, $CDCl_3$) δ 10.09 (s, 1H, CHO), 8.21 (d, 2H, $J=8.6$ Hz, H-Ar), 7.94 (d, 2H, $J=8.6$ Hz, H-Ar), 4.51 (t, 2H, $J=4.8$ Hz, $O=C-OCH_2$), 3.84 (t, 2H, $J=4.8$ Hz, $O=C-OCH_2-CH_2$), 3.58–3.71 (m, 13H, OH, $6 \times O-CH_2$). ^{13}C NMR (125 MHz, $CDCl_3$) δ 191.5, 165.3, 138.9, 134.8, 130.0, 129.2, 72.3, 70.4, 70.3, 70.0, 68.8, 64.4, 61.4. FAB-MS: m/z : 327 ($[M+1]^+$). Anal. Calcd for $C_{16}H_{22}O_7$: C, 58.89; H, 6.80. Found: C, 58.14; H, 7.04.

4.1.2. Synthesis of 11-(2',5',7'-trinitrofluorenone-4'-carboxylate)-3,6,9-trioxaundecyl *p*-formylbenzoate (6**).** A mixture of **4** (790 mg, 2.1 mmol), 2,5,7-trinitrofluorenone-4-carboxylic acid chloride (690 mg, 2.1 mmol), DMAP (20 mg, 0.2 mmol) and dichloromethane (25 ml) was stirred for 48 h under argon at room temperature. The reaction mixture was washed with sodium bicarbonate solution and water. After the solvent was evaporated under reduced pressure, the crude material was purified by column

chromatography (eluent hexane/ethyl acetate 1:2), to yield the pure product as an orange oil (500 mg, 35%). FT-IR (Ge-ATR) ν_{\max} 1724, 1540, 1347 1277, 1103 cm^{-1} . ^1H NMR (300 MHz, CDCl_3) δ 10.07 (s, 1H, CHO), 8.94 (d, 1H, $J=2.1$ Hz, H-TNF), 8.89 (d, 1H, $J=2.2$ Hz, H-TNF), 8.81 (d, 1H, $J=2.1$ Hz, H-TNF), 8.75 (d, 1H, $J=2.2$ Hz, H-TNF), 8.18 (d, 2H, $J=8.3$ Hz, H-Ar), 7.92 (d, 2H, $J=8.3$ Hz, H-Ar), 4.53–4.47 (m, 4H, $2\times\text{CH}_2\text{-O-C=O}$), 3.88–3.83 (m, 4H, $2\times\text{CH}_2\text{-CH}_2\text{-O-C=O}$), 3.73–3.67 (m, 8H, $4\times\text{CH}_2\text{-O}$). ^{13}C NMR (125 MHz, CDCl_3) δ 191.3, 184.6, 165.0, 164.1, 149.2, 149.0, 146.2, 143.1, 139.3, 138.8, 138.5, 137.4, 134.6, 131.7, 130.4, 129.9, 129.1, 125.0, 122.1, 121.4, 70.3, 68.7, 68.2, 65.8, 64.3. MALDI-TOF (dithranol+NaI): m/z : 690 ($[\text{M}+\text{Na}]^+$). Anal. Calcd for $\text{C}_{30}\text{H}_{25}\text{N}_3\text{O}_{15}$: C, 53.98; H, 3.78; N, 6.29. Found: C, 53.9; H, 4.13; N, 5.72.

4.1.3. Synthesis of 11-(2',5',7'-trinitrofluorenone-4'-carboxylate)-3,6,9-trioxaundecyl *p*-(*N*-methyl-3,4-fulleropyrrolidin-2-yl)benzoate (2). A mixture of C_{60} (180 mg, 0.3 mmol), **6** (500 mg, 0.7 mmol), sarcosine (70 mg, 0.8 mmol) and 1,2-dichlorobenzene (30 ml) was heated under argon for 7 h. After flash chromatography (eluent toluene/diethyl ether 9:1) the desired product was isolated as a brown solid (110 mg, 31%). ^1H NMR (300 MHz, CDCl_3) δ 8.95 (d, 1H, $J=2.1$ Hz, H-TNF), 8.90 (d, 1H, $J=2.2$ Hz, H-TNF), 8.82 (d, 1H, $J=2.1$ Hz, H-TNF), 8.75 (d, 1H, $J=2.2$ Hz, H-TNF), 8.10 (d, 2H, $J=8.1$ Hz, H-Ar), 7.90 (m, 2H, H-Ar), 5.01 (d, 2H, $J=9.6$ Hz, CHHN), 5.00 (s, 1H, CHN), 4.53 (t, 2H, $J=4.7$ Hz, TNF-CO₂-CH₂), 4.43 (t, 2H, $J=4.9$ Hz, Ar-CO₂-CH₂), 4.29 (d, 1H, $J=9.6$ Hz, CHHN) 3.91–3.63 (m, 12H, $6\times\text{CH}_2\text{-O}$), 2.81 (s, 3H, N-CH₃). ^{13}C NMR (125 MHz, CDCl_3) δ 184.6, 166.2, 164.3, 155.9, 153.7, 152.8, 152.6, 149.4, 149.1, 147.3, 147.2, 146.4, 146.3, 146.2, 146.1, 146.0, 145.9, 145.7, 145.6, 145.4, 145.3, 145.2, 145.1, 144.6, 144.5, 144.3, 143.2, 143.1, 142.9, 142.6, 142.5, 142.4, 142.1, 142.0, 141.9, 141.8, 141.7, 141.6, 141.5, 140.1, 139.8, 139.4, 139.3, 138.5, 137.4, 136.9, 136.3, 135.9, 135.6, 131.8, 130.5, 130.0, 129.0, 125.0, 122.2, 21.6, 83.0, 70.6, 70.0, 69.0, 68.5, 66.1, 65.8, 64.1, 40.0. FT-IR (KBr) ν_{\max} 1736, 1613, 1594, 1538, 1343, 1093 cm^{-1} . MALDI-TOF (dithranol): m/z : 1415 ($[\text{M}+1]^+$), 695 ($[\text{M}+1]^+ - \text{C}_{60}$). Anal. Calcd for $\text{C}_{92}\text{H}_{30}\text{N}_4\text{O}_{14}$: C, 78.08; H, 2.14; N, 3.96. Found: C, 78.12; H, 2.55; N, 3.90.

4.1.4. Synthesis of 11-(2',5',7'-trinitro-9'-dicyanomethylenfluorene-4'-carboxylate)-3,6,9-trioxaundecyl *p*-(*N*-methyl-3,4-fulleropyrrolidin-2-yl)benzoate (3). A mixture of **2** (30 mg, 0.02 mmol), malononitrile (20 mg, 0.3 mmol) and dry DMF (20 ml), was stirred under argon at room temperature for 72 h. The reaction mixture was diluted with ethyl acetate and washed with brine and water. The organic layer was dried, concentrated and the residue was washed with methanol and diethyl ether to give the product as a brown solid (20 mg, 64%). FT-IR (KBr) ν_{\max} 2199, 1720, 1611, 1537, 1342, 1104 cm^{-1} . ^1H NMR (300 MHz, CDCl_3) δ 9.69 (d, 1H, $J=1.8$ Hz, H-TNDCF), 9.60 (d, 1H, $J=2.0$ Hz, H-TNDCF), 8.98 (d, 1H, $J=1.9$ Hz, H-TNDCF), 8.93 (d, 1H, $J=2.1$ Hz, H-TNDCF), 8.06 (d, 2H, $J=8.9$ Hz, H-Ar), 7.91 (m, 2H, H-Ar), 4.99 (d, 2H, $J=9.6$ Hz, CHHN), 4.99 (s, 1H, CHN), 4.48 (t, 2H, $J=4.8$ Hz, TNDCF-CO₂-CH₂, Ar-CO₂-CH₂), 4.35 (t, 2H, $J=5.1$ Hz), 4.28 (d, 1H, $J=9.6$ Hz, CHHN) 3.84–3.62 (m, 12H,

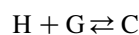
$6\times\text{CH}_2\text{-O}$), 2.81 (s, 3H, N-CH₃). ^{13}C NMR (125 MHz, CDCl_3) δ 166.3, 164.1, 156.0, 153.8, 153.3, 152.9, 152.7, 149.2, 148.7, 147.3, 146.9, 146.5, 146.3, 146.2, 146.1, 145.9, 145.8, 145.7, 145.5, 145.4, 145.3, 145.2, 145.1, 144.7, 144.5, 144.4, 144.3, 143.1, 143.0, 142.6, 142.5, 142.2, 142.1, 142.0, 141.9, 137.6, 137.0, 136.4, 136.0, 135.9, 135.6, 132.5, 130.3, 130.0, 129.0, 124.6, 123.7, 123.0, 111.5, 111.4, 83.1, 70.7, 70.0, 69.2, 69.1, 68.6, 66.3, 65.8, 64.1, 40.0. MALDI-TOF (dithranol): m/z : 1463 ($[\text{M}+1]^+$), 743 ($[\text{M}+1]^+ - \text{C}_{60}$). Anal. Calcd for $\text{C}_{95}\text{H}_{30}\text{N}_6\text{O}_{13}$: C, 77.98; H, 2.07; N, 5.74. Found: C, 77.47; H, 2.36; N, 5.81.

4.1.5. Synthesis of methyl 2,5,7-trinitrofluorenone-4-carboxylate (10). To a mixture of 2,5,7-trinitrofluorenone-4-carboxylic acid (400 mg, 1.1 mmol), DCC (280 mg, 1.4 mmol), DMAP (10 mg, 0.1 mmol) in 10 ml of dry toluene, 0.45 ml (11.1 mmol) of dry methanol were slowly added. The mixture was heated at 65 °C for 20 h under argon atmosphere. After the solvent was evaporated, the crude material was purified by column chromatography (eluent hexane/ethyl acetate 4:1), to afford the pure product as a pale yellow solid (210 mg, 51%). FT-IR (KBr) ν_{\max} 1736, 1616, 1594, 1543, 1345 cm^{-1} . ^1H NMR (300 MHz, CDCl_3) δ 8.97 (d, 1H, $J=2.1$ Hz, H-TNF), 8.89 (d, 1H, $J=2.2$ Hz, H-TNF), 8.83 (d, 1H, $J=2.1$ Hz, H-TNF), 8.78 (d, 1H, $J=2.2$ Hz, H-TNF), 4.00 (s, 3H, CO₂CH₃).

4.1.6. Synthesis of methyl 2,5,7-trinitro-9-dicyanomethylenfluorene-4-carboxylate (11). A mixture of **10** (100 mg, 0.3 mmol), malononitrile (100 mg, 1.5 mmol) and dry DMF (5 ml), was stirred and heated at 50 °C, under argon, for 14 h. The reaction mixture was diluted with ethyl acetate and the residue was washed with brine and water. The organic layer was dried, concentrated and washed with methanol to give the product as a yellow-green solid (70 mg, 62%). FT-IR (KBr) ν_{\max} 2232, 1734, 1602, 1536, 1350 cm^{-1} . ^1H NMR (300 MHz, CDCl_3) δ 9.70 (d, 1H, $J=1.9$ Hz, H-TNDCF), 9.62 (d, 1H, $J=2.0$ Hz, H-TNDCF), 9.00 (d, 1H, $J=1.8$ Hz, H-TNDCF), 8.91 (d, 1H, $J=2.0$ Hz, H-TNDCF), 4.00 (s, 3H, CO₂CH₃).

Determination of K_a : ^1H NMR titration method

The uncomplexed dyad (Host, H) and ethylcarbazole (Guest, G) are in equilibrium with the 1:1 complex (C)



The association constant K_a is defined by Eq. 1

$$K_a = \frac{[\text{C}]}{[\text{H}][\text{G}]} \quad (1)$$

and can be rewritten as Eq. 2

$$K_a = \frac{[\text{C}]}{([\text{H}_0] - [\text{C}])([\text{G}_0] - [\text{C}])} \quad (2)$$

where $[\text{H}_0]$ and $[\text{G}_0]$ are the starting concentrations of the dyad and *N*-ethylcarbazole, respectively.

Under fast-exchange conditions the observed chemical shift δ_{obs} of the dyad will be an averaged value between free (δ_{H})

and complexed host (δ_C), as we can see in Eq. 3

$$\delta_{\text{obs}} = \frac{[\text{H}]}{[\text{H}] + [\text{C}]} \delta_{\text{H}} + \frac{[\text{C}]}{[\text{H}] + [\text{C}]} \delta_{\text{C}} \quad (3)$$

Combination of Eqs. 2 and 3 leads to Eq. 4, that gives the observed shift for the host as a function of $[\text{H}_0]$, $[\text{G}_0]$, δ_{H} , δ_{C} and K_{a}

$$\delta_{\text{obs}} = \delta_{\text{H}} - \frac{\delta_{\text{H}} - \delta_{\text{C}}}{2} \left[\left(1 + \frac{[\text{G}_0]}{[\text{H}_0]} + \frac{1}{[\text{H}_0]K_{\text{a}}} \right) - \sqrt{\left(1 + \frac{[\text{G}_0]}{[\text{H}_0]} + \frac{1}{[\text{H}_0]K_{\text{a}}} \right)^2 - 4 \frac{[\text{G}_0]}{[\text{H}_0]}} \right] \quad (4)$$

The NMR studies were performed on a Bruker Avance DRX 500 MHz at 298 ± 1 K in CDCl_3 , the concentration of the dyad was fixed at 0.99×10^{-3} and 0.83×10^{-3} M for dyad **2** and dyad **3**, respectively. Increasing amounts of ECZ were added while the total volume of the resulting solution was kept constant (0.5 ml), and the complexation-induced shift of the protons of the fluorene moiety (δ_{obs}) were observed. Fitting of these data to the 1:1 binding isotherm by iterative methods²⁵ delivered the parameters K_{a} and $\Delta\delta_{\text{max}} = \delta_{\text{H}} - \delta_{\text{C}}$.

Acknowledgements

This work was financially supported by the Spanish Government (CICYT Grant no. BQU2002-04513-C02-01), by the Spanish Generalitat Valenciana (Grant no. CTIDIA/2002/33) and by the US National Science Foundation (Grant CHE-0135786).

References and notes

- Solymar, L.; Webb, D. J.; Grunnet-Jepsen, A. In *The Physics and Applications of Photorefractive Materials*; Clarendon: Oxford, 1996.
- Ashkin, A.; Boyde, G. D.; Dziedzic, J. M.; Smith, R. G.; Ballman, A. A.; Levenstein, J. J.; Nassau, K. *Appl. Phys. Lett.* **1966**, *9*, 72–74.
- Günter, P.; Huignard, J.-P. In *Photorefractive Materials and Their Applications I and II*; Springer: Berlin, 1988.
- Ostroverkhova, O.; Moerner, W. E. *Chem. Rev.* **2004**, *104*, 3267–3314.
- Sutter, K.; Günter, P. *J. Opt. Soc. Am. B* **1990**, *7*, 2274–2278.
- Ducharme, S.; Scott, J. C.; Twieg, R. J.; Moerner, W. E. *Phys. Rev. Lett.* **1991**, *66*, 1846–1849.
- (a) Moerner, W. E.; Silence, S. M. *Chem. Rev.* **1994**, *94*, 127–155. (b) Moerner, W. E.; Grunnet-Jepsen, A.; Thompson, C. L. *Ann. Rev. Mater. Sci.* **1997**, *27*, 585–623.
- (a) Wang, Y.; West, R.; Yuang, C.-H. *J. Am. Chem. Soc.* **1993**, *115*, 3844–3845. (b) Wang, Y. *Nature (London)* **1992**, *356*, 585–587. (c) Silence, S. M.; Walsh, C. A.; Scott, J. C.; Moerner, W. E. *Appl. Phys. Lett.* **1992**, *61*, 2967–2969.
- Meerholz, K.; Volodin, B. L.; Sandalphon, B.; Kippelen, B.; Peyghambarian, N. *Nature (London)* **1994**, *371*, 497–500.
- Würthner, F.; Wortmann, R.; Meerholz, K. *Chem. Phys. Chem.* **2002**, *3*, 17–31.
- (a) Wright, D.; Diaz-Garcia, M. A.; Casperson, J. D.; DeClue, M.; Moerner, W. E.; Twieg, R. J. *Appl. Phys. Lett.* **1998**, *73*, 1490–1492. (b) Diaz-Garcia, M. A.; Wright, D.; Casperson, J. D.; Smith, B.; Glazer, E.; Moerner, W. E.; Sukhomlinova, L. I.; Twieg, R. J. *Chem. Mater.* **1999**, *11*, 1784–1791.
- Pope, M.; Swenberg, C. E. In *Electronic Processes in Organic Crystals and Polymers*; Oxford University Press: New York, 1999.
- Martín, N.; Sánchez, L.; Illescas, B.; Pérez, I. *Chem. Rev.* **1998**, *98*, 2527–2548 and references cited therein.
- Hendrickx, E.; Zhang, Y. D.; Ferrio, K. B.; Herlocker, J. A.; Anderson, J.; Armstrong, N. R.; Mash, E. A.; Persoons, A. P.; Peyghambarian, N.; Kippelen, B. *J. Mater. Chem.* **1999**, *9*, 2251–2258.
- Guldi, D. M.; Martín, N. In *Fullerenes: From Synthesis to Optoelectronic Properties*; Kluwer Academic: The Netherlands, 2002.
- Mecher, E. H.; Brauchle, C.; Horhold, H. H.; Hummelen, J. C.; Meerholz, K. *Phys. Chem. Chem. Phys.* **1999**, *1*, 1749–1756.
- Perepichka, D. F.; Bryce, M. R.; Perepichka, I. F.; Lyubchik, S. B.; Christensen, C. A.; Godbert, N.; Batsanov, A. S.; Levillain, E.; McInnes, J. L. E.; Zhao, J. P. *J. Am. Chem. Soc.* **2002**, *124*, 14227–14238 and references cited therein.
- Kippelen, B.; Marder, S. R.; Hendrickx, E.; Maldonado, J. L.; Guillemet, G.; Volodin, B. L.; Steele, D. D.; Enami, Y.; Sandalphon, Y. J.; Wang, J. F.; Rockel, H.; Erskine, L.; Peyghambarian, N. *Science* **1998**, *279*, 54–57.
- Würthner, F.; Yao, S.; Schilling, J.; Wortmann, R.; Redi-Abshiro, M.; Mecher, E.; Gallego-Gomez, F.; Meerholz, K. *J. Am. Chem. Soc.* **2001**, *123*, 2810–2824.
- Ostroverkhova, O.; Wright, D.; Gubler, U.; Moerner, W. E.; He, M.; Sastre-Santos, A.; Twieg, R. *Adv. Funct. Mater.* **2002**, *12*, 621–629.
- Mecher, E.; Gallego-López, F.; Tillmann, H.; Hörhold, H.-H.; Hummelen, J. C.; Meerholz, K. *Nature (London)* **2002**, *418*, 959–964.
- Ortiz, J.; Fernández-Lázaro, F.; Sastre-Santos, A.; Quintana, J. A.; Villalvilla, J. M.; Boj, P.; Díaz-García, M. A.; Rivera, J.; Stepleton, S.; Cox, C.; Echegoyen, L. *Chem. Mat.* **2004**, *16*, 5021–5026.
- (a) Sulzberg, T.; Cotter, R. J. *J. Org. Chem.* **1970**, *35*, 2762–2769. (b) Perepichka, I. F.; Popov, A. F.; Orekhova, T. V.; Bryce, M. R.; Vdovichenko, A. N.; Batsanov, A. S.; Goldenberg, L. M.; Howard, J. A. K.; Sokolov, N. I.; Megson, J. L. *J. Chem. Soc., Perkin Trans. 2* **1996**, 2453–2469. (c) Perepichka, D. F.; Bryce, M. R.; Batsanov, A. S.; McInnes, E. J. L.; Zhao, J. P.; Farley, R. D. *Chem. Eur. J.* **2002**, *8*, 4656–4669.
- (a) Maggini, M.; Scorrano, G.; Prato, M. *J. Am. Chem. Soc.* **1993**, *115*, 9798–9799. (b) Prato, M.; Maggini, M. *Acc. Chem. Res.* **1998**, *31*, 519–526.
- A nonlinear regression analysis of Eq. 4 (see Section 4) was performed by the program OriginPro 7.5.

Self-organization of amphiphilic [60]fullerene derivatives in nanorod-like morphologies

Peter Brough, Davide Bonifazi and Maurizio Prato*

Dipartimento di Scienze Farmaceutiche, Università degli Studi di Trieste, 34127 Trieste, Italy

Received 3 June 2005; revised 29 August 2005; accepted 30 August 2005

Available online 21 November 2005

Abstract—The aggregation of four charged C₆₀ derivatives has been investigated by TEM, SEM, and AFM microscopies. In all molecules a short aliphatic chain connects an ammonium cation to the fullerene sphere and the variation comes in the counter anions. In water, remarkably well-ordered structures that resemble nanorod-like aggregates are formed. They have a cross-sectional diameter and a length in the range of 30–60 and 100–900 nm, respectively. Fine topographical details were elucidated by atomic force microscopy, in which the height was found up to a maximum of 60 nm. Scanning electron microscopy shows that both the shape and morphology of the aggregates is consistent throughout the material. Nanorods of uniform shape were obtained with all molecules containing inorganic counter anions, BF₄⁻, Br⁻, and Cl⁻.

© 2005 Elsevier Ltd. All rights reserved.

1. Introduction

Since the discovery of C₆₀ by Kroto and Smalley¹ this novel form of carbon has enticed the curiosity of both the chemist and physicist owing to its fascinating properties that hold great promise in many emerging areas of nanotechnology.^{2,3,4} Amongst these are the exceptional electron acceptor properties⁵ and the absorption across the UV–vis wavelength region.⁶ Many synthetic modifications have been developed in order to harness and tailor the molecular properties of C₆₀ by attaching covalently linked addends.^{7,8,9} Control of structure superior to the molecular level involves supramolecular chemistry, which employs non-covalent bonding interactions and has been used to design and build molecules that organize themselves into regular organic nanostructures.¹⁰

Self-organization of molecules in 1-, 2-, and 3-dimensional nanostructures is a recognized goal, with the aim of controlling both the shape and physical properties of new materials.¹¹ Fullerenes, with their highly hydrophobic carbon cage, are well suited to self-organization, and clusters of aggregated pristine fullerenes and their derivatives are already known especially in polar solvents.^{12,13,14,15} Thus, tailoring these groups and study of the consequent effects on the material is a pre-requisite for the design of shaped and size-controlled assemblies.

Studies of macro assemblies have begun appearing, in which a variety of structures have been observed from amphiphilic fullerene molecules. Nakashima has described rod-like ensembles, that is, ‘nanorods’, from a quaternary alkyl bromide addend giving particle sizes in the range of 150–600 nm.¹⁶ In general, the solubility of functionalized fullerenes tends to be poor in water so that ultrasound is often used as an aid to dissolution. However, Tour found that sonication tended to shorten or disrupt the assemblies of fullerene-*N,N*-dimethylpyrrolidinium iodide, which otherwise gave long nanorods of up to 70 μm when prepared by two phase solvent mixtures.¹⁷ Additionally vesicle-type assemblies were obtained by tuning the conditions of sonication. Other functional species have been appended to fullerene amphiphiles in our laboratory, such as porphyrin and phthalocyanine moieties.^{18,19} Interestingly, when aggregated, the latter molecule has been shown to have fast charge separation and very slow charge recombination in photochemical processes. These groups also provided an extra element of ordering, by π-stacking, and in both of these cases finely shaped rod-like materials were obtained. It is clear that there are many factors that could regulate the assembly process, hydrophobic–hydrophilic balances, solvents polarities, and concentration amongst others. Addressing some of these fundamental questions, De Maria et al. have studied the solvent-induced aggregation effect of fullerenes in aqueous solutions, and also in mixed organic/aqueous systems.^{20,21} Spectroscopic evidence inferred that the polarity of the solvent medium and also the presence of H₂O influenced the formation and structural properties of the assemblies.

Keywords: Fullerenes; Organization; Aggregates; Microscopy-AFM-TEM-STM.

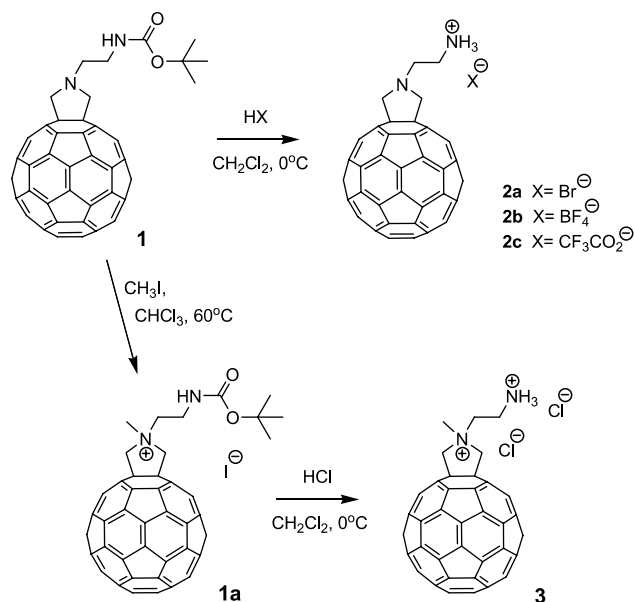
* Corresponding author. Fax: +39 040 52572;

e-mail addresses: prato@units.it; prato@univ.trieste.it

In this work, we report the preparation of uniformly shaped rods at the nanometer scale, containing amphiphilic fullerene derivatives bearing one or two ammonium moieties. All the structures were analyzed in detail by means of TEM, AFM, and SEM microscopies. Additionally, the influence of counter anion in the structural morphology was also investigated.

2. Results and discussion

The well established 1,3-dipolar cycloaddition of azo-methine ylides to C_{60} was used to synthesize precursor compound **1**.⁷ The *tert*-butoxy carbonyl protecting group was easily cleaved with various acids, giving ammonium-bearing fullerenes **2a–c** (Scheme 1). For compound **3**, the



Scheme 1. Synthesis of short-chain fullerene amphiphiles **2a–c** and **3**.

pyrrolidine group was first methylated using methyl iodide prior to the deprotection step.

The essential characteristics of compounds **2a–c** are the presence of at least one positive charge and the hydrophobic fullerene cage. The balance of hydrophobicity–hydrophilicity gives rise to molecules that are partially water soluble and having a propensity to aggregate. We synthesized several compounds bearing different counterions because of their significant influence in the aggregation process.²² Included in these is the trifluoroacetate anion, which is quite different in size and polarity to the inorganic ions.

The TEM samples of **2a–c** and **3** were prepared by sonication of the appropriate compound in water. Following centrifugation, removing undissolved solid, the suspensions were deposited on grids, which were dried and then examined under a TEM microscope.

In general, under TEM microscopy all fullerene compounds, except **2c**, gave aggregates resembling rods or blocks with nanoscopic dimensions. Representative images are shown in Figure 1 and more have been deposited in the Supplementary information. Several zones of every grid were checked for consistency and these aggregates were found to be distributed homogeneously throughout. In the case of molecule **2b** containing the BF_4^- counterion, the nanorods were extremely well defined and measurements indicated very little variation in the width (50–70 nm). Much more variation was observed in the lengths, which were in the range of 100–900 nm. Close-up views of some of the rods, showed much darker zones towards the middle and lighter ones towards the boundaries suggesting the presence of tube-like structures. The remarkable morphological uniformity of these structures, with only major variation in length, indicates a possible template growth effect in one direction only. The aggregates appear both

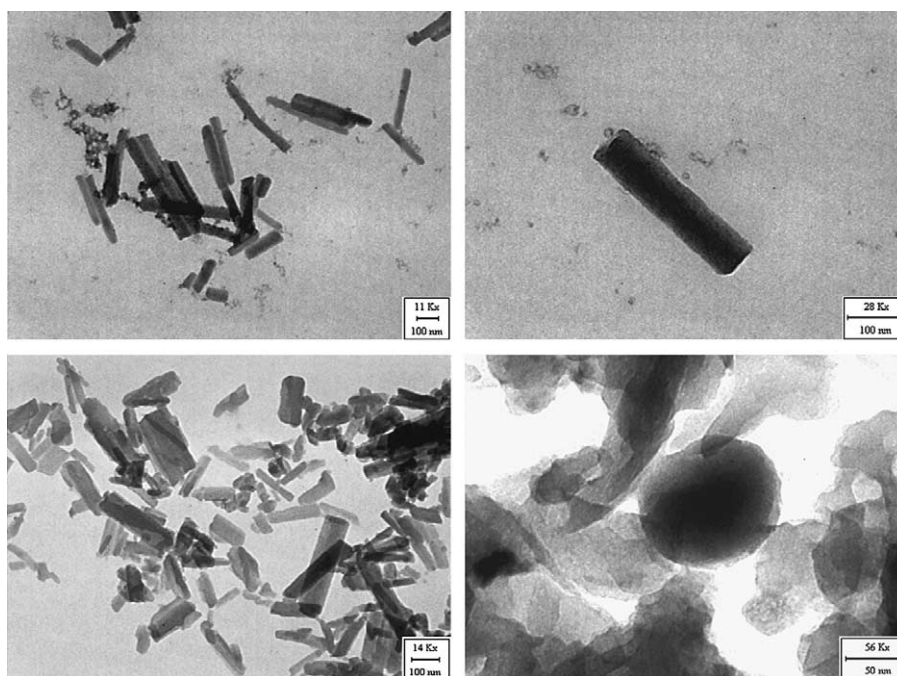


Figure 1. TEM images of rod-like aggregates formed by amphiphilic fullerene derivatives **2b** (upper-left and upper-right), **2a** (lower-left), **2c** (lower-right).

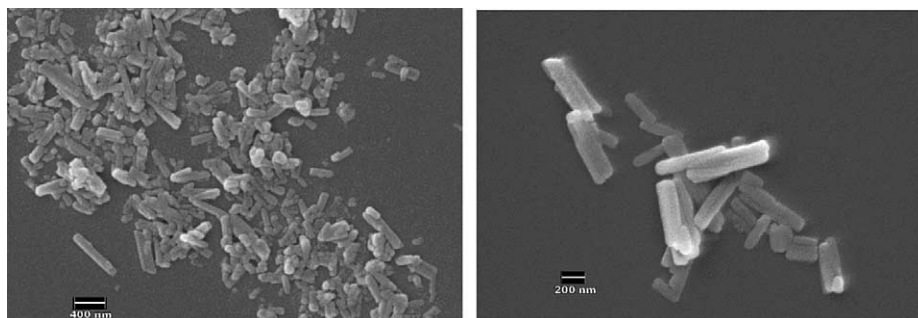


Figure 2. SEM images of fullerene aggregates containing molecules **3** (left) and **2b** (right) deposited on silicon substrate by spin coating.

alone and sometimes overlapping, suggesting the absence of inter-rod interactions.

The assemblies of molecule **3** bearing an extra positive charge, the pyrrolidinium cation, retained the same shapes as of those singly charged and showed a higher solubility in water. The aggregates of molecule **2a** and **3** were structurally similar to those of **2b** even though they were not so well defined and contained a mixture of broad and short rods. The distribution in length and in width was in the range of 80–500 and 20–90 nm, respectively.

The effect of changing to an organic trifluoroacetate counterion, such as compound **2c**, was very pronounced, specifically a large proportion of the material was revealed to be composed of amorphous solids that could not be resolved at any level. We speculate that the weak ammonium– CF_3COO^- ion-pairing interaction and its hydrophilic nature preclude the formation of the rod-like structures.^{23,24}

Interestingly, TEM analysis of materials deposited from a non-sonicated suspension of compound **2b** did not show the formation of any organized structures.

In order to exclude a template effect of the TEM grids, SEM

and AFM analyses were pursued, in which the material was deposited onto silicon surfaces by spin coating.

On SEM images, the nanorods appear remarkably similar to those previously studied by TEM, of which representative images are shown in Figure 2. These show that the formation of the rod-like fullerene-containing aggregates is independent from both substrate and deposition methods. The latter observation infers that such rod-like organization is an intrinsic property of the fullerenes amphiphiles, when suspended in aqueous phases.

The aggregates were sparsely scattered in **2b**, whereas there was a copious coating of rods in **3**, and we attribute this to the difference in solubility between the single charged and doubly charged species.

The fullerene-containing aggregates were also investigated by means of tapping mode atomic force microscopy (TP-AFM). All AFM images were repeatedly observed and were stable under experimental conditions. AFM measurements of aqueous dispersions containing positively charged fullerene derivatives **2b** and **3** spin-coated on silicon substrates, reproducibly revealed the presence of rectangular objects, that is, rod-like aggregates (Fig. 3).

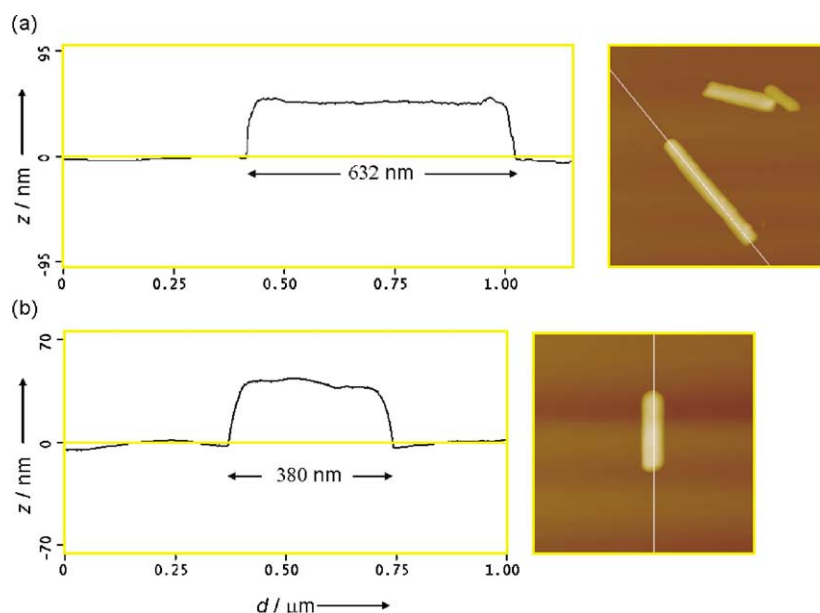


Figure 3. TP-AFM (right) and cross section profiles (left) of the aggregates containing fullerene derivative (a) **2b** (average vertical profile: 50 nm) and (b) **3** (average vertical profile: 43 nm) deposited by spin-coating on silicon surfaces.

The average dimensions of the objects were ranging from 200 to 700 nm in length, from 40 to 100 nm in width, and from 40 to 60 in height. Although the rod-like aggregates were the major fraction, some amorphous material was also observed. These results are in excellent agreement with those obtained from TEM and SEM measurements. Higher resolution images of a rod-like aggregate, showed the presence of terraces on top of the objects, with smooth steps of several nanometers, accounting for a layer-by-layer growth of the fullerene aggregate. Similar AFM images were also obtained with fullerene compound **2a**, whereas no regular aggregates have been observed upon spin-coating of an aqueous dispersion of fullerene **2c**.

3. Conclusion

In summary, we have shown that short chain C₆₀ amphiphiles organize into rod-like aggregates, having well defined dimensions. Investigations using TEM, SEM, and AFM microscopies reveal highly reproducible materials, which are independent of both substrate and sampling method, and are homogeneously dispersed throughout the substrate. The counterion of the ammonium salt plays a crucial role in determining the morphology of the materials, in which organized structures are obtained using BF₄⁻, Br⁻, and Cl⁻ anions. In contrast, the trifluoroacetate counter anion gave unresolved amorphous materials. Fullerenes bearing ammonium groups are promising materials for the construction of organized nano-materials and are worthy candidates for the further integration of optically and electrically active groups.

4. Experimental

Fullerene molecule **1** was prepared according to literature procedures.²⁵ Reagents and solvents were purchased reagent grade and used without further purification. Mass spectra were taken with 7070H VG Microsoma (MS-EI) and PESCIEX API 1 (MS-ES) spectrometers and compounds were dissolved in methanol unless otherwise noted. TEM images were taken on a Philips TEM 208 at an accelerating voltage of 100 kV. AFM analysis was carried out on a TP-AFM measurements in air at 298 K, using a Nanoscope IIIa (Digital Instruments Metrology Group, USA) instrument, model: MMAFMLN. The tips used in all measurements were phosphorous-doped silicon cantilevers ($T=20\text{--}80\text{ mm}$, $L=115\text{--}135\text{ mm}$, $f_0=200\text{--}400\text{ kHz}$, $k=20\text{--}80\text{ N m}^{-1}$, VEECO, USA) working at a resonant frequency of ca. 316 kHz.

Molecule **1a** was prepared according to our reported procedure,²⁵ by refluxing **1** (50.0 mg, 0.0551 mmol, in CH₂Cl₂, 2 mL) in the presence of a large excess of CH₃I (3 mL), for a duration of 24 h. The suspension was filtered (Millipore Fluorophore) and washed with dichloromethane (3 × 20 mL) and then toluene (3 × 20 mL) furnishing compound **1a** as a brown solid (23.2 mg, 0.0219 mmol, 39.7%). m/z (CHCl₃/CH₃OH 1:1) 921 M⁺.

The compounds **2a–c** and **3** were prepared using the following procedure: fullerene **1a** was dissolved in CH₂Cl₂ (5 mL) and then HBF₄ (54% in Et₂O, 2 mL) added dropwise,

under ice cooling. The solution was brought to room temperature and stirred for 1 h giving a brown suspension. After solvent removal in vacuo, the solid was filtered (Millipore, PTFE, 0.22 μm) and washed with diethyl ether (3 × 20 mL) and toluene (3 × 20 mL). Drying under vacuum gave a powder-like brown solid of **2b**, 22 mg, 0.0246 mmol, 89% yield, m/z (CH₃OH) 807 M⁺. UV–vis (THF): λ_{max} nm 704, 471, 429, 322, 271; UV–vis (H₂O) 726, 356, 284; IR-DRIFT (KBr): 2897, 1653, 1446, 1088, 758.

Compounds **2a** and **2c** were synthesized following similar protocols but using different acids, namely for molecule **2a** CH₃CO₂H/HBr (71% yield, UV–vis (THF): λ_{max} nm 716, 489, 324, 256; UV–vis λ_{max} nm (H₂O): 726, 348, 280); IR-DRIFT (KBr): 2934, 1475, 1189, 1041, 785, 548. And for **2c**, TFA (89% yield, UV–vis (THF): λ_{max} nm 704, 473, 431, 320, 255; UV–vis (H₂O) λ_{max} nm: 725, 488, 347, 279); IR-DRIFT (KBr): 2924, 2854, 1685, 1553, 1211, 1140, 852, 782, 735. Molecule **3** m/z (CH₃OH) 822 M⁺ (UV–vis (THF): λ_{max} nm 718, 503, 362, 279; UV–vis (H₂O) λ_{max} nm: 712, 332, 263); IR-DRIFT (KBr): 2925, 1465, 1191, 1007, 777.

Preparation of TEM samples. The fullerene compound (0.5 mg and 0.2 mg for **2a–c** and **3**, respectively) was weighed into a glass centrifuge tube and then suspended in water (1 mL, distilled and filtered through Millipore, Ionophore filter). Sonication in an ultrasound bath three times for 5 min with 5 min intervals gave a finely dispersed brown suspension. After centrifugation (30 min, 3000 rpm) one drop of the transparent brown solution was transferred to a TEM grid (Formvar film). The grid was wicked dry using a filter paper from the underneath and dried for 12 h at room temperature prior to TEM microscopy.

Preparation of AFM and SEM samples. The sonication technique was the same as described for TEM sample, except that the dispersion containing the fullerene derivatives in H₂O was spin-coated (spinning rate: 1800 rpm) on to clean silicon surfaces ((100), p-doped with B, $\rho \sim 10\ \Omega\ \text{cm}^{-2}$). The silicon substrates were previously cleaned using boiling 1,1',2,2'-tetrachloroethane for 10 min, copiously rinsed with acetone, and dried with a nitrogen stream. Further dilution (10 mL of water) of **3** was necessary in order to prevent complete coverage of the surface. For the purposes of consistency and reproducibility, the same samples were used for both AFM and SEM measurements.

Acknowledgements

We are deeply indebted to Mr. Claudio Gamboz for the skilled TEM manipulation, Mr. Tito Ubaldini for the SEM images, and Dr. Fabio Hollan for the mass spectra. This work was supported by European Union, Human Potential Networks WONDERFULL, contract HPRN-CT-2002-00177 and also by the University of Trieste and MIUR (PRIN 2004, prot. 2004035502).

Supplementary data

Supplementary data associated with this article can be found, in the online version, at doi:10.1016/j.tet.2005.08.125. The data supplied contain mass spectra of the individual

compounds **1a**, **2a–c**, and **3**. In addition, photos of TEM, SEM, and AFM microscopies are included. Also, example UV spectra of molecule **2c** in organic and aqueous phases are supplied.

References and notes

1. Kroto, H. W.; Heath, J. R.; O'Brien, S. C.; Curl, R. F.; Smalley, R. E. *Nature* **1985**, *318*, 162–163.
2. Segura, J. L.; Martin, N.; Guldi, D. M. *Chem. Soc. Rev.* **2005**, *34*, 31–47.
3. Joachim, C.; Gimzewski, J. K.; Tang, H. *Phys. Rev. B* **1998**, *58*, 116407–116411.
4. Mirkin, C. A.; Caldwell, W. B. *Tetrahedron* **1996**, *52*, 5113–5130.
5. Echegoyen, L.; Echegoyen, L. E. *Acc. Chem. Res.* **1998**, *31*, 593–601.
6. Isaacs, L.; Wehrsig, A.; Diederich, F. *Helv. Chim. Acta* **1993**, *76*, 1231–1250.
7. Maggini, M.; Scorrano, G.; Prato, M. *J. Am. Chem. Soc.* **1993**, *115*, 9798–9799.
8. Langa, F.; De la Cruz, P.; Espildora, E.; De la Hoz, A.; Bourdelande, J. L.; Sanchez, L.; Martin, N. *J. Org. Chem.* **2001**, *66*, 5033–5041.
9. Bingel, C. *Chem. Ber.* **1993**, *126*, 1957–1959.
10. Diederich, F.; Gómez-López, M. *Chem. Soc. Rev.* **1999**, *28*, 263–277.
11. Whiteside, G. M.; Boncheva, M. *Proc. Natl. Acad. Sci. U.S.A.* **2002**, *99*, 4769–4774.
12. Sun, Y. P.; Bunker, C. *Nature* **1993**, *365*, 398–401.
13. Alargova, R.; Deguchi, S.; Tsujii, K. *J. Am. Chem. Soc.* **2001**, *123*, 10460–10467.
14. Zhou, S.; Burger, C.; Chu, B.; Sawamura, M.; Nagahama, N.; Toganoh, M.; Hackler, U. E.; Isobe, H.; Nakamura, E. *Science* **2001**, *291*, 1944–1947.
15. Guldi, D. M.; Zerbetto, F.; Georgakilas, V.; Prato, M. *Acc. Chem. Res.* **2005**, *38*, 38–43.
16. Nakashima, N.; Ishii, T.; Shirakusa, M.; Nakanishi, T.; Murakami, H.; Sagara, T. *Chem. Eur. J.* **2001**, *7*, 1766–1772.
17. Cassell, A. M.; Asplund, C. K.; Tour, J. M. *Angew. Chem., Int. Ed.* **1999**, *38*, 2403–2405.
18. Guldi, D. M.; Goulomis, A.; Vazquez, P.; Torres, T.; Georgakilas, V.; Prato, M. *J. Am. Chem. Soc.* **2005**, *127*, 5811–5813.
19. Georgakilas, V.; Pellarini, F.; Prato, M.; Guldi, D. M.; Melle-Franco, M.; Zerbetto, F. *Proc. Natl. Acad. Sci. U.S.A.* **2002**, *99*, 5075–5080.
20. Angelini, G.; De Maria, P.; Fontana, A.; Pierini, M.; Maggini, M.; Gasparrini, F.; Zappia, G. *Langmuir* **2001**, *17*, 6404–6407.
21. Angelini, G.; Cusan, C.; De Maria, P.; Fontana, A.; Maggini, M.; Pierini, M.; Prato, M.; Schergna, S.; Villani, C. *Eur. J. Org. Chem.* **2005**, *9*, 1884–1891.
22. Myers, D. *Surfactant Science and Technology*; VCH: New York, 1988.
23. Guo, D.; Mant, C. T.; Hodges, R. S. *J. Chromatogr.* **1987**, *386*, 205–222.
24. Zielinski, R.; Szymusiak, H. *Int. J. Quantum Chem.* **2004**, *99*, 724–734.
25. Kordatos, K.; Da Ros, T.; Bosi, S.; Vazquez, E.; Bergamin, M.; Cusan, C.; Pellarini, F.; Tomberli, V.; Baiti, B.; Pantarotto, D.; Georgakilas, V.; Spalluto, G.; Prato, M. *J. Org. Chem.* **2001**, *66*, 4915–4920.

Dendritic liquid-crystalline fullerene–ferrocene dyads

Stéphane Campidelli,^a Laura Pérez,^b Julián Rodríguez-López,^b Joaquín Barberá,^{c,*}
Fernando Langa^{b,*} and Robert Deschenaux^{a,*}

^a*Institut de Chimie, Université de Neuchâtel, Avenue de Bellevaux 51, Case Postale 2, 2007 Neuchâtel, Switzerland*

^b*Facultad de Ciencias del Medio Ambiente, Universidad de Castilla-La Mancha, 45071 Toledo, Spain*

^c*Química Orgánica, Facultad de Ciencias-Instituto de Ciencia de Materiales de Aragón, Universidad de Zaragoza-CSIC, 50009 Zaragoza, Spain*

Received 14 June 2005; revised 8 October 2005; accepted 10 October 2005

Available online 1 December 2005

Dedicated to Prof. David I. Schuster on the occasion of his 70th birthday

Abstract—First- and second-generation ferrocene-based dendrimers, fullerene and a second-generation liquid-crystalline poly(arylester) dendrimer carrying four cyanobiphenyl units were assembled to elaborate polyfunctional materials displaying mesomorphic and electronic properties. The targeted compounds gave rise to enantiotropic smectic A phases and organized into bilayer structures within the smectic layers. Cyclic voltammetry investigations revealed oxidation and reduction processes in agreement with the presence of both ferrocene and fullerene units. Finally, strong quenching of the fluorescence was obtained for the fullerene–ferrocene dyads suggesting efficient electron transfer from the ferrocene-based dendrimer to fullerene.

© 2005 Elsevier Ltd. All rights reserved.

1. Introduction

A rich variety of electron donors, including TTF,¹ conjugated oligomers,² porphyrins³ and ferrocenes,⁴ were associated to [60]fullerene (C₆₀) in order to generate efficient intramolecular electron transfer. The design of photoactive [60]fullerene-based materials for applications in photovoltaic^{2a,b,5} and organic light emitting diode⁶ technologies strongly motivated synthetic efforts in this research area. Furthermore, recent developments in liquid crystal technology demonstrated that columnar phases, in which high-hole mobility along the columns was observed, were found to be a suitable medium for photovoltaic applications.⁷ Therefore, functionalized liquid-crystalline fullerenes are promising materials for applications in electronic and optical nanotechnologies as they combine the unique properties of C₆₀ with the characteristics of liquid crystals.

We designed liquid-crystalline ferrocene–fullerene dyads in which photoinduced electron transfer was observed.⁸ Such materials could act as photoactive supramolecular switches providing the lifetime of the charge separated state is long enough. The switching mechanism would be based on the different intermolecular interactions generated by either the neutral ferrocene species (light off) or the cationic ferrocenium

species (light on): we were able to obtain either smectic A or rectangular columnar phases from the oxidation of non-mesomorphic ferrocene derivatives.⁹ This behavior could be extended to liquid-crystalline ferrocene–fullerene dyads.

To further explore the properties of liquid-crystalline dyads based on ferrocene and C₆₀, we decided to use a dendritic-like ferrocene architecture as a source of electrons. Ferrocene-based dendrimers display remarkable electrochemical properties and have been used for the construction of batteries¹⁰ and sensors.¹¹ The association of a ferrocene-containing dendrimer and C₆₀ within a liquid-crystalline structure could lead to polyfunctional materials displaying interesting mesomorphic, photophysical and electrochemical properties.

We report, herein, the synthesis, liquid-crystalline properties, supramolecular organization, electrochemical and photophysical behavior of fullerene–ferrocene dyads **1** and **2** containing two and four ferrocene units, respectively. A second-generation poly(arylester) dendrimer functionalized with cyanobiphenyl units was used as liquid-crystalline promoter (Chart 1).

2. Results and discussion

2.1. Synthesis

The synthetic procedure used for the preparation of **1** and **2** is shown in Scheme 1. Fulleropyrrolidines **5** and **6** were

Keywords: Ferrocene; Fullerene; Supramolecular organization.

* Corresponding authors. Fax: +34 925268840 (F.L.); e-mail addresses: jbarbera@unizar.es; fernando.lpuente@uclm.es; robert.deschenaux@unine.ch

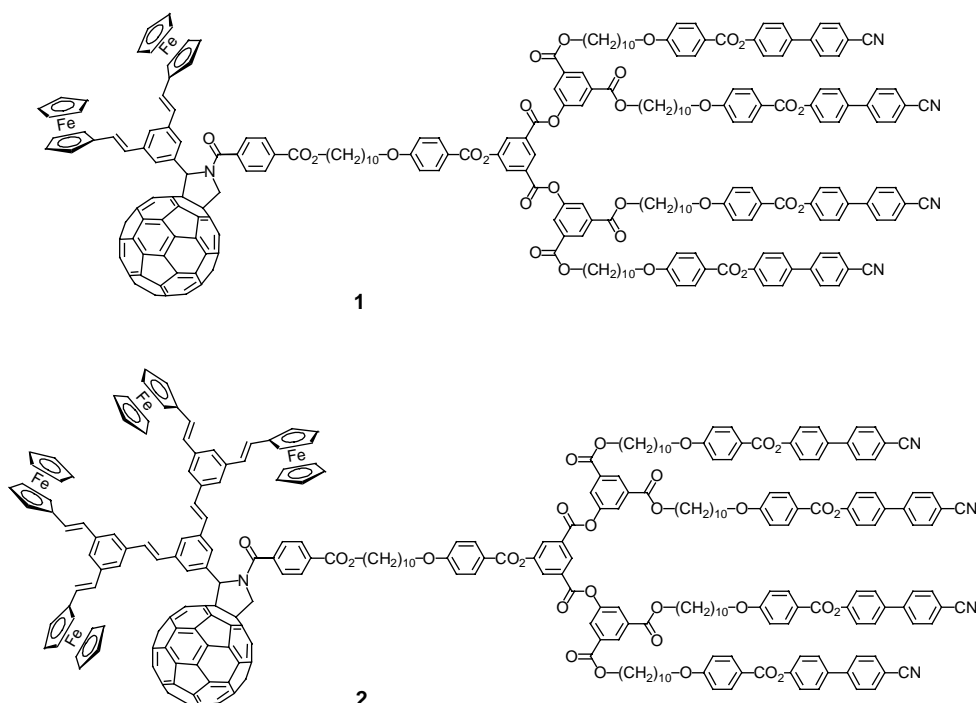


Chart 1.

prepared by 1,3-dipolar cycloaddition of C_{60} with the azomethine ylide¹² generated in situ from aldehyde functionalized dendrons **3** or **4** and glycine in refluxing chlorobenzene. Monoadducts **5** and **6** were obtained in 32 and 30% yield, respectively, after purification by column chromatography (silica gel, toluene/hexane 7:3). The synthesis of targeted compounds **1** and **2** involved reaction of acid **7a** with thionyl chloride in CH_2Cl_2 to prepare the corresponding acid chloride **7b** followed by condensation of the latter with **5** or **6** in refluxing CH_2Cl_2 (quantitative yields), and purification by column chromatography (silica gel, toluene/hexane 4:1).

All new compounds were characterized by 1H and ^{13}C NMR, FT-IR and MALDI-TOF mass spectrometry. The analytical data were in agreement with the structures. High resolution 1H NMR spectra of *NH*-fulleropyrrolidines **5** and **6** showed all the expected signals. The ferrocene protons are shown between 4 and 5 ppm as two groups of signals; the typical pyrrolidine protons [two doublets (AB system) and one singlet] appeared in the 4–5 ppm range. The *E*-configuration of the vinyl hydrogens in the ferrocene-based dendrimer ($J=16$ – 17 Hz) is observed. In target structures **1** and **2**, the signals described for precursors **5** and **6** remain, appearing together with the typical signature of mesogenic dendrimers.^{8,9} MALDI-TOF mass spectrometry showed the $M+1$ molecular ion peak for **1** and **2** and the M molecular ion peak for **5** and **6**. UV–vis spectra revealed the typical dihydrofullerene absorption band at around 430 nm. The synthesis of **3**, **4** and **7a** will be reported separately with other dendritic materials.

2.2. Liquid-crystalline properties

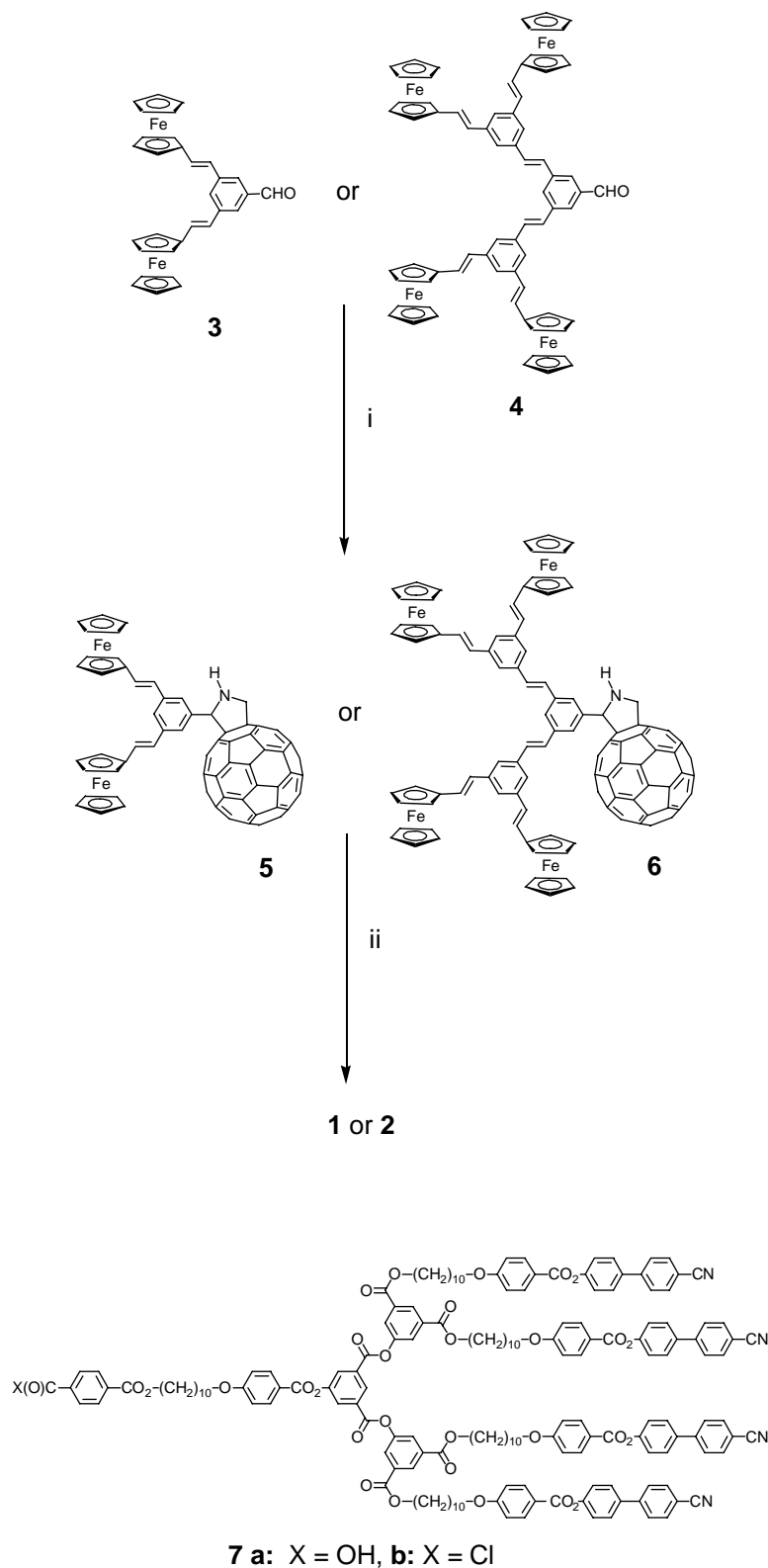
The thermal and liquid-crystalline properties of **1**, **2** and **7a** were investigated by polarized optical microscopy (POM)

and differential scanning calorimetry (DSC). The mesomorphic behavior of **1** and **2** was also analyzed by X-ray diffraction (XRD). The phase transition temperatures and enthalpies are reported in Table 1.

Compounds **1**, **2** and **7a** gave rise to smectic A phases, which were identified by POM from the observation of typical focal-conic and homeotropic textures. Fullerene derivatives **1** and **2** showed a lower clearing point than liquid-crystalline dendrimer **7a**. This behavior is in agreement with results obtained for other fullerene-containing liquid crystals,¹³ and is attributed to the presence of bulky ferrocene and C_{60} units.

The X-ray diffraction patterns recorded at room temperature from as-obtained samples of **1** and **2** were consistent with the formation of smectic A phases. They contained a set of two equally-spaced maxima at low angles, which are typical of lamellar systems. These maxima were sharp and corresponded to the first and second order reflections. By applying Bragg's law to these maxima, layer spacings of 93 and 105 Å were obtained for **1** and **2**, respectively. No reflections were found at middle and high angles, except for a diffuse scattering halo, which was characteristic of the liquid-like packing inside the smectic layers. This halo, which corresponded to an average distance of about 4.5 Å for **1** and 4.3 Å for **2**, is usually found in X-ray diffractograms of liquid crystal phases and confirms the mesomorphic nature of the room temperature phases displayed by **1** and **2**.

The diffraction patterns did not change after thermal treatment of the samples, which were heated above the clearing point and then cooled to room temperature. In the case of **1**, experiments were carried out at different temperatures between the glass transition temperature and



Scheme 1. Reagents and conditions: (i) C_{60} , glycine, chlorobenzene, reflux, 8 h, yield: 32% for **5**, 30% for **6**; (ii) **7a**, thionyl chloride, CH_2Cl_2 , reflux, 7 h, then **5** or **6**, CH_2Cl_2 , pyridine, room temperature, 2 h, quantitative yields.

the clearing point. These experiments confirmed that the mesophase was smectic A in nature within the mesomorphic domain. No differences were observed between the X-ray patterns recorded below and above the glass transition. This result meant that the room temperature phase was a frozen

smectic A phase with the same structure as the high-temperature liquid crystal phase but lacking fluidity. When the possible temperature dependence of the layer thickness was tested, the measured values were found to be constant within the accuracy of the measurements. Thus, it can be

Table 1. Phase-transition temperatures and enthalpy changes of **1**, **2** and **7a**^a

Compound	T_g (°C) ^b	$S_A \rightarrow I$ (°C)	ΔH (kJ/mol)
1	47	171 ^c	7.3
2	34	168 ^c	13.3
7a	45	203 ^d	18.6

^a T_g =glass transition temperature, S_A =smectic A phase, I =isotropic liquid.

^b Determined during the first cooling run.

^c Determined as the maximum of the peak obtained during the second heating run.

^d Determined as the onset of the peak obtained during the second heating run.

concluded that the temperature had no significant effect on the molecular conformations or on the extent of interdigitation (see below).

2.3. Supramolecular organization

The molecular lengths (L) of **1** and **2**, in their extended conformation, were estimated by means of HyperChem software, and were estimated to be 70 Å for **1** and 77 Å for **2**. The d/L ratio of 1.33 for **1** and of 1.36 for **2** revealed that **1** and **2** organized into a bilayer smectic structure with alternate sublayers of cyano-biphenyl units, fullerene units and ferrocene units (Fig. 1). Such a supramolecular organization is driven by steric constraints resulting from the difference of the cross-sectional area of C_{60} (90–100 Å²), ferrocene (45 Å²) and the four mesogenic groups (22–25 Å²)

per mesogenic unit). For **1**, there is a good adequacy of the cross-sectional areas of each part of the molecule (four mesogenic units, one C_{60} unit and two ferrocene units), and an average value of about 100 Å² is obtained. In **2**, there are four ferrocene units, leading to a cross-sectional area of about 180 Å², that is, twice as much than in **1**. For **2**, the difference in cross-sectional areas is, most likely, compensated by a different orientation of the poly(arylester) dendrimer, so efficient space filling is obtained. Finally, interdigitation of the cyanobiphenyl units from one layer to the adjacent one should contribute to the stabilization of the layers.

2.4. Electrochemistry

The determination of the redox potentials in donor–acceptor systems is important to evaluate the energetics of electron transfer reactions. We performed a systematic study to evaluate the redox properties of **1**, **2**, **5**, **6**, **7a**, and of ferrocene and C_{60} used for comparative purposes, using cyclic (CV) and Osteryoung square wave voltammetry (OSWV) (Table 2, Fig. 2). As illustrated in Figure 2 for **1**, the CV curves of **1**, **2**, **5** and **6** showed that they were electrochemically active in both anodic and cathodic sweep directions between +1.0 and –2.5 V. In the cathodic scan, three reversible reduction waves were observed and presumably, fullerene centred, but shifted to more negative values than those observed for C_{60} because of the saturation of one double bond of the C_{60} cage.¹² An additional non-reversible reduction wave was observed for **1** and **2** at

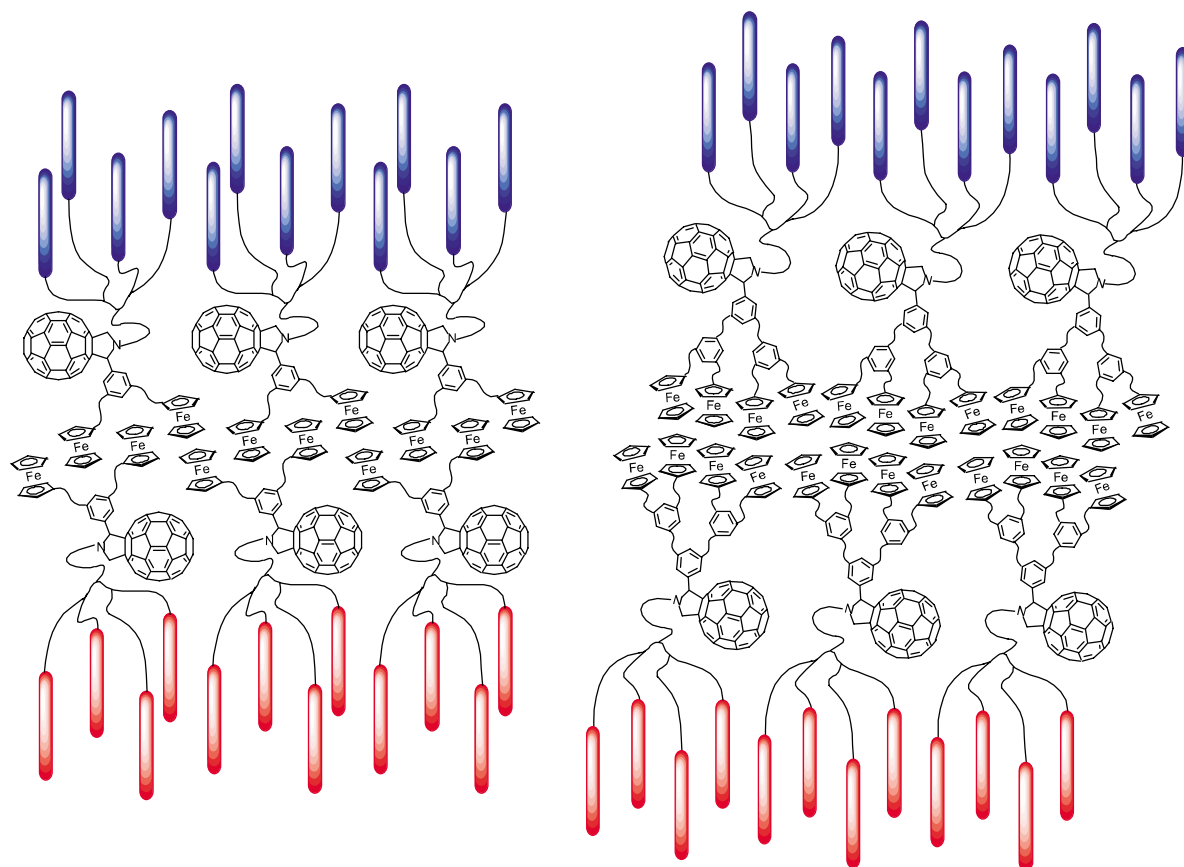
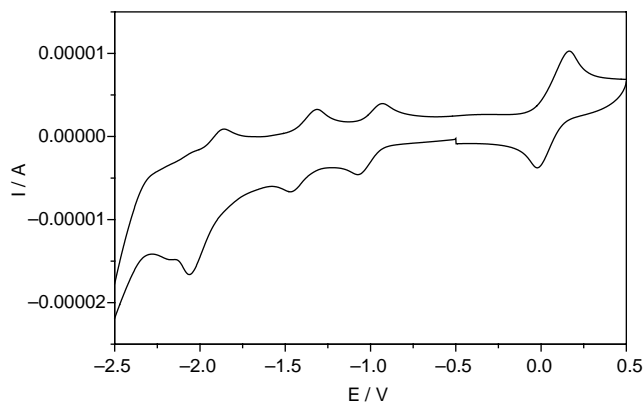


Figure 1. Postulated supramolecular organization of **1** (left) and **2** (right) within the smectic A phase.

Table 2. Osteryoung square wave voltammetry (OSWV) data in *o*-dichlorobenzene–acetonitrile (4/1)^a

	E_{red}^1 (V)	E_{red}^2 (V)	E_{red}^3 (V)	E_{red}^4 (V)	E_{ox}^1 (V)
1	−1.02	−1.41	−1.96	−2.11	0.01
2	−1.01	−1.40	−1.96	−2.08	−0.03
5	−1.10	−1.49	−2.00		0.03
6	−1.04	−1.44	−1.98		
7a				−2.08	
C ₆₀	−0.99	−1.38	−1.85		
Ferrocene					0.04

^a V versus Ag/AgNO₃; glassy carbon electrode as the working electrode; 0.1 M TBAP; scan rate = 100 mV s^{−1}; concentration: 1.4 × 10^{−3} M.

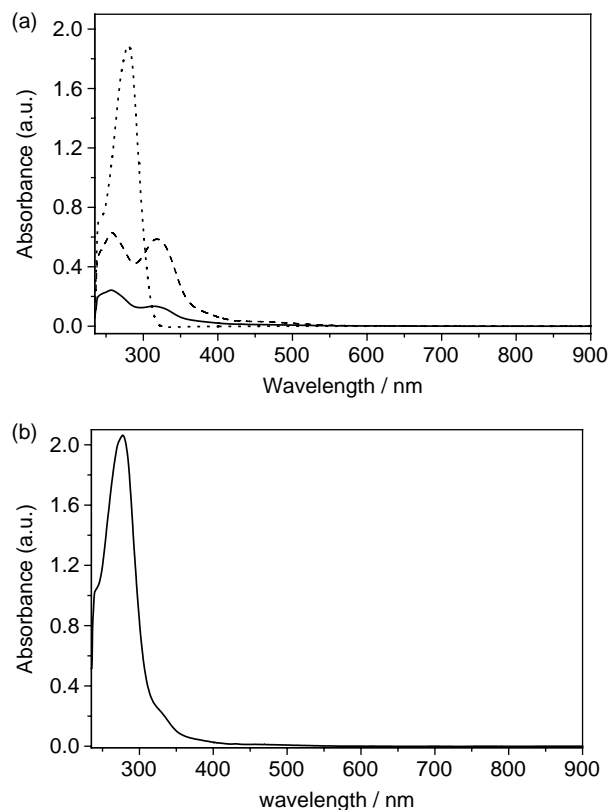
**Figure 2.** Cyclic voltammogram of **1**.

around −2.10 V, which was assigned to the reduction of the mesogenic dendrimer by comparison with the reduction wave observed for **7a**. In the anodic scan, the observed oxidation process is ferrocene-based because no oxidation can be observed for **7a** in this region. The experimentally determined HOMO–LUMO gap (ΔE) is lower (0.98 eV) for the second-generation ferrocene dendrimer derivative **2** compared with that of **1** (1.03 eV). The same trend is found for precursor *NH*-fulleropyrrolidine **6** (1.04 eV) with respect to **5** (1.13 eV).

2.5. Photophysical studies

The absorption spectra of **5** and **6** were measured in CHCl₃ (Fig. 3a) and display λ_{max} values at 257 nm (log ϵ = 4.38) and 313 nm (log ϵ = 4.13) for **5** and 258 nm (log ϵ = 4.80) and 318 nm (log ϵ = 4.77) for **6** indicating that conjugation is not extended by *meta*-substitution. Consequently, **5** and **6** behave as an assembly of two and four vinylferrocene moieties sharing a phenyl ring. Both fullerene–ferrocene dendrimers show the typical small band for [6,6]-bridged fullerene derivatives at 431 nm. On the other hand, **7a** show only one λ_{max} value at 279 nm (log ϵ = 5.28). Absorption spectra of **1** and **2** in CHCl₃ are dominated by the mesogenic moiety, showing maxima at 279 nm, and were essentially the sum of the spectra of the corresponding components (**5** or **6**) and **7a** (Fig. 3b). Weak absorptions typical for fulleropyrrolidines were observed around 430 and 700 nm, respectively (not shown).

The fluorescence of functionalized fullerene derivatives is a sensitive parameter, which can be used to probe

**Figure 3.** (a) Absorption spectra in chloroform (10^{−5} M) of **5** (solid line), **6** (dashed line) and **7a** (dotted line). (b) Absorption spectra in chloroform (10^{−5} M) of **1**.

intramolecular transfer processes in donor–acceptor systems.¹⁴ Emission spectra of *N*-methylfulleropyrrolidine, used as reference, show maxima around 710 nm,^{3b,15} independently of the polarity of solvent. We studied the room temperature fluorescence spectra of **1**, **2**, **5** and **6** using *N*-methylfulleropyrrolidine as reference, in toluene and benzonitrile with excitation at 430 nm, wavelength where only the fullerene cage is excited.¹⁶ In toluene, the fluorescence observed at 714 nm for *N*-methylfulleropyrrolidine was almost totally quenched in **5** and **6** (only a weak emission at 704 nm is observed) independently of the generation of the dendrimer (Fig. 4a). When the most polar benzonitrile solvent was used, the fluorescence was totally quenched. These findings suggested the occurrence of an efficient electron transfer process from the ferrocene-based dendrimer to C₆₀. Efficient electron transfer processes in fullerene–ferrocene dyads were previously observed.^{4a,17} Similar behavior was observed for **1** and **2** (Fig. 4b), with respect to the properties observed for **5** and **6**, indicating that the newly incorporated mesogenic dendrimer did not influence the photophysical behavior of the studied materials.

3. Conclusion

We have designed a novel family of liquid-crystalline fullerene–ferrocene dyads by assembling a first- or second-generation ferrocene-based dendrimer, a second-generation mesomorphic poly(arylester) dendrimer carrying

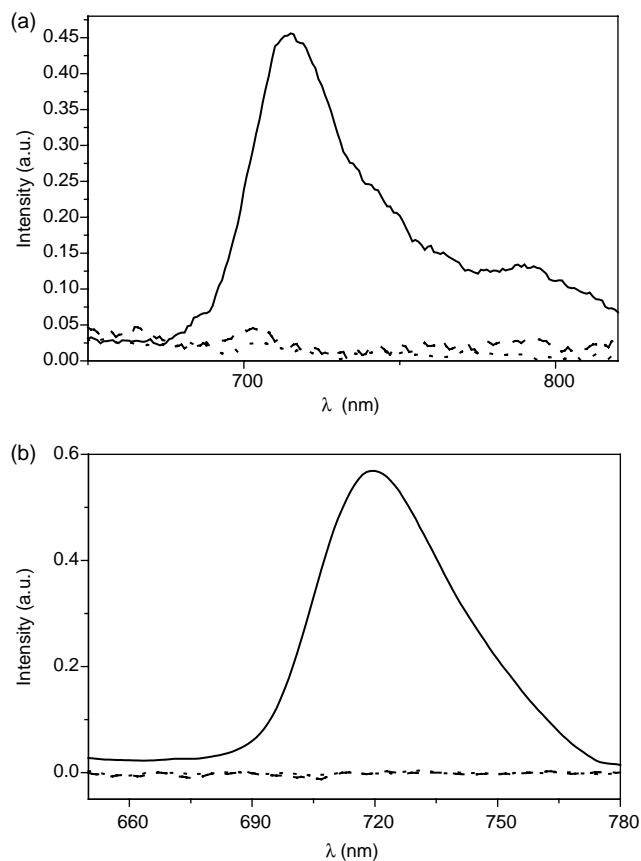


Figure 4. (a) Steady-state fluorescence ($\lambda_{\text{exc}}=430$ nm) of **5** (dashed line), **6** (dotted line) and *N*-methylpyrrolidino[60]fullerene (solid line) measured in toluene. (b) Steady-state fluorescence ($\lambda_{\text{exc}}=430$ nm) of **1** (dashed line), **2** (dotted line) and *N*-methylpyrrolidino[60]fullerene (solid line) measured in benzonitrile.

cyanobiphenyl units and fullerene. The materials displayed smectic A phases, and the supramolecular organization was governed by steric constraints. The electrochemical behavior was in agreement with the redox-activity of the building-blocks. Steady-state emission spectra showed that the fluorescence was totally quenched, suggesting the existence of an efficient electron transfer process from the ferrocene dendrimer to C_{60} . Therefore, the use of ferrocene-based dendrimers as electron donor moieties could be appealing to elaborate supramolecular switches based on fullerene and ferrocene.

4. Experimental

4.1. General procedures

All the cycloaddition reactions were performed under argon. C_{60} was purchased from MER Corporation (Tucson, AZ, USA) and the commercial starting materials were purchased from ACROS. Cycloaddition reactions were monitored by TLC using Merck silica gel 60-F₂₅₄. ^1H and ^{13}C NMR spectra were recorded on a Varian Mercury 200 apparatus. UV–vis absorption spectra were obtained on a Shimadzu spectrophotometer. FT-IR spectra were recorded on a Nicolet AVATAR 370 spectrophotometer on KBr discs.

Transition temperatures (onset point) and enthalpies were determined with a differential scanning Mettler DSC 822 calorimeter, under N_2/He , at a rate of $10^\circ\text{C}/\text{min}$. Optical studies were conducted using a Zeiss-Axioscope polarizing microscope equipped with a Linkam-THMS-600 variable-temperature stage, under N_2 . The XRD patterns were obtained with a pinhole camera (Anton-Paar) operating with a point-focussed Ni-filtered $\text{Cu K}\alpha$ beam. The samples were held in Lindemann glass capillaries (1 mm diameter) and heated, when necessary, with a variable-temperature oven. The patterns were collected on flat photographic films. The capillary axis and the film are perpendicular to the X-ray beam. Spacings were obtained via Bragg's law. MALDI-TOF mass spectra were obtained on a Voyager DE-STR from Applied Biosystems, using ditranol as a matrix. Cyclic voltammetry measurements were obtained using a Versastat PAR EG and G potentiostat with analytical electrochemical software (Mod. 250). The measurements were made in a double-walled cell (Metrohm EA 876-20). A glassy carbon working electrode (Metrohm 6.0804.010) was used after being polished with alumina ($0.3\ \mu$) for 1 min, and platinum wire was used as counter electrode. An Ag/AgNO_3 electrode, used as a reference electrode, was separated from the solution by a solution of tetrabutylammonium perchlorate, which was used as the supporting electrolyte in toluene/acetonitrile 4:1. The samples were purged with argon prior to measurement.

4.1.1. Synthesis of 5. A mixture of C_{60} (122.4 mg, 0.17 mmol), **3** (20 mg, 0.038 mmol) and glycine (14.3 mg, 0.19 mmol) was heated under reflux for 8 h in degassed anhydrous chlorobenzene (30 mL) under inert atmosphere. After removal of the solvents, the residue was purified over silica gel (toluene/hexane 7:3). The product was centrifuged with CH_3OH and *n*-pentane to give **5** (32%) as a dark brown solid. ^1H NMR (200 MHz, CDCl_3): δ 4.14 (s, 10H, C_5H_5), 4.31 (t, 4H, $J=1.8$ Hz, HCp), 4.50 (t, 4H, $J=1.8$ Hz, HCp), 4.87 (A of AB_q , 1H, $J=10.2$ Hz, $\text{H}_2\text{C}_{\text{pyrrol}}$), 5.17 (B of AB_q , 1H, $J=10.2$ Hz, $\text{H}_2\text{C}_{\text{pyrrol}}$), 5.84 (s, 1H, $\text{HC}_{\text{pyrrol}}$), 6.74 (A of AB_q , 2H, $J=16.2$ Hz, $\text{CH}=\text{}$), 6.95 (B of AB_q , 2H, $J=16.2$ Hz, $\text{CH}=\text{}$), 7.44 (s, 1H, H_{arom}), 7.75 (s, 2H, H_{arom}). ^{13}C NMR (125 MHz, CDCl_3): δ 155.95, 153.77, 153.47, 152.78, 147.04, 146.74, 146.34, 146.22, 146.01, 145.81, 145.62, 145.41, 145.32, 145.08, 144.83, 144.52, 144.27, 143.10, 142.91, 142.62, 142.40, 142.22, 142.07, 141.94, 141.70, 141.64, 141.50, 140.15, 140.11, 139.79, 139.56, 138.49, 137.02, 136.49, 136.35, 136.04, 135.81, 135.54, 128.22, 128.13, 127.82, 125.54, 123.77, 123.61, 123.37, 122.94, 82.93, 77.59, 77.08, 69.28, 69.20, 66.98, 61.72, 53.37. UV–vis λ_{max} (nm) ($\log \epsilon$, CHCl_3): 257 (4.38), 313 (4.13), 431 (3.14). IR (KBr) ν (cm^{-1}) 1510, 835, 538. MALDI-MS, *m/e* 1259.1 (M).

4.1.2. Synthesis of 6. Prepared as **5** from **4** (44 mg, 0.038 mmol). Yield: 30%. ^1H NMR (200 MHz, CDCl_3): δ 4.17 (s, 20H, C_5H_5), 4.33 (t, 8H, $J=1.6$ Hz, HCp), 4.51 (t, 8H, $J=1.8$ Hz, HCp), 4.92 (A of AB_q , 1H, $J=10.4$ Hz, $\text{H}_2\text{C}_{\text{pyrrol}}$), 5.16 (B of AB_q , 1H, $J=10.4$ Hz, $\text{H}_2\text{C}_{\text{pyrrol}}$), 5.86 (s, 1H, $\text{HC}_{\text{pyrrol}}$), 6.75 (A of AB_q , 4H, $J=16.2$ Hz, $\text{CH}=\text{}$), 6.98 (B of AB_q , 4H, $J=16.0$ Hz, $\text{CH}=\text{}$), 7.24 (s broad, 4H, $\text{CH}=\text{}$), 7.39 (s, 2H, H_{arom}), 7.48 (s broad, 4H, H_{arom}), 7.74 (s, 1H, H_{arom}), 7.90 (s, 2H, H_{arom}). ^{13}C NMR (50 MHz, CDCl_3): δ 156.08, 153.88, 153.30, 150.78,

150.60, 150.29, 149.80, 149.40, 148.40, 148.24, 147.60, 147.47, 147.24, 146.70, 146.33, 146.29, 145.72, 145.52, 145.32, 145.06, 144.45, 143.09, 142.87, 142.42, 142.27, 141.93, 140.50, 138.93, 138.79, 138.47, 138.38, 137.48, 135.85, 134.12, 133.96, 133.74, 133.53, 133.31, 130.77, 130.02, 129.64, 127.95, 127.74, 127.71, 125.99, 123.57, 122.73, 83.50, 81.36, 73.04, 69.55, 69.45, 69.44, 67.18. UV–vis λ_{\max} (nm) (log ϵ , CHCl₃): 258 (4.80), 318 (4.77), 431 (3.57). IR (KBr) ν (cm⁻¹) 1531, 625, 528. MALDI-MS, *m/e* 1883.2 (M).

4.1.3. Synthesis of 1. A mixture of **7a** (100 mg, 0.036 mmol) and thionyl chloride (0.1 mL, 1.3 mmol) was heated under reflux for 7 h in anhydrous CH₂Cl₂. The solvent was evaporated under reduced pressure and added to a solution of **5** (20 mg, 0.016 mmol) in 25 mL of CH₂Cl₂ and anhydrous pyridine (1.5 mg, 0.02 mmol). The mixture was stirred at room temperature for 2 h. After evaporation of the solvent under reduced pressure, the residue was purified by column chromatography (toluene/hexane 4:1). A further purification by centrifugation with CH₃OH afforded **1** in quantitative yield as a dark brown solid. ¹H NMR (200 MHz, CDCl₃): δ 1.24–1.70 (m broad, 60H, H_{aliph.}), 1.72–1.92 (m broad, 20H, 5 × CO₂CH₂CH₂ + 5 × CH₂CH₂O), 4.03 (t, 10H, *J* = 6.4 Hz, CH₂O), 4.14 (s, 10H, C₅H₅), 4.36 (m, 14H, 4 × HCp + 5 × CO₂CH₂), 4.50 (t, 4H, *J* = 1.8 Hz, HCp), 5.80 (AB_q, 2H, H₂C_{pyrrol.}), 6.22 (s, 1H, HC_{pyrrol.}), 6.80 (A of AB_q, 2H, *J* = 16.0 Hz, CH=), 6.94 (B of AB_q, 1H, CH=), 6.97 (m, 11H, *J* = 8.8 Hz, 10 × H_{arom.} + CH=), 7.15–7.36 (m, 8H, *J* = 8.4 Hz, H_{arom.}), 7.60 (s, 1H, H_{arom.}), 7.61–7.75 (m, 24H, H_{arom.}), 7.90 (d, 2H, *J* = 8.4 Hz, H_{arom.}), 8.12–8.20 (m, 16H, H_{arom.}), 8.21 (s, 2H, H_{arom.}), 8.37 (t, 2H, *J* = 1.5 Hz, H_{arom.}), 8.65 (t, 2H, *J* = 1.5 Hz, H_{arom.}), 8.94 (t, 1H, *J* = 1.5 Hz, H_{arom.}). ¹³C NMR (50 MHz, CDCl₃): δ 165.54, 164.69, 164.61, 164.20, 163.90, 163.49, 163.06, 162.95, 162.80, 155.23, 152.68, 151.67, 151.43, 150.39, 150.12, 147.47, 146.26, 146.08, 146.00, 145.88, 145.76, 145.59, 145.43, 145.24, 145.11, 145.04, 144.72, 144.46, 144.35, 144.17, 143.95, 143.09, 142.62, 142.12, 141.92, 141.86, 141.67, 140.14, 139.52, 139.17, 137.76, 136.93, 136.85, 136.55, 135.20, 134.35, 132.58, 132.49, 132.28, 130.02, 128.72, 128.28, 127.62, 126.98, 123.59, 123.28, 121.17, 120.27, 118.87, 114.55, 111.00, 95.91, 82.89, 82.80, 70.09, 69.72, 69.52, 68.62, 68.52, 67.36, 67.18, 66.07, 65.79, 30.04, 29.80, 29.42, 28.98, 21.83. UV–vis λ_{\max} (nm) (log ϵ , CHCl₃): 279 (5.31). IR (KBr) ν (cm⁻¹) 2223, 1726, 1598, 1055, 845, 538. MALDI-MS, *m/e* 3989.1 (M + 1).

4.1.4. Synthesis of 2. Prepared as **1** from **6** (18.8 mg, 0.01 mmol). Dark brown solid. Quantitative yield. ¹H NMR (200 MHz, CDCl₃): δ 0.70–1.70 (m broad, 60H, H_{aliph.}), 1.71–2.0 (m broad, 20H, 5 × CO₂CH₂CH₂ + 5 × CH₂CH₂O), 4.04 (t, 10H, *J* = 6.4 Hz, CH₂O), 4.17 (s, 20H, C₅H₅), 4.37 (m, 18H, 8 × HCp + 5 × CO₂CH₂), 4.53 (t, 8H, *J* = 1.8 Hz, HCp), 5.83 (AB_q, 2H, H₂C_{pyrrol.}), 6.25 (s, 1H, HC_{pyrrol.}), 6.76 (A of AB_q, 4H, *J* = 16.0 Hz, CH=), 6.97 (m, 14H, *J* = 8.8 Hz, 10 × H_{arom.} + 4 × CH=), 7.15–7.36 (m, 12H, *J* = 8.4 Hz, 8 × H_{arom.} + 4 × CH=), 7.40 (s, 2H, H_{arom.}), 7.50 (s, 4H, H_{arom.}), 7.57–7.90 (m, 27H, H_{arom.}), 8.09–8.16 (m, 16H, H_{arom.}), 8.19 (s, 2H, H_{arom.}), 8.36 (t, 2H, *J* = 1.5 Hz, H_{arom.}), 8.63 (t, 2H, *J* = 1.5 Hz, H_{arom.}), 8.93 (t,

1H, *J* = 1.5 Hz, H_{arom.}). ¹³C NMR (50 MHz, CDCl₃): δ 165.08, 164.96, 164.59, 164.33, 163.93, 163.48, 163.30, 163.26, 160.65, 155.89, 153.99, 151.88, 151.84, 151.48, 150.82, 150.79, 150.63, 149.22, 148.42, 148.22, 148.01, 147.46, 147.25, 146.72, 146.63, 146.59, 146.57, 145.60, 145.26, 145.25, 145.11, 145.09, 144.77, 144.71, 144.54, 143.39, 143.28, 142.88, 144.21, 142.01, 141.74, 140.16, 137.11, 136.90, 133.46, 132.96, 132.84, 132.72, 132.54, 131.71, 131.40, 131.27, 130.73, 130.36, 130.21, 129.68, 128.51, 127.89, 127.16, 122.74, 121.54, 120.63, 118.99, 114.80, 114.62, 111.31, 81.01, 80.37, 70.70, 69.71, 68.58, 67.85, 66.07, 65.77, 53.57, 45.53, 29.89, 29.51, 29.42, 28.88, 28.58, 26.17, 22.87, 22.52. UV–vis λ_{\max} (nm) (log ϵ , CHCl₃): 279 (5.37). IR (KBr) ν (cm⁻¹) 2218, 823, 533. MALDI-MS, *m/e* 4613.4 (M + 1).

Acknowledgements

R.D. thanks the Swiss National Science Foundation (Grant no. 200020-103424) for financial support. This work was supported by the EU (RTN contract “FAMOUS”, HPRN-CT-2002-00171), the Ministerio of Educación y Ciencia of Spain (Project CTQ2004-00364/BQU) and FEDER funds. L.P. thanks a grant from the Ministerio de Educación y Ciencia of Spain.

References and notes

- Martín, N.; Sánchez, L.; Illescas, B.; Pérez, I. *Chem. Rev.* **1998**, *98*, 2527.
- (a) Nierengarten, J.-F.; Eckert, J.-F.; Nicoud, J.-F.; Ouali, L.; Krasnikov, V.; Hadziioannou, G. *Chem. Commun.* **1999**, 617. (b) Eckert, J.-F.; Nicoud, J.-F.; Nierengarten, J.-F.; Liu, S.-G.; Echegoyen, L.; Barigelletti, F.; Armaroli, N.; Ouali, L.; Krasnikov, V.; Hadziioannou, G. *J. Am. Chem. Soc.* **2000**, *122*, 7467. (c) Peeters, E.; van Hal, P. A.; Knol, J.; Brabec, C. J.; Sariciftci, N. S.; Hummelen, J. C.; Janssen, R. A. J. *J. Phys. Chem. B* **2000**, *104*, 10174. (d) Marcos Ramos, A.; Rispens, M. T.; van Duren, J. K. J.; Hummelen, J. C.; Janssen, R. A. J. *J. Am. Chem. Soc.* **2001**, *123*, 6714. (e) Zerza, G.; Röthler, B.; Sariciftci, N. S.; Gómez, R.; Segura, J. L.; Martín, N. *J. Phys. Chem. B* **2001**, *105*, 4099. (f) Guldi, D. M.; Swartz, A.; Luo, C.; Gómez, R.; Segura, J. L.; Martín, N. *J. Am. Chem. Soc.* **2002**, *124*, 10875. (g) Martineau, C.; Blanchard, P.; Rondeau, D.; Delaunay, J.; Roncali, J. *Adv. Mater.* **2002**, *14*, 283.
- (a) Imahori, H.; Sakata, Y. *Eur. J. Org. Chem.* **1999**, 2445. (b) Guldi, D. M. *Chem. Commun.* **2000**, 321. (c) Guldi, D. M. *Chem. Soc. Rev.* **2002**, *31*, 22.
- (a) Guldi, D. M.; Maggini, M.; Scorrano, G.; Prato, M. *J. Am. Chem. Soc.* **1997**, *119*, 974. (b) Guldi, D. M.; Prato, M. *Acc. Chem. Res.* **2000**, *33*, 695.
- (a) Yu, G.; Gao, J.; Hummelen, J. C.; Wudl, F.; Heeger, A. J. *Science* **1995**, *270*, 1789. (b) Brabec, C. J.; Sariciftci, N. S.; Hummelen, J. C. *Adv. Funct. Mater.* **2001**, *11*, 15. (c) Shaheen, S. E.; Brabec, C. J.; Sariciftci, N. S.; Padinger, F.; Fromherz, T.; Hummelen, J. C. *Appl. Phys. Lett.* **2001**, *78*, 841.
- Hutchison, K.; Gao, J.; Schick, G.; Rubin, Y.; Wudl, F. *J. Am. Chem. Soc.* **1999**, *121*, 5611.

7. (a) Schmidt-Mende, L.; Fechtenkötter, A.; Müllen, K.; Moons, E.; Friend, R. H.; MacKenzie, J. D. *Science* **2001**, *293*, 1119. (b) Pisula, W.; Tomović, Ž.; El Hamaoui, B.; Watson, M. D.; Pakula, T.; Müllen, K. *Adv. Funct. Mater.* **2005**, *15*, 893.
8. (a) Deschenaux, R.; Even, M.; Guillon, D. *Chem. Commun.* **1998**, 537. (b) Even, M.; Heinrich, B.; Guillon, D.; Guldi, D. M.; Prato, M.; Deschenaux, R. *Chem. Eur. J.* **2001**, *7*, 2595. (c) Campidelli, S.; Vázquez, E.; Milic, D.; Prato, M.; Barberá, J.; Guldi, D. M.; Marcaccio, M.; Paolucci, D.; Paolucci, F.; Deschenaux, R. *J. Mater. Chem.* **2004**, *14*, 1266.
9. (a) Deschenaux, R.; Schweissguth, M.; Levelut, A.-M. *Chem. Commun.* **1996**, 1275. (b) Deschenaux, R.; Schweissguth, M.; Vilches, M.-T.; Levelut, A.-M.; Hautot, D.; Long, G. L.; Luneau, D. *Organometallics* **1999**, *18*, 5553.
10. Ruiz, J.; Pradet, C.; Varret, F.; Astruc, D. *Chem. Commun.* **2002**, 1108.
11. (a) Valério, C.; Fillaut, J.-L.; Ruiz, J.; Guittard, J.; Blais, J.-C.; Astruc, D. *J. Am. Chem. Soc.* **1997**, *119*, 2588. (b) Casado, C. M.; González, B.; Cuadrado, I.; Alonso, B.; Morán, M.; Losada, J. *Angew. Chem., Int. Ed.* **2000**, *39*, 2135. (c) Alonso, B.; Casado, C. M.; Cuadrado, I.; Morán, M.; Kaifer, A. E. *Chem. Commun.* **2002**, 1778. (d) Daniel, M.-C.; Ba, F.; Ruiz Aranzaes, J.; Astruc, D. *Inorg. Chem.* **2004**, *43*, 8649.
12. (a) Prato, M.; Maggini, M. *Acc. Chem. Res.* **1998**, *31*, 519. (b) Tagmatarchis, N.; Prato, M. *Synlett* **2003**, 768.
13. Chuard, T.; Deschenaux, R. *J. Mater. Chem.* **2002**, *12*, 1944.
14. Bracher, P. J.; Schuster, D. I. In *Fullerenes: From Synthesis to Optoelectronic Properties*; Guldi, D. M., Martín, N., Eds.; Kluwer Academic, 2002; pp 163–212.
15. Gust, D.; Moore, T. A.; Moore, A. L. *Acc. Chem. Res.* **2001**, *34*, 40.
16. A residual absorption of light by the ferrocene dendrimer cannot be excluded.
17. (a) D'Souza, F.; Zandler, M. E.; Smith, P. M.; Deviprasad, G. R.; Arkady, K.; Fujitsuka, M.; Ito, O. *J. Phys. Chem. A* **2002**, *106*, 649. (b) Zandler, M. E.; Smith, P. M.; Fujitsuka, M.; Ito, O.; D'Souza, F. *J. Org. Chem.* **2002**, *67*, 9122.

Guanosine and fullerene derived de-aggregation of a new phthalocyanine-linked cytidine derivative

Jonathan L. Sessler,^{a,*} Janarthanan Jayawickramarajah,^a Andreas Gouloumis,^b G. Dan Pantos,^a Tomás Torres^{b,*} and Dirk M. Guldi^{c,*}

^aDepartment of Chemistry and Biochemistry and Institute for Cellular and Molecular Biology, 1 University Station, A5300, University of Texas at Austin, Austin, TX 78712-0165, USA

^bUniversidad Autónoma de Madrid, Departamento de Química Orgánica, Campus de Cantoblanco, Madrid, Spain

^cUniversität Erlangen, Institute for Physical and Theoretical Chemistry, 91058 Erlangen, Germany

Received 20 April 2005; accepted 4 May 2005

Available online 21 November 2005

Abstract—Electronic absorption and emission properties of a new cytidine tethered zinc phthalocyanine **2** were used to probe the aggregation and guanosine/C₆₀ derived de-aggregation of this nucleobase linked phthalocyanine. These experiments revealed that **2** aggregates even at low concentrations in a competitive solvent system (1.1 × 10⁻⁶ M in 20% DCM/toluene). Nucleobase–metal coordination and slipped co-facial π-stacking interactions are both important in aggregate formation. Guanosine **5**, C₆₀ **6**, and a guanosine–C₆₀ chimera **4** were employed as potential aggregate disruptors. These experiments revealed that both guanosine and fullerene subunits are effective in disrupting the aggregate formed by **2**. Such findings support the conclusion that base-pairing, π-stacking, as well as nucleobase–metal coordination interactions play important roles in the de-aggregation of **2**.

© 2005 Elsevier Ltd. All rights reserved.

1. Introduction

Phthalocyanines (Pcs), and their metallated congeners, are an important class of non-natural organic pigments that have received considerable attention in recent years.¹ These 18 π-electron macrocyclic systems have shown considerable promise for a wide range of applications, including as materials for optical data storage² and nonlinear optics,³ as well as photosensitizers for photodynamic therapy.⁴ The common denominator in these applications is the useful photophysical properties of Pcs. In fact, these highly colored molecules absorb intensely in the 700 nm spectral range, a region where the solar photon flux is a maximum. Furthermore, once illuminated Pcs are capable of efficient electron donation to fullerene acceptors.⁵ These attributes render Pcs especially attractive as possible components in photovoltaic devices that can harvest and convert solar energy into chemical energy.

The propensity of Pcs to self-aggregate through coplanar

association of the Pc rings to form dimers and higher order aggregates is well known.⁶ This tendency, can cause Pcs to be insoluble in many solvents and can also dramatically affect their photochemical properties. For instance, aggregation has been shown to cause a decrease in light absorption^{6,7} and has also been found to induce a large reduction in fluorescence quantum yield.⁸ On the other hand, the formation of well-defined Pc aggregates is useful in materials applications where the self-assembly of Pc cores in close proximity is beneficial.^{9,2a} In light of such considerations, it is not surprising that methods to manipulate the aggregation/de-aggregation properties of Pcs are being actively pursued.¹⁰

We and others have focused our efforts on using non-covalent synthesis as a strategy to assemble Pcs in conjunction with efficient electron acceptors such as fullerenes to study photoinduced electron transfer.¹¹ These systems have been assembled through various non-covalent interactions such as, ligand–metal coordination, π-stacking, and hydrogen bonding interactions. In this paper, we report the use of these non-covalent interactions to effect the aggregation and de-aggregation of a cytidine tethered zinc phthalocyanine (ZnPc) **2**. Specifically, we show how guanosine **5**, C₆₀ **6**, and a guanosine–C₆₀ hybrid **4** may be used to induce the de-aggregation of ZnPc **2** in solution.

Keywords: Phthalocyanine aggregation; Phthalocyanine de-aggregation; Fullerenes; Nucleobases; Non-covalent interactions; Electronic spectra.

* Corresponding authors. Tel.: +1 512 471 5009; fax: +1 512 471 7550 (J.L.S.); tel.: +34 91 497 4151; fax: +34 91 497 3966 (T.T.); tel.: +49 9131 852 7341; fax: +49 9131 852 8307 (D.M.G.); e-mail addresses: ssessler@mail.utexas.edu; tomas.torres@uam.es; dirk.guldi@chemie.uni-erlangen.de

2. Aggregation/de-aggregation of phthalocyanines

In general Pc aggregation is thought to reflect coplanar interactions involving the macrocycle ring.⁶ These interactions occur as a result of favorable van der Waals forces, π -stacking interactions, and solvent effects. The aggregation process of Pcs can be easily probed using electronic spectroscopy. Upon formation of higher order complexes, the coupling between the electronic states of individual monomeric Pc units causes significant spectral perturbations. For example, monomeric Pcs exhibit strong absorption bands in the 300 and 700 nm spectral regions, termed the B and Q bands, respectively. The presence of higher order Pc systems can be observed in the Q band region of the electronic absorption spectrum. Typically, Pc aggregation results in a decrease in intensity in the components of the Q band corresponding to the monomeric species, meanwhile a new, broader and blue-shifted band is seen to increase in intensity. This shift to lower wavelengths corresponds to H-type aggregates. Rare cases of Pc aggregation causing red-shifted bands, corresponding to J-type aggregation, have also been observed.

3. Results and discussion

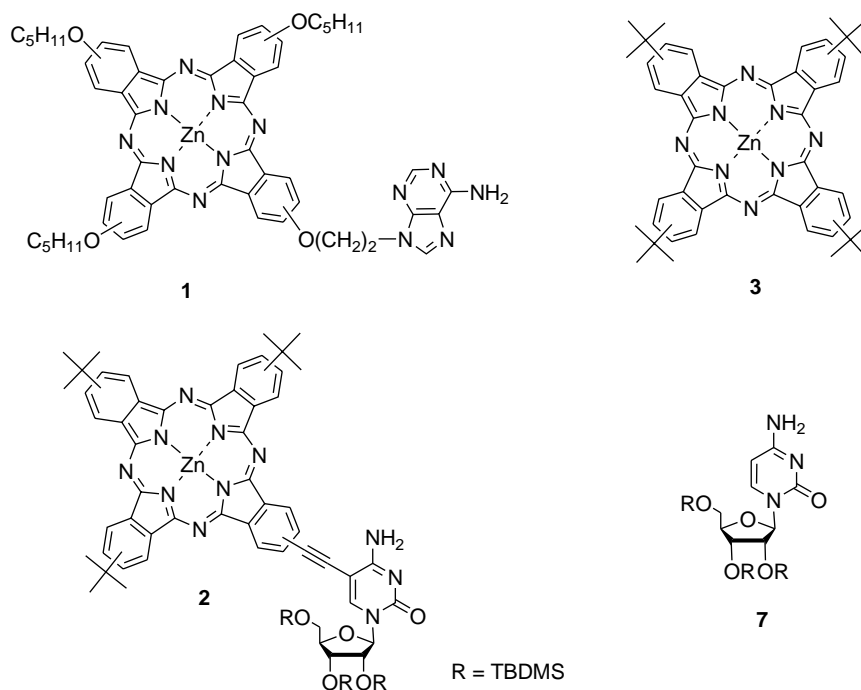
3.1. Aggregation behavior of nucleobase appended zinc phthalocyanines

A recent study by Ng and co-workers demonstrated that phthalocyanine-nucleobase conjugates, such as the adenine derivative **1**, can be prepared.^{10f} Additionally, it was found that these phthalocyanine conjugates possess a tendency to aggregate as a result of a variety of interaction modes. These intermolecular interactions include the typical π - π interactions between the macrocycle cores that one would expect for Pcs, as well as possible hydrogen bonding interactions due to the nucleobase unit. Another potential mode of interaction, proposed by the

authors, is through axial coordination of adenine to the zinc(II) center of the phthalocyanine macrocycle. A further advantage of using nucleobase tethered systems is the possibility of forming Watson–Crick base-pairs by the addition of a complementary nucleobase. Accordingly, in the same paper, Ng and colleagues have also investigated the base-pairing capability of adenine substituted Pcs with a thymine derivative.

Inspired by these initial nucleobase linked ZnPc systems, we have prepared cytidine tethered ZnPc **2**. It was rationalized that this novel nucleobase appended ZnPc should form stronger Watson–Crick base-pairing interactions than Pc **1**, because, the cytidine motif can form three-point hydrogen bonding interactions with a guanine moiety, whilst the adenine–thymine base-pair is only stabilized by two hydrogen bonds.¹² Furthermore, in this new system, a rigid alkynyl linker was used to tether the pyrimidine nucleobase to the ZnPc subunit. It was anticipated that increasing the rigidity of the system would lead to the formation of better-defined self-assemblies, as well as supporting stronger Watson–Crick type base-pairing interactions.¹³ In order to enhance solubility in organic solvents, lipophilic *tert*-butyl and *tert*-butyldimethylsilyl (TBDMS) groups were incorporated on the ZnPc and cytidine subunits, respectively.

Given that electronic absorption spectroscopy has been extensively used to determine the formation of Pc aggregation,⁶ we carried out our initial studies of aggregation effects with ZnPc **2** using this method. A typical spectrum of **2** (3.9×10^{-6} M), in dichloromethane (DCM), is shown in Figure 1. Two major bands are visible at 347 and 679 nm, respectively. These, so-called B and Q absorption bands are considered to originate from ligand-based π - π^* transitions.¹⁴ As is clearly evident from an inspection of Figure 1, the Q-band is rather broad with a significant blue-shifted shoulder appearing at ca. 630 nm. This result is consistent



with the conclusion that even at this low concentration regime ZnPc **2** displays significant aggregation behavior. Interestingly, adenine tethered ZnPc **1** at similar concentrations (6.3×10^{-6} – 1.0×10^{-4} M) was found to be free of aggregation in DCM as judged by UV–vis spectroscopy.^{10f} Thus, under the conditions of the above experiment, ZnPc **2** has a greater tendency to self-aggregate than the previously reported nucleobase derived ZnPc, system **1**.

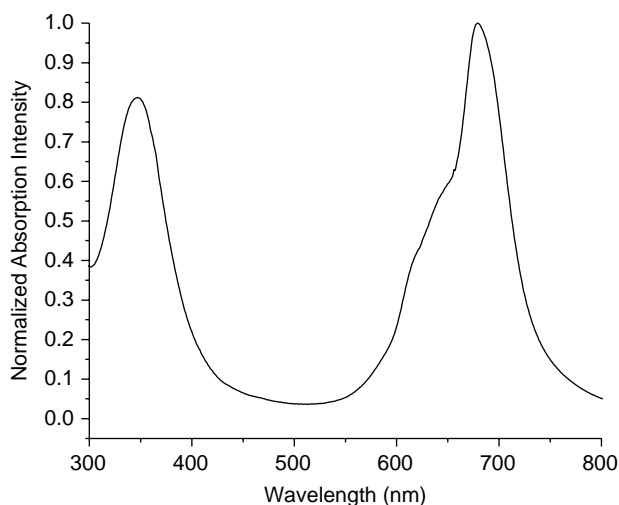


Figure 1. Normalized electronic absorption spectrum of the B- and Q-band regions of ZnPc **2** (3.9×10^{-6} M) in dichloromethane.

UV–vis experiments were also carried out in a more competitive solvent system (20% DCM in toluene), in order to test the stability of the self-aggregate and to elucidate the signature peaks corresponding to the monomeric form of **2**. Toluene was included in the mixture, since it was expected to act as a π – π interaction disruptor. Interestingly, even in this solvent system, at a concentration of 5.7×10^{-5} M, ZcPc **2** is predominantly aggregated (see Fig. 2). Under these conditions, the Q-band region of compound **2** is

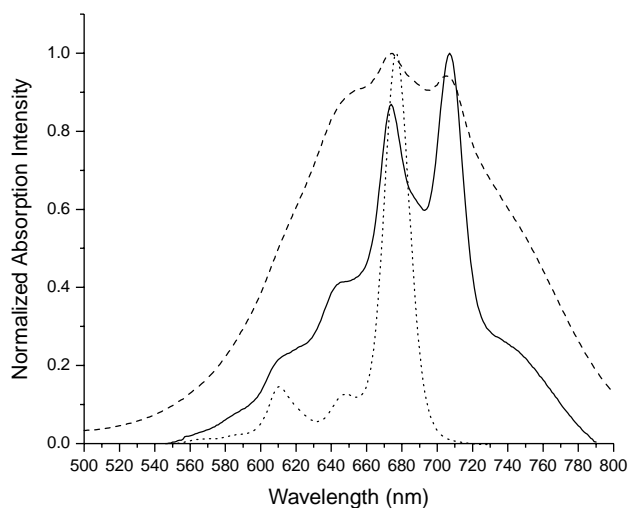


Figure 2. Normalized absorption spectra of the Q-band region of ZnPc **2** (dashed line corresponds to $[2] = 5.7 \times 10^{-5}$ M, solid line corresponds to $[2] = 1.1 \times 10^{-6}$ M) and control **3** (dotted line: $[3] = 2.5 \times 10^{-6}$ M) in 20% DCM/toluene.

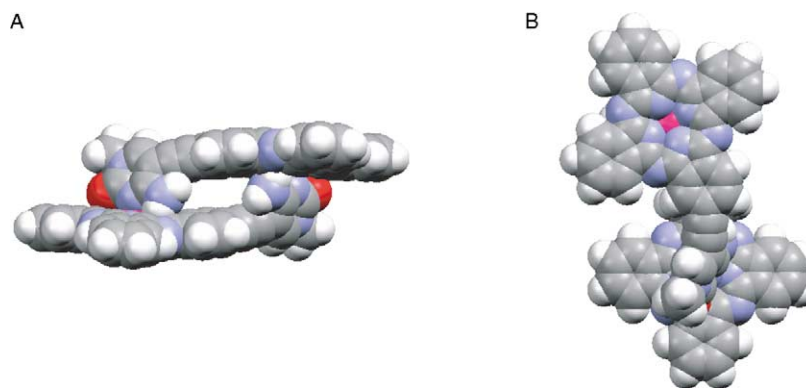
characterized by a very broad band, almost void of structure except for one small hump corresponding to a maximum at 674 nm and a second smaller hump at 708 nm. The broadness of the Q-band (the width of which is ca. 127 nm at half height) is considered to be clear evidence of substantial aggregation.

When ZnPc **2** is diluted to a concentration of 1.1×10^{-6} M, evidence of aggregation is still apparent. For instance, the presence of a shoulder at ca. 750 nm is typical of aggregation. However, at this concentration, the absorption features corresponding to the monomeric species are also evident. For instance, a clearly split Q-band, with peaks at 674 and 708 nm, attributed to the monomeric species, is visible.¹⁵ The reason for the split in the Q-band region is thought to reflect the unsymmetric nature of the ZnPc moiety, arising from the introduction of the cytidine motif onto the isoindole ring. Two minor vibrational satellites corresponding to the monomeric species are also observable at ca. 613 and 644 nm. Still, it must be noted that the features present in this region (600–662 nm) are rather broadened, leading us to suggest the underlying presence of a low intensity, blue-shifted absorption band corresponding to one or more aggregated species.

The blue shifting and the broadening in the Q-band region of **2**, ascribed to aggregation are both features that are consistent with linearly stacked Pc monomers.⁶ In an effort to understand better the nature of the aggregates formed in the case of **2** and to determine the influence imparted by the cytidine subunit on the overall aggregation process, control studies using tetra-*tert*-butyl ZnPc **3** (lacking the nucleobase functionality) were carried out. As illustrated in Figure 2, ZnPc **3** showed no evidence of aggregation at 2.5×10^{-6} M in 20% DCM/toluene. Rather, an absorption band corresponding only to the monomeric form was observed. In particular, a sharp absorbance maximum at 677 nm (the width of which is ca. 18 nm at half height) was seen, as well as two vibrational satellites at 611 and 648 nm, respectively.

The above mentioned UV–vis experiments indicate that the cytidine subunit and the ZnPc macrocycle are both important in the observed aggregation of **2**. Furthermore, the mode of aggregation results, at least in part, from stacked ZnPc monomers. A proposed mode of aggregation is illustrated in Scheme 1, wherein the aggregate is stabilized by axial coordination of the cytidine subunit to the zinc(II) center that acts in conjunction with slipped cofacial π – π interactions between the Pc macrocycles.

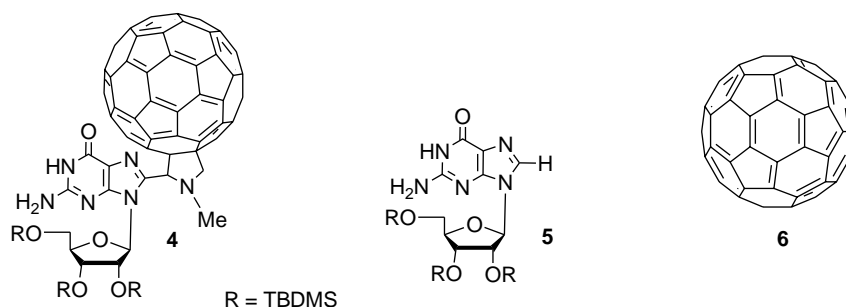
Control studies, involving ZnPc **3** and 2',3',5'-tri-*O*-*tert*-butyldimethylsilyl protected cytidine **7**, were performed to verify that the cytidine moiety can interact with the ZnPc macrocycle. As cytidine **7** (0 – 2.1×10^{-5} M) is titrated into a solution containing **3** (2.5×10^{-6} M) in 20% DCM/toluene, a decrease in the absorption maximum at 677 nm is seen. A plot of the change in absorption at 677 nm versus concentration of cytidine **7** displays typical binding behavior (Fig. 3a). Based on these findings, and in analogy to the findings of Ng^{10f} and others,¹⁶ it is thought that the cytidine motif interacts with the Pc moiety in **2** through axial coordination to the metal center. Presumably, this occurs through the N3 nitrogen (see Scheme 1), since it is



Scheme 1. Computer generated model showing the side view (A) and top view (B) of one possible aggregation mode for ZnPc **2** (for clarity the ribose unit has been replaced by a methyl group and the *t*-butyl motifs have been omitted).

the most basic nitrogen center present on the nucleobase. Further evidence supporting the notion that axial metal coordination may play an important role in the aggregation of ZnPc **2** came from the addition of pyridine into a solution of **2** in 20% DCM/toluene (Fig. 3b). Pyridine is an effective axial ligand for Zn(II) centers constrained within a macrocyclic framework,^{18a} and not surprisingly complete disruption of aggregation is seen, as evidenced by the clean monomer-type spectrum.

to complement the functionalities present on ZnPc **2**. For instance, it was envisaged that the guanosine motif on **4** would base-pair with the cytidine subunit of **2**, thus inducing a break up of the self-aggregation normally caused by this subunit. Similarly, the fullerene motif was included since it is known that fullerenes can bind porphyrinoid macrocycles through π - π interactions, and more specifically, that Pcs can interact with fullerenes in solution and in the solid state.^{18,5c} In particular, it was thought that the fullerene



3.2. Disruption of aggregation using guanosine-appended fulleropyrrolidine (**4**)

In order to promote the disassembly of ZnPc **2**, guanosine derivative **4** was synthesized.¹⁷ This molecule was designed

subunit would induce break up of the aggregate by participating in non-covalent π - π interactions involving ZnPc **2**. Nucleobase **5** and commercially available C₆₀ **6** were used as controls to gage the effectiveness of each subunit separately in terms of effecting aggregate breakup.

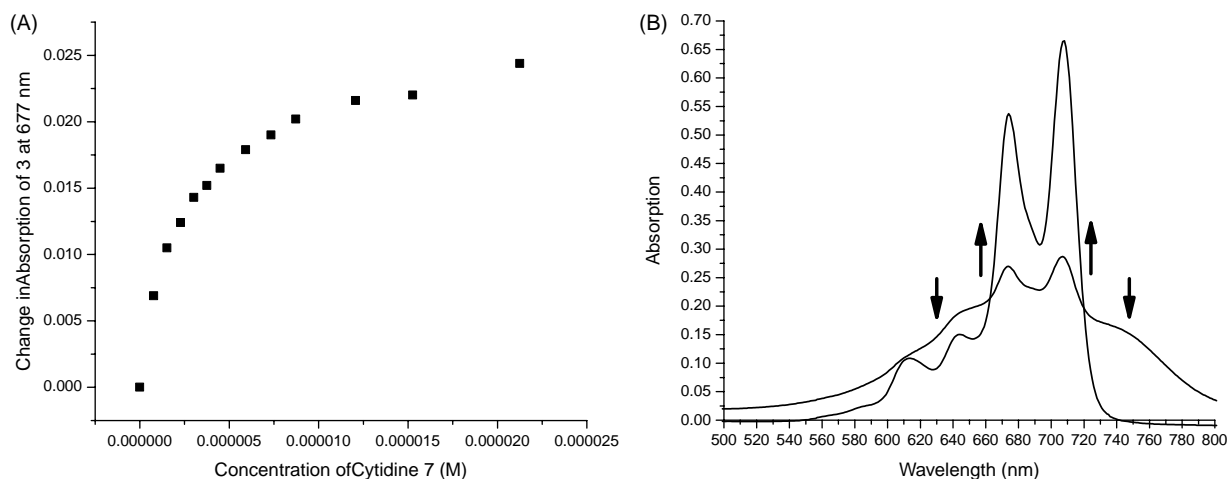


Figure 3. (A) A plot depicting the change in ZnPc **3** (2.5×10^{-6} M) absorption at 677 nm versus increasing concentration of cytidine **7** (0 – 2.1×10^{-5} M), in 20% DCM/toluene. (B) Change in the absorption spectrum of ZnPc **2** (ca. 2.0×10^{-6} M) in 20% DCM/toluene upon addition of a drop of pyridine.

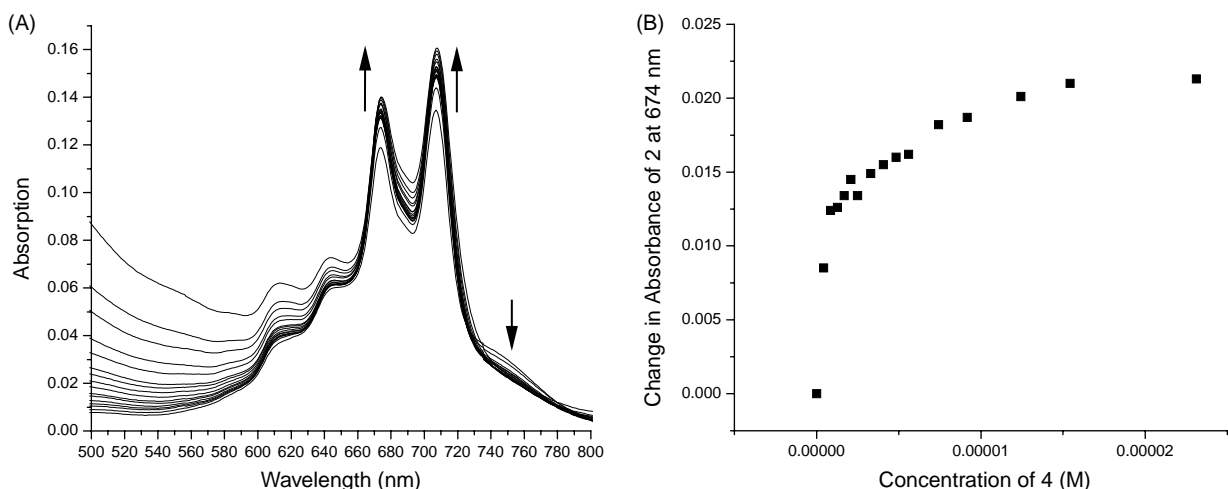


Figure 4. (A) Changes in the absorption spectrum of ZnPc **2** (1.0×10^{-6} M) seen upon the addition of increasing concentrations of **4** (0 – 2.3×10^{-5} M) in 20% DCM/toluene. (B) Plot showing the change in ZnPc **2** (1.0×10^{-6} M) absorption intensity at 674 nm versus concentration of **4** (0 – 2.3×10^{-5} M) in 20% DCM/toluene.

Electronic absorption spectroscopy was employed to detect the de-aggregation process caused by the addition of guanosine tethered fullerene **4**. For this experiment, the conditions were chosen such that the monomeric species of **2** as well as the aggregated form are both present in solution (i.e., $[2] \sim 1.0 \times 10^{-6}$ M in 20% DCM/toluene). The results from this experiment are shown in Figure 4. The Q-band region corresponding to the monomeric species is seen to increase upon increasing concentration of **4** (0 – 2.3×10^{-5} M). In fact, a plot of absorption at 674 nm (a band that is attributed to the monomeric species) versus concentration of guanosine **4** (see Fig. 4b), results in a sharp increase followed by a plateau. This behavior is interpreted as being caused by an increase in monomer concentration as a result of the addition of increasing aliquots of **4**.

More evidence for de-aggregation came from the observation that the broad shoulder at 750 nm decreases in intensity, albeit by a small amount. Unfortunately, a decrease of the low intensity, blue-shifted, aggregate band, which overlaps the vibrational bands of the monomer was not observed. The reason for this is due to the concomitant increase of a rather high intensity absorption band of **4** in this region of the spectrum.

3.3. De-aggregation experiments with guanosine (**5**) and C_{60} (**6**)

Similar de-aggregation experiments were pursued using the guanosine control compound **5** to confirm that the guanosine subunit was capable of base-pairing with the cytidine subunit of **2** and as a consequence, disrupting self-aggregation. The results (Fig. 5) show a clear increase in the monomeric bands at 674 (see Fig. 5b) and 708 nm upon the addition of increasing quantities of guanosine **5** (0 – 6.9×10^{-5} M). In addition, the region between 600–660 nm shows spectral features characteristic of de-aggregation. In particular, the broad band ascribed to the aggregated species was seen to decrease in intensity, while the vibrational satellites corresponding to the monomeric species became more distinct. The shoulder at 750 nm was also seen to disappear upon adding increasing

concentrations of **5**. These observations, in conjunction with the presence of clean isosbestic points at 662 and 723 nm, are considered as prima facie evidence that the guanosine motif is capable of de-aggregating the ensemble(s) resulting from the self-assembly of the cytidine-linked ZnPc **2**.

UV–vis titrations of ZnPc **2** with C_{60} **6** in 20% DCM/toluene were also carried out in an effort to determine whether the fullerene moiety is also capable of breaking up aggregates formed from ZnPc **2**. As shown in Figure 6, titration of C_{60} **6** (0 – 2.2×10^{-5} M) into a solution of **2** (1.3×10^{-6} M) gives rise to typical de-aggregation behavior. Here, the absorption corresponding to the monomer increases in intensity (see Fig. 6b), while spectral features corresponding to the aggregate decrease in intensity. These findings, support the notion that fullerene, with electron accepting capabilities, can interact with ZnPc which possesses electron donating features.

These de-aggregation studies lead us to suggest that both guanosine and C_{60} motifs can effect de-aggregation of ZnPc–cytidine conjugate **2**. In addition, the de-aggregation is thought to occur, for the most part, as a result of either base-pairing (in the case of compounds **4** and **5**) or π – π interactions (in the case of **4** and **6**).

3.4. Control studies with ZnPc (**3**)

While it is not surprising that guanosine derivatives **4** and **5** can disrupt ZnPc–cytidine **2** aggregation as a result of base-pairing, other interactions (such as axial ligation of guanosine with the metal center) should also be taken into account. Control experiments, involving ZnPc **3** and the aggregation disruptors **4**, **5** and **6** in 20% DCM/toluene, were undertaken in an effort to gain a further understanding of how these latter species can interact with the macrocycle core. Titrations involving all three guest compounds gave rise to similar observations. Specifically, the absorption maximum at 677 nm is seen to decrease in intensity upon addition of all three guests. A typical spectrum is shown in Figure 7a. Despite the relatively small change in absorbance

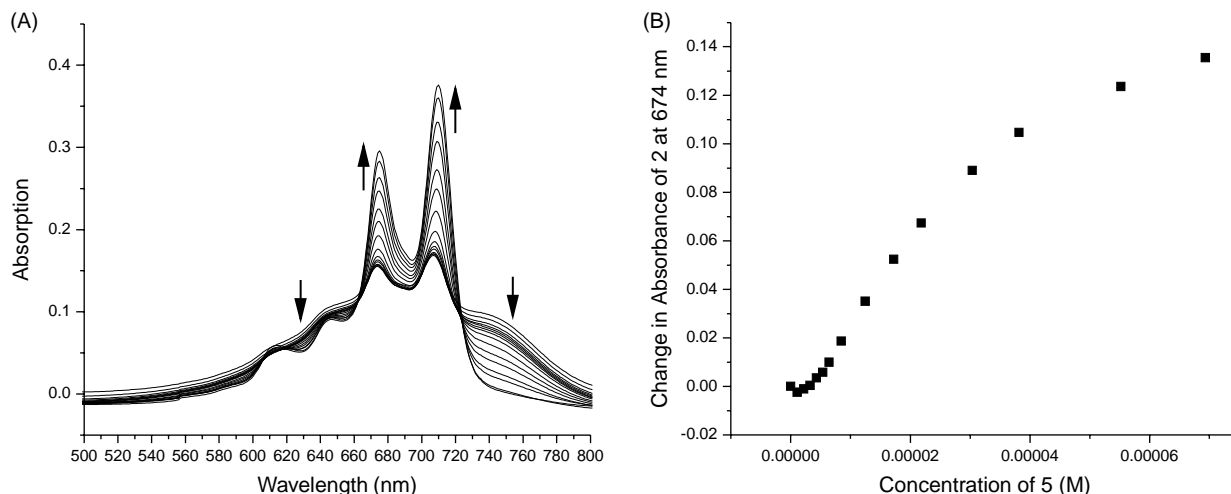


Figure 5. (A) Changes in the absorption spectrum of ZnPc **2** (1.3×10^{-6} M) seen upon the addition of increasing concentrations of guest **5** (0 – 6.9×10^{-5} M) in 20% DCM/toluene. (B) Plot depicting the change in absorption intensity of **2** (1.3×10^{-6} M) at 674 nm versus concentration of guest **5** (0 – 6.9×10^{-5} M) in 20% DCM/toluene.

intensity seen over the course of the titration, the structures of the resulting curves (Fig. 7b) suggest that all three guest molecules are involved in binding.¹⁹ These results serve to verify that the C₆₀ subunit can interact with the ZnPc core. More interestingly, the results also lead to the inference that the guanosine motif per se also has some affinity for the ZnPc core. One possible mode of interaction of guanosine with ZnPc **3** is through coordination of the N7 nitrogen to the central Zn atom.¹⁶

3.5. Fluorescence spectroscopy

Fluorescence spectroscopy can also be used as a tool to investigate aggregation in Pc systems, since aggregate formation results in significant quenching of fluorescence.^{6,7} Accordingly, the fluorescence emission of ZnPc **2** was monitored as increasing aliquots of disruptor molecules **4**, **5**, and **6**, respectively, in 20% DCM/toluene, were added. As expected, addition of guanosine **5** and C₆₀ **6** resulted in an increase in the fluorescence emission followed by saturation

behavior (Fig. 8b). These observations are consistent with the UV–vis studies (see Sections 3.3 and 3.4 supra), and support the proposal that the addition of either **5** or **6** induces de-aggregation of ZnPc **2**.

Interestingly, the maximum increase in fluorescence emission upon the addition of guanosine **5** ($I/I_0 = 2.4$) is significantly larger than the maximum for C₆₀ **6** ($I/I_0 = 1.7$). The reason for the lower I/I_0 value is thought to reflect photoinduced electron transfer from the photoexcited ZnPc **2** to C₆₀ **6**.⁵ In accord with such an explanation, titration of fulleropyrrolidine **4** into a solution of ZnPc **2** (see Fig. 8a), showed almost no increase in fluorescence intensity (maximum value for $I/I_0 \sim 1.0$). Instead, a clear decrease in the intensity of fluorescence emission is observed. While not yet studied in detail, this decrease in intensity is attributed to intra-complex photoinduced electron transfer, which outweighs any increase in fluorescence emission resulting from effecting the de-aggregation of **2**. The nature and time scale of the photoinduced electron transfer process

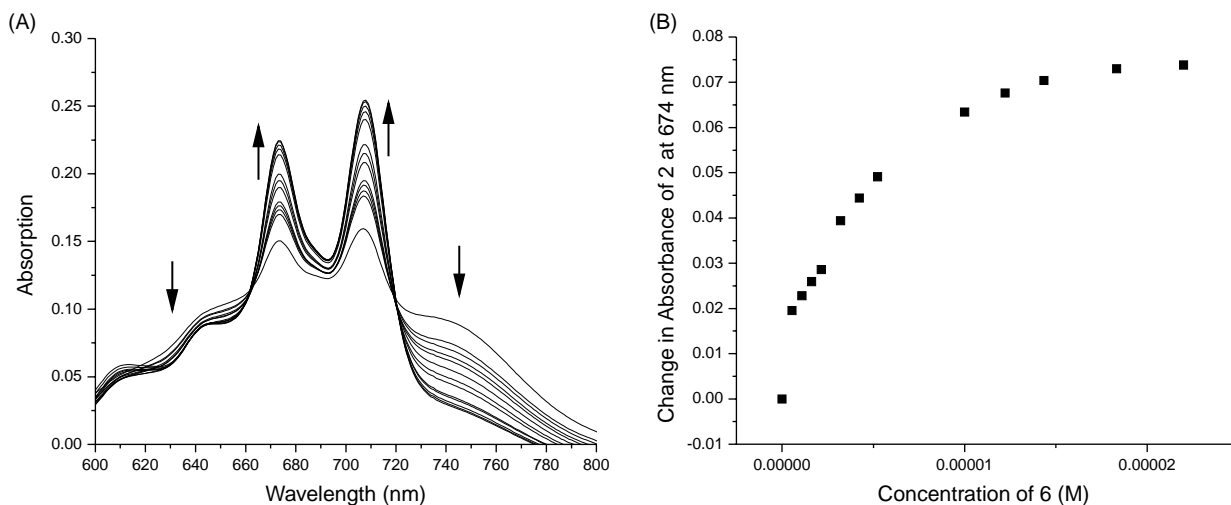


Figure 6. (A) Changes in the absorption spectrum of ZnPc **2** (1.3×10^{-6} M) seen upon the addition of increasing concentrations of guest **6** (0 – 2.2×10^{-5} M) in 20% DCM/toluene. (B) A plot illustrating the change in ZnPc **2** (1.3×10^{-6} M) absorption at 674 nm versus concentration of **6** (0 – 2.2×10^{-5} M) in 20% DCM/toluene.

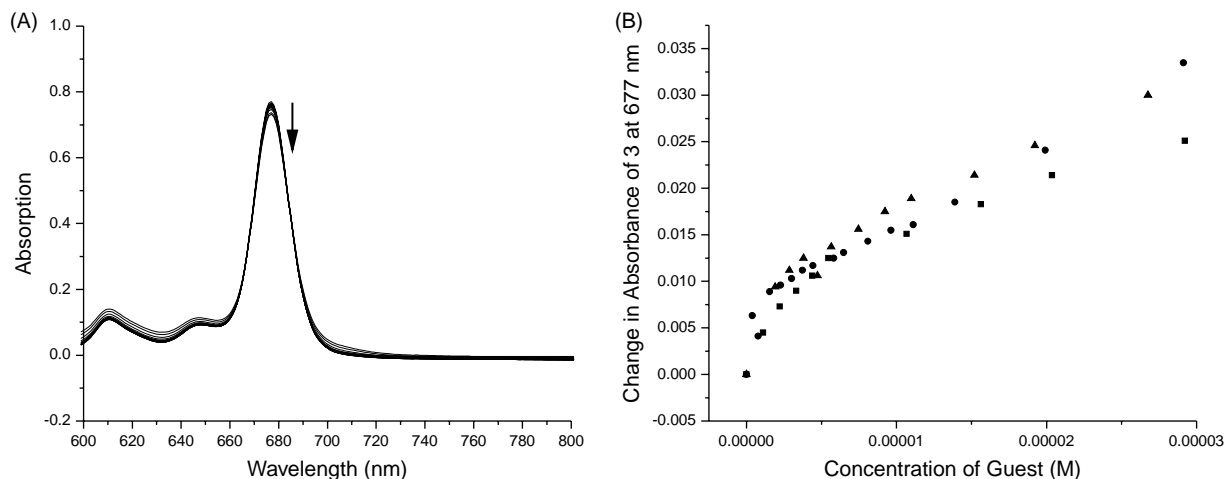


Figure 7. (A) Changes in the absorption spectrum of ZnPc **3** (2.5×10^{-6} M) seen upon the addition of increasing concentrations of **4** ($0\text{--}2.9 \times 10^{-5}$ M) in 20% DCM/toluene. (B) Plot depicting the change in ZnPc **3** ($\sim 3.0 \times 10^{-6}$ M) absorption intensity at 677 nm versus concentration of guest (**4** (●), **5** (■), and **6** (▲)) in 20% DCM/toluene.

between ZnPc–cytidine **2** and fullerene tethered guanosine **4** is currently being investigated in our laboratories. Results from these studies will be published in due course.

4. Conclusion

Taken in concert the above results indicate that the cytidine–ZnPc hybrid **2** is highly ‘narcissistic’; as it undergoes self-assembly even at low concentrations in 20% DCM/toluene as a result of using both π – π interactions and cytidine macrocycle interactions. The resulting aggregate(s) can be broken up by the addition of guanosine, a nucleic acid base that can serve to tie up the cytidine functionality through base-pairing interactions. Additionally, guanosine can also directly interact with the metal center of the macrocycle. An alternative method of de-stabilizing the aggregate is to use the fullerene motif. This motif can compete with macrocycle–macrocycle π – π stacking interactions. The results of this paper thus serve to illustrate that fullerene and

guanosine, icon-like entities in supramolecular chemistry, can be used to modulate phthalocyanine aggregation.

5. Experimental

5.1. General

Melting points were determined using a Buchi melting point apparatus and are uncorrected. ¹H NMR spectra were obtained on a Bruker AC-300 (300 MHz) spectrometer. Mass-spectra were determined on a VG AUSTOspec apparatus. Elemental analyses were performed on a Perkin-Elmer 2400 CHN elemental analyzer. UV–vis spectra were taken on a Beckman DU 540 spectrophotometer. Fluorescence measurements were obtained using a SPEX-332 spectrofluorimeter. Fluorescence titrations were carried out by exciting the samples at the isosbestic points, where possible. Otherwise, the fluorescence emission was corrected for variations in the absorptions. The solvents

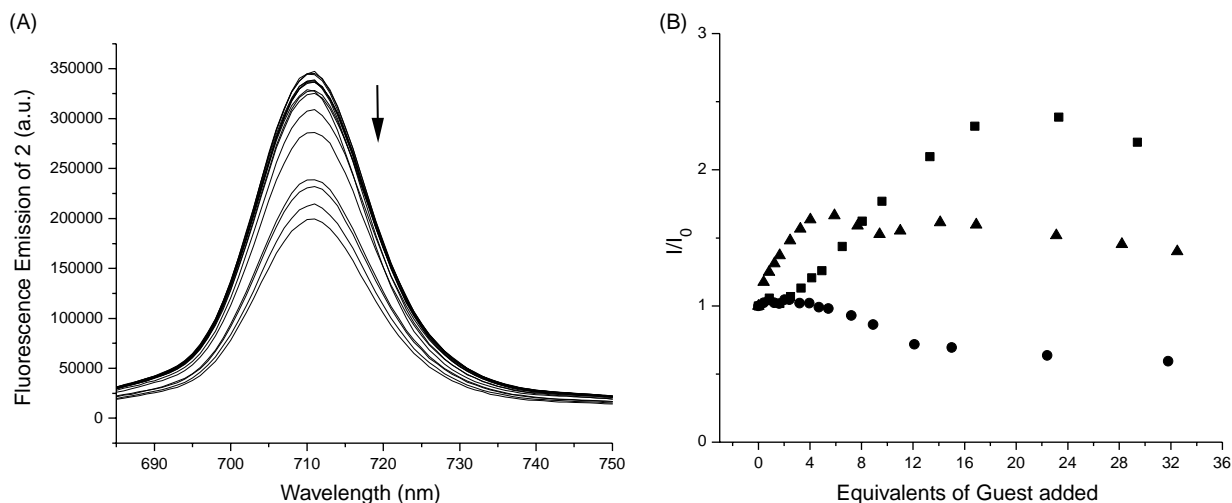


Figure 8. (A) Changes in the emission spectrum of **2** (1.0×10^{-6} M) seen upon the addition of **4** ($0\text{--}3.3 \times 10^{-5}$ M) in 20% DCM/toluene; excitation wavelength 660 nm. (B) Plot of the change in fluorescence intensity of **2** as a ratio of I/I_0 versus equivalents of guest (**4** (●), **5** (■), and **6** (▲)) in 20% DCM/toluene. For titration of **2** with **4**: (excitation at 660 nm), $[2] = 1.0 \times 10^{-6}$ M and $[4] = 0\text{--}3.3 \times 10^{-5}$ M. For titration of **2** with **5**: (excitation at 662 nm), $[2] = 1.3 \times 10^{-6}$ M and $[5] = 0\text{--}3.8 \times 10^{-5}$ M. For titration of **2** with **6**: (excitation at 662 nm), $[2] = 1.3 \times 10^{-6}$ M and $[6] = 0\text{--}4.2 \times 10^{-5}$ M.

used for spectroscopic analyses were ACS spectranalyzed DCM (Fischer) and spectrophotometric grade toluene (ACROS).

Control **3** was prepared using a standard procedure.²⁰ Fullerene **6** was used as purchased from MER corporation. Nucleobases **5** and **7** were synthesized using standard protection protocols.²¹ Synthetic compound **4** was prepared as described elsewhere.¹⁷

5.1.1. 4-Amino-5-[5'-ethynyl-tri-tert-butylphthalocyaninatoZn(II)]-1-[2',3',5'-tri-O-(tert-butyl-dimethylsilyl)-β-D-ribofuranosidyl]-pyrimidin-2-one (2). To a mixture of tri-tert-butyl(ethynyl)phthalocyaninatozinc²² (77 mg, 0.1 mmol) and iodocytidine²³ (86 mg, 0.12 mmol) in dry toluene (10 ml) and triethylamine (1 ml) under argon atmosphere, CuI (2 mg, 10 μmol) and Pd(PPh₃)₄ (11.5 mg, 10 μmol) were added. The reaction mixture was then stirred and heated at 50 °C overnight. After cooling, the solvents were removed in vacuo and the crude product was purified by flash column chromatography (SiO₂, methanol/dichloromethane 1:100), yielding **2** as a green solid (75 mg, 55%): mp > 250 °C (decomp.); UV-vis (CH₂Cl₂) λ_{max} (nm) (log ε): 679 (5.12), 347 (5.03); ¹H NMR (300 MHz, CD₂Cl₂ with a drop of CD₃OD) δ 8.9–7.2 (br×m, 12H), 5.9–5.7 (m, 1H), 4.3–4.0 (m 4H), 3.8 (m 1H), 1.9–1.5 (m, 27H), 1.07 (s, 9H), 0.95 (s, 9H), 0.93 (s, 9H), 0.32 (s, 6H), 0.17 (s, 3H), 0.14 (s, 3H), 0.13 (s, 3H), 0.09 (s, 3H); ¹³C NMR (75 MHz, CD₂Cl₂ with a drop of CD₃OD) δ 163.2, 153.5, 148.9, 143.2, 142.5, 138.5, 133.8, 133.4, 131.00, 128.9, 126.6, 125.7, 120.3, 118.7, 95.0, 90.7, 89.0, 83.9, 80.3, 76.0, 70.0, 61.8, 36.1, 32.3, 29.1, 25.6, 24.8, 17.8, 17.5, 17.2, –5.2, –5.5, –5.9; ESI-MS: m/z 1354–1358 [M]⁺: calcd for **2** C₇₃H₉₃N₁₁O₅Si₃Zn: C 64.74, H 6.92, N 11.38; found C 64.32, H 6.83, N 11.06.

Acknowledgements

This work was supported by the Robert A. Welch Foundation grant (F-1018 to J.L.S.), the EU (RTN network 'WONDERFULL' SFB-583), and the Office of Basic Energy Sciences of the U.S. Department of Energy (NDRL 4651), as well as by the Ministerio de Educación y Ciencia and Comunidad de Madrid, Spain (CTQ-2005-08933-BQU and GR/MAT/0513/2004, respectively). J.L.S. would like to express his appreciation to the Spanish Ministry of Education for a Sabbatical Fellowship (SAB2002-0153). J.J. would like to thank the Dorothy B. Banks Foundation for a research fellowship at the University of Texas at Austin.

References and notes

- (a) Kadish, K. M., Smith, K. M., Guillard, R., Eds.; *The Porphyrin Handbook*; Academic: San Diego, 2003; Vols. 15–20. (b) Leznoff, C. C., Lever, A. B. P., Eds.; *Phthalocyanines: Properties and Applications*; VCH: Weinheim, 1989, 1993, 1996; Vols. 1–4. (c) Hanack, M.; Heckmann, H.; Polley, R. In Schaumann, E., Ed.; *Methods in Organic Chemistry*; Thieme: Stuttgart, 1998; Vol. E9d, p 717. (d) de la Torre, G.;

- Nicolau, M.; Torres, T. In *Phthalocyanines: Synthesis, Supramolecular Organization and Physical Properties*; Nalwa, H. S., Ed.; Academic: New York, 2001.
- (a) Fabian, J.; Nakazumi, H.; Matsuoka, M. *Chem. Rev.* **1992**, *92*, 1197. (b) Schmidt, H.-W. *Adv. Mater.* **1989**, *1*, 218. (c) Birkett, D. *Chem. Ind.* **2000**, *5*, 178. (d) Kuder, J. E. *J. Imaging Sci.* **1988**, *32*, 51.
- (a) de la Torre, G.; Vázquez, P.; Agulló-López, F.; Torres, T. *J. Mater. Chem.* **1998**, *8*, 1671. (b) de la Torre, G.; Vázquez, P.; Agulló-López, F.; Torres, T. *Chem. Rev.* **2004**, *104*, 3723.
- (a) Bonnett, R. *Chem. Soc. Rev.* **1995**, *24*, 19. (b) Xue, L. Y.; Chiu, S. M.; Oleinick, N. L. *Oncogene* **2001**, *20*, 3420.
- (a) Linszen, T. G.; Durr, K.; Hanack, M.; Hirsch, A. *J. Chem. Soc., Chem. Commun.* **1995**, 103. (b) El-Khouly, M. E.; Ito, O.; Smith, P. M.; D'Souza, F. *J. Photochem. Photobiol., C* **2004**, *5*, 79. (c) Nojiri, T.; Alam, M. M.; Konami, H.; Watanabe, A.; Ito, O. *J. Phys. Chem. A* **1997**, *101*, 7943. (d) Guldi, D. M.; Gouloumis, A.; Vázquez, P.; Torres, T. *Chem. Commun.* **2002**, 2056. (e) Guldi, D. M.; Zilbermann, I.; Gouloumis, A.; Vázquez, P.; Torres, T. *J. Phys. Chem. B* **2004**, *108*, 18485. (f) Loi, M. A.; Denk, P.; Hoppe, H.; Neugebauer, H.; Winder, C.; Meissner, D.; Brabec, C. J.; Sariciftci, N. S.; Gouloumis, A.; Vázquez, P.; Torres, T. *J. Mater. Chem.* **2003**, *13*, 700.
- Snow, A. W. In Kadish, K. M., Smith, K. M., Guillard, R., Eds.; *The Porphyrin Handbook*; Academic: San Diego, 2003; Vol. 17, p 129.
- George, R. D.; Snow, A. W.; Shirk, J. S.; Barger, W. R. *J. Porphyrins Phthalocyanines* **1988**, *2*, 1.
- (a) Martin, P. C.; Gouterman, M.; Pepich, B. V.; Renzoni, G. E.; Schindele, D. C. *Inorg. Chem.* **1991**, *30*, 3305. (b) Dhami, S.; de Mello, A. J.; Rumbles, G.; Bishop, S. M.; Phillips, D.; Beeby, A. *Photochem. Photobiol.* **1995**, *61*, 341.
- (a) Cook, M. J.; Chambrier, I. In Kadish, K. M., Smith, K. M., Guillard, R., Eds.; *The Porphyrin Handbook*; Academic: San Diego, 2003; Vol. 17, p 37. (b) Law, K.-Y. *Chem. Rev.* **1993**, *93*, 449.
- (a) See Ref. 6 (b) Schutte, W. J.; Sluyters-Rehbach, M.; Sluyters, J. H. *J. Phys. Chem.* **1993**, *97*, 6069. (c) Fujiki, M.; Tabei, H.; Kurihara, T. *J. Phys. Chem.* **1988**, *92*, 1281. (d) de la Escosura, A.; Martínez-Díaz, V. M.; Thordarson, P.; Rowan, A. E.; Nolte, R. J. M.; Torres, T. *J. Am. Chem. Soc.* **2003**, *125*, 12300. (e) Engel, M. K.; Bassoul, P.; Bosio, L.; Lehmann, H.; Hanack, M.; Simon, J. *Liq. Cryst.* **1993**, *15*, 709. (f) Li, X.-Y.; Ng, D. K. P. *Tetrahedron Lett.* **2001**, 305.
- (a) Martínez-Díaz, V. M.; Fender, N. S.; Rodríguez-Morgade, S. M.; Gómez-López, M.; Diederich, F.; Echegoyen, L.; Stoddart, F. J.; Torres, T. *J. Mater. Chem.* **2002**, *12*, 2095. (b) Guldi, D. M.; Ramey, J.; Martínez-Díaz, V. M.; de la Escosura, A.; Torres, T.; Da Ros, T.; Prato, M. *Chem. Commun.* **2002**, 2774. (c) Guldi, D. M.; Gouloumis, A.; Vázquez, P.; Torres, T.; Georgakilas, V.; Prato, M. *J. Am. Chem. Soc.* **2005**, *127*, 5811.
- For a review on synthetic ensembles prepared through base-pairing interactions see: Sessler, J. L.; Jayawickramarajah, J. *Chem. Commun.* **2005**, 1939.
- Increasing the rigidity of the linkers in nucleobase derived systems can dramatically enhance association through base-pairing interactions. See: Sessler, J. L.; Wang, B.; Harriman, A. *J. Am. Chem. Soc.* **1993**, *115*, 10418.
- Lee, L. K.; Sabelli, N. H.; LeBreton, P. R. *J. Phys. Chem.* **1982**, *86*, 3926.
- The split Q-band is attributed to the monomeric species and not to aggregation. This is because when pyridine (a ligand

- that can coordinate to the Zn metal center and thereby effect de-aggregation) is added to the solution, the split Q-band persists. In contrast, the aggregation bands (centered at 630 and 750 nm, respectively) completely disappear.
16. For examples of nucleobases coordinating through axial ligation to metal centers within a macrocyclic framework see: (a) Ogoshi, H.; Hatakeyama, H.; Yamamura, K.; Kuroda, Y. *Chem. Lett.* **1990**, 51. (b) Ogoshi, H.; Hatakeyama, H.; Kotani, J.; Kawashima, A.; Kuroda, Y. *J. Am. Chem. Soc.* **1991**, *113*, 8181.
 17. Sessler, J. L.; Jayawickramarajah, J.; Gouloumis, A.; Torres, T.; Guldi, D. M.; Maldonado, S.; Stevenson, K. J. *Chem. Commun.* **2005**, 1892.
 18. (a) Satake, A.; Kobuke, Y. *Tetrahedron* **2005**, *61*, 13 and references therein. (b) Boyd, P. D. W.; Hodgson, M. C.; Rickard, C. E. F.; Oliver, A. G.; Chaker, L.; Brothers, P. J.; Bolskar, R. D.; Tham, F. S.; Reed, C. A. *J. Am. Chem. Soc.* **1999**, *121*, 10487. (c) Mizuseki, H.; Igarashi, N.; Belosludov, R. V.; Farajian, A. A.; Kawazoe, Y. *Synth. Met.* **2003**, *138*, 281. (d) El-Khouly, M. E.; Islam, S. D.-M.; Fujitsuka, M.; Ito, O. *J. Porphyrins Phthalocyanines* **2000**, *4*, 713. (e) Kessler, B. *Appl. Phys. A* **1998**, *67*, 125.
 19. To confirm that compounds **4**, **5**, and **6** were indeed binding with control **3**, fluorescence emission of **3** was monitored (excitation at 656 nm) as a function of increasing concentrations of **4**, **5**, and **6**, respectively. Addition of all three compounds resulted in a decrease in fluorescence (monitored at 684 nm), substantiating the notion that they can interact with ZnPc **3**.
 20. Mosers, F. M.; Thomas, A. L. In *Phthalocyanines*, Vol. 2; CRC: Boca Raton, FL, 1983; Chapter 1.
 21. Hayakawa, H.; Haraguchi, K.; Tanaka, H.; Miyasaka, T. *Chem. Pharm. Bull.* **1987**, *35*, 72.
 22. Maya, E. M.; Vázquez, P.; Torres, T. *Chem. Eur. J.* **1999**, *5*, 2004.
 23. Sessler, J. L.; Brown, C. T.; Wang, R.; Hirose, T. *Inorg. Chim. Acta* **1996**, *251*, 135.